Finite element modelling of transportation tunnels

Haluk Bayrakdar

FINITE ELEMENT MODELLING OF TRANSPORTATION TUNNELS

VOLUME I

By
Haluk Bayrakdar
B.Sc., M.Sc.

This thesis is submitted to the University of Durham for the Degree of Doctor of Philosophy

School of Engineering
University of Durham
September, 1995

VOLUME I

CONTENTS

VOLUME II

APPENDICES

Dedicated to my parents who brought me up,

to Imge who has taken me on,

and to Prof. Attewell and to Dr. Bermek who made it possible.

DECLARATION

I declare that the work reported in this thesis was carried out by the candidate. It has not previously been submitted for any degree and all material in this thesis is original except where indicated by reference to other work.

STATEMENT OF COPYRIGHT

FINITE ELEMENT MODELLING OF TRANSPORTATION TUNNELS

ABSTRACT

by
Haluk Bayrakdar

The aim of this thesis is to determine the ground deformation and stress distribution around highway tunnels at various stages of excavation and for several support conditions using finite element modelling techniques.

When ground is excavated and material removed the subsequent redistribution of stress in the remaining surrounding material needs to be treated by one of three methods. These are the gravity difference method, the stress reversal technique and the relaxation approach. The first two methods were chosen for the simulation of excavation in this study.

The tunnel data are in the form of the dimensions of the tunnel, heights of the rock layers, details of the shotcrete lining and tunnel support systems. A pre-processing program was written to transform this information into a finite element mesh in a format suitable for use by PAFEC-FE software. This enables different tunnel models and meshes to be produced with minimum error and time.

The lack of adequate post-processing facilities available in PAFEC-FE dictated that computer programs needed to be written in order to reformat the textual output files and process the mesh stress and displacement outputs for graphical display using UNIRAS. In this way repeated use could be made of PAFEC-FE without time-consuming and error-prone manual retrieval of data.

The tunnels were modelled at various stages of excavation and with such support provided at those stages as to allow the computed displacements to be compared with measurements made on highway tunnels in Turkey. The stresses generated in the tunnel supports and surrounding ground were also calculated to enable the possibility of damage or failure of the support structure or ground to be assessed and the selection of an optimal support system. Insertion of a support system into the model has a marginal effect on the development of rock strength around an excavation boundary.

ACKNOWLEDGEMENTS

The work described in this thesis was financed jointly by a construction company and by the University of Durham, and I wish to express my thanks to both of these bodies. I am also indebted to the staff of the Istanbul Technical University for their help and support.

I am extremely grateful to my supervisors Prof. Peter Attewell and Dr. John Wilson for the initial setting up of the project and for their advice, support, helpful comment and information through this study.

I am especially grateful to my friend and colleague Dr. Jonathan Welch, with whom I have had many interesting and enlightening discussions about modelling. I am also extremely grateful to Dr. Norman James Powell for introducing me to the finite element method and mesh design. The advice and additional support provided by Dr. David Toll and my colleagues Rory Barr and Bob Bement were also greatly appreciated.

I would like to thank the staff of both the School of Engineering and the Computer Service (especially the night operator) for the support provided during the project. Thanks to Wendy Lister, Val Yorkston and Janet Barclay for their sensible approach to secretarial work.

I am indebted to Diana Mihalopoulou, Andy Oliver, Vicky Malandraki, Liam Keating, Marlene Lopez, Adnan Bashir and Antonis Giolas for their support and friendship during my time in Durham. I am also grateful to Alex, Bernei, Steve, Emad, Hugh, Michael, Graham, Alamin, Sophia and many others who have put up with me over the years.

Lastly I would like to thank Ayse Kizilersü for her unfailing encouragement and understanding during my time in Durham.

LIST OF FIGURES

LIST OF TABLES

NOTATION

CHAPTER 1

B_{eq}	Equivalent dimensions of the excavation
B	Excavation span
ESR	Excavation support ratio
g	The value of acceleration due to gravity
h	Depth below surface
J_a	Degree of alteration or filling along the weakest joint
J_n	Number of joint sets
J_r	Roughness of the most unfavourable joint or discontinuity
J_w	Water inflow
Q	Rock classification (Barton et al., 1974)
RQD	Rock quality designation
SRF	Stress conditions express in terms of the stress reduction factor
ν	Poisson's ratio
K	Ratio of the horizontal stress to the vertical stress
ρ	Density of overburden
$\sigma_x = \sigma_z$	Horizontal component of the ground stress
τ_{xy}, τ_{yz},τ_{zx}	Shear stresses
$\sigma_y = \sigma_v$	Vertical component of the ground stress
σ_z	Z-(third) directional component of ground stress

CHAPTER 2

A, B, C	Identified rock classes for lithologies
E	Young's modulus
r_1, r_5	Radii of the tunnel geometry
RMR	Rock mass ratio

RMR	Rock mass ratio
SCR	Solid core rate
TCR	Total core rate
ν	Poisson's ratio

CHAPTER 3

a	The tunnel radius
e	Volumetric strain (dilation)
E	Young's modulus
F', $F'_{(x)}$, $F'_{(y)}$	Reversed excavation surface forces
F, $F_{(x)}$, $F_{(y)}$	Projected excavation surface forces
G	Shear modulus
r	Any radial distance
u	The radial displacement with a positive sign denoting movement towards the origin
U_r	Resultant displacement
U_x, U_y, U_z	Excavated ground directional displacements
U'_x, U'_y, U'_z	Unexcavated ground directional displacements
u, v, w	Three components of displacements along the x, y, z directions
σ_h , σ_v	Horizontal and vertical stresses
σ_r	Resultant radial stress at distance r from the centre of the tunnel and angle θ from x axis
υ	The circumferential displacement
σ_{eq}	The equivalent (Von Mises) stress
σ_θ	The hoop (tangential) stress
θ	The polar co-ordinate angle with respect to the x horizontal axis
$\tau_{r\theta}$	The shear stress in the element
τ_m'	Uniaxial Von Mises stress

σ_{yield}	Uniaxial yield stress
τ_m	Von Mises stress
$\sigma_{xx}, \sigma_{yy}, \sigma_{zz}$	Excavated ground directional stresses
$\sigma_{xy}, \sigma_{yz}, \sigma_{zx}$	Excavated ground directional stresses
$\sigma'_{xx}, \sigma'_{yy}, \sigma'_{zz}$	Unexcavated ground directional stresses
$\sigma'_{xy}, \sigma'_{yz}, \sigma'_{zx}$	Unexcavated ground directional stresses
λ	Lamé's constant
ν	Poisson's ratio
σ_x , σ_y , σ_z	The three normal stresses, assumed positive if compressive
ε_x , ε_y , ε_z	Three normal strains, assumed positive if compressive
τ_{xy} , τ_{yz} , τ_{zx}	The three independent shear stresses and six corresponding strain components
γ_{xy} , γ_{yz} , γ_{zx}	Three shear strains

CHAPTER 4

ANG1(θ)	Local axis direction
ASTR	Averaged stresses
DSTR	Directional stresses
E	Young's modulus
ESTR	Gravity difference method Von Misses stress
EXCT	Excavated ground
F(1), F(2), F(3)	Directional forces along the x, y, z respectively
Fx, Fy, Fz	Directional forces
g	The value of acceleration due to gravity (9.81 m/s^2) used by PAFEC
GDIF	Gravity difference
IA	Axis set
IE	Element number
IG	Group number

IL	Load case
IN	Node number
IT	Element type
IYY, IZZ	Two principal second moments area of the beam element section
KPSH(8)	Number of pafblocks in distinct regions of shell calculation
LOC	Local axis
MSYM	Symmetric model
N1, N2, N5	Reference subdivision number in the mesh module
NBS	Number of pafblock in each shell
NCOL	Number of columns
NDIM	Total number of dimension
NNS	Number of nodes in each shell
NOELS	Total number of elements
NONOS	Total number of nodes
NPLR	Number of pafblock from last ring inside the tunnel
NPOT	Number of pafblock outside the tunnel
NPSIDE	Number of pafblocks besides the tunnel
NROW	Number of rows
NU	Poisson's ratio
RO	Mass density
UNEX	Unexcavated ground
USTR	Unaveraged stresses
VSTR	Von Mises stresses
XC(10), YC(10)	Co-ordinates of the tunnel centres
XE, YE, ZE	Excavated ground directional displacements
XGVALUE	The value of x directional acceleration due to gravity
XU, YU, ZU	Unexcavated ground directional displacements
YGVALUE	The value of y directional acceleration due to gravity
ZGVALUE	The value of z directional acceleration due to gravity
ZY, ZZ	Sectional module of the beam element

CHAPTER 5

D1MAX	Maximum dimension of each pafblock for DIM(1)
D1MIN	Minimum dimension of each pafblock for DIM(2)
D2MAX	Maximum dimension of each pafblock for DIM(3)
D2MIN	Minimum dimension of each pafblock for DIM(4)
DIM(4)	Dimensions of each pafblock of xy plane
H(3)	Major and minor heights of steel arch along the y axis
IPAF	Pafblock number counter
K(0:8)	Number of extra levels in region A and C
KPSH(8)	Number of pafblocks in distinct regions of shell calculation
N1, N2, N5	Reference pafblock subdivision number in the mesh module
NBS	Number of pafblock in each shell
NCOL	Number of columns
NDIM	Total number of dimension
NNS	Number of nodes in each shell
NPLR	Number of pafblock from last ring inside the tunnel
NPOT	Number of pafblock outside the tunnel
NPSIDE	Number of pafblocks besides the tunnel
NROW	Number of rows
NSIZE	Maximum size of the elements
NSUBCO	Column pafblock subdivision
NSUBRO	Row pafblock subdivision
NSUBSH	Shell pafblock subdivision
NZ	Number of subdivision made of the minimum pafblock (resolution number)
RATIO	Aspect ratio of an element (14.9)
SAMAJ	Half width of steel arch flange
SAMAJ2	Half width of steel arch along the y axis

SAMIN	Half width of steel arch web
SANCH	Half circular cross-section of the anchorage
X(NODELE)	X co-ordinate of node
XDIM	X-dimension of pafblock
XMAX	Maximum pafblock size along the x-axis
XMIN	Minimum pafblock size along the x-axis
Y(NODELE)	Y co-ordinate of node
YDIM	Y-dimension of pafblock
YMAX	Maximum pafblock size along the y-axis
YMIN	Minimum pafblock size along the y-axis
Z(5)	Lengths of longitudinal-section of the tunnel (period)
ZMAX	Maximum pafblock size along the z-axis
ZMIN	Minimum pafblock size along the z axis

CHAPTER 6

ASTR	Averaged stresses
NU	Total number of element
RASTR	Rearrange average stresses
SIG MISES	Von Mises stresses
USTR	Unaveraged stresses

CHAPTER 7

Ux	X-directional displacement
Uy	Y-directional displacement
U	Resultant displacement
U_{DL}	Left hand side of the tunnel diagonal displacement
U_{DR}	Right hand side of the tunnel diagonal displacement
U_{H}	Horizontal displacement

CHAPTER 1

INTRODUCTION

1.1 Definition of Tunnel

A tunnel may be defined as a "long, narrow, essentially linear excavated underground opening with a length greatly exceeding its width or height." Most tunnels are driven substantially on the level, or with a shallow inclination, but for special purposes may be driven at angles up to 30 degrees. Long, linear sub-surface excavations at angles greater than 30 degrees from the horizontal are generally referred to as shafts or adits.

1.2 Tunnel Design and Tunnelling Techniques

When people started living in the Eastern Mediterranean countries, one of the most urgent problems was that of bringing water from considerable distances to those places. For centuries, starting with the Romans in about 1200 BC, to the declining years of the Roman Empire, tunnels were constructed as part of elaborate aqueduct systems. The modern tunnel age started with construction of the railroads and development of rapid transit systems, and infrastructure generation in urban areas.

1.2.1 Tunnel Design

Figure 1.1 shows a general design procedure for tunnelling. There are two main steps in the design of underground openings in rock as follows.

i) Modelling of underground openings in terms of geometry, dimensions, rock mass characterisation and boundary conditions, including in situ stresses based on observation and experiments.

ii) Selecting an approach for analysis of problems in terms of stress concentrations, deformations based on theory and/or support mechanism.

The design of tunnels in rock currently utilises five main approaches; experimental, empirical, observational, analytical and numerical.

In view of the very complex nature of rock masses and difficulties encountered with their characterisation, the analytical approach is the least used in the present engineering practice. The reason for it does not lie in the analytical techniques themselves. Analytical solutions have been developed to a high degree of sophistication but they are unable to furnish the necessary input data as the ground conditions are rarely enough explored. Consequently, such analytical techniques are mainly useful for assessing the influence of the various parameters or processes and for comparing alternative design schemes.

The observational and experimental approach are based on observations and monitoring of tunnel behaviour during construction and selecting or modifying the support as the project proceeds. The New Austrian Tunnelling Method (NATM) is the good example of the observational approach. The support is adjusted during construction to meet the changes in ground conditions. In practice, a combination of rock bolts and shotcrete is used to prevent excessive loosening in the rock mass but allowing it to deform sufficiently to develop arching and self support characteristics. However the problem with this approach is that it requires special contractual provisions.

The empirical approach relates the experience encountered at previous projects to the conditions anticipated at a proposed site. If an empirical design is supported by a systematic approach to ground classification, it can effectively utilise the valuable practical experience gained at many projects. Rock classifications, which form the empirical design approach, are widely employed in rock tunnelling and most of tunnels constructed at present in Turkey use of classification system. The most extensively used and best known of these are the Rock Mass Rating (RMR) system (or geomechanics classification), the Q-system and the Terzaghi classification which was introduced over 40 years ago.

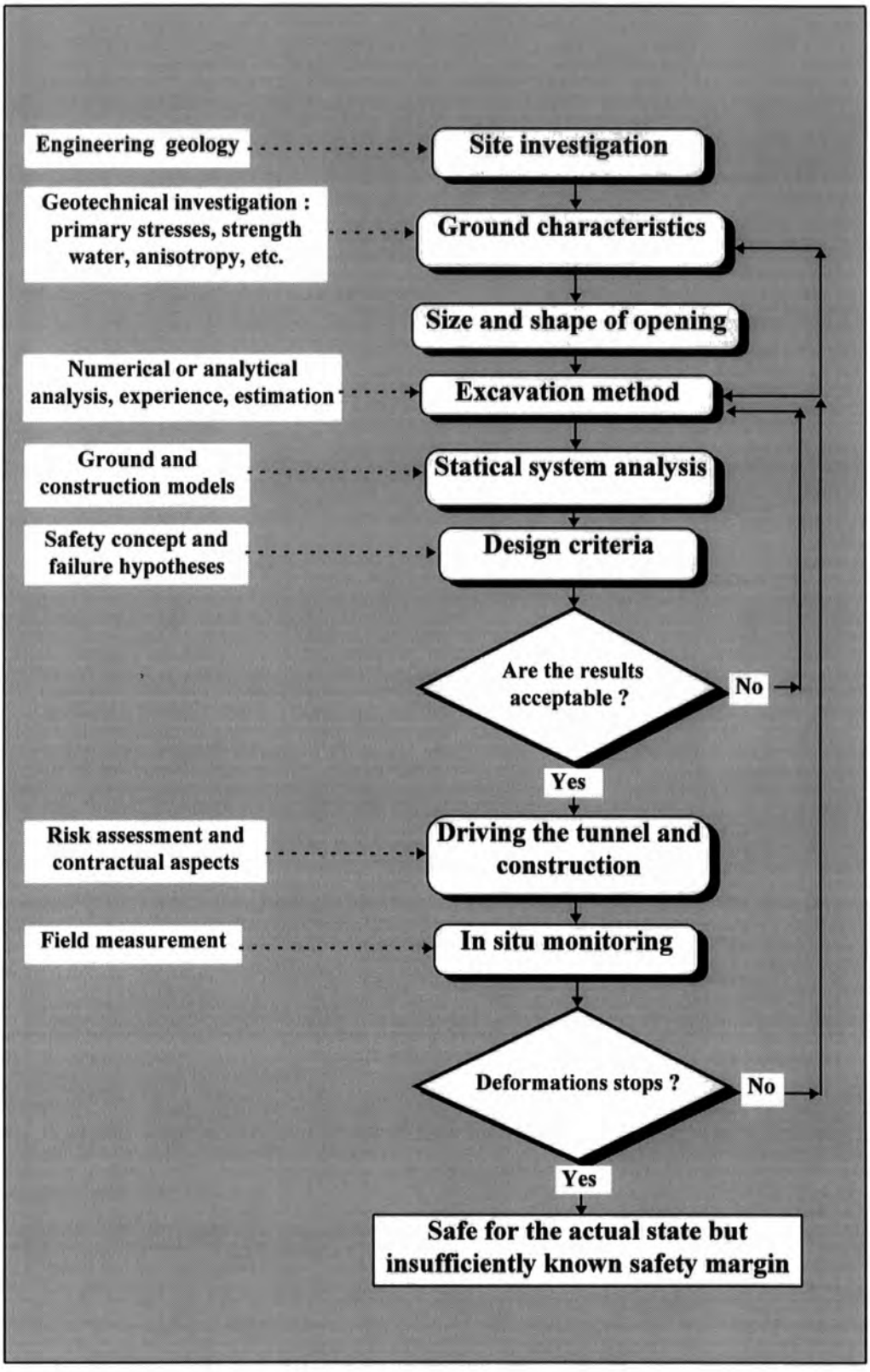

Fig. 1.1 General design procedure for tunnelling (after Duddeck, 1991)

The empirical approach may be especially reasonable if experiences from a successful tunnelling project can be applied to a similar one. Such a transfer of information is justified only when;

i) the ground conditions, including groundwater, are comparable,
ii) the dimensions of the tunnel and its cross-sectional shape are similar,
iii) the depths of overburden are approximately the same, and
iv) the tunnelling methods to be employed are the same.

The disadvantages of the empirical approach are that an appropriate tunnel design can be applied without a consistent safety assessment and the structure may be designed over-conservatively. Consequently, construction costs will be higher.

The capability of numerical approaches is large (Zienkwiecz, 1989), although it is still difficult to cover collapse modes by numerical analyses. Plasticity, viscosity, fracture of the rock, non-linear stress-strain and deformation behaviour etc. may be covered by special assumptions for material laws and applying numerical methods like those of the finite element method, the boundary element method, or a combination of both (Swoboda, 1990). For tunnel structures the ground provides the principal stability of the opening in rock and the geometrical properties of the underground opening can be modelled by numerical analysis. For instance, in the case of tunnels, a continuum or discontinuum model is necessary.

1.2.2 Tunnelling Techniques

The excavation and construction methods can significantly affect the support system requirements. Support loading can be minimised by the use of construction methods such as controlled blasting, full face machine excavation using a tunnel boring machine (TBM) or the NATM which should cause minimum overbreak or damage to the rock near to the tunnel surface. Geological conditions also change from one section of a tunnel to another. As a result, support system requirements may need to be altered during tunnel construction. Therefore the support system should be capable of responding to these changes by providing for

variations in strength or system modifications. The loosened rock remaining in place loads the primary or 'initial' support (shotcrete, steel arch or rock bolts). Its thickness may be twice as great as a result of using control blasting rather than full face machine excavation. Machine excavation generally can result in less overbreak than with blasting methods and create minimum disturbance to the ground at depth. As noted above, the essential function of support in a tunnel excavation is to re-establish the equilibrium of forces disturbed by excavation. For instance, the use of shotcrete alone for initial support is not recommended when large overbreak exists at the tunnel periphery because the resulting non-uniform stress concentration can seriously reduce the stabilising influence of the shotcrete (Attewell, 1995).

A tunnel support system can include a primary (initial) lining (shotcrete, anchorages or rock bolts, steel arches) and a secondary (final) lining, often of cast in situ or slip-formed concrete. Most tunnels are lined in two stages. The first stage is the primary lining constructed as soon as possible after the excavation process. The function of this lining is to provide support for the ground and to inhibit the direct, unimpeded entry of water. Steel arches, the function of which is to provide transfer of force from rock to support, may form part of the primary support. The term "rock reinforcement" refers to the placement of dowels or rock bolts, usually in the form of rock anchors at a fairly uniform spacing to consolidate the rock and reinforce the rock's natural tendency to support itself. In general, when tunnelling in rock, initial support should be installed immediately behind the tunnel face whether the support consists of rock bolts, shotcrete or steel arches, or a combination of these. In this manner, further rock loosening is prevented or minimised and maximum advantage is taken of the inherent ability of the rock to support itself. The second stage is a secondary or final (permanent) lining placed to prevent the effects of any additional loads which may develop after construction of the primary lining. A final lining is also placed to provide a smooth internal profile for the tunnel.

The NATM system may be characterised by the following three points.

i) It is rooted in the basic principle of tunnelling, i.e. "the tunnel should be supported by the surrounding ground as much as possible".

ii) For adhering to the basic principle of tunnelling and preserving the strength of the surrounding ground, a flexible support system such as shotcrete and or rock bolts is efficiently applied based on a second principle of tunnelling, i.e., "permit elastic deformation in ground, but exclude loosening it".

iii) Field measurements in the form of in situ monitoring are efficiently applied in order to confirm whether the flexible support system is functioning satisfactorily and to indicate when the time is right for placement of the final tunnel lining.

Kovàri (1994) demonstrates that these basic principles of tunnelling are not exclusive to the NATM but have been adopted on basic of experience for tunnel constructions throughout the world over a period of many years. Irrespective of the NATM, it is important to clarify and understand the mechanical behaviour of the surrounding ground in connection with tunnelling.

1.3 Rock Mass Classification Systems

Rock mass properties more than any other factor determine the degree of difficulty and the cost of excavating and supporting an underground opening of a given size. This is because the ground conditions greatly influence the choice of excavation method which in turn affects construction costs. Discontinuities are present in all rock masses in the form of planes or surfaces separating intact blocks of rock. Geologically these discontinuities are recognised as joints, faults, bedding planes or cleavage planes.

The strength and deformation characteristics of a rock mass are influenced in part by the physical properties of intact blocks of rock and in part by the properties of the discontinuities between the blocks. When evaluating discontinuities between blocks. consideration should be given to the spacing, orientation, extent of chemical alteration, and condition of joint in filling material.

For example, joints filled with low shear strength clay material can cause serious support problems during excavation of the tunnel. The principal aims of any rock classification system in connection with tunnelling operations can be summarised as follows ;

i) to predict rock behaviour in comparison with behaviour observed in other tunnels,

ii) to divide a particular tunnelling job into sections according to expected rock behaviour so that support details can be planned and the tunnelling work priced on the basis of reference ground conditions.

Some classification systems permit a direct estimate of the design loads or of the stand-up time.

Engineering classifications of rock masses for the design of tunnel support are detailed in many publications such as, Bieniawski (1984, 1989 and 1992), Hoek and Brown (1980), Mahtab and Grasso (1992), Sinha (1991), Whittaker and Frith (1990). Major rock classifications currently in use are given in Table 1.1. In practice most of these indexing systems have been correlated with a wide variety of rock mass properties. The classification developed by the Terzaghi (1946) is for determining rock loads on steel sets. Lauffer's (1958) classification was developed for estimating the stand-up time, the maximum elapsed time that can be allowed between excavation and support installation.

One particular rock classification system, based on the Rock Quality Designation (RQD) was proposed by Deere (1963). Barton et al. (1974) combine empirical correlations based on numerous case studies together with geomechanical parameters that should be entered in a classification scheme for tunnel support determinations.

The engineering intact rock classification proposed by Deere and Miller (1966) has been widely recognised as particularly realistic and convenient for use in the field of rock mechanics. The International Society of Rock Mechanics (ISRM) commission on rock classification recommended different ranges of values for intact rock strength (ISRM, 1981).

Name of classification	*Originator and date*	*Country of origin*	*Applications*
Stand-up time	**Lauffer, 1958**	**Austria**	**Tunnelling**
Intact rock strength	**Deere & Miller, 1966**	**USA**	**Communication**
Geomechanics classification (RMR system)	**Bieniawski, 1973**	**S. Africa & USA**	**Tunnels, mines, foundations**
Strength/block size	**Franklin, 1975**	**Canada**	**Tunnelling**

Table 1.1 Major rock classifications currently in use (Bieniawski, 1984)

The RMR geomechanic rock classification proposed by Bieniawski (1973) for jointed rock masses is generally used for the design of underground excavations. The RMR classification takes into account a combination of five basic parameters as described below ;

i) uniaxial compressive strength of intact rock: Bieniawski uses the classification of the uniaxial compressive strength of intact rock proposed by Deere and Miller (1966),

ii) drill core quality: the Deere (1963) RQD classification is used as a measure of drill core quality,

iii) spacing of joints: in this context, the term joint is used to mean all discontinuities which may be joints; faults; bedding planes and other surfaces of weakness,

iv) condition of joints: this parameter accounts for the separation or aperture of joints; their continuity; the surface roughness and presence of filling materials in the joints,

v) ground water conditions.

A number of points, or a rating, is allocated to each range of values for each parameter and an overall value for the rock mass is arrived at by adding the ratings for each of the parameters. Bieniawski (1984) relates his rock mass rating (or total rating score for the rock mass) to the stand-up time of an active unsupported span as originally proposed by Lauffer. The proposed relationship, unsupported length of tunnel and other details of the RMR rock classification are given by Bieniawski (1984, 1989).

The Q system which is also known as the NGI (Norwegian Geotechnical Institute) tunnelling quality index was developed by Barton and co-workers of the Norwegian Geotechnical Institute. The Q-system is based on a numerical assessment of the rock mass quality using six different parameters;

i) RQD;

ii) number of joint sets (J_n);

iii) roughness of the most unfavourable joint or discontinuity (J_r);

iv) degree of alteration or filling along the weakest joint (J_a);

v) water inflow (J_w); and

vi) stress conditions express in terms of the stress reduction factor (SRF).

Numerical values of each of above parameters are given as a table by Barton et al. (1974). The Q value is calculated by the formula:

$$Q = \left(RQD / J_n \right) x \left(J_r / J_a \right) x \left(J_w / SRF \right) \qquad (1.1)$$

The Q value is related to tunnel support requirements by defining the equivalent dimensions (B_{eq}) of the excavation which is calculated as :

$$B_{eq} = \frac{B}{ESR} \qquad (1.2)$$

where B is excavation span, diameter, or height and ESR is defined as the excavation support ratio which is given as a table according to the excavation category by Barton et al. (1974).

In the case of the subdivision of a tunnel profile the classification can apply to the top heading of the tunnel. If the rock in the lower portion of the tunnel (bench and invert) differs considerably from that in the top heading, the support is adapted to conform to the actual rock conditions. The behaviour of the rock at the face of a tunnel excavation is time dependent, in the sense that a trend towards instability will be faster in poor quality rock and with long free spans of unsupported rock. Accordingly, the maximum length of advance that can be excavated before instability develops is a function of rock quality and can be a parameter in the overall rock classification.

1.4 In Situ Stress Changes and Deformation

1.4.1 In Situ Stress State

In situ stresses are natural stresses which exist in the rock mass prior to any excavation. The initial ground state of stress at a point in a rock mass is the product of various events in the geological history of the rock mass. Therefore, the natural stresses present may be the resultant of many earlier states of stress.

1.4.1.1 In Situ Stresses due to Gravity

If a geologically undisturbed rock mass is considered, the vertical component of the ground stress (σ_v) is due to the effect of gravity on the mass of the above rock. In a homogeneous rock mass, when the rock density (ρ) is constant, the vertical stress is the pressure exerted by the weight of a column of overlying rock of unit cross-sectional area. Taking the origin to be at the surface and directing the y-axis vertically downwards, the vertical component of the ground stress is

$$\sigma_y = \sigma_v = \rho\, g\, h \qquad (1.3)$$

where g is the acceleration due to gravity and h is the depth below surface. In the case of a horizontally stratified rock mass, either a mean density is used in equation (1.3) or a summation process is employed as indicated by the following equation.

$$\sigma_v = \sum_{i=1}^{n} \rho_i\, g\, h_i \qquad (1.4)$$

In equation (1.4) ρ_i and h_i denote the density and thickness of the individual strata beds respectively. Most measurement carried out to determine the initial states of stress indicates that, for geological undisturbed rock masses, equation (1.4) gives an acceptable value for the vertical component of ground stresses.

The horizontal ground stress components are also found to be dependent on the depth below surface. In relatively undisturbed rock mass, both horizontal components are generally found to be equal, $\sigma_x = \sigma_z$. Their relationship to the vertical stress is usually specified by a constant K, where

$$\sigma_x = \sigma_z = K\, \sigma_v\ . \qquad (1.5)$$

It is considerably more difficult to determine the horizontal stresses (and hence the value of K) than the magnitude of the vertical ground stress component acting at a point. The lowest possible limiting value of 'K' for a set of conditions is generally derived from the assumption that, on loading an isotropic, linearly-elastic rock element by the overlying column of rock, the horizontal movement is inhibited by the presence of the neighbouring rock elements. It is easy to show that in this case, K is dependent on Poisson's ratio (ν) of the rock. and is given by

$$K = \frac{\nu}{1-\nu} \quad . \tag{1.6}$$

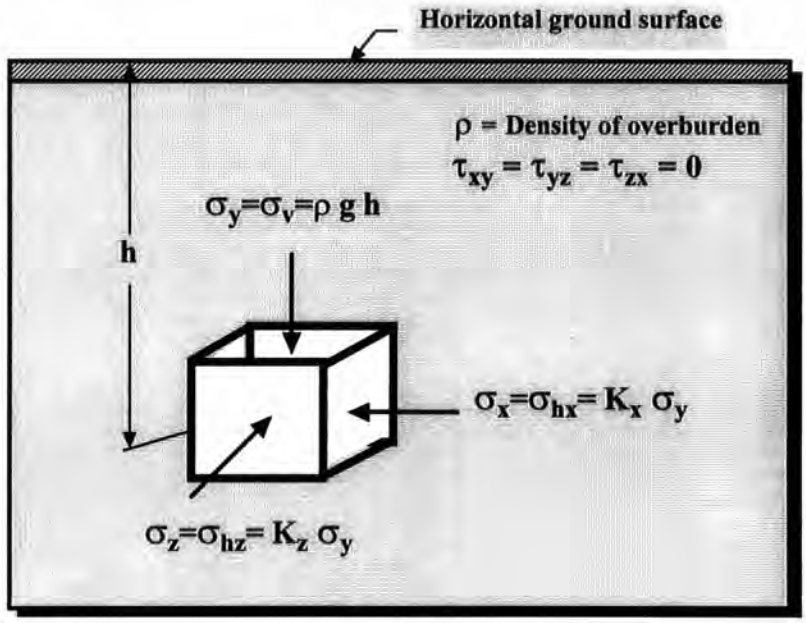

Fig. 1.2 In situ stress field

Since Poisson's ratio for most rock is between 0.20 an 0.33, the value of K should lie between 0.25 and 0.50. The magnitude of the horizontal stress components can be expected to be the same as that of the vertical component if the rock behaves plastically or elastoplastically.

1.4.1.2 Tectonic and Residual Stresses

In some instances the horizontal stresses may differ considerably from those predicted by equation (1.6) due principally to the existence of tectonic and residual stresses. Tectonic stresses are due to previous and/or present-day straining of the earth's crust. They may arise from regional uplift, downwarping, faulting, folding and surface irregularities. The superposition of these tectonic stresses on the gravity induced stress field can result in substantial changes in both direction and the magnitude of the resultant ground stresses in comparison with those of the original stress field.

Residual stresses are defined as stresses remaining in rock masses even after their causes have been removed. The existence of residual stress is usually explained in the following manner. During the previous history of a rock mass, it may have been subjected to higher stresses than it is subjected to at the present time. On removal of the load causing the higher stresses, the relaxation of the rock is resisted by the interlocking mineral grains, the shear stresses along fractures. Thus part of the earlier existing high stresses remain locked in the rock as residual stress. If the stresses are locked in on a scale less than the representative dimension of the excavation, then the residual stresses will affect only the strength of the rock. However, if the stresses are locked in on a scale larger than the dimension of the excavation, the residual stresses will be added to the load applied to rock mass.

Consequently, neither tectonic nor residual stresses magnitudes are possible to predict even to a fair degree of certainty without the measurement of in situ stresses. In order to obtain a reasonable knowledge of the state of virgin stress in a region, one must be familiar with its geology, collect and analyse the results of previous stress measurements, and observe the effects of natural stresses on existing structures in rock.

1.4.2 Stress Changes due to Tunnelling

Underground rock masses are usually in a state of static equilibrium and subjected to states of stress under the action of gravity and tectonic forces of various origins before disturbance by engineering construction. Forces in the ground have been acting for so long a period that all variations of material deformation with time have subsided unless renewed by tectonic activity. The forces on each element of ground, and the compression produced by these forces, are fixed and substantially in static equilibrium. In particular, the forces acting inwards on the proposed tunnel periphery are balanced exactly by the forces acting outwards in the rock or soil mass within the periphery. Extraction of ground to form a tunnel removes some of the force-carrying components, disturbs the pre-

existing equilibrium, and causes a redistribution of the forces acting on the remaining elements of ground. The change in force acting on a component in turn produces a change in deformation. If the deformation is excessive, the rock surrounding the tunnel moves inwards at the void. Deformations continue until the forces are re-equilibrated within the ground. Provided that the redistribution of forces in rock does not produce excessive rotation of blocks of ground or tension across any fractures such as joints (the effects which may occur depending on load distribution and joint orientation) then the system will approach equilibrium, or stabilise with inward deformation. It is possible, however, that the tangential (compressive) forces that must be developed in the unsupported peripheral ground for equilibrium to be established require intolerably high deformations and/or exceed the compressive strength of the ground, so leading to failure of the wall of the excavation.

In such cases it becomes necessary to install a resistant tunnel lining, or 'initial (primary) support'. The rate at which the readjustments occur depends on the nature of the ground and any discontinuities in it, the intensity of the stress change compared to the strength of the ground mass, and the extent to which the excavation procedures have weakened the ground. These factors will dictate the so-called "stand-up time " of the opening that is, the length of the time after excavation that a section of tunnel can be left unsupported. Lauffer (1958) attempted to formulate stand-up times for tunnels in rock under various geological conditions. His work has been discussed and noted by Bieniawski (1984). A support system cannot replace in technical effectiveness the action of the rock that was excavated. As soon as deformation starts, which is usually deep into the face, some of the load that was carried by the excavated rock is transferred to the rock surrounding the tunnel. For the tunnel walls to be able to sustain these loads, it is necessary that they maintain some degree of integrity. Even the rock that is broken by the action of support withdrawal can offer some support to the redistributed load, but only if it is prevented from falling out of the tunnel roof and walls. Rational and economic design of a tunnel lining has to be based on an understanding of the ground-support interaction. Even though an exact calculation

is not possible, formulation of a realistic model should always be a guideline for design calculations. All calculations involve to a greater or lesser degree simplifications and idealisations of the real problem. However, tunnel design methods are much less sound approximations to the true structural behaviour of the ground than are most other civil engineering design methods because of the complexity of the problem, the general lack of information about the ground at depth (one of the principal components in the structure), and the paucity of field investigations which could provide more practical guidelines.

1.4.3 Deformation due to Tunnelling

Factors affecting the type and magnitude of ground movements associated with tunnelling can be summarised as follows.

i) The geological factor is dominant in the determination of ground deformation associated with tunnel excavations.

ii) This factor, together with the properties of the rock influence to some extent the choice of type of excavation and supporting system.

iii) The geometrical factor is also important for stability of excavations. The dimension ratio (depth / clear width) of the tunnel is directly related to stability of tunnel.

iv) Ground movements are also dependent on the particular details of the construction and its progress and upon the quality of the equipment used.

Taking account of the particular character of the ground stress regime, the engineer chooses the appropriate type of support (shotcrete, anchorages, inner lining or pre-cast segments and so on) and decides on the suitable method of excavation. In the case of difficult ground conditions, in the form of longitudinal variations of lithology and structure along the tunnel axis and centre line, ground stabilisation might be an effective way of preventing severe and unacceptable ground deformation. Geotechnical processes, although very useful, in unfavourable ground conditions, must be used with care especially when the tunnel

is driven beneath urban areas because it can happen that the stabilisation of the ground around the tunnel may only be at the cost of inducing ground instability in the foundations of the nearby buildings (Attewell, 1995).

It may be argued that ground movements will always occur during construction whatever the effectiveness of the supporting system. These deformations usually take the form of;

i) an inward movement of rock on the side walls,

ii) an upward movement of the base (invert) of excavation

and iii) a surface settlement resulting from the ground loss of the side walls.

The third type of movement is probably the most serious because it is the most likely to occur, and thus place at risk the foundations of nearby buildings.

1.5 Numerical Methods in Tunnelling

Computation procedures to investigate the stability of engineering structures in rock must be able to deal with general three-dimensional states of stress as well as the usual elastic-viscoplastic and anisotropic rock and soil mass characteristics. It is not possible to include these aspects in a mathematical solution using analytical approaches. The only way to solve such complex problems lies in the application of numerical procedures of computation. One of them is known as the finite element method and has been developed significantly in recent years. However, this computational procedure also needs to be specially adapted for geotechnical engineering purposes.

The analysis method uses a numerical finite element model for a simulated elastic, homogeneous or heterogeneous body. Numerical modelling is particularly suitable for non-circular and irregular tunnel cross-sections. It is unlikely that circular cross-section tunnels driven in soil for the purposes of low pressure water or sewage transfer, and lined-out with long-established support systems, will need to have their lining support design and checked for structural integrity as a routine procedure. On the other hand, transportation tunnels of non-circular configuration driven in variable rock, often intrinsically weak and highly discontinuous, and

using several support systems will invariably require the installation of some quite sophisticated monitoring equipment. But such installations should also require the use of one or more suitable modelling systems, specifically these days of a computational nature. Models that are answerable to the sequential changes of the geometrical variables and of the ground and lining are a prime requirement. Computationally the modelling systems can take several forms, of which the finite element, boundary element and finite difference forms are the best known. A finite element form of modelling, in which a solid is discretized for better internal and boundary definition of displacements, strains and stresses, was thought to be most appropriate for modelling tunnels. But finite element (FE) models need to be calibrated, and this can be done only by using in-tunnel data from actual tunnels.

1.6 Aim and Organisation of Thesis

The aim of the present thesis is to examine ground displacement and ground stress concentration in association with primary and secondary support for two tunnels being constructed in Turkey, namely the Kisikli and Tantavi tunnels. For these tunnels the magnitude of the ground deformation is normally higher in the vicinity of opening where ground failure takes place. In this context, the main question is the prediction of the magnitude and quantity of the main parameters of the ground deformation and its numerical modelling conditions associated with tunnel support systems such as shotcrete , anchorage, steel arches and inner lining.

This is probably understandable from the point of view of simple economics, since the establishment of a numerical model of ground is far simpler and cheaper than the sinking of boreholes and the operation of continuous subsurface surveys with the aid of inclinometers, magnetic detectors and other instrumentation. Therefore, it is not surprising that during that last ten years, well-documented case histories for numerical modelling of geotechnical engineering problems have appeared in the literature.

A commercial software package (PAFEC-FE, version 7.4, marketed by a Nottingham-based international company) has been used for this modelling work

but, as is always the case with such packages, adaptation to a specific problem can be filled with difficulty. Some of these difficulties are described later in the thesis.

In order to perform a tunnel simulation with PAFEC-FE it has been necessary to first form a text file containing details of model mesh (nodal co-ordinates and element topologies, type of element used, material properties), list of control commands, dictating the type of simulation to be performed, the restraints and conditions to be applied to the model. Output from the program consisted of text files containing the requested values (stresses, displacements and so on) for the model. These output files can be examined and analysed. Simulation runs could take between a few minutes and many hours to complete, depending on model complexity, test type and system load. The most time-consuming part of producing the input file is in establishing the finite element mesh. The qualities of the mesh are important for the success of the simulation. This process can be simplified by making use of automatic or semi-automatic mesh generation. PAFEC-FE pafblocks are used for this purpose and their usage will be described later. Mesh generation may also be aided by a pre- processor. In the case of PAFEC-FE , there is the PIGS (PAFEC-Program Interactive Graphics System) but this is fairly limited. This means that for any reasonable analysis it is necessary for the user to write programs capable of pre-processing tunnel input data and which transform the tunnel parameters into a finite element mesh.

The input data are in the form of the dimensions of the tunnel, height of overburden, number of the rock layers of different heights and their material properties, reinforcing anchorages, steel arches, shotcrete, inner lining and finally excavation type which, in the case of the Turkish tunnels, is the NATM. A FORTRAN program first transforms this information into a series of pafblocks having varying dimensions and then divides each pafblock into a mesh of individual elements. Many variations of the problem can be described by simply altering the input file.

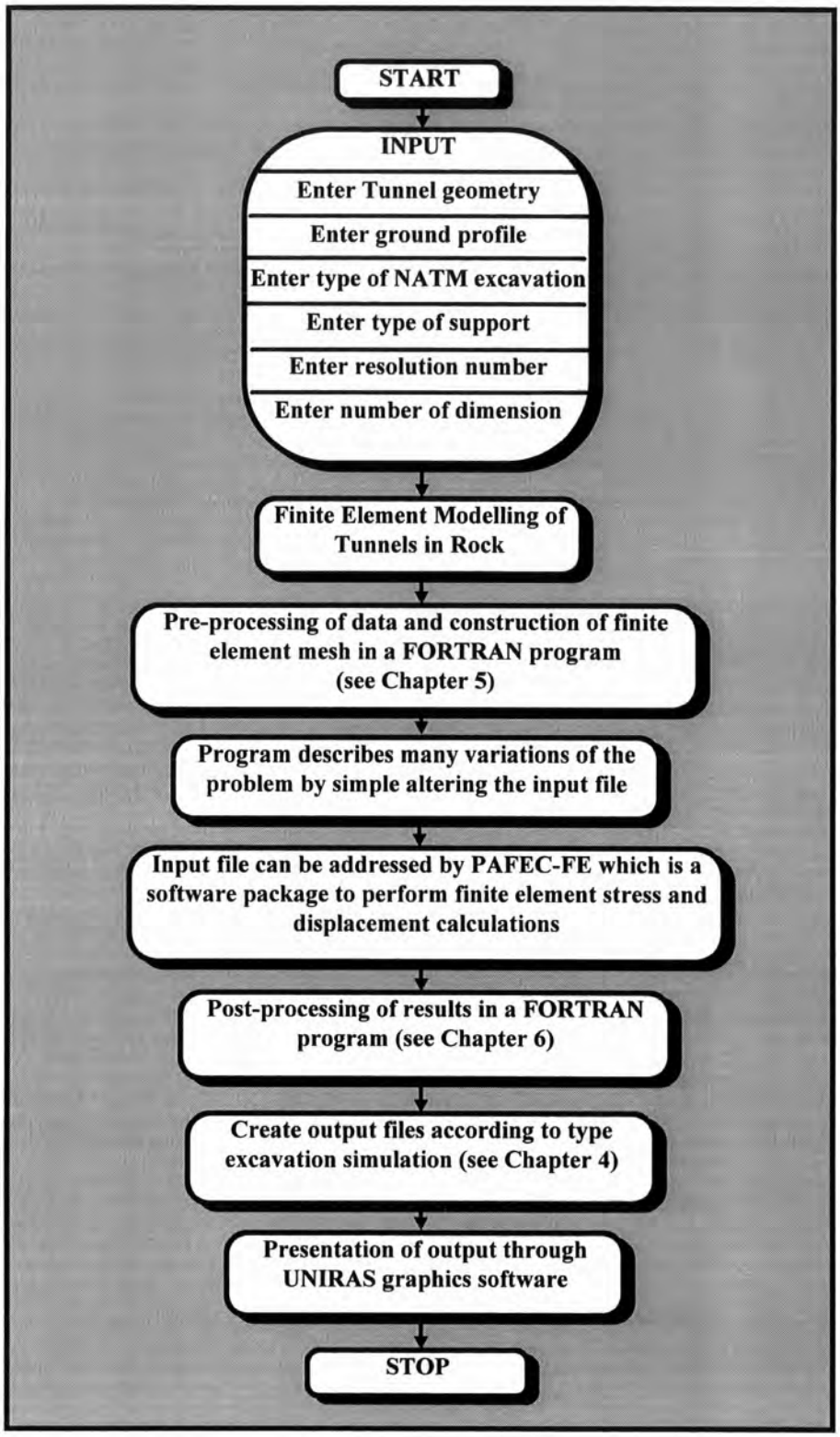

Fig. 1.3 Main Outline Flowchart

After that, simulation can be addressed by PAFEC-FE performing finite element stress and displacement analyses as shown in Fig. 1.3.

Unfortunately, PAFEC-PIGS has only a limited capability for the display of its results in simplified or graphical form, and its output files containing results are massive for a model of any complexity. For example, in the case of a model containing 5000 nodes in its mesh, no displaced shape plot was automatically produced by PAFEC-PIGS for representing distortion of a model, but the print output file contains individual nodal displacements in the three Cartesian directions for each node. This means that for any reasonable analysis of the results to be performed it is necessary to write a FORTRAN program capable of extracting stress and displacement values from the various results files and displaying them in a suitable format, usually with coloured contours representing the values superimposed on a three-dimensional solid model. Because of this difficulty, post-processing of results has accordingly been performed through UNIRAS graphics software. UNIRAS is the collective name given to a suite of programs, some dedicated to data mapping, graphing and image processing in addition to a library of graphics subroutines available for use in the user's own programs.

Having outlined the aim of the work which forms the basis of this thesis this introductory chapter is concluded by mentioning the contents of the remaining chapters.

The second chapter of this thesis deals with the description of Istanbul Kisikli and Tantavi highway tunnels project and design methods. Topics dealt with include tunnel design and construction techniques under the NATM, methods of controlling tunnel deformations, and modelling techniques applied to tunnel design and analysis.

A review of the stress analysis, the application of the finite element method to tunnel design and the other numerical methods are discussed in Chapter 3.

Special consideration is given to the basic structure and requirements of the computer program (PAFEC-FE) in Chapter 4. There is included a brief description of modules (commands) which are available in the PAFEC-FE library and the

necessary input data for automatic finite element mesh generation. A detailed description of how to implement an excavation process using finite element analysis also is described in Chapter 4. There are three possible methods;

i) the gravity difference method,

ii) the relaxation approach ,

and iii) the stress reversal technique.

Simulation of the excavation process was implemented for the purposes of this thesis by employing the gravity difference method and stress reversal technique.

Chapter 5 describes the pre processing FORTRAN program used for PAFEC-FE input data file generation and stages in the modelling process. The chapter is, in effect, designed to take the form of a user manual. There is an explanation of the program its design and objectives. A detailed description of tunnel mesh design is included together with diagrams.

Post processing programs are analysed in Chapter 6. Examples are chosen to investigate the influence of the different PAFEC-FE stress and displacement output files. Each case includes a description and result sections.

Chapter 7 contains the final summary of the most important results obtained in the thesis. Displacement results are compared with measured tunnel convergence obtained from the project.

Chapter 8 deals with the general discussion and finally, conclusions and recommendations are then made in Chapter 9 for future work that could usefully be pursued on the basis of the developments described in this thesis.

Volume II contains Appendices A to F which consist of the pre- and post-processing programs operational procedure, examples of PAFEC-FE input and output files, full lists of the pre- and post- processing programs, shell node co-ordinate calculations and details of beam elements for anchorages and steel arches.

CHAPTER 2

KISIKLI AND TANTAVI TUNNELS

2.1 Introduction

2.1.1 Tunnels in Turkey

The importance of underground construction has been increasing in Turkey during recent years. Outside the field of mining, there are clear indications that more civil engineering works involving tunnels have been undertaken and that demand is growing. Contributing factors towards this are economic, technical, and environmental. Tunnel use is increasing in areas of urban development, particularly in the railway or metro, water supply, sewerage and road construction areas. The increase in both population and industrial demand have led to greater water consumption, and consequently more and larger works for disposal of industrial and domestic waste water. Tunnels are a fundamental element in the disposal. Rapid transit systems are in existence in Istanbul and under construction in Ankara, Izmir, Adana and Bursa. Other City Councils have drawn up plans for an underground railway network. The main stumbling block at the moment affecting execution of these schemes is one of finance, but the decision by the Turkish government to accept design reports on the scheme in principle is an encouraging sign. Because of the mountain ranges between the coastal ports and the hinterland, there are many railway tunnels in existence. With the increasing development of the agricultural, mining and industrial areas, faster rail communications and new lines are being sought and constructed. There are few tunnels within the existing national road network, and the few in place are of short length. However, the planning of a high speed motorway often requires a number of major road tunnels.

In the last decades, Turkey has been a gateway for international traffic in the east-west direction only. Up to now, the Trans-Turkey Highway, which is a part of the Trans-Europe Motorway (TEM) Project, has served as a link between Europe and the Middle East through Iran, Iraq and Syria. However, since the emergence of several transition countries such as Georgia, Azerbaijan, Armenia, Russia around

the Caspian Sea region, new connections have been added to the existing Trans-Turkey Highway network in eastern Turkey. Similarly new connections have become important for the economic development of western Black Sea countries such as Romania and Bulgaria (Erden, 1994). The NATM system of tunnelling has been widely adopted in Turkey. More than 15 highway tunnels have been constructed using this system and many others are now under construction or at the planning stage.

The work described in this thesis is mainly based on the Istanbul Altunizade-Umraniye highway project (part of the TEM project) in Turkey which includes two sets of twin tunnels in rock as shown in Fig 2.1. One set of tunnels carries the highway beneath Kisikli town where open cut techniques are not practical. With respect to the second set of tunnels the open cut techniques are not permitted by the owner due to preservation of the Tantavi Park. Kisikli tunnel, 690 m long, is located under Kisikli town and it takes the form of two curved tubes that follow different alignments. Tantavi tunnel, 165 m long, is located under Tantavi park and it also consists of two tubes but the tunnel alignment is straight. The following chapter gives more details on the Kisikli and Tantavi tunnels project. It is important to analyse as accurately as possible the influence of the construction techniques and support system on the stability of the tunnel at the time when construction recommendations are made. The principal factors which affect the ground-support interaction should be considered in support system selection and design. The load distribution between the rock (as in the case of the Turkish tunnels) and the support depends on the relative stiffness of each. The rock mass must have sufficient inherent strength to carry its share of the load, or it must be reinforced and the support then be strong enough to carry its share of the load and to provide the necessary composite strength to the rock. Quantitative estimation of the interactive effects of construction techniques and ground support is possible by iteratively examining the effect of variations of one upon the other, but it does require sophisticated analysis.

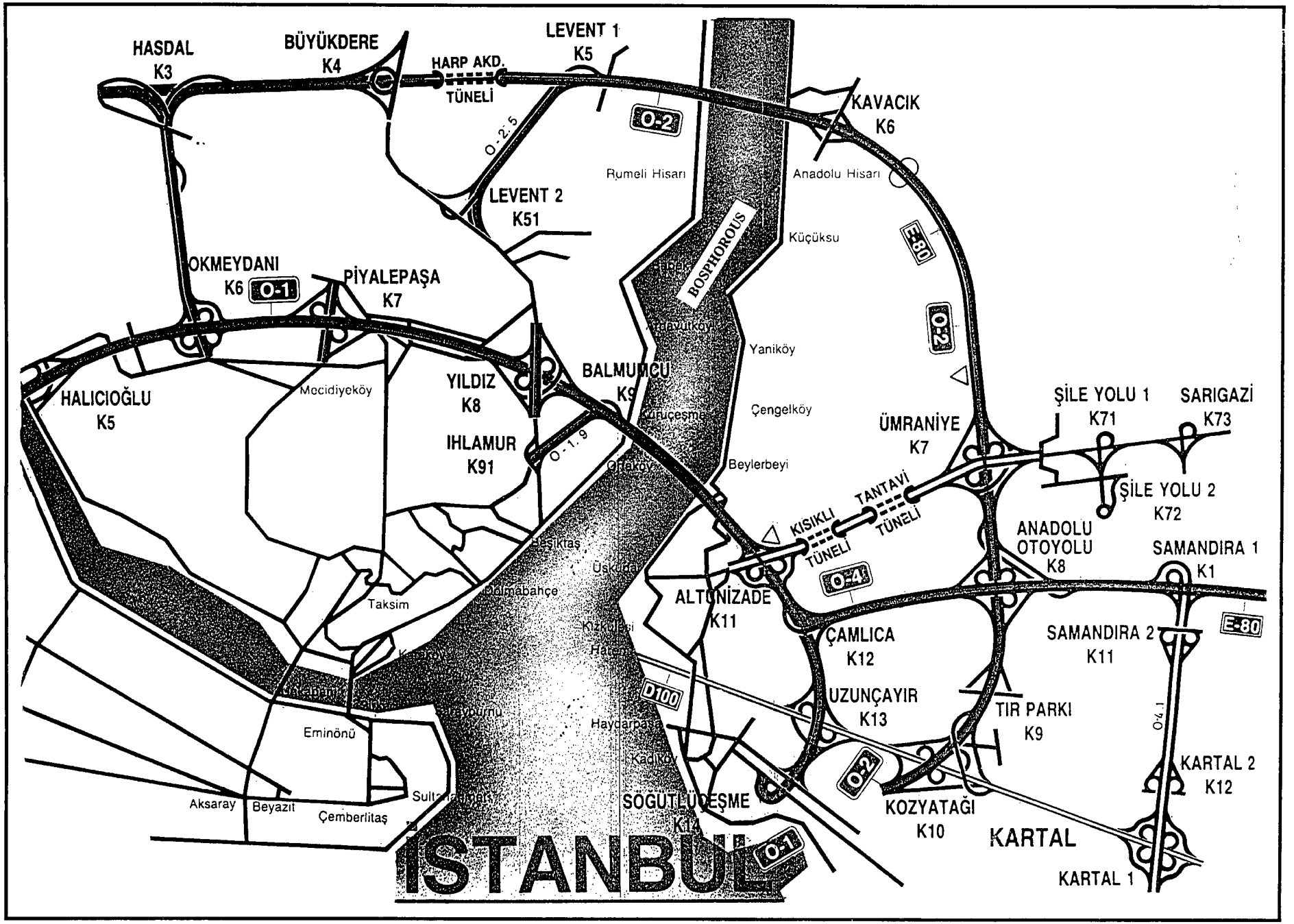

Fig. 2.1 The road networks in Bosphorous area of Istanbul and tunnel locations

2.1.2 Kisikli and Tantavi Tunnels

This chapter does not attempt to provide a full description of Kisikli and Tantavi tunnel project design and construction specifications but it does provide an introduction to the project and techniques used in the construction of these tunnels. A full description of the tunnel design was described in the final design report of STFA Construction Co. (1992).

The Istanbul Altunizade-Umraniye Highway, with construction contracted to Sezai Turkes Fevzi Akkaya (STFA) Construction Company by the General Directorate of Highways 17th Division, passes in separate tunnels under the centre of Kisikli town and Tantavi park.

	KISIKLI TUNNEL	TANTAVI TUNNEL
Tunnel shape	**Inverted horseshoe**	**Inverted horseshoe**
Length of tunnel	**515 m**	**105m**
Length of cut and cover	**175 m**	**60 m**
Total length of tunnel	**690m**	**165 m**
Number of line	**2+1**	**2+1**
Separation distance	**3.0-24.0 m**	**8.0 m**
Clear height (H)	**7.45 m**	**7.45 m**
Clear width (B)	**13.0 m**	**13.0 m**
Maximum ascending gradient	**1%**	**1%**
Volume of excavation	**160000 m3**	**54000 m3**
Volume of reinforced concrete	**32300 m3**	**12000 m3**
Shelter steel arch mass	**2800 tonne**	**810 tonne**
Total anchoring length	**58 km**	**22 km**
Total mass of steel	**400 tonne**	**240 tonne**
Total injection hole length	**62 km**	**36 km**
Total number of lights	**430**	**300**
Total length of lighting cable	**2500 m**	**1000 m**
Number of ventilation fans	**2**	**-**
Number of fire alarms	**2**	**2**
Number of fire hoses	**1**	**-**

Table 2.1 Some technical properties of Kisikli and Tantavi tunnels

STFA Construction Company appointed Acer Consultants Limited to undertake the design and specification of the tunnels. Some of the major construction and design parameters are given in Table 2.1. The Istanbul Altunizade-Umraniye Highway consists of two lanes in each direction. In addition to these two lanes of 3.5 m width, the tunnels were designed to incorporate a subsidiary lane dictating an overall clear width of 13 m. A clear height of 7.45 m is provided over the invert of tunnel. Two 0.75 m wide walkways having a clear height of 2 m are provided each side of the carriageway.

Tunnel construction was performed according to the principles of the NATM as described in Section 2.6. A top heading and bench method of excavation were used together with a primary lining of shotcrete, rock bolts, forepoling and steel arches when necessary. The secondary (final) lining was of plain concrete as described in Section 2.6.

The electro-mechanical fittings include power supply and emergency power supply, lighting, ventilation, fire alarms and emergency call systems, fire fighting, traffic signals and traffic signs. The electro-mechanical system to be installed in the tunnels is always run in automatic mode unless a manual mode is selected by the authorised person. Since the length of Tantavi tunnel is relatively short, an automatic lighting system only was installed in this tunnel. Ducts are provided each side of the carriageway to accommodate drainage and cables for electricity, fire alarms, telephones and monitoring. The tunnel invert accommodates the materials necessary to form a suitable road surface.

2.2 Kisikli Tunnels

2.2.1 Project Description

The Kisikli tunnel is located on the route of the Istanbul Umraniye-Altunizade Highway as it passes through beneath the centre of Kisikli town, in the south eastern suburbs of Istanbul. The separation distance of the two tunnel tubes amounts to 24.0 m at maximum and decreases to a minimum value of 3.0 m

towards the ends of the drive. The portals, to be built by open construction method subsequently, have lengths of 135 m and 40 m .

2.2.2 Engineering Geology

Thirteen cored borings were made for the Kisikli tunnel, probing in general to 2 m below tunnel invert level. Information from the boreholes, however, does not provide sufficient information for formulating a clear picture of the structure. It is probable, in retrospect, that more detailed investigation could have provided a significantly clearer picture of the geological structure through which the tunnels are driven. The main features of the geological structure are as follows.

i) Significant folding, including possible overfolding (recumbent folding) of all the strata has occurred.

ii) Significant faulting has occurred, particularly towards the western end of the proposed tunnel alignment. The faults seem to include a low inclination thrust fault close to the junction of the quartzite/micaceous sandstone, siltstone, claystone sequence and the underlying arkose. Arkose and quartzite, which outcrop in Kisikli region, are the oldest Palaeozoic rocks in Istanbul.

iii) All rocks have been intruded by volcanic dykes

As can be seen from the geological longitudinal cross section, a geological profile, characterised by a heterogeneous alteration sequence of the rock types noted below, lies above the entire line of the tunnel centre is shown in Table 2.2. Rock cores recovered from the boreholes 1 to 13 point to relatively strong fissuring in all rock layers. The total core rate (TCR), solid core rate (SCR) and rock quality designation (RQD) values were measured for each of the cores. No subsurface water-level is indicated on the engineering geological cross-section.

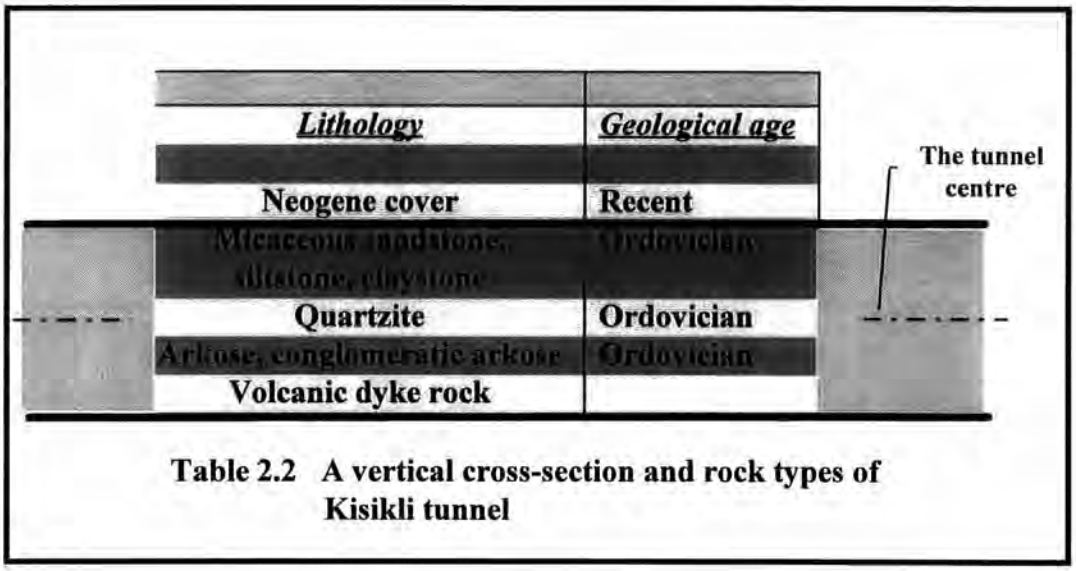

Table 2.2 A vertical cross-section and rock types of Kisikli tunnel

2.2.2.1 Neogene Cover

Under this heading have been included all the superficial "soil-like" materials encountered during the borings. All regions, except the high sections of hills, are predominantly blanketed with a young sediment. The materials are generally less than 5.0 m thick and consist principally of gravely silty clays and gravely clayey silts. The recorded thickness increased generally as the ground elevation increased, suggesting that in part the material is derived from weathering of the underlying rocks.

2.2.2.2 Quartzite

On the logs the quartzite is described as a very hard pinkish greyish white jointed quartzitic sandstone. The variable surface exposures indicated that it can be moderately strong to strong. Recorded RQD values vary considerably from 0% to 70%, although the majority of values ranged from 0% to 20%, indicating that the formation was substantially fractured.

2.2.2.3 Micaceous Sandstone Siltstone Claystone

It is considered that the clayey siltstone and the micaceous sandstone (described on the logs as a sandstone siltstone alternation) are all part of the same stratigraphic unit; that is, a series of interbedded layers of sandstone and siltstone. Sandstone is the dominant type of lithology. From the drilling records it appears to be highly fractured and moderately weathered.

2.2.2.4 Arkose

The arkose consists of a conglomerate of quartzite and feldspar fragments set in a fine-grained matrix. The highest recorded RQD was 20% although most of the values were less than 10%. It is possible that significant weathering has taken place, quite a large proportion of the material being highly or completely weathered. The fracturing and weathering together indicate a rock stratum that is relatively weak.

2.2.2.5 Volcanic Dyke

This was recorded as being of andesite. RQD values were generally low, being at or close to 0%. Occasionally a significant RQD was recorded; this may well represent the less weathered core of the volcanic dyke. The evidence indicates that the igneous dyke rock is weak in the mass as a result of the high discontinuity spatial density as shown in Table 2.2.

2.2.3 Hydrogeology

It is noted that some of the strata could have a significant primary or secondary porosity. However, several wells shown on the site plans produced show that there are no major aquifers but that some strata are able to yield small quantities of groundwater.

2.3 Tantavi Tunnels

2.3.1 Project Description

The site of the tunnels is located about 2 km east of Kisikli, on the crest of a hill. Thus, the approaches to the tunnel particularly from the north east are on significant uphill gradients. As noted earlier, the area over the proposed tunnel is part of Tantavi Park, an area of grassland and trees. The park forms a locally important visual feature and an established environmental amenity.

The Tantavi tunnel scheme consists of two tunnel tubes each having a clear width of 13.0 m and clear height of 7.45 m . The separation distance of the two tunnel tubes is constant at 8.0 m along the tunnel route. The tunnels are driven through relatively uniform and weak ground. Cover to roof of the tunnels is low, typically between 4.0 and 9.0 m. While other methods of tunnel construction (for example open-cut) are possible given this low depth of cover, the need to preserve Tantavi Park has led to adoption of a mined tunnel.

2.3.2 Engineering Geology

Although the tunnels have been excavated through relatively uniform ground, this ground is very weak in rock terms. The site is underlain by Ordovician siltstone intruded by volcanic dykes. A total of six boreholes were drilled on the Tantavi tunnel alignment with depths varying between 15.50 m and 19.0 m. In general, the ground conditions are relatively uniform, consisting of superficial deposits (Neogene cover) overlying clayey siltstone as shown in Table 2.3.

2.3.2.1 Neogene Cover

These superficial deposits consist of between 2.0 to 3.0 m of silty clay to clayey silt. It is likely that the material is the weathered residue of the siltstone.

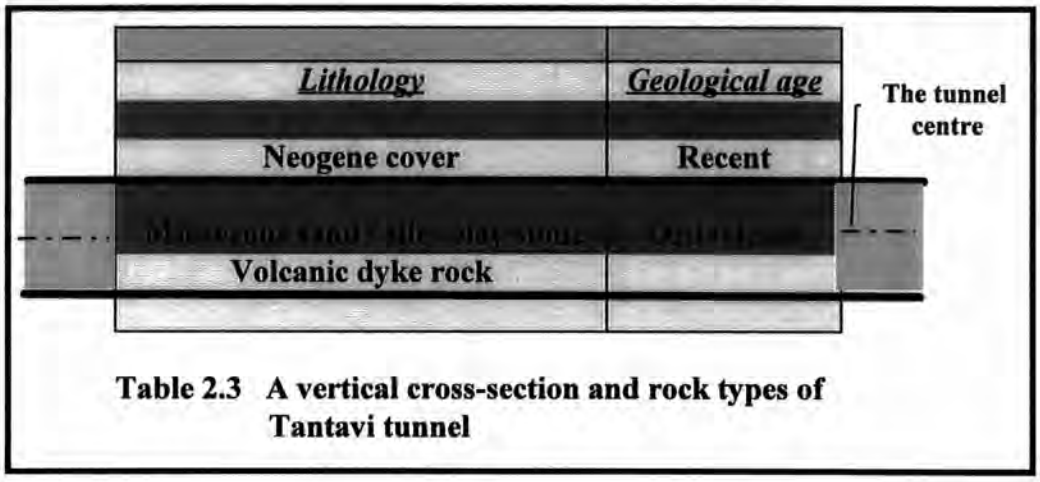

Table 2.3 A vertical cross-section and rock types of Tantavi tunnel

2.3.2.2 Micaceous Sandstone Siltstone Claystone

This consists of a yellow grey clayey siltstone sandstone. RQD values were generally at or close to 0%. Examination of exposures in the highway cutting to the north east indicates a heavily-jointed very weak siltstone. In some instances the material could be broken by hand. A number of the boreholes encountered heavily fractured rock, probably associated with fault zones. Information on the bedding appears to indicate that it dips at around 20% to 45% to the south/south west.

2.3.2.3 Volcanic Dykes

Generally the investigation data appear to indicate a very weak, highly weathered and heavily jointed andesite, although it appears that there are occasional bands of harder rock. RQD values were generally low, being at or close to 0%.

2.3.3 Hydrogeology

The available data indicate that while groundwater heads are likely to be positive, there appear to be no zones of high permeability. It is noted that the cutting to the north east of the site is relatively dry.

2.4 Material Properties

This specification covers material properties required for the Kisikli and Tantavi tunnels in any type of rock and soil formation encountered. Mechanical properties of both soil and rock samples obtained from borings were determined at approved laboratories. Uniaxial compressive strength, tensile strength, modulus of elasticity, Poisson's ratio and seismic velocities were assessed for the samples. Material property values are based on the geotechnical report prepared by STFA Construction Company. The values obtained from laboratory tests may be used for various purposes.

For instance if information on the discontinuities justifies the use of continuum methods for estimating the stability of the tunnel, laboratory tests can provide upper values for properties such as the modulus of elasticity, Poisson's ratio and rock strength. The tests may be useful in differentiating sections along the tunnel according to rock properties. Also the test results could aid estimation of boring, drilling and blasting efficiency by comparison with past performance in rocks of similar character. For instance the unconfined compressive strength of a rock is an indexing parameter used for selection of cutters for boring machines. Hardness and abrasiveness also strongly affect the performance of tunnel boring machines.

2.4.1 Material Properties of Kisikli Tunnel

A summary of material properties of Kisikli tunnel is given Table 2.4. As can be seen in this table, the compressive strength of the quartzite is very high but that of the andesite (volcanic dyke) and micaceous sandstone is low. These values from laboratory tests reasonably cannot reflect the actual conditions on site. The quartzites, which are amongst the stronger rocks, are brittle but the others have been weathered to a greater or lesser extent.

LITHOLOGY	*UNCONFINED COMPRESSIVE STRENGTH* *(MPa)*	*YOUNG'S (ELASTICITY) MODULUS E* *(GPa)*	*POISSON'S RATIO* ν	*MASS DENSITY* γ *(kg/m³)*	*COHESION C* *(MPa)*	*INTERNAL FRICTION ANGLE* ϕ *(degrees)*
Micaceous sand/silt/clay Stone	**3.5**	**0.7**	**0.27**	**2200**	**0.176**	**34**
Arkose, Conglomeratic Arkose	**26**	**15**	**0.26**	**2600**	**0.083**	**31**

Table 2.4 Material properties in Kisikli tunnel

2.4.2 Material Properties of Tantavi Tunnel

A summary of material properties of Tantavi tunnel is given Table 2.5.

LITHOLOGY	*UNCONFINED COMPRESSIVE STRENGTH* *(MPa)*	*YOUNG'S (ELASTICITY) MODULUS E* *(GPa)*	*POISSON'S RATIO* ν	*MASS DENSITY* γ *(kg/m³)*	*COHESION C* *(MPa)*	*INTERNAL FRICTION ANGLE* ϕ *(degrees)*
Neogene cover (soil)		**0.09**	**0.35**	**2060**		
Volcanic dyke rock	**6**	**1.86**	**0.28**	**2300**	**0.136**	**31**

Table 2.5 Material properties in Tantavi tunnel

2.5 Rock Classification

Material properties of rock samples obtained from the drillings along Kisikli and Tantavi tunnels were determined at soil and rock mechanics laboratories of STFA Contraction Company. These rock parameters were incorporated by the designer into RMR and Q classification for the Kisikli and Tantavi tunnels. The results based on the geotechnical interpretation range of RMR and Q values for typical rocks to be encountered along Kisikli and Tantavi tunnels are given in sections 2.5.1 and 2.5.2, respectively.

2.5.1 Kisikli Tunnel Rock Classification

Based on the results of the suitable laboratory and the site (ground) investigation the various strata were classified by the designer using the RMR and Q methods. Table 2.6 shows the rock classification factor of the each of the strata. In general the rock classification indicates poor rock engineering conditions, with low stand-up times and with the need to provide significant support as early as possible.

The maximum spans and stand-up times in Table 2.7 were derived by the designer from the typical RMR values. It should be noted that the results of the investigation show highly variable values. Thus a flexible approach could have been adopted. For the values given in Table 2.7 it was assumed the general dip of strata was in the range of 20° and 45° for RMR rock classification. While this is not strictly the case, it is considered reasonable for the purposes of classification.

	RMR			*Q*		
Micaceous sandstone / siltstone / claystone	**15 - 35**	**30**	**Poor**	**0.1 - 0.7**	**0.2**	**Very poor**
Arkose	**15 - 40**	**30**	**Poor**	**0.1 - 0.7**	**0.2**	**Very poor**

Table 2.6 Kisikli tunnel rock classification

Strata	*RMR*	*Maximum span*	*Stand-up time*
Micaceous sandstone/ siltstone / claystone	**30**	**4.0**	**2**
Arkose	**30**	**2.4**	**4**

Table 2.7 Kisikli tunnel maximum spans and stand-up times

2.5.2 Tantavi Tunnel Rock Classification

Based on the results of the investigation, the RMR and Q values were assessed by the designer for Tantavi tunnel as follows.

Lithology	Range proposed value	Class	Range proposed value	Class
Micaceous sand/silt/clay stone	**20**	**Very poor**	**0.07**	**Extremely poor**
[illegible]	[illegible]	[illegible]	[illegible]	[illegible]

Table 2.8 Tantavi Tunnel rock classification

Strata	*RMR*	*Maximum span (m)*	*Stand-up time (hours)*
[illegible]	[illegible]	[illegible]	[illegible]
Volcanic dyke	**24**	**2.5**	**0.3**

Table 2.9 Tantavi tunnel maximum spans and stand-up times

2.6 Construction Procedure

A typical tunnel cross-section is shown in Fig. 2.2. The method of constructing a tunnel, as well as the care taken in preserving the integrity of the remaining rock, can have a large effect on loads that are carried by the initial support system. If the construction procedure causes excessive overbreak, the effective diameter of the tunnel will be correspondingly increased. This can result in an increase in the supported height of rock above the crown which may be proportionately larger than the diameter increase.

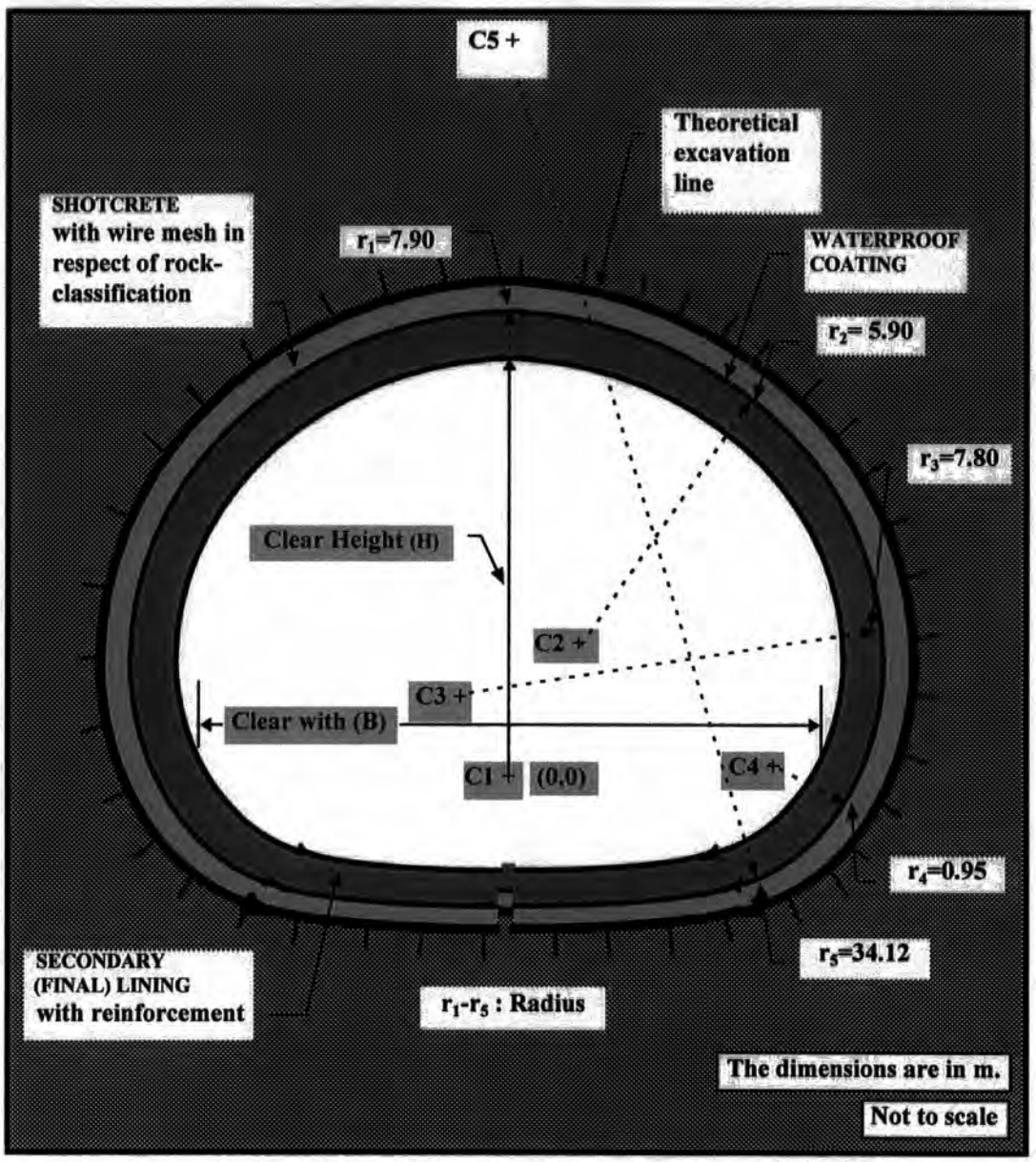

Fig. 2.2 Standard cross - section invert to arch

Tunnel support was by the NATM. Since with the NATM the rock adjacent to the excavation is an integral part of the ground support system, it very important that the rock strength is maintained as far as possible. For the traffic tunnels, the importance of instrument monitoring, observation, a flexibility of contract style within the NATM concept becomes obvious whenever continuously changing rock conditions are encountered.

Following geotechnical appraisal of both tunnels three types of rock were classified based on RMR and Q values, and support systems to be used for each rock type were classified. The lithologies, identified as units A, B and C on Table 2.10, reflect the state of knowledge of the engineering geological nature of the tunnel sites as obtained from site investigations. These categories are a form of reference ground conditions and are for information and contract pricing only, since the actual conditions encountered at the tunnel face may be different. This specification defines a rock classification system in terms of the rock structure and its stability when subjected to excavation. This classification has been used by the contractor for all distances in the tunnels, in the top heading and bench, in order to identify the particular rock class (A to C). All rock classification types (A, B and C) were expected to occur in Kisikli tunnel but rock type C only was expected in the Tantavi tunnel. Shotcrete (primary) lining, anchorages, steel supports type, inner (final) lining have been designed for each category, taking account of the respective loading likely to be imposed as shown in Table 2.10.

2.6.1 Underground Excavation

The cross-section and dimensions of the excavation, depending upon the different rock conditions (type A, B and C) have been varied as shown in Figs. 2.3 to 2.5. Top heading and bench methods of excavation were used in the tunnel construction. Following excavation of a heading at the top of the tunnel, the lower ground is then removed in benches as shown in Fig. 2.6. Tunnel excavation is performed either by means of wheeled roadheaders, or by blasting depending on the rock classification. Selection of the excavation method to be applied was made on cost-efficiency grounds and also on environmental grounds; for example, restriction on the use of blasting under built-up areas. 'Smooth blasting' has been using to limit the overbreak and to prevent shattering of the cut rock surface.

Type	*Classification*		*Support*	*Comment*
	RMR	*Q*		
A	**>40**	**>0.7**	**4 m. long anchorages (rock bolts) at 1.5 to 2.0 m in crown and walls plus 50 to 100 mm of mesh reinforced shotcrete**	**Advanced, 1.5 to 3.0 m generally; some sub-division of face may be required**
B	**21 - 40**	**0.1 - 0.7**	**4 to 5 m. long anchorages in crown and wall; light to medium steel arches spaced at 1.0 to 1.5 m, centres where required, plus 100 to 150 mm shotcrete lagging**	**Sub-division of this class will be possible. Progressive excavation will be required, based on an initial upper heading. Advance 1.0 to 1.5 m**
C	**<21**	**< 0.1**	**4 to 6 m. long anchorages in crown and walls and medium to heavy steel arches at 0.75 to 1.0 m plus 150 to 250 mm shotcrete lagging. Forepoles / grouted dowels to form "umbrella support also required**	**Major sub-division of face will be required, for excavation. Advance of face 0.75 to 1.0 m**
		Notes	**1. These classes will be reviewed and refined on site during construction once observations of rock conditions and deformation measurements are available.**	**2. The boundaries between the above classes and types of support should not be taken as rigid. Variations should be made based on the actual condition encountered**

Table 2.10 Rock support systems - preliminary assessment

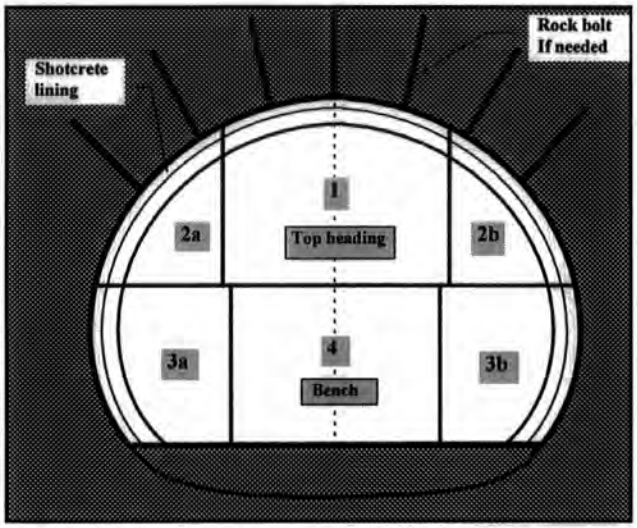

Fig. 2.3 NATM excavation sequence section for rock type A

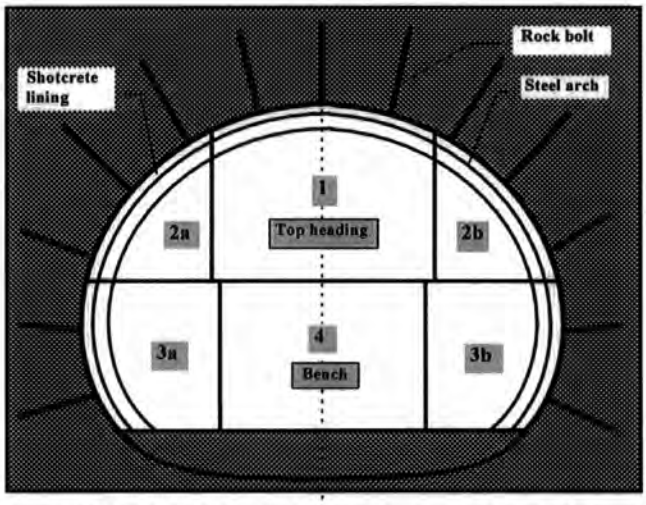

Fig. 2.4 NATM excavation sequence section for rock type B

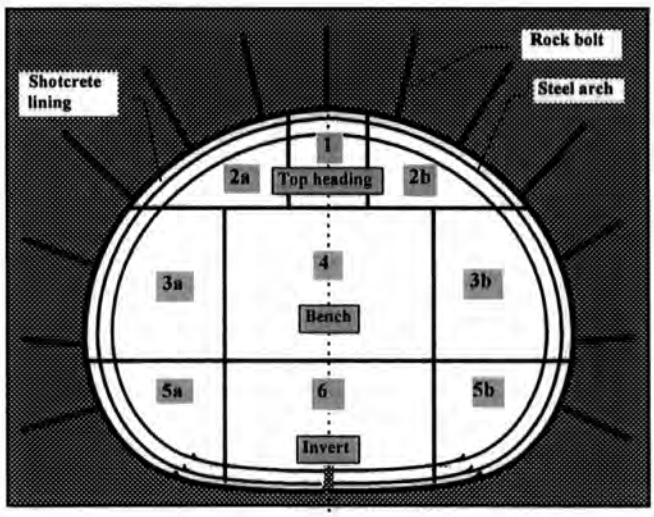

Fig. 2.5 NATM excavation sequence section for rock type C

Any mechanical equipment for underground excavation works and the means of transportation of the spoil have to be suitable for the works, as specified with respect both to performance and to current Turkish safety regulations, as well as for compliance with the requirements of the construction program.

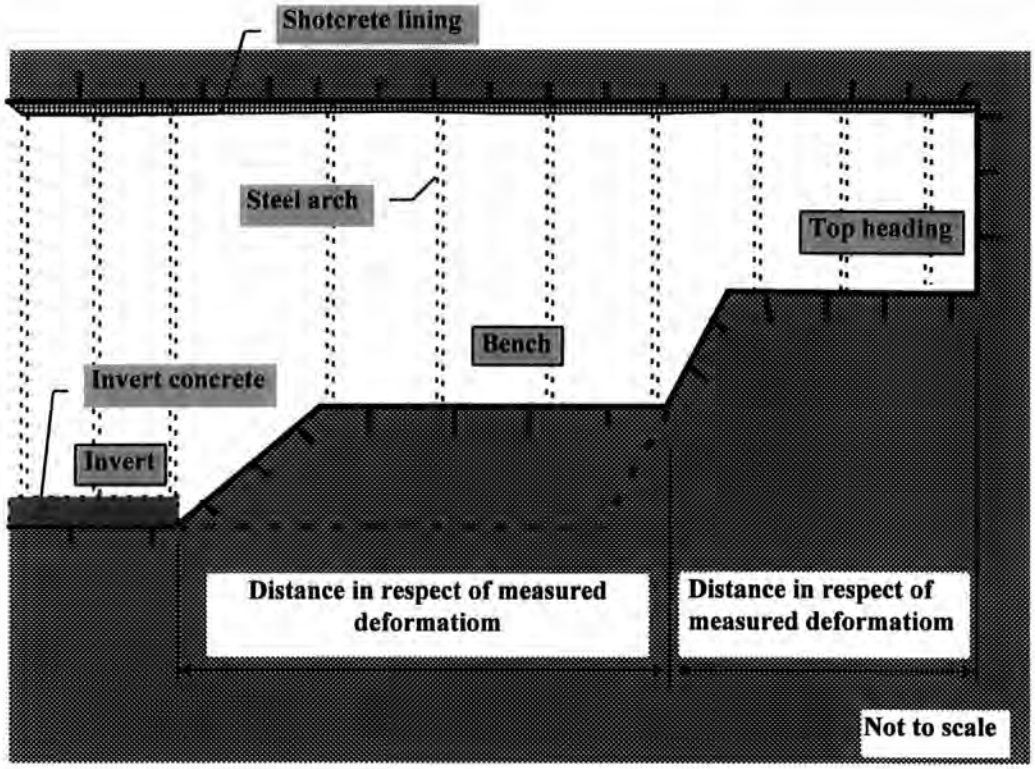

Fig. 2.6 Excavation longitudinal section

2.6.2 Primary (Shotcrete) Lining

Shotcrete is a concrete slurry which is transported by pipe and compacted by jetting onto a surface at high velocity. Alternatively, the cement with any admixtures can be transferred in a dry state and the water added at the nozzle. The primary tunnel lining has been designed separately for Tantavi and Kisikli tunnels. At Tantavi tunnel the cover is about 5 m so all the load is assumed to act on the primary lining. For most of Kisikli tunnel the cover is 12.0 to 15.0 m. Arching of the rock has been considered for type A and B rocks in the design of this primary

lining. All available rock types are expected in Kisikli tunnel. The shotcrete lining has been designed to an average thickness of 200 mm for each tunnel taking account of the respective loads on the tunnels as shown in Figs. 2.3-2.5

2.5.3 Steel Arches

Steel arches are used as support in the underground excavation if they are required. Steel arches are effective as protection and primary support immediately after excavation, and they subsequently act as reinforcement and load distributing members for the shotcrete lining.

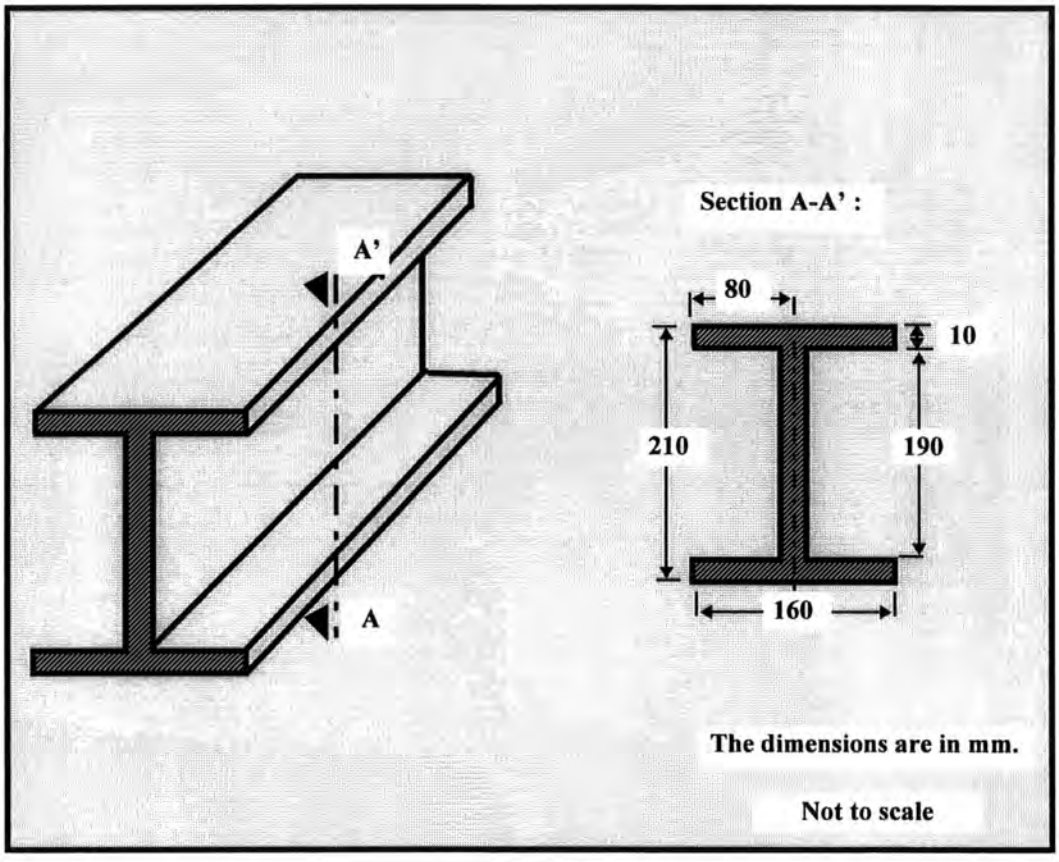

Fig. 2.7 Schematic diagram of steel arch

The steel arches have been manufactured to meet the geometrical requirements of each of the rock classes requiring their use i.e. rock class B and C. For steel arches, hot-rolled "H-profiles" have been used.

The dimensions of the steel arches are as indicated in Fig. 2.7. The steel arches consist of structural steel with a minimum yield strength of 280 MPa and comply with BS4 part 1 (1993) or BS 4848 part 2 (1991). Steel ribs are erected to the lines and levels. Tie bars have been used to connect the ribs to the adjacent steel arch and fix it securely in place. Tie bars are steel rods of 22 mm diameter, bent and connected to the arch. The steel arches have been embedded in shotcrete in order to obtain maximum contact between rock and steel arch through a solid shotcrete packing which was designed to have a minimum thickness of 50 mm .

2.5.4 Anchorages

All rock anchorages (rock bolts) have been installed either locally as required or in a systematic pattern in the roof, side walls and invert of the tunnels as shown in Figs. 2.3 to 2.5. Anchorages are an integral part of the primary support system, with the purpose of activating the requisite composite action between the surrounding rock and the shotcrete, so contributing to the load bearing capacity of the primary tunnel lining. Anchorages have been made of steel bars having specified properties and fully bonded with the surrounding rock by means of cement mortar. They have been used as the conditions demanded and installed according to the depths and configurations for each relevant standard support system. These patterns and lengths were varied according to the rock conditions. Holes for all rock bolts have been drilled to the depths required by the lengths of rock bolts specified for the respective rock class and at diameters which ensured efficiency for grouting and installation. The minimum diameter of the holes was 10 mm larger than the diameter of the rock bolts to be installed which have a 28 mm diameter as shown in Fig. 2.8.

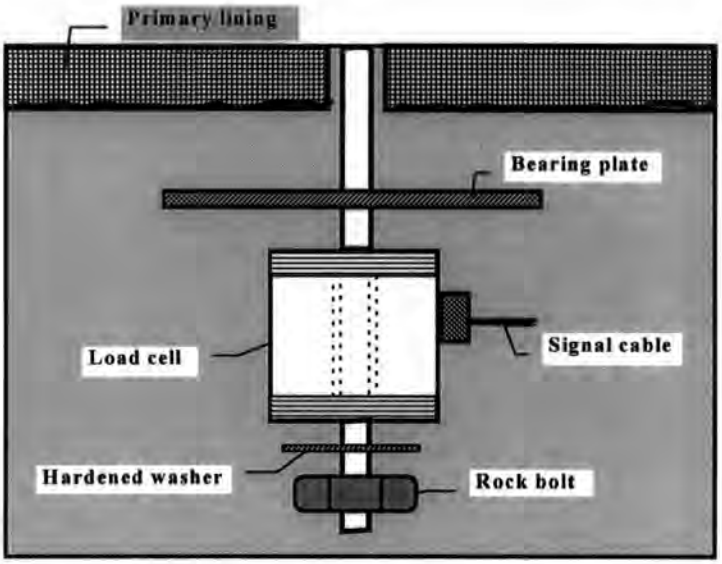

Fig. 2.8 Rock bolt and load cell

At the distal (tunnel perimeter) end each bolt is fitted with suitable thread for receiving an anchor plate and fixing nut. All rock bolts have a minimum breaking load of 250 kN. Anchor plates, washers and nuts have been designed to allow satisfactory transfer of the anchor force at the head of the rock bolt, to the shotcrete, steel rib or rock surface, even if the anchor plate cannot be fitted exactly perpendicular to the rock bolt. The cement mortar grout consists of sand, cement and water. Tests with available cement and sand were carried out to determine an appropriate mix design which would achieve the specified strength and a proper workability in association with the grouting device used. The following mix was found to be suitable ;

Two parts of sand (grain size 0.5 mm) one part cement and water, so that the mortar has a plastic consistency. The water/cement ratio is between approximately 0.5 and 0.6. The grout has a minimum compressive strength of 8 MPa after 24 hours and 20 MPa after 28 days and was tested on 50 mm cubes. At least five cube samples were taken weekly from the grouting hose at the nozzle.

Prior to the installation of each rock bolt, the entire hole was filled with cement mortar by inserting the grout pipe to the full depth of the hole and withdrawing as the grout was pumped in. The nozzle is kept buried in the grout as the pipe was withdrawn so that air is displaced as the hole is filled. The bolt was

the pushed into the hole. The nuts of the grouted rock bolts were tightened not earlier than 6 hours but not later than 8 hours after installation in order to achieve a force at the anchor plate of approximately 20 kN. This force was verified by means of a calibrated torque wrench.

2.5.5 Insulation and Final Lining

According to the principles of the NATM, there is a clear distinction between primary lining and final lining. The final lining, of placed in-situ concrete, is in the present case sealed against the primary lining by a waterproof coating. The individual sealing strips are welded together to ensure continuity of water proofing. Water collected by the seal above the tunnel cross-section is diverted by drainage pipes located in the area of the side wall footings. The waterproof membrane insulation is protected against and separated from the shotcrete by a watertight membrane. In order to permit the individual blocks of the final lining to move a certain extent in response creeping and shrinking of the concrete, block joints are arranged in regular sections. It is thus possible to achieve a high measure of safety against cracking. Assumptions made in the calculation of the tunnel final lining concrete are as follows.

i) Loads on the section are based on material (geotechnical) properties of rocks. The depth of overburden above the crown level was taken into account. Full hydrostatic pressures were applied.
ii) The material properties of the rock were assumed to be elastic and characterised by Young's modulus (E) and Poisson's ratio (ν). For ground, minimum and maximum Young's Modulus values were taken and results calculated.
iii) Any arching of the rock will be ignored as the tunnels are considered to be shallow (overburden ranges between 4 and 10 metres); thus Kisikli and Tantavi tunnels were considered to lie at a sufficiently shallow depth that arching was not assessed.

A static model was used to design the final lining by computer software. It was assumed that the ground would not be affected by tension and that the predominant rock type existed throughout the tunnel drives.

The final lining consists of three sections : arch, toe, invert. Calculations based on the above assumptions gave concrete thicknesses of 450 mm, 1000 mm and 500 mm, respectively without reinforcement. Invert concrete was not designed for rock types A and B. The final tunnel lining comprised 450 mm thick unreinforced concrete as shown in Fig 2.2.

2.6.6 Geomechanical Measurements (Monitoring)

Monitoring, combined with a degree of flexibility in the placement of ground support, is an essential part of good tunnel design and construction, especially with the NATM method. The data obtained from monitoring in Turkish tunnels has been used to check on the design of the primary lining and its in situ deformation.

The following observations have been taken for each heading and for the whole tunnel;

i) a visual examination of the tunnel lining,

ii) convergence pins cast into the primary lining to check on relative movement of the tunnel and surrounding ground (see Fig. 2.9),

iii) movement of the ground towards the tunnel,

iv) settlement of the ground surface,

v) movement of the structures above and close to the tunnel alignment,

vi) face logging of the geology and ground conditions encountered.

Deformation is dealt with by means of geomechanical measurements as an integral part of this construction method. This requirement is being taken into consideration with all NATM projects by means of a comprehensive measurement programme.

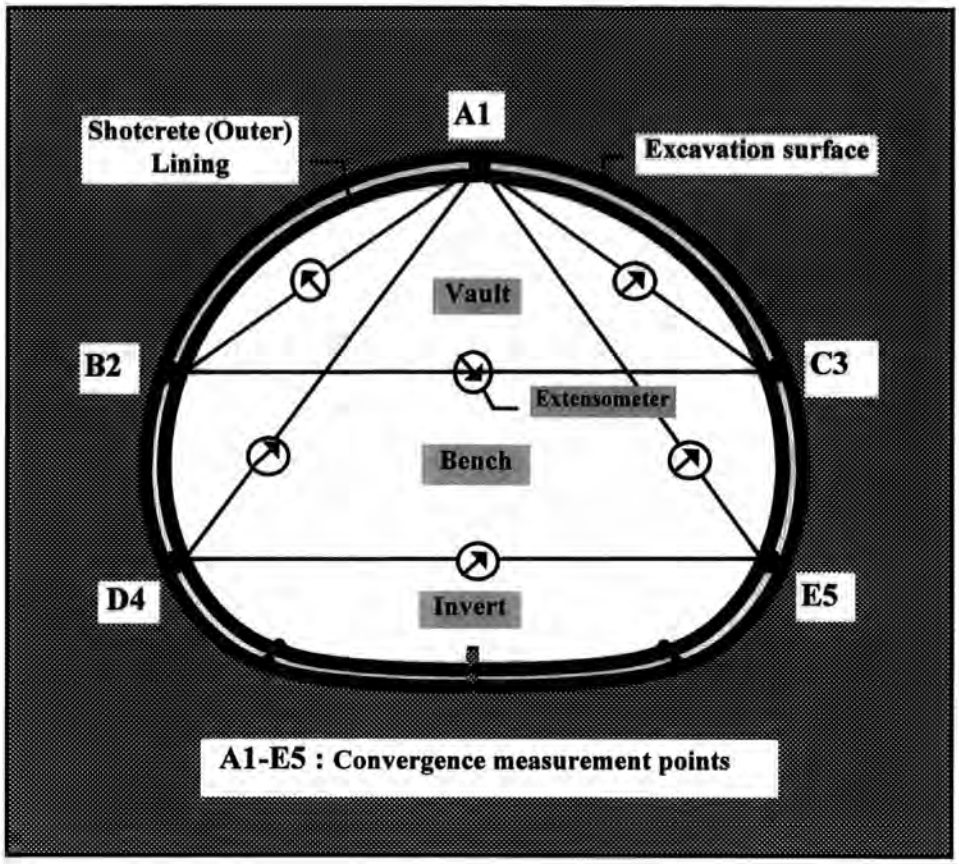

Fig. 2.9 Location of extensometer and convergence measuring cross-section

The measurement of forces and deformations is also the basis of on-going empirical design. Rock behaviour as measured becomes the basis for further construction progress by calibration of an updated static model. Convergence pins were inserted in order to monitor the tunnel deformation after the shotcrete lining was applied. Readings were taken daily, and then weekly when construction was completed at the point under construction. As the tunnel faces advanced beyond the instrumented area the frequency of readings could then be reduced to weekly or possibly monthly cycles. However, should any large movements be recorded, the frequency of reading would then be increased to at least daily until the movement ceased. Detailed requirements for monitoring are shown in Fig. 2.9. Further details of the in situ convergence measurements are given in Chapter 7.

CHAPTER 3

ANALYSIS METHODS

3.1 Introduction

This chapter describes the finite element analysis and proposed solution technique. It will begin with a discussion of ways in which stress analysis can be performed and then will give a brief description and comparison of four standard ways of analysing stresses.

When a body is subjected to gravitational or external loads it deforms. The way of deformation can be described by specifying components of displacement or strain at every point in the body. These are related to stress components throughout the body. The prediction of these stresses, strains and displacements is the matter of stress analysis.

For certain classes of engineering problem, it is possible to predict the stresses and strains in a structure with a high degree of certainty. This is particularly so when the material properties can be measured accurately and the mechanical characteristics of the components of a structure are consistent and well understood.

Unfortunately soil and rock are not so easily described. Tunnels or shafts usually pass through the inhomogeneous and discontinuous rock mass. The initial state of stress in the rock mass is known only approximately. A stress analysis requires exact and detailed description of the body and applied loads, boundary conditions. The design of any tunnel or tunnel lining is definitely based on some model in which loads are distributed in the surrounding rock. Stress analyses need values for the idealised properties of the rock then stress analyses produce numbers that are roughly related to the displacements or stresses that might be measured in the field. These numbers can serve only as a guide and not as an instruction for design. One set of results may be compared with another, making different

assumptions or showing the effect of some change in design but the analysis should never be treated as an absolute answer.

3.2 Mathematical Analysis of Stress and Strain

3.2.1 Theory of Elasticity

Many text books provide a discussion of the theory of elasticity; Obert and Duvall (1967), Timoshenko and Goodier (1970), Jaeger and Cook (1979), Brown (1987), Brady and Brown (1985), Wittke (1990), Mahtab (1992). For the purpose of this section it is not intended to repeat the essential equations of linear elasticity, but merely to describe their basic use.

The exact analytical solution requires certain conditions to be met. Firstly the body is a continuum. All deformations are continuous, single valued and finite. Thus when a body is strained, the resulting displacements produce no gaps between small adjacent elements of the body. This leads to the first set of equations based essentially on geometry known as the compatibility equations.

Secondly the body, and all parts of it, are in equilibrium. Under these conditions, Newton's Laws are universally applicable to all parts and this leads to a set of partial differential equations expressed, in terms of stresses and their derivatives, called equilibrium equations. All the forces on any element of a body are balanced, so that a static equilibrium exists.

The third set of equations form constitutive or stress-strain relationships. These are based on the deformational behaviour of material under load and link the first two sets of equation. In the simplest case the stress-strain relationships will be linear, isotropic, elastic and can be expressed in terms of two material constants, usually Young's modulus and Poisson's ratio.

In addition the appropriate boundary conditions of stresses and displacements must be satisfied on all the surface of the body.

Mathematical solutions can usually be found only for the simplest of cases where the rock mass is homogeneous and behaves in a linear elastic manner, the loading is fairly simple and boundaries have simple geometric shapes.

Mathematical solutions usually assume conditions of plane stress or strain or some type of symmetry which reduce the complexity of the analysis.

Problems in three dimensional elastic theory involve the following parameters, expressed in terms of a Cartesian co-ordinate system. These comprise six stress components as shown in Fig. 3.1.

σ_x , σ_y , σ_z the three normal stresses, assumed positive if compressive, and

τ_{xy} , τ_{yz} , τ_{zx} the three independent shear stresses,

and six corresponding strain components ;

ε_x , ε_y , ε_z the three normal strains, assumed positive if compressive, and

γ_{xy} , γ_{yz} , γ_{zx} the three shear strains.

In addition there are three components of displacements *u, v, w.*

3.2.1.1 Stress-Strain Relations

To calculate from given stresses the resulting strains or displacements in the material, the material properties need to be known. These are expressed in terms of a constitutive law or stress-strain relationship for the material as applicable. For a linear, isotropic material obeying Hooke's law, the stress-strain relationship requires only two constants, the Young's modulus (E) and Poisson's ratio (ν). The shear modulus is related to Young's modulus and Poisson's ratio by the equation

$$E = 2G\,(1+\nu) \tag{3.1}$$

For principal or normal stresses and strains this behaviour may be expressed as

$$\sigma_x = (\lambda + 2G)\,\varepsilon_x + \lambda\,\varepsilon_y + \lambda\,\varepsilon_z \tag{3.2a}$$

$$\sigma_y = \lambda\,\varepsilon_x + (\lambda + 2G)\varepsilon_y + \lambda\,\varepsilon_z \tag{3.2b}$$

$$\sigma_z = \lambda\,\varepsilon_x + \lambda\,\varepsilon_y + (\lambda + 2G)\varepsilon_z \tag{3.2c}$$

where λ, known as Lamé's constant, is given by

$$\lambda = \frac{\nu E}{(1+\nu)(1-2\nu)} \quad . \tag{3.2d}$$

This form is chosen to express the fact that one constant, (λ + 2G), connects stress and strain in same direction, while a different one, λ, relates stress and strain in two perpendicular directions which must be on the same footing.

The shear stresses and strains are related by

$$\tau_{xy} = G\,\gamma_{xy} \tag{3.3a}$$

$$\tau_{yz} = G\,\gamma_{yz} \tag{3.3b}$$

$$\tau_{zx} = G\,\gamma_{zx} \tag{3.3c}$$

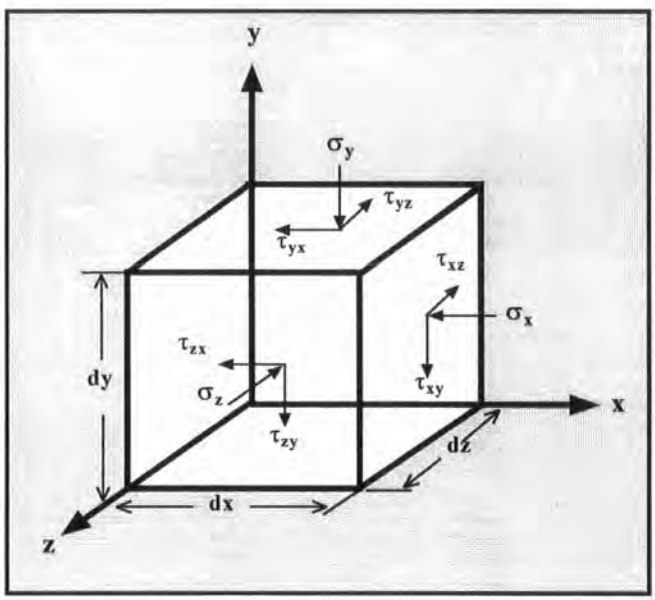

Fig. 3.1 Components of stress

The volumetric strain (dilation) is given as,

$$e = \varepsilon_x + \varepsilon_y + \varepsilon_z \tag{3.4}$$

Equations (3.2a) to (3.2c) can be alternatively written as;

$$\sigma_x = \lambda\, e + 2G\varepsilon_x \tag{3.5a}$$

$$\sigma_y = \lambda\, e + 2G\varepsilon_y \tag{3.5b}$$

$$\sigma_z = \lambda e + 2G\varepsilon_z \tag{3.5c}$$

or as

$$\varepsilon_x = \frac{1}{E}\left[\sigma_x - \nu\sigma_y - \nu\sigma_z\right] \tag{3.6a}$$

$$\varepsilon_y = \frac{1}{E}\left[\sigma_y - \nu\sigma_x - \nu\sigma_z\right] \tag{3.6b}$$

$$\varepsilon_z = \frac{1}{E}\left[\sigma_z - \nu\sigma_y - \nu\sigma_x\right] \tag{3.6c}$$

These relationships express the *principle of superposition.*

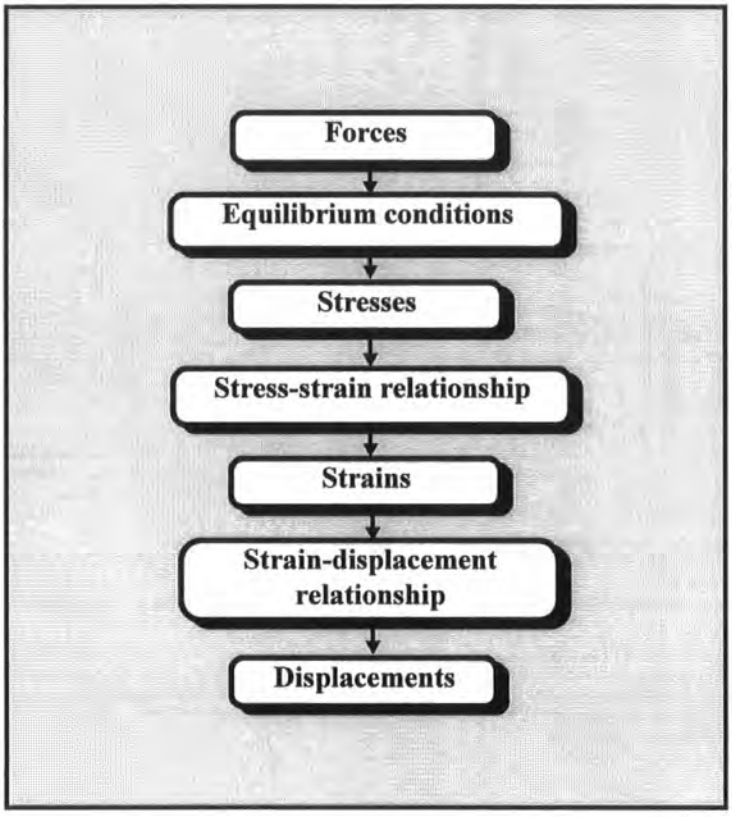

Fig 3.2 The calculation path from forces to displacements

3.2.1.2 Strain-Displacement Relations

Displacements can be calculated from components of normal strain (ε) and shear strain (γ) as given below.

$$\varepsilon_x = \frac{\partial u}{\partial x} \tag{3.7a}$$

$$\varepsilon_y = \frac{\partial v}{\partial y} \tag{3.7b}$$

$$\varepsilon_z = \frac{\partial w}{\partial z} \tag{3.7c}$$

$$\gamma_{xy} = \frac{\partial u}{\partial y} + \frac{\partial v}{\partial x} \tag{3.8a}$$

$$\gamma_{yz} = \frac{\partial v}{\partial z} + \frac{\partial w}{\partial y} \tag{3.8b}$$

$$\gamma_{zx} = \frac{\partial w}{\partial x} + \frac{\partial u}{\partial z} \tag{3.8c}$$

3.2.1.3 Plane Stress and Plane Strain

The general problem of elasticity is to determine the stresses and displacements in three dimensions. However two special cases which are essentially two dimensional are of importance. These are *the plane stress* and *plane strain* cases.

All physical structures are inherently three-dimensional, but their behaviour may be characterised as two-dimensional. The theory of elasticity specifies a special class of problem, plane problems, which may be solved more readily than the general three-dimensional problem, since certain simplifying assumptions are made. The structure should consist of a region of uniform thickness bounded by two parallel planes, oriented normal to the prescribed z-axis. The thickness of the structure may either be very thin or very thick. These represent the most desirable cases for plane static analysis. Generally plane stress is employed where the structure is relatively thin in relation to its lateral dimension, while plane strain is used when the structure is very thick relative to this dimension. Plane strain assumes that there is no strain perpendicular to the plane, while plane stress assumes that there is no stress normal to the surface. The bending stresses are also

negligible. Stresses and displacements may be determined for a two-dimensional finite element static approach by using either the plane stress or plane strain approach, but because of the length of a tunnel in the z direction, plane strain analysis is used here.

3.2.1.3.1 Plane Stress

A plane stress condition is a condition where all stresses are in or parallel to the plane of interest. An example is given of a thin plate which is subjected to stresses uniformly distributed over the thickness of the plate in the x-y plane to form a state of plane stress as shown in Fig. 3.3.

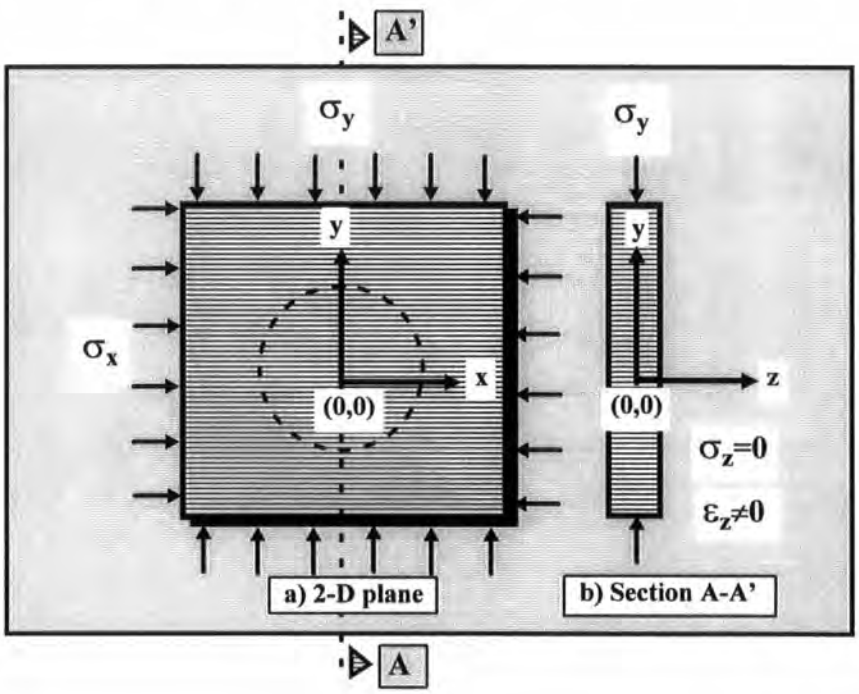

Fig. 3.3 Plane stress condition

Several theory of elasticity solutions for two-dimensional boundary problem are given for the plane stress case using the assumptions as given below

$$\sigma_z = \gamma_{xz} = \gamma_{yz} = 0 \tag{3.9}$$

$$\varepsilon_z \neq 0 \tag{3.10}$$

Substituting equations (3.9-3.10) in the general form of Hooke's law (equations (3.6a-3.6c)) the plane stress condition, gives

$$\varepsilon_x = \frac{1}{E}\left(\sigma_x - \nu\sigma_y\right) \tag{3.11a}$$

$$\varepsilon_y = \frac{1}{E}\left(\sigma_y - \nu\sigma_x\right) \tag{3.11b}$$

$$\varepsilon_z = \frac{-\nu}{E}\left(\sigma_y + \sigma_x\right) \tag{3.11c}$$

and similarly for the shear strain

$$\gamma_{xy} = \frac{\tau_{xy}}{G} \tag{3.11d}$$

The stresses acting in the plane for plane stress condition are obtained by inversion of equations (3.11a-3.11d) as given below;

$$\sigma_x = \frac{E}{1-\nu^2}\left(\varepsilon_x + \nu\varepsilon_y\right) \tag{3.12a}$$

$$\sigma_y = \frac{E}{1-\nu^2}\left(\varepsilon_y + \nu\varepsilon_x\right) \tag{3.12b}$$

$$\tau_{xy} = G\gamma_{xy} \tag{3.12c}$$

3.2.1.3.2 Plane Strain

A plane strain case is a case where stresses are applied in two-dimensional plane (the x-y plane) but deformation in the third orthogonal direction, the z-axis, is prevented completely. The case of plane strain can be illustrated by an infinitely long cylindrical underground opening such as tunnel. If z-axis represents the axis of opening, the displacements of all points in the plane of cross section are not zero but shear stress strains (γ_{yz} and γ_{xz}) associated with the z-direction are zero. Thus a plane strain condition is characterised by the given formula;

$$\varepsilon_z = 0 \tag{3.13a}$$

$$\gamma_{yz} = \gamma_{xz} = 0 \tag{3.13b}$$

The displacement components are independent of the z-direction and are functions of x and y only.

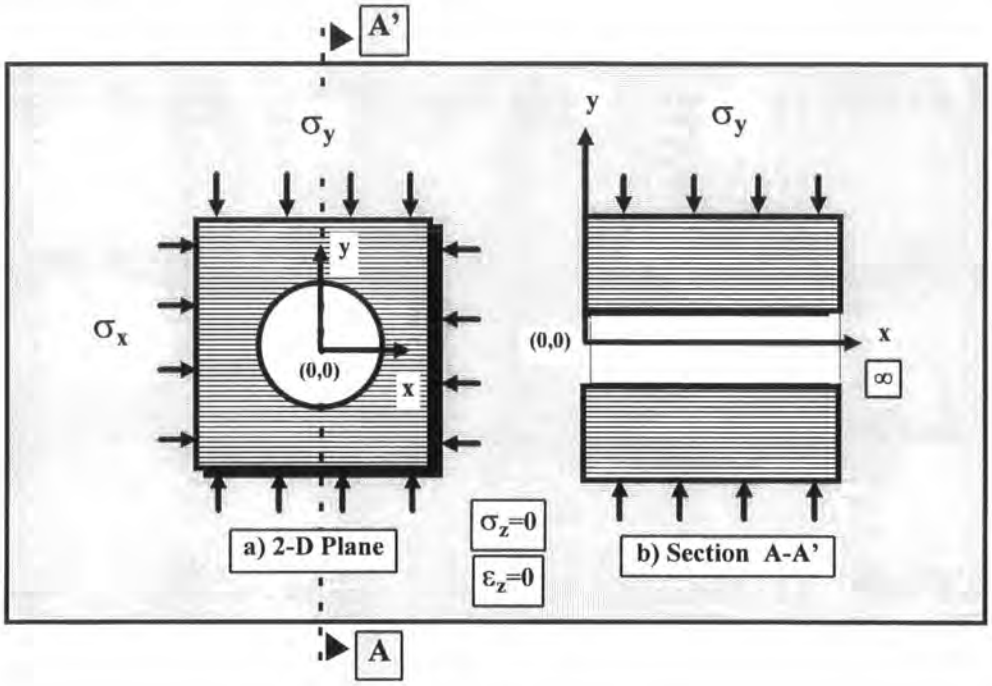

Fig. 3.4 Plane strain condition

Substituting equations (3.13a and 3.13b), in equations (3.2a-3.2c and 3.3a) the plane strain condition leads to

$$\sigma_x = (\lambda + 2G)\,\varepsilon_x + \lambda\,\varepsilon_y \qquad (3.14a)$$

$$\sigma_y = (\lambda + 2G)\,\varepsilon_y + \lambda\,\varepsilon_x \qquad (3.14b)$$

$$\sigma_z = \nu\,(\sigma_x + \sigma_y) \qquad (3.14c)$$

$$\tau_{xy} = G\,\gamma_{xy} \qquad (3.14d)$$

This shows that strains around underground openings are different for the case of plane stress (free slice) and plane strain (constrained slice).

These expressions break down when Poisson's ratio (ν) equals 0.5, as the quantity (1-2ν) in equation (3.2d) becomes zero and the above expressions become infinite. The problem may be overcome by using a Poisson's ratio that is slightly less than 0.5, typically 0.49 is used for an appropriately deforming medium, such

as a plastic soil. However Zienkiewicz (1971) warns that this results in a deterioration of the solution. In geotechnical applications the plane strain conditions are not strictly valid, even though the structure may fully satisfy the plane strain conditions, because the orientation of the axes of the principal initial stresses (geostatic stresses) may not coincide with the plane of analysis.

3.2.1.3.3 Von Mises Stresses and Resultant Displacement

The solution of structural problems in which the strain-displacement and stress-strain relationship are linear is relatively straightforward because the solution is obtained from a quadratic energy function and the resulting equations are linear. Von Mises shear strain energy criterion is often presented as being based on the idea that yielding of a ductile material under a general state of stress will occur when the density of shear strain energy is equal to the density of shear strain energy at the yield point in a sample tension test. It is often referred to as Von Mises criterion, after the German-American mathematician Richard Von Mises (1883-1953). An equivalent way of deriving it is to base yielding not just on the absolute maximum shear stress in the material, but on the root mean square maximum shear stress, thereby taking into account the shear stresses on planes at right angles to that of absolute maximum.

Using maximum shear stresses equations associated with each of the three principal planes, the root mean square maximum shear stress for a complex three-dimensional state of stress is

$$\tau_m = \sqrt{\left\{ \frac{1}{3} \left[\left(\frac{\sigma_x - \sigma_y}{2} \right)^2 + \left(\frac{\sigma_y - \sigma_z}{2} \right)^2 + \left(\frac{\sigma_z - \sigma_x}{2} \right)^2 \right] \right\}} \qquad (3.15)$$

In simple uniaxial tension, with $\sigma_x=\sigma_1$, $\sigma_y=0$ and $\sigma_z=0$, this becomes

$$\tau_m' = \frac{\sigma_1}{\sqrt{6}} \qquad (3.16)$$

and the yield criterion is obtained by equating τ_m and τ_m' to give

$$(\sigma_x - \sigma_y)^2 + (\sigma_y - \sigma_z)^2 + (\sigma_z - \sigma_x)^2 = 2\sigma_1^2 \qquad (3.17)$$

Another way of expressing the same result is to define a Von Mises equivalent stress

$$\sigma_{eq} = \frac{1}{\sqrt{2}} \sqrt{(\sigma_x - \sigma_y)^2 + (\sigma_y - \sigma_z)^2 + (\sigma_z - \sigma_x)^2} \qquad (3.18)$$

The equivalent stress (Von Mises) and resultant displacement are given, as in PAFEC 75 (1976) respectively, by

$$\sigma_{eq} = \frac{1}{\sqrt{2}} \sqrt{\begin{matrix}(\sigma_{xx} - \sigma_{yy})^2 + (\sigma_{yy} - \sigma_{zz})^2 + (\sigma_{zz} - \sigma_{xx})^2 + \\ 6(\sigma_{xy}^2 + \sigma_{yz}^2 + \sigma_{zx}^2)\end{matrix}} \qquad (3.19)$$

$$U_r = \sqrt{U_x^2 + U_y^2} \qquad (3.20)$$

To relate two and three dimensional problems to the one dimensional uniaxial case it is convenient to work with the equivalent stress. In other words, the equivalent stress is the stress in uniaxial case which is equivalent to the complex state of stress according to the Von Mises criterion. When the equivalent stress becomes greater than the uniaxial yield stress, then yielding takes place PAFEC-75 (1976).

$$\sigma_{eq} > \sigma_{yield} \qquad (3.21)$$

The equivalent stress is therefore a useful parameter with which to characterise a state of stress, which is why it was chosen in this research.

3.2.2 Stresses Around a Circular Hole

A major cause of stresses in a rock and soil mass is the weight of overburden rock and soil. It is called the primary, or initial , or roof pressure of rock or soil and varies in magnitude with depth from ground surface.

Near the ground surface, natural rock stresses are influenced by the weight of the rock, tectonic forces caused by folding of the earth's crust, jointing, fractures, restraint against lateral expansion.

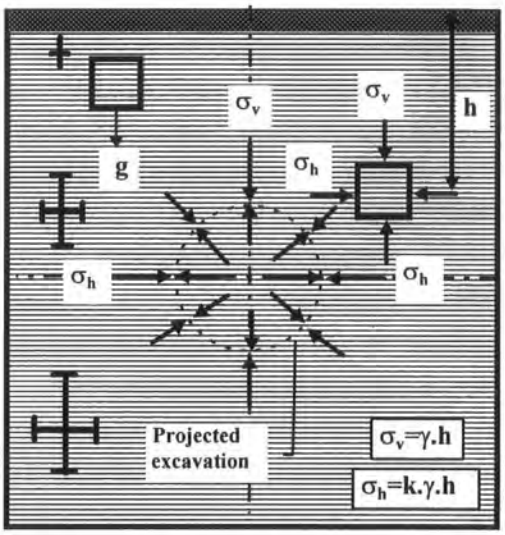

a) **Before the excavation is made, the stress field around the projected tunnel boundary is determined by geological conditions and can have any orientation with respect to the tunnel.**

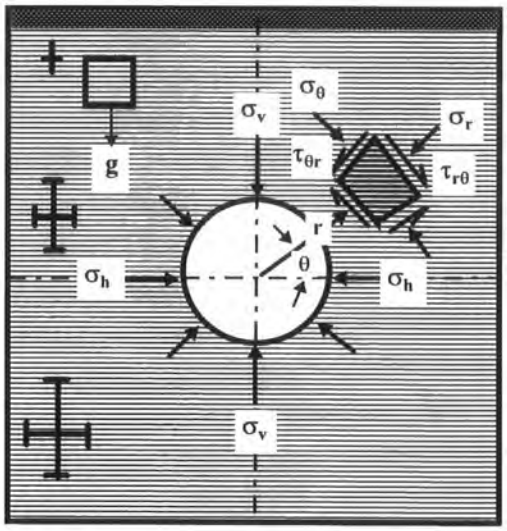

b) **Upon excavation, the boundary of the tunnel becomes free of normal stress, and this results in readjustment of the original stress field, especially in the vicinity of the boundary. This readjustment brings about rock displacements and rotations.**

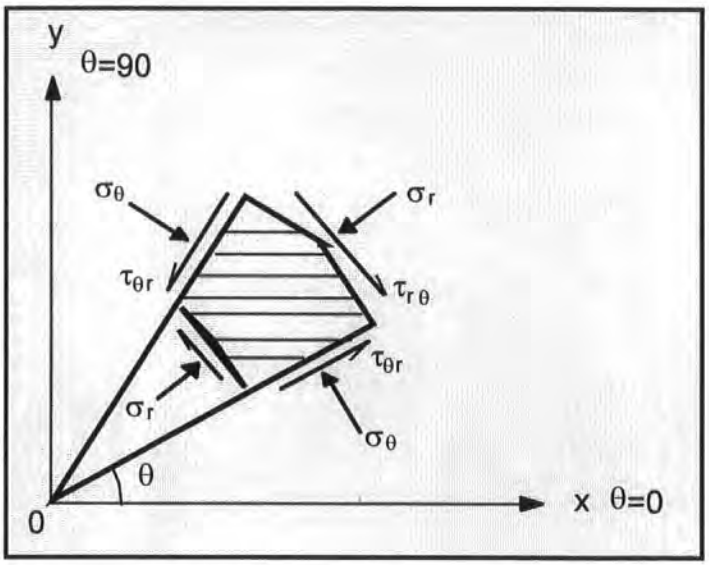

c) **Parameters and stress components for a circular hole in an infinite plane. All stresses are compressive positive.**

Fig. 3.5 Excavation of a tunnel changes the stress distribution in the ground around the opening.

The magnitude and direction or initial of primary stress in the rock and soil or the state of stress before excavation depends upon the stress field. Excavations bring about a new distribution of secondary stresses around the excavations. The magnitude of those secondary stresses is influenced by shape and size of the opening and by in-situ physical and mechanical properties of the rock and soil mass.

Assuming the rock is a homogeneous material, and knowing its exact elastic properties, the calculations of stresses in rock and soil, weakened by openings, can be made in a reasonable manner by means of the theory of elasticity. It should be said, however, that in practice these assumptions are very seldom met. Take the homogeneous, isotropic elastic case and assume that a long horizontal tunnel can be approximated by a circular hole in a plate of infinite extent. The necessary conditions for specifying the stress field in the general vicinity of the opening have been set out by Obert and Duvall (1967) and the solution was first obtained by Kirsch (1898). The standard solutions given by Attewell (1980) are ;

$$\sigma_r = \frac{1}{2}(\sigma_h + \sigma_v)\left(1-\frac{a^2}{r^2}\right) + \frac{1}{2}(\sigma_h - \sigma_v)\left(1+\frac{3a^4}{r^4}-\frac{4a^2}{r^2}\right)\cos 2\theta \qquad (3.22)$$

$$\sigma_\theta = \frac{1}{2}(\sigma_h + \sigma_v)\left(1+\frac{a^2}{r^2}\right) - \frac{1}{2}(\sigma_h - \sigma_v)\left(1+\frac{3a^4}{r^4}\right)\cos 2\theta \qquad (3.23)$$

$$\tau_{r\theta} = -\frac{1}{2}(\sigma_h - \sigma_v)\left(1-\frac{3a^4}{r^4}+\frac{2a^2}{r^2}\right)\sin 2\theta \qquad (3.24)$$

where

σ_h , σ_v are horizontal and vertical stresses ,

r is any radial distance,

a is the tunnel radius,

θ is the polar co-ordinate angle with respect to the x horizontal axis,

σ_r is a resultant radial stress at distance r from the centre of the tunnel and angle θ from x axis,

σ_θ is the hoop (tangential) stress,

$\tau_{r\theta}$ is the shear stress in the element

It is sometimes useful to be able to estimate the elastic displacement in the rock which result from external stresses σ_h and σ_v. Pender (1980) adopts a plane stress condition and provides the solutions in his pre-stress post-construction analysis, of the form

$$u = \frac{1}{2E}(1+\nu)\left\{(\sigma_h + \sigma_v)\left(\frac{a^2}{r}\right) + (\sigma_h + \sigma_v)\left[(1-\nu)\frac{4a^2}{r} - \frac{a^4}{r^3}\right]\cos 2\theta\right\} \quad (3.25)$$

$$\upsilon = \frac{1}{2E}(1+\nu)\left\{-(\sigma_h + \sigma_v)\left[(1-2\nu)\frac{2a^2}{r} + \frac{a^4}{r^3}\right]\sin 2\theta\right\} \quad (3.26)$$

where

u is the radial displacement with a positive sign denoting movement towards the origin,

υ is the circumferential displacement again with a positive sign as shown in Fig. 3.5,

ν is Poisson's ratio for the ground,

E is Young's modulus.

Edwards (1951), Terzaghi and Richart (1952) and Savin (1961), published series of papers which examined ground movement and treated it as an elastic phenomenon. Timoshenko and Goodier (1970) used a heterogeneous isotropic elastic model, plane elasticity to investigate excavated circular tunnels.

3.3 Photoelasticity

Until the advent of numerical methods, photoelasticity was the only practical method available for stress analysis of problems with complicated boundaries. For simple boundaries such as planes, circles, ellipses etc., exact analytical solutions are available. Photoelasticity is an optical method and relies on the optical properties of certain isotropic materials when they are stressed.

The method can be applied to determine the stress distribution around two- and three-dimensional excavations. Photoelasticity provides a graphical illustration of the stress distribution that develops when a body is loaded. An

extension discussion of the theory and application of photoelasticity is given by Obert and Duvall (1967).

Photoelastic methods are being almost completely replaced by numerical modelling techniques such as finite element methods, finite difference methods, boundary element methods etc.

3.4 Laboratory Models

Scaled models of tunnels and tunnel linings can be prepared from special materials in the laboratory. These can be instrumented suitably with strain or deformation gauges and loaded in compressive testing machine. A discussion of scaled models and their uses is given by Stagg and Zienkiewicz (1968).

Tests are usually performed under conditions of plane stress rather than the most realistic conditions of plane strain. Problems may be encountered in finding suitable materials which satisfy similarity. The failure behaviour of the material can have a very marked effect on the extent of failure or disintegration. This will have an effect on loads and deformation. Actual rock tends to dilate during disintegration.

Engineers are generally familiar with the use of laboratory models to help visualise stress and deformation patterns. Numerical models discussed below can be approached in the same way and with the same philosophy. However it is important to note that numerical modelling is not an exact solution to ground problems.

3.5 Numerical Methods

Analytical methods such as Kirsch's solution may be used to solve the governing equations exactly over a simple circular tunnel problem domain. The extension of the analytical solution to more complex domains (e.g. non-circular highway tunnels) requires simplifying assumptions to be made concerning the problem of geometry, material properties and/or boundary conditions. The finite

element (FE) method is an alternative technique in which the partial differential equations are solved approximately for more realistic problem descriptions. The finite element method is just one of a complementary set of numerical techniques that have been employed to solve partial differential equations. The finite difference method and the boundary integral element method are also commonly used to solve problems involving tunnelling. The finite difference method breaks the model down into a grid. The finite element method uses a mesh and the boundary element just uses elements on boundary of element as shown in Fig 3.6. A comparison of these methods is beyond both the scope of this thesis. Each of these techniques has advantages in certain particular cases.

One common feature of almost all quantitative investigations of realistic problems in engineering is that the boundary geometry of the region of interest is too irregular for analytical solution. Some form of numerical solution which may usually be obtained by the use of computational procedures, becomes necessary. Computational methods fall into two distinct categories: differential methods and integral methods. In differential methods, the governing differential equations are solved directly in the form which they are derived without any further mathematical manipulation. This is usually done either by approximating the differential operations in the localised algebraic equations valid at a serious of nodes within the region, as in the finite difference method, or by representing the region itself by finite elements of material which are assembled to provide an approximation to the real system, as in the finite element method. All such methods involve whole body discretization which require the solution of very large systems of algebraic equations. These methods generate the solution at all internal nodes used.

The essence of the integral equation techniques is the transformation of the differential equations into equivalent sets of integral equations as the first step in their solution. From such an operation a set of equations is obtained which would involve only values of the variables on the boundaries of the region of interest for example boundary element method.

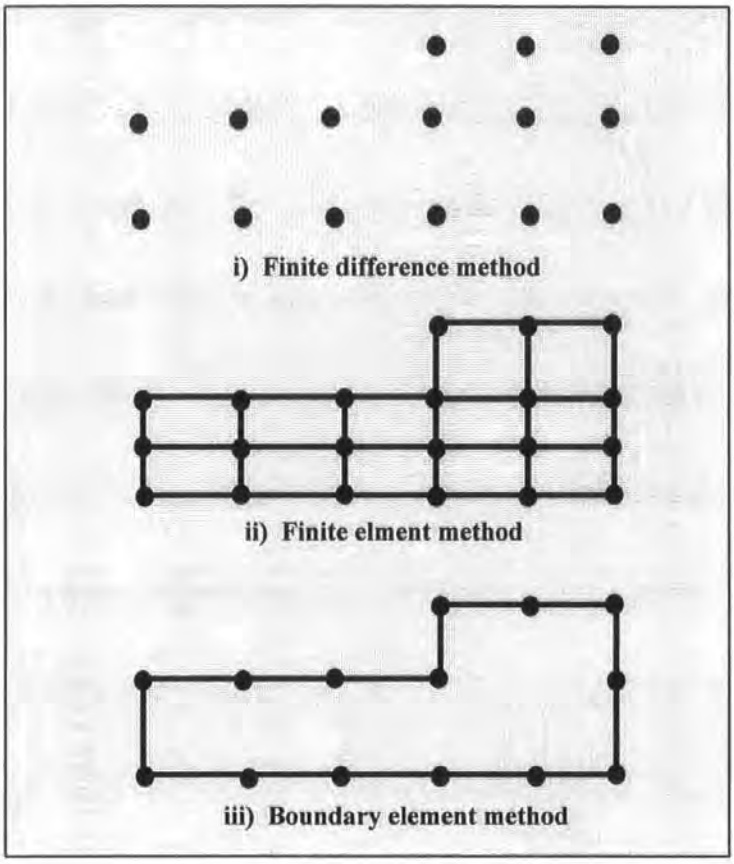

Fig. 3.6 Numerical methods

3.5.1 Finite Difference Method

Before the finite element method, the finite difference method was perhaps the main numerical technique employed. The application of finite difference method was discussed by Timoshenko and Goodier (1970) and Desai and Christian (1977). The finite difference method requires the entire region of interest to be discretized into an assemblage of grid nodes and it seeks an exact solution by approximating the differential equation (Jaeger and Cook 1979). For simple configurations such as rectangular regions, we can adjust the mesh points to coincide with the boundaries. Special procedures are necessary to account for irregular boundaries. With the finite element method such special procedures are not required. Use of different types of elements can solve modelling of irregular boundary problem.

3.5.2 Finite Element Method

3.5.2.1 Introduction

Numerous excellent works have been written on the subject of the theory belong to the finite element method and it is not the author's intention to discuss in any detail the mathematics of the method in this thesis.

The basic concept behind finite element analysis is the replacement of a complex problem by one that can be simply enacted so that the solution can be approximated. This idea was used by mathematicians more than two thousand years ago. For example, Archimedes approximated the circumference of a circle by the edge of a polygon (Woodford et al., 1992). Finite element analysis in its modern form is a very powerful computational technique. Zienkiewicz & Taylor, (1989) describe how the finite element method developed in the field of structural engineering. It has been use widely in structural engineering over the past twenty years, and has gained acceptance throughout engineering and the applied sciences. The initial development of the finite element method for aerospace and structural engineering was soon followed by application of the method to problems in soil and rock mechanics. The nature of soils and rocks, however, is highly complex and requires different considerations from the relatively prescribed materials used in structures. A realistic appraisal of the complexities imposed by such natural features as joints and other discontinuities would often require that soils and rocks be treated as discontinuous media. Nevertheless, approximate but acceptable solutions can be obtained by considering them as continuous masses. In most applications of the finite element method, the continuum approach is used. The fundamentals of finite element analysis are detailed in many publications such as, for example, Clough (1960, 1980), Zienkiewicz (1971), Norrie and Vries (1973, 1978), Desai and Abel (1972), Rockey et. al., (1975), Segerlind (1976), Tottenham and Brebbia (1977), Owen and Hinton (1980), Irons and Ahmad (1980), Akin (1986), Smith and Griffiths (1988), Rao (1989), Zienkiewicz and Taylor (1989), Ottosen and Petersson (1992) and Carlton (1993).

3.5.2.2 Basic Concepts

Initially the body or structure is divided into sub-regions known as finite elements. Their shape, size, number and arrangement are chosen to mirror the original body as closely as possible. The choice of element type is partly determined by the geometry and spatial co-ordinates of the body, with one, two or three dimensional elements being used, each having a variable number of nodal points (nodes) along element boundaries. Element size directly influences the accuracy of the solution, smaller elements producing more accurate results but requiring more computational time. Several sizes of elements are usually included within one structure. The aspect ratio describes the element shapes within the group, and elements with an aspect ratio near to unity give the best results. For two-dimensional elements the aspect ratio is the largest to smallest dimension. A structure that has unexpected changes in geometry or material properties requires nodes to be located at those places. By using more elements accuracy is improved, but this generates a large number of degrees of freedom, requiring larger matrices which may exceed the available computer memory. If the shape and external conditions of the structure are symmetrical, then it is only necessary to model half of the structure but these conditions need to be incorporated into the solution procedure. In geotechnical problems the area boundaries are generally not clearly defined, it is however possible to consider only the area expected to be affected.

The finite element analysis of practical problems frequently generates banded matrix equations and, by minimising the band width, both storage requirements and solution time are minimised. In simple systems, it easy to label nodes manually in order to minimise the band width, but in complex systems this is almost impossible. The development of automatic mesh generation algorithms which can divide any geometry into efficient finite element meshes, without user interruption, overcomes this problem. The minimum requirement is that the topology of the original geometry is maintained. Development of the finite

element procedure advances through the following stages (Zienkiewicz and Taylor, 1989). Assumptions concerning the element geometry are listed. A displacement function is chosen to model the state of displacement at any point in the element. The coefficients of this function are expressed in terms of the nodal displacement. The strains at any point in the finite element are now related to the displacements at that point and to the nodal displacement equation. The internal stresses occurring in the element are then related to the strains through the elasticity matrix. The loads are related to the nodal displacements through the established relationships defining the required element stiffness matrix. Finally a stress displacement matrix is used to relate the internal stresses in the finite element to the nodal displacements, thus enabling the internal stresses in the composite model to be evaluated.

PROGRAM NAME	*2-D*	*3-D*	*USA & CANADA*	*EUROPE*
ABAQUS	+	+	+	+
PHASE	+	+	+	+
UMFES	+	+	+	+
BEFE	+	+	+	-
SIGMA/W	+	+	+	-
FLAC	+	+	+	+
SHAKE	+	+	+	+
FLUSH	+	+	+	+
PAFEC	+	+	-	+

Table 3.1 Commercial softwares for stress and displacement analyses

Several software products exist which include a number of features useful for geotechnical problems, such as time-dependent movement, anisotropic behaviour, joint elements, and a facility to simulate rock fracture. However, there is always some difficulty when considering the use of inelastic model in assessing the type of inelastic behaviour. Some software currently on the market is listed in Table 3.1.

3.5.2.3 Use of the Finite Element Method for Soil and Rock Masses

Important factors affecting the solution of a geotechnical problem are the structure, the validity of the structural model, together with the analysis and the results obtained from the analysis. The geometry, boundary conditions and material composition of the structure must be considered and restrictions on movement within the model taken into account.

Deformation behaviour of soils and rocks is influenced by a number of factors, such as the physical structure (mineralogical composition, internal cracking), porosity, density, stress history, loading characteristics, and macroscopic fracturing. In addition, such geologic features as faults, joints, crushed zones, fissures, folds and other tectonic effects produce behaviour significantly different from that derived on the assumption of a continuum. These factors can make the stress-deformation behaviour highly complex and non-linear. No currently available analytical solution method can handle them all.

The model structure is designed by a mesh of simple geometric shape. The mathematical properties of these meshes designed replicate accurately the structure's physical characteristics. The environment of the model structure embodies the specification of external force, supports and boundary conditions. Analysis is performed on the individual elements, taking account of the interaction between each element and its immediate neighbours, and the imposed boundary conditions on the structure. The response in terms of stress, strain and displacement from the individual elements are combined to produce results which apply to the composite.

In the development of a typical finite element computational rock and soil mass model for static analysis, the following procedure should be adopted:

i) Firstly it is necessary to select a suitable mathematical model for the solving of problem of the structural interaction between the tunnel support and the surrounding ground. This should include consideration of symmetry required in order to reduce the analysis if the geometry of

the structure itself is symmetric and the boundary conditions, static loads and restrains are also symmetric.

ii) A finite element discretization is then applied. The structure is sub-divided into a mesh of finite elements which might consist of two-dimensional triangular and/or quadrilateral or three-dimensional brick and/or wedge elements. Furthermore, the appropriate boundary details are defined in terms of specified static loading and constraint conditions that characterise the structure under consideration. After a computer run, the next step involves the presentation and interpretation of the static analysis results. The results can be presented graphically in the form of displaced shape, stress vector plots and stress contour plots.

iii) A computer run without any error or warning messages does not show that the static analysis is correct. The expected stress distribution and unrealistic results must be checked. Alternatively a different mesh and perhaps a more accurate type of element must be used. The accuracy of the results and analysis depend on a good finite element mesh.

The principle of using the finite element method in the study of geotechnical engineering problems has to be the design of an optimum mesh which not only will offer the greatest possible degree of detail around the excavation, but will also reduce the number of nodes away from the opening where detailed accuracy may not be required. This is even more important when a three dimensional model is used because the number of nodes is significantly increased over an equivalent two dimensional model.

3.5.2.4 A Review of the Application of the Finite Element Method to Tunnelling

Of particular note for the finite element approach in connection with geotechnical engineering applications are the contributions by many authors given below.

Goodman (1966) discussed the effect of constructing circular tunnels in layered rocks as opposed to homogeneous rocks in his paper. The results represent solutions to plane strain boundary value problems using a finite element analysis.

Blake (1966) described the finite element method of analysis and its use in solving typical underground stress problems in his paper. The effects of non-homogeneities surrounding an circular opening were shown in computer plots of maximum shear stress contours, stress trajectories and principal stress directions.

Anderson and Dodd (1966) showed an example model for determining the stress field acting about a rectangular underground opening in a faulted rock mass using finite element method.

Salvador and Deere (1966) analysed stress concentrations around circular openings in an infinite medium for arbitrary values of yield parameters and initial state of stress.

Stagg and Zienkiewicz (1968) discussed the application of the finite element method to stress studies and an example of lined tunnel was shown in the stresses when the lining was considered in section eight of their book.

Agarwal and Boshkov (1969) discussed finite element analyses of stress and displacement fields for some combined loading conditions and comparison of plane stress and strain solution for a circular tunnel.

Desai and Abel (1972) described finite element method for soil and rock mechanics and a few typical application of a circular tunnel mesh and loading in their books.

Barla (1972) studied the influence of a horizontal pulling-free surface on the stresses in the near vicinity of a single circular underground opening using finite element method.

Kulhawy (1974) presented modelling criteria for plane strain finite element analyses of a circular underground opening in homogeneous, linear elastic rock .

Chang and Nair (1974) described a simple computer program for the evaluation of the stability of openings in rock using finite element method and demonstrated its capacity through an analysis of case histories.

Barla and Ottoviani (1974) solved the problem of determining the stresses and displacements around two adjacent, circular openings, located near to a horizontal ground surface using finite element method.

Monaco et al. (1974) illustrated problems belonging to underground openings for three large pumped-storage plants and usefulness of the finite element method.

Kulhawy (1975) presented the significance of material properties, initial stresses, excavation sequences and opening shapes on the resulting stresses and displacements around underground openings in homogeneous rock masses using finite element method.

Wittke (1977a) discussed static analysis for underground openings in jointed rock using finite element method and importance of underground openings such as traffic tunnels, water power tunnels, irrigation project.

Wittke (1977b) presented the evaluation of the stability and the amount of required safety measures and lining for underground openings in jointed rock and a new design concept based on the finite element method.

Gudehus (1977) discussed generally geomechanics and finite element methods and knowledge of basic continuum mechanics. The equilibrium state around an excavated tunnel and finite set of variables were presented

Orr, Atkinson and Worth (1978) discussed a detailed comparison between the observed displacements around two circular model tunnels and those from finite element computations based on two non-linear models of soil behaviour. They showed that much theoretical research and development work is still required and it is not possible to solve all design problem yet.

Vollstedt and Duddeck (1978) showed that analytical methods cannot deal with non-linearities therefore numerical methods are needed as the different variations of the finite element methods and examples of non-linearities were classified.

Naylor and Pande (1981) presented the application of finite element in geotechnical engineering and some tunnel case histories.

Smith (1982) described programming the finite element method with application to geomechanics and some program examples chosen involves creation of a mesh of four noded elements for the stress analysis of a tunnel in linear elastic ground.

Swoboda (1982) discussed the use of finite element calculation for tunnel models when planning tunnels make necessary solving a number of very different problems and the starting parameters only allow an estimation of the actual conditions.

Ohnishi et al. (1982) presented that the study in detail the effects of delayed construction of the tunnel support and the behaviour of the ground mass around the face of advancing tunnel must quantitatively be analysed. Since this problem is not simple and cannot be solved by closed form analyses, it must be solved numerically using three-dimensional techniques like finite element method.

Attewell, Yeates and Selby (1986) described solutions to soil-structure interaction at three levels of analysis which involve common simplifying assumptions and discussed finite element analyses of the prediction of response of a soil-structure system to tunnelling.

Pan and Hudson (1988) carried out a non-linear axisymmetric finite element simulation of tunnelling in a rock mass to investigate the stresses and displacements behind an advancing tunnel face.

Mertz and Swoboda (1989) described a CAD program that was specially developed for the generation of three-dimensional finite element meshes as were used in tunnel construction.

Wittke (1990) presented computation of stresses and strains due to underground openings in rock masses using the finite element method in his book.

Juemin and Huanqian (1990) analysed the special problem of the tunnel with three-dimensional finite element method and they showed that results of the computation were consistent with that of in-situ measurement.

Swoboda (1990), showed the approximations necessary for two-dimensional analysis using finite element analysis and increasing significance for three-dimensional tunnel models.

Duddeck (1991) reviewed the application of finite element method in tunnelling, the achievements and presented the future tasks for closing the gap between real ground behaviour in critical tunnelling situations.

Kielbassa and Duddeck (1991) presented some results of elastic three-dimensional finite element analyses in consecutive steps of the sectional excavation of circular and non-circular tunnels.

Mahtab and Grasso (1992) presented rock characterization for tunnel design and numerical analysis methods and design criteria were introduced in their book.

Woodford, Passaris and Bull (1992) published a book to provide an introduction and guide to good finite element practise using PAFEC-FE finite element software for engineering analysis and engineering design. Geotechnical engineering application section of this book contains excavation simulation methods, modelling of underground excavation support systems and an example of a near surface excavation using PAFEC-FE.

Soliman, Duddeck and Ahrens (1993) presented the results of a finite element approach to these problems for shield-driven tunnels, as well as for tunnels driven by excavation and shotcreting. The results showed the relative changes in stresses and deformations and it was suggested that single -tunnel solutions can be used to find double-tube solutions.

Peila (1994) discussed a three-dimensional, elasto-plastic finite element tunnel analyses results. Tunnel face reinforcement was simulated and the stresses, plastic zones and displacements in the ground were studied for face reinforcement.

Carter and Xiao (1994) described a coupled finite element and boundary element formulation for the analysis of excavation in jointed rock. Good agreement has been found between numerical and analytical solutions for several example problems. Numerical solutions were also presented for the problems of a deep circular tunnel in a variety of jointed rock masses.

Bernaud, Buhan and Maghous (1995) presented finite element simulations of a bolt-supported circular tunnel and calculating its convergence as the excavation proceeds. The results of this numerical simulation prove to agree perfectly well with those derived from an analytical model.

Pelia and Oreste (1995) presented a new analytical axisymmetric model for the evaluation of the ground response curve when a zone with better geomechanical properties is presented around the tunnel. For a simple geometric condition, the results obtained with the proposed analytical approach and a numerical finite difference model using 2-D FLAC software have been compared obtaining a good agreement.

The intention here is to examine the finite element method in the light of its applicability to geotechnical problems, and its development in the field of rock mechanics is reviewed. If an elastic solution can be made to predict ground mass behaviour to a reasonable degree of accuracy the assumptions and approximations made can be more clearly defined than if a highly complex model were chosen. It was with this philosophy in mind that an examination of the types of solution available was carried out.

3.5.3 Boundary Integral Method

The boundary element method has been establish as an important alternative technique to the numerical methods in continuum mechanics (Brebbia, 1978). The technique basically consists of the transformation of the partial differential equation, describing the behaviour of the unknowns inside and on the boundary of the domain, into an integral equation relating only boundary values and the numerical solution of this equation. If values at internal points are required, they are calculated afterwards from the boundary data. Since all numerical approximations take place only at the boundaries, the dimension of the problem is reduced by one and smaller system of equation obtained in comparison with those achieved through differential methods. Discretization would only involve subdivision of the boundary surface of the body. Since the surface of the body only is defined and discretized, the boundary element methods effectively provide a unit reduction in the dimensional order of a problem, which especially in three dimensions, leads to an appreciable reduction in the number of algebraic

equation generated for solution and simplified data preparation. The integral methods are distinguished by either direct or indirect formulation.

3.6 Excavation Simulation

3.6.1 Introduction

Several procedures for simulating excavation operation have been proposed by Goodman and Brown (1963), Brown and King (1966), Dunlop and Duncan (1970), Desai and Abel (1972), Kulhawy (1974), Naylor and Pande (1981) and Budari (1983). The basic concept is that the rock is in equilibrium and at rest in an initially stressed state. Under excavation the removal of material and subsequent redistribution of stress in the remaining material must be treated by one of three methods. These are the gravity difference method, the relaxation approach and the stress reversal technique. Both the gravity difference method and stress reversal technique were chosen for the simulation of excavation for this study.

3.6.2 Gravity Difference Method

In the gravity difference method (alternatively known as the gravity turn on method by Dunlop and Duncan (1970)) two analyses must be conducted. Firstly, gravity load is applied to a block of ground having no opening, and, secondly, the process is repeated with the same block of ground but with openings or sometimes with the excavated elements (air elements) given a very low modulus value (approximating to air material properties). The stress and displacement differences between the two analyses are the ground stresses and displacements caused by the creation of the opening as shown in Fig. 3.7. The gravity difference method is limited in its application. It cannot model a tunnel having a shotcrete, secondary lining and steel arch as shown in Fig. 3.8.

There is a displacement of rock due to the application of gravity load to the unexcavated rock. The excavated displacements are calculated by comparison with the gravity loaded excavated and unexcavated grounds.

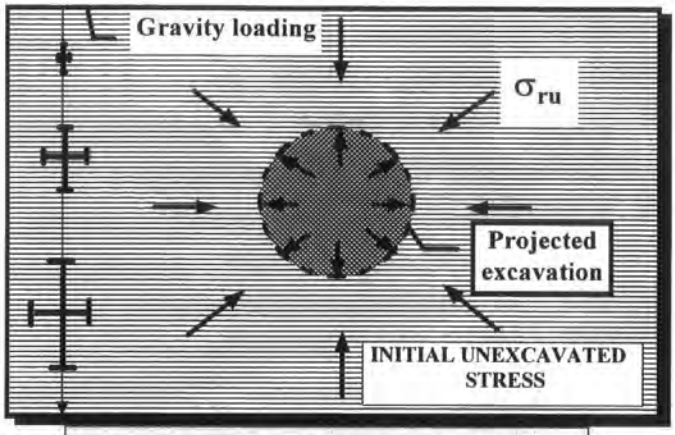

Initial ground stress due to gravity = σ_{ru}
Initial displacement due to gravity = U_{ru}

a) Unexcavated ground with gravity load

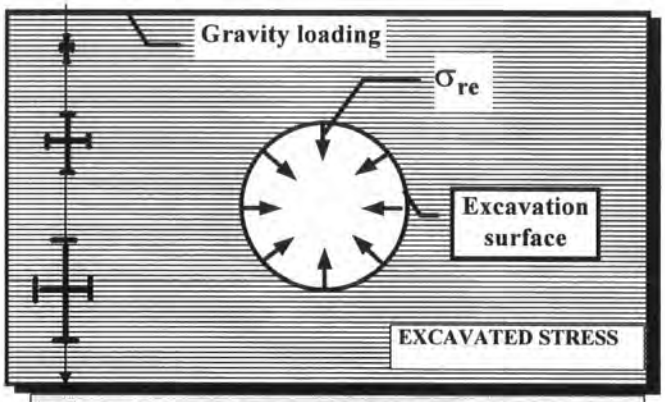

Excavated ground stress due to gravity = σ_{re}
Excavated ground displacement due to gravity = U_{re}

b) Excavated ground with gravity load

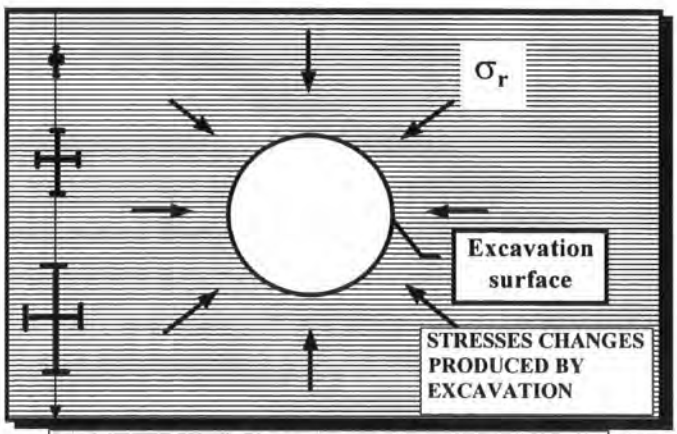

Stress due to excavation = $\sigma_r = \sigma_{re} - \sigma_{ru}$
Displacement due to excavation = $U_r = U_{re} - U_{ru}$

c) Gravity difference

Fig. 3.7 Gravity difference method

When the ground support is applied at the excavation surface it is positioned in the rock before gravity loading has been applied. When the gravity loading is exerted it has to work against the support to achieve the displacement expected from gravity-loaded ground having no excavation. The resulting displacement is significantly less above the supports, indicating that the presence of the supports make the surface rise as shown in Fig. 3.8.

The gravity difference method requires the differences between two analyses to produce the stresses and displacements that result from the creation of ground excavation. This is because in the gravity difference method displacements (vectoral quantities) can be subtracted but stresses need to be carefully considered. Von Mises (the equivalent stress) should not be subtracted but the equivalent stress is calculated from global stress tensor components which can be subtracted.

The Von Mises stress difference between the two analyses can be recalculated from subtracted stress tensor components by using equation (3.19). The resultant Von Mises stress is

$$\sigma_r = \frac{1}{\sqrt{2}} \sqrt{\begin{aligned} &\left[\left(\sigma_{xx} - \sigma'_{xx}\right) - \left(\sigma_{yy} - \sigma'_{yy}\right)\right]^2 + \\ &\left[\left(\sigma_{yy} - \sigma'_{yy}\right) - \left(\sigma_{zz} - \sigma'_{zz}\right)\right]^2 + \\ &\left[\left(\sigma_{zz} - \sigma'_{zz}\right) - \left(\sigma_{xx} - \sigma'_{xx}\right)\right]^2 + \\ &6\left[\left(\sigma_{xy} - \sigma'_{xy}\right)^2 - \left(\sigma_{yz} - \sigma'_{yz}\right)^2 + \left(\sigma_{zx} - \sigma'_{zx}\right)^2\right] \end{aligned}} \tag{3.27}$$

and resultant displacement difference between the two analysis by using equation (3.20) is

$$U_r = \sqrt{\left(U_x - U'_x\right)^2 + \left(U_y - U'_y\right)^2} \tag{3.28}$$

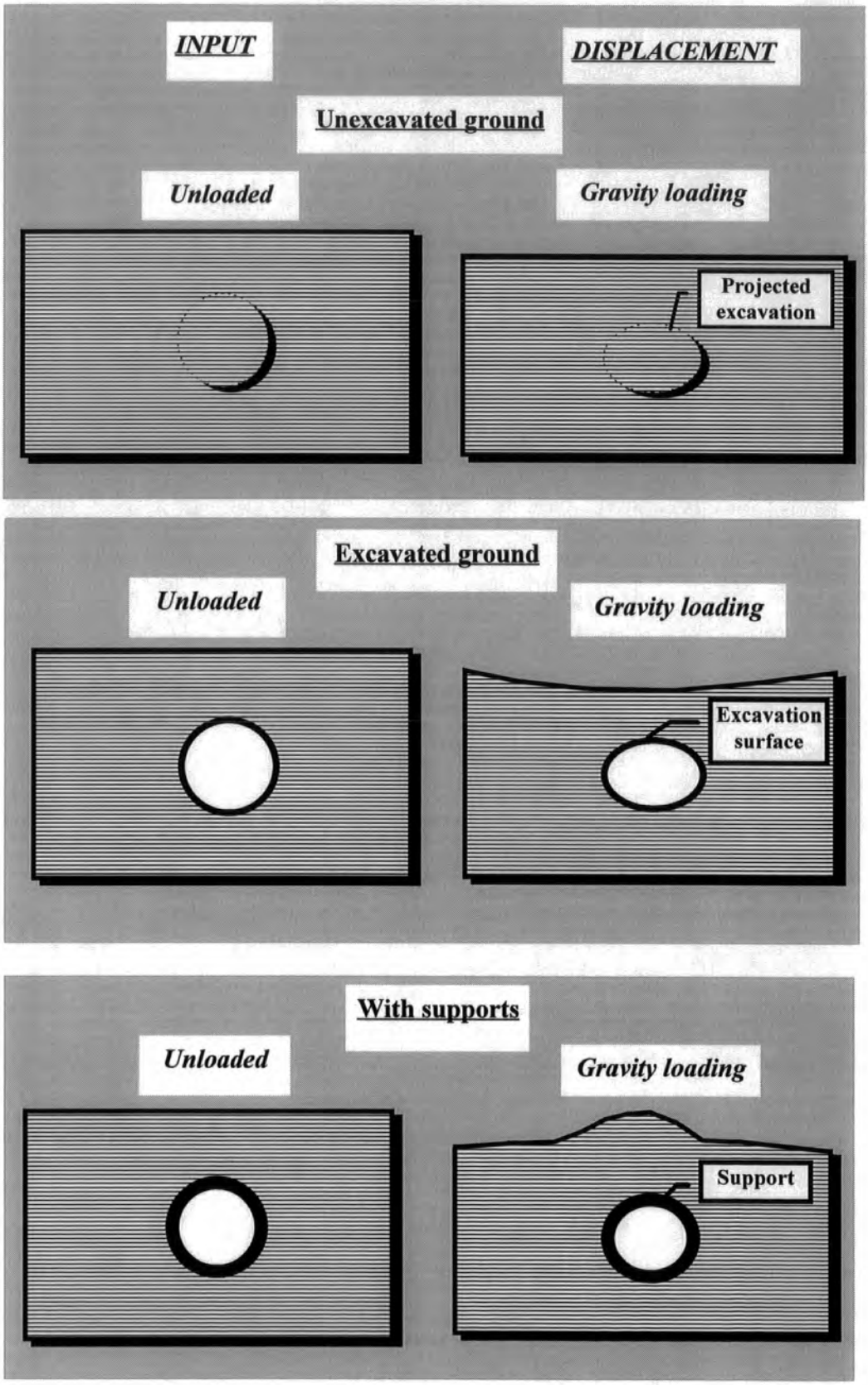

Fig. 3.8 Gravity difference method and its limitation

3.6.3 Relaxation Approach

In the relaxation or residual stress approach, the final geometry of the opening is usually established in the initial finite element mesh. The elements representing the surrounding rock mass are initially stressed to some desired values which are subsequently relaxed to provide a final equilibrium stress state around the opening as shown in Fig. 3.9. With this approach it is difficult to follow a construction sequence, and also the relaxation is controlled exclusively by stresses existing in the elements which form the rock mass surrounding the excavation.

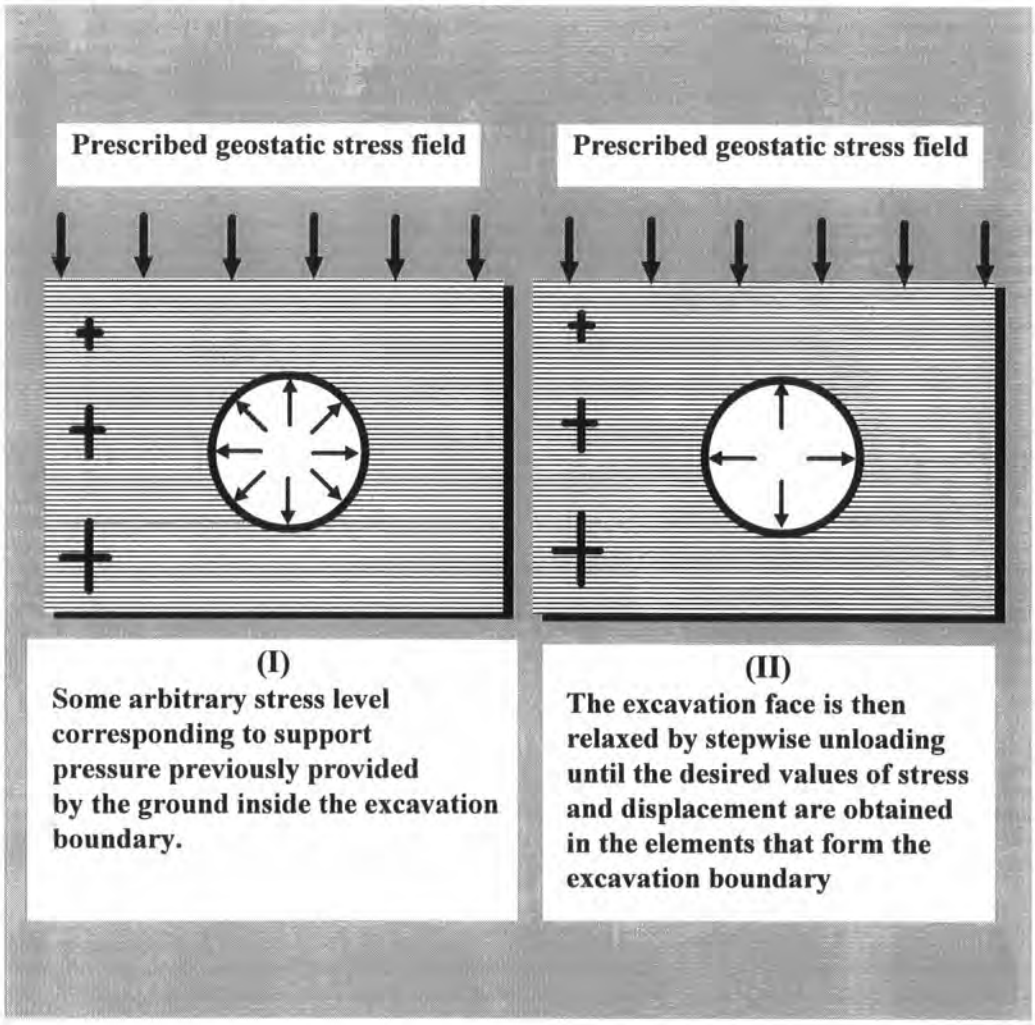

Fig. 3.9 Relaxation approach

3.6.4 Stress Reversal Technique

The stress reversal approach considers the stresses existing in the finite elements on both sides of a proposed excavation boundary at any stage of excavation. The excavation is simulated by applying a gravity load to the mesh and evaluating the stresses along the potential excavation surface. From these stresses, the equivalent forces at the nodes along the excavation surface are computed and their signs are reversed. A second run then applies computed forces to the excavation surface. Any body subjected to external force exhibits an opposite reaction ; in other words, internal forces develop in it, tending to restore its original shape as shown in Fig 3.10.

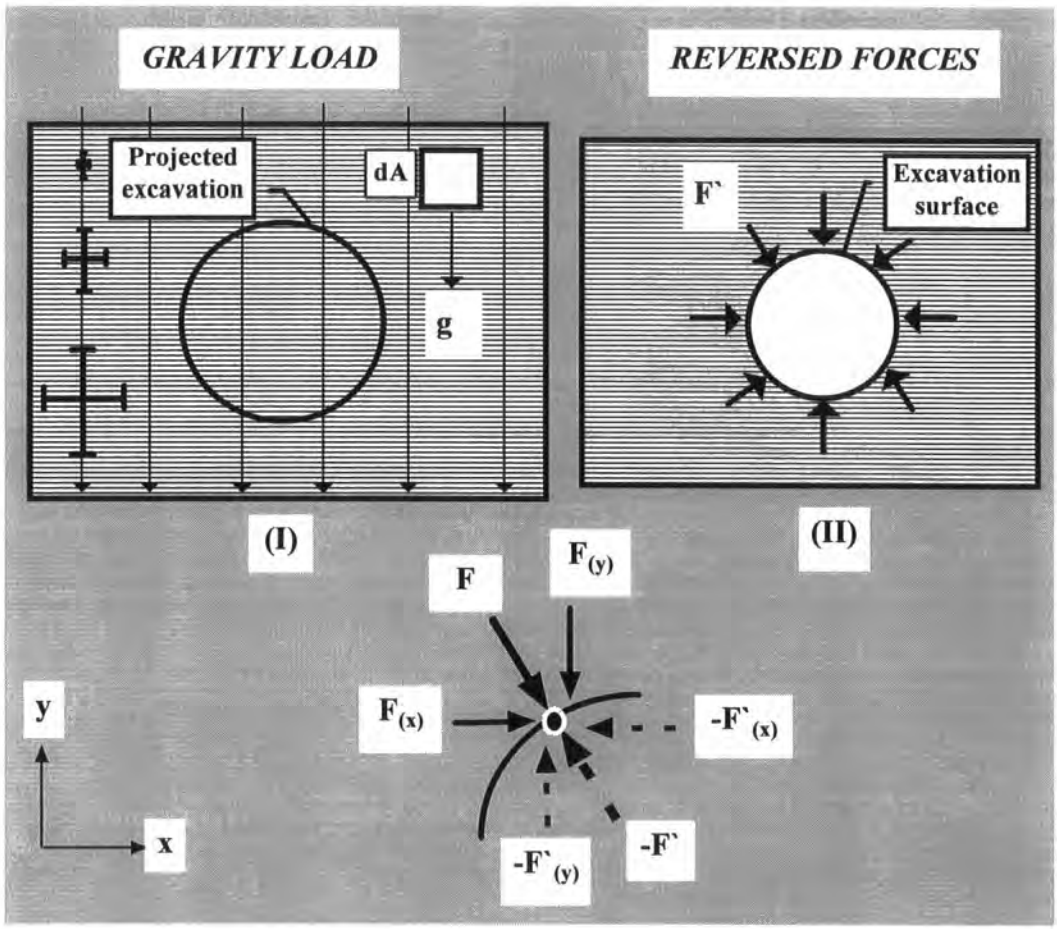

Fig. 3.10 Stress reversal technique

The computed stresses, strains and displacements from the two runs are then compared to give the results of a particular excavation step. A typical application of the stress reversal technique is used for simulating the excavation of underground openings and the application of supports.

The stress reversal approach considers the stresses existing in the elements on both sides of a proposed excavation boundary at any stage of excavation, and based upon these stresses evaluates the equivalent nodal forces to be applied along the boundary. Stresses on the excavation boundary have to be defined in terms of local direction for front and back planes in a three-dimensional model.

In the finite element method, stresses are commonly determined at either the centres of the elements or midway between two opposing nodal points, depending upon the type of element used, but excavation boundaries pass between elements. Therefore, a technique must be employed to interpolate from the centre stresses to the nodal or boundary stresses. The stress reversal technique was the method chosen for the analyses included in this thesis.

The implementation of the gravity difference method and reverse stress technique in PAFEC-FE will be discussed in Chapter 4.

CHAPTER 4

EXCAVATION SIMULATION USING PAFEC-FE

4.1 General Structure of PAFEC-FE System

4.1.1 Introduction

PAFEC is an a acronym for 'Programs for Automatic Finite Element Calculations'. It was first developed in 1960's at Nottingham University but has been continuously developed and extended and is now very widely used both in industrial and academic institutions. PAFEC-FE is a general purpose, three-dimensional finite element system for structural and thermal analysis (PAFEC Ltd., 1992). It employs free-format input with engineering keyword identifiers and has a library of over 80 elements. These include beams, springs, masses, plates, shells, bricks, and wedges for use in one, two or three dimensions. Applied loads include gravity, pressure and point loads.

PAFEC-FE consists primarily of two systems. The first performs the actual finite element analysis (PAFEC.EXE) and second handles the interaction of the program with the computer on which it is running. The second is referred to as the PAFEC-FE driver (front end program). PAFEC.EXE is always same but the driver is different for PC, SUN and UNIX systems. There are ten separate phases corresponding to subroutines in a complete single run of PAFEC using a particular data file. These are shown in Fig. 4.1 and generated displacements and stresses are written to a particular output file related to each phase. The version of PAFEC-FE used and described here was 7.4.

4.1.2 Application of PAFEC-FE

The first step in modelling any problem with PAFEC-FE is construction of an input data file which is a computer file containing all the information which is necessary to run PAFEC-FE completely. This data has to be in a format which

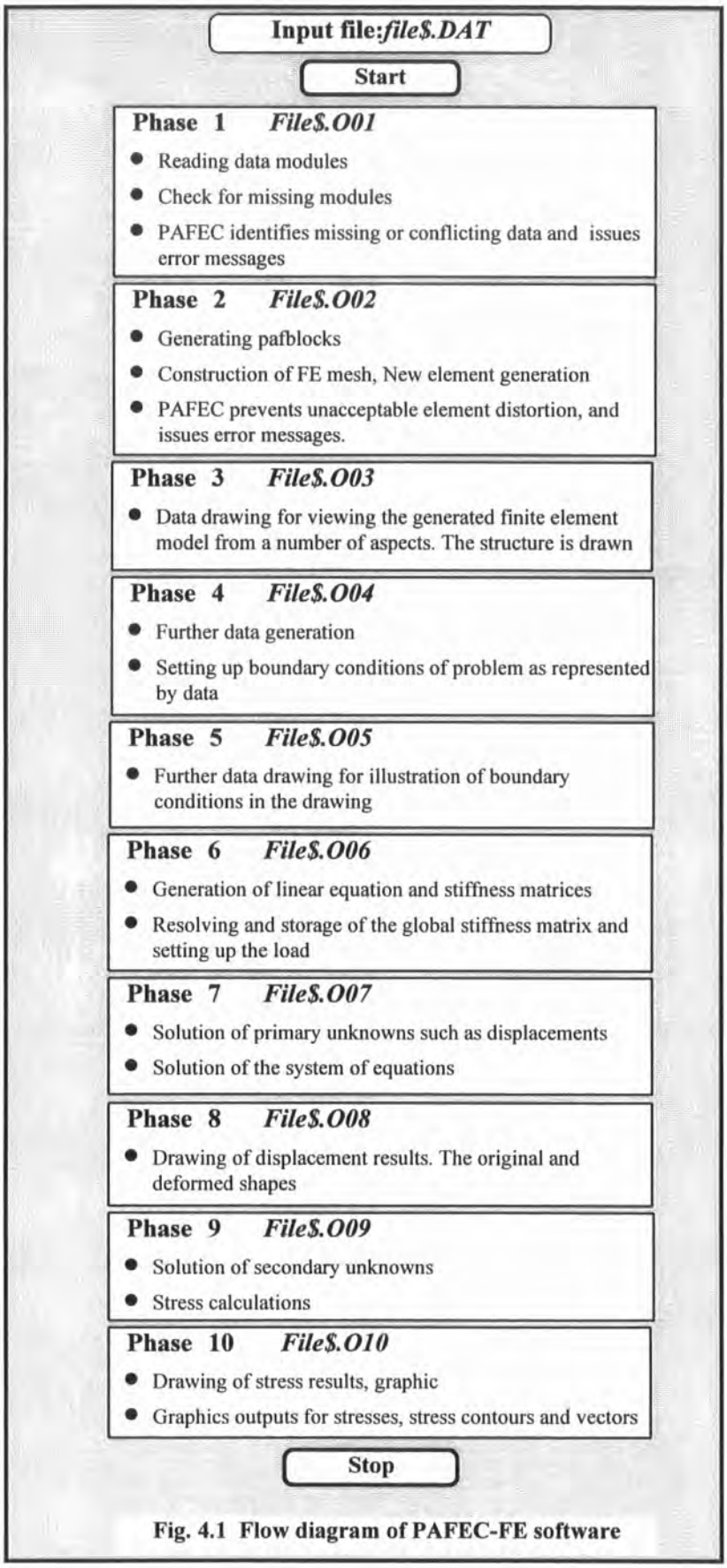

Fig. 4.1 Flow diagram of PAFEC-FE software

PAFEC-FE can recognise and read in and must be expressed in terms of the basic SI units. The input data file comprises information called PAFEC-FE modules. Many modulus are optional but there are certain modules which appear in every data file and without them the program cannot be run. Each module contains a module header and headings for the columns forming the rest of module. Comment lines in the data file which start with letter 'C' are ignored by PAFEC-FE. The main modules used in this work are described below.

4.1.2.1 NODES module

Node is a point at the corner of an element or midway between two corners on the element edge. The locations of nodes are defined by co-ordinates using NODES module in the data file. This module is a list of the nodes and their x, y, z co-ordinates. The node numbers should increase in magnitude through the module but not necessarily in steps of one. The format of this module in the data file is as shown in Fig. 4.2. The default set is standard Cartesian and is the only one used in the analyses

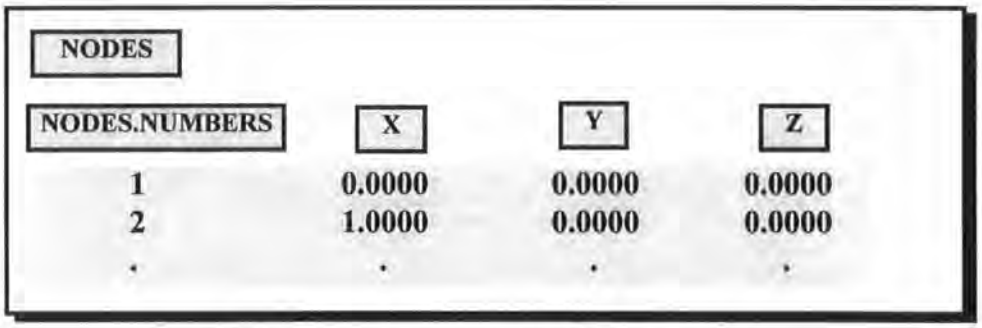

Fig. 4.2 Data format for NODES module

4.1.2.2 PAFBLOCKS module

This module allows automatic mesh generation. The pafblock is a comparatively large region of material forming a simple shape defined by the position of its nodes which is automatically subdivided into a mesh of individual elements each of which is of similar shape and type to the large block. The

pafblock is defined by the block number, pafblock type, element type, properties, reference subdivision number N1 to N5 and position of pafblock nodes (topology) as shown in Fig. 4.3.

PAFBLOCKS

BLOCK.NUMBER	TYPE	ELEMENT TYPE	PROPERTIES	N1	N2	N5	TOPOLOGY
1	1	36210	1	1	1	0	12340000

Fig. 4.3 Data format for PAFBLOCKS module

The block number column contains the number of pafblock being defined which must increase in magnitude through the module. The type column refers to the pafblocks being used for the analysis. Element type column contains element being used for the analysis, whether two- or three-dimensional, linear or quadrilateral. The two types element used in the analysis are referred to as 36210 (2-D) and 37110 (3-D). The properties column contains the number of the set of properties assigned to a particular element. The topology column contains a list of the nodes which are in the pafblock geometry.

4.1.2.3 PLATES AND SHELLS module

This module is used for only two-dimensional models. It is defined by plate number, material number and element thickness. The plate number should increase with material number. The properties column in the pafblock module refers to the plate number being used. The material number column contains the number of the set of properties in MATERIAL module as shown in Fig. 4.4.

PLATES.AND.SHELLS

PLATE.NUMBER	MATERIAL.NUMBER	THICKNESS
1	11	1
2	12	1

Fig. 4.4 Data format for PLATES AND SHELL module

4.1.2.4 MATERIAL module

This module is defined by a material number. The properties for material '1' to '10' are pre-programmed into the PAFEC-FE code, e.g. mild steel to concrete, but different properties can be supplied via a material module. Young's modulus (E), Poisson's ratio (NU) and mass density (RO) are used to specify the mechanical characteristics of the geological and other materials which are involved in the analysis and PLATES AND SHELLS module in a two-dimensional approach. The format of this module in the data file as shown in Fig. 4.5.

MATERIAL			
MATERIAL.NUMBER	E	NU	RO
11	90E+6	0.35	2060
12	0.7E+9	0.27	2200
.	.	.	.

Fig. 4.5 Data format for MATERIAL module

4.1.2.5 GRAVITY module

Gravity module simulates the effect of the vertical gravitational stress field, normally imposed on geological formations. The format of the gravity module is as shown in Fig. 4.6. In the GRAVITY module the sign in the YGVALUE is negative, indicating that gravity acts in the vertical downwards direction. The XGVALUE and ZGVALUE directions columns contain an entry similar in meaning to restraints direction.

GRAVITY				
LOAD.CASE	XGVALUE	YGVALUE	ZGVALUE	AXIS.NUMBER
1	0	-1	0	1

Fig. 4.6 Data format for GRAVITY module

MATERIAL NUMBER	MATERIAL DESCRIPTION
11	Neogen cover
12	Micaceous sandstone, siltstone and claystone
13	Quartzite
14	Arkose, conglomeratic arkose
15	Volcanic dyke
16	Schotcrete lining
17	Inner lining
18	Mild steel for anchorages and steel arch
19	Elements inside the tunnel for excavation have air material properties

Table 4.1 Materials used for simulation

MATERIAL NUMBER	YOUNG'S (ELASTICITY) MODULUS E (GPa)	POISSON'S RATIO ν	MASS DENSITY ρ (kg/m^3)
11	0.090	0.35	2060
12	0.7	0.27	2200
13	68	0.16	2600
14	15	0.26	2600
15	1.9	0.28	2300
16	15	0.20	2000
17	30	0.20	2400
18	209	0.30	7800
19	0.0	0.499	0.00

Table 4.2 Initial mechanical properties of materials used for simulation

4.1.2.6 RESTRAINTS module

This module essentially defines the restrictions on movement of certain nodes or planes in any combination of the three principal directions. The format of the module is as shown in Fig. 4.7. The node number column contains the number of the nodes at which the restraint is to be applied. The plane column contains a number which defines how the restraint affects the node in the previous column.

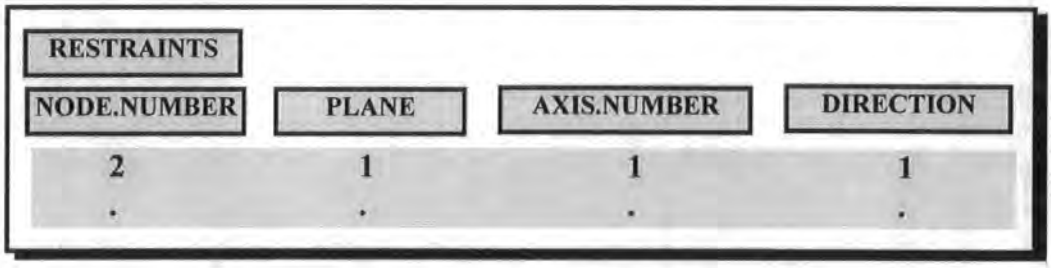

Fig. 4.7 Data format for RESTRAINTS module

A zero means that the restraint only applies to the node mentioned whereas a 1, 2 or 3 means that restraint applies to a plane of constant x, y or z through the node mentioned. The entry in the direction column refers to the degree of freedom to be restrained at the node or plane in question. Numbers of 1 to 3 refer to x, y, z displacements and 4 to 6 refer to x, y, z rotations. Any combination of numbers may be used in this column.

4.1.2.7 CONTROL module

This module contains commands controlling the way in which the analysis is run. PAFEC-FE provides a default mechanism by which the program is run if no commands are inserted in the module. The format of the module is as shown in Fig. 4.8.

Fig. 4.8 Data format for CONTROL module

CONTROL module for two-dimensional model allows plane strain and plane stress analysis to be applied where required.

4.1.2.8 PROCESSING FOR PRINT OUTPUT module

This module requests suitable outputs including stress orders and displacements. The format of the module is as shown in Fig. 4.9. Order refers to type of stress or stress component referred to a given axis set.

PROCESSING.FOR.PRINTED.OUTPUT

ORDER	FORMAT.TYPE	LOCAL.AXIS	WINDOW
1	1	1	0
2	1	1	0

Fig. 4.9 Data format for PROCESSING FOR PRINTED OUTPUT module

4.1.2.9 ORDER FOR PRINT OUTPUT module

This module specifies the type of order related to the stresses and displacements. The format of the module is as shown in Fig. 4.10. The code numbers to be used in the LIST OF TYPES determine the different stress types are given in PAFEC-FE user manual as shown in Table 4.3.

ORDER.FOR.PRINTED.OUTPUT

ORDER	LIST.OF.TYPES
1	101 103 102 4 8 9 10 11 12 13
2	101 102 4 8 9 10 11 12 13

Fig. 4.10 Data format for ORDER FOR PRINTED OUTPUT module

Order 1 and 2 refer to two and three-dimensional models respectively.

The code numbers	Description
4	Von Mises stress
8	Sigma-XX
9	Sigma-YY
10	Sigma-ZZ
11	Tau-XY
12	Tau-YZ
13	Tau-ZX
101	Loadcase
102	Node number
103	Element number

Table 4.3 The code numbers to be used in the LIST OF TYPES column

4.1.2.10 BEAMS module

The format of this module in the data file is as shown in Fig. 4.11. Beam element is defined in BEAMS module by section number, mater4ial number depending on material type and various section properties, i.e. the cross section area, the two principal second moments of area and corresponding section moduli.

BEAMS

SECTION	MATERIAL	AREA	IYY	IZZ	ZY	ZZ
20	18	.242E-03	.280E-01	.560E-01	.200E+01	.200E+01
21	18	.180E-02	.103E-04	.322E-02	.128E-03	.153E-01

Fig. 4.11 Data format for BEAMS module

The format of BEAMS module in the data file is as shown in Fig. 4.11. SECTION number is referred to in the properties column of the ELEMENT module. MATERIAL NUMBER refers to the material number in the MATERIAL

module. IYY and IZZ are two principal second moments area of the section and they are calculated as follows.

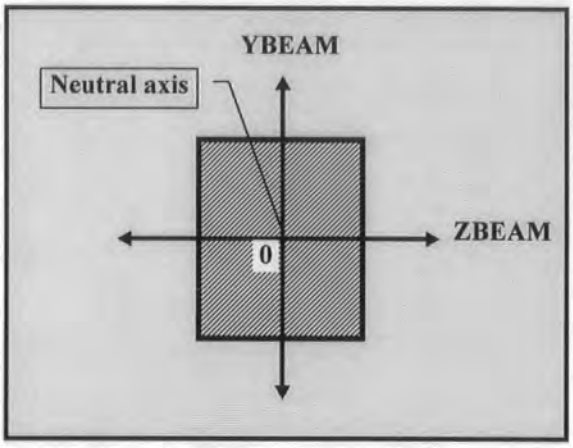

Fig. 4.12 Orientation of a beam in space

$$IYY = \int Z_A^{\,2}\, dA \tag{4.1}$$

$$IZZ = \int Y_A^{\,2}\, dA \tag{4.2}$$

where Z and Y are the element directions. Sectional module ZY and ZZ of the beam for stressing purposes are then

$$ZY = \frac{IYY}{z_{\max}} \tag{4.3}$$

$$ZZ = \frac{IZZ}{y_{\max}} \tag{4.4}$$

where z_{max} and y_{max} are the maximum distance from the neutral axes as shown in Fig. 4.12

4.1.2.11 AXES module

This module references nodes in local co-ordinates which are applicable to the geometry of the ground structure under consideration. The format of the module is as shown in Fig. 4.13 and more explanation is given in the subsequent section.

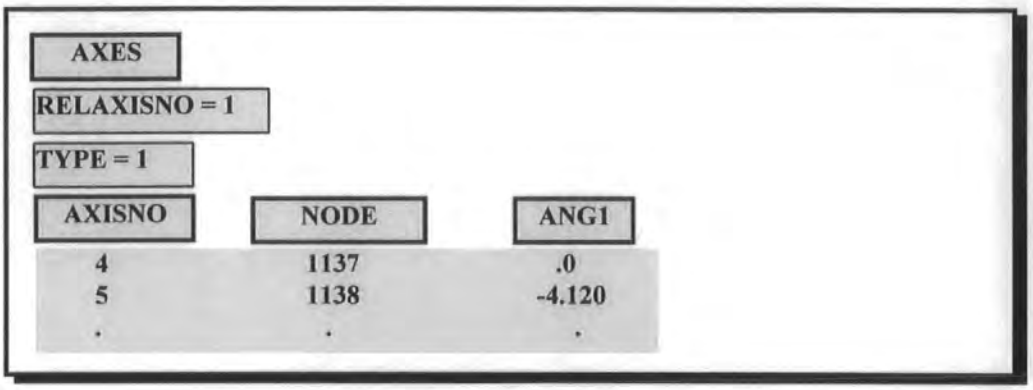

Fig. 4.13 Data format for AXES module

4.1.2.12 EXTERNAL FORCE module

This module requests the calculation of forces acting on specific nodes and in specific direction as a result of the application of prescribed loading conditions. The format of this module is as shown in Fig. 4.14.

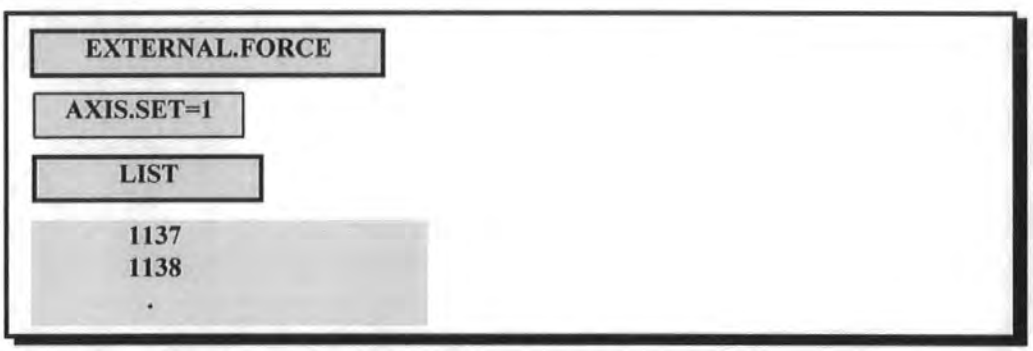

Fig 4.14 Data format for EXTERNAL FORCE module

4.1.2.13 LOCAL DIRECTIONS module

This module specifies an axis related to the element face that forms part of the model boundary, in order to input radial loads which have been calculated using EXTERNAL FORCE module. The format of this module is as shown in Fig. 4.15.

LOCAL.DIRECTIONS	
NODE.NUMBER	**LOCAL.AXIS**
1137	4
1138	5
.	.

Fig. 4.15 Data format for LOCAL DIRECTIONS module

Forces on the excavation boundary have to be defined in terms of a local direction for finding the radial component of forces on elements for reverse stress technique. Any number of axes sets may be defined by using the standard Cartesian type axis (axis type =1) as shown in Fig. 4.16.

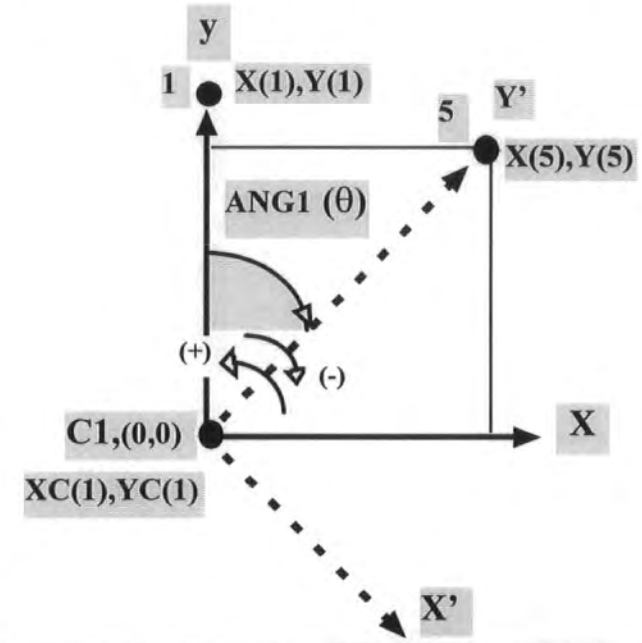

ANG1(θ)=DATAN2(X(5) - XC(1), Y(5) - YC(1) / DRAD

```
C Define local axis and directions
AXISNO   NODE     -ANG1
  4        C1        0          (Node1)
  .        .         .            .
  8        C1       -45         (Node5)
```

Fig. 4.16 Typical example of user defined axis set

The rotation is always clockwise when viewed along the axis from the origin. Any number of axes sets maybe defined by using axis types under the NODES module. It is not possible to define axes sets with numbers 1, 2 or 3 since these numbers are considered standard axes (type 1 : right handed Cartesian set, type 2 : right handed cylindrical polar set, type 3 : right handed spherical polar set) in PAFEC-FE.

These cannot be overwritten. Axes set 4 to any number can be defined by the user. AXISNO in the AXES module relates directly to AXIS NUMBER in the NODES module and to other modules. For a special user- defined axis set which may have a rotation (local direction, ANG1 (θ)) from the global origin, an entry for AXISNO must be started from '4' to any number as shown in Fig 4.16. For nodes on the excavation surface, it is necessary to define sets of axes using the LOCAL DIRECTIONS module. LOCAL AXIS in the LOCAL DIRECTIONS module refers to AXISNO in the AXES module and it is used to describe local directions of nodes on the excavation boundary.

4.1.3 Types of Element Used for the Analysis

The PAFEC-FE program provides a range of elements including one dimensional beam element, two-dimensional triangular and quadrilateral elements and three-dimensional brick elements. The element types used for the analysis were as follows;

i) Beam element (type 34000)
ii) Two-dimensional element (type 36210)
iii) Three-dimensional element (type 37110)

A uniform beam element (type 34000) having two nodes was used to construct the frame structure of the steel arch and anchorages. The beam element appears as a line connecting two nodal points as shown in Fig. 4.17. The properties of beam elements are provided in the BEAMS module as described in Section 4.1.2.10. The beam element is essentially one dimensional although it may be curved and it may be used to form a three-dimensional structure. Beam elements should only be

used where the part of the physical model is acting as a beam e.g. length to depth ratio greater than five. The mathematical formulation assumes that a linear direct strain variation exists over the depth or width of the beam. A more detailed explanation of beam element is given in Appendix F.

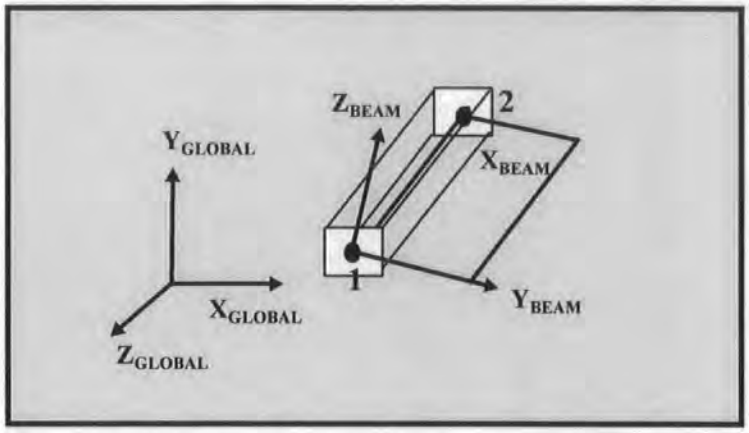

Fig. 4.17 Simple beam element (type 34000)

The particular element used to model the tunnel in a two-dimensional analysis is a quadrilateral PAFEC-FE (type 36210) element with eight nodes and two degree of freedom at each node, U_x and U_y as shown in Fig. 4.18. It is based on the isoparametric formulation and carries in-plane loads. It does not have central node therefore it is not 'serendipity' type element. The element has a constant thickness within which the stresses do not vary. Reasonable distortion from a square are permitted. If midside node numbers are omitted from the topology entry in the elements module the corresponding sides are taken as straight. The plane strain mode is used when it is reasonable to assume that there is no strain perpendicular to the plane. The stiffness and loading matrices are all calculated by transforming the curved shape to a square using the isoparametric method. All bending and twisting effects acting out of the plane of the element are ignored.

The output listing gives the principal stresses at each of the eight nodes plus a central point for isotropic elements. In the stress output listing (*file$.O09*) an asterisk (*) indicates central point of an element. When this type of element is used in the plane stress mode, which is the default option, the normal stress on the plane is printed as zero.

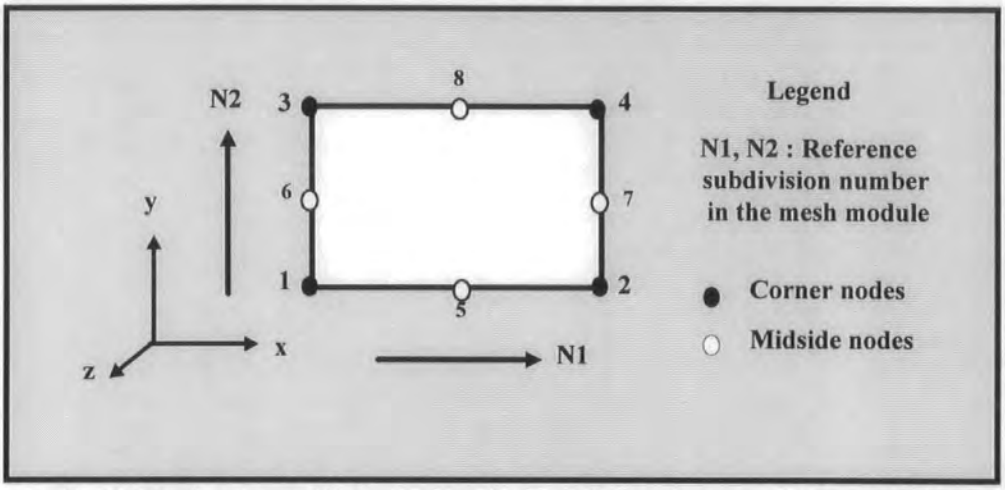

Fig. 4.18 Eight noded isoparametric quadrilateral element (type 36210)

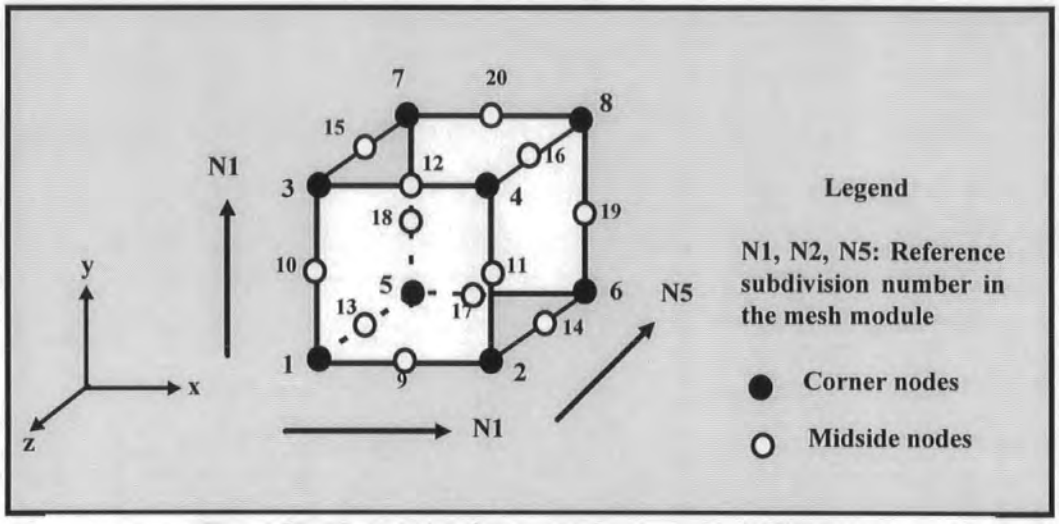

Fig. 4.19 20 noded brick type element (type 37110)

The element used to model the ground in a three-dimensional analysis is the brick shaped PAFEC-FE element (type 37110) having six faces, twelve edges and twenty nodes as shown in Fig. 4.19. There are three degrees of freedom at each node along the orthogonal axes, U_x, U_y and U_z . This element is based on the isoparametric principle. Reasonable distortion from the basic cubical shape is permitted. If the midside node numbers are omitted from the 'TOPOLGY' entry in the 'ELEMENT' module then corresponding sides are taken as straight. Three-dimensional elements are expensive to use and should only be employed when the stresses vary in three-dimensions. For isoparametric elements the principle stresses are given at each of the nodes and also at the centres of the six faces and the centre of the element.

4.1.4 Stress and Displacement Outputs

The stresses are created in phase 9 (*file$.O09*) of the PAFEC-FE output file. The basic information written to the file consists of two parts for each load case: the stresses on each element and the averaged nodal stresses. Information for every element is written to the file, with the exception of the beam elements. If they occur within a particular job, then a beam stress file (*file$.*SB) is created, which contains shear forces, bending moments and stresses for each user specified point along the beam, and for each load case. The averaged and unaveraged directional stresses can be written to requested file *file$.SP* using ORDER FOR PRINTED OUTPUT module. In PAFEC-FE the sign convention for tensor components of stress is as follows. The compressive stresses are negative whereas tensile are positive. The nodal displacements are calculated in phase 7 and written into the file *file$.O07*. A more detailed explanation of these output files is given in Chapter 6 and Appendix B.

4.2 Use of PAFEC-FE For Excavation Simulation

4.2.1 Tunnel Models

All transportation tunnels studied by the author were in the form of an inverted horseshoe. Because of their shape, no closed form analytical solution was possible and hence the finite element method was adopted for the solution.

This study used PAFEC-FE to simulate tunnel structure, excavation, supports, ground movements, and their effect on adjacent structures. The tunnel geometry chosen for model has a clear width of 13.0 m and an overburden height of rock varying from one to 15 metres in depth. A variety of supports inside the tunnel were introduced into the models which included an outer shotcrete lining, an inner final lining of varying thickness, steel arches and anchorages of varying angle as described in Chapter 2.

The tunnels were modelled at various stages of excavation and with such support provided at those stages so that the unsupported displacements and stresses

could be compared with measurements made in situ. The stresses and displacements generated in the supports were also calculated, to enable the probability of damage or failure of the support structure to be assessed. The finite element analysis was initially undertaken for two-dimensional models, using plane strain analysis. Subsequently three-dimensional analyses were undertaken.

4.2.2 Position of Model Boundary

Finite element models must have finite boundaries at which known conditions are applied. In the case of modelling tunnels, an artificial finite boundary must be chosen. The distance that this boundary should be away from an opening has been discussed fairly widely. Wittke (1990) states that five times the opening diameter is sufficient for reasonable accuracy when modelling a tunnel. Kulhawy (1974) presents a number of graphs of the displacements along, and stresses near the face of a circular opening calculated from theory, and these are compared with results from finite element analyses with the boundary at varying distances. Finite element analysis results from several solutions showed that the boundary can be located six radii away from the centre of the opening.

4.2.3 Gravity Loading

In finite element analysis, the geometry of a structure and the load imposed on the system are very important. In general any number of load cases can be supplied with particular analysis. For all the models in this thesis the geostatic stresses were introduced by using gravity loading and the simulation of the excavation process was implemented by employing the gravity difference method and stress reversal technique. Therefore two consecutive PAFEC-FE finite element analyses were necessary for both of these methods. During the first analysis the conditions before the excavation were simulated.

In the second analysis the excavation was simulated by eliminating the appropriate (air) elements within the tunnel boundary. In the finite element method

excavation means the removal of elements and the creation of new surfaces. One of the problems that had to be overcome is that PAFEC-FE changes midside node numbers according to the new pafblock positions after removing pafblocks. So it is difficult to control the node number and position of nodes around the excavation surface for the application of the gravity difference method and stress reversal technique. The geostatic stress can be simulated in finite element analysis by applying gravity loading to the unstressed ground model. This was achieved by using the GRAVITY module to increase the stress according to the depth below the loaded surface as shown in Fig. 4.20. In some structure such as tunnels, dams and earthworks the loading due to gravity forms an important and sometimes the only load. GRAVITY module describes the pressures applied to the nodes. Gravity is normally imposed on the geological formations surrounding a ground structure.

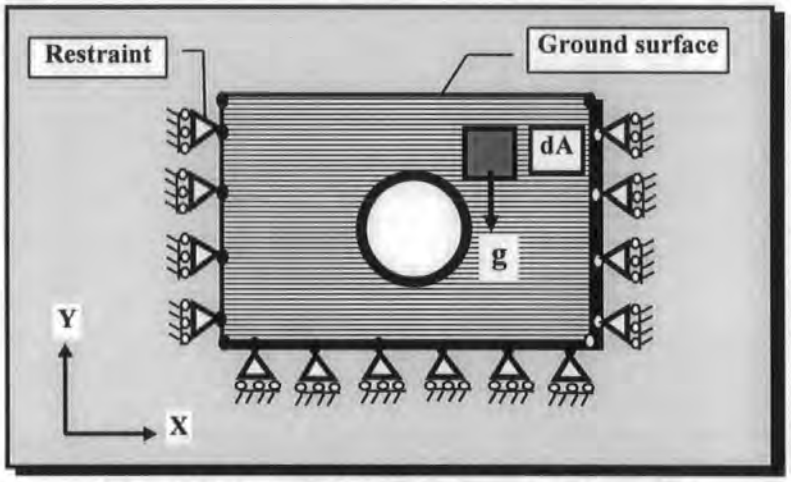

Fig. 4.20 Gravity loading case of 2-D model

It is often convenient to automatically determine equivalent nodal loads. PAFEC-FE does this by using the value of density that is input with the element data and assuming that gravity acts in any direction chosen by the user. The default direction for gravity is the negative global y-direction (YGVALUE). The value of acceleration due to gravity programmed in to PAFEC-FE is 9.81 m/s^2 The GRAVITY module is used to increment the stress according to the depth of the model below the load surface. The horizontal geostatic stress may be introduced by either the application of constant pressure to the side boundaries of the mesh, using one of the pressure modules. The pressure is set equal to the value of the

pressure applied to the top surface of the model mesh and multiplied by the appropriate K value (K=ν/(1-ν)) or by using RESTRAINTS to ensure that the side boundaries of the mesh are free to move only in the vertical direction, thus introducing horizontal stresses as a result of the lateral confinement. In this case k_0 is a function of Poisson's ratio of geological materials involved and such is automatically determined by the PAFEC-FE. At points located above and below an underground opening, the actual horizontal stress component is expected to vary linearly with depth below the surface. However in the case of tunnels where opening size is often relatively small in comparison with depth (tunnel depth), it is acceptable to assume that the horizontal geostatic stress component may be modelled as a constant pressure loading (Woodford et. al., 1992).

4.2.4 General Criteria for Mesh Generation

For greater accuracy a fine mesh is required in areas where stresses are varying more rapidly i.e. around the boundary of the excavation. For this purpose, a FORTRAN pre-processing program was written to produce a mesh according to the criteria given in Chapter 5.

4.2.5 Chosen Excavation Methods Using PAFEC-FE

4.2.5.1 Gravity Difference Method

In particular the gravity difference method needs subtraction of stresses and displacements from excavated and unexcavated models using data post processing programs 'gdstress' and 'gddisp' as shown in Figs. 4.21 to 4.24 and full listings of these programs are given in Appendix D. For that reason node numbers and their position must be same for unexcavated and excavated runs. Otherwise the wrong displacement and stress values are subtracted from each other. Accordingly, excavation simulation has been undertaken without removing elements or pafblocks inside the tunnel but instead by using air material properties for those elements.

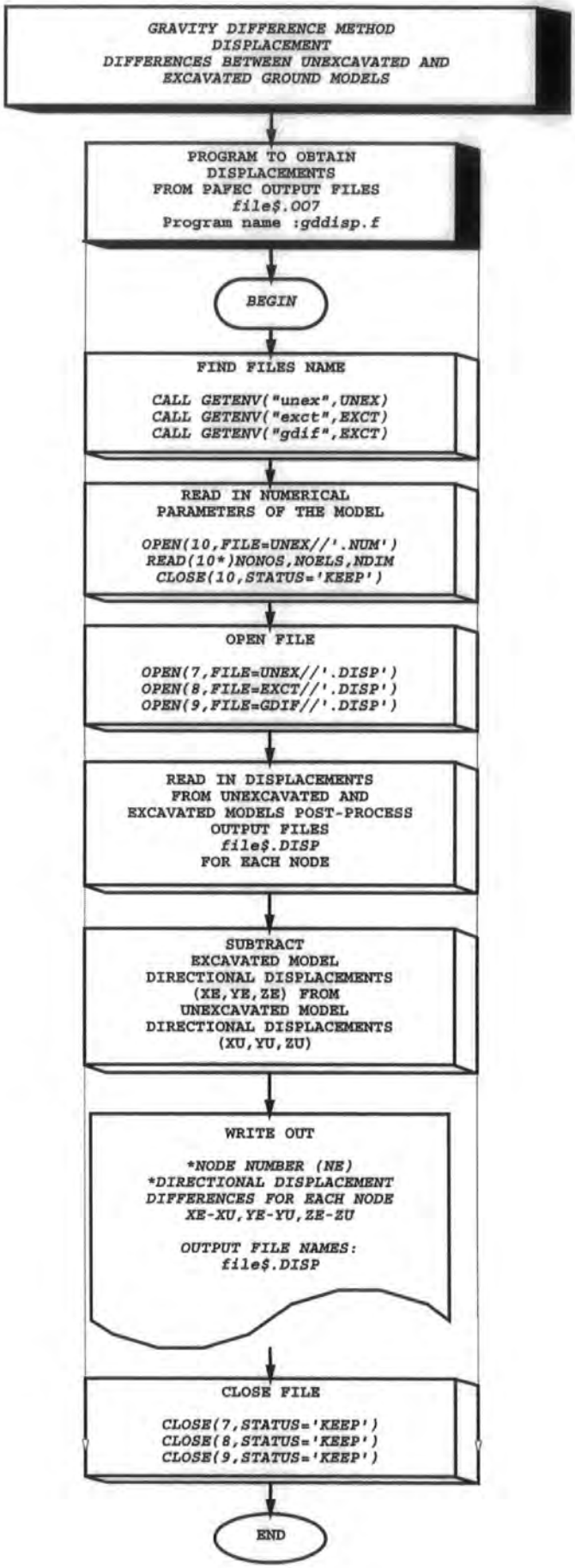

Fig. 4.21 Processing of displacement results for gravity difference method

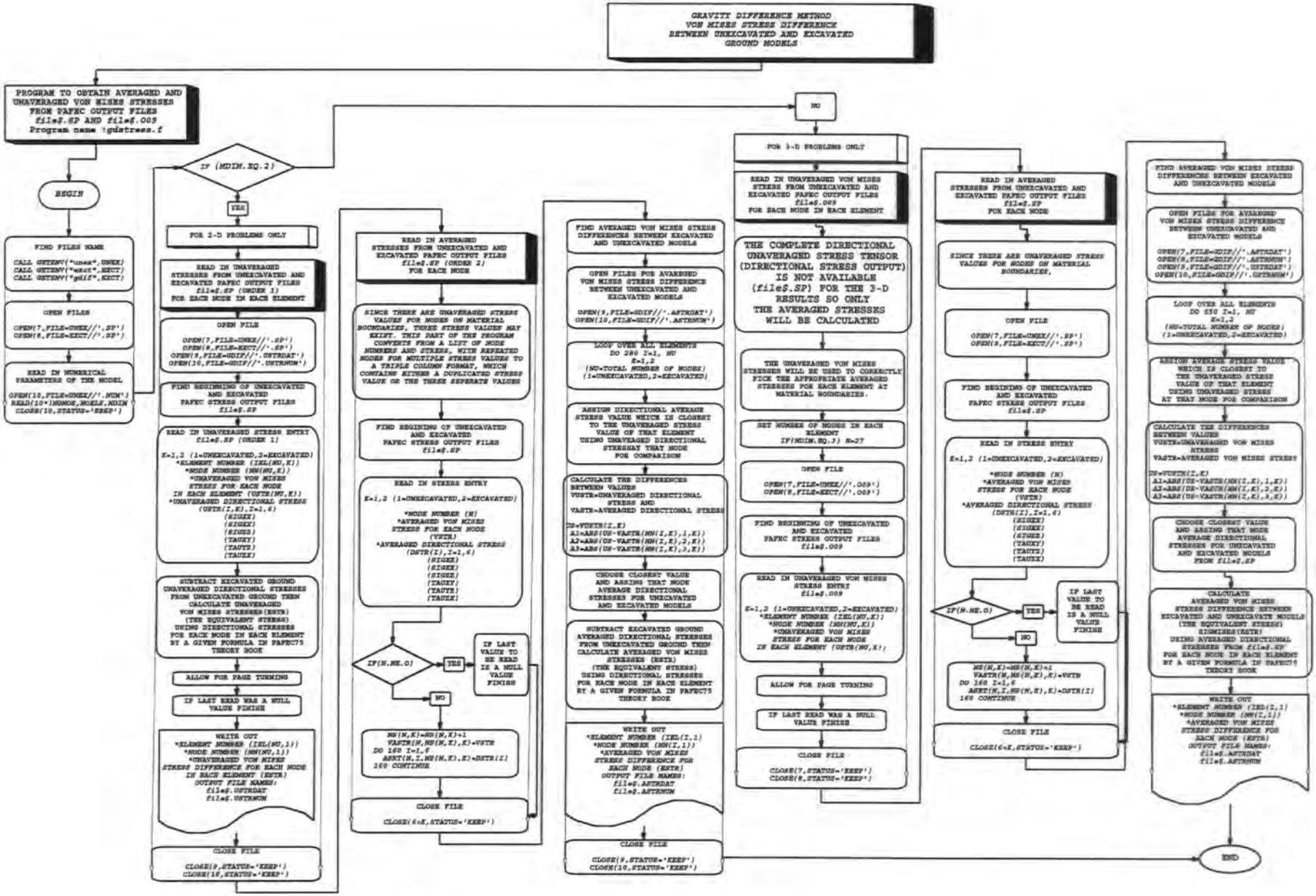

Fig. 4.22 Processing of stress results for gravity difference method

```
************************************************************************
*    PROGRAM TO OBTAIN Unaveraged & Averaged Stresses
*           PAFEC OUTPUT FILES from .SP files   File name: gdstress.f
************************************************************************


    PARAMETER (MXNOS1 = 80 000)
    PARAMETER (MXELS  = 25 00)
    PARAMETER (MXEN   = 20*MXELS )


    CHARACTER*6 UNEX, EXCT, GDIF, TEST
    CHARACTER*1 CHRU, CHAR1, ELNO*12
    INTEGER IEL(MXEN,2), NN(MXEN,2), NONO(3), NS(MXEN,2)
    REAL  VUSTR(MXEN,2)
    REAL  USTR(6,3)
    REAL  ASTR(MXEN,6,3,2), VASTR(MXEN,3,2), DSTR(6)


C Find files name

    CALL GETENV ("unex",UNEX)
    CALL GETENV ("exct",EXCT)
    CALL GETENV ("gdif",GDIF)

    OPEN(7,FILE=UNEX//'.SP')
    OPEN(8,FILE=EXCT//'.SP')

    OPEN(10,FILE=UNEX//'.NUM')
    READ(10,*)NONOS,NOELS,NDIM
    CLOSE(10,STATUS='KEEP')


C For 2-D Problems only

    IF (NDIM.EQ.2) THEN
*
      OPEN(7,FILE=UNEX//'.SP')
      OPEN(8,FILE=EXCT//'.SP')
      OPEN(9,FILE=GDIF//'.USTRDAT')
      OPEN(10,FILE=GDIF//'.USTRNUM')
*
C
```

Continued on next page

Continued from previous page

```
C=======================================================================
C Read in Directional Stresses for each node in each element
C=======================================================================
C
C Find Beginning of Tables

      NU = 1

      DO 20 K=1,2
 10      READ(6+K,101)TEST
         IF (TEST.NE.'  ELEM') GO TO 10
        READ(6+K,101)TEST
        READ(6+K,101)TEST
 20    CONTINUE
C Read in Stress Entry
 30     DO 60 K=1,2
 40      READ(6+K,103,ERR=50)
     *   CHRU,IEL(NU,K),NN(NU,K),VUSTR(NU,K),(USTR(I,K),I=1,6)
 50      CONTINUE
         IF (CHRU.EQ.'1') THEN
          DO 55 I=1,7
 55          READ(6+K,101)CHAR1
         ENDIF
         IF (CHRU.EQ.'1') GO TO 40
         IF (IEL(NU,K).EQ.0)   GO TO 100
 60     CONTINUE

        IF (NN(NU,K) .NE. 0) THEN
         DO 70 I=1,6
 70         USTR(I,3) = USTR(I,2) - USTR(I,1)
         ESTR = SQRT ( ( (USTR(1,3)-USTR(2,3))**2 +
     *                 (USTR(2,3)-USTR(3,3))**2 +
     *                 (USTR(3,3)-USTR(1,3))**2 +
     *       6.0 * (USTR(4,3)**2+USTR(5,3)**2+USTR(6,3)**2) )
     *                                / 2.0 )
         WRITE(9,104)IEL(NU,1),NN(NU,1),ESTR
         NU = NU+1
        ENDIF
      GO TO 30
 100   NU=NU-1
      WRITE(6,*)'Unaverage Stresses: ',NU
      WRITE(9,*)'*'
      WRITE(10,*)NU
      CLOSE(9,STATUS='KEEP')
      CLOSE(10,STATUS='KEEP')
 101   FORMAT(A6)
 103   FORMAT(A1,2I7,E14.4,6E13.4)
 104   FORMAT(3X,2I7,E14.5)
=======================================================================
                 MAJORITY OF CODES OMITTED
=======================================================================
```

Fig. 4.23 Program to obtain stresses from PAFEC output file for gravity difference method

```
************************************************************************
*    PROGRAM TO OBTAIN DISPLACEMENTS FROM
*          PAFEC OUTPUT FILES from .O07 files    File name: gddisp.f
************************************************************************

    CHARACTER*6 UNEX, EXCT, GDIF

C Find files name

    CALL GETENV ("unex",UNEX)
    CALL GETENV ("exct",EXCT)
    CALL GETENV ("gdif",GDIF)

    OPEN(10,FILE=UNEX//'.NUM')
    READ(10,*)NONOS,NOELS,NDIM
    CLOSE(10,STATUS='KEEP')
*
    OPEN(7,FILE=UNEX//'.DISP')
    OPEN(8,FILE=EXCT//'.DISP')
    OPEN(9,FILE=GDIF//'.DISP')
*
    DO 200 I=1,NONOS

      READ(7,*)NU,XU,YU,ZU
      READ(8,*)NE,XE,YE,ZE
      WRITE(9,*)NE,XE-XU,YE-YU,ZE-ZU

200  CONTINUE

    WRITE(6,*)'Gravity Difference Dispacemants ',NONOS
    CLOSE(7,STATUS='KEEP')
    CLOSE(8,STATUS='KEEP')
    CLOSE(9,STATUS='KEEP')

    STOP
    END
```

Fig. 4.24 Program to obtain displacements form PAFEC output file for gravity difference method

4.2.5.2 Stress Reversal Technique

During the first analysis for excavated ground using the stress reversal technique the stresses that would exist along the proposed excavation surface, as a result of the geostatic loading applied by the gravity module, were evaluated. These were calculated in terms of the equivalent forces at each element node. In the second analysis on excavated ground the forces obtained from the first analysis were then applied to the excavation surface after their sign had been reversed. PAFEC-FE then calculates the resulting stresses and displacements on the excavation boundary. The implementation of this is described in more detail below and full listings of programs are given in Appendix D.

The forces acting on individual elements, the numbers of which are given in the LIST module, are calculated and printed by using the EXTERNAL FORCES module. These forces on the projected excavation will be caused by the gravity loading condition for the unexcavated ground. The force distribution on elements depends on the displacement shape functions used in formulating the element stiffness matrices. The forces are in fact calculated by multiplying the element stiffness matrix by the appropriate vector of element nodal displacements.

The axis set in the EXTERNAL FORCE module determines axis types for the forces which are to be resolved when printed. The axis set entry '1' is the default value in the reverse stress technique FORTRAN program called 'revforce2' as shown in Fig. 4.28. A flow diagram for this program is shown in Fig. 4.25. If axis set is equal to zero then the forces at nodes are given along element axes. If the axis set entry is the default then forces at the nodes having local directions will be shown resolved in those directions. The list of elements on the projected excavation boundary which is used for the extraction of the external forces given by this program. The numbering system for elements selected for the application of external forces has to be changed since there is an extra ring (shotcrete lining, steel arch and final lining) of elements in the model for the particular NATM construction considered in this work. External forces for elements on the projected excavation boundary are calculated.

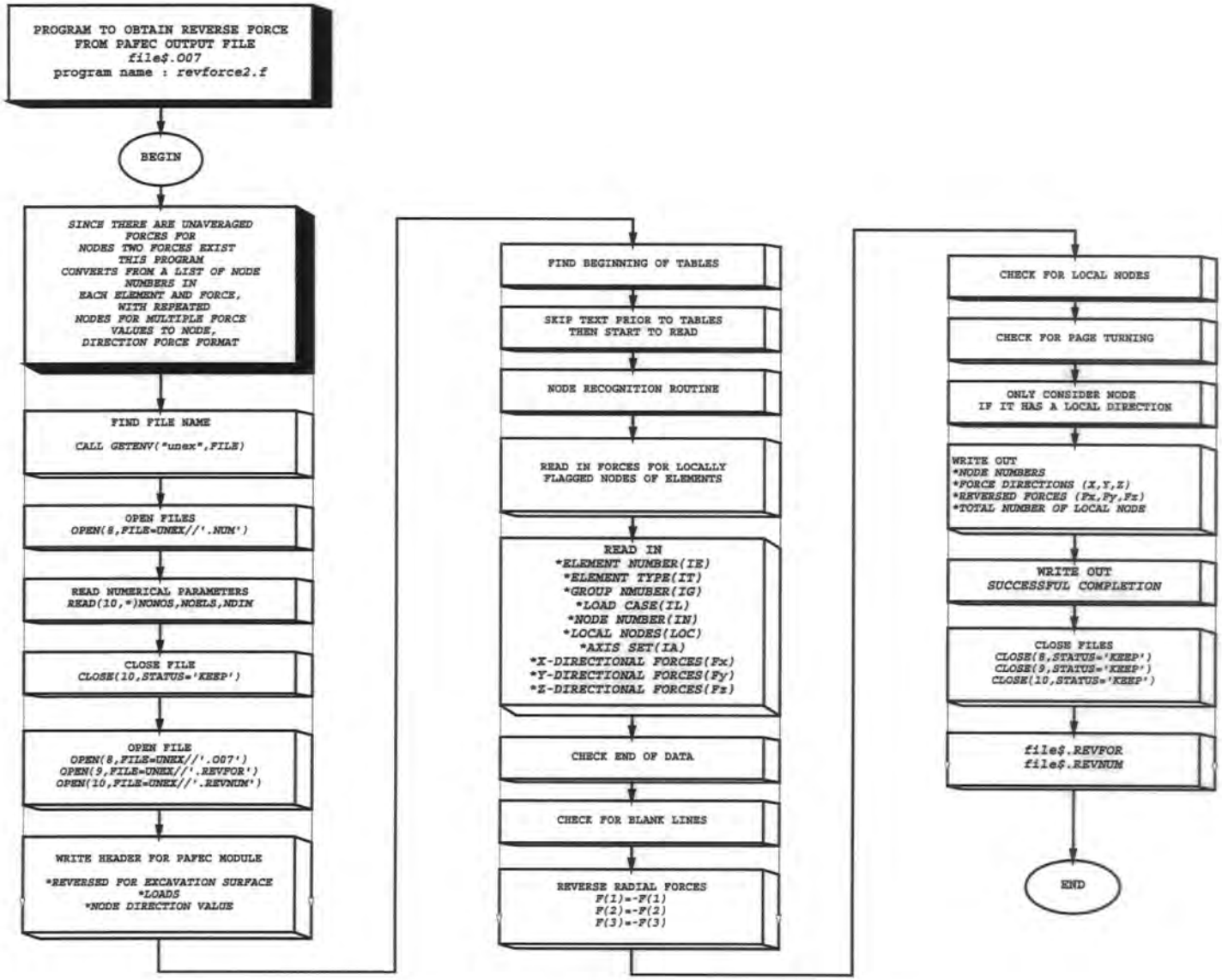

Fig. 4.25 Processing of reversed forces for excavation surface

Initially an unexcavated phase has to be run with the GRAVITY LOAD and EXTERNAL FORCE modules before running the model for excavated ground using reversed forces. Forces on elements appear in the PAFEC-FE run phase 7. An 'E' in the axis set column in the PAFEC-FE 'O07' file indicates that the forces on each element are given in local element axis set as shown in Fig 4.26. Element axis is formed by an X-axis positive from the first node in the topology to second. The Y-axis passes through the first node normal to the X-axis in the plane of the first three nodes and is positive towards the third as shown in the figure.

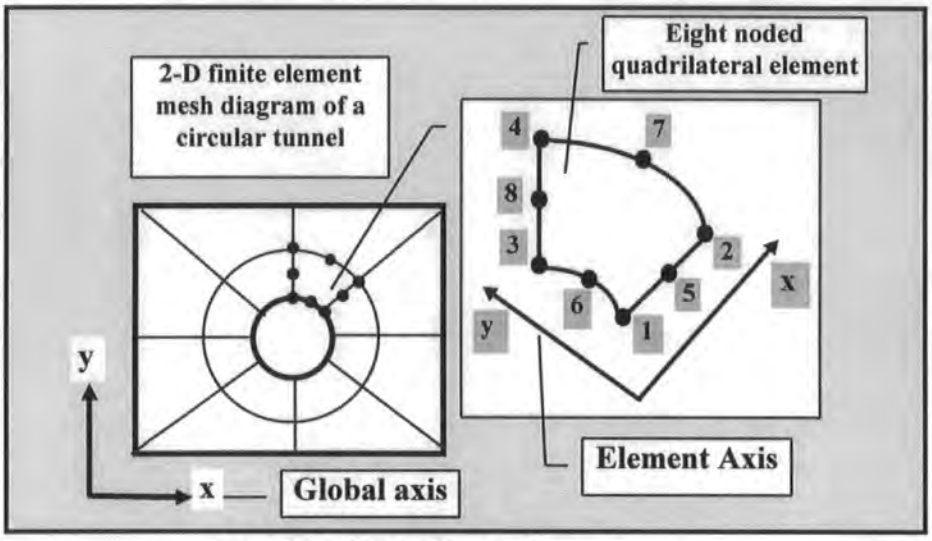

Fig. 4.26 Global and element axes

4.2.5.3 Local Axis and Directions for Reversed Forces

Program 'revforce2' extracts a list of node numbers in each element and forces on the projected excavation surface and reverses forces, placing them in files adopting a format suitable for use by an excavated ground input file with reverse stresses as described above. The requirement for the results of unexcavated ground stresses with EXTERNAL FORCE and LOCAL DIRECTION module to form the input for the reverse stress calculation using excavated ground and a lack of facilities for post processing of results dictated that subroutine 'exloc' needed to be written as shown in Fig 4.27 and full listing of this program is given in Appendix C. In this way, repeated use could be made of the stress reversal technique without time-consuming and inaccurate manual retrieval of data.

```
C ==========================================================
C SUBROUTINE EXCLOC WRITES LOCAL DIRECTIONS FOR
C EXCAVATION SURFACE
C ==========================================================
      SUBROUTINE EXCLOC

      IMPLICIT DOUBLE PRECISION  (A-H,O-Z)
      PARAMETER(NNODES=5000)
      COMMON / CNODES / X(NNODES), Y(NNODES)
      COMMON / CFLAG  / MSYM, MDIM
      COMMON / CKEYPR /K(0:8),NNS,NBS,NPOT,NPLR,NNODE,NPAF
      COMMON / COUNT / KPSH(8), NPSIDE, NCOL, NROW
      COMMON / CCENPR / XC(10), YC(10)
      COMMON / CZNOD / Z(5), NDEPTH

      DRAD=DACOS(0D0)/90D0
      WRITE(8,*)'C'
      WRITE(8,*)'C Define local axis and directions'
      WRITE(8,*)'C'
      WRITE(8,*)'AXES'
      WRITE(8,*)'RELAXISNO = 1'
      WRITE(8,*)'TYPE = 1'
      WRITE(8,*)'AXISNO   NODE   ANG1'
      IF (MSYM.EQ.0) N = NNS
      IF (MSYM.EQ.1) N = (NNS/2)+1
      DO 15 L=1,mdim-1
        DO 10 I=1,N
          IF (I .LE.(2*KPSH(2) + 1)) THEN
            ICEN=1
```

MAJORITY OF CODES OMITTED

```
IO = NNODE*(NDEPTH+1)+ICEN
          IP = I + 2*NNS
          ANG = DATAN2(X(IP)-XC(ICEN),Y(IP)-YC(ICEN)) / DRAD
          IF(I.EQ.((NNS/2)+1)) ANG=180.0
          WRITE(8,*) 3+I+(L-1)*NNS, IO + (L-1)*10,  -ANG
10      CONTINUE
15    CONTINUE
      WRITE(8,*)'C'
      WRITE(8,*)'C'
      WRITE(8,*)'LOCAL.DIRECTIONS'
      WRITE(8,*)'NODE.NUMBER  LOCAL.AXIS '
      DO 25 L=1,mdim-1
        DO 20 I=1,N
          INODE = I+2*NNS+(L-1)*NNODE
          IAX   = 3+I+(L-1)*NNS
          WRITE(8,*) INODE,  IAX
20      CONTINUE
```

MAJORITY OF CODES OMITTED

Fig. 4.27 Subroutine 'exloc' for local direction of nodes on the excavation surface

```
************************************************************************
*    PROGRAM TO OBTAIN Reverse Forces          *
*    PAFEC OUTPUT FILES from .O07 files   File name: revforce2.f  *
************************************************************************

      PARAMETER (MXNOS1 = 80 000)
      CHARACTER*6 TEST,CHAR*2,CHAR1*2,LOC*1, UNEX
      REAL F(3)
C
C=======================================================================
C Read in Forces for locally flagged nodes of elements
C=======================================================================
C
C Since there are unaveraged foces for nodes two forces exist.
C This program converts from a list of node numbers in each element
C  and force, with repeated nodes for multiple
C  force values to node, direction force format,
C
C
C Find files name

      CALL GETENV ("unex",UNEX)

      OPEN(10,FILE=UNEX//'.NUM')
      READ(10,*)NONOS,NOELS,NDIM
      CLOSE(10,STATUS='KEEP')

      OPEN(8,FILE=UNEX//'.O07')
      OPEN(9,FILE=UNEX//'.REVFOR')
      OPEN(10,FILE=UNEX//'.REVNUM')

C Write Header for PAFEC Module

      WRITE(9,*)'C'
      WRITE(9,*)'C Reversed Forces for Excavation Surface'
      WRITE(9,*)'C'
      WRITE(9,*)'LOADS'
      WRITE(9,*)'NODE    DIRECTION    VALUE'

C Find Beginning of Tables

 10  READ(8,901)TEST
     IF (TEST.NE.' F O R') GO TO 10

C Skip Text prior to Tables

     DO 20 I=1,24
 20    READ(8,901)TEST

     NONOS=0
```

Continued on next page

Continued from previous page

```
*
*    *** NODE RECOGNITION ROUTINE ***
*
 40    READ(8,903,ERR=45)
   *    CHAR,IE,IT,IG,IL,IN,LOC,IA,(F(I),I=1,NDIM)
      write(6,903)CHAR,IE,IT,IG,IL,IN,LOC,(F(I),I=1,3)
 45    CONTINUE

C Check for end of Data
      IF (CHAR.EQ.' C') GO TO 100

C Check for Blank Lines
      IF (IN.EQ.0) GO TO 40

C Reverse Radial Force
      F(2)=-F(2)
      F(1)=-F(1)
      F(3)=-F(3)
C Check for local nodes
      IF (LOC.EQ.'L') L=1
      IF (LOC.NE.'L') L=0

C Check for Page Turning
      IF (CHAR.EQ.'1 ') THEN
        READ(8,901)CHAR1
        READ(8,901)CHAR1
        write(6,901)'end test',CHAR1
C Check for end of Data
        IF (CHAR1.EQ.' C') GO TO 100
        READ(8,901)CHAR1
        READ(8,901)CHAR1
      ENDIF
      IF (CHAR.EQ.'1') GO TO 40

C Only Consider node if it has a local direction
      IF (L.EQ.1) THEN
        NONOS=NONOS+1
        DO 110 I=1,NDIM
110         WRITE(9,904) IN, I, F(I)
      ENDIF
    GO TO 40
100  WRITE(6,*)'Successful Completion',NONOS
    WRITE(10,*)NONOS
    CLOSE(8,STATUS='KEEP')
    CLOSE(9,STATUS='KEEP')
    CLOSE(10,STATUS='KEEP')
    STOP
901  FORMAT(A6)
903  FORMAT(A2,I5,I6,I7,2I6,A1,I4,2X,3F11.3)
904  FORMAT(3X,2I7,F14.3)
    END
```

Fig. 4.28 Program to obtain forces on the excavation surface from PAFEC output file

CHAPTER 5

PRE-PROCESSING PROGRAM

5.1 Introduction

An operating system has two main aims, to manage efficiently the computer's hardware resources and to make it easy to use. The improvement in computer systems has resulted in the development of 'multi-tasking' and 'multi-user' system. Multi-tasking is the capability for handling more than one program at once and tasks are divided into sections and completed at high speed, therefore appearing to occur simultaneously. Multi-user systems employ the same basic principle as multi-tasking, enabling more than one person to use the machine at once.

5.1.1 The UNIX Operating System

UNIX is a multi-tasking, multi-user operating system, which with modification can be used on most types of computer and with thousands of programs. UNIX is composed of four basic interrelating parts, the kernel, the file system, the shell and the tools. The kernel is the nucleus of the operating system, controlling the computer hardware and translating UNIX commands into hardware commands. The file system stores information, with UNIX treating all files equally, enabling easy access by the user on UNIX. The shell is an interface program between the user and kernel. The tools are all programs that can be run by the shell to perform various tasks.

The following characteristics result in a very convenient system for programmers and users. UNIX is written in C language, enabling any programmer to understand, modify and integrate the operating system. It also supports other languages, including FORTRAN, BASIC and PASCAL. It is a true multi-tasking, multi-user system allowing multiple users each to have several tasks executing at once. Additionally UNIX 'hides' the machine architecture from the user, making it

easier to write programs that run on different hardware implementations. UNIX employs simple very powerful user interfaces, which can be readily customised to user's requirements. It provides a large number of basic programs (primitives), which can be combined to simplify the task of writing larger and more complex applications.

The UNIX file system is hierarchical, and the structure is simple and efficient, permitting easy maintenance and ready use by application programs. UNIX treats all disk drivers, terminals, printers and other attached frameworks as standard devices, allowing the use of a consistent interface.

5.1.2 The Durham Computer Network

Durham University computer centre manages several major systems based on UNIX, SUN and MS-DOS. There are four time-sharing UNIX computers available for general use in Durham known as vega, deneb, altair, and pehang. A large amount of software such as PAFEC-FE and UNIRAS is held on these machines. PCs are linked via a network, known as the Novell network. A large number of software including word-processing, spreadsheets, databases , Microsoft Windows-based packages are available on this network.

5.1.3 Supplementary Program Running

To enable rapid and error-free mesh generation for the tunnel finite element models in PAFEC-FE and to process the output to allow for excavation simulation, pre- and post-processing programs respectively were written in FORTRAN. These supplementary source programs were compiled on UNIX using the FORTRAN 77 compiler to provide object programs.

After compilation, the object program is usually stored on disk and may be executed immediately by a command. When the program is to be executed, by default the object code is stored into an executable file named 'a.out'. To write object code to some file other than 'a.out', the '-o' compiler option is used to make a file script as shown in Appendices A and C. The program then takes control of

the computer which performs the tasks specified by the programmer. This involves reading input data, decision-making and producing output using this data in calculations.

The shell is a computer program that interprets requests to run programs and is the most important program for most UNIX users. The UNIX shell is not typical of command interpreters. It lets the user run commands in the usual way because it is a programming language. The other features, such as shell files are really provided by the kernel. The shell gives a natural syntax for creating tasks or files and this increases the capabilities of the system. The shell sets up pipes which are connections to the kernel which can move the data through them.

Several shell programs have been written by the author to perform various tasks, but other shell programs with several names already exist within the system. For example the shell program 'make' written by the author reads a specification of how the components of a program depend on each other and how to run them in a complicated order. 'make' also understands the multi-step processes. Tasks can be put into a 'make' specification without spelling out the individual steps.

5.2 Pre-Processing Program

The program for pre-processing the input data for the tunnel and ground parameters consists of six main subroutines as shown in Figs. 5.1 and 5.2. The tunnel data is in the form of the dimensions of the tunnel, heights of the rock layers, details of the tunnel support system and shotcrete linings. The pre-processing program transforms this information into a finite element mesh with varying dimensions and material properties in a format suitable for use by PAFEC-FE.

The program itself is versatile and enables different tunnel models and meshes to be produced with minimum error and time. Appendix C contains a full list of pre-processing programs that have been written, their uses and filenames.

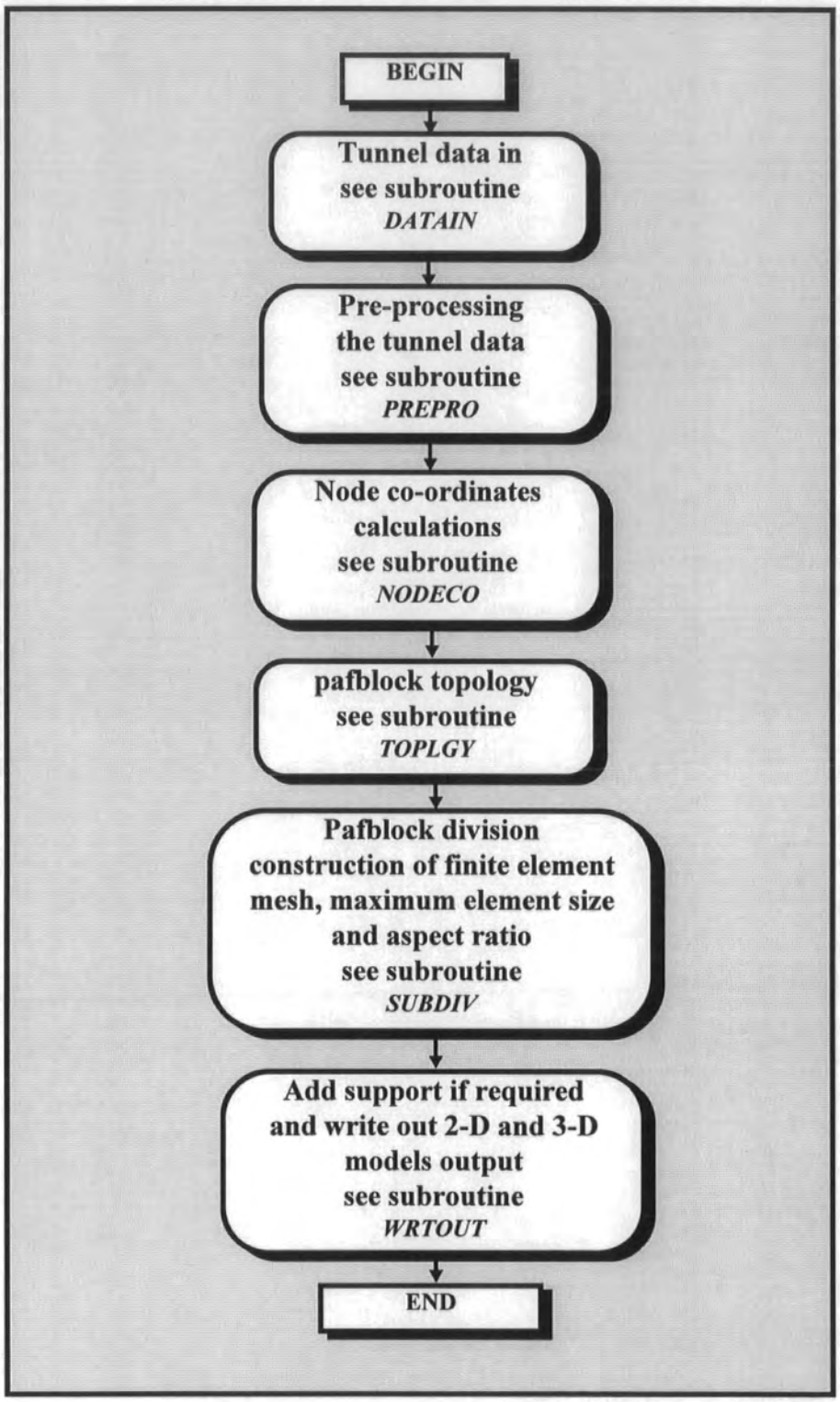

Fig. 5.1 Main flow diagram for pre-processing of program

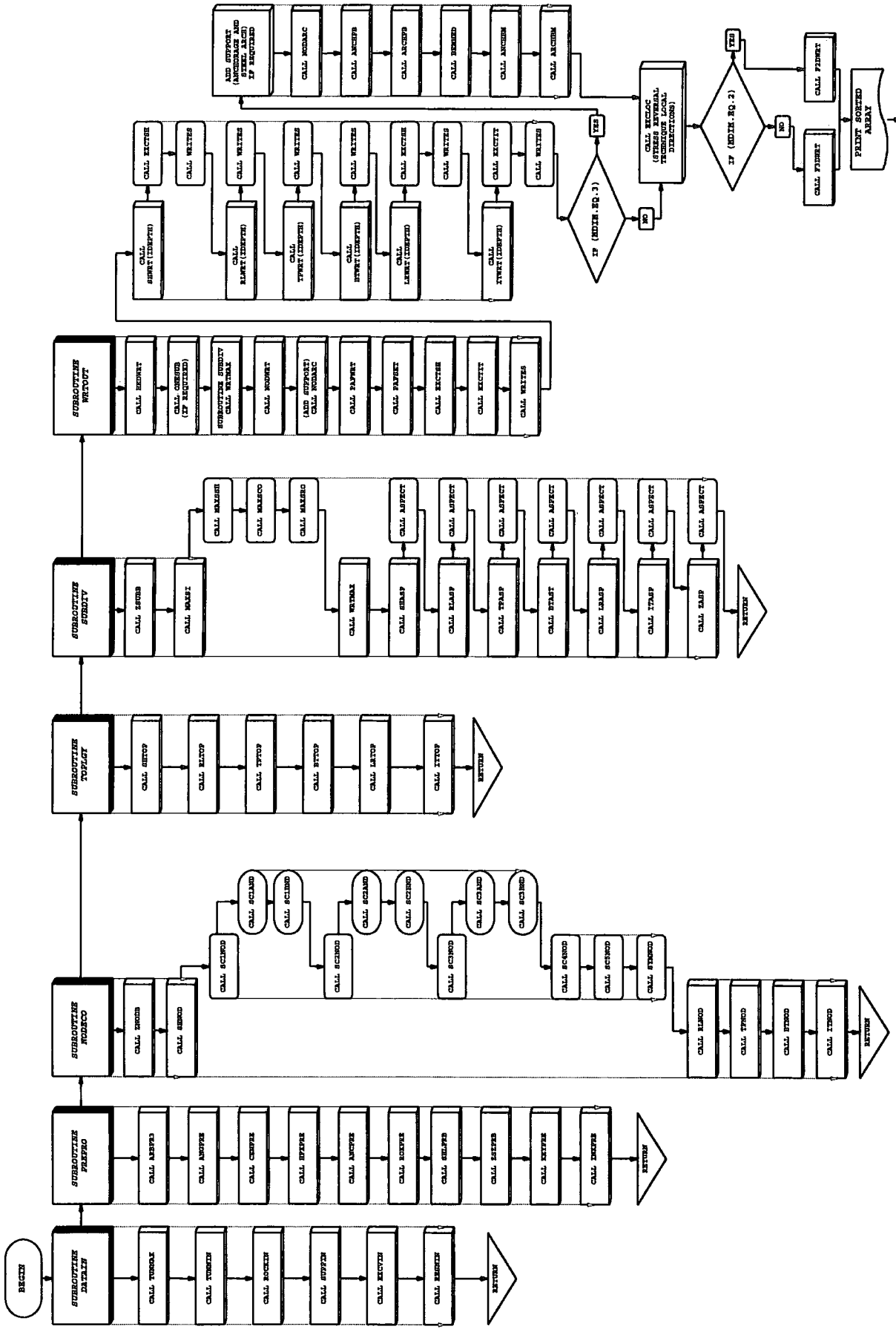

Fig. 5.2 Detailed flow diagram for pre-processing program

5.2.1 Strategy for Simulation

In order to deal with the simulation of the excavation by the NATM method and the provision of a variety of support systems, it was necessary to produce both two-dimensional and three-dimensional finite element models of the tunnel and ground. This was achieved by the versatile feature of the pre-processing program.

In the case of the three-dimensional finite element meshes, it was necessary to reduce the problem to a small region. This was achieved by making use of the periodicity of the support structure, the period being determined by the repetition of the steel arches and anchorages. A periodic structure that is symmetrical can be modelled by taking a natural boundary condition at the planes of symmetry, hence reducing the problem to one half of the period.

The versatility inherent in the program structure enabled the actual Turkish transportation tunnels and ground conditions to be used as a practical example of the modelling techniques. Potentially the techniques described in this thesis could be used to investigate the integrity of numerous alternative ground conditions and tunnel support designs and their consequent costs.

In order to successfully model tunnel behaviour it was necessary to specify a structure and tunnel supports (shotcrete outer lining, concrete final lining, anchorages and steel arch) that could be used to establish the input data. Ideally the structure should be simple, brief and designed to produce self consistent output to aid accuracy in measurement and modelling. Examples of a two-dimensional tunnel with an outer lining (shotcrete) and a three-dimensional periodic tunnel having anchorages, steel arches, shotcrete lining are shown respectively in Figs. 5.3 and 5.4. Examples of the corresponding input data files are shown in Table 5.1.

Details of the model conditions and tunnel geometry would form the basis for simulating the actual tunnelling projects in Turkey by taking different cross sections along the lengths of the tunnels. Appendix B contains a full list of two and three-dimensional input data files.

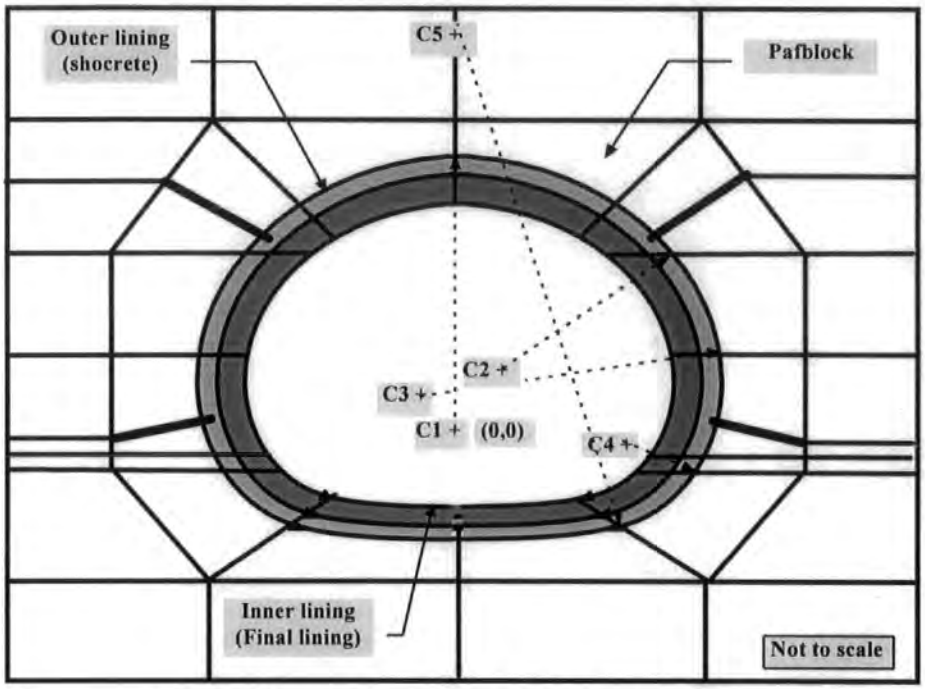

Fig. 5.3 Numerical modelling of the transportation tunnel

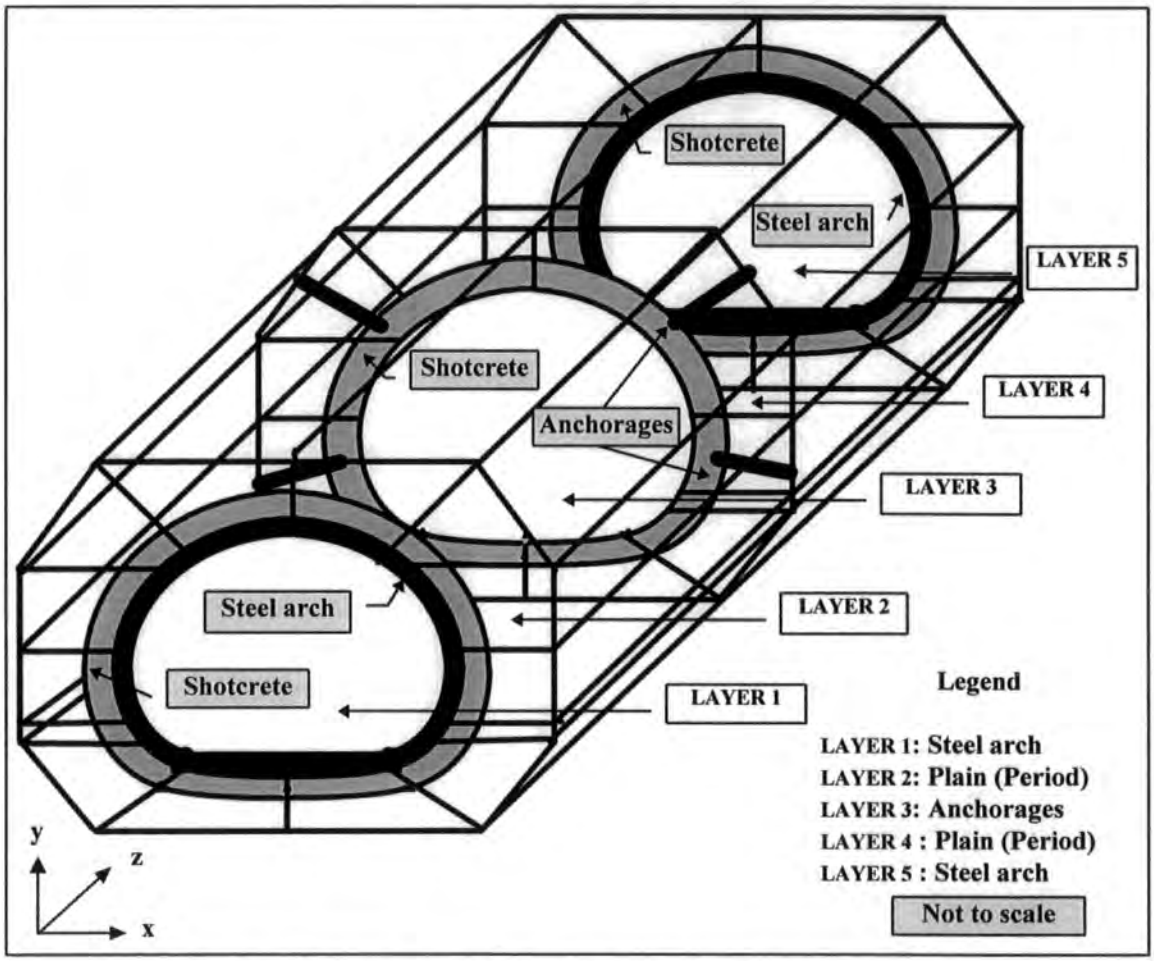

Fig. 5.4 Three-dimensional model and stage of construction

THREE-DIMENSIONAL TUNNEL MODEL - INPUT LIST

TWO-DIMENSIONAL TUNNEL MODEL - INPUT LIST

	TEST2D-1	TEST3D-1
	0+300	0+300
INPUT CLEAR HEIGHT OF TUNNEL IN METRES	7.9	7.9
INPUT HEIGHT OF OVERBURDEN IN METRES	4.5	4.5
INPUT HEIGTH UNDER TUNNEL IN METRES	4.5	4.5
INPUT NUMBER OF ROCK LAYERS	4	4
	1.0	1.0
	1	1
	8.0	8.0
	2	2
	11.0	11.0
	3	3
	17.0	17.0
	4	4
INPUT MATERIAL PROPERTY OF REST OF GROUND	5	5
MINOR (1/2) WIDTH OF STEEL ARCH = ? (SAMIN)	0.005	0.005
MAJOR (1/2) WIDTH OF STEEL ARCH ALONG THE Z AXIS = ? (SAMAJ)	0.08	0.08
MAJOR (1/2) WIDTH OF STEEL ARCH ALONG THE Y AXIS = ? (SAMAJ2)	0.105	0.105
IS A STEEL ARCH PRESENT ? 0) NO, 1) YES	0	1
WHAT IS THE MATERIAL PROPERTY OF THE STEEL ARCH USED	18	18
HEIGHT OF ANCHORAGES 1 AND 2= ?	6.0 0.5	6.0 0.5
LENGTH OF ANCHORAGES 1 AND 2= ?	4.0 4.0	4.0 4.0
RADIUS OF ANCHORAGES = ?	0.014	0.014
ANGLE OF ANCHORAGES 1 AND 2= ?	25 -10	25 -10
ARE ANCHORAGES PRESENT ? 0) NO, 1) YES'	0	1
WHAT IS THE MATERIAL PROPERTY OF THE ANCHORAGES USED ?	18	18
LENGTH OF (1/2) PERIOD = ?	0.35	0.35
INPUT WHAT ROCK TYPE OF EXCAVATION ?, 0)A,B OR 1)C	1	1
REGION: 1 C FOR EACH REGION INDICATE 0) IF EXCAVATED OR 1) IF NOT'	1 1	1 1
REGION: 2a C AND	1 1	1 1
REGION: 2b C IS THERE AN OUTER (SHOTCRETE) LINING? 0) NO, 1) YES'	1 1	1 1
REGION: 3a	1 1	1 1
REGION: 3b	1 1	1 1
REGION: 4	1 1	1 1
REGION: 5a	1 1	1 1
REGION: 5b	1 1	1 1
REGION: 6	1 1	1 1
WHAT IS THE MATERIAL PROPERTY OF THE SHOTCRETE USED ?	6	6
THICKNESS OF SHOTCRETE	0.45	0.45
IS THERE AN INNER LINING ? 0) NO, 1) YES	0	0
WHAT IS THE MATERIAL PROPETY OF THE INNER LINING USED ?	7	7
THICKNESS OF INNER LINING	0.5	0.5
RESOLUTION (increase resolution number to achieve fine mesh)	1	1
IS THIS EXAMPLE A SYMMETRICAL MODEL ? MSYM.EQ 0) NO or 1) YES	0	0
NUMBER OF DIMENSIONS	2	3

Table. 5.1 List of two- and three-dimensional input files

5.2.2 Assumptions and Limitation for Model Generation

The tunnel geometry for various input data is transferred into the pafblock design for mesh generation for two and three-dimensional models. The tunnel geometry for the excavation is defined by five radii, C1 to C5 as shown in Fig 5.3. Simple geometry and trigonometry were used to find the relationship between the centres of the tunnel curvature and the beginning and end points of the curves described.

These relationships were expressed in terms of the clear height and width of the tunnel as shown in Fig 2.2. and details of calculations are given in Appendix E.

The approach taken in this work, that of studying tunnel behaviour, has already been established and this approach is defined through the assumptions made in fixing the conditions for the finite element simulations. The major considerations are outlined as follows.

5.2.2.1 General Tunnel Model

The aim was to develop a system which would contain all the relevant programs and data files to be able to perform a complete analysis of a problem with the very minimum of input. A tunnel pafblock model is developed by the pre-processing program in the six stages as shown in Figs. 5.5 to 5.10. These are outlined below and relate mainly to the two-dimensional model, but are also applicable with some minor modification to the three-dimensional model. For the practical aspects of modelling it was decided that for the first simple analyses, very general PAFEC-FE features were taken into account for generating the pafblock model.

To avoid the unnecessary complication, some aspects of the model development have not been explained in detail. The pre-processing program contains detailed iterative calculations for generation of pafblocks. After establishing the pafblock model the complete mesh design was developed as described in this chapter.

i) Stage 1. Outer and Inner Boundaries

This stage involves setting the excavation surface, lining boundaries and the external boundary as defined by the input parameters as shown in Fig. 5.5. As can be seen from Fig. 5.5 the information required for this stage to be modelled consists only of the clear height of tunnel, height of overburden, height below the tunnel and position of the outer vertical boundary. The height of overburden and the distance between the bottom of the tunnel and bottom boundary must both be greater than 1 m in order to satisfy the PAFEC-FE geometry limits for pafblocks.

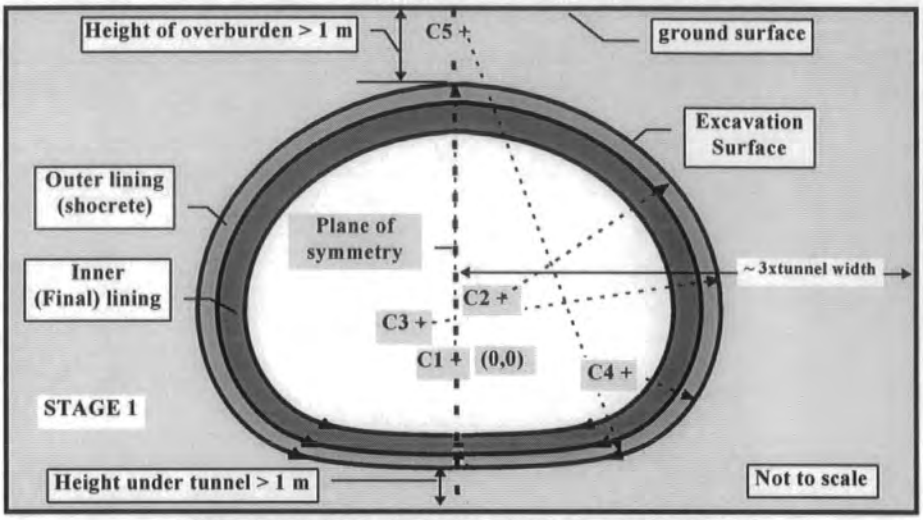

Fig. 5.5 Setting the outer and inner boundaries

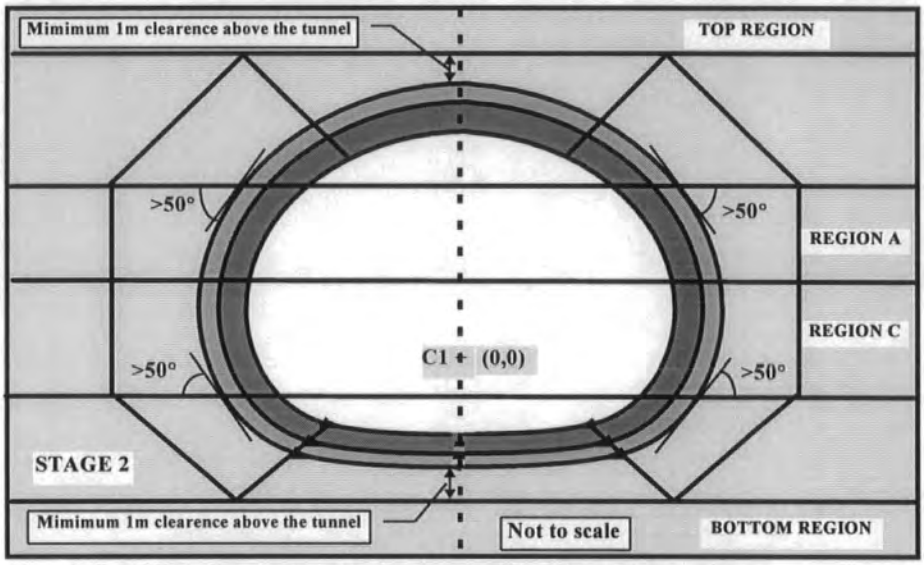

Fig. 5.6 Setting the region levels and shell boundaries

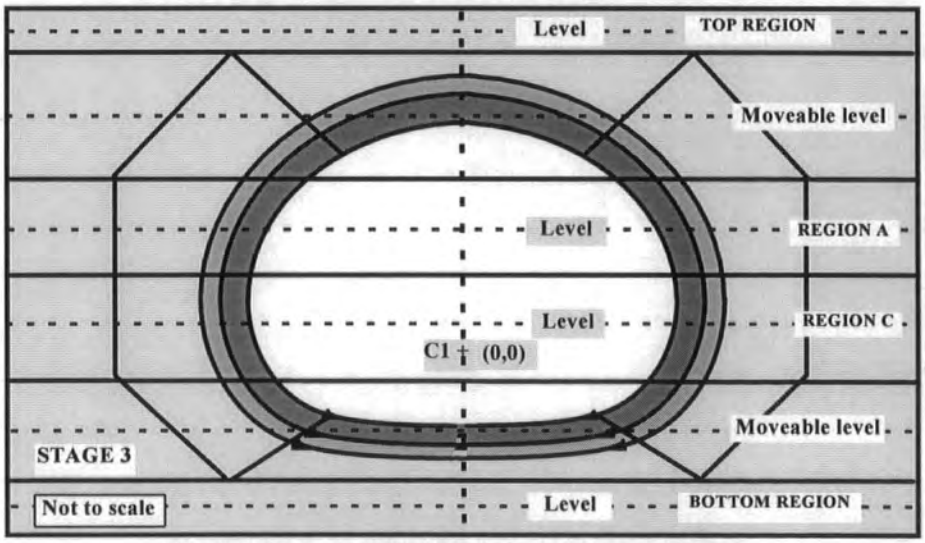

Fig. 5.7 Superposition of levels forming rock layers

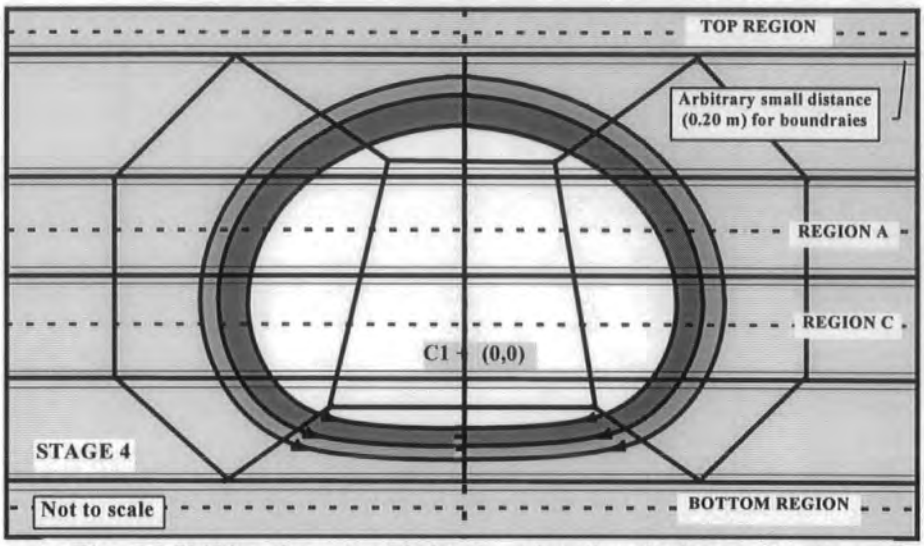

Fig. 5.8 Shifting the moveable levels and setting the internal regions

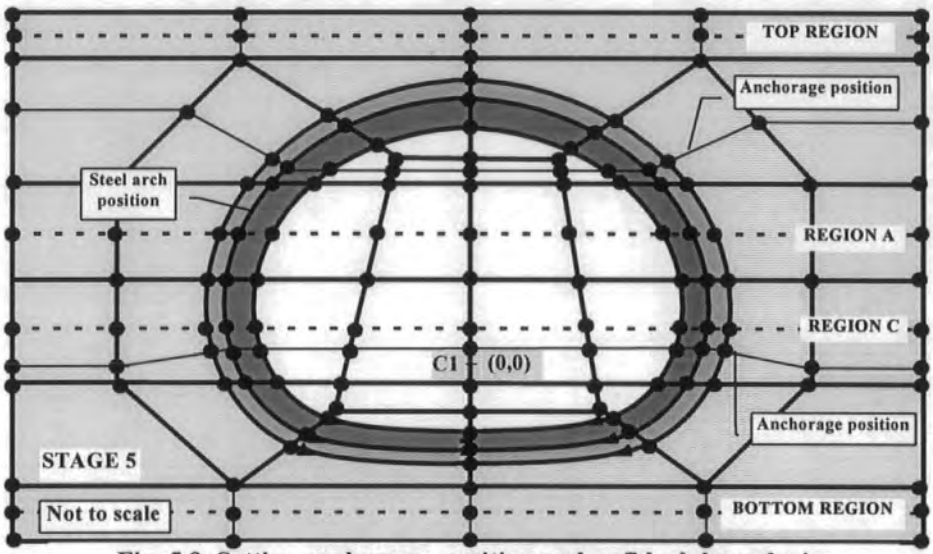

Fig. 5.9 Setting anchorages position and pafblock boundaries

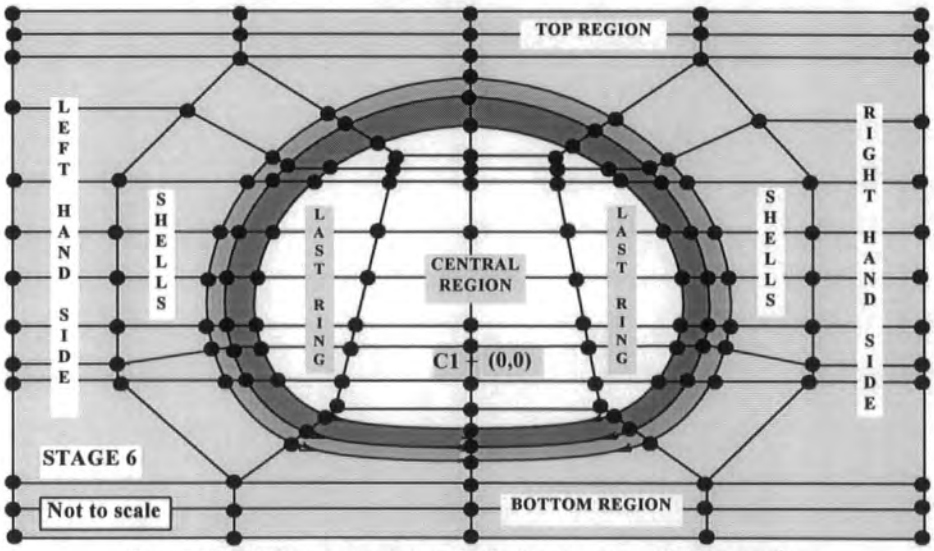

Fig. 5.10 Pafblock model and choice of computation regions

The positioning of the outer boundary has been discussed in section 4.2.2.1 and has been chosen as shown in Fig. 5.5 as at least three times the tunnel width.

ii) Stage 2. Region Boundaries

The consideration of the correct pafblock geometry had to be fulfilled namely, the angle of each corner of a pafblock has to be greater than 45^{O} and less then 135^{O} ($45^{O} < \theta < 135^{O}$) and the aspect ratio (ratio of the pafblock side lengths) of the resulting pafblock is required to be less than 15:1. Errors and warnings are produced by PAFEC-FE if these limits are violated or approached respectively. In order to ensure that such problems do not occur the angular limit was set at 50°. At this stage the region and shell boundaries can be set to ensure that this condition is avoided as shown in Fig. 5.6.

iii) Stage 3. Superposition of Levels Forming Rock Layers

The inclusion of the rock layers needed to be combined with the geometry of the tunnel. Incorporation of this factor into a finite element solution would require an iterative process that significantly separates the layers as shown in Fig. 5.7. In order to avoid any difficulties with a level forming the boundary between rock layers meeting the tunnel at a shallow angle, such a level must be moved as shown in the next stage.

iv) Stage 4. Shifting the Moveable Levels and Setting the Internal Regions

At this stage, any levels forming rock layers in the regions at the top and bottom of the tunnel are moved up or down to the corresponding fixed region boundaries as shown in Fig. 5.8. A further complication arises because due to the final configuration of the pafblocks, it was not possible to represent all the levels. This required additional regions to be put 0.20 m from the fixed boundaries to avoid narrow pafblocks and the levels forming rock layers are then moved to be combined into one fixed boundary outside these 0.20 m regions as shown in Fig. 5.11. However the rock layers could be accurately represented in regions A and C around the tunnel and in the outer regions.

Pafblock meshes are used inside the tunnel to form regions specifically to include the different forms of NATM excavation sequence for rock types A, B and C as shown in Figs. 5.12 and 5.13. The regions are defined either by a single pafblock or a small group of pafblocks. The excavated regions can be progressively omitted by the pre-processing program to simulate the excavation of the tunnel. It is also necessary to match the boundaries of excavation regions inside the tunnel to the fixed geometry of the ground outside the tunnel. Therefore the pafblock topology inside the tunnel includes the fixed boundaries for both forms of excavation. DO loops inside the pre-processing program automatically generate these patterns and IF blocks separate these patterns out.

v) Stage 5. Support System and Pafblock Boundaries

The inner and outer linings must be of uniform thickness and the pafblocks must be in the form of second order quadrilaterals to provide a good description of the stresses. If a support system consisting of steel arches and anchorages is required, it is necessary to use a three-dimensional model. In such a model these are represented by beam elements and it is necessary to ensure that the pafblock mesh matches these as shown in Fig. 5.4.

Uniform straight beam elements having two nodes are used to construct the frame structure for the steel arches and the anchorages which can be positioned so that they connect two adjacent pafblocks in the three-dimensional model as shown in Fig. 5.9 The inclusion of these support systems in the model permitted a useful investigation into the reinforcement of the tunnel. The beam element can have any cross-section described by second moments of area IYY, IZZ and area A as described in Section 5.2.6.2. At this stage the regions can be divided into suitably shaped pafblocks.

vi) Stage 6. Pafblock Model

The final stage of the pafblock model is shown in Fig. 5.10 with the regions reclassified for subsequent processing and the pafblock topology can be generated automatically for input to PAFEC-FE. Pafblocks inside the tunnel include the fixed boundaries for both sequences of excavation as shown in Figs 5.12 and 5.13..

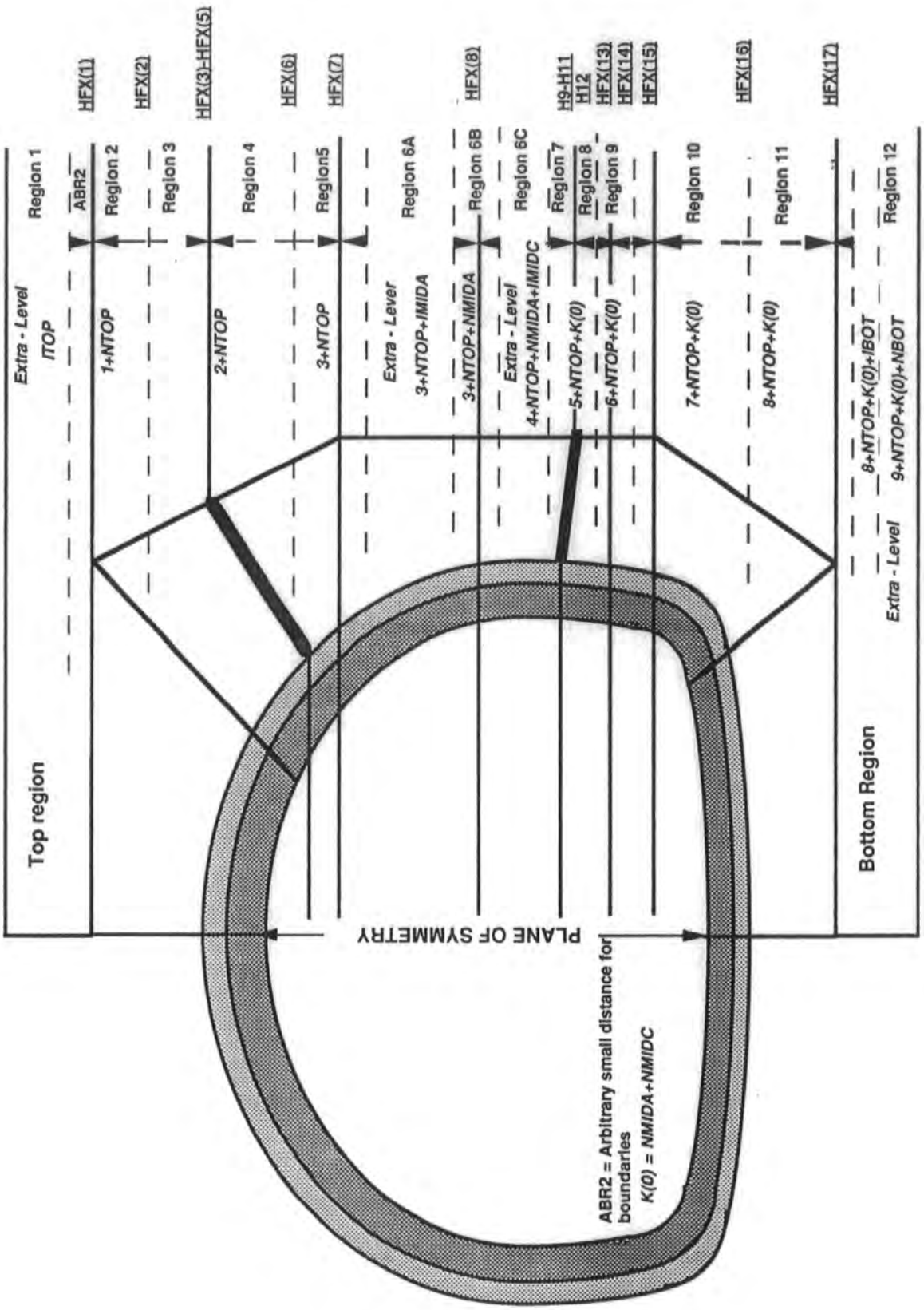

Fig. 5.11 General structure of region boundaries

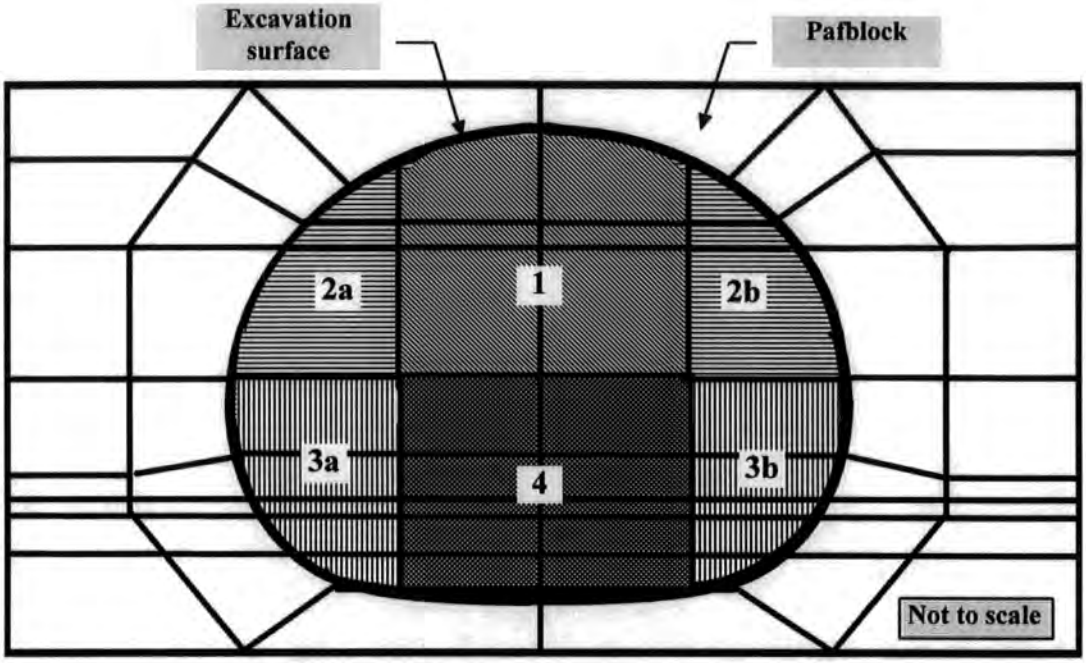

Fig. 5.12 Excavation sequence section and pafblock model for rock type A and B

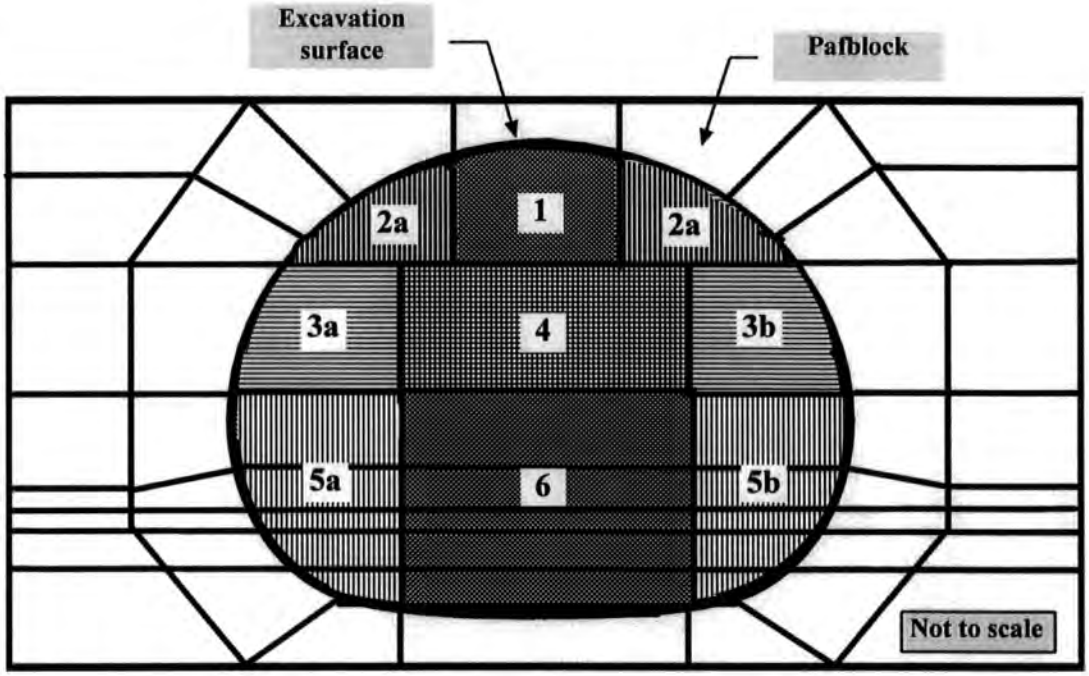

Fig. 5.13 Excavation sequence section and pafblock model for rock type C

5.2.2.2 Material Properties

Nearly all the material properties change with the rock layer variations with the exception of the outer lining (shotcrete), steel arch, anchorages and inner lining. The material properties of each rock layer and those for the support system, if required, are in the input data file assigned of the pre-processing program and allocated by the program to the pafblocks.

5.2.2.3 Model Loads

To simulate the existence of the geostatic stress field by incorporating gravity into the model, the GRAVITY module is used to increment the stress according to the depth of the model below the loaded surface as described in Chapter 4. The horizontal geostatic stress also can be simulated by applying constant pressure to the side boundaries of the mesh, using one of the PRESSURE modules. The pressure is set equal to the value of the pressure applied to the top surface of the mesh. Alternatively it is possible to use RESTRAINTS to ensure that the side boundaries of the mesh are free to move only in the vertical direction.

5.2.3 Limitation of Model Accuracy

It was accepted that there would be limitations on the accuracy of the model attributable to the required versatility. The greatest of these concerns the definition of the PAFEC-FE angle and aspect ratio errors. Mesh quality also has a significant effect on the error of the numerical results, although there are established techniques of mesh design and ways of checking the quality of a mesh with respect to aspect ratio and angle errors. Steps were taken in the model validation phase to ensure that most efficient combination of numbers of elements and subdivision numbers (N1, N2 and N5) were employed and that the resulting mesh was suitable. It is therefore very important that it is well conditioned for the purpose of mesh quality, since the FORTRAN program generates pafblock subdivision numbers depending on the element size compared with the required maximum aspect ratio (15:1). If this

comparison fails then the number of subdivisions must be increased so that the comparison no longer fails.

5.2.4 Mesh Generation

The finite element mesh is at the heart of the finite element method. The number and type of elements and the variation of the element size are all important, and guidelines exist for the determination of each. On the whole the greater the number of nodes and elements, the more accurate are the results that the mesh will generate. Also higher order elements produce more accurate results than lower order for a given mesh size. Thus quadratic elements are preferable to linear elements for the purposes of stress calculation. In general it is advisable to use large elements where stress concentrations are low and smaller elements in a denser mesh where stress concentrations are high in order to produce a combination of solution efficiency and accuracy. It is also advisable to maintain as smooth as possible the rate of change of size from one element to the next. However when very large numbers of elements are used for a mesh resulting in a computational model with a large number of degrees of freedom, not only does the computation time increase disproportionately but also there is the possibility that round-off errors will form an increasingly large proportion of the total error.

5.2.5 Model Restraints

In order to accurately simulate the behaviour of a model it is necessary to establish physical restraints. These are required to fully describe the fixed conditions of the model, in other words the quantities that remain constant through out the simulation. According to the specific details of the restraints, different constraining effects can be applied, typically rotation without translational displacement. It is therefore important that these restraints be applied carefully and fully, otherwise unexpected behaviour is likely to occur. The sides and bottom of the model were restrained as shown in Fig. 4.20.

5.2.6 Modelling of Tunnel Support System

Applications of support systems are necessary to establish the permanent stability of the excavated tunnel if required. This application covers all main support elements to be applied such as shotcrete lining, anchorages, steel arch and final lining. The type and amount of tunnel support to be installed is directly related to the rock strength as established immediately after excavation. However as a consequence of variations from the anticipated rock conditions the standard support system as shown in Fig 5.4. for each rock class may require modification and adjustment during construction.

A three-dimensional periodic structure is required to solve problems with anchorages and steel arches. In order to implement a periodic boundary condition, both sides of the model have the same boundary conditions. If the system has mirror symmetry at the boundaries then this could be modelled using the natural boundary condition to form an additional plane of symmetry as shown in the Fig. 5.15. Under such conditions the deformation in the z direction is constrained but those in the x and y directions are free, or the displacements at the nodes at one boundary must be made to have the same values as those at the other boundary, hence making the system periodic. Because the plane of symmetry contains the steel 'I' section used to form the support arch as shown in Fig. 5.14, the section properties used for the beam element were halved. Attempts to model the beam section as an equivalent solid rectangular section based on the full flange width using pafblocks were unsuccessful because they invalidated the restrictions on aspect ratio imposed by the PAFEC-FE program.

5.2.6.1 Shotcrete and Final Linings

The initial shotcrete and final concrete linings for the tunnels are respectively 200 mm and 500 mm thick. Their dimensions are determined with reference to the excavation boundary. Because the linings are relatively thin, modelling them as pafblocks poses problems due to the need to match them with adjacent pafblocks

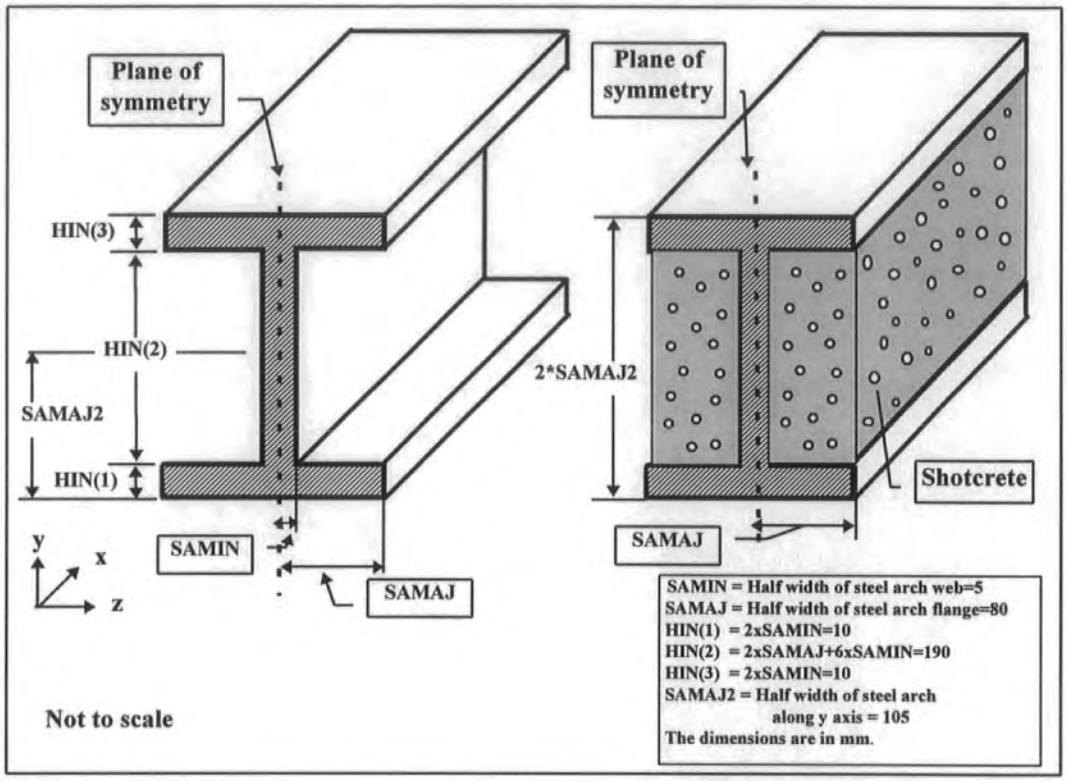

Fig. 5.14 Modification of 'I'cross-section steel arch to a solid steel arch of the same size

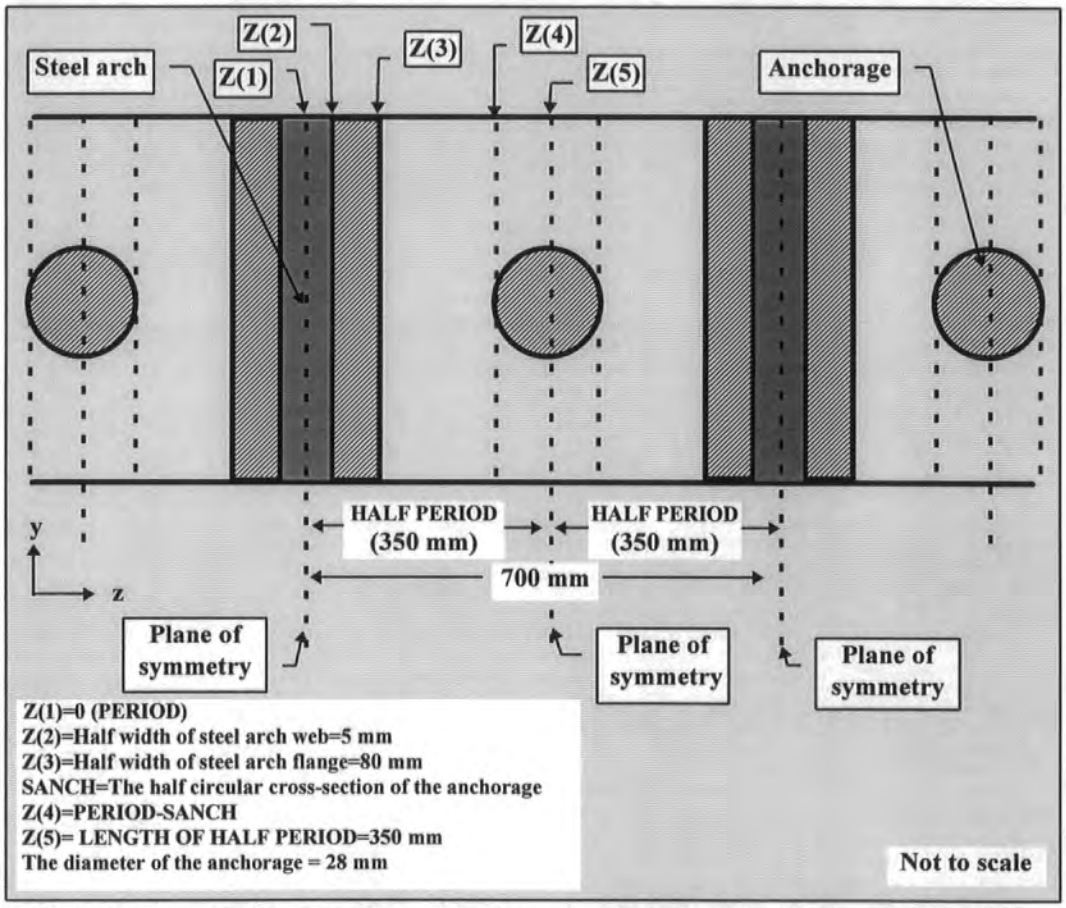

Fig. 5.15 Longitudinal-section of the tunnel and simulation of the support system

inside and outside the tunnel and the consequent limitations on aspect ratios and angles. Several different types of pafblock models were tried. Finally these linings were modelled by quadrilateral plane strain elements with 8 nodes (PAFEC type 36210) for the two-dimensional model and 20 noded brick elements (PAFEC type 37110) for the three-dimensional model as shown in Figs. 5.3 and 5.4 respectively. These elements are capable of providing a good description of the stresses and were used in preference to equivalent triangular elements commonly used.

5.2.6.2 Anchorages

A possible description of the behaviour of an anchorage is that it is not free to move independently but is constrained to move with the rock to which it is attached. To achieve this type of behaviour with pafblocks can only be accomplished using the RIGID LINKS module. This cannot be achieved with the RESTRAINTS or DISPLACEMENTS PRESCRIBED modules which apply the constraints globally and therefore will not model these conditions correctly. Using the RIGID LINK module consideration of local directions and nodal connectivity is important. Because the anchorage used has a 28 mm diameter, it is extremely thin and modelling using pafblocks again causes problems due to aspect ratio limitations. Therefore linear bar or beam elements must be used to model the anchorages. Initially the tension bar element (PAFEC type 34400) was used. Unfortunately no output was produced using this in PAFEC-FE and discussions with the company promised a modification in a later PAFEC-FE release Therefore the simple beam element 34000 was used to model anchorages which end in the first and last flattened shells as shown in Figs. 5.9 and 5.10.

Beam elements are geometrically the simplest of all finite elements and hence the cheapest. The beam element is essentially one dimensional although it may be curved and it may be used to form a three dimensional structure. The simple beam element used in PAFEC-FE is a straight beam element with two nodes and six degree of freedom and at each node U_x, U_y, U_z, $\varnothing_x$, $\varnothing_y$ and $\varnothing_z$. It provides bending in two directions, an axial force and a twisting moment. The cross-section is described by the second moments of area IYY and IZZ, the area and the torsional

constant. This element assumes that shear forces, twisting moments and axial forces are all constant along its length. The beam element is normally used if length to depth ratio is greater than five. The end points of each anchorage are found from simple geometry. Implementation of the anchorages in the pre-processing program is given in the subroutine 'support' in Appendix C. The derivation of the equivalent section properties for the anchorage beam elements is given in Appendix F.

5.2.6.3 Steel Arch

Initially curved beam elements (the three-noded PAFEC type 34800 and two-noded PAFEC type 34300) were used to model the steel arch. However unfortunately no printed output was obtained using these PAFEC-FE elements and discussions with the company indicated that modifications would be provided in a future version 8.1 of the program. Finally the simple beam element (PAFEC type 34000) was adopted as shown in Fig. 5.16. The derivation of the equivalent section properties for the steel arch is given in Appendix F.

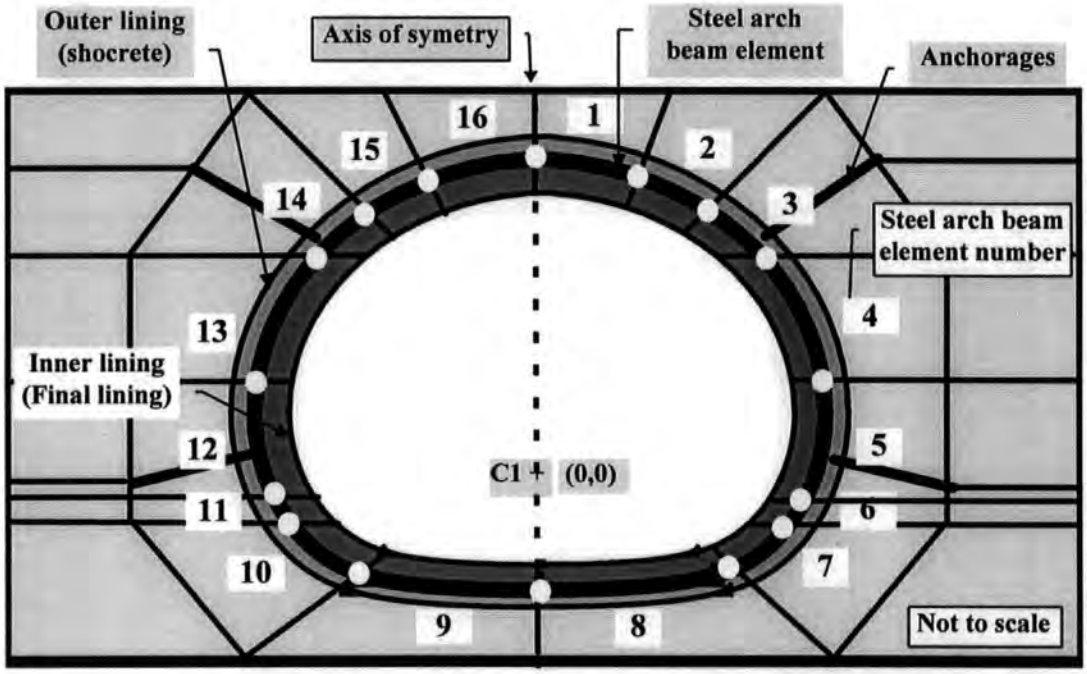

Fig. 5.16 Modelling of steel arch using beam element

5.3 Finite Element Mesh Design

This chapter describes in detail the refinement of the initial pafblock mesh to form a new arrangement of pafblocks which satisfied not only the angular limits but also the limits on aspect ratio. Error messages are produced by PAFEC-FE if the aspect ratio exceeds 15 and warnings if this exceeds 5. In order to retain some flexibility in the pafblock subdivision, it was decided to ignore any such warnings. The process of pafblock refinement is shown in the flowchart of Fig. 5.17. The final stage is to produce the finite element mesh for the pafblocks.

5.3.1 Two-Dimensional Pafblock Subdivision

The subdivision of the two-dimensional pafblocks requires choosing the values for two subdivision numbers N1 and N2 which are used in a similar manner to equivalent reference numbers in the pafblock subdivision used in PAFEC-FE to form the finite element mesh.

There are three groups of pafblock subdivisions as shown in Fig. 5.18.

i) Shell pafblock subdivision (NSUBSH)
ii) Row pafblock subdivision (NSUBRO)
iii) Column pafblock subdivision (NSUBCO)

Three arrays were necessary for these groups. The shell, row and column pafblock subdivision values were assigned such that all angle and aspect ratio errors disappear in file$.O02 of the PAFEC-FE output file. The reference numbers were assigned for the regions given in stage 6 of Section 5.2.2.

The criteria for the resulting mesh are the same as for the generation of the pafblocks.

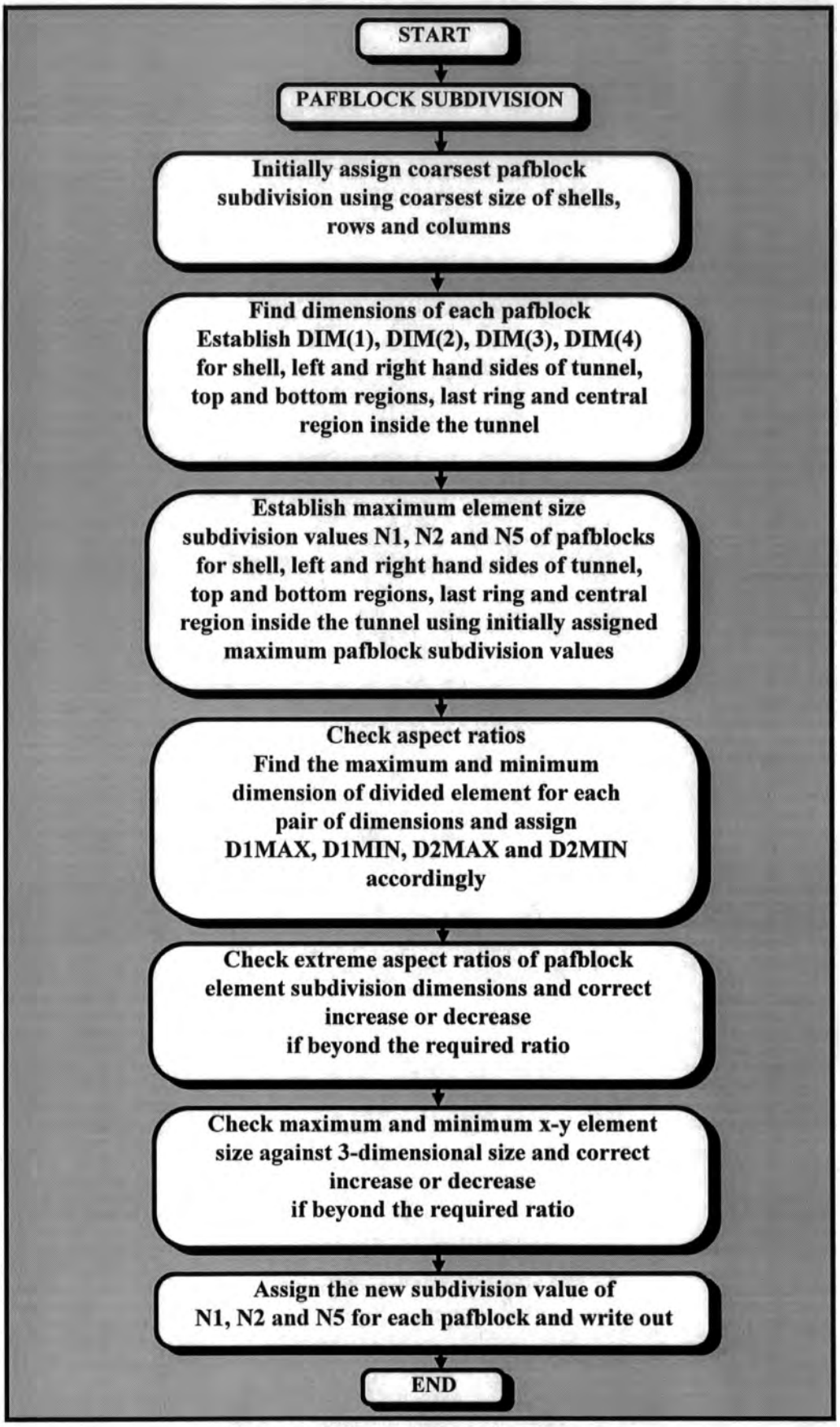

Fig. 5.17 Pafblock subdivision flowchart

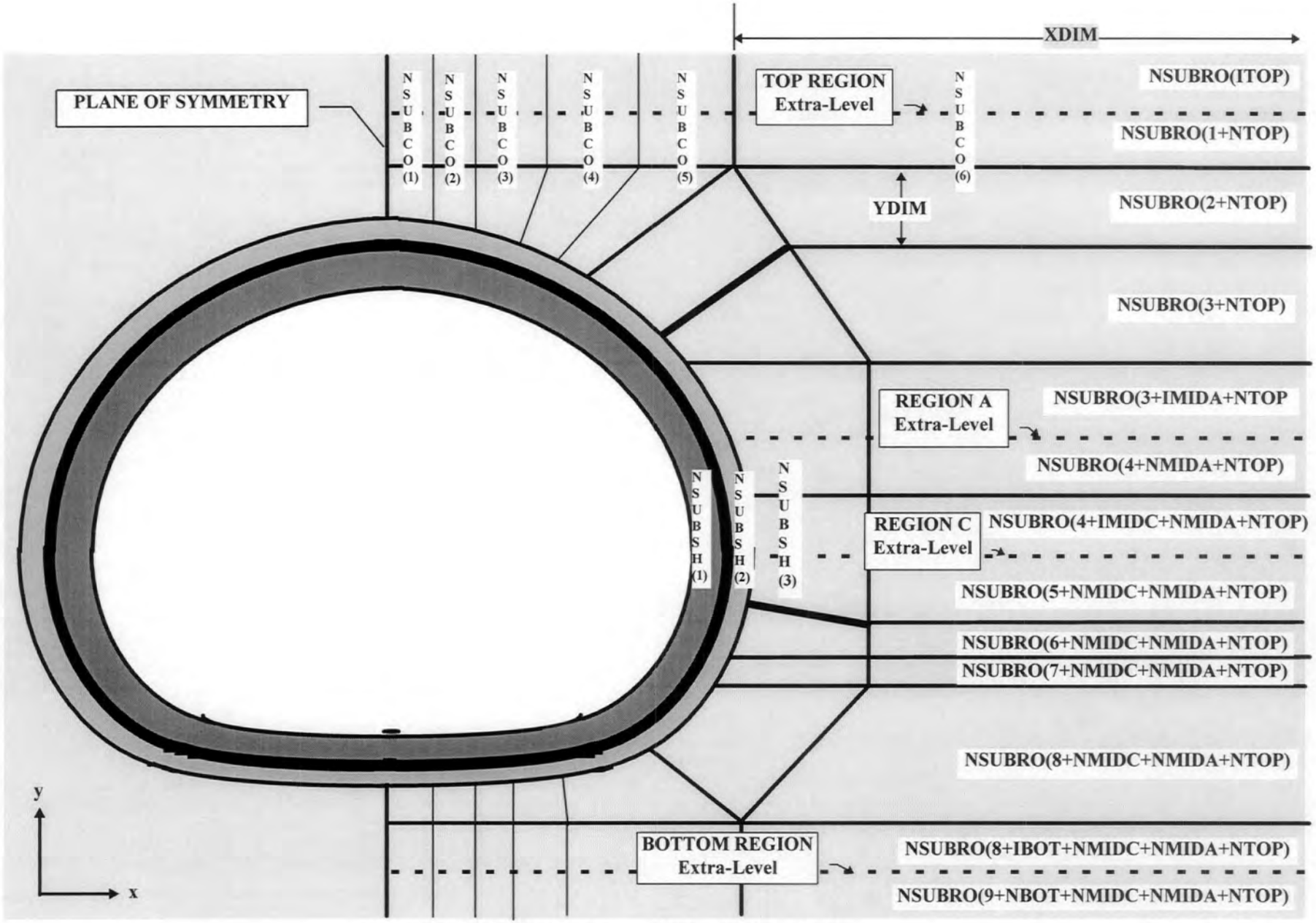

Fig. 5.18 Pafblock topology and indexing formulas

The stages in the production of the finite element mesh involve

i) The dimensions of pafblocks along the row were fixed from column 1 to 6 (SUBCO(1) to SUBCO(6)) as shown in Fig. 5.18. However the vertical dimensions are variable because of extra levels produced by the inclusion of the rock layers.

ii) The coarsest dimensions (XDIM, YDIM) of each pafblock have to be found for each shell, column and row. The appropriate subdivision of shells, columns and rows then can be calculated using equations (5.1) to (5.10) below.

iii) If there are extra layers in the top region, region A, region C and the bottom region, the values of YDIM for each of the layers in each region is found.

iv) Resolution of the mesh depends on the maximum element size (Z) defined by the user in the input data.

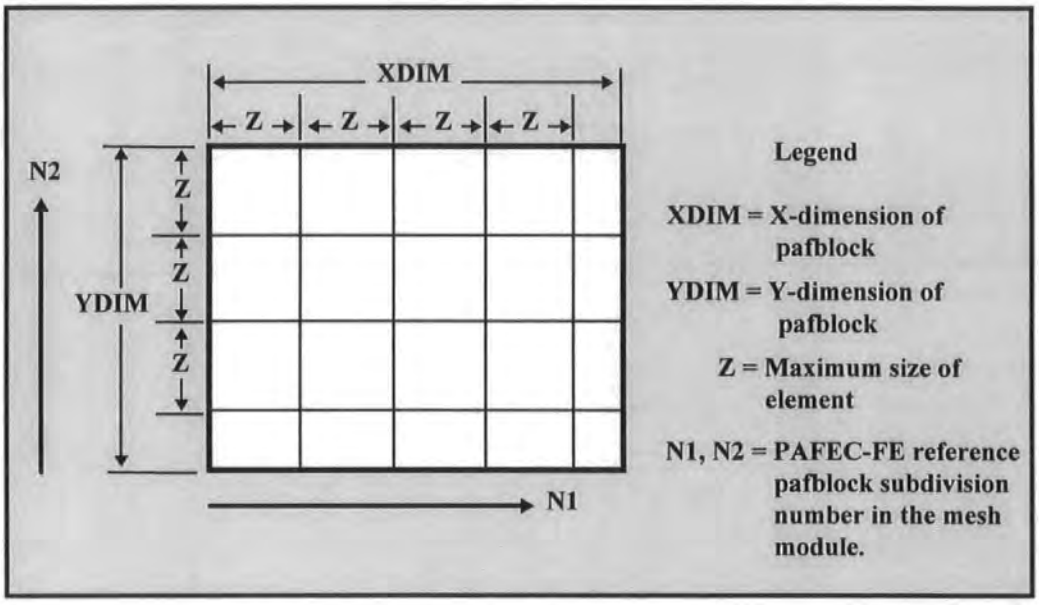

Fig. 5.19 An example of pafblock subdivisions

The number of Z-sized elements which can fit into XDIM and YDIM can be found simply from equations (5.1a)and (5.1b) respectively.

$$N1 = NSUBCO = 1 + \frac{XDIM}{Z}. \qquad (5.1a)$$

$$N2 = NSUBRO = 1 + \frac{YDIM}{Z}. \qquad (5.1b)$$

The problem of exact division by Z was solved by adding '1' to each formula to make the number of Z-sized elements round up according to the rules of FORTRAN 77.

5.3.1.1 Pafblock Subdivision Using Coarsest Pafblock Size

The appropriate coarsest pafblock sizes were assigned for shell, column and row arrays. Using these arrays then the pafblocks were divided using the initial subdivision values N1 and N2. There are three groups of subdivisions;

i) shell subdivisions, NSUB(ISHELL),

ii) column subdivisions, NSUB(ICOL),

and iii) row subdivisions, NSUB(IROW) as shown in Fig. 5.20.

```
C ================================================================
C SUBROUTINEMAXSI SUBDIVIDE PAFBLOCKS USING MAXIMUM
C PAFBLOCK SIZE
C ================================================================

      SUBROUTINE MAXSI

C THERE ARE THREE GROUP OF SUBDIVISIONS
C 1. NSHELL = NSUB(I)
C    1.1. NSUB(ISHELL)  ISHELL=1, NSHELL
C    1.2. NSUB(0)  LAST RING
C 2. NCOLUMN = NSUB(NSHELL+I)
C 3. NROW = NSUB(NSHELL+NCOL+I)

      CALL MAXSSH
      CALL MAXSCO
      CALL MAXSRO

      RETURN
      END
```

Fig. 5.20 Pafblock subdivision using coarsest pafblock size

5.3.1.1.1 Coarsest Pafblock Subdivision for Shell

The largest height of each shell was used for the coarsest subdivision size of the shell. This was found by subtraction of each shell height from the one before. The height between the last flattened shell and the one before is the largest height as shown in Fig 5.22. The largest dimension of the last ring was used in the subdivision of the last ring. This lies on the border between regions A and C inside the tunnel. Subroutine 'MAXSSH' was used for this process and as shown in Fig. 5.21.

```
C ==========================================================
C SUBROUTINE MAXSSH MAXIMUM PAFBLOCK SUBDIVISION FOR SHELL
C ==========================================================
      SUBROUTINE MAXSSH

      IMPLICIT DOUBLE PRECISION  (A-H,O-Z)
      PARAMETER(NNODES=5000)
      COMMON / CNODES / X(NNODES), Y(NNODES)
      COMMON / CSHLPR / NSHELL, HIN(5),SUMR
      COMMON / CKEYPR /K(0:8),NNS,NBS,NPOT,NPLR,NNODE,NPAF
      COMMON / CSUBDV / NSUB(0:50),MASPCT
      COMMON / CRESNI / NZ, ZSIZE, RATIO
      COMMON / CROKPR / MATPRO(20), HTOP(4), HMIDA(4), HMIDC(4),
     &                  HBOT(4),NMIDA,NMIDC,NTOP,NBOT
      COMMON / COUNT  / KPSH(8), NPSIDE, NCOL, NROW

C LARGEST HEIGTH OF SHELLS IS USED THE CALCULATION OF
C DIVIDING THE SHELLS
C THE HEIGTH BETWEEN LAST SHELL AND ONE BEFORE IS THE
C LARGEST HEIGTH

      DO 1190 ISHELL=1,NSHELL
 1190   NSUB(ISHELL)=1+( X(2*KPSH(4)+1+NNS*ISHELL)-
     &                  X(2*KPSH(4)+1+NNS*(ISHELL-1)) )/ZSIZE

C LAST RING PAFBLOCK TOPOLOGY SUBDIVISION N1=NSUBSH(0)
C LARGEST DIMENSION OF LAST RING IS USED THE CALCULATION OF
C DIVIDING THE LAST RING
C LARGEST DIMENSION OF LAST RING IS BORDER BETWEEN REGION A AND C
      NSUB(0)=1+( X(2*KPSH(4)+1+NNS)
     &        -X(2*NCOL*(4+NMIDA)+K(6)-1) )/ZSIZE
      RETURN
      END
```

Fig. 5.21 Coarsest pafblock subdivision for shell

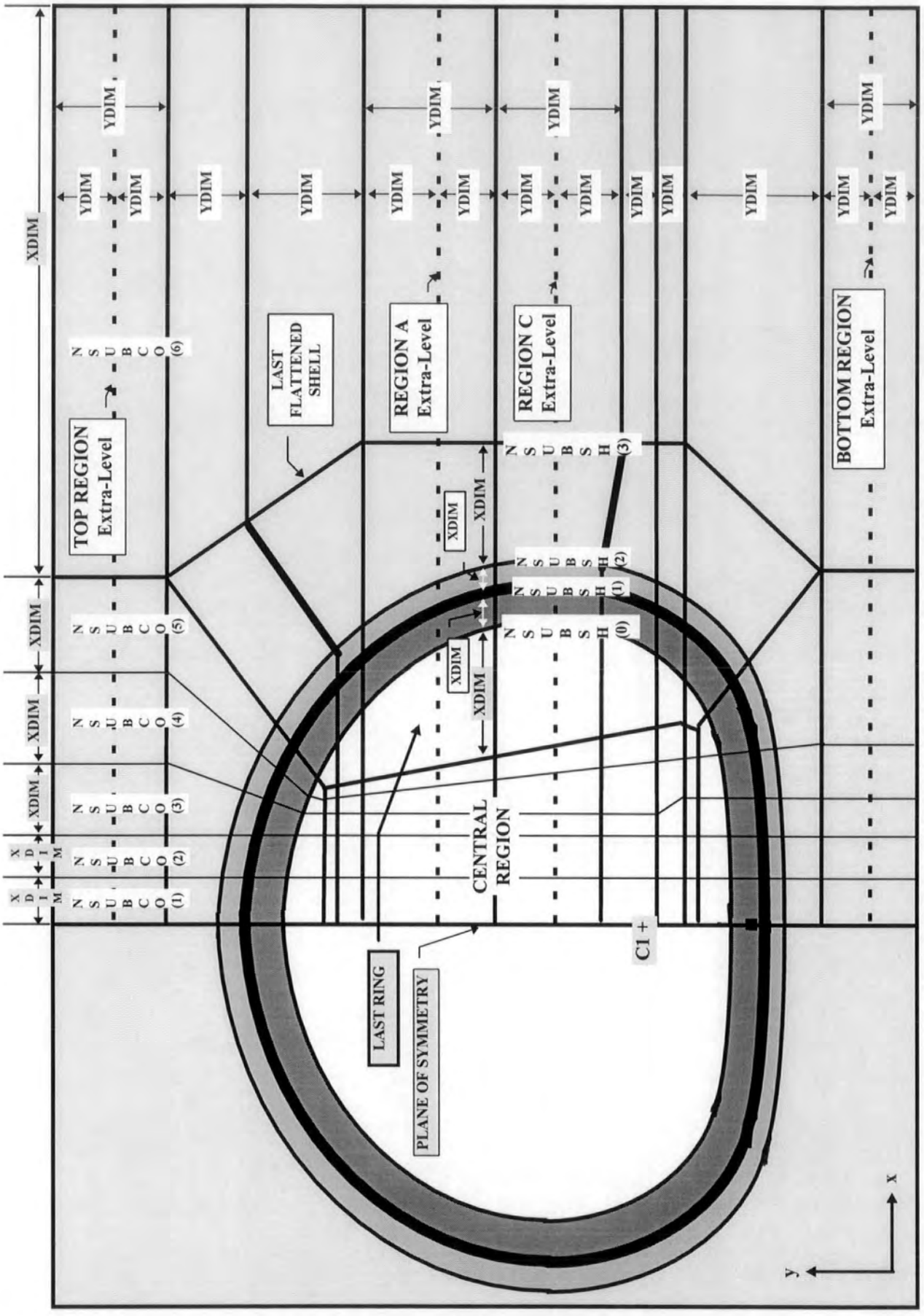

Fig. 5.22 Coarsest pafblock sizes for column, row and shell subdivisions

5.3.1.1.2 Coarsest Pafblock Subdivision for Column

The largest dimension of each column was used to find coarsest subdivision of the columns as shown in Fig. 5.22. This was undertaken in the subroutine 'MAXSCO' which is shown in Fig. 5.23.

```
C ==========================================================
C SUBROUTINE MAXSCO MAXIMUM PAFBLOCK SUBDIVISION
C FOR COLUMN
C ==========================================================

      SUBROUTINE MAXSCO

      IMPLICIT DOUBLE PRECISION  (A-H,O-Z)
      PARAMETER(NNODES=5000)
      COMMON / CNODES / X(NNODES), Y(NNODES)
      COMMON / CKEYPR /K(0:8),NNS,NBS,NPOT,NPLR,NNODE,NPAF
      COMMON / CSUBDV / NSUB(0:50),MASPCT
      COMMON / CRESNI / NZ, ZSIZE, RATIO
      COMMON / COUNT  / KPSH(8), NPSIDE, NCOL, NROW
      COMMON / CSHLPR / NSHELL, HIN(5),SUMR

C LARGEST DIMENSION OF EACH COLUMNS IS USED THE CALCULATION
C OF DIVIDING THE COLUMNS
      DO 10 I=1,NCOL
         XDIM=X(2*I+1+K(5))-X(2*I-1+K(5))
 10      NSUB(NSHELL+I)=1+(XDIM/ZSIZE)

      RETURN
      END
```

Fig. 5.23 Coarsest pafblock subdivision for column

5.3.1.1.3 Coarsest Pafblock Subdivision for Row

The largest dimensions of the top region, the right hand side of tunnel and the bottom region were used to find the coarsest row pafblock subdivision as shown in Fig. 5.22. This was calculated using the subroutine 'MAXSRO' as shown in Fig. 5.24.

```
C ================================================================
C SUBROUTINE MAXSRO MAXIMUM PAFBLOCK SUBDIVISION FOR ROW
C ================================================================

      SUBROUTINE MAXSRO

      IMPLICIT DOUBLE PRECISION  (A-H,O-Z)
      PARAMETER(NNODES=5000)

      COMMON / CNODES / X(NNODES), Y(NNODES)
      COMMON / CSHLPR / NSHELL, HIN(5),SUMR
      COMMON / CKEYPR /K(0:8),NNS,NBS,NPOT,NPLR,NNODE,NPAF
      COMMON / CSHTOP / NODELE(5000,8)
      COMMON / CROKPR / MATPRO(20), HTOP(4), HMIDA(4), HMIDC(4),
     &                  HBOT(4),NMIDA,NMIDC,NTOP,NBOT
      COMMON / CSUBDV / NSUB(0:50),MASPCT
      COMMON / CRESNI / NZ, ZSIZE, RATIO
      COMMON / CSUPIN / SAMIN, SAMAJ, HANCH(2), DANCH(2),
     &                  RANCH,AANCH(2),PERIOD, SANCH, SAMAJ2,
     &                  MARCH,MPARCH,MANCH,MPANCH
      COMMON / COUNT  / KPSH(8), NPSIDE, NCOL, NROW

C MAXIMUM PAFBLOCK SUBDIVISION FOR ROW
      DO 10 J=1,NROW
        IF (J.LE.NTOP) THEN
C EXTRA LAYERS IN TOP REGION
          YDIM = Y(1+4*(NPSIDE+1)+K(3)+(4*NCOL+2)*(J-1))
     &         - Y(1+4*(NPSIDE+1)+K(3)+(4*NCOL+2)*J)
        ELSE IF (J.EQ.NTOP+1) THEN
C TOP REGION
          YDIM = Y(1+4*(NPSIDE+1)+K(3)+(4*NCOL+2)*NTOP)
     &         - Y(1+K(3))
        ELSE IF (J.LE.1+NTOP+NPSIDE) THEN
C RIGHT SIDE OF TUNNEL
          YDIM = SQRT( ( X(2*NCOL-1+2*(J-(2+NTOP))+NNS*NSHELL)
     &                  -X(2*NCOL+1+2*(J-(2+NTOP))+NNS*NSHELL) )**2
     &                 +( Y(2*NCOL-1+2*(J-(2+NTOP))+NNS*NSHELL)
     &                  -Y(2*NCOL+1+2*(J-(2+NTOP))+NNS*NSHELL) )**2 )
C PAFBLOCKS BELOW 2ND ANCHORAGE ARE LARGER IN TUNNEL
          IF (J.EQ.NTOP+NPSIDE-1) YDIM=Y(2*KPSH(5)+1)-Y(2*KPSH(5)+3)
        ELSE IF (J.EQ.NTOP+2+NPSIDE) THEN
          YDIM = Y(2*NPSIDE+1+K(3))
     &         - Y(1+K(5)+(4*NCOL+2)*NBOT)
        ELSE
          YDIM = Y(1+K(5)+(4*NCOL+2)*(11+NTOP+K(0)+NBOT+1-J))
     &         - Y(1+K(5)+(4*NCOL+2)*(11+NTOP+K(0)+NBOT  -J))
        ENDIF
        NSUB(NSHELL+NCOL+J)=1+(YDIM/ZSIZE)
 10   CONTINUE

      RETURN
      END
```

Fig. 5.24 Coarsest pafblock subdivision for row

5.3.1.2 Dimensions of Pafblocks

The size of each pafblock can be found using the nodal co-ordinates. Array 'NODELE' was used to store the topology of each pafblock. The pafblock dimensions were established as array DIM for the shells, the left and right hand sides, the top and bottom regions, the last ring inside the tunnel and the central region using equations (5.2). Later, with the geometry of the each pafblock checked, they can be divided into elements using N1 and N2 as shown in Fig. 5.25. This is similar to the method used to form the original pafblock mesh for the tunnel as shown in Fig. 5.10.

$$DIM(1) = \left| X\left(NODELE(IPAF,2)\right) - X\left(NODELE(IPAF,1)\right) \right| \tag{5.2a}$$

$$DIM(2) = \left| X\left(NODELE(IPAF,4)\right) - X\left(NODELE(IPAF,3)\right) \right| \tag{5.2b}$$

$$DIM(3) = \left| Y\left(NODELE(IPAF,3)\right) - Y\left(NODELE(IPAF,1)\right) \right| \tag{5.2c}$$

$$DIM(4) = SQRT\left[\begin{array}{l} \left(Y\left(NODELE(IPAF,4)\right) - Y\left(NODELE(IPAF,2)\right)\right)^2 + \\ \left(X\left(NODELE(IPAF,4)\right) - X\left(NODELE(IPAF,2)\right)\right)^2 \end{array} \right] \tag{5.2d}$$

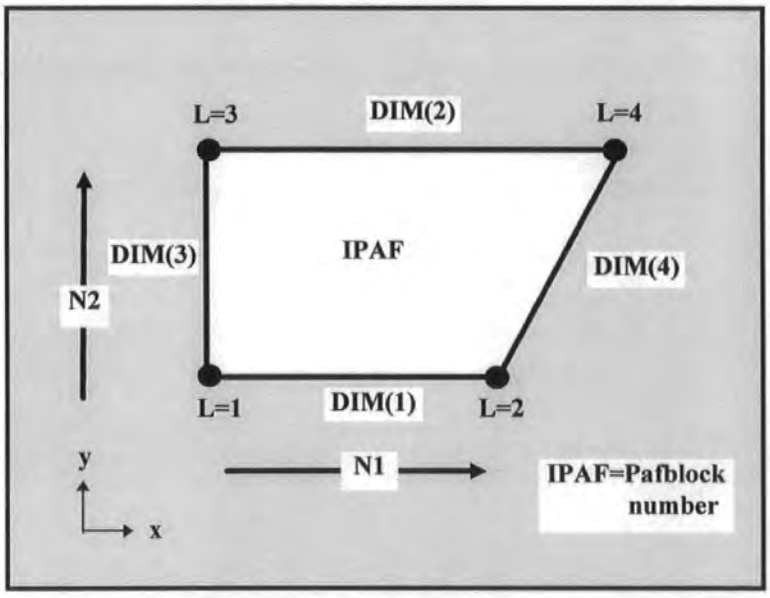

Fig. 5.25 Dimensions of a quadralateral pafblock

DIM(1)/N1, DIM(2)/N1, DIM(3)/N2 and DIM(4)/N2 are the element dimensions. The aspect ratio of the elements then can be found and compared with required maximum aspect ratio 14.9.

5.3.1.2.1 Dimensions of the Shell Pafblocks

The shell pafblocks dimensions DIM(1) and DIM(2) are always arcs and these can be found by dividing them into two right angled triangles as shown in Fig 5.26. The equations (5.3) were derived from such division. DIM(3) and DIM(4) are equal the radial dimension differences between the shells and always straight lines as shown in the figure.

$$CORD1 = SQRT\left[\begin{array}{l}\left(X\left(NODELE\left(IPAF,1\right)\right) - X\left(NODELE\left(IPAF,2\right)\right)\right)^2 + \\ \left(Y\left(NODELE\left(IPAF,1\right)\right) - Y\left(NODELE\left(IPAF,2\right)\right)\right)^2\end{array}\right] \tag{5.3a}$$

$$CORD2 = SQRT\left[\begin{array}{l}\left(X\left(NODELE\left(IPAF,3\right)\right) - X\left(NODELE\left(IPAF,4\right)\right)\right)^2 + \\ \left(Y\left(NODELE\left(IPAF,3\right)\right) - Y\left(NODELE\left(IPAF,4\right)\right)\right)^2\end{array}\right] \tag{5.3b}$$

$$ANGLE1 = 2 * ARCSIN\left(\frac{CORD1}{2Q1}\right) \tag{5.3c}$$

$$ANGLE2 = 2 * ARCSIN\left(\frac{CORD2}{2Q2}\right) \tag{5.3d}$$

ANGLE1 and ANGLE2 are the central angles in radians and circumference DIM(1) and DIM(2) are calculated by equations (5.3e) and (5.3f).

$$DIM(1) = Q1 \times ANGLE1 \tag{5.3e}$$

$$DIM(2) = Q2 \times ANGLE2 \tag{5.3f}$$

The last flattened shell dimension DIM(2) is a straight line as shown in Fig. 5.26. Therefore DIM(2) is calculated using the equation (5.3g).

$$DIM(2) = SQRT\left[\begin{array}{l}\left(X\left(NODELE\left(IPAF,4\right)\right) - X\left(NODELE\left(IPAF,3\right)\right)\right)^2 + \\ \left(Y\left(NODELE\left(IPAF,4\right)\right) - Y\left(NODELE\left(IPAF,3\right)\right)\right)^2\end{array}\right] \tag{5.3g}$$

DIM(3) and DIM(4) are always straight lines and calculated using the Pythagorean theorem as shown in equations (5.3h) and (5.3j).

$$DIM(3) = SQRT\left[\begin{array}{l}\left(X\left(NODELE\left(IPAF,1\right)\right) - X\left(NODELE\left(IPAF,3\right)\right)\right)^2 + \\ \left(Y\left(NODELE\left(IPAF,1\right)\right) - Y\left(NODELE\left(IPAF,3\right)\right)\right)^2\end{array}\right] \quad (5.3h)$$

$$DIM(4) = SQRT\left[\begin{array}{l}\left(X\left(NODELE\left(IPAF,2\right)\right) - X\left(NODELE\left(IPAF,4\right)\right)\right)^2 + \\ \left(Y\left(NODELE\left(IPAF,2\right)\right) - Y\left(NODELE\left(IPAF,4\right)\right)\right)^2\end{array}\right] \quad (5.3j)$$

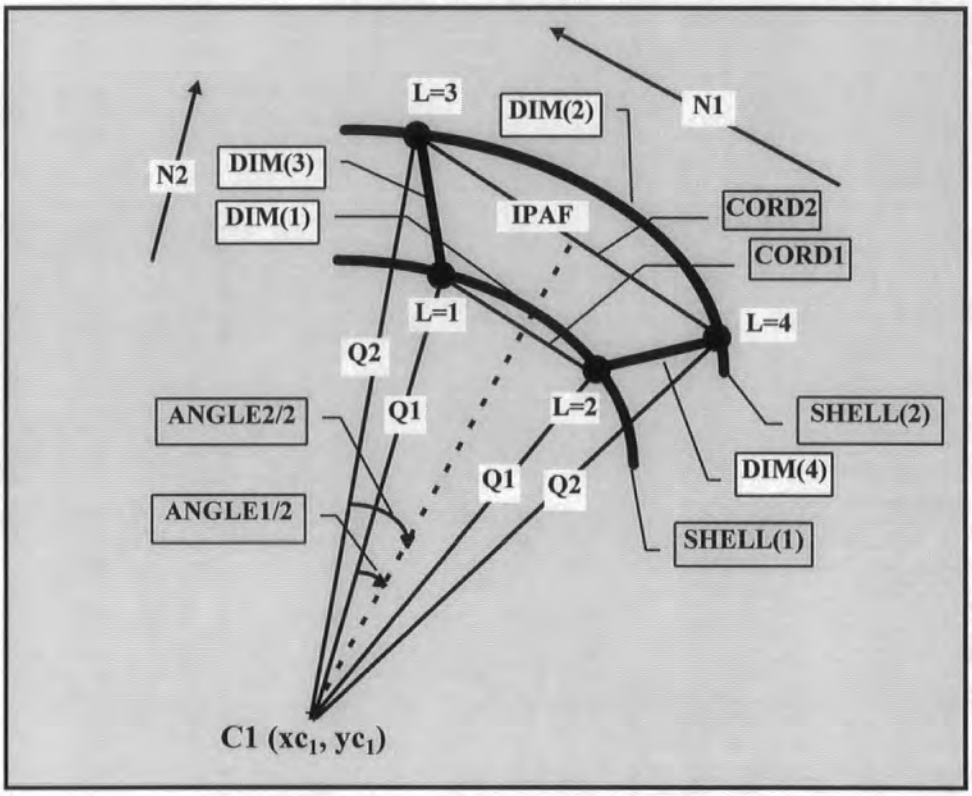

Fig. 5.26 Dimensions of shell pafblocks

5.3.1.2.2 Dimensions of the Right and Left Hand Sides of Tunnel Pafblocks

The right hand side of the tunnel pafblock dimensions are always straight lines and DIM(1) belongs to the last flattened shell as shown in Fig. 5.27. The dimensions then are defined by equations (5.4).

$$DIM(1) = SQRT\left[\begin{array}{l}\left(X\left(NODELE\left(IPAF,1\right)\right) - X\left(NODELE\left(IPAF,2\right)\right)\right)^2 + \\ \left(Y\left(NODELE\left(IPAF,1\right)\right) - Y\left(NODELE\left(IPAF,2\right)\right)\right)^2\end{array}\right] \quad (5.4a)$$

$$DIM(2) = \left|Y\left(NODELE\left(IPAF,3\right)\right) - Y\left(NODELE\left(IPAF,4\right)\right)\right| \quad (5.4b)$$

$$DIM(3) = \left| X\left(NODELE\left(IPAF,3\right)\right) - X\left(NODELE\left(IPAF,1\right)\right)\right| \quad (5.4c)$$

$$DIM(4) = \left| X\left(NODELE\left(IPAF,4\right)\right) - X\left(NODELE\left(IPAF,2\right)\right)\right| \quad (5.4d)$$

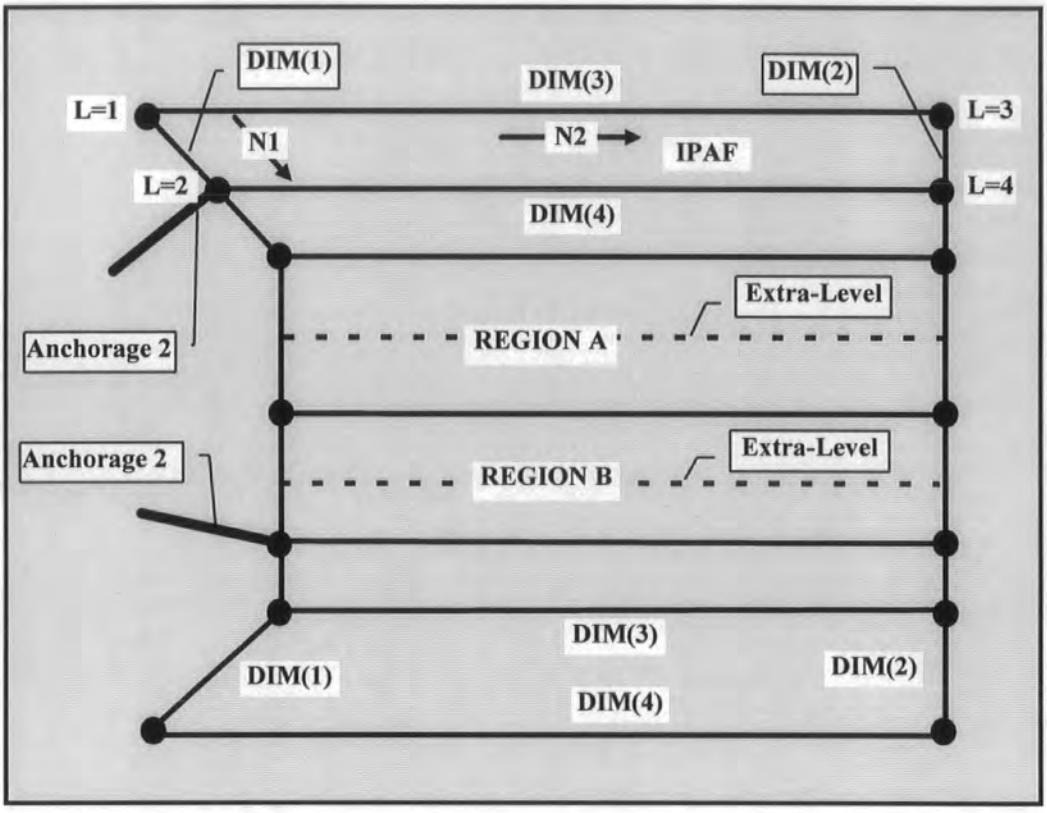

Fig. 5.27 Right hand side of the shell pafblock topology

5.1.3.2.3 Dimensions of the Top and Bottom Regions Pafblocks

The pafblock dimensions of the top and bottom regions are always straight lines as shown in Fig. 5.28 and these are obtained by equations (5.5) and (5.6) respectively.

$$DIM(1) = \left| X\left(NODELE\left(IPAF,2\right)\right) - X\left(NODELE\left(IPAF,1\right)\right)\right| \quad (5.5a)$$

$$DIM(2) = \left| X\left(NODELE\left(IPAF,4\right)\right) - X\left(NODELE\left(IPAF,3\right)\right)\right| \quad (5.5b)$$

$$DIM(3) = \left| Y\left(NODELE\left(IPAF,3\right)\right) - Y\left(NODELE\left(IPAF,1\right)\right)\right| \quad (5.5c)$$

$$DIM(4) = \left| Y\left(NODELE\left(IPAF,4\right)\right) - Y\left(NODELE\left(IPAF,2\right)\right)\right| \quad (5.5d)$$

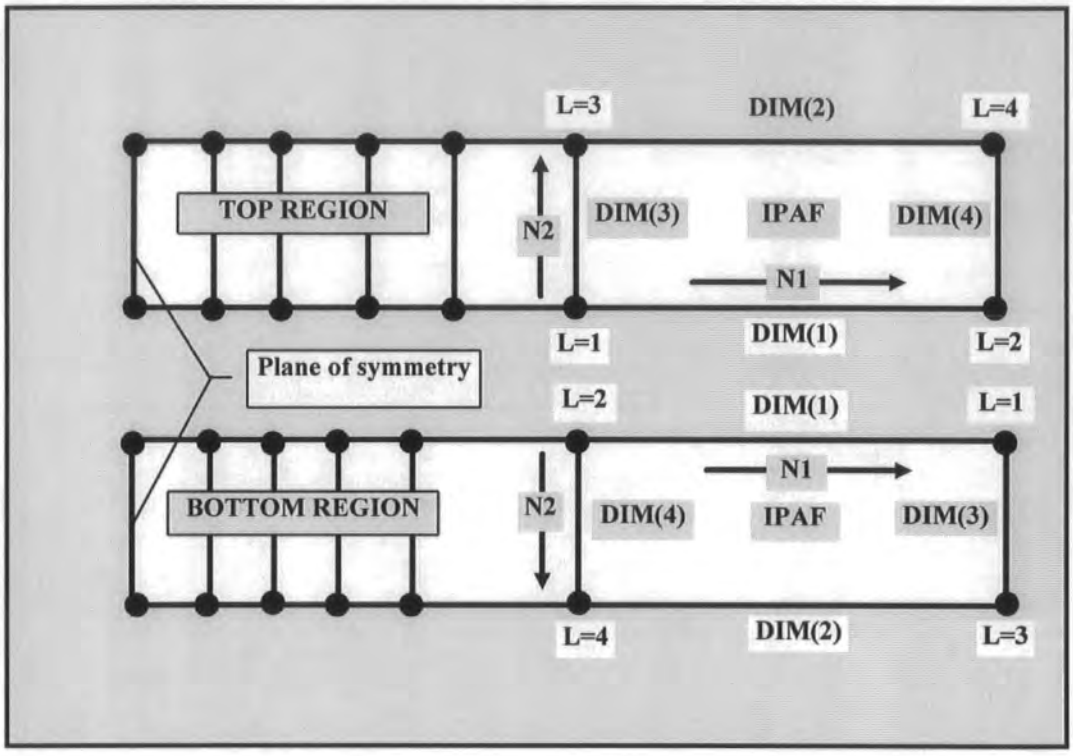

Fig. 5.28 Pafblock dimensions of top and bottom regions

$$DIM(1) = \left| X\left(NODELE\left(IPAF,1\right)\right) - X\left(NODELE\left(IPAF,2\right)\right)\right| \quad (5.6a)$$

$$DIM(2) = \left| X\left(NODELE\left(IPAF,3\right)\right) - X\left(NODELE\left(IPAF,4\right)\right)\right| \quad (5.6b)$$

$$DIM(3) = \left| Y\left(NODELE\left(IPAF,1\right)\right) - Y\left(NODELE\left(IPAF,3\right)\right)\right| \quad (5.6c)$$

$$DIM(4) = \left| Y\left(NODELE\left(IPAF,2\right)\right) - Y\left(NODELE\left(IPAF,4\right)\right)\right| \quad (5.6d)$$

5.3.1.2.4 Dimensions of the Last Ring Pafblocks Inside the Tunnel

The last ring pafblock dimensions inside the tunnel DIM(1), DIM(3) and DIM(4) are always straight lines but DIM(2) is an arc as shown in Fig. 5.29. The simple expressions for pafblocks dimensions are given by equations (5.7).

$$DIM(1) = SQRT\left[\begin{array}{l}\left(X\left(NODELE\left(IPAF,1\right)\right) - X\left(NODELE\left(IPAF,2\right)\right)\right)^2 + \\ \left(Y\left(NODELE\left(IPAF,1\right)\right) - Y\left(NODELE\left(IPAF,2\right)\right)\right)^2\end{array}\right] \tag{5.7a}$$

$$CORD1 = SQRT\left[\begin{array}{l}\left(X\left(NODELE\left(IPAF,3\right)\right) - X\left(NODELE\left(IPAF,4\right)\right)\right)^2 + \\ \left(Y\left(NODELE\left(IPAF,3\right)\right) - Y\left(NODELE\left(IPAF,4\right)\right)\right)^2\end{array}\right] \tag{5.7b}$$

$$ANGLE1 = 2 * ARCSIN\left(\frac{CORD1}{2Q1}\right) \tag{5.7c}$$

$$DIM(2) = Q1 \times ANGLE1 \tag{5.7d}$$

$$DIM(3) = SQRT\left[\begin{array}{l}\left(X\left(NODELE\left(IPAF,1\right)\right) - X\left(NODELE\left(IPAF,3\right)\right)\right)^2 + \\ \left(Y\left(NODELE\left(IPAF,1\right)\right) - Y\left(NODELE\left(IPAF,3\right)\right)\right)^2\end{array}\right] \tag{5.7e}$$

$$DIM(4) = SQRT\left[\begin{array}{l}\left(X\left(NODELE\left(IPAF,2\right)\right) - X\left(NODELE\left(IPAF,4\right)\right)\right)^2 + \\ \left(Y\left(NODELE\left(IPAF,2\right)\right) - Y\left(NODELE\left(IPAF,4\right)\right)\right)^2\end{array}\right] \tag{5.7f}$$

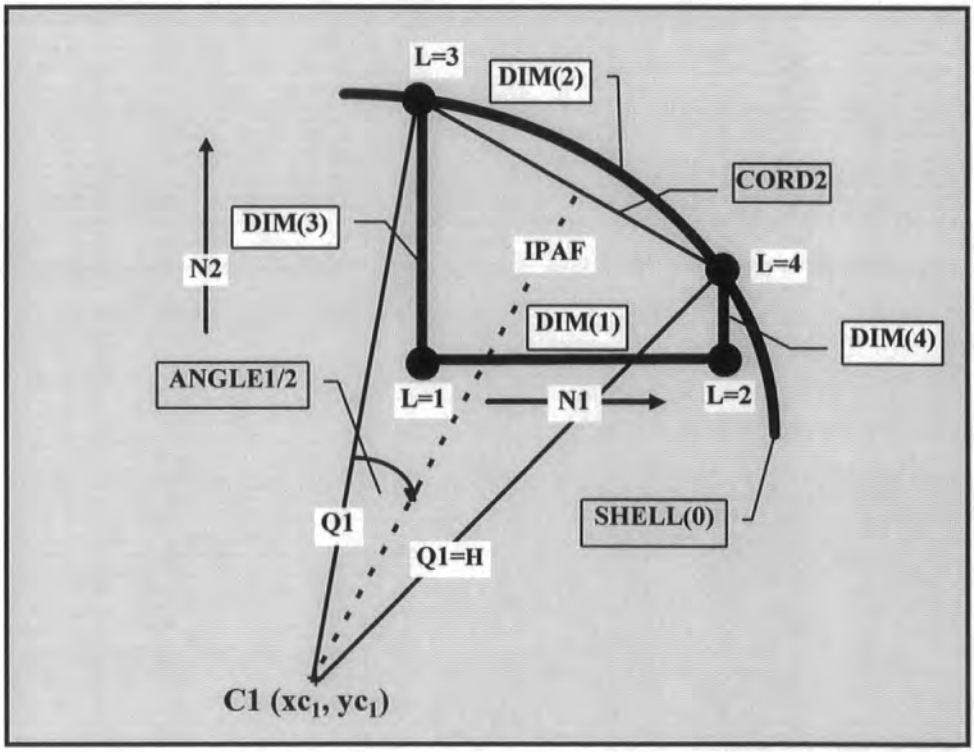

Fig. 5.29 Dimensions of the last ring pafblocks inside the tunnel

5.3.1.2.5 Dimensions of the Central Pafblocks Inside the Tunnel

The analysis represented in equations (5.8) is very simple one which uses the model shown in Fig. 5.30. The central pafblock dimensions are always straight lines as shown in the figure and these are determined from the equations as follows.

$$DIM(1) = \left| X\left(NODELE(IPAF,1)\right) - X\left(NODELE(IPAF,2)\right) \right| \tag{5.8a}$$

$$DIM(2) = \left| X\left(NODELE(IPAF,3)\right) - X\left(NODELE(IPAF,4)\right) \right| \tag{5.8b}$$

$$DIM(3) = \left| Y\left(NODELE(IPAF,1)\right) - Y\left(NODELE(IPAF,3)\right) \right| \tag{5.8c}$$

$$DIM(4) = \left| Y\left(NODELE(IPAF,2)\right) - Y\left(NODELE(IPAF,4)\right) \right| \tag{5.8d}$$

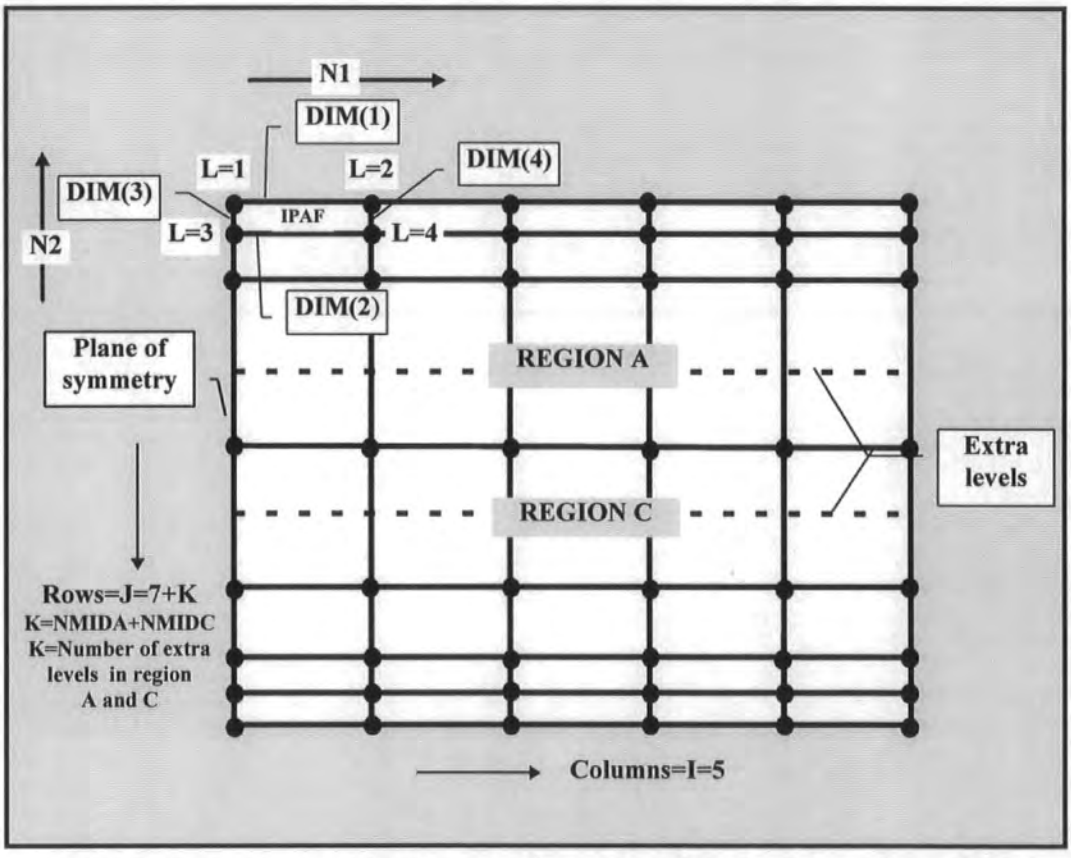

Fig. 5.30 Dimensions of the central region pafblocks inside the tunnel

5.3.1.3 Maximum Element Size Subdivision Values of Pafblocks

The maximum element size subdivision values of the pafblock for the shell, left and the right hand side of the tunnel, the top and bottom region, the last ring and inside the tunnel were assigned according to the maximum size of the shells, rows and columns as shown in Fig 5.18 before the checks on aspect ratio were performed. The complete solution of pafblock subdivision into finite elements requires the determination of the aspect ratio in addition to the methods introduced above.

5.3.2 Aspect Ratio of the Elements

It was important to ensure the aspect ratio of any element produced does not exceed the value of aspect ratio 15. In order to avoid possibilities of errors being generated by pafblocks approaching this ratio, a slightly lower value of 14.9 was adopted in practice. The dimensions of the subdivided pafblock elements can be found by dividing the pafblock dimensions by N1 and N2. Each pair of the pafblock dimensions were found as maximum and minimum dimensions and they were used to assign, D1MIN, D1MAX, D2MIN and D2MAX as shown in Fig. 5.31 and Table 5.2. The maximum and minimum orthogonal dimension can be found by given conditions. The global maximum and minimum pafblock sizes were initialised with dummy values for DMIN of 100 and DMAX of zero. The pre-processing program then finds D1MAX, D1MIN, D2MIN and D2MAX by means of the subroutine 'ASPCHK' as shown in Fig. 5.32.

The aspect ratio of an element then can be found and compared with the lower aspect ratio as follows.

$$\frac{D1MAX/N1}{D2MIN/N2} < 14.9 \qquad (5.9a)$$

$$\frac{D2MAX/N2}{D1MIN/N1} < 14.9 \qquad (5.9b)$$

Figure 5.31 shows the results of the subdivision calculations carried out for a sample pafblock. In this problem, the angles forming the pafblock have an important influence on the dimensions and shapes of the elements.

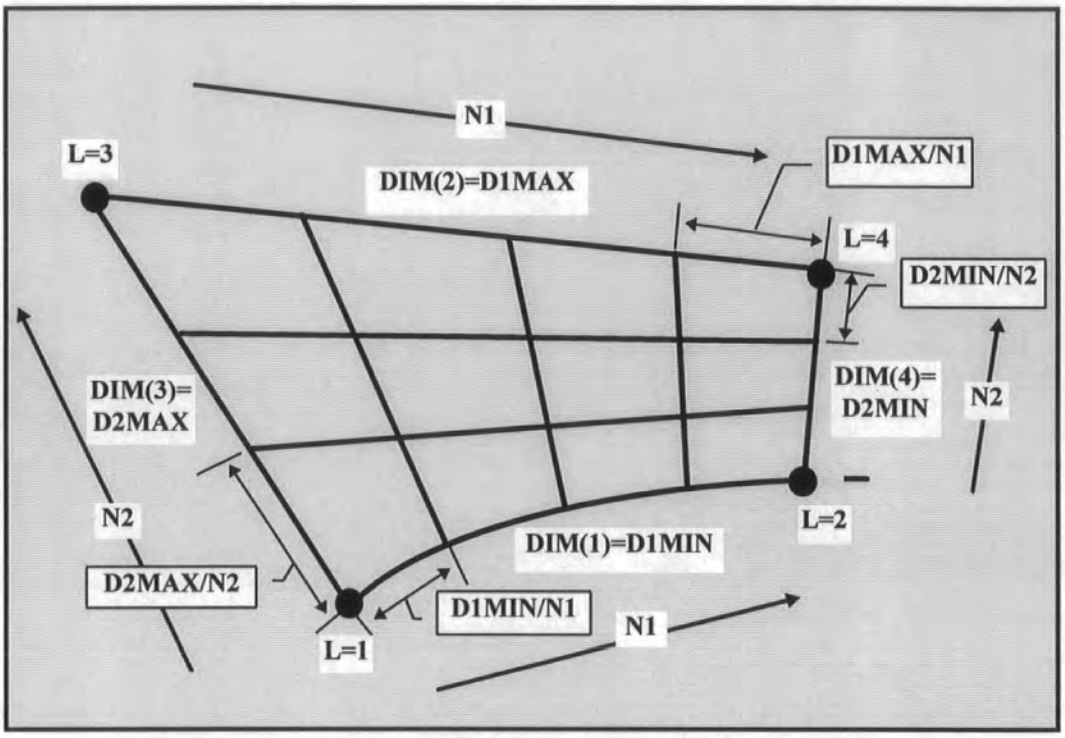

Fig. 5.31 Extreme ratios of pafblock elements subdivision dimensions

Pafblock dimensions	Subdivision numbers	Dimensions of subdivided element
D1MIN (DIM1)	N1	D1MIN/N1
D1MAX (DIM2)	N1	D1MAX/N1
D2MAX (DIM3)	N2	D2MAX/N2
D2MIN (DIM4)	N2	D2MIN/N2

Table 5.2 Dimensions of divided elements

```
C ==========================================================
C SUBROUTINE ASPECT RATIO CHECK
C ==========================================================

      SUBROUTINE ASPCHK (IPAF,N1,N2)

      IMPLICIT DOUBLE PRECISION  (A-H,O-Z)

      COMMON / CDIM   / DIM(4), DMIN, DMAX, IPMAX, IPMIN
      COMMON / CRESNI / NZ, ZSIZE, RATIO
      COMMON / CSUBDV / NSUB(0:50),MASPCT

c     WRITE(6,*)'DIMENSIONS OF PAFBLOCK ',IPAF
c     WRITE(6,*)DIM(1)
c     WRITE(6,*)DIM(2)
c     WRITE(6,*)DIM(3)
c     WRITE(6,*)DIM(4)

C FIND THE MAXIMUM AND MINIMUM DIMENSION FOR EACH PAIR OF
C DIMENSIONS AND ASSIGN D1MAX,D1MIN,D2MAX,D2MIN ACCORDINGLY

      IF (DIM(1).GT.DIM(2)) THEN
        D1MAX=DIM(1)
        D1MIN=DIM(2)
      ELSE
        D1MAX=DIM(2)
        D1MIN=DIM(1)
      ENDIF

      IF (DIM(3).GT.DIM(4)) THEN
        D2MAX=DIM(3)
        D2MIN=DIM(4)
      ELSE
        D2MAX=DIM(4)
        D2MIN=DIM(3)
      ENDIF

C CHECK EXTREME ASPECT RATIOS OF PAFBLOCK ELEMENT SUBDIVISION
C DIMENSIONS AND CORRECT IF BEYOND THE REQUIRED RATIO

c     WRITE(6,*)'PREVIOUS SUBDIVISIONS'
c     WRITE(6,*)N1,N2

      IF ((D1MAX/N1)/(D2MIN/N2).GT.RATIO) THEN
c       write(6,*)Ipaf
c       WRITE(6,*)'Old N1 VALUE = ',N1
        N1=1+N2*D1MAX/(RATIO*D2MIN)
        MASPCT = 1
c       WRITE(6,*)'NEW N1 VALUE = ',N1
      ENDIF
```

Fig. 5.32 Aspect ratio check

If these comparisons defined by equations (5.9a) and (5.9b) fail then the number of the subdivisions must be increased so that the comparisons no longer fail. New subdivision values of N1 and N2 then are defined by equations (5.36).

$$\frac{D1\,MAX}{N1} < 14.9 \times \frac{D2\,MIN}{N2} \tag{5.10a}$$

$$\frac{D1\,MAX}{N1} < 14.9 \times \frac{D2\,MIN}{N2} \tag{5.10b}$$

$$\frac{N2 \times D1\,MAX}{14.9 \times D2\,MIN} < N1 \tag{5.10c}$$

$$N1 = \frac{N2 \times D1\,MAX}{14.9 \times D2\,MIN} \tag{5.10d}$$

When the same rules are applied to equation (5.10a), N2 can be found from equation (5.10e).

$$N2 = \frac{N1 \times D2\,MAX}{14.9 \times D1\,MIN} \tag{5.10e}$$

If the comparison is successful then no further action is required. The calculations for N1 and N2 are repeated until there are no more changes to be made subject to the condition for mesh continuity across the boundaries of adjacent pafblocks. The shell, the right and left hand sides, the top and bottom regions, the last ring and the central region inside the tunnel pafblocks were each subdivided in order. The subdivision of any other regions was checked to ensure conformity with the earlier subdivision of the regions. Once any subdivision of a region had been undertaken, there was no way to revert to a previous subdivision. The selection of appropriate subdivision numbers is set by the clear flag 'MASPCT'.

```
C CLEAR FLAG, MASPCT, WHICH IS SET WHEN THE SUBDIVISIONS CHANGE

 20       MASPCT = 0

===========================================================
                 MAJORITY OF CODES OMITTED
===========================================================

C CHECK EXTREME ASPECT RATIOS OF PAFBLOCK ELEMENT SUBDIVISION
C DIMENSIONS AND CORRECT IF BEYOND THE REQUIRED RATIO

c     WRITE(6,*)'PREVIOUS SUBDIVISIONS'
c     WRITE(6,*)N1,N2

    IF ((D1MAX/N1)/(D2MIN/N2).GT.RATIO) THEN
c       write(6,*)Ipaf
c       WRITE(6,*)'Old N1 VALUE = ',N1
      N1=1+N2*D1MAX/(RATIO*D2MIN)
      MASPCT = 1
c       WRITE(6,*)'NEW N1 VALUE = ',N1
    ENDIF
IF ((D2MAX/N2)/(D1MIN/N1).GT.RATIO) THEN
c       write(6,*)Ipaf
c       WRITE(6,*)'OLD N2 VALUE = ',N2
      N2=1+N1*D2MAX/(RATIO*D1MIN)
      MASPCT = 1
c       WRITE(6,*)'NEW N2 VALUE = ',N2
    ENDIF

===========================================================
                 MAJORITY OF CODES OMITTED
===========================================================
C REPEAT ASPECT RATIO CHECK UNTIL THERE ARE NO MORE CHANGES TO
C THE SUBDIVISIONS

       IF ( MASPCT .NE. 0 ) GO TO 20

C CLEAR FLAG, MASPCT, WHICH IS SET WHEN THE SUBDIVISIONS CHANGE

       MASPCT = 0

C CHECK THAT RESULTING SUBDIVISION IS COMPATABLE WITH
C Z - SUBDIVISION

       CALL ZASP

C REPEAT SUBDIVISION UNTIL Z SUBDIVISION IS SATISFIED

    IF ( MASPCT .NE. 0 ) GO TO 10
    RETURN
    END
```

Fig. 5.33 Repeated aspect ratio check

The new subdivisions values of N1 and N2 then were assigned to the appropriate variable NSUBCO(-), NSUBRO(-) and NSUBSH(-) depending on the column, row and shell pafblocks respectively.

5.3.3 Extension to Three-Dimensional Problem

In the case of a three-dimensional problem the two-dimensional subdivision has to be fitted to the subdivision in the third dimension (z-direction). Two planes of nodes, the front and back, having the same two-dimensional pafblock subdivision are positioned so that they are separated by the period defined by the symmetry of the tunnel as shown in Fig. 5.34. This forms a rectangular block which can be simply subdivided into three-dimensional finite elements by the means of parallel planes, according to the previously established rules for the aspect ratio of the elements as given by equations (5.11). Since the shape of the pafblocks is prismatic a regular mesh can be used in this direction.

$$\frac{XMAX}{ZMIN} < 14.9 \tag{5.11a}$$

$$\frac{YMAX}{ZMIN} < 14.9 \tag{5.11b}$$

The maximum z-direction size of any pafblock subdivided element can be set and defined by equations (5.12).

$$\frac{XMAX}{ZMIN} \leq RATIO=14.9 \Rightarrow XMAX = RATIO \times ZMIN \tag{5.12a}$$

$$\frac{YMAX}{ZMIN} \leq RATIO=14.9 \Rightarrow YMAX = RATIO \times ZMIN \tag{5.12b}$$

$$\frac{XMIN}{ZMAX} \leq RATIO = 14.9 \Rightarrow XMIN = \frac{ZMAX}{RATIO} \tag{5.12c}$$

$$\frac{YMIN}{ZMAX} \leq RATIO = 14.9 \Rightarrow YMIN = \frac{ZMAX}{RATIO} \tag{5.12d}$$

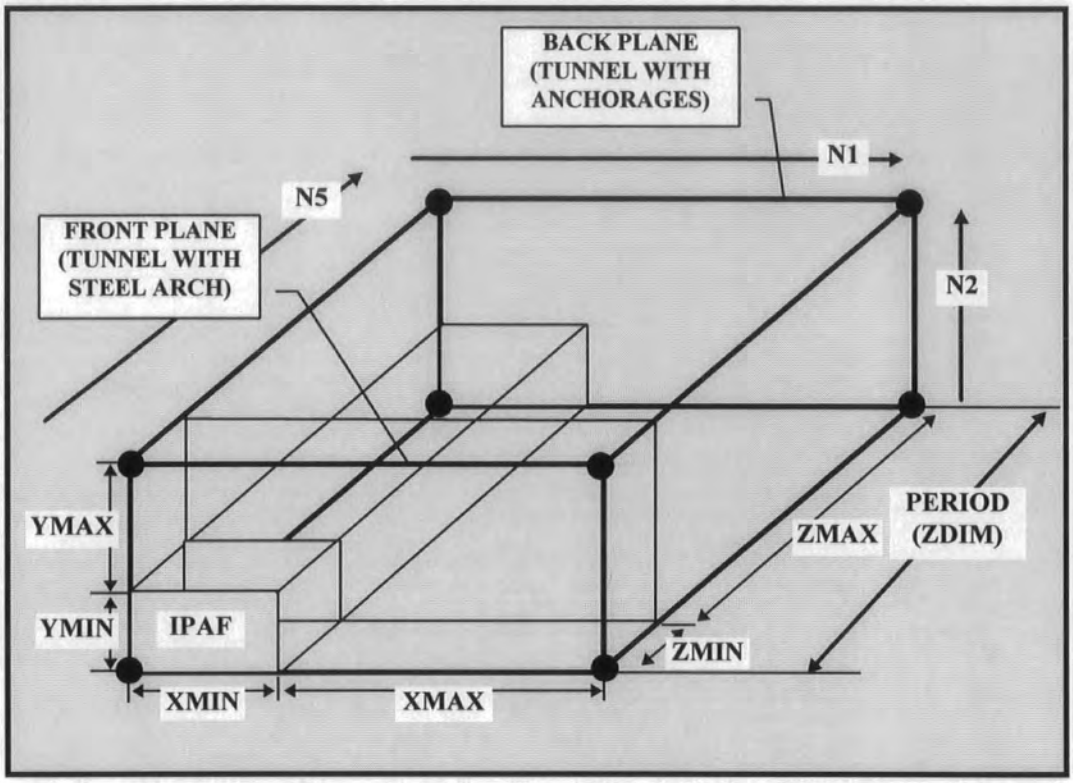

Fig. 5.34 A three-dimensional pafblock maximum and minimum sizes

The requirements for a three-dimensional pafblock subdivisions are shown in Table. 5.3.

$\frac{XMAX}{ZMAX} < 14.9$	$\frac{XMIN}{ZMAX} < 14.9$	$\frac{XMAX}{ZMIN} < 14.9$	$\frac{XMIN}{ZMIN} < 14.9$
$\frac{YMAX}{ZMAX} < 14.9$	$\frac{YMIN}{ZMAX} < 14.9$	$\frac{YMAX}{ZMIN} < 14.9$	$\frac{YMIN}{ZMIN} < 14.9$

Table 5.3 Requirements for a three-dimensional pafblock subdivision

The maximum and minimum dimension ratios of each direction were needed to find for each shell, column and row pafblock subdivided into elements for a three-dimensional model. This requires division of equation (5.12a) by (5.12c) and (5.12b) by (5.12d) as follows.

$$\frac{XMAX \le RATIO \times ZMIN}{\frac{ZMAX}{RATIO} \le XMIN} \tag{5.13a}$$

$$\frac{XMAX}{XMIN} \le (RATIO)^2 \times \frac{ZMIN}{ZMAX} \tag{5.13b}$$

$$\frac{YMAX \le RATIO \times ZMIN}{\frac{ZMAX}{RATIO} \le YMIN} \tag{5.13c}$$

$$\frac{YMAX}{YMIN} \le (RATIO)^2 \times \frac{ZMIN}{ZMAX} \tag{5.13d}$$

where the ratio is equal 14.9. Equations (5.13b) and (5.13d) automatically satisfy the requirements for the aspect ratio for any element in each subdivided pafblock. Equations (5.13b) and (5.13d) can be rewritten as follows.

$$\frac{DMAX}{DMIN} \le (RATIO)^2 \times \frac{ZMIN}{ZMAX} \tag{5.14}$$

If the resulting three-dimensional subdivisions cause warnings in aspect ratios, then the two-dimensional mesh has to be refined until the three-dimensional mesh is acceptable. This is undertaken by the subroutine 'SUBDIV' as shown in Fig. 5.35. If the iteration for the subdivision changes is repeated more than ten times pre-processing program stops and gives warning as 'conflict in geometry'. The resolution number then has to be increased to achieve a finer mesh.

```
C ==========================================================
C SUBROUTINE SUBDIV FOR PAFBLOCK SUBDIVISION, FOR MAX ELEMENT
C SIZE AND ASPECT RATIO ASPECT
C ==========================================================

      SUBROUTINE SUBDIV

      IMPLICIT DOUBLE PRECISION  (A-H,O-Z)

      COMMON / CSUBDV / NSUB(0:50),MASPCT
      COMMON / CDIM   / DIM(4), DMIN, DMAX, IPMAX, IPMIN

C SUBDIVIDE Z DIRECTION
      ipmax = 0
      ipmin = 0

      CALL ZSUBB

      IT=0

C SET MAXIMUM SIZE OF ELEMENTS

 10   CALL MAXSI
      CALL WRTMAX

C CLEAR FLAG, MASPCT, WHICH IS SET WHEN THE SUBDIVISIONS CHANGE

 20     MASPCT = 0

C ITERATION COUNTER

        IT=IT+1
        WRITE(6,*)'ITERATION = ',IT

C STOP IF REPEATED MORE THAN 10 TIMES

        IF (IT .GT. 10) WRITE(6,*)'Conflict in Geometry !!'
        IF (IT .GT. 10) STOP

C INITIALIZE GLOBAL MINIMUM AND MAXIMUM ELEMENT SIZE
C WITH DUMMY VALUES
        DMIN = 1D2
        DMAX = 0D0

C ASPECT RATIO CHECK
        CALL SHASP
        CALL RLASP
        CALL TPASP
        CALL BTASP
        CALL LRASP
        CALL ITASP
```

Continued on next page

Continued from previous page

```
C ==========================================================
C SUBROUTINE ASPCHT RATIO CHECK
C ==========================================================

      SUBROUTINE ASPCHK (IPAF,N1,N2)

      IMPLICIT DOUBLE PRECISION  (A-H,O-Z)

      COMMON / CDIM   / DIM(4), DMIN, DMAX, IPMAX, IPMIN
      COMMON / CRESNI / NZ, ZSIZE, RATIO
      COMMON / CSUBDV / NSUB(0:50),MASPCT
==========================================================
                MAJORITY OF CODES OMITTED
==========================================================
C CHECK MAXIMUM ELEMENT SIZE AGAINST ZSIZE
      IF (D1MAX/N1.GT.ZSIZE) THEN
c       write(6,*)Ipaf
c       WRITE(6,*)'Old N1 VALUE = ',N1
        N1=1+D1MAX/ZSIZE
        MASPCT = 1
c       WRITE(6,*)'NEW N1 VALUE = ',N1
      ENDIF
      IF (D2MAX/N2.GT.ZSIZE) THEN
c       write(6,*)Ipaf
c       WRITE(6,*)'OLD N2 VALUE = ',N2
        N2=1+D2MAX/ZSIZE
        MASPCT = 1
c       WRITE(6,*)'NEW N2 VALUE = ',N2
      ENDIF
c     WRITE(6,*)'NEW SUBDIVISIONS'
c     WRITE(6,*)N1,N2

C FIND MAXIMUM AND MINIMUM ELEMENT SIZES OF XY-PLANE

      IF (D1MAX/N1.GT.DMAX) IPMAX=10000+IPAF
      IF (D2MAX/N2.GT.DMAX) IPMAX=20000+IPAF
      IF (D1MAX/N1.GT.DMAX) DMAX=D1MAX/N1
      IF (D2MAX/N2.GT.DMAX) DMAX=D2MAX/N2
      IF (D1MIN/N1.LT.DMIN) IPMIN=10000+IPAF
      IF (D2MIN/N2.LT.DMIN) IPMIN=20000+IPAF
      IF (D1MIN/N1.LT.DMIN) DMIN=D1MIN/N1
      IF (D2MIN/N2.LT.DMIN) DMIN=D2MIN/N2

      RETURN
      END
```

Fig. 5.35 General structure of the pafblock subdivision and aspect ratio

The z-direction subdivision provides the required aspect ratio for the extreme element dimension in the x-y plane and it was checked that z-subdivision is compatible with the minimum and maximum x-y element size as shown in Fig. 5.36. If this is not compatible a new subdivision is started using the subroutine 'ZASP' as shown in figure.

```
C=======================================================================
C SUBROUTINE ZASP FOR Z-DIRECTION SUBDIVISION
C ASPECT RATIO INSIDE THE TUNNEL
C=======================================================================
      SUBROUTINE ZASP
      IMPLICIT DOUBLE PRECISION  (A-H,O-Z)
      COMMON / CDIM   / DIM(4), DMIN, DMAX, IPMAX, IPMIN
      COMMON / CRESNI / NZ, ZSIZE, RATIO
      COMMON / CSUBDV / NSUB(0:50),MASPCT
      COMMON / CZNOD  / Z(5), NDEPTH
      COMMON / CSHLPR / NSHELL, HIN(5),SUMR
      COMMON / COUNT  / KPSH(8), NPSIDE, NCOL, NROW
      COMMON / CSUPIN / SAMIN, SAMAJ, HANCH(2), DANCH(2),
     &                  RANCH,AANCH(2),PERIOD, SANCH, SAMAJ2,
     &                  MARCH,MPARCH,MANCH,MPANCH
C CHECK IF A Z-SUBDIVISION WHICH PROVIDES THE REQUIRED
C ASPECT RATIO
C FOR THE EXTREME ELEMENT DIMENSIONS IN THE XY-PLANE IS
C POSSIBLE. IF IMPOSSIBLE STOP PROGRAM.
      IF (DMAX/DMIN.GE.RATIO*RATIO)
     &  WRITE(6,*)'Geometry Conflict in Z-Subdivision'
      IF (DMAX/DMIN.GE.RATIO*RATIO) STOP
C FOR EACH PLANE OF PAFBLOCKS
      DO 10 I=1,NDEPTH
        J=I+NSHELL+NCOL+NROW
        ZDIM = DABS (Z(I+1) - Z(I))
C ENSURE THAT Z-SUBDIVISION IS COMPATABLE WITH MINIMUM
C XY-ELEMENT SIZE
        IF (DMIN*RATIO.LT.ZDIM/NSUB(J)) THEN
          NSUB(J) = 1+ ZDIM / (RATIO * DMIN)
        ENDIF
C CHECK THAT Z-SUBDIVISION IS COMPATABLE WITH MAXIMUM
C XY-ELEMENT SIZE
C IF NOT REDO SUBDIVISION FROM START WITH NEW MAXIMUM
C ELEMENT SIZE
        IF (DMAX/RATIO.GT.ZDIM/NSUB(J)) THEN
          MASPCT = 1
          ZSIZE = RATIO*ZDIM/NSUB(J)
        ENDIF
 10   CONTINUE
      RETURN
      END
```

Fig. 5.36 Third dimension pafblock subdivision and aspect ratio

CHAPTER 6

POST-PROCESSING PROGRAMS

6.1 Introduction

The textual output files from PAFEC-FE just consist of rows of numbers and cannot be directly formatted to suit the requirements of the user. Although PAFEC-FE does have interactive graphics software (PIGS) this is fairly limited in its ability to process large amounts of data. This lack of adequate post-processing facilities dictated that a number of additional supplementary computer programs were written to reformat the textual output files and process the mesh, stress and displacement outputs for graphical display. In this way repeated use could be made of PAFEC-FE without time-consuming and error prone manual retrieval of data either for further computation or graphical output. There are two main categories of programs as shown in Fig. 6.1.

The first type of programs 'getin', 'dispget' and 'stressget' that were developed for this work were concerned with data post processing. Many of these were created to extract mesh information and results, and place them in files with formats suitable for use by the second type of post-processing program. This type of program was developed to deal with the transformation of the output text files of the first type of program and convert them to graphical output producing coloured representations of the model stresses and distortions. The output from these files appears much the same as other graphical output from other finite element packages.

In order to produce pictures of this quality and flexibility, the second type of program 'indistress' was written and UNIRAS subroutines were used. This library of subroutines contains ready pieces of FORTRAN code for a large number of applications from hidden line removal, shading and contouring to data manipulation such as complex grid interpolation routines.

The programs themselves are versatile. Post-processing programs have to be called and run depending on the particular output required such as diagrams of unexcavated ground showing rock strata, model mesh diagrams, shaded contour diagrams, displaced shape diagrams and diagrams of the excavated tunnel with

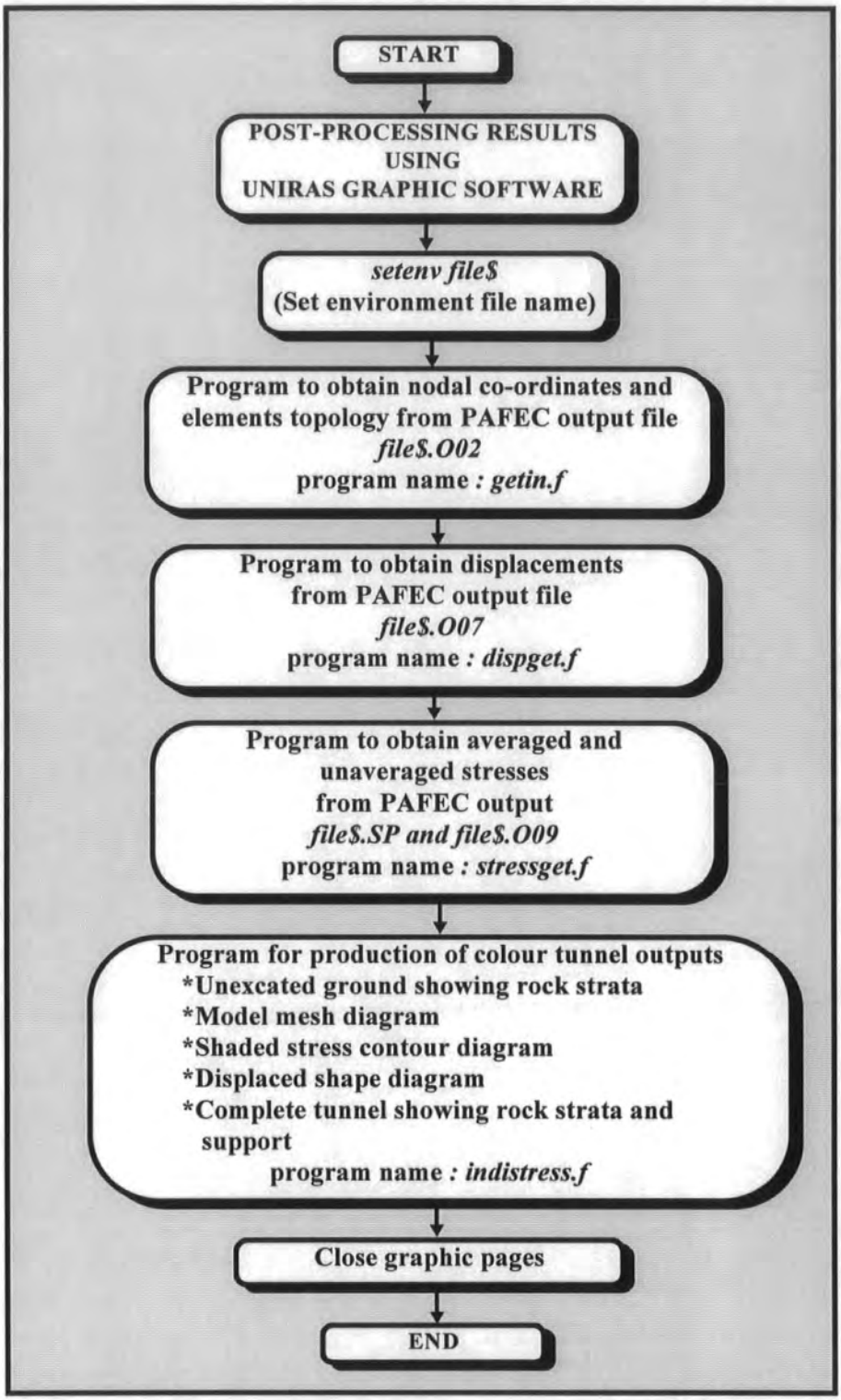

Fig. 6.1 Main flow diagram for post-processing of programs

support systems and complete diagrams showing the rock strata and support. They collectively form a very acceptable post-processor for PAFEC-FE.

The majority of post-processing programs were straightforward to design and performed the production of different models with greater accuracy and speed than any produced by PIGS. Although each one had a single function all could be adapted by changing variables to perform that operation on different models and meshes of any size. A very efficient system was thus created which could perform a very practical use. The post processing program output results can also be imported into spreadsheets using file transfer programs (ftp) to get more detailed analysis. It was relatively simple to construct a sheet containing all the nodes and their stress and displacement results.

6.2 Data Processing Programs

The FORTRAN post-processing programs provide respectively node co-ordinates and element topologies, displacements and stress data for the simulations. The program 'getin' was written to retrieve data from the PAFEC-FE output file *(file$.O02)*. It obtains geometric data from the node co-ordinates and element topologies for the creation of the solid models as shown in Fig. 6.2. Programs 'dispget' and 'stressget' concern displacement and stress values and these retrieve data from PAFEC-FE output files *(file$.O07)* and *(file$.O09)* respectively as shown in Figs. 6.3 and 6.4. All data from these programs were stored and superimposed on the solid models in a suitable format to be used by the graphic generation program 'indistress' as shown in Fig 6.11. Data processing programs also rearrange retrieved values from the files created and produce a list of stresses and displacements for each node and element.

Two post-processing programs were written for specific tasks, namely gravity difference method and reverse stress technique. 'stressget' was written to retrieve data from PAFEC-FE output files*(file$.O09, file$.SP)* for reverse stress technique and store it in a suitable format files *(file$.ASTRDAT or file$.USTRDAT)* and to be used by the graphics generation program UNIRAS. Second program 'gdstress' was written for gravity difference method as described in Chapter 4.

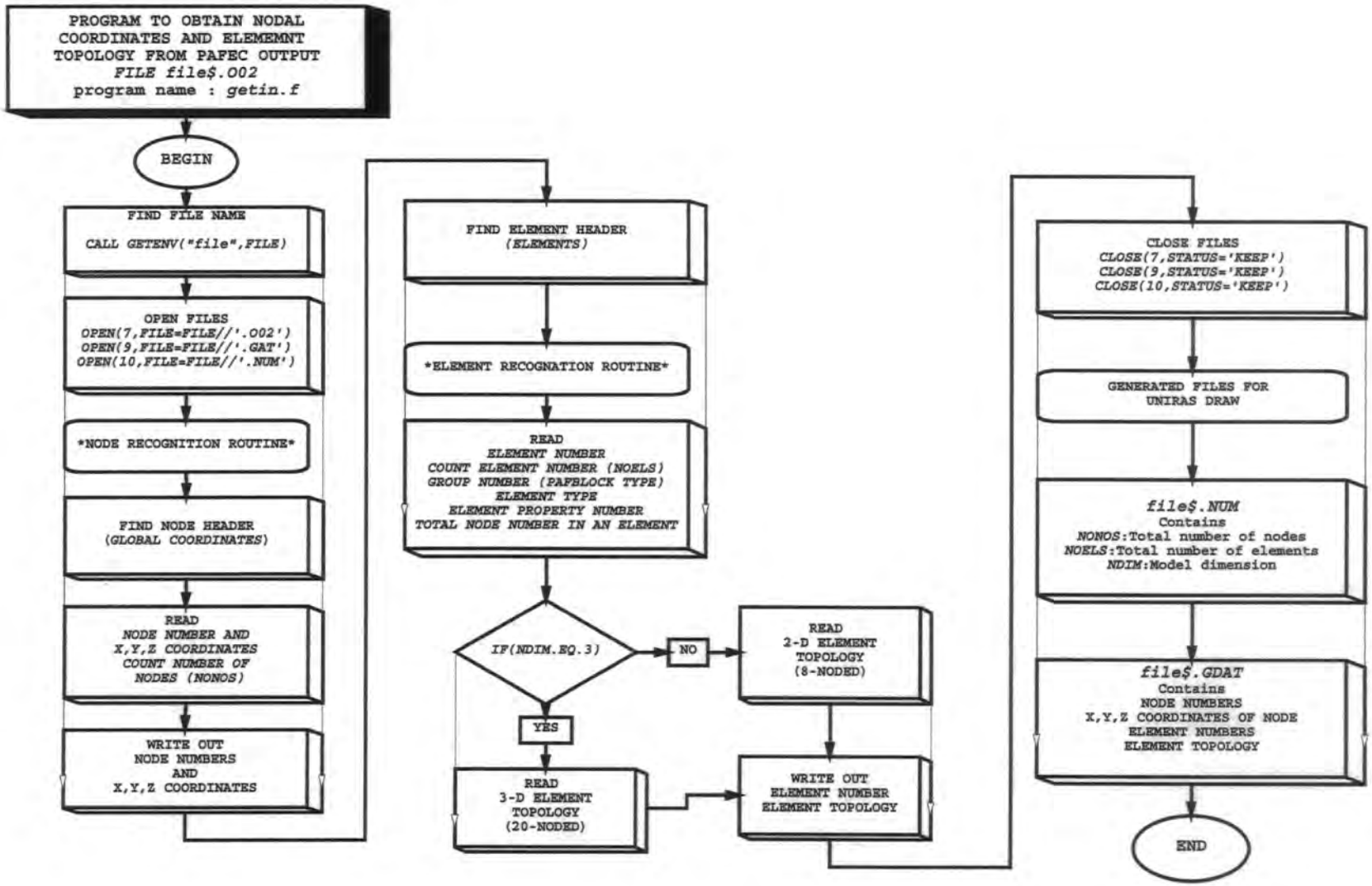

Fig. 6.2 Post-processing of nodal co-ordinates and element topology

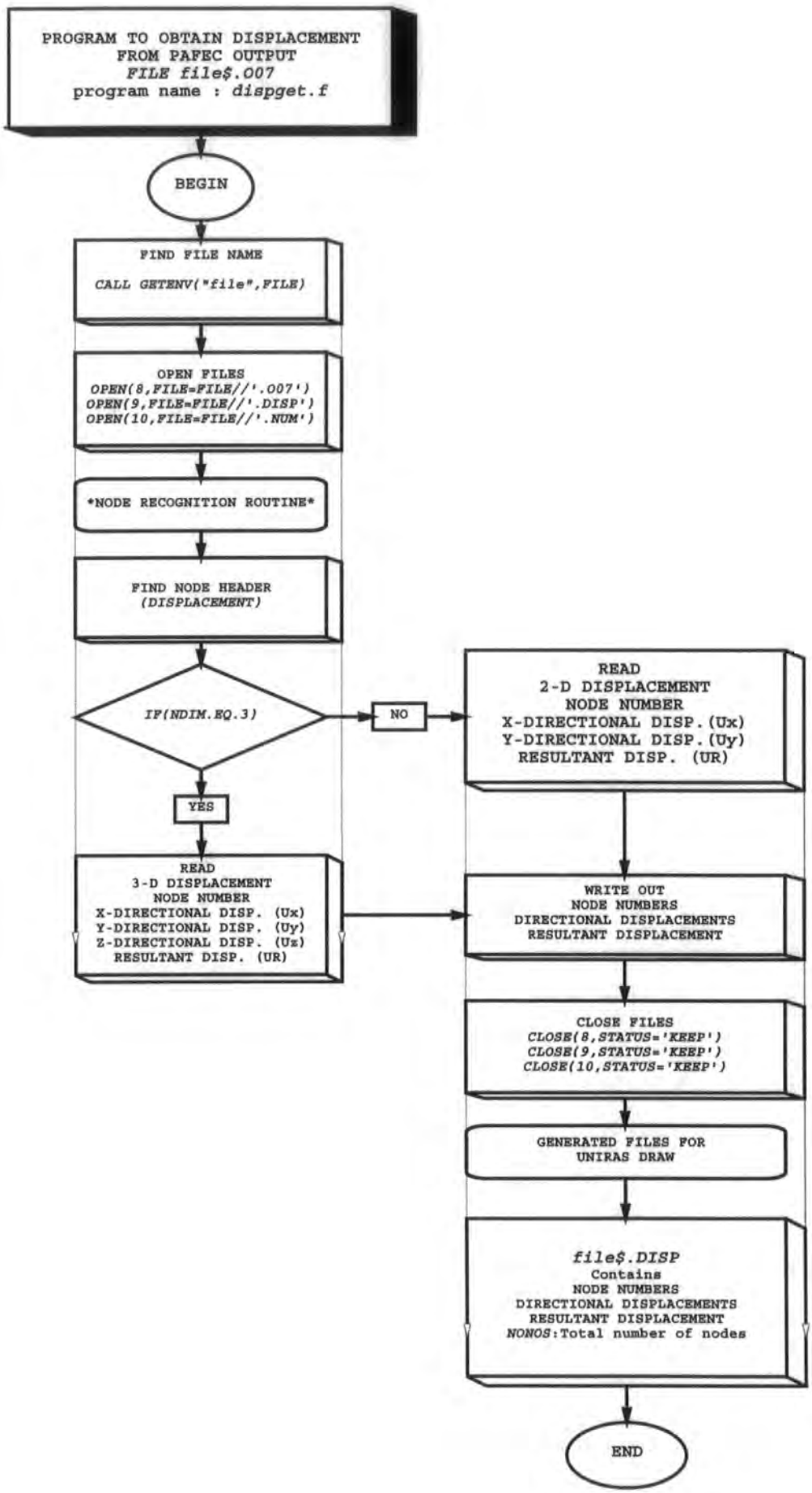

Fig. 6.3 Post-processing of displacement results

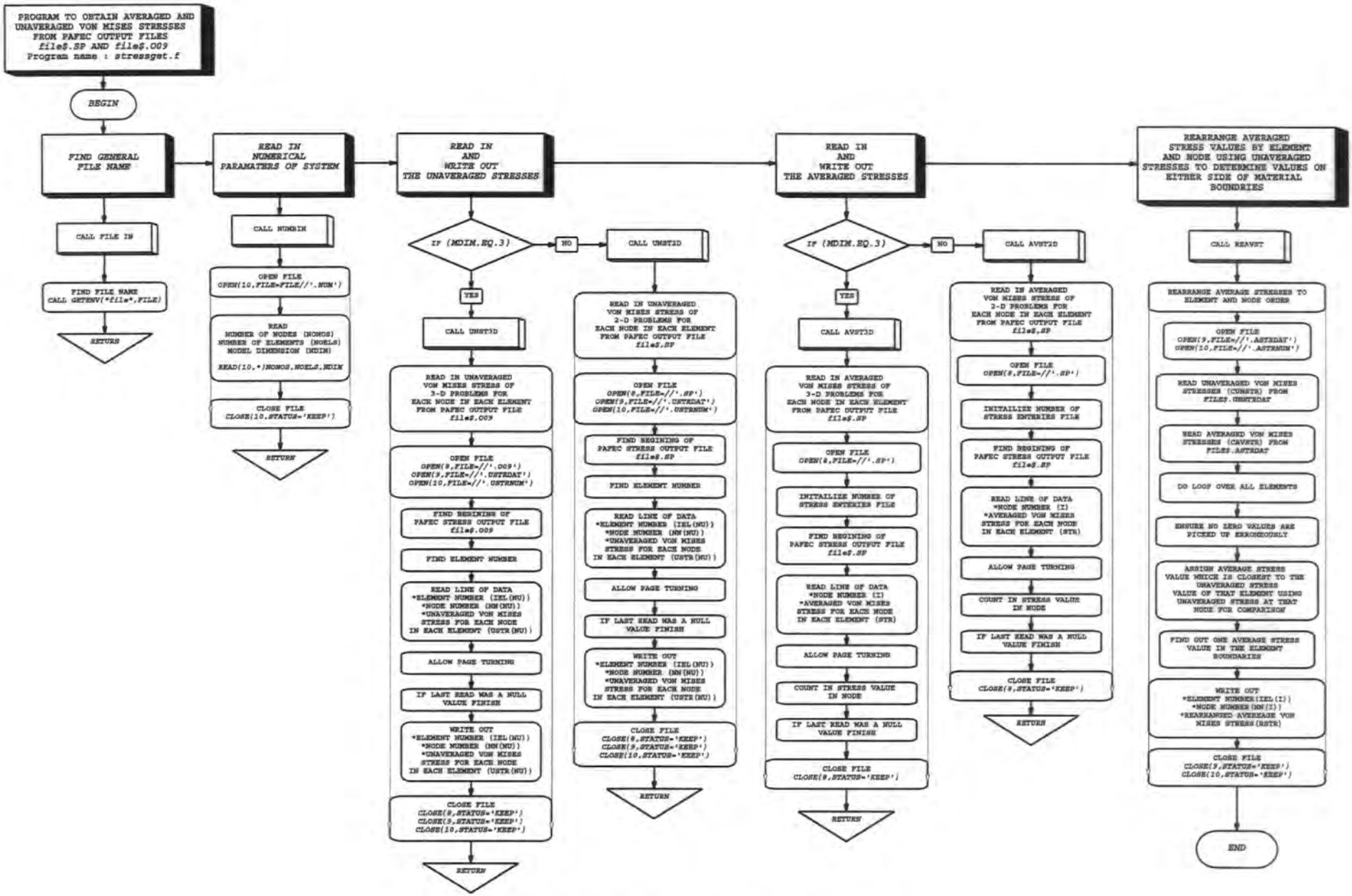

Fig. 6.4 Post-processing of stress results

6.2.1 Averaged and Unaveraged Stress Concept

After a period of investigation it was decided that the following outline would be implemented. Two post-processing programs were written for specific tasks, namely the gravity difference method and the reverse stress technique and averaged and unaveraged stress data were retrieved from the output files*(file$.O09, file$.SP)* and stored in a suitably formatted files *(file$.ASTRDAT or file$.USTRDAT)* to be used by the graphics generation program UNIRAS.

During gravity difference analysis Von Mises (the equivalent) stress should not be subtracted directly. However the equivalent stress is calculated from global stress tensor components (σ_{xx}, σ_{yy}, σ_{zz}, τ_{xy}, τ_{yz}, τ_{zx}) which can be subtracted. The *file$.O09* stress output file of PAFEC-FE does not provide the shear stress values (τ_{xy}, τ_{yz}, τ_{zx}) hence the directional stresses are incompletely known and their differences can not be obtained. However directional stresses can be written to the file *(file$.SP)* using the ORDER FOR PRINTED OUTPUT module which uses code numbers for required stress types. The code number '103' to be used in the LIST OF TYPES column in the ORDER FOR PRINTED OUTPUT module refers to the element numbers. If the reference code '103' appears in the LIST OF TYPES then the output values will be unaveraged nodal stresses for each element. The code number '102' refers to node numbers. If '102' appears in the LIST OF TYPES column then the output values will be averaged values of nodal Von Mises and directional stresses which are stored in a suitably formatted file *(file$.ASTRDAT)*. Only unaveraged values are available in the output of stresses for beam elements.

For two-dimensional examples, the averaged and unaveraged stresses are written to the file *(file$.SP)*. For the three-dimensional case when unaveraged stresses are requested the output file *(file$.SP)* does not appear. In this case only the unaveraged nodal Von Mises stresses for each element are obtained from the file *(file$.O09)* and stored in a suitably formatted file *(file$.USTRDAT)*, because shear stress values (τ_{xy}, τ_{yz}, τ_{zx}) are not available in the output file *(file$.O09)*.

Because stresses depend on the material properties, the averaged stresses have two values at the material boundaries and determining which stress belongs to which material is uncertain. In this case for the two- and three-dimensional heterogeneous models, it is not possible to tell from the output file *(file$.SP)* for the averaged stresses to which element the nodal stress refers. In order to resolve this it is necessary to return to the unaveraged nodal stresses for each element output file *(file$.SP)* to determine this and hence relate the outputs from both files. The stages required to carry out this are as shown in Fig. 6.4.

Normally for two-dimensional examples this is decided with reference to the unaveraged stress order file *(file$.SP)*. Therefore in order to make the same decision without the unaveraged directional stresses *(file$.SP)* for the three-dimensional model, the averaged stresses are read in from *file$.SP* for unexcavated and excavated models and then unaveraged Von Mises stresses are read in from *file$.O09* for unexcavated and excavated models. After that the unaveraged Von Mises stress values which are closest to the averaged values for the unexcavated and excavated models are used to determine average stresses in the material boundary. Finally, using the values of the rearranged average Von Mises stress, the average directional stresses are found from the file *(file$.SP)* and stored in suitably formatted files *(file$.ASTRDAT or file$.USTRDAT)* to be used by the graphics generation program UNIRAS.

For the gravity difference method, the values of the average directional stresses for the excavated ground are subtracted from those for the unexcavated ground. Then the averaged Von Mises stress for each node is calculated by a given formula in Chapter 3.

In the case of averaged nodal stress output for the three-dimensional heterogeneous model, it is not possible to tell from the output to which element the nodal stress refers. In order to resolve this it is necessary to return to the output file *(file$.O09)* in order to determine this and hence relate the outputs from both files.

The stages required to carry out these procedures are as follows. The post-processor allows sorting of the output where the user specifies a particular stress. The PROCESSING FOR PRINTED OUTPUT module references an other module

ORDER FOR PRINTED OUTPUT as described in Chapter 4. These modules form a set in a prescribed order. The set must be separately specified for two-dimensional and three-dimensional output and must not be mixed. The ORDER column is determined by the order of the code numbers for stress types given in the LIST OF TYPES module. The ORDER column in the ORDER FOR PRINTED OUTPUT module is the same as the ORDER column in the PROCESSING FOR PRINTED OUTPUT module. The code numbers of the different stress types are as follows. There is no set code number for two- or three-dimensional output. If required, at least one of the code numbers '101', '102' and '103' must be given in the LIST OF TYPE column. The directional stress can be written to the requested *file$.SP* file using ORDER FOR PRINTED OUTPUT module. The code numbers to be used in the LIST OF TYPES column are shown in Table 4.3.

6.2.1.1 Two-Dimensional Model

The eight noded quadrilateral element was used for the two-dimensional model as shown in Fig. 4.18. Two types of output can be obtained, averaged and unaveraged. For the averaged stress output, values from elements attached to a particular node are averaged. Partial averaging occurs when averaged output has been requested, but cannot be performed at the nodes joining elements in different materials.

For the homogeneous model as shown in Fig. 6.5, nodes 3, 4 and 10 have one nodal averaged stress value for each element number and a separate value for each adjacent element. The unaveraged stress output file *(file$.O09)* from phase 9 for a two-dimensional homogeneous model and the averaged stress output file *(file$.SP)* are shown in Tables 6.1 and 6.2 respectively.

For the heterogeneous model, as shown in Fig. 6.6, the averaged nodal stress has one value apart from material boundaries where it has one value for each material. The unaveraged nodal stresses for each element have separate values for each adjacent element at a material boundary. Material boundaries are not important for unaveraged stress values. For example, nodes 3 and 4 have four and node 10 has

two stress values. The stress output file *(file$.O09)* from phase 9 and the averaged and unaveraged stress output files *(file$.SP)* for the two-dimensional heterogeneous model are shown in Tables 6.3, 6.4 and 6.5 respectively. The underlined data in the tables are the important stress values for the nodes connecting the elements 1 and 2 in different materials as shown in Figs. 6.5 to 6.8.

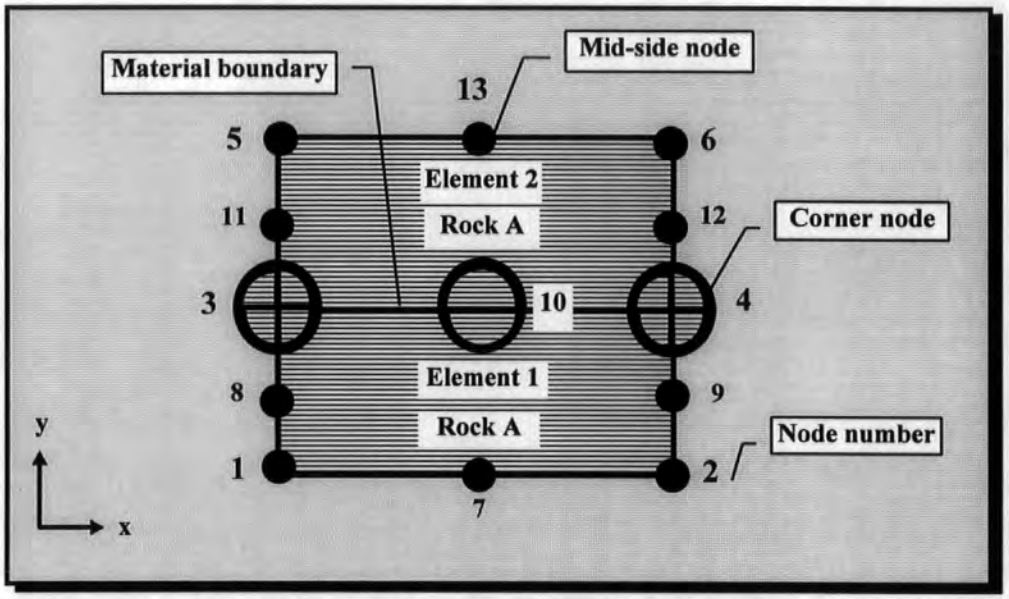

Fig. 6.5 Two-dimensional homogeneous model

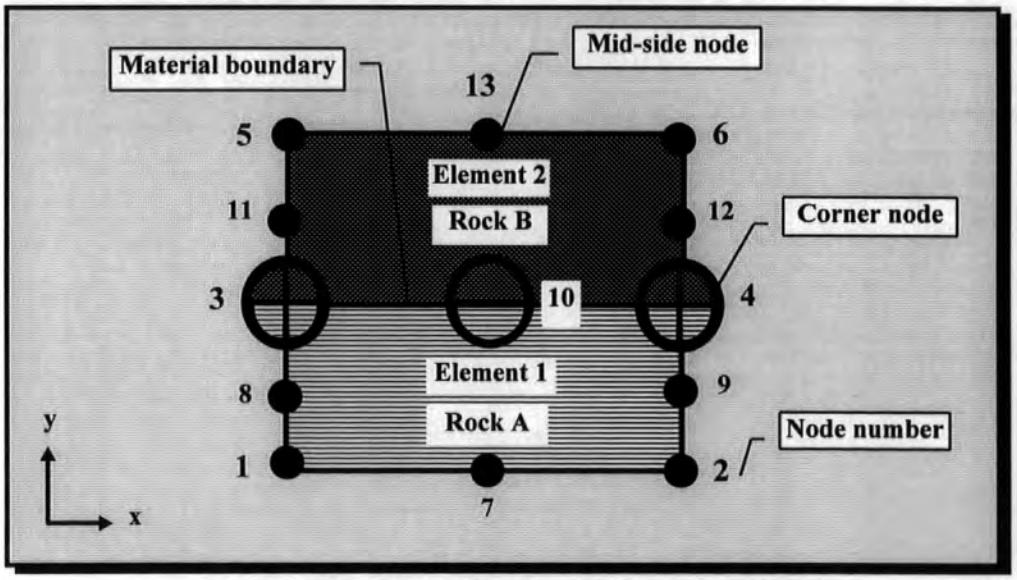

Fig. 6.6 Two-dimensional heterogeneous model

ELEM NO	LOAD CASE	NODE NO	PRINCIPAL.STRESSES SIGMA-1	SIGMA-2	SIGMA-3	MAX.SHEAR STRESS	ANG.OF.SIG-1 LOCAL	GLOBAL	ELEMENT.STRESSES SIGMA-X	SIGMA-Y	SIGMA-XY
1	1	1	-1.37E+04	-2.55E+04	-1.37E+04	5.89E+03	.0	.0	-1.37D+04	-2.55D+04	.00D+00
1	1	7	-1.37E+04	-2.55E+04	-1.37E+04	5.89E+03	.0	.0	-1.37D+04	-2.55D+04	-8.81D-13
1	1	2	-1.37E+04	-2.55E+04	-1.37E+04	5.89E+03	.0	.0	-1.37D+04	-2.55D+04	.00D+00
1	1	8	-1.03E+04	-1.91E+04	-1.03E+04	4.41E+03	.0	.0	-1.03D+04	-1.91D+04	4.85D-04
1	1	*	-1.03E+04	-1.91E+04	-1.03E+04	4.41E+03	.0	.0	-1.03D+04	-1.91D+04	-8.81D-13
1	1	9	-1.03E+04	-1.91E+04	-1.03E+04	4.41E+03	.0	.0	-1.03D+04	-1.91D+04	-4.85D-04
1	1	3	-6.87E+03	-1.28E+04	-6.87E+03	2.94E+03	.0	.0	-6.87D+03	-1.28D+04	9.70D-04
1	1	10	-6.87E+03	-1.28E+04	-6.87E+03	2.94E+03	.0	.0	-6.87D+03	-1.28D+04	-8.81D-13
1	1	4	-6.87E+03	-1.28E+04	-6.87E+03	2.94E+03	.0	.0	-6.87D+03	-1.28D+04	-9.70D-04
2	1	3	-6.87E+03	-1.28E+04	-6.87E+03	2.94E+03	.0	.0	-6.87D+03	-1.28D+04	9.70D-04
2	1	10	-6.87E+03	-1.28E+04	-6.87E+03	2.94E+03	.0	.0	-6.87D+03	-1.28D+04	9.16D-13
2	1	4	-6.87E+03	-1.28E+04	-6.87E+03	2.94E+03	.0	.0	-6.87D+03	-1.28D+04	-9.70D-04
2	1	11	-3.43E+03	-6.38E+03	-3.43E+03	1.47E+03	.0	.0	-3.43D+03	-6.38D+03	4.85D-04
2	1	*	-3.43E+03	-6.38E+03	-3.43E+03	1.47E+03	.0	.0	-3.43D+03	-6.38D+03	-2.43D-04
2	1	12	-3.43E+03	-6.38E+03	-3.43E+03	1.47E+03	.0	.0	-3.43D+03	-6.38D+03	-9.70D-04
2	1	5	-3.22E-03	-6.48E-03	-3.40E-03	1.63E-03	13.3	13.3	-3.40D-03	-6.31D-03	7.28D-04
2	1	13	2.43E-04	-2.43E-04	.00E+00	2.43E-04	45.0	45.0	.00D+00	.00D+00	2.43D-04
2	1	6	8.42E-03	4.51E-03	4.53E-03	1.96E-03	-86.4	-86.4	4.53D-03	8.41D-03	-2.43D-04

Table 6.1 2-D homogeneous model, elements 1 and 2 stress output *file$.O09*

NODE NO.	SIG MISES	SIG XX	SIG YY	SIG ZZ	TAU XY	TAU YZ	TAU ZX
1	1.1772E+04	-1.3734E+04	-2.5506E+04	-1.3734E+04	-3.0702E-01	-9.2107E-02	-2.3991E-06
2	1.1772E+04	-1.3734E+04	-2.5506E+04	-1.3734E+04	-3.0702E-01	-9.2107E-02	-2.3991E-06
3	5.8860E+03	-6.8670E+03	-1.2753E+04	-6.8670E+03	4.6755E-02	4.6053E-02	-3.6880E-07
4	5.8860E+03	-6.8670E+03	-1.2753E+04	-6.8670E+03	-1.5421E-01	-4.6054E-02	-1.2033E-06
5	3.1715E-03	-3.3955E-03	-6.3058E-03	-3.3954E-03	7.2761E-04	2.3779E-08	-4.2328E-09
6	3.9032E-03	4.5273E-03	8.4078E-03	4.5273E-03	-2.4256E-04	-3.0428E-08	1.7763E-09
7	1.1772E+04	-1.3734E+04	-2.5506E+04	-1.3734E+04	-3.0702E-01	-9.2107E-02	-2.3991E-06
8	8.8290E+03	-1.0301E+04	-1.9130E+04	-1.0301E+04	6.9080E-02	6.9079E-02	-5.4389E-07
9	8.8290E+03	-1.0301E+04	-1.9130E+04	-1.0301E+04	-2.3026E-01	-6.9080E-02	-1.7956E-06
10	5.8860E+03	-6.8670E+03	-1.2753E+04	-6.8670E+03	-1.5351E-01	-4.6054E-02	-1.1995E-06
11	2.9430E+03	-3.4335E+03	-6.3765E+03	-3.4335E+03	2.3377E-02	2.3026E-02	-1.8440E-07
12	2.9430E+03	-3.4335E+03	-6.3765E+03	-3.4335E+03	-7.7807E-02	-2.3027E-02	-6.0722E-07
13	4.2008E-04	0.0000E+00	3.7835E-09	0.0000E+00	2.4253E-04	2.6836E-09	0.0000E+00

Table 6.2 2-D homogeneous model, elements 1 and 2 averaged stress output *file$.SP*

ELEM NO	LOAD CASE	NODE NO	..PRINCIPAL.STRESSES.. SIGMA-1	SIGMA-2	SIGMA-3	MAX.SHEAR STRESS	ANG.OF.SIG-1 LOCAL	GLOBAL	ELEMENT.STRESSES..... SIGMA-X	SIGMA-Y	SIGMA-XY
1	1	1	-1.27E+04	-2.35E+04	-1.27E+04	5.43E+03	.0	.0	-1.27D+04	-2.35D+04	.00D+00
1	1	7	-1.27E+04	-2.35E+04	-1.27E+04	5.43E+03	.0	.0	-1.27D+04	-2.35D+04	-4.98D-05
1	1	2	-1.27E+04	-2.35E+04	-1.27E+04	5.43E+03	.0	.0	-1.27D+04	-2.35D+04	.00D+00
1	1	8	-9.24E+03	-1.72E+04	-9.24E+03	3.96E+03	.0	.0	-9.24D+03	-1.72D+04	4.85D-04
1	1	*	-9.24E+03	-1.72E+04	-9.24E+03	3.96E+03	.0	.0	-9.24D+03	-1.72D+04	-4.98D-05
1	1	9	-9.24E+03	-1.72E+04	-9.24E+03	3.96E+03	.0	.0	-9.24D+03	-1.72D+04	-4.85D-04
1	1	3	-5.81E+03	-1.08E+04	-5.81E+03	2.49E+03	.0	.0	-5.81D+03	-1.08D+04	9.70D-04
1	1	10	-5.81E+03	-1.08E+04	-5.81E+03	2.49E+03	.0	.0	-5.81D+03	-1.08D+04	-4.98D-05
1	1	4	-5.81E+03	-1.08E+04	-5.81E+03	2.49E+03	.0	.0	-5.81D+03	-1.08D+04	-9.70D-04
2	1	3	-7.19E+03	-1.08E+04	-7.19E+03	1.80E+03	.0	.0	-7.19D+03	-1.08D+04	4.68D-05
2	1	10	-7.19E+03	-1.08E+04	-7.19E+03	1.80E+03	.0	.0	-7.19D+03	-1.08D+04	1.38D-05
2	1	4	-7.19E+03	-1.08E+04	-7.19E+03	1.80E+03	.0	.0	-7.19D+03	-1.08D+04	-4.68D-05
2	1	11	-3.60E+03	-5.40E+03	-3.60E+03	8.99E+02	.0	.0	-3.60D+03	-5.40D+03	1.17D-04
2	1	*	-3.60E+03	-5.40E+03	-3.60E+03	8.99E+02	.0	.0	-3.60D+03	-5.40D+03	1.38D-05
2	1	12	-3.60E+03	-5.40E+03	-3.60E+03	8.99E+02	.0	.0	-3.60D+03	-5.40D+03	-1.17D-04
2	1	5	7.64E-05	-3.22E-04	-9.84E-05	1.99E-04	34.9	34.9	-5.41D-05	-1.92D-04	1.87D-04
2	1	13	1.44E-04	8.98E-05	9.35E-05	2.72E-05	74.7	74.7	9.35D-05	1.40D-04	1.38D-05
2	1	6	-1.56E-04	-5.33E-04	-2.76E-04	1.89E-04	-41.3	-41.3	-3.20D-04	-3.69D-04	-1.87D-04

Table 6.3 2-D heterogeneous model, elements 1 and 2 *stress* output *file$.O09*

NODE NO.	SIG MISES	SIG XX	SIG YY	SIG ZZ	TAU XY	TAU YZ	TAU ZX
1	1.0866E+04	-1.2678E+04	-2.3544E+04	-1.2678E+04	-2.8340E-01	-8.5022E-02	-2.2054E-06
2	1.0866E+04	-1.2678E+04	-2.3544E+04	-1.2678E+04	-2.8340E-01	-8.5022E-02	-2.1979E-06
3	4.9805E+03	-5.8105E+03	-1.0791E+04	-5.8105E+03	3.9562E-02	3.8968E-02	-3.1292E-07
3	3.5970E+03	-7.1940E+03	-1.0791E+04	-7.1940E+03	2.8144E-02	2.8143E-02	-2.1979E-07
4	4.9805E+03	-5.8105E+03	-1.0791E+04	-5.8105E+03	-1.2979E-01	-3.8968E-02	-1.0096E-06
4	3.5970E+03	-7.1940E+03	-1.0791E+04	-7.1940E+03	-1.4072E-01	-2.8144E-02	-1.0952E-06
5	3.4624E-04	-5.4093E-05	-1.9197E-04	-9.8427E-05	1.8710E-04	2.2198E-09	1.1939E-10
6	3.3404E-04	-3.2010E-04	-3.6931E-04	-2.7577E-04	-1.8710E-04	-2.1334E-09	-6.2481E-10
7	1.0866E+04	-1.2678E+04	-2.3544E+04	-1.2678E+04	-2.8340E-01	-8.5022E-02	-2.2054E-06
8	7.9235E+03	-9.2440E+03	-1.7168E+04	-9.2440E+03	6.2939E-02	6.1994E-02	-4.9174E-07
9	7.9235E+03	-9.2440E+03	-1.7168E+04	-9.2440E+03	-2.0759E-01	-6.1995E-02	-1.6168E-06
10	4.9805E+03	-5.8105E+03	-1.0791E+04	-5.8105E+03	-1.2989E-01	-3.8968E-02	-1.0133E-06
10	3.5970E+03	-7.1940E+03	-1.0791E+04	-7.1940E+03	2.8144E-02	2.8143E-02	-2.1979E-07
11	1.7985E+03	-3.5970E+03	-5.3955E+03	-3.5970E+03	1.4286E-02	1.4072E-02	-1.1176E-07
12	1.7985E+03	-3.5970E+03	-5.3955E+03	-3.5970E+03	-7.0573E-02	-1.4072E-02	-5.5134E-07
13	5.2551E-05	9.3549E-05	1.4032E-04	9.3548E-05	1.3831E-05	3.8937E-10	7.5834E-11

Table 6.4 2-D heterogeneous model, elements 1 and 2 averaged stress output *file$.SP*

ELEMENT NUMBER	NODE NO.	SIG MISES	SIG XX	SIG YY	SIG ZZ	TAU XY	TAU YZ	TAU ZX
1	1	1.0866E+04	-1.2678E+04	-2.3544E+04	-1.2678E+04	0.0000E+00	0.0000E+00	0.0000E+00
1	7	1.0866E+04	-1.2678E+04	-2.3544E+04	-1.2678E+04	-4.9792E-05	0.0000E+00	0.0000E+00
1	2	1.0866E+04	-1.2678E+04	-2.3544E+04	-1.2678E+04	0.0000E+00	0.0000E+00	0.0000E+00
1	8	7.9235E+03	-9.2440E+03	-1.7168E+04	-9.2440E+03	4.8506E-04	0.0000E+00	0.0000E+00
1	9	7.9235E+03	-9.2440E+03	-1.7168E+04	-9.2440E+03	-4.8506E-04	0.0000E+00	0.0000E+00
1	3	4.9805E+03	-5.8105E+03	-1.0791E+04	-5.8105E+03	9.7013E-04	0.0000E+00	0.0000E+00
1	10	4.9805E+03	-5.8105E+03	-1.0791E+04	-5.8105E+03	-4.9792E-05	0.0000E+00	0.0000E+00
1	4	4.9805E+03	-5.8105E+03	-1.0791E+04	-5.8105E+03	-9.7013E-04	0.0000E+00	0.0000E+00
2	3	3.5970E+03	-7.1940E+03	-1.0791E+04	-7.1940E+03	4.6774E-05	0.0000E+00	0.0000E+00
2	10	3.5970E+03	-7.1940E+03	-1.0791E+04	-7.1940E+03	1.3830E-05	0.0000E+00	0.0000E+00
2	4	3.5970E+03	-7.1940E+03	-1.0791E+04	-7.1940E+03	-4.6774E-05	0.0000E+00	0.0000E+00
2	11	1.7985E+03	-3.5970E+03	-5.3955E+03	-3.5970E+03	1.1694E-04	0.0000E+00	0.0000E+00
2	12	1.7985E+03	-3.5970E+03	-5.3955E+03	-3.5970E+03	-1.1694E-04	0.0000E+00	0.0000E+00
2	5	3.4624E-04	-5.4092E-05	-1.9197E-04	-9.8427E-05	1.8710E-04	0.0000E+00	0.0000E+00
2	13	5.2551E-05	9.3548E-05	1.4032E-04	9.3548E-05	1.3830E-05	0.0000E+00	0.0000E+00
2	6	3.3404E-04	-3.2010E-04	-3.6931E-04	-2.7577E-04	-1.8710E-04	0.0000E+00	0.0000E+00

Table 6.5 2-D Heterogeneous model, elements 1 and 2 unaveraged stress output *file$.SP*

6.2.1.2 Three-Dimensional Model

The twenty noded brick type element was used for the three-dimensional model as shown in Fig. 4.19. However in this case the stress output file (*file$.O09*) produced in phase 9 contains 27 stresses for each element as shown in Table 6.6. Stresses are given for 8 corner nodes, 12 midside nodes, 6 face centres and the element centre as shown in Figs. 6.7 and 6.8. For the three-dimensional example, unaveraged stresses are written to the *file$.O09* file as shown in Tables 6.6 and 6.7 respectively. Only averaged stress values are available in the *file$.SP* output as shown in Table 6.8.

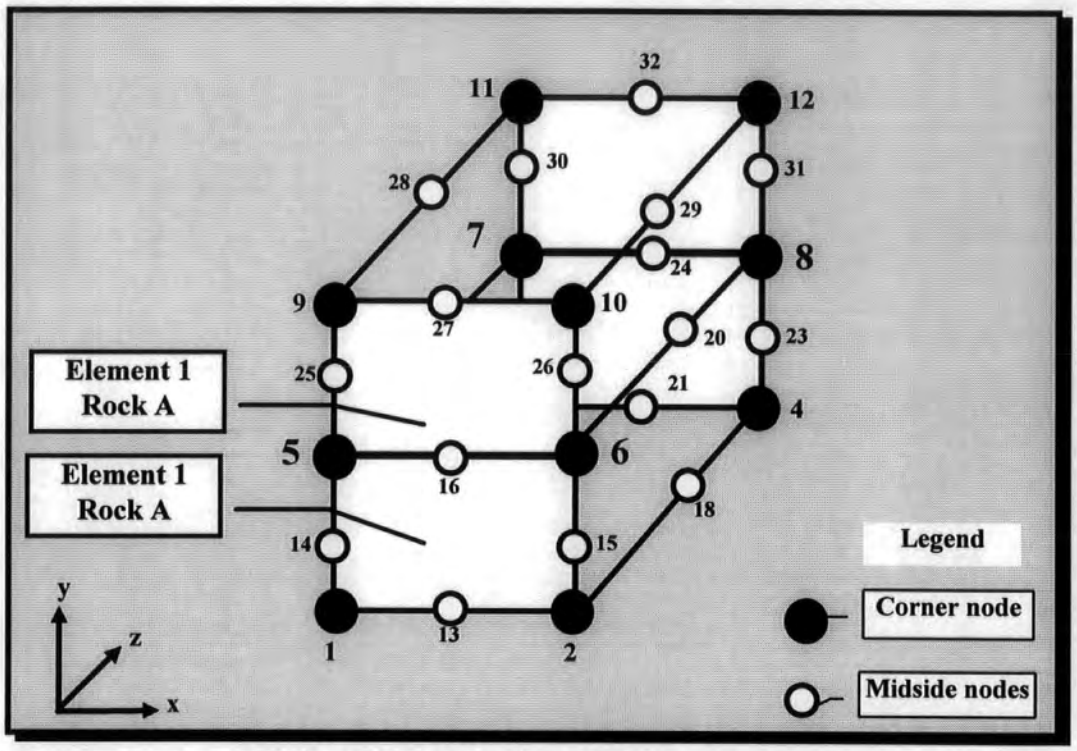

Fig. 6.7 Three-dimensional homogeneous model

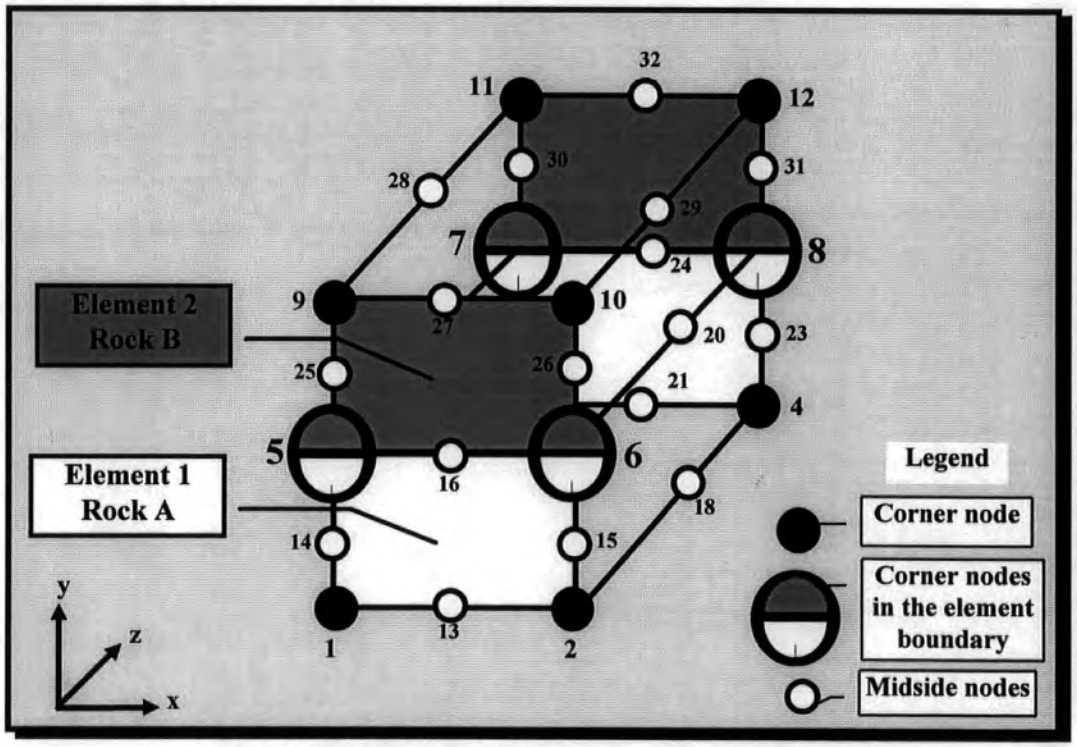

Fig. 6.8 Three-dimensional heterogeneous model

LOAD CASE	NODE NO	GLOBAL.STRESSES.... SIGMA- X	SIGMA- Y	SIGMA-Z	PRINCIPAL.STRESSES.. SIGMA-1	SIGMA-2	SIGMA-3	VON.MISES STRESS	ANGS.OF.PRINCIPAL.DIRECTIONS AX	AY	AZ	BX	BY	BZ
ELEMENT NO. 1														
1	1	-1.27D+04	-2.35D+04	-1.27D+04	-1.27D+04	-1.27D+04	-2.35D+04	1.09D+04	90	90	0	0	90	90
1	17	-1.27D+04	-2.35D+04	-1.27D+04	-1.27D+04	-1.27D+04	-2.35D+04	1.09D+04	84	89	5	5	90	95
1	3	-1.27D+04	-2.35D+04	-1.27D+04	-1.27D+04	-1.27D+04	-2.35D+04	1.09D+04	90	90	0	0	90	90
1	14	-9.24D+03	-1.72D+04	-9.24D+03	-9.24D+03	-9.24D+03	-1.72D+04	7.92D+03	0	89	89	89	90	17
1	0	-9.24D+03	-1.72D+04	-9.24D+03	-9.24D+03	-9.24D+03	-1.72D+04	7.92D+03	71	90	18	18	89	10
1	22	-9.24D+03	-1.72D+04	-9.24D+03	-9.24D+03	-9.24D+03	-1.72D+04	7.92D+03	89	89	1790		89	89
1	5	-5.81D+03	-1.08D+04	-5.81D+03	-5.81D+03	-5.81D+03	-1.08D+04	4.98D+03	0	89	89	89	90	17
1	19	-5.81D+03	-1.08D+04	-5.81D+03	-5.81D+03	-5.81D+03	-1.08D+04	4.98D+03	11	89	78	78	89	16
1	7	-5.81D+03	-1.08D+04	-5.81D+03	-5.81D+03	-5.81D+03	-1.08D+04	4.98D+03	0	89	90	89	90	0
1	13	-1.27D+04	-2.35D+04	-1.27D+04	-1.27D+04	-1.27D+04	-2.35D+04	1.09D+04	5	89	84	84	89	17
1	0	-1.27D+04	-2.35D+04	-1.27D+04	-1.27D+04	-1.27D+04	-2.35D+04	1.09D+04	44	89	45	45	89	13
1	21	-1.27D+04	-2.35D+04	-1.27D+04	-1.27D+04	-1.27D+04	-2.35D+04	1.09D+04	84	89	5	5	89	95
1	0	-9.24D+03	-1.72D+04	-9.24D+03	-9.24D+03	-9.24D+03	-1.72D+04	7.92D+03	13	89	76	76	90	16
1	0	-9.24D+03	-1.72D+04	-9.24D+03	-9.24D+03	-9.24D+03	-1.72D+04	7.92D+03	45	90	44	44	90	13
1	0	-9.24D+03	-1.72D+04	-9.24D+03	-9.24D+03	-9.24D+03	-1.72D+04	7.92D+03	76	90	13	13	89	10
1	16	-5.81D+03	-1.08D+04	-5.81D+03	-5.81D+03	-5.81D+03	-1.08D+04	4.98D+03	25	89	64	64	90	15
1	0	-5.81D+03	-1.08D+04	-5.81D+03	-5.81D+03	-5.81D+03	-1.08D+04	4.98D+03	44	90	45	45	90	13
1	24	-5.81D+03	-1.08D+04	-5.81D+03	-5.81D+03	-5.81D+03	-1.08D+04	4.98D+03	64	90	25	25	89	11
1	2	-1.27D+04	-2.35D+04	-1.27D+04	-1.27D+04	-1.27D+04	-2.35D+04	1.09D+04	0	90	90	90	90	0
1	18	-1.27D+04	-2.35D+04	-1.27D+04	-1.27D+04	-1.27D+04	-2.35D+04	1.09D+04	5	89	84	84	90	17
1	4	-1.27D+04	-2.35D+04	-1.27D+04	-1.27D+04	-1.27D+04	-2.35D+04	1.09D+04	0	90	90	90	90	0
1	15	-9.24D+03	-1.72D+04	-9.24D+03	-9.24D+03	-9.24D+03	-1.72D+04	7.92D+03	0	90	89	89	89	17
1	0	-9.24D+03	-1.72D+04	-9.24D+03	-9.24D+03	-9.24D+03	-1.72D+04	7.92D+03	18	90	71	71	90	16
1	23	-9.24D+03	-1.72D+04	-9.24D+03	-9.24D+03	-9.24D+03	-1.72D+04	7.92D+03	0	90	89	89	89	17
1	6	-5.81D+03	-1.08D+04	-5.81D+03	-5.81D+03	-5.81D+03	-1.08D+04	4.98D+03	89	90	1790		90	89
1	20	-5.81D+03	-1.08D+04	-5.81D+03	-5.81D+03	-5.81D+03	-1.08D+04	4.98D+03	78	89	11	11	90	10
1	8	-5.81D+03	-1.08D+04	-5.81D+03	-5.81D+03	-5.81D+03	-1.08D+04	4.98D+03	89	90	1790		90	89

Table 6.6 3-D Heterogeneous model element 1 stress output *file$.O09*

LOAD CASE	NODE NO	GLOBAL.STRESSES.... SIGMA- X	SIGMA- Y	SIGMA-Z	PRINCIPAL.STRESSES..VON.MISES SIGMA-1	SIGMA-2	SIGMA-3	STRESS	ANGS.OF.PRINCIPAL.DIRECTIONS AX	AY	AZ	BX	BY	BZ
ELEMENT NO. 2														
1	5	-7.19D+03	-1.08D+04	-7.19D+03	-7.19D+03	-7.19D+03	-1.08D+04	3.60D+03	0	89	89	89	90	17
1	19	-7.19D+03	-1.08D+04	-7.19D+03	-7.19D+03	-7.19D+03	-1.08D+04	3.60D+03	11	89	78	78	89	16
1	7	-7.19D+03	-1.08D+04	-7.19D+03	-7.19D+03	-7.19D+03	-1.08D+04	3.60D+03	0	89	90	89	90	0
1	25	-3.60D+03	-5.40D+03	-3.60D+03	-3.60D+03	-3.60D+03	-5.40D+03	1.80D+03	89	89	0	0	89	90
1	0	-3.60D+03	-5.40D+03	-3.60D+03	-3.60D+03	-3.60D+03	-5.40D+03	1.80D+03	78	90	11	11	89	10
1	30	-3.60D+03	-5.40D+03	-3.60D+03	-3.60D+03	-3.60D+03	-5.40D+03	1.80D+03	89	89	1790		89	89
1	9	-1.93D-03	-2.45D-03	-1.82D-03	-1.55D-03	-1.84D-03	-2.81D-03	1.14D-03	44	58	62	60	85	14
1	28	-4.39D-04	-4.49D-04	-3.55D-04	-6.64D-05	-3.53D-04	-8.23D-04	6.61D-04	45	45	95	81	89	8
1	11	4.91D-04	7.09D-04	5.46D-04	1.39D-03	5.36D-04	-1.77D-04	1.36D-03	53	41	10765		88	24
1	16	-7.19D+03	-1.08D+04	-7.19D+03	-7.19D+03	-7.19D+03	-1.08D+04	3.60D+03	25	90	64	64	90	15
1	0	-7.19D+03	-1.08D+04	-7.19D+03	-7.19D+03	-7.19D+03	-1.08D+04	3.60D+03	45	90	44	44	90	13
1	24	-7.19D+03	-1.08D+04	-7.19D+03	-7.19D+03	-7.19D+03	-1.08D+04	3.60D+03	64	90	25	25	89	11
1	0	-3.60D+03	-5.40D+03	-3.60D+03	-3.60D+03	-3.60D+03	-5.40D+03	1.80D+03	41	90	48	48	89	13
1	0	-3.60D+03	-5.40D+03	-3.60D+03	-3.60D+03	-3.60D+03	-5.40D+03	1.80D+03	44	90	45	45	90	13
1	0	-3.60D+03	-5.40D+03	-3.60D+03	-3.60D+03	-3.60D+03	-5.40D+03	1.80D+03	48	89	41	41	89	13
1	27	4.21D-04	6.31D-04	4.21D-04	8.41D-04	4.40D-04	1.92D-04	5.68D-04	68	34	11640		89	49
1	0	1.17D-04	1.75D-04	1.17D-04	2.85D-04	9.93D-05	2.46D-05	2.33D-04	54	13871		76	10216	
1	32	8.42D-04	1.26D-03	8.42D-04	1.31D-03	8.39D-04	7.98D-04	4.92D-04	84	17	73	11	97	81
1	6	-7.19D+03	-1.08D+04	-7.19D+03	-7.19D+03	-7.19D+03	-1.08D+04	3.60D+03	89	90	1790		90	89
1	20	-7.19D+03	-1.08D+04	-7.19D+03	-7.19D+03	-7.19D+03	-1.08D+04	3.60D+03	78	89	11	11	90	10
1	8	-7.19D+03	-1.08D+04	-7.19D+03	-7.19D+03	-7.19D+03	-1.08D+04	3.60D+03	89	90	1800		90	89
1	26	-3.60D+03	-5.40D+03	-3.60D+03	-3.60D+03	-3.60D+03	-5.40D+03	1.80D+03	0	90	89	89	89	17
1	0	-3.60D+03	-5.40D+03	-3.60D+03	-3.60D+03	-3.60D+03	-5.40D+03	1.80D+03	11	90	78	78	89	16
1	31	-3.60D+03	-5.40D+03	-3.60D+03	-3.60D+03	-3.60D+03	-5.40D+03	1.80D+03	0	90	90	89	89	0
1	10	1.88D-03	2.38D-03	1.77D-03	3.01D-03	1.88D-03	1.13D-03	1.64D-03	88	14454		2	89	92
1	29	-1.01D-03	-1.73D-03	-1.09D-03	-6.68D-04	-1.09D-03	-2.07D-03	1.25D-03	34	11973		70	88	16
1	12	-1.29D-03	-1.90D-03	-1.34D-03	-8.04D-04	-1.32D-03	-2.40D-03	1.41D-03	45	12311		556	88	33

Table 6.7 3-D Heterogeneous model element 2 stress output *file$.O09*

LOAD CASE	NODE NO.	SIG MISES	SIG XX	SIG YY	SIG ZZ	TAU XY	TAU YZ	TAU ZX
1	1	1.09E+04	-1.27E+04	-2.35E+04	-1.27E+04	8.50E-02	8.50E-02	-1.98E-01
1	2	1.09E+04	-1.27E+04	-2.35E+04	-1.27E+04	8.50E-02	8.50E-02	-1.98E-01
1	3	1.09E+04	-1.27E+04	-2.35E+04	-1.27E+04	8.50E-02	8.50E-02	-1.98E-01
1	4	1.09E+04	-1.27E+04	-2.35E+04	-1.27E+04	8.50E-02	8.50E-02	-1.98E-01
1	5	4.98E+03	-5.81E+03	-1.08E+04	-5.81E+03	5.36E-02	2.01E-02	-7.32E-02
1	5	3.60E+03	-7.19E+03	-1.08E+04	-7.19E+03	3.78E-02	1.26E-02	-9.08E-02
1	6	4.98E+03	-5.81E+03	-1.08E+04	-5.81E+03	4.53E-02	2.98E-02	-8.67E-02
1	6	3.60E+03	-7.19E+03	-1.08E+04	-7.19E+03	3.36E-02	2.14E-02	-1.07E-01
1	7	4.98E+03	-5.81E+03	-1.08E+04	-5.81E+03	5.25E-02	-2.40E-02	-1.37E-02
1	7	3.60E+03	-7.19E+03	-1.08E+04	-7.19E+03	3.69E-02	-1.50E-02	-1.68E-02
1	8	4.98E+03	-5.81E+03	-1.08E+04	-5.81E+03	5.23E-02	-1.74E-02	-1.83E-02
1	8	3.60E+03	-7.19E+03	-1.08E+04	-7.19E+03	3.78E-02	-1.26E-02	-2.22E-02
1	9	1.14E-03	-1.93E-03	-2.45E-03	-1.82E-03	5.15E-04	2.34E-04	-6.90E-09
1	10	1.64E-03	1.88E-03	2.38E-03	1.77E-03	-4.68E-05	-8.89E-04	1.80E-08
1	11	1.36E-03	4.91E-04	7.09E-04	5.46E-04	7.02E-04	-3.27E-04	8.69E-09
1	12	1.41E-03	-1.29E-03	-1.90E-03	-1.34E-03	-6.08E-04	4.21E-04	-1.41E-08
1	13	1.09E+04	-1.27E+04	-2.35E+04	-1.27E+04	8.29E-02	8.46E-02	-1.98E-01
1	14	7.92E+03	-9.24E+03	-1.72E+04	-9.24E+03	8.25E-02	3.16E-02	-1.19E-01
1	15	7.92E+03	-9.24E+03	-1.72E+04	-9.24E+03	7.20E-02	-4.88E-02	-5.74E-03
1	16	4.98E+03	-5.81E+03	-1.08E+04	-5.81E+03	4.41E-02	-3.23E-02	-1.46E-03
1	16	3.60E+03	-7.19E+03	-1.08E+04	-7.19E+03	2.83E-02	2.80E-02	-1.13E-01
1	17	1.09E+04	-1.27E+04	-2.35E+04	-1.27E+04	8.55E-02	8.33E-02	-1.97E-01
1	18	1.09E+04	-1.27E+04	-2.35E+04	-1.27E+04	8.81E-02	-8.32E-02	-5.96E-05
1	19	4.98E+03	-5.81E+03	-1.08E+04	-5.81E+03	4.31E-02	-3.44E-02	-1.16E-03
1	19	3.60E+03	-7.19E+03	-1.08E+04	-7.19E+03	3.53E-02	1.84E-02	-1.03E-01
1	20	4.98E+03	-5.81E+03	-1.08E+04	-5.81E+03	4.18E-02	3.53E-02	-8.90E-02
1	20	3.60E+03	-7.19E+03	-1.08E+04	-7.19E+03	2.83E-02	2.80E-02	-1.13E-01
1	21	1.09E+04	-1.27E+04	-2.35E+04	-1.27E+04	8.34E-02	8.41E-02	-1.98E-01
1	22	7.92E+03	-9.24E+03	-1.72E+04	-9.24E+03	6.20E-02	-6.29E-02	1.06E-06
1	23	7.92E+03	-9.24E+03	-1.72E+04	-9.24E+03	7.84E-02	-3.92E-02	-1.42E-02
1	24	4.98E+03	-5.81E+03	-1.08E+04	-5.81E+03	4.44E-02	-3.41E-02	-1.34E-03
1	24	3.60E+03	-7.19E+03	-1.08E+04	-7.19E+03	3.98E-02	-1.50E-03	-5.20E-02
1	25	1.80E+03	-3.60E+03	-5.40E+03	-3.60E+03	1.88E-02	-7.06E-03	-9.28E-03
1	26	1.80E+03	-3.60E+03	-5.40E+03	-3.60E+03	1.41E-02	-1.43E-02	3.37E-07
1	27	5.68E-04	4.21E-04	6.31E-04	4.21E-04	1.94E-04	-2.34E-04	1.90E-05
1	28	6.61E-04	-4.39E-04	-4.49E-04	-3.55E-04	3.74E-04	-5.45E-05	1.17E-05
1	29	1.25E-03	-1.01E-03	-1.73E-03	-1.10E-03	-5.61E-04	-2.24E-04	1.17E-05
1	30	1.80E+03	-3.60E+03	-5.40E+03	-3.60E+03	1.98E-02	3.42E-03	-3.80E-02
1	31	1.80E+03	-3.60E+03	-5.40E+03	-3.60E+03	1.96E-02	1.01E-03	-2.98E-02
1	32	4.92E-04	8.42E-04	1.26E-03	8.42E-04	3.84E-05	1.40E-04	1.90E-05

Table 6.8 3-D Heterogeneous model elements 1 and 2 averaged stress output *file8.SP*

6.2.2 Rearrangement of Heterogeneous Model Average Stresses

In this case the stresses are dependent on the material properties and hence the average stresses in the output file (*file$.SP*) have two values on the material boundaries and three values at the rock in the boundary between both rock and shotcrete as shown in Fig. 6.9. Again determining which stress belongs to which material is uncertain. Therefore in order to make some decision using the unaveraged stresses, the averaged stresses were rearranged. Average stress values were assigned for each node in the material boundary according to which average stress value was closest to the unaveraged stress value of that element, using the unaveraged stress at that node for comparison. When an ambiguous node (a node having two or three stress values in the averaged stress output file (*file$.SP*)) is found, the value closest to the unaveraged nodal value in the unaveraged stress output file (*file$.USTRDAT*) as shown in Tables 6.9 and 6.11 is used to rearrange the average stresses on the material boundaries as shown in Tables 6.10 and 6.12. For both two- and three-dimensional models the rearranged average stress results are calculated using a subroutine 'REAVST' as shown in Fig. 6.10.

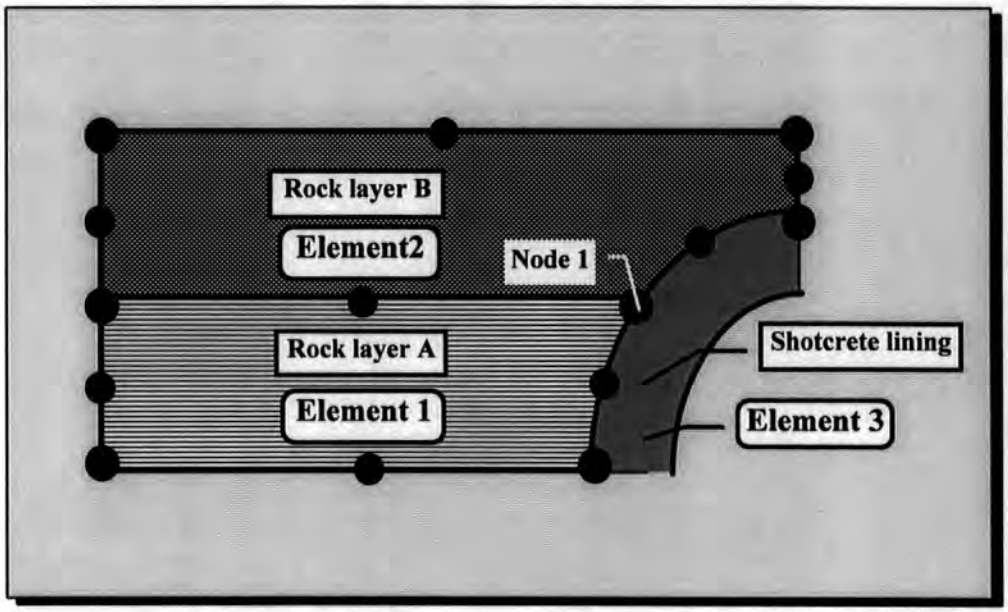

Fig. 6.9 Node 1 joining elements in three different materials

```
C=======================================================
C SUBROUTINE REAVST REARRANGE AVERAGE STRESSES TO
C ELEMENT AND NODE ORDER
C=======================================================
      SUBROUTINE REAVST

      PARAMETER (MXNOS1 = 80 000)
      PARAMETER (MXELS  = 25 000)
      PARAMETER (MXEN   = 20*MXELS )

      CHARACTER FILE*6
      COMMON / FILNAM / FILE
      COMMON / NUMBRS / NONOS, NOELS, NDIM
      COMMON / CUNSTR / NU,IEL(MXEN),NN(MXEN),USTR(MXEN)
      COMMON / CAVSTR / NS(MXNOS1), ASTR(MXNOS1,3)

      OPEN(9,FILE=FILE//'.ASTRDAT')
      OPEN(10,FILE=FILE//'.ASTRNUM')

C Loop over all elements
      DO 50 I=1,NU

C Ensure no Zero Values are picked up erroneously
        DO 10 J=1,3
 10       IF (ASTR(NN(I),J).EQ.0.0) ASTR(NN(I),J) = -9E29

C Assign average stress value which is closest to the
C  unaveraged stress value of that element
C Using Unaveraged Stress at that Node for comparison
        US = USTR(I)
C Calclulate the differences between Values
        A1 =  ABS(US-ASTR(NN(I),1))
        A2 =  ABS(US-ASTR(NN(I),2))
        A3 =  ABS(US-ASTR(NN(I),3))
C Write out closest value
        IF ((A1.LE.A2).AND.(A1.LE.A3)) THEN
            RSTR = ASTR(NN(I),1)
        ELSE IF (A2.LE.A3) THEN
            RSTR = ASTR(NN(I),2)
        ELSE
           RSTR = ASTR(NN(I),3)
        ENDIF
        WRITE(9,904)IEL(I),NN(I),RSTR
 50   CONTINUE
      WRITE(6,*)'Average Stresses: ',NU
      WRITE(9,*)'*'
      WRITE(10,*)NU
904   FORMAT(3X,2I7,E11.4)
      CLOSE(9,STATUS='KEEP')
      CLOSE(10,STATUS='KEEP')
      RETURN
      END
```

Fig. 6.10 Averaged stresses for the heterogeneous model

File name : square1.USTRDAT

2-D Heterogeneous model unaveraged Von Mises stress

Elements	Nodes	Von Mises
1	1	.10866E+05
1	7	.10866E+05
1	2	.10866E+05
1	8	.79235E+04
1	9	.79235E+04
1	3	.49805E+04
1	10	.49805E+04
1	4	.49805E+04
2	3	.35970E+04
2	10	.35970E+04
2	4	.35970E+04
2	11	.17985E+04
2	12	.17985E+04
2	5	.34624E-03
2	13	.52551E-04
2	6	.33404E-03
*		

Table 6.9 Post-processing of unaveraged stresses for 2-D heterogeneous model

File name : square1.ASTRDAT

2-D Heterogeneous model averaged Von Mises stress

Elements	Nodes	Von Mises
1	1	.1087E+05
1	7	.1087E+05
1	2	.1087E+05
1	8	.7924E+04
1	9	.7924E+04
1	3	.4981E+04
1	10	.4981E+04
1	4	.4981E+04
2	3	.3597E+04
2	10	.3597E+04
2	4	.3597E+04
2	11	.1799E+04
2	12	.1799E+04
2	5	.3462E-03
2	13	.5255E-04
2	6	.3340E-03
*		

Table 6.10 Post-processing of averaged stresses for 2-D heterogeneous model

File name : cubes2.USTRDAT

3-D Heterogeneous model unaveraged Von Mises stress

Elements	Nodes	Von Mises
1	1	.1090E+05
1	17	.1090E+05
1	3	.1090E+05
1	14	.7920E+04
1	22	.7920E+04
1	5	.4980E+04
1	19	.4980E+04
1	7	.4980E+04
1	13	.1090E+05
1	21	.1090E+05
1	16	.4980E+04
1	24	.4980E+04
1	2	.1090E+05
1	18	.1090E+05
1	4	.1090E+05
1	15	.7920E+04
1	23	.7920E+04
1	6	.4980E+04
1	20	.4980E+04
1	8	.4980E+04
2	5	.3600E+04
2	19	.3600E+04
2	7	.3600E+04
2	25	.1800E+04
2	30	.1800E+04
2	9	.1140E-02
2	28	.6610E-03
2	11	.1360E-02
2	16	.3600E+04
2	24	.3600E+04
2	27	.5680E-03
2	32	.4920E-03
2	6	.3600E+04
2	20	.3600E+04
2	8	.3600E+04
2	26	.1800E+04
2	31	.1800E+04
2	10	.1640E-02
2	29	.1250E-02
2	12	.1410E-02

*

Table 6.11 Post-processing of unaveraged stresses for 3-D heterogeneous model

File name : cubes2.ASTRDAT

3-D Heterogeneous model averaged Von Mises stress

Elements	Nodes	Von Mises
1	1	.1087E+05
1	17	.1087E+05
1	3	.1087E+05
1	14	.7924E+04
1	22	.7924E+04
1	5	.4981E+04
1	19	.4981E+04
1	7	.4981E+04
1	13	.1087E+05
1	21	.1087E+05
1	16	.4981E+04
1	24	.4981E+04
1	2	.1087E+05
1	18	.1087E+05
1	4	.1087E+05
1	15	.7924E+04
1	23	.7924E+04
1	6	.4981E+04
1	20	.4981E+04
1	8	.4981E+04
2	5	.3597E+04
2	19	.3597E+04
2	7	.3597E+04
2	25	.1799E+04
2	30	.1799E+04
2	9	.1139E-02
2	28	.6613E-03
2	11	.1355E-02
2	16	.3597E+04
2	24	.3597E+04
2	27	.5675E-03
2	32	.4917E-03
2	6	.3597E+04
2	20	.3597E+04
2	8	.3597E+04
2	26	.1799E+04
2	31	.1799E+04
2	10	.1640E-02
2	29	.1247E-02
2	12	.1411E-02
2	0	-.9000E+30

*

Table 6.12 Post-processing of averaged stresses for 3-D heterogeneous model

6.3 Graphics Generation

The stress and displacement results are superimposed on the solid models by the post-processing program 'indistress' using UNIRAS which produces coloured stress contour plots and displaced shape plots.

The graphics generation program 'indistress' uses the specific values from the suitably formatted output files *(file$.ASTRDAT or file$.USTRDAT)* of the data processing programs to generate the graphical output seen throughout this thesis as shown in Fig. 6.11. It produces illuminated solid models of any model mesh and enables better visualisation. After that it generates coloured contour plots for stresses and produces displaced shape plots allowing the deformation of any mesh to be assimilated very quickly. Distributed stresses and deformation values across the nodes on the tunnel model mesh were achieved with the help of UNIRAS mapping and interpolation routines. This post processing program lies at the heart of the method for using the stress and displacement results from data processing programs directly to generate very accurate finite element tunnel model colour outputs and displaced shape plots.

The specific values from the files *(file$.ASTRDAT or file$.USTRDAT)* created by the data post processing programs are used to compile summary tables for stress and displacement as shown in Tables 6.9 to 6.12. Analysis of other models could be completed more quickly and more accurately by repeating the same process with both the gravity different method and stress reversal technique.

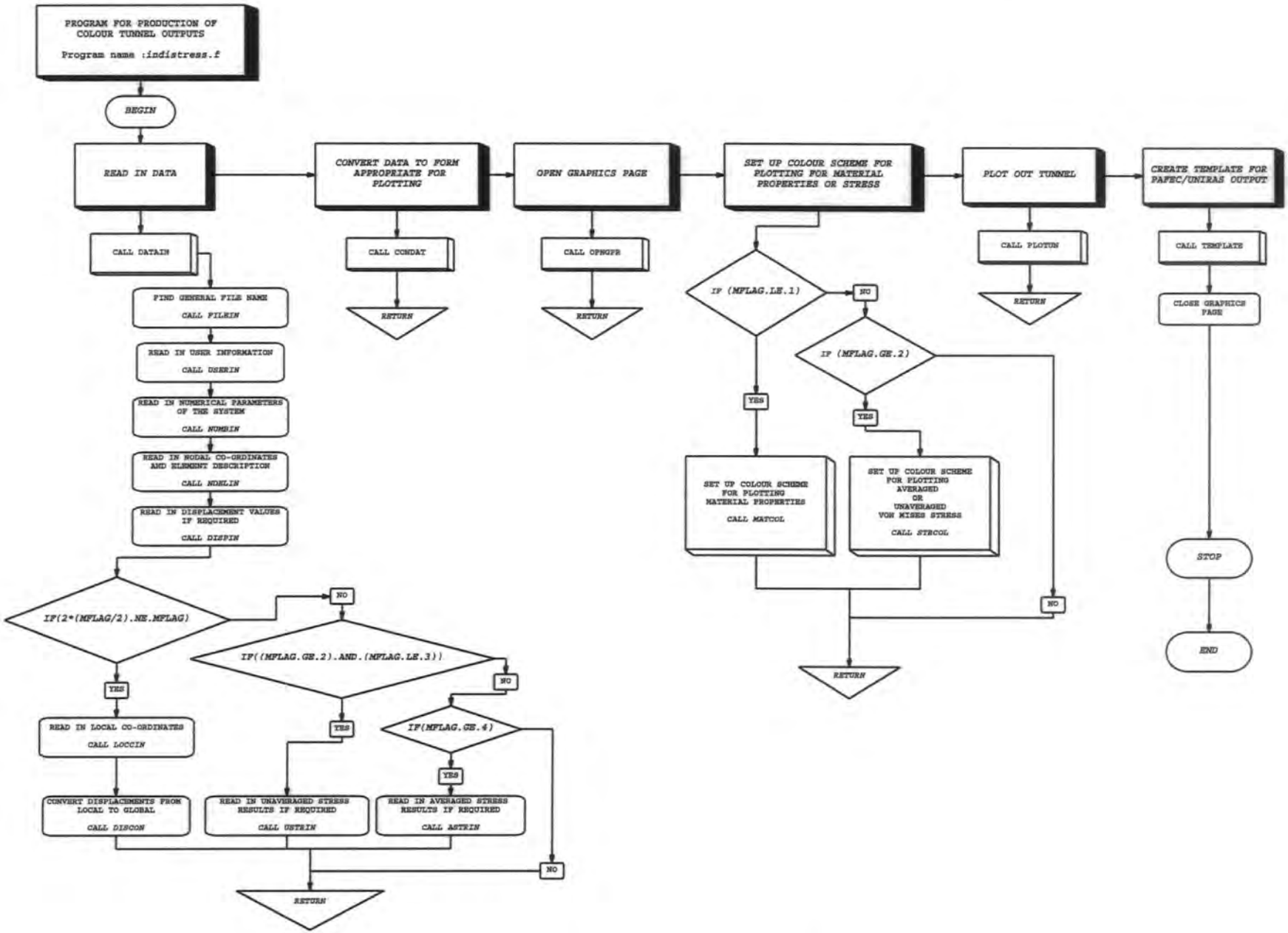

Fig. 6.11 Production of colour tunnel outputs using UNIRAS graphics software

CHAPTER 7

CONVERGENCE MEASUREMENTS AND SIMULATION RESULTS

7.1 Introduction

This chapter contains results from analyses of the computer models after checking the programs with simple, circular cross-section tunnels. The classical analytical method after Kirsch (1898) - outlined by Attewell (1980) - suitably describes a tunnel perforation of circular configuration in an elastic homogeneous body (ground). Initially two-dimensional circular single and dual tunnel finite element results were compared with analytical Kirsch method. Simple models have been chosen for the first phase of investigation and their adoption depends on what is discovered at that time. Complex modelling should only be adopted after developing an understanding of such displacement and stress mechanisms. It was considered very doubtful whether the method Kirsch used to obtain these formulae could be adapted to suit the tunnel geometry and ground conditions applicable to this present tunnel project. It was quite apparent that the support system and the in situ conditions needed to be analysed by an alternative procedure, and clearly a rather different approach was required to solve this more complex type of problem to any degree of accuracy. Most of the simulations were performed on cross-sections of the Kisikli tunnel project in Turkey, because cover to roof of the Tantavi tunnels is low, typically between 4.0 and 9.0 m.

For each simulation run, the results and the interpretation of these results are given according to the construction sequence of the tunnel. Due to the volume of the computer output obtained at the end of each analysis it is not feasible to produce all the stress and displacement outputs in this thesis although one example is given in Appendix B. Instead, the results for each analysis are represented graphically and then compared. The results are also presented in the form of

stress-shaded colour and displaced shape diagrams. A comparison between the gravity difference method and stress reversal technique has been done for the stresses and displacements.

There were four main stages of computational test using the gravity difference method or stress reversal technique, as shown in Figs. 7.1 and 7.2. The first stage uses a homogeneous model for testing the excavation methods for two- and three-dimensional tunnel models. The second stage adopts a heterogeneous tunnel model without any support. The third stage demonstrates different heterogeneous models having different shotcrete lining thicknesses and includes a comparison of partially and fully excavated tunnel models. Finally the fourth stage utilises three-dimensional tunnel models having anchorages, steel arches and inner lining, for the investigation of both ground and support displacements and stresses induced by tunnelling.

It was decided to match the same cross-sections of tunnel used for simulation with the sections used for convergence measurements. The cross-sections were taken from the longitudinal section and related to several distances of tunnel advance. The changes in the displacements and stresses obtained were observed and computed displacements were compared with measured displacements.

The values of Young's Modulus for the simulation presented in Chapter 4 refer to the general values used in the models. Due to the highly fractured nature of the ground around the tunnel, reduced values of modulus equal to 10% and 50% were used to give a best correlation with field measurements. An increase of 0.05 on the 'intact' specimen value was used throughout the models for the Poisson's ratio. Some tests were conducted in order to establish the effect on the model of different material properties. The following diagrams, tables and graphs in this section contain the relevant information for the Kisikli heterogeneous model and allow comparison of the results of the analysis as a function of the different material properties.

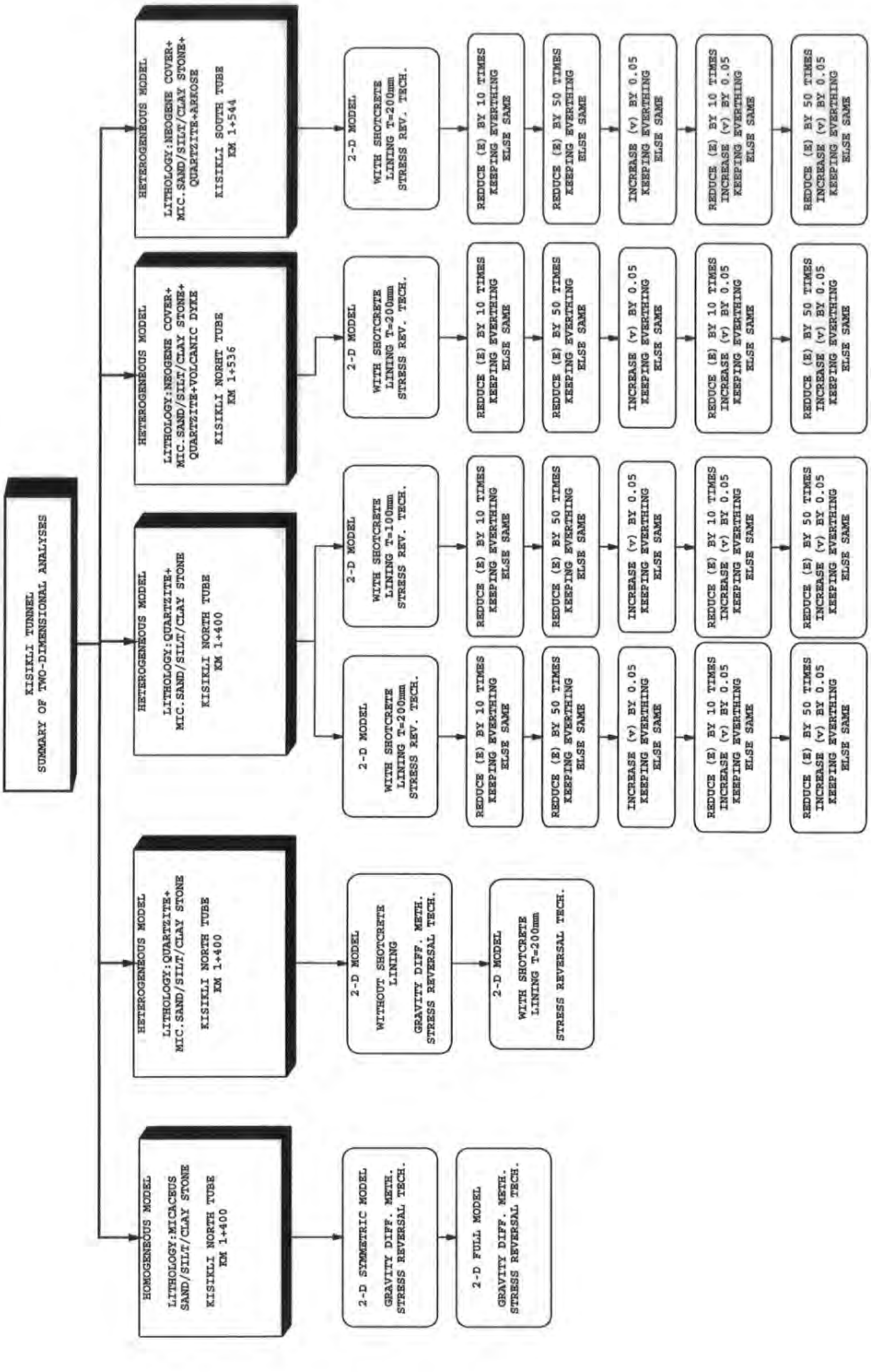

Fig. 7.1 Summary of two-dimensional analyses

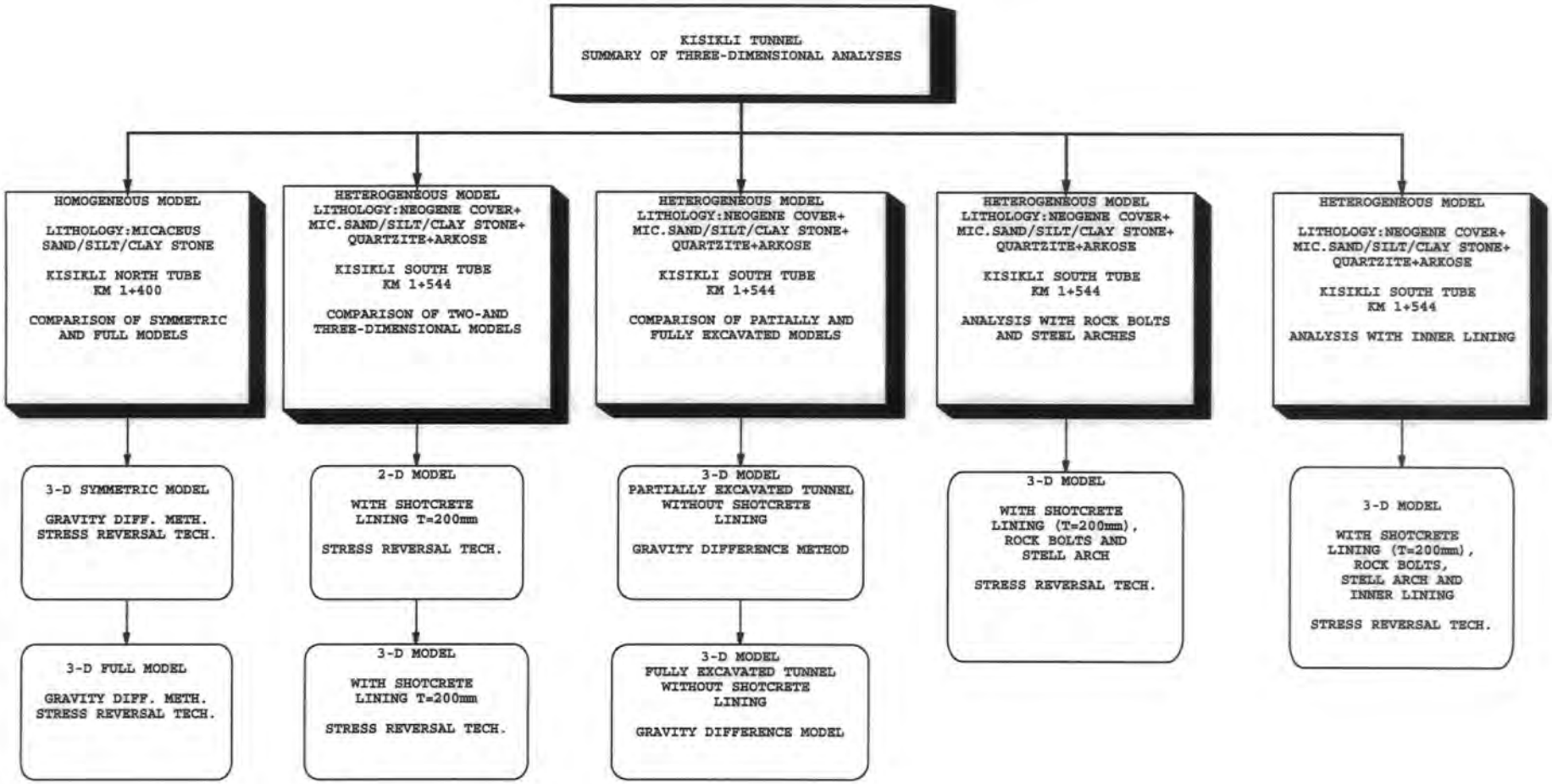

Fig. 7.2 Summary of Three-dimensional analyses

Several different simulation runs were also performed, with the different section depths being varied from 3 to 15 metres using three-dimensional tunnel models having support systems.

The finite element development of the two- and three-dimensional tunnel models described in Chapter 5 and the examples given in this chapter incorporate the following basic features.

a) The stratigraphical geometry of the ground
b) The stress and deformation characteristics of unexcavated and excavated ground.
c) Partial excavation.
d) The shotcrete lining.
e) Features of the anchorage and steel arch.
f) The inner lining pressure.

In a graphical representation of the stress and displacement results an individual plot will have two features in order to define accurately the origin of the data.

a) Name of the tunnel and location.
b) The variable or parameter being represented and the conditions pertaining to the variable or parameter, i.e. unexcavated or excavated ground, partially excavated ground, type of support system.

7.2 Convergence Results

Convergence pins were inserted as shown in Fig. 7.3 in order to monitor the tunnel deformation after the shotcrete lining was applied. The data obtained from monitoring the Kisikli tunnels has been used to check the design of the primary lining. Extensometer wires were positioned between pairs of pins enabling four diagonal and two horizontal measurements of convergence to be recorded.

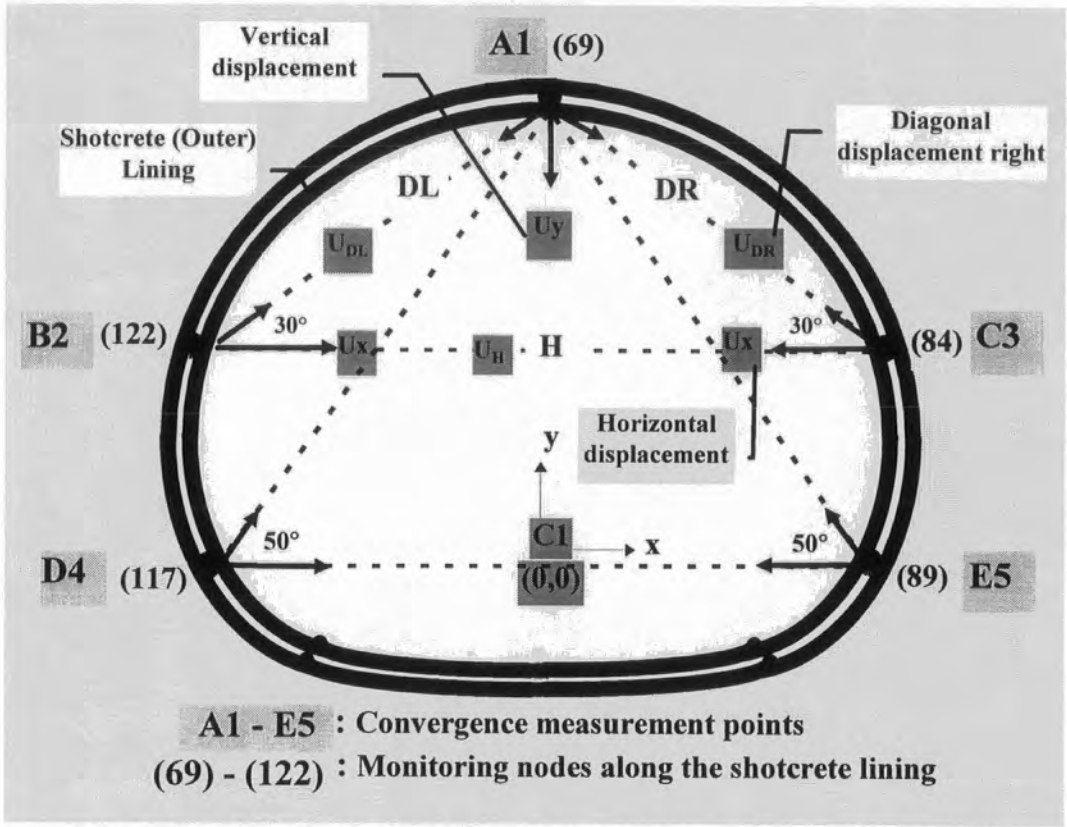

Fig. 7.3 Location of extensometers and convergence measurment cross-section

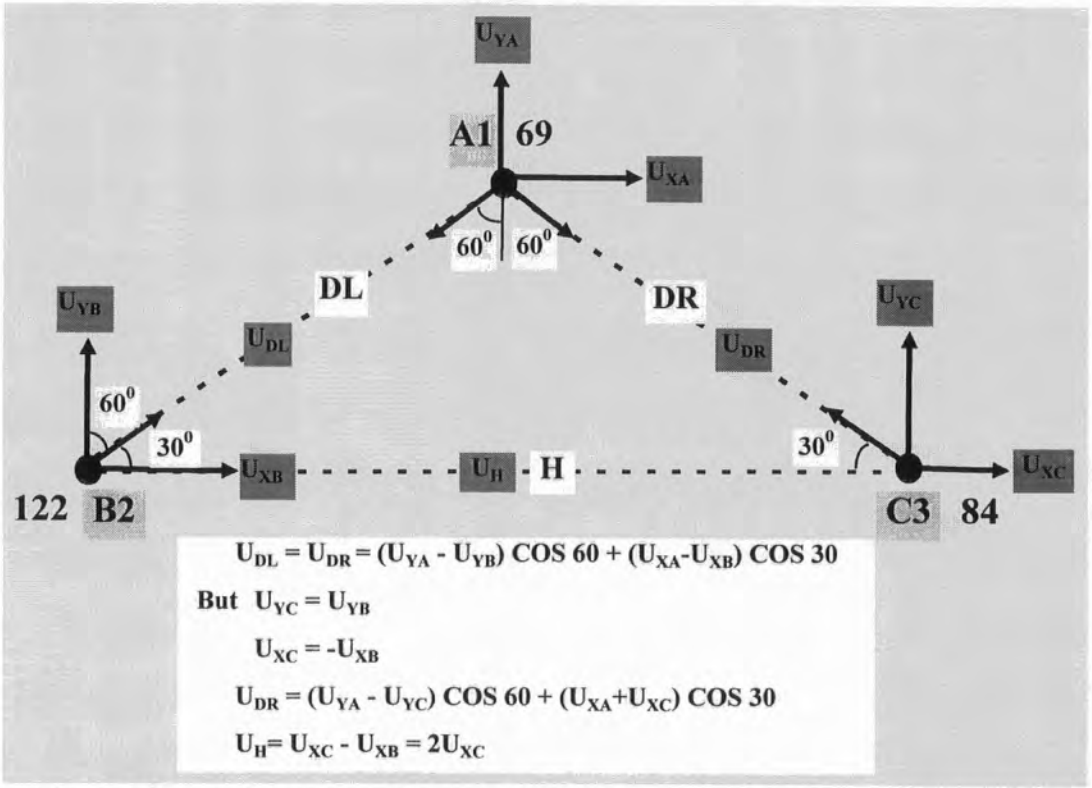

Fig. 7.4 Determining the settlements from the computed results of measurements along the horizontal and diagonal convergence measuring gauges.

Readings were taken daily, and then weekly when construction was completed at the point under consideration. As the tunnel faces advanced beyond the instrumented area the frequency of readings could then be reduced to weekly or possibly monthly cycles. However, should any large movements be recorded, the frequency of reading would then be increased to at least daily until the movement ceased.

In order to compare the measured and computed displacements it was necessary to transform the output from PAFEC-FE, in terms of orthogonal displacement components Ux and Uy, to calculate the diagonal and horizontal convergence between any two measuring points as shown in Fig. 7.4.

The measured displacements from Kisikli north tube (km 1+400 and 1+536) and Kisikli south tube (km 1+536) indicate a general trend of movement towards the tunnel origin as shown in Tables 7.1 to 7.3 and Figs. 7.5 to 7.7 respectively. Furthermore, it can be seen that the region of in situ displacement is also shown to be similar to the trend of the creep curve.

The length of time for the measured displacements is 151 days for the Kisikli north tube at km 1+400 and general trend of displacement changes between 0.20 and 0.40 mm as shown in Fig. 7.5. Cumulative tunnel convergence at the same section for the arrays A1-B2, A1-C3 and B2-C3 are 0.36, 0.29 and 0.39 mm as shown in Table 7.1 respectively. The convergence measurements for Kisikli north tube at km 1+536 were carried out 46 days and the general trend of displacement at the same section is between 0.40 and 1.40 mm as shown in Fig. 7.6. Cumulative tunnel convergence at the same section for the arrays A1-B2, A1-C3 and B2-C3 are 1.33, 0.71 and 1.36 mm as shown in Table 7.2 respectively. Finally the length of time for measured displacements at the Kisikli south tube (km 1+544) is 41 days. The general trend of displacement changes between 0.10 and 0.45 mm as shown in Fig. 7.7. Cumulative tunnel convergence at the same section for arrays A1-B2, A1-C3 and B2-C3 are 0.50, 0.15 and 0.45 mm as shown in Table 7.3 respectively.

EXTENSOMETER MONITORING
KISIKLI NORTH TUNNEL, (km 1+400)
THICKNESS OF SHOTCRETE LINING = 200 mm

	ARRAY A1-B2			ARRAY A1-C3			ARRAY A1-D4			ARRAY A1-E5			ARRAY B2-C3			ARRAY D4-E5		
	MOVEMENT			MOVEMENT			MOVEMENT			MOVEMENT			MOVEMENT			MOVEMENT		
DATE	READING	LAST	TOTAL	READING	LAST	TOTAL	READING	LAST	TOTAL	READING	LAST	TOTAL	READING	LAST	TOTAL	READING	LAST	TOTAL
	mm			mm			mm			mm			mm			mm		
1	7551.81	0.00	0.00	6109.66	0.00	0.00							12767.92	0.00	0.00			
9	7551.84	0.03	0.03	6109.71	0.05	0.05							12767.77	-0.15	-0.15			
15	7551.78	-0.06	-0.03	6109.58	-0.13	-0.08							12767.67	-0.10	-0.25			
22	7551.69	-0.09	-0.12	6109.54	-0.04	-0.12							12767.61	-0.06	-0.31			
30	7551.60	-0.09	-0.21	6109.51	-0.03	-0.15							12767.66	0.05	-0.26			
78	7551.62	0.02	-0.19	6109.47	-0.04	-0.19							12767.58	-0.08	-0.34			
85	7551.51	-0.11	-0.30	6109.47	0.00	-0.19							12767.70	0.12	-0.22			
94	7551.43	-0.08	-0.38	6109.58	0.11	-0.08							12767.42	-0.28	-0.50			
101	7551.47	0.04	-0.34	6109.44	-0.14	-0.22							12767.88	0.46	-0.04			
111	7551.30	-0.17	-0.51	6109.36	-0.08	-0.30							12767.61	-0.27	-0.31			
124	7551.26	-0.04	-0.55	6109.41	0.05	-0.25							12767.68	0.07	-0.24			
128	7551.20	-0.06	-0.61	6109.42	0.01	-0.24							12767.72	0.04	-0.20			
135	7551.42	0.22	-0.39	6109.58	0.16	-0.08							12767.61	-0.11	-0.31			
143	7551.35	-0.07	-0.46	6109.51	-0.07	-0.15							12766.57	-1.04	-1.35			
151	7551.45	0.10	**-0.36**	6109.37	-0.14	**-0.29**							12767.53	0.96	**-0.39**			

Table 7.1 Measured tunnel displacements for Kisikli north tube (Km 1+400)

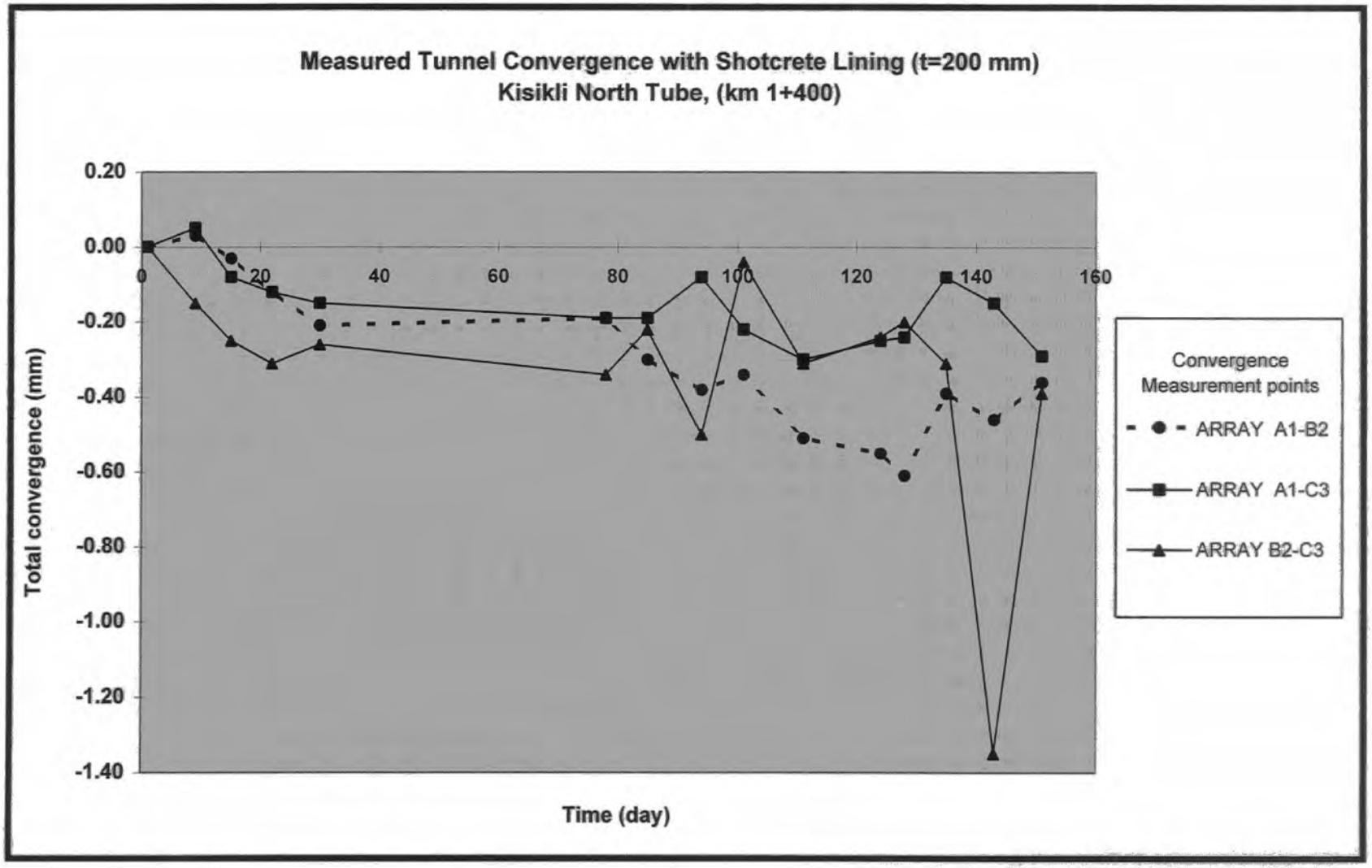

Fig. 7.5 Measured tunnel displacements for Kisikli north tube (km 1+400)

EXTENSOMETER MONITORING
KISIKLI NORTH TUNNEL, (km 1+536)
THICKNESS OF SHOTCRETE LINING = 200 mm

	ARRAY A1B2			ARRAY A1C3			ARRAY A1D4			ARRAY A1E5			ARRAY B2C3			ARRAY D4E5		
	MOVEMENT			MOVEMENT			MOVEMENT			MOVEMENT			MOVEMENT			MOVEMENT		
DATE	READING	LAST	TOTA	READING	LAST	TOTA	READING	LAST	TOTAL	READING	LAST	TOTAL	READING	LAST	TOTAL	READING	LAST	TOTA
	mm			mm			mm			mm			mm			mm		
1	6214.47	0.00	0.00	6512.81	0.00	0.00							11901.77	0.00	0.00			
2	6214.14	-0.33	-0.33	6512.48	-0.33	-0.33							11901.68	-0.09	-0.09			
3	6214.08	-0.06	-0.39	6512.57	0.09	-0.24							11901.43	-0.25	-0.34			
4	6214.11	0.03	-0.36	6512.44	-0.13	-0.37							11901.51	0.08	-0.26			
5	6214.27	0.16	-0.20	6512.38	-0.06	-0.43							11901.38	-0.13	-0.39			
8	6214.14	-0.13	-0.33	6512.47	0.09	-0.34							11901.42	0.04	-0.35			
9	6213.98	-0.16	-0.49	6512.33	-0.14	-0.48							11900.96	-0.46	-0.81			
10	6213.88	-0.10	-0.59	6512.41	0.08	-0.40							11900.82	-0.14	-0.95			
11	6213.74	-0.14	-0.73	6512.54	0.13	-0.27							11900.62	-0.20	-1.15			
16	6213.68	-0.06	-0.79	6512.48	-0.06	-0.33							11900.52	-0.10	-1.25			
17	6213.62	-0.06	-0.85	6512.38	-0.10	-0.43							11900.64	0.12	-1.13			
18	6213.54	-0.08	-0.93	6512.51	0.13	-0.30							11900.56	-0.08	-1.21			
19	6213.56	0.02	-0.91	6512.48	-0.03	-0.33							11900.66	0.10	-1.11			
20	6213.52	-0.04	-0.95	6512.36	-0.12	-0.45							11900.58	-0.08	-1.19			
22	6213.48	-0.04	-0.99	6512.44	0.08	-0.37							11900.54	-0.04	-1.23			
23	6213.53	0.05	-0.94	6512.54	0.10	-0.27							11900.61	0.07	-1.16			
24	6213.50	-0.03	-0.97	6512.46	-0.08	-0.35							11900.63	0.02	-1.14			
25	6213.56	0.06	-0.91	6512.42	-0.04	-0.39							11900.57	-0.06	-1.20			
26	6213.47	-0.09	-1.00	6512.46	0.04	-0.35							11900.58	0.01	-1.19			
27	6213.54	0.07	-0.93	6512.44	-0.02	-0.37							11900.61	0.03	-1.16			
29	6213.42	-0.12	-1.05	6512.38	-0.06	-0.43							11900.61	0.00	-1.16			
30	6213.56	0.14	-0.91	6512.48	0.10	-0.33							11900.55	-0.06	-1.22			
31	6213.59	0.03	-0.88	6512.41	-0.07	-0.40							11900.51	-0.04	-1.26			
32	6213.52	-0.07	-0.95	6512.43	0.02	-0.38							11900.58	0.07	-1.19			
33	6213.37	-0.15	-1.10	6512.33	-0.10	-0.48							11900.53	-0.05	-1.24			
34	6213.33	-0.04	-1.14	6512.38	0.05	-0.43							11900.48	-0.05	-1.29			
36	6213.41	0.08	-1.06	6512.44	0.06	-0.37							11900.56	0.08	-1.21			
37	6213.45	0.04	-1.02	6512.36	-0.08	-0.45							11900.44	-0.12	-1.33			
38	6213.38	-0.07	-1.09	6512.33	-0.03	-0.48							11900.47	0.03	-1.30			
39	6213.51	0.13	-0.96	6512.27	-0.06	-0.54							11900.38	-0.09	-1.39			
40	6213.42	-0.09	-1.05	6512.31	0.04	-0.50							11900.47	0.09	-1.30			
41	6213.38	-0.04	-1.09	6512.18	-0.13	-0.63							11900.35	-0.12	-1.42			
43	6213.46	0.08	-1.01	6512.34	0.16	-0.47							11900.39	0.04	-1.38			
44	6213.41	-0.05	-1.06	6512.21	-0.13	-0.60							11900.46	0.07	-1.31			
45	6213.32	-0.09	-1.15	6512.17	-0.04	-0.64							11900.37	-0.09	-1.40			
46	6213.34	0.02	**-1.13**	6512.10	-0.07	**-0.71**							11900.41	0.04	**-1.36**			

Table 7.2 Measured tunnel displacements for Kisikli north tube (km 1+536)

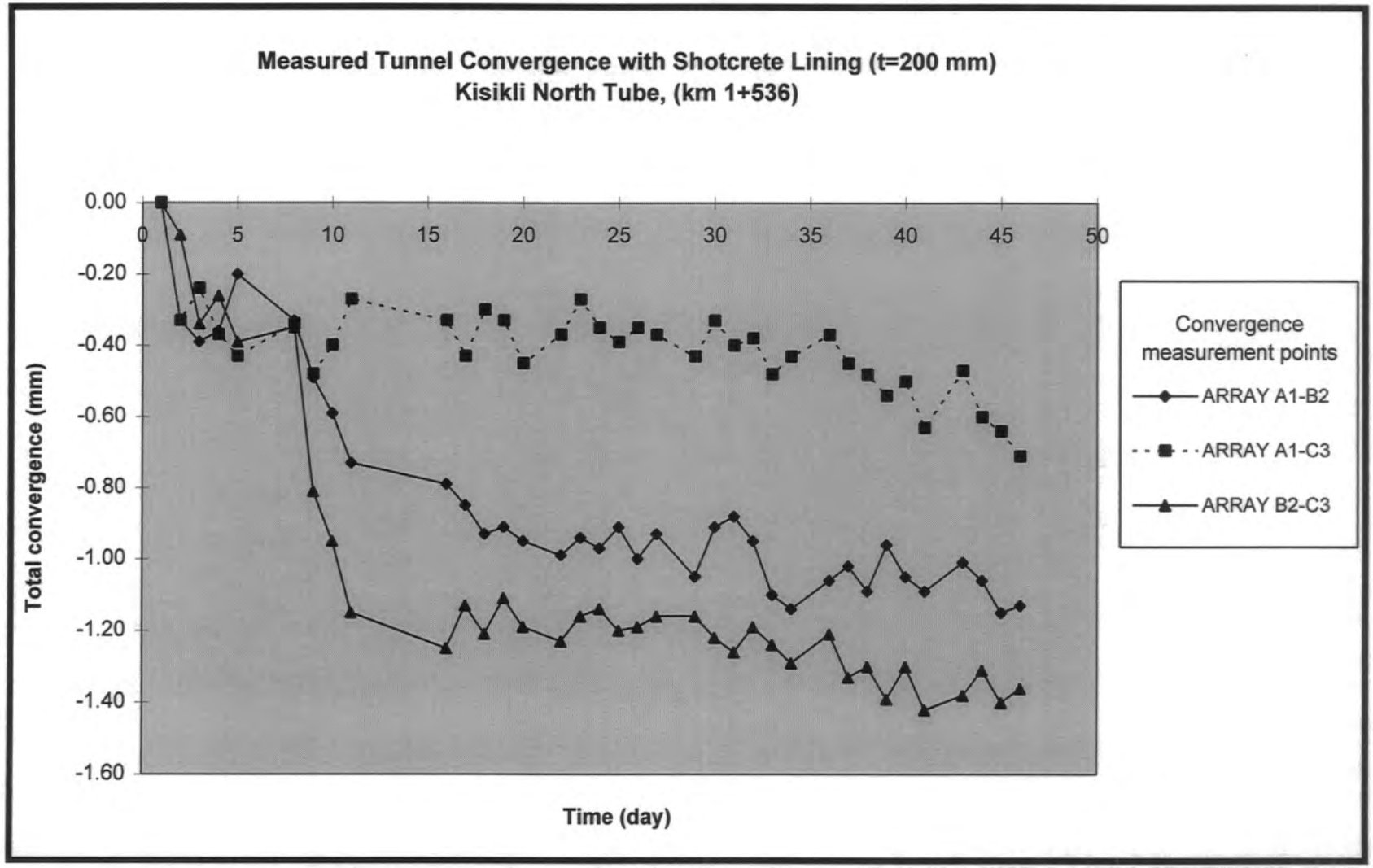

Fig. 7.6 Measured tunnel displacements for Kisikli north tube (km 1+536)

EXTENSOMETER MONITORING
KISIKLI SOUTH TUNNEL, (km 1+544)
THICKNESS OF SHOTCRETE = 200 mm

	ARRAY A1B2			ARRAY A1C3			ARRAY A1D4			ARRAY A1E5			ARRAY B2C3			ARRAY D4E5		
	MOVEMENT			MOVEMENT			MOVEMENT			MOVEMENT			MOVEMENT			MOVEMENT		
DATE	READING	LAST	TOTAL	READING	LAST	TOTAL	READING	LAST	TOTAL	READING	LAST	TOTAL	READING	LAST	TOTAL	READING	LAST	TOTAL
	mm			mm			mm			mm			mm			mm		
1	7498.81	0.00	0.00	6119.42	0.00	0.00							12605.87	0.00	0.00			
4	7498.66	-0.15	-0.15	6119.38	-0.04	-0.04							12605.72	-0.15	-0.15			
5	7498.59	-0.07	-0.22	6119.33	-0.05	-0.09							12605.64	-0.08	-0.23			
6	7498.48	-0.11	-0.33	6119.27	-0.06	-0.15							12605.55	-0.09	-0.32			
7	7498.44	-0.04	-0.37	6119.30	0.03	-0.12							12605.64	0.09	-0.23			
12	7498.54	0.10	-0.27	6119.36	0.06	-0.06							12605.68	0.04	-0.19			
13	7498.51	-0.03	-0.30	6119.31	-0.05	-0.11							12605.77	0.09	-0.10			
14	7498.55	0.04	-0.26	6119.34	0.03	-0.08							12605.73	-0.04	-0.14			
15	7498.47	-0.08	-0.34	6119.28	-0.06	-0.14							12605.66	-0.07	-0.21			
16	7498.53	0.06	-0.28	6119.33	0.05	-0.09							12605.64	-0.02	-0.23			
18	7498.46	-0.07	-0.35	6119.35	0.02	-0.07							12605.60	-0.04	-0.27			
19	7498.44	-0.02	-0.37	6119.26	-0.09	-0.16							12605.66	0.06	-0.21			
20	7498.48	0.04	-0.33	6119.24	-0.02	-0.18							12605.71	0.05	-0.16			
21	7498.51	0.03	-0.30	6119.30	0.06	-0.12							12605.58	-0.13	-0.29			
22	7498.53	0.02	-0.28	6119.28	-0.02	-0.14							12605.64	0.06	-0.23			
23	7498.42	-0.11	-0.39	6119.36	0.08	-0.06							12605.73	0.09	-0.14			
25	7498.47	0.05	-0.34	6119.31	-0.05	-0.11							12605.67	-0.06	-0.20			
26	7498.40	-0.07	-0.41	6119.39	0.08	-0.03							12605.69	0.02	-0.18			
27	7498.48	0.08	-0.33	6119.33	-0.06	-0.09							12605.61	-0.08	-0.26			
28	7498.51	0.03	-0.30	6119.38	0.05	-0.04							12605.66	0.05	-0.21			
29	7498.41	-0.10	-0.40	6119.34	-0.04	-0.08							12605.57	-0.09	-0.30			
30	7498.45	0.04	-0.36	6119.31	-0.03	-0.11							12605.55	-0.02	-0.32			
32	7498.44	-0.01	-0.37	6119.35	0.04	-0.07							12605.51	-0.04	-0.36			
33	7498.38	-0.06	-0.43	6119.40	0.05	-0.02							12605.48	-0.03	-0.39			
34	7498.47	0.09	-0.34	6119.32	-0.08	-0.10							12605.61	0.13	-0.26			
35	7498.45	-0.02	-0.36	6119.28	-0.04	-0.14							12605.66	0.05	-0.21			
36	7498.48	0.03	-0.33	6119.36	0.08	-0.06							12605.59	-0.07	-0.28			
37	7498.43	-0.05	-0.38	6119.25	-0.11	-0.17							12605.55	-0.04	-0.32			
39	7498.37	-0.06	-0.44	6119.21	-0.04	-0.21							12605.51	-0.04	-0.36			
40	7498.35	-0.02	-0.46	6119.34	0.13	-0.08							12605.46	-0.05	-0.41			
41	7498.31	-0.04	**-0.50**	6119.27	-0.07	**-0.15**							12605.42	-0.04	**-0.45**			

Table 7.3 Measured tunnel displacements for Kisikli south tube (km 1+544)

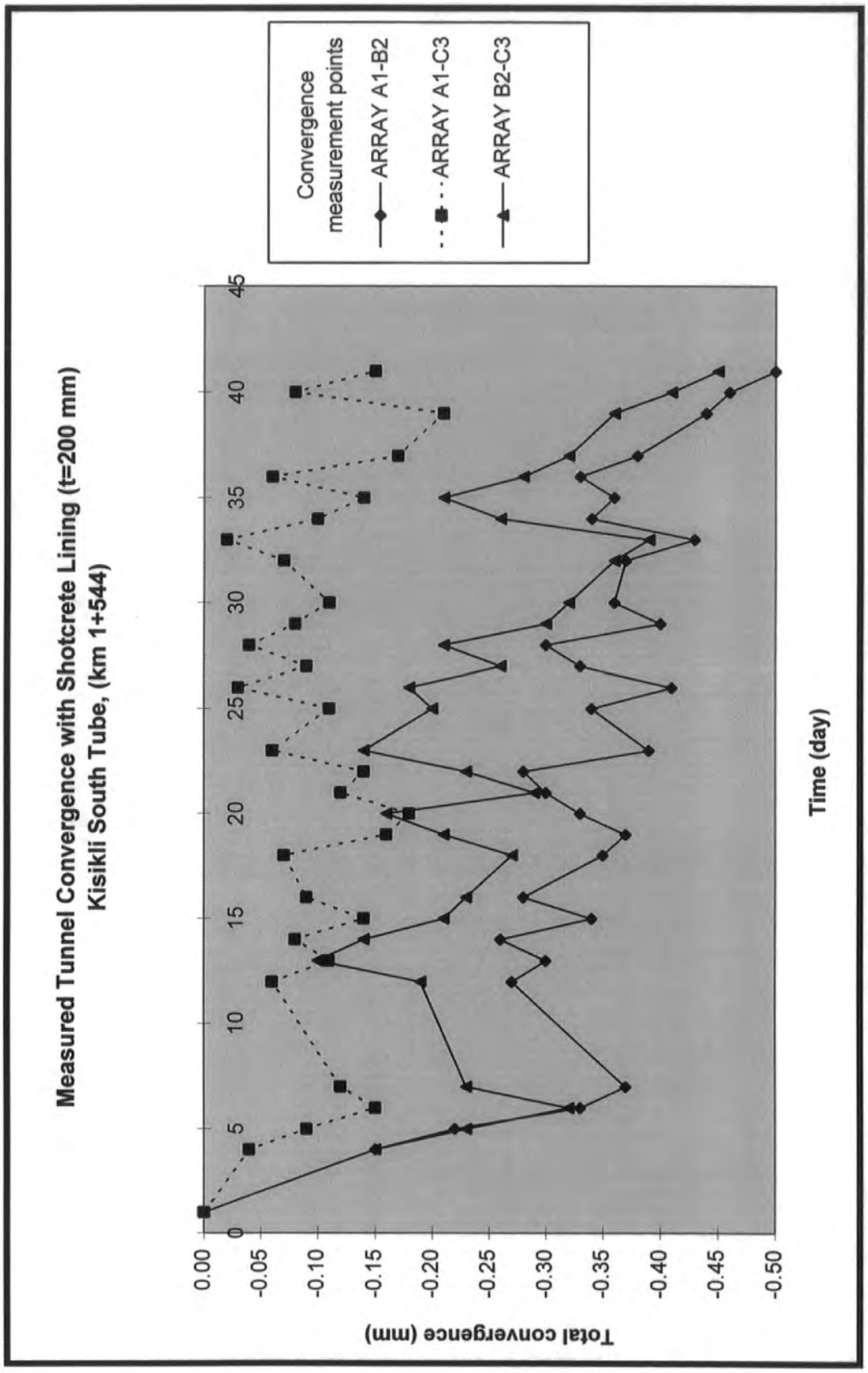

Fig. 7.7 Measured tunnel convergence for Kisikli south tube (km 1+544)

7.3 Simulation Results and Comparisons

Simulation of ground movements around the tunnel and the resulting settlement at ground surface can be achieved using a two-dimensional finite element model. However, it is necessary to adopt a three-dimensional model when considering the periodic support system, steel arches and anchorages. Ideally, the block of ground was modelled having the tunnel support systems and partial excavation. The boundaries of the model were approximately three times the tunnel width from the tunnel centre.

There were no differences between the displacements and stresses on the excavation boundary when the gravity difference method and stress reversal techniques were used. Summary results of the Kisikli north tube for Von Mises stresses and displacements resulting from the gravity difference method and stress reversal technique are given in several tables in the present section. Comparison between stresses and displacements also are given in several figures within this section of the thesis.

The gravity difference method uses air elements inside the tunnel, as explained in Chapter 4. Results stemming from the extraction of elements inside the tunnel model and the excavated tunnel simulation with air elements were compared and they proved to be the same. Subtractions of displacements and of stresses from excavated and unexcavated runs were calculated by means of the post-processing program written by the author for the gravity difference method.

Initially two- and three-dimensional symmetric and full tunnel model stress and displacement results were compared with those measured in the Kisikli north tube without a support system. There were no differences between the results for the symmetric and full model conditions.

7.3.1 Kisikli North Tube (km 1+400)

Two-dimensional model dimensions, material properties and geological conditions of this section of the Kisikli north tube at km 1+400 are shown in Fig. 7.9. Fig. 7.10 shows the overall tunnel model mesh diagram produced by the pre-processing programs. The node and element numbers along the excavation surface are shown in Fig. 7.11. There were 384 elements and 1736 nodes in the mesh diagram. This number of elements and nodes was only achieved by the lowest resolution number in the input data file for the finite element mesh generation. Fig. 7.12 shows the node numbers along the shotcrete lining. It should be noted that Figs. 7.10 to 7.12 are produced using PAFEC-PIGS rather than UNIRAS because it provides a PostScript file of the model mesh diagram having node and element numbers. A detail of the mesh and geological conditions produced by the post-processing program using UNIRAS is also shown in Fig. 7.13. The results of these analyses using both the gravity difference method and stress reversal technique are presented in Figs. 7.14 to 7.24 and summarised in Tables 7.4 to 7.7.

7.3.1.1 Comparison of Gravity Difference Method and Stress Reversal Technique

Stress and displacement results for the gravity difference and stress reversal techniques are plotted for comparison purposes along the excavation surface and at various points in chosen directions within the surrounding rock as shown in Fig. 7.8.

Table 7.4 shows a comparison of the Von Mises stresses obtained using the gravity difference method and stress reversal technique for the Kisikli north tube (km 1+400). The variations in stress along the chosen directions are also shown graphically in Fig. 7.14 for comparison. Using both techniques, Von Mises stresses along the excavation surface at the same tunnel section are shown in

Table 7.5 and are plotted as a polar diagram as shown in Fig. 7.15. The results obtained using both techniques are very similar.

Table 7.6 shows a comparison of the gravity difference method and the stress reversal technique for component and resultant displacements at points along the chosen directions. The same results are presented in Fig. 7.16 for visual comparison. Fig. 7.17 shows deformed and undeformed mesh diagrams for this section of the Kisikli tunnel. It can be seen that the roof and invert area of the tunnel have quite extensive convergence. The component and resultant displacements at points along the excavation surface obtained using both techniques are shown in Table 7.7 and are presented in Fig. 7.18. The resultant displacements are also presented in Fig. 7.19 using a polar diagram. From the displacement results it can be seen that the model is deformed symmetrically. Finally a comparison of Von Mises stresses and resultant displacements along the excavation surface is shown in Fig. 7.20. This figure illustrates relative changes in stresses and displacements. It can be seen that where the displacement is low, the resulting stress is high and also when the displacement is high, the resulting stress is low.

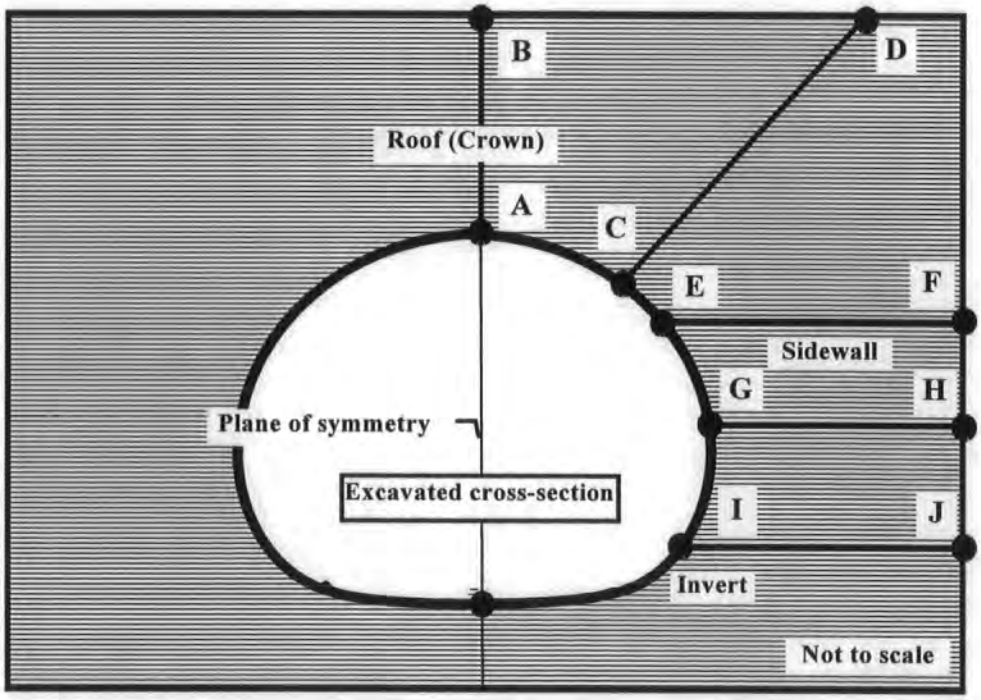

Fig. 7.8 Chosen directions for the analysis of surrounding rock

Figs. 7.21 to 7.24 are examples of graphical colour output for the two-dimensional model of the Kisikli north tube at km 1+400. Fig. 7.21 shows the Von Mises stress distribution in colour and the slightly deformed shape of the unexcavated ground under the action of gravity. Fig. 7.22 shows a similar diagram for the excavated ground. The gravity difference method uses the differences between the two analyses to produce the stresses and displacements shown in Fig. 7.23 that result from the ground excavation. Fig. 7.24 shows a similar colour diagram using the stress reversal technique. In comparing Von Mises stresses and displacements from the gravity difference method and stress reversal technique, it can be seen that the outputs are very similar and show quite convincingly the deformation style of the model.

It is possible to estimate the Von Mises stress and displacement of the rock layer on the boundary of excavation. A failure zone will be produced in the rock mass around the excavation when induced stresses are greater than the rock strength. The extent of the high stress zone produced by excavation of the tunnel can be assessed from a consideration of Von Mises criterion. In each example the zones of increased stress are indicated on each colour diagram, by the change in colour from red to blue indicating the reduction in field stress away from the tunnel excavation boundary.

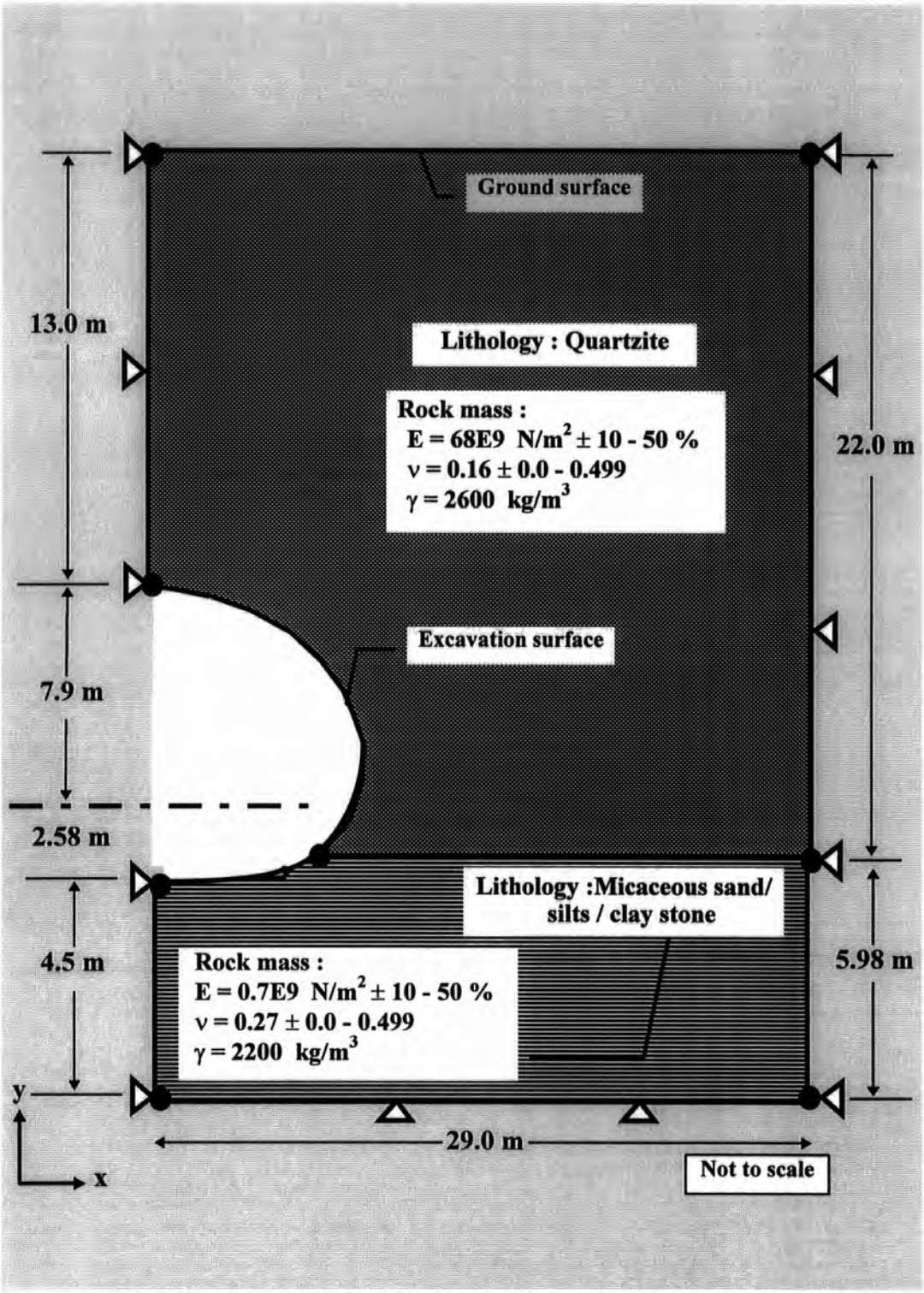

Fig. 7.9 Model dimensions, material properties and geological conditions of Kisikli north tube (km 1+400)

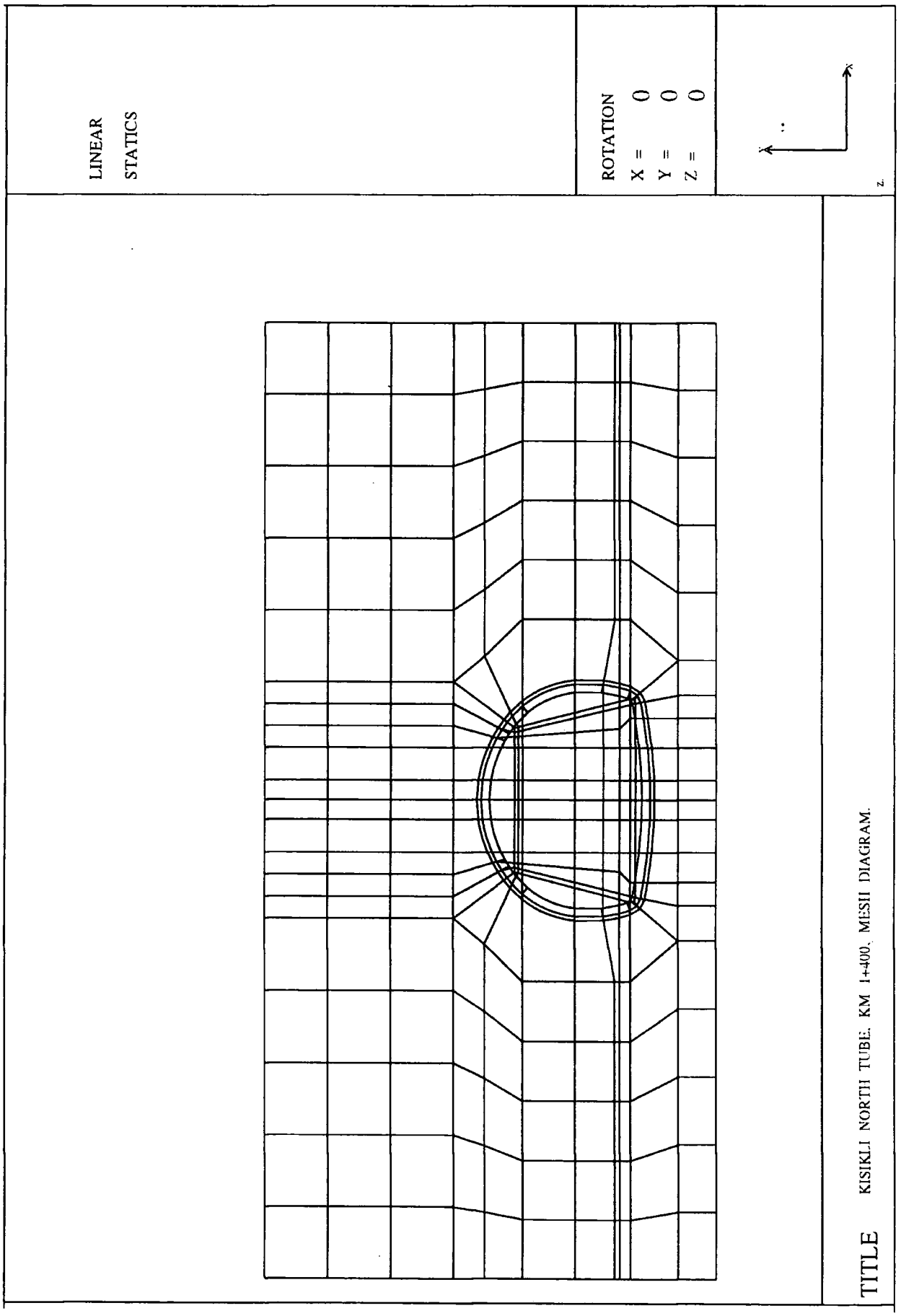

Fig. 7.10 Mesh diagram of Kisikli north tube (km 1+400)

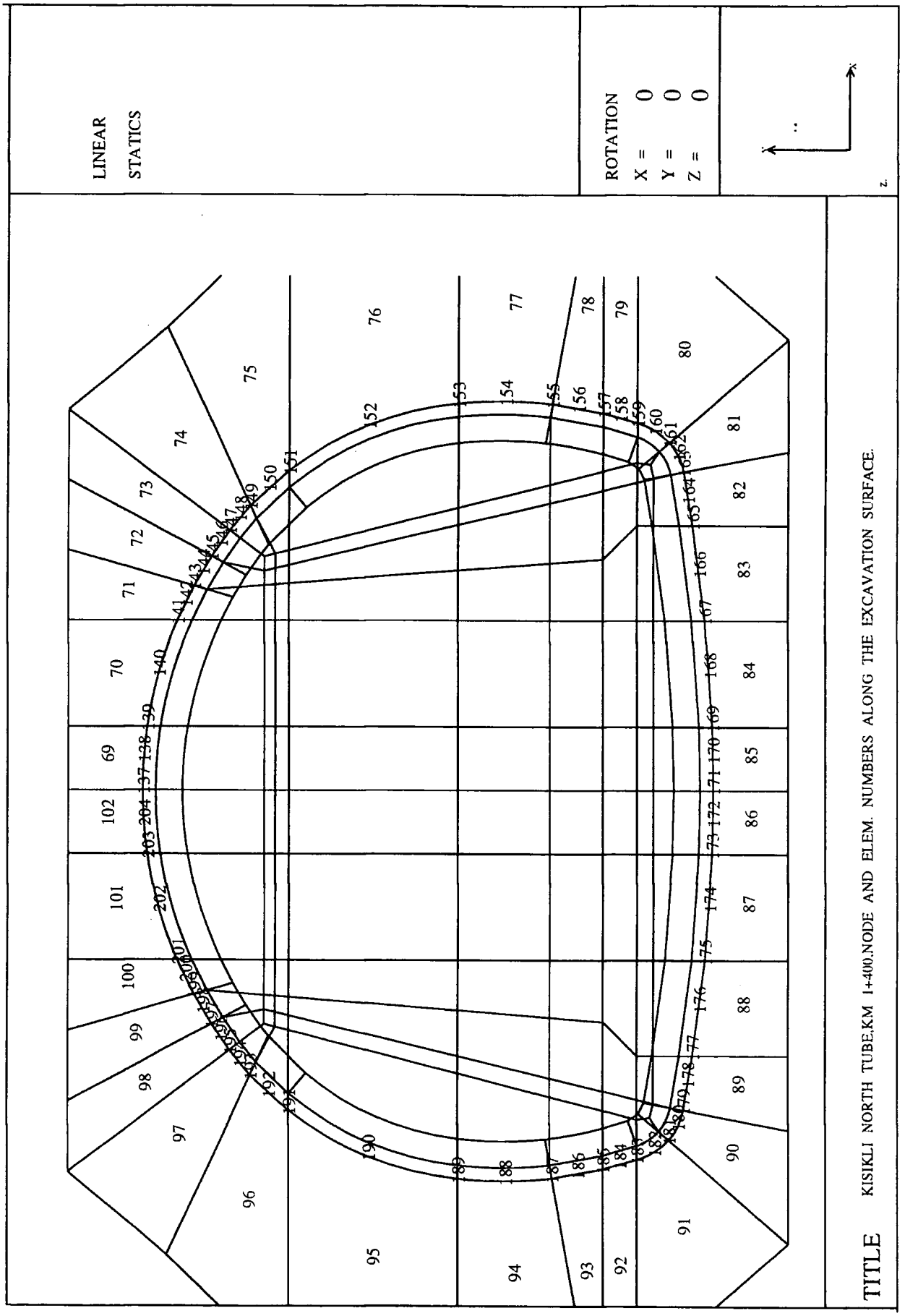

Fig. 7.11 Node and element numbers along the excavation surface of Kisikli north tube (km 1+400)

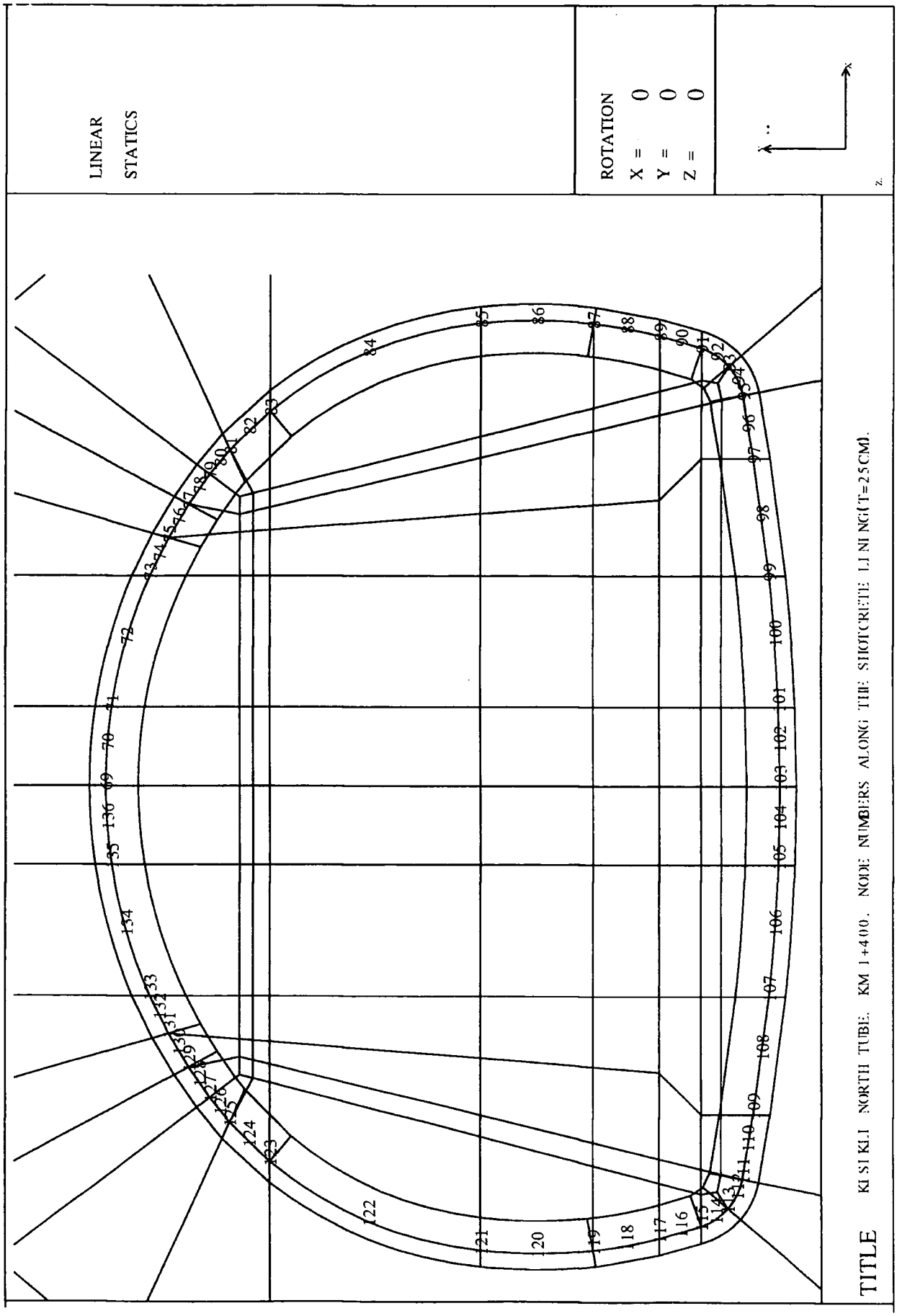

Fig. 7.12 Node numbers along the free surface of the shotcrete lining of Kisikli north tube (km 1+400)

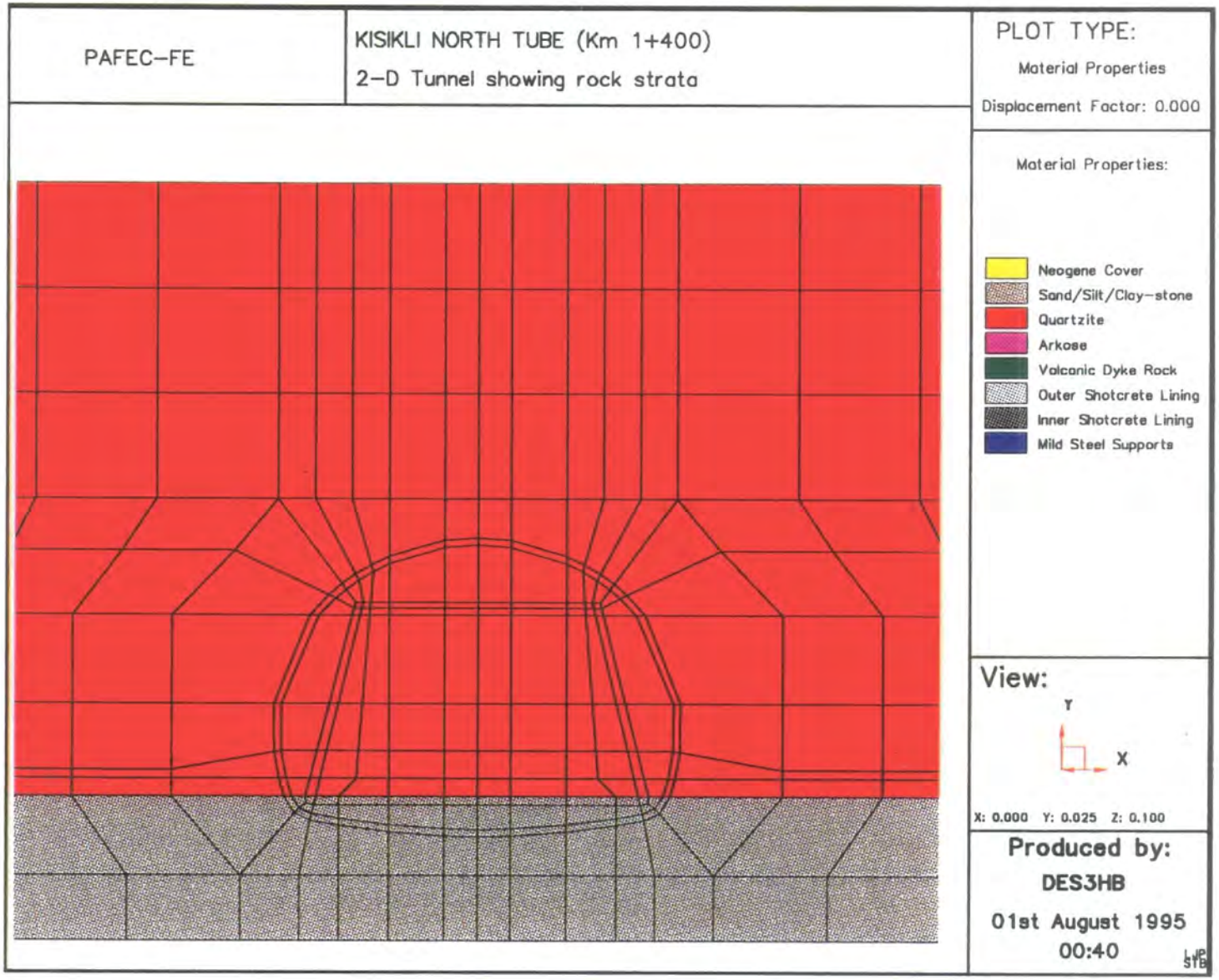

Fig. 7.13 Mesh diagram and colour output of geological conditions of Kisikli north tube (km 1+400)

KISIKLI NORTH TUBE					*GRAVITY DIFFERENCE*	*STRESS REVERSAL*
km 1+400					*METHOD*	*TECHNIQUE*
WITHOUT SHOTCRETE LINING						
HETEROGENEOUS MODEL					*Number of nodes =1650*	*Number of nodes =1650*
LITHOLOGY : QUARTZITE + MICACEOUS SAND / SILT / CLAY STONE					*Number of elements =356*	*Number of elements =356*
	NODE				*Number of d.o.f =2175*	*Number of d.o.f =2175*
	NUMBER					
	A LONG THE	COMPUTED			AVERAGED	AVERAGED
ELEMENT	Y-AXIS	RESULT	AXIAL	AXIAL DIS. /	VON MISES	VON MISES
NUMBER	(A-B)	LOCATIONS	DISTANCE (m)	HOLE RAD.	STRESS (N/m^-2)	STRESS (N/m^-2)
69	137	1	8.15	1.03	2.12E+05	2.14E+05
69	983	2	8.85	1.12	2.34E+05	2.38E+05
173	205	3	9.55	1.21	2.63E+05	2.64E+05
173	1239	4	11.44	1.45	2.41E+05	2.37E+05
174	1241	5	13.33	1.69	1.97E+05	1.90E+05
174	1244	6	15.22	1.93	1.68E+05	1.60E+05
175	1246	7	17.12	2.17	1.52E+05	1.42E+05
175	1249	8	19.01	2.41	1.82E+05	1.68E+05
175	305	9	20.90	2.65	2.45E+05	2.26E+05
	A LONG THE					
	DIAGONAL					
	(C-D)					
73	147	10	8.15	1.03	4.45E+05	4.39E+05
73	988	11	10.04	1.27	3.24E+05	3.17E+05
188	215	12	11.96	1.51	2.86E+05	2.78E+05
194	1290	13	17.64	2.23	1.51E+05	1.36E+05
200	1307	14	23.37	2.96	7.23E+04	6.29E+04
200	1324	15	26.27	3.33	1.03E+05	9.28E+04
	A LONG THE					
	X-AXIS					
	(E-F)					
75	151	16	6.05	0.77	6.45E+05	6.48E+05
75	991	17	8.52	1.08	2.80E+05	2.76E+05
108	219	18	11.00	1.39	1.23E+05	1.22E+05
108	1056	19	12.80	1.62	9.96E+04	8.81E+04
109	1058	20	14.60	1.85	1.23E+05	1.13E+05
109	1059	21	16.40	2.08	1.24E+05	1.16E+05
110	1061	22	18.20	2.30	1.22E+05	1.14E+05
110	1062	23	20.00	2.53	1.06E+05	9.91E+04
111	1064	24	21.80	2.76	9.27E+04	8.76E+04
111	1065	25	23.60	2.99	7.45E+04	7.05E+04
112	1067	26	25.40	3.22	6.13E+04	5.85E+04
112	1068	27	27.20	3.44	5.01E+04	4.83E+04
112	277	28	29.00	3.67	4.62E+04	4.48E+04
	A LONG THE					
	X-AXIS					
	(G-H)					
76	153	29	7.32	0.93	1.06E+06	1.08E+06
76	993	30	9.16	1.16	2.44E+05	2.40E+05
113	221	31	11.00	1.39	1.42E+05	1.35E+05
113	1070	32	12.80	1.62	1.83E+05	1.75E+05
114	1072	33	14.60	1.85	2.01E+05	1.98E+05
114	1073	34	16.40	2.08	1.57E+05	1.54E+05
115	1075	35	18.20	2.30	1.40E+05	1.38E+05
115	1076	36	20.00	2.53	1.11E+05	1.09E+05
116	1078	37	21.80	2.76	9.27E+04	9.09E+04
116	1079	38	23.60	2.99	7.55E+04	7.38E+04
117	1081	39	25.40	3.22	6.41E+04	6.23E+04
117	1082	40	27.20	3.44	5.65E+04	5.48E+04
117	279	41	29.00	3.67	5.38E+04	5.20E+04
	A LONG THE					
	X-AXIS					
	(I-J)					
79	159	42	6.95	0.88	1.70E+06	1.71E+06
79	996	43	8.98	1.14	7.33E+05	7.43E+05
128	227	44	11.00	1.39	5.54E+05	5.68E+05
128	1109	45	12.80	1.62	2.77E+05	2.88E+05
129	1111	46	14.60	1.85	2.35E+05	2.46E+05
129	1112	47	16.40	2.08	1.44E+05	1.53E+05
130	1114	48	18.20	2.30	9.33E+04	1.01E+05
130	1115	49	20.00	2.53	7.28E+04	7.76E+04
131	1117	50	21.80	2.76	6.24E+04	6.22E+04
131	1118	51	23.60	2.99	6.00E+04	5.61E+04
132	1120	52	25.40	3.22	6.22E+04	5.46E+04
132	1121	53	27.20	3.44	6.37E+04	5.50E+04
132	285	54	29.00	3.67	6.54E+04	5.58E+04

Table 7.4 Comparison of stresses along the chosen directions for Kisikli north tube, (km 1+400), using gravity difference and stress reversal techniques

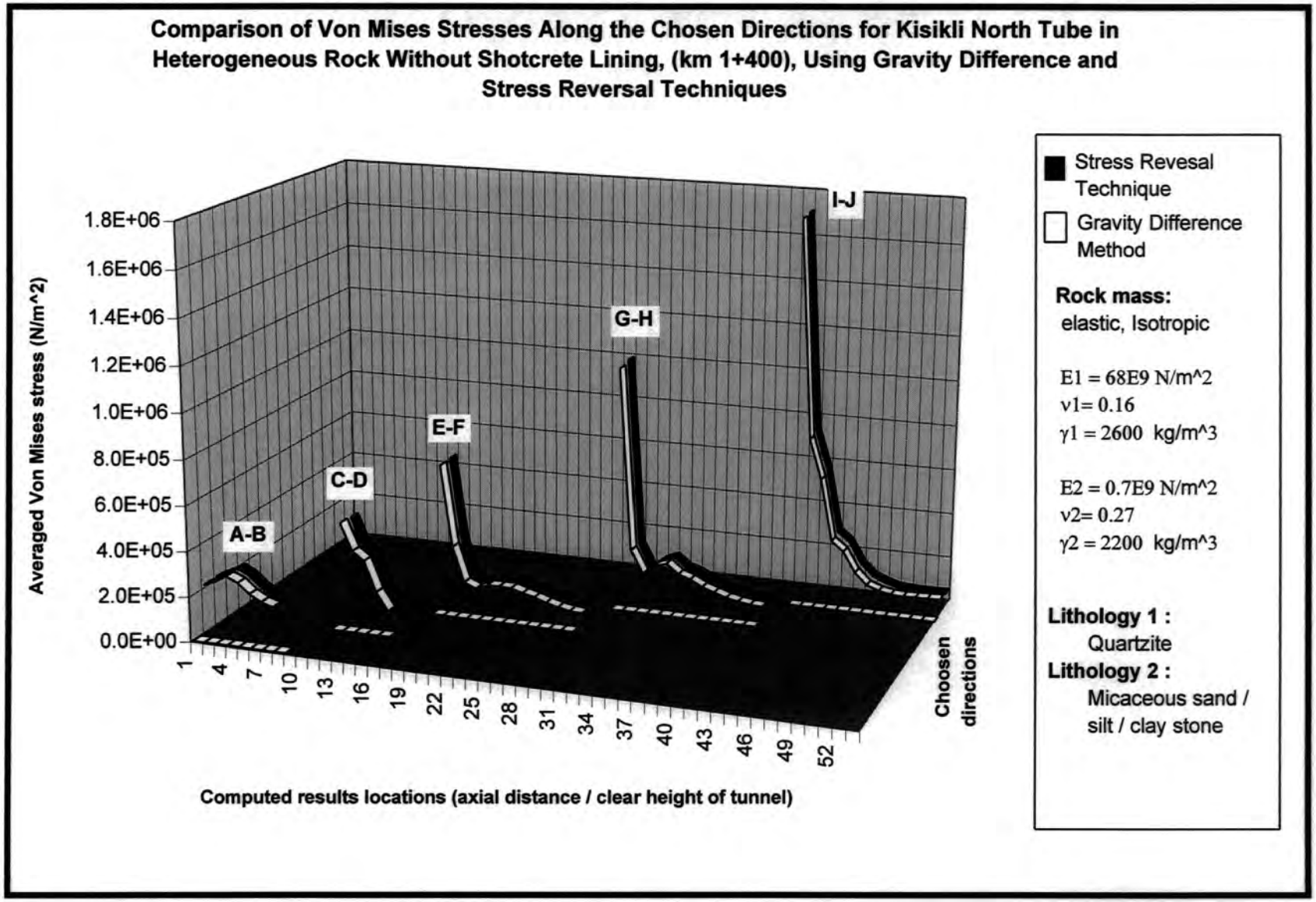

Fig 7.14 Comparison of stresses along the chosen directions for Kisikli north tube, (km 1+400), using gravity difference and stress reversal techniques

KISIKLI NORTH TUBE		*GRAVITY DIFFERENCE*	*STRESS REVERSAL*
km 1+400		*METHOD*	*TECHNIQUE*
WITHOUT SHOTCRETE LINING			
HETEROGENEOUS MODEL		*Number of nodes =1650*	*Number of nodes =1650*
LITHOLOGY : QUARTZITE + MICACEOUS SAND /		*Number of elements =356*	*Number of elements =356*
SILT / CLAY STONE		*Number of d.o.f =2175*	*Number of d.o.f =2175*
ELEMENT	NODE		
NUMBER	NUMBER		
ALONG THE	ALONG THE	AVERAGED	AVERAGED
EXCAVATION	EXCAVATION	VON MISES	VON MISES
SURFACE	SURFACE	STRESS (N/m^2)	STRESS (N/m^2)
69	137	2.12E+05	2.14E+05
69	138	2.14E+05	2.11E+05
70	139	2.16E+05	2.20E+05
70	140	2.50E+05	2.44E+05
71	141	2.93E+05	2.97E+05
71	142	3.24E+05	3.23E+05
72	143	3.51E+05	3.48E+05
72	144	3.80E+05	3.77E+05
73	145	4.08E+05	4.05E+05
73	146	4.38E+05	4.34E+05
74	147	4.45E+05	4.39E+05
74	148	4.93E+05	4.91E+05
75	149	5.51E+05	5.56E+05
75	150	6.22E+05	6.21E+05
76	151	6.45E+05	6.48E+05
76	152	8.17E+05	8.23E+05
77	153	1.06E+06	1.08E+06
77	154	1.25E+06	1.28E+06
78	155	1.35E+06	1.36E+06
78	156	1.46E+06	1.48E+06
79	157	1.46E+06	1.48E+06
79	158	1.57E+06	1.58E+06
80	159	1.70E+06	1.71E+06
80	160	9.11E+05	9.00E+05
80	161	7.94E+05	7.85E+05
81	162	5.72E+05	5.68E+05
81	163	4.53E+05	4.54E+05
82	164	3.99E+05	4.04E+05
82	165	3.71E+05	3.71E+05
83	166	3.99E+05	4.06E+05
83	167	4.07E+05	4.04E+05
84	168	4.43E+05	4.50E+05
84	169	4.73E+05	4.69E+05
85	170	4.77E+05	4.82E+05
85	171	4.80E+05	4.81E+05
86	172	4.77E+05	4.82E+05
86	173	4.73E+05	4.69E+05
87	174	4.43E+05	4.50E+05
87	175	4.07E+05	4.04E+05
88	176	3.99E+05	4.06E+05
88	177	3.71E+05	3.71E+05
89	178	3.99E+05	4.04E+05
89	179	4.53E+05	4.54E+05
90	180	5.72E+05	5.68E+05
90	181	7.94E+05	7.85E+05
91	182	9.11E+05	9.00E+05
91	183	1.70E+06	1.71E+06
92	184	1.57E+06	1.58E+06
92	185	1.46E+06	1.48E+06
93	186	1.46E+06	1.48E+06
93	187	1.35E+06	1.36E+06
94	188	1.25E+06	1.28E+06
94	189	1.06E+06	1.08E+06
95	190	8.17E+05	8.23E+05
95	191	6.45E+05	6.48E+05
96	192	6.22E+05	6.21E+05
96	193	5.51E+05	5.56E+05
97	194	4.94E+05	4.91E+05
97	195	4.45E+05	4.39E+05
98	196	4.38E+05	4.34E+05
98	197	4.08E+05	4.05E+05
99	198	3.79E+05	3.77E+05
100	199	3.51E+05	3.48E+05
100	200	3.24E+05	3.23E+05
101	201	2.92E+05	2.97E+05
101	202	2.49E+05	2.44E+05
102	203	2.17E+05	2.20E+05
102	204	2.14E+05	2.11E+05

Table 7.5 Comparison of stresses along the excavation surface for Kisikli north tube, (km 1+400), using gravity difference and stress reversal techniques

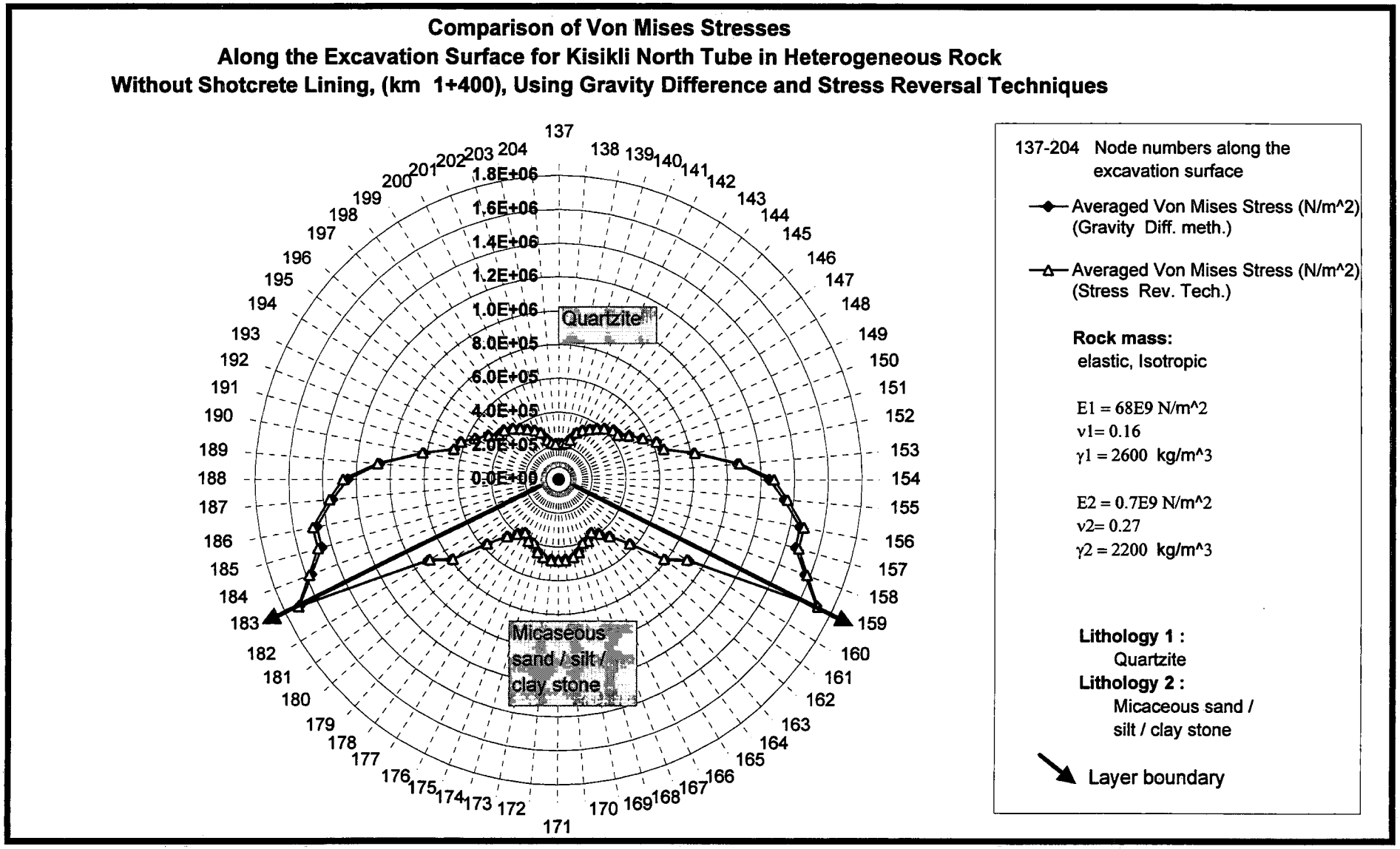

Fig. 7.15 Comparison of stresses along the excavation surface for Kisikli north tube, (km 1+400), using gravity difference and stress reversal techniques

KISIKLI NORTH TUBE					*GRAVITY DIFFERENCE*			*STRESS REVERSAL*		
km 1+400					*METHOD*			*TECHNIQUE*		
WITHOUT SHOTCRETE LINING										
HETEROGENEOUS MODEL					*Number of nodes =1650*			*Number of nodes =1650*		
LITHOLOGY : QUARTZITE + MICACEOUS SAND / SILT / CLAY STONE					*Number of elements =356*			*Number of elements =356*		
	NODE				*Number of d.o.f =2175*			*Number of d.o.f =2175*		
	NUMBER									
	A LONG THE	COMPUTED								
ELEMENT	Y-AXIS	RESULT	AXIAL	AXIAL DIS. /	DISPLACEMENT (m)			DISPLACEMENT (m)		
NUMBER	(A-B)	LOCATIONS	DISTANCE (m)	HOLE RAD.	Ux	Uy	U	Ux	Uy	U
69	137	1	8.15	1.03	0.0000	-0.6971	0.6971	0.0000	-0.6415	0.6415
69	983	2	8.85	1.12	0.0000	-0.6941	0.6941	0.0000	-0.6385	0.6385
173	205	3	9.55	1.21	0.0000	-0.6912	0.6912	0.0000	-0.6355	0.6355
173	1239	4	11.44	1.45	0.0000	-0.6839	0.6839	0.0000	-0.6284	0.6284
174	1241	5	13.33	1.69	0.0000	-0.6786	0.6786	0.0000	-0.6232	0.6232
174	1244	6	15.22	1.93	0.0000	-0.6749	0.6749	0.0000	-0.6197	0.6197
175	1246	7	17.12	2.17	0.0000	-0.6726	0.6726	0.0000	-0.6174	0.6174
175	1249	8	19.01	2.41	0.0000	-0.6711	0.6711	0.0000	-0.6160	0.6160
175	305	9	20.90	2.65	0.0000	-0.6698	0.6698	0.0000	-0.6148	0.6148
	A LONG THE									
	DIAGONAL									
	(C-D)									
73	147	10	8.15	1.03	0.0093	-0.6731	0.6732	0.0084	-0.6176	0.6177
73	988	11	10.04	1.27	0.0015	-0.6592	0.6592	0.0010	-0.6042	0.6042
188	215	12	11.96	1.51	-0.0018	-0.6510	0.6510	-0.0020	-0.5966	0.5966
194	1290	13	17.64	2.23	-0.0061	-0.6318	0.6318	-0.0056	-0.5796	0.5796
200	1307	14	23.37	2.96	-0.0118	-0.6169	0.6170	-0.0106	-0.5666	0.5667
200	1324	15	26.27	3.33	-0.0158	-0.6060	0.6062	-0.0139	-0.5572	0.5574
	A LONG THE									
	X-AXIS									
	(E-F)									
75	151	16	6.05	0.77	0.0100	-0.6573	0.6574	0.0086	-0.6019	0.6020
75	991	17	8.52	1.08	0.0078	-0.6325	0.6326	0.0066	-0.5784	0.5784
108	219	18	11.00	1.39	0.0068	-0.6243	0.6243	0.0056	-0.5719	0.5719
108	1056	19	12.80	1.62	0.0052	-0.6200	0.6200	0.0040	-0.5687	0.5687
109	1058	20	14.60	1.85	0.0037	-0.6155	0.6155	0.0025	-0.5652	0.5652
109	1059	21	16.40	2.08	0.0026	-0.6107	0.6107	0.0014	-0.5613	0.5613
110	1061	22	18.20	2.30	0.0019	-0.6059	0.6059	0.0008	-0.5572	0.5572
110	1062	23	20.00	2.53	0.0013	-0.6014	0.6014	0.0004	-0.5533	0.5533
111	1064	24	21.80	2.76	0.0010	-0.5974	0.5974	0.0003	-0.5498	0.5498
111	1065	25	23.60	2.99	0.0007	-0.5942	0.5942	0.0001	-0.5470	0.5470
112	1067	26	25.40	3.22	0.0005	-0.5918	0.5918	0.0001	-0.5449	0.5449
112	1068	27	27.20	3.44	0.0000	-0.5908	0.5908	0.0000	-0.5436	0.5436
112	277	28	29.00	3.67	0.0000	-0.5898	0.5898	0.0000	-0.5431	0.5431
	A LONG THE									
	X-AXIS									
	(G-H)									
76	153	29	7.32	0.93	0.0044	-0.6138	0.6138	0.0017	-0.5584	0.5584
76	993	30	9.16	1.16	0.0072	-0.6162	0.6162	0.0045	-0.5624	0.5624
113	221	31	11.00	1.39	0.0044	-0.6206	0.6206	0.0017	-0.5683	0.5683
113	1070	32	12.80	1.62	0.0030	-0.6188	0.6188	0.0005	-0.5676	0.5676
114	1072	33	14.60	1.85	0.0030	-0.6144	0.6144	0.0006	-0.5643	0.5643
114	1073	34	16.40	2.08	0.0029	-0.6094	0.6094	0.0007	-0.5602	0.5602
115	1075	35	18.20	2.30	0.0029	-0.6041	0.6041	0.0010	-0.5556	0.5556
115	1076	36	20.00	2.53	0.0029	0.5992	0.5992	0.0012	-0.5513	0.5513
116	1078	37	21.80	2.76	0.0026	-0.5949	0.5949	0.0013	-0.5475	0.5475
116	1079	38	23.60	2.99	0.0022	0.5914	0.5914	0.0011	-0.5444	0.5444
117	1081	39	25.40	3.22	0.0016	-0.5889	0.5889	0.0009	-0.5422	0.5422
117	1082	40	27.20	3.44	0.0008	-0.5874	0.5874	0.0005	-0.5408	0.5408
117	279	41	29.00	3.67	0.0000	-0.5868	0.5868	0.0000	-0.5403	0.5403
	A LONG THE									
	X-AXIS									
	(I-J)									
79	159	42	6.95	0.88	-0.0573	-0.5322	0.5353	-0.0632	-0.4753	0.4795
79	996	43	8.98	1.14	-0.0313	-0.6054	0.6062	-0.0367	-0.5516	0.5528
128	227	44	11.00	1.39	-0.0106	-0.6150	0.6151	-0.0155	-0.5629	0.5631
128	1109	45	12.80	1.62	-0.0036	-0.6155	0.6155	-0.0080	-0.5646	0.5647
129	1111	46	14.60	1.85	0.0024	-0.6112	0.6112	-0.0016	-0.5614	0.5614
129	1112	47	16.40	2.08	0.0053	-0.6060	0.6060	0.0018	-0.5571	0.5571
130	1114	48	18.20	2.30	0.0069	-0.6005	0.6005	0.0038	-0.5523	0.5523
130	1115	49	20.00	2.53	0.0072	-0.5955	0.5955	0.0046	-0.5479	0.5479
131	1117	50	21.80	2.76	0.0066	-0.5912	0.5912	0.0045	-0.5441	0.5441
131	1118	51	23.60	2.99	0.0055	-0.5877	0.5877	0.0039	-0.5410	0.5410
132	1120	52	25.40	3.22	0.0039	-0.5852	0.5852	0.0028	-0.5387	0.5387
132	1121	53	27.20	3.44	0.0020	-0.5836	0.5836	0.0015	-0.5374	0.5374
132	285	54	29.00	3.67	0.0000	-0.5831	0.5831	0.0000	-0.5369	0.5369

Table 7.6 Comparison of displacements along the chosen directions for Kisikli north tube, (km 1+400), using gravity difference and stress reversal techniques

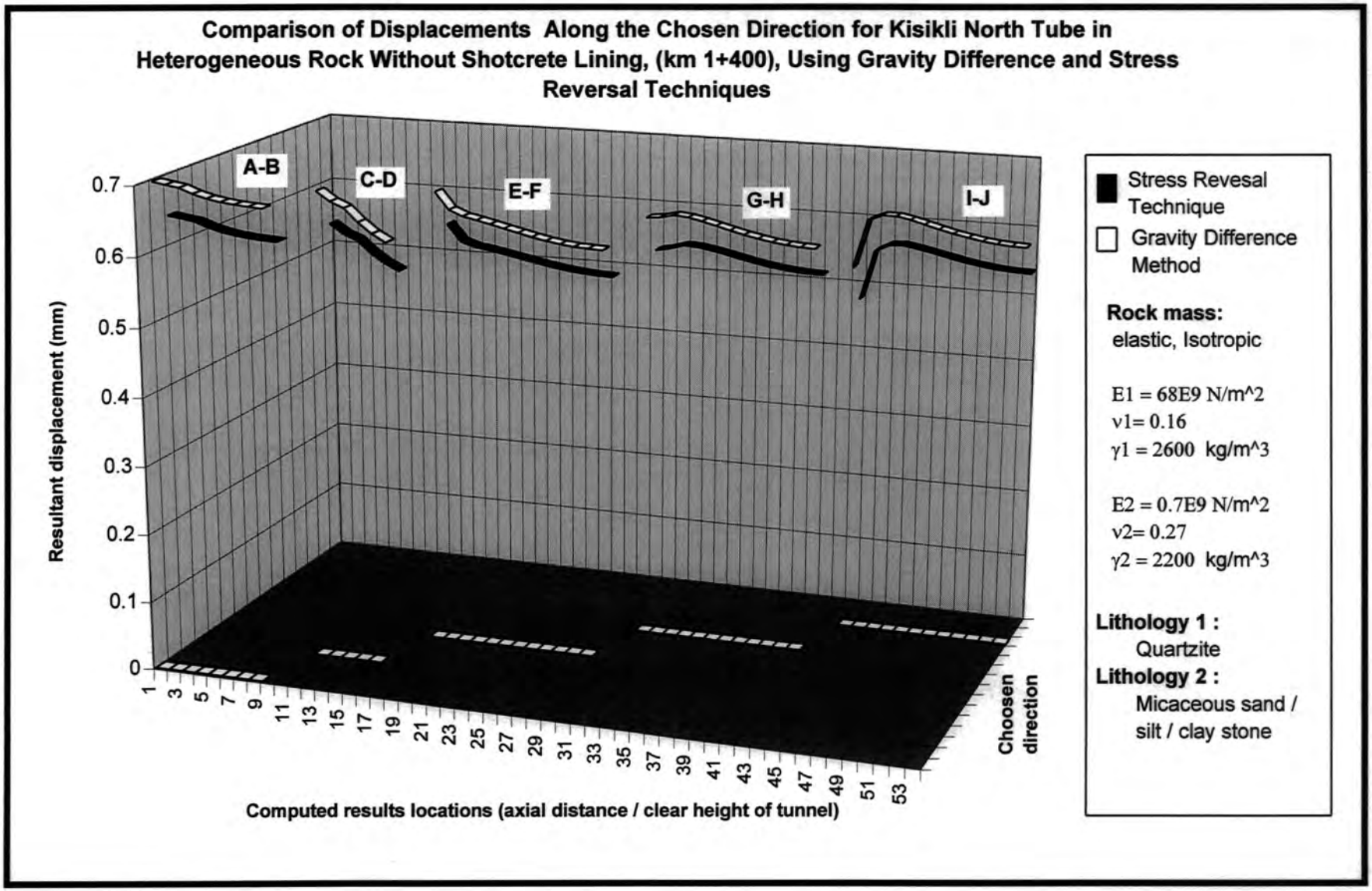

Fig. 7.16 Comparison of diplacements along the chosen directions for Kisikli north tube, (km 1+400), using gravity difference and stress reversal techniques

KISIKLI NORTH TUBE		*GRAVITY DIFFERENCE*			*STRESS REVERSAL*		
km 1+400		*METHOD*			*TECHNIQUE*		
WITHOUT SHOTCRETE LINING							
HETEROGENEOUS MODEL		*Number of nodes =1650*			*Number of nodes =1650*		
LITHOLOGY : QUARTZITE + MICACEOUS		*Number of elements =356*			*Number of elements =356*		
SAND / SILT / CLAY STONE		*Number of d.o.f =2175*			*Number of d.o.f =2175*		
ELEMENT	NODE						
NUMBER	NUMBER						
ALONG THE	ALONG THE	DISPLACEMENT (mm)			DISPLACEMENT (mm)		
EXCAVATION	EXCAVATION	Ux	Uy	U	Ux	Uy	U
SURFACE	SURFACE						
69	137	0.0000	-0.6971	**0.6971**	0.0000	-0.6415	**0.6415**
69	138	0.0014	-0.6968	**0.6968**	0.0013	-0.6411	**0.6411**
70	139	0.0027	-0.6959	**0.6959**	0.0026	-0.6403	**0.6403**
70	140	0.0050	-0.6928	**0.6928**	0.0046	-0.6368	**0.6368**
71	141	0.0070	-0.6877	**0.6877**	0.0064	-0.6322	**0.6322**
71	142	0.0076	-0.6856	**0.6856**	0.0069	-0.6300	**0.6300**
72	143	0.0081	-0.6832	**0.6832**	0.0074	-0.6276	**0.6276**
72	144	0.0085	-0.6809	**0.6810**	0.0078	-0.6252	**0.6252**
73	145	0.0089	-0.6783	**0.6784**	0.0081	-0.6227	**0.6228**
73	146	0.0091	-0.6759	**0.6760**	0.0083	-0.6202	**0.6203**
74	147	0.0093	-0.6731	**0.6732**	0.0084	-0.6176	**0.6177**
74	148	0.0096	-0.6704	**0.6705**	0.0087	-0.6148	**0.6149**
75	149	0.0098	-0.6675	**0.6676**	0.0087	-0.6119	**0.6120**
75	150	0.0098	-0.6628	**0.6629**	0.0086	-0.6072	**0.6073**
76	151	0.0100	-0.6573	**0.6574**	0.0086	-0.6019	**0.6020**
76	152	0.0089	-0.6367	**0.6368**	0.0070	-0.5809	**0.5809**
77	153	0.0044	-0.6138	**0.6138**	0.0017	-0.5584	**0.5584**
77	154	0.0011	-0.5967	**0.5967**	-0.0023	-0.5408	**0.5408**
78	155	-0.0085	-0.5787	**0.5788**	-0.0124	-0.5227	**0.5228**
78	156	-0.0170	-0.5668	**0.5671**	-0.0214	-0.5105	**0.5109**
79	157	-0.0283	-0.5539	**0.5546**	-0.0333	-0.4974	**0.4985**
79	158	-0.0410	-0.5434	**0.5449**	-0.0464	-0.4867	**0.4889**
80	159	-0.0573	-0.5322	**0.5353**	-0.0632	-0.4753	**0.4795**
80	160	-0.1622	0.0408	**0.1673**	-0.1667	0.1022	**0.1955**
80	161	-0.3627	0.8022	**0.8804**	-0.3592	0.8448	**0.9180**
81	162	-0.4200	1.2867	**1.3535**	-0.4205	1.3340	**1.3987**
81	163	-0.4032	1.7156	**1.7623**	-0.4018	1.7475	**1.7931**
82	164	-0.4270	2.2107	**2.2516**	-0.4263	2.2508	**2.2908**
82	165	-0.4726	2.4991	**2.5434**	-0.4710	2.5202	**2.5638**
83	166	-0.5128	2.7951	**2.8418**	-0.5114	2.8361	**2.8818**
83	167	-0.5094	2.9019	**2.9463**	-0.5085	2.9116	**2.9557**
84	168	-0.3995	2.9313	**2.9584**	-0.3995	2.9680	**2.9948**
84	169	-0.2383	2.9265	**2.9362**	-0.2397	2.9338	**2.9436**
85	170	-0.1215	2.9195	**2.9220**	-0.1223	2.9433	**2.9458**
85	171	0.0000	2.9173	**2.9173**	0.0000	2.9291	**2.9291**
86	172	0.1215	2.9195	**2.9220**	0.1222	2.9433	**2.9458**
86	173	0.2383	2.9265	**2.9362**	0.2397	2.9338	**2.9436**
87	174	0.3995	2.9313	**2.9584**	0.3994	2.9680	**2.9948**
87	175	0.5094	2.9019	**2.9463**	0.5085	2.9116	**2.9557**
88	176	0.5128	2.7951	**2.8418**	0.5114	2.8361	**2.8818**
88	177	0.4726	2.4991	**2.5434**	0.4709	2.5202	**2.5638**
89	178	0.4270	2.2107	**2.2516**	0.4262	2.2508	**2.2908**
89	179	0.4032	1.7156	**1.7623**	0.4017	1.7474	**1.7930**
90	180	0.4200	1.2867	**1.3535**	0.4204	1.3340	**1.3987**
90	181	0.3627	0.8022	**0.8804**	0.3591	0.8448	**0.9180**
91	182	0.1622	0.0408	**0.1673**	0.1666	0.1021	**0.1954**
91	183	0.0573	-0.5322	**0.5353**	0.0631	-0.4753	**0.4795**
92	184	0.0410	-0.5434	**0.5449**	0.0463	-0.4867	**0.4889**
92	185	0.0283	-0.5539	**0.5546**	0.0332	-0.4974	**0.4985**
93	186	0.0170	-0.5668	**0.5671**	0.0213	-0.5105	**0.5109**
93	187	0.0085	-0.5788	**0.5789**	0.0123	-0.5227	**0.5228**
94	188	-0.0011	-0.5967	**0.5967**	0.0023	-0.5408	**0.5408**
94	189	-0.0044	-0.6138	**0.6138**	-0.0017	-0.5584	**0.5584**
95	190	-0.0089	-0.6367	**0.6368**	-0.0070	-0.5809	**0.5809**
95	191	-0.0100	-0.6573	**0.6574**	-0.0086	-0.6019	**0.6020**
96	192	-0.0098	-0.6628	**0.6629**	-0.0086	-0.6072	**0.6073**
96	193	-0.0098	-0.6675	**0.6676**	-0.0087	-0.6119	**0.6120**
97	194	-0.0096	-0.6704	**0.6705**	-0.0087	-0.6148	**0.6149**
97	195	-0.0093	-0.6731	**0.6732**	-0.0084	-0.6176	**0.6177**
98	196	-0.0091	-0.6759	**0.6760**	-0.0083	-0.6202	**0.6203**
98	197	-0.0089	-0.6783	**0.6784**	-0.0081	-0.6227	**0.6228**
99	198	-0.0085	-0.6809	**0.6810**	-0.0078	-0.6252	**0.6252**
100	199	-0.0081	-0.6832	**0.6832**	-0.0074	-0.6276	**0.6276**
100	200	-0.0076	-0.6856	**0.6856**	-0.0070	-0.6299	**0.6299**
101	201	-0.0070	-0.6877	**0.6877**	-0.0064	-0.6322	**0.6322**
101	202	-0.0050	-0.6928	**0.6928**	-0.0046	-0.6368	**0.6368**
102	203	-0.0027	-0.6959	**0.6959**	-0.0026	-0.6403	**0.6403**
102	204	-0.0014	-0.6968	**0.6968**	-0.0013	-0.6411	**0.6411**

Table 7.7 Comparison of displacements along the excavation surface for Kisikli north tube, (km 1+400), using gravity difference and stress reversal techniques

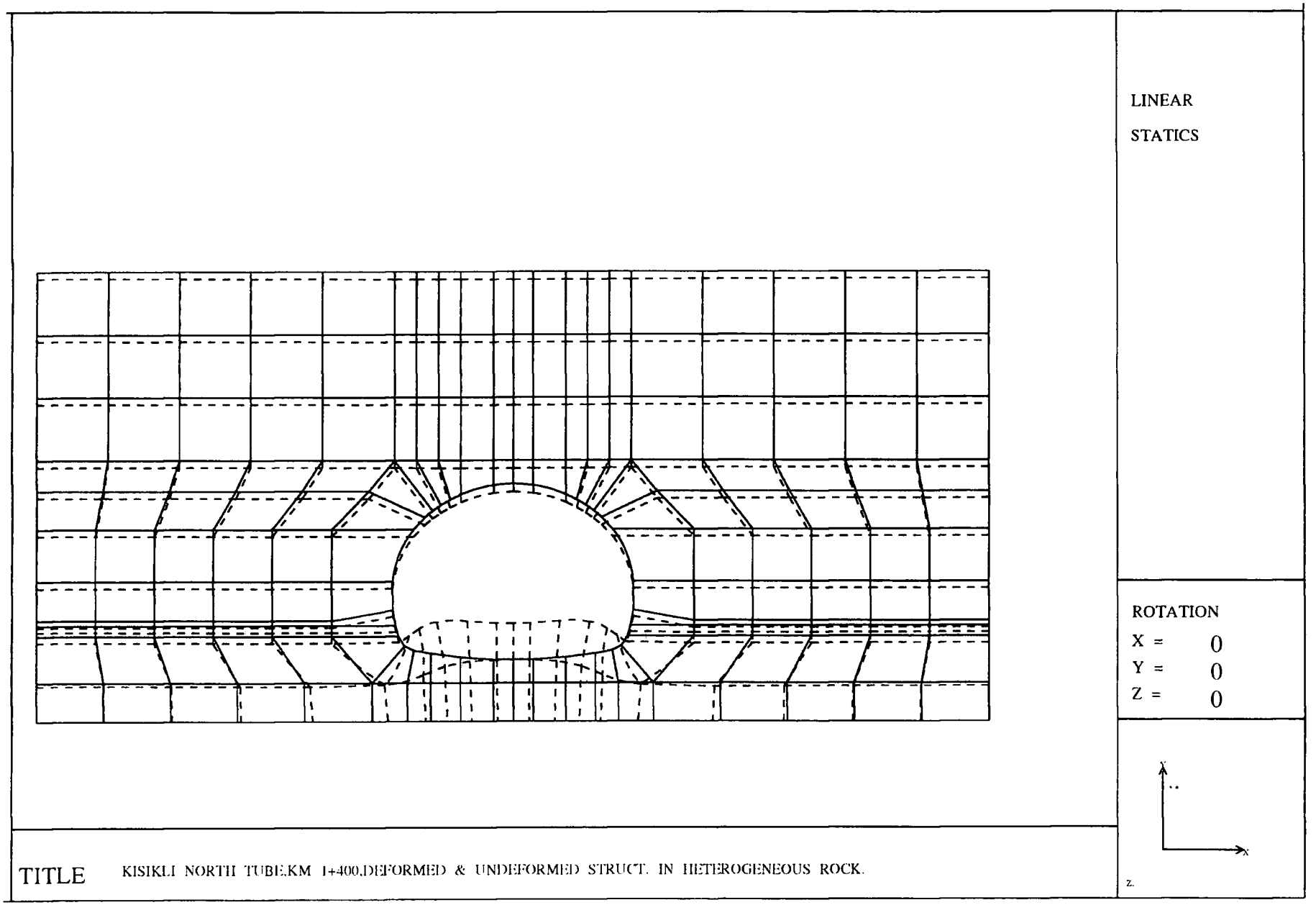

Fig. 7.17 Deformed and undeformed meshes of Kisikli north tube (km 1+400)

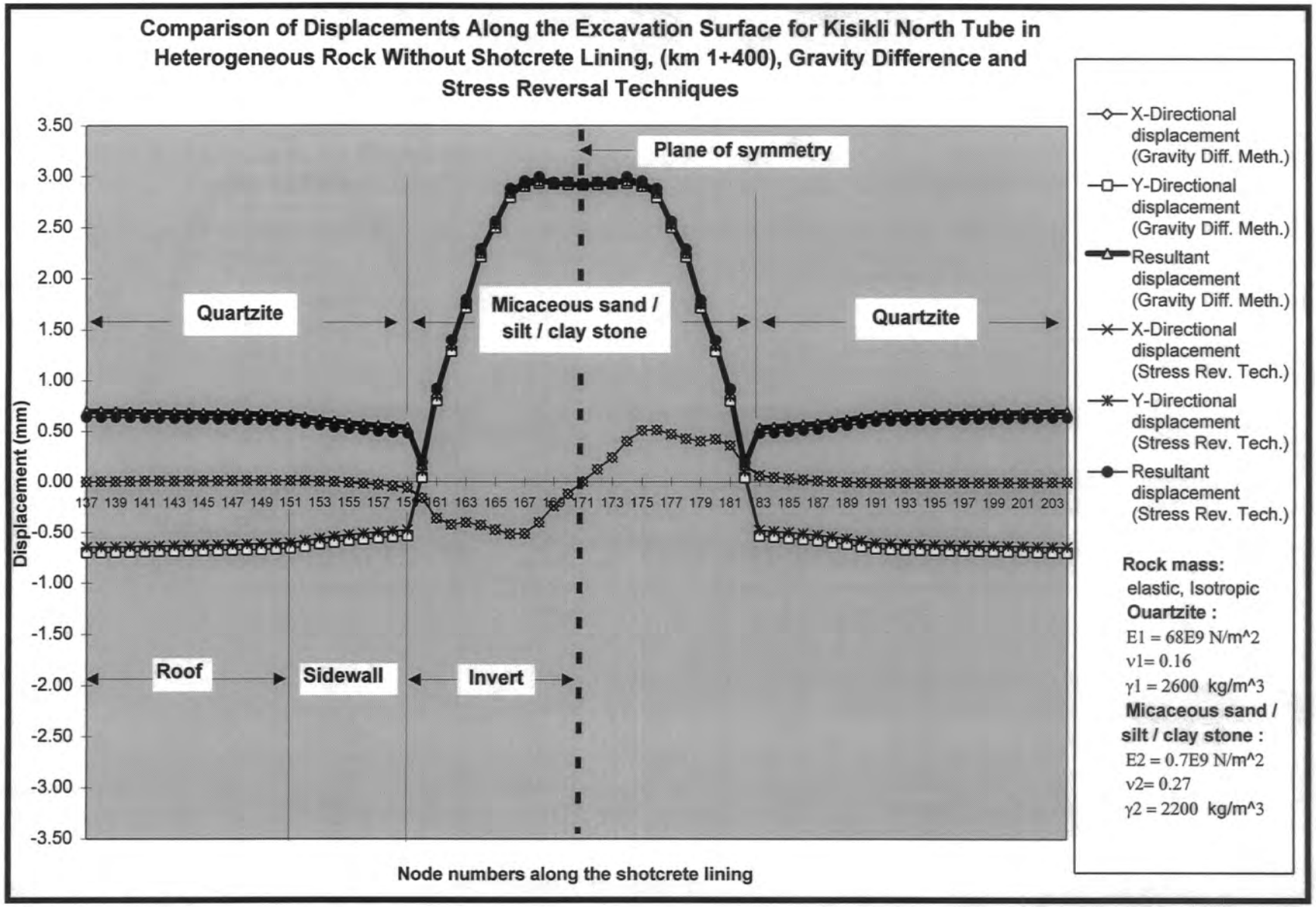

Fig. 7.18 Comparison of displacements along the excavation surface for Kisikli north tube, (km 1+400), using gravity difference and stress reversal techniques

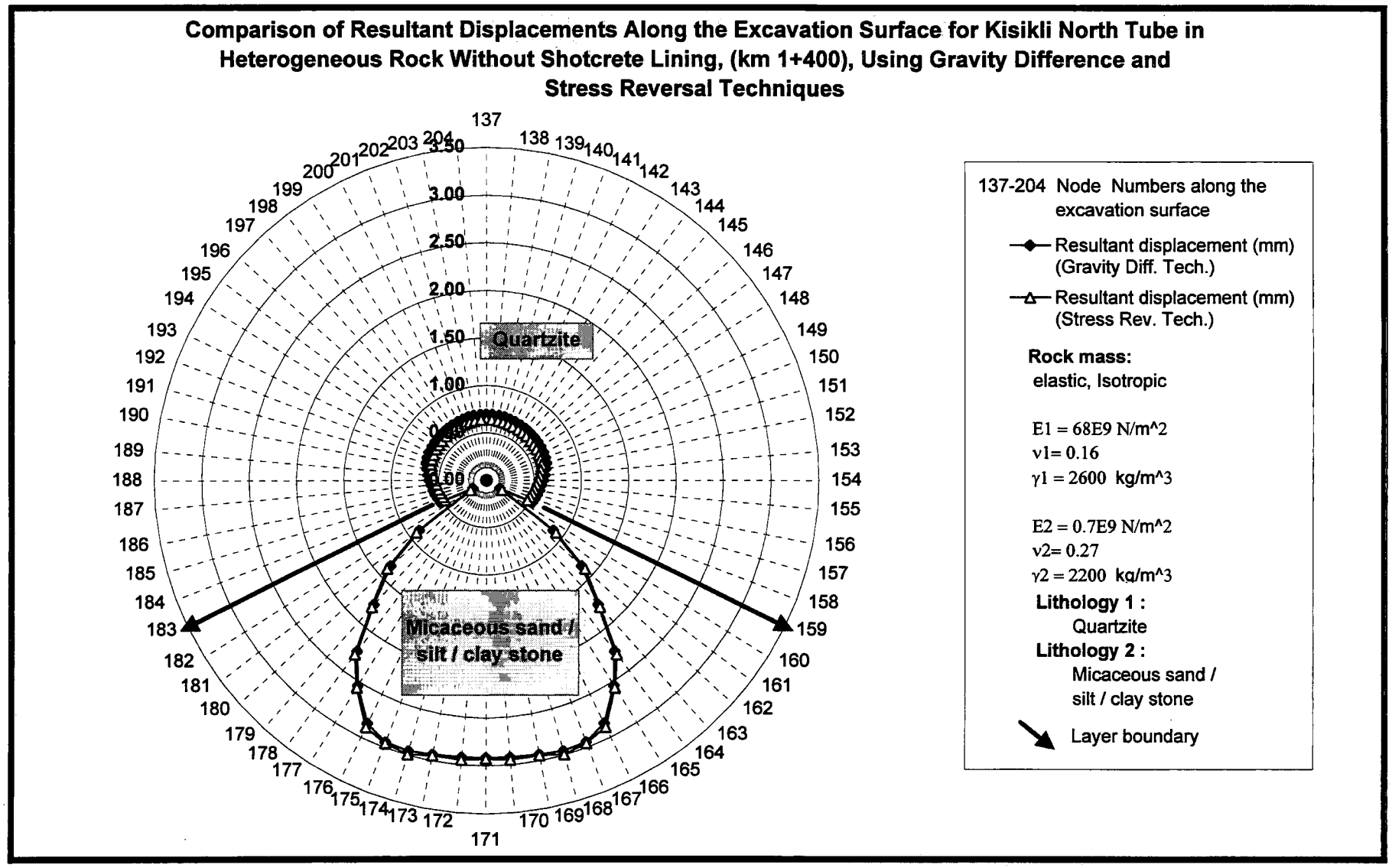

Fig. 7.19 Comparison of resultant displacements along the excavation surface for Kisikli north tube, (km 1+400), using gravity difference and stress reversal techniques

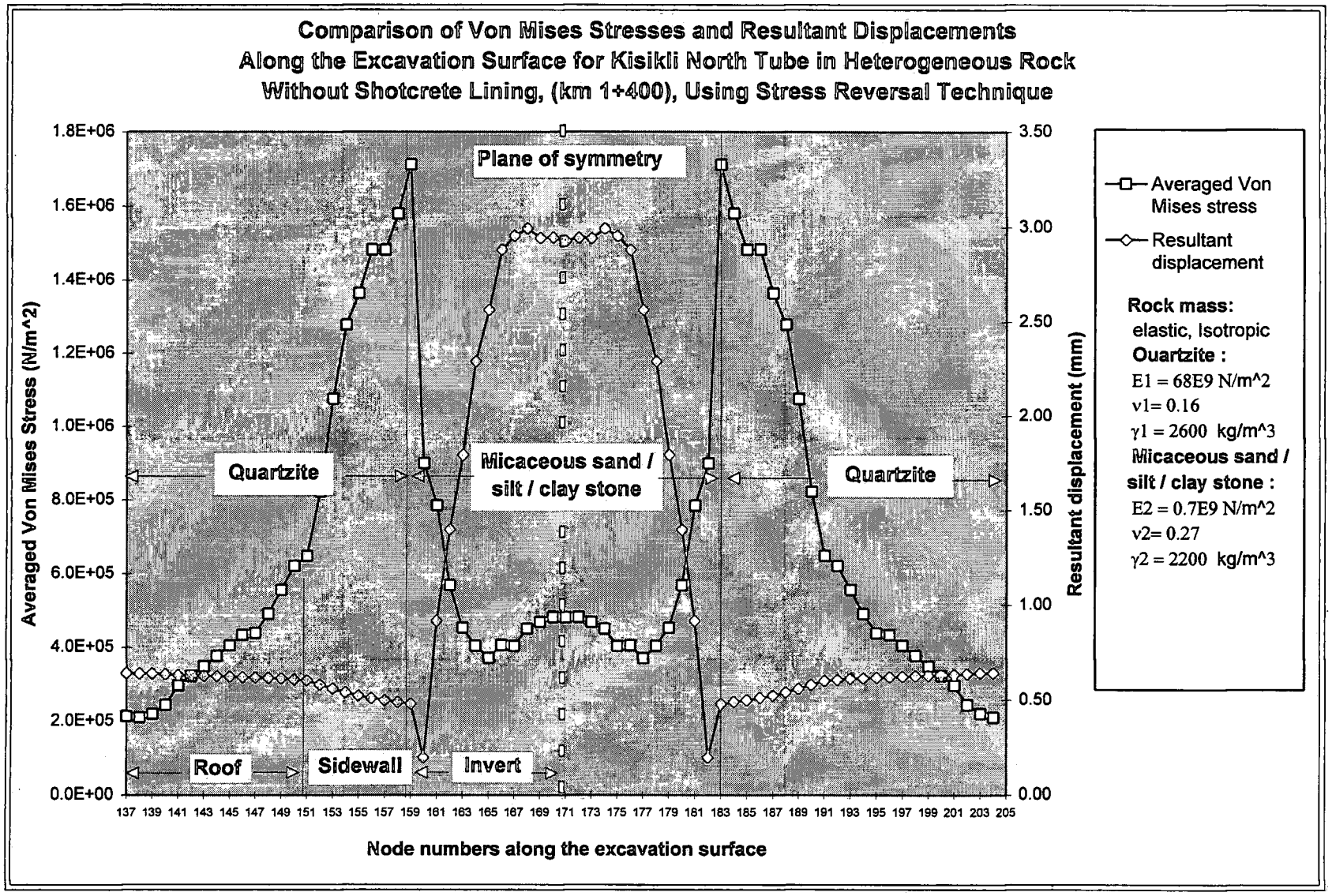

Fig. 7.20 Comparison of stresses and displacements along the excavation surface for Kisikli north tube (km 1+400)

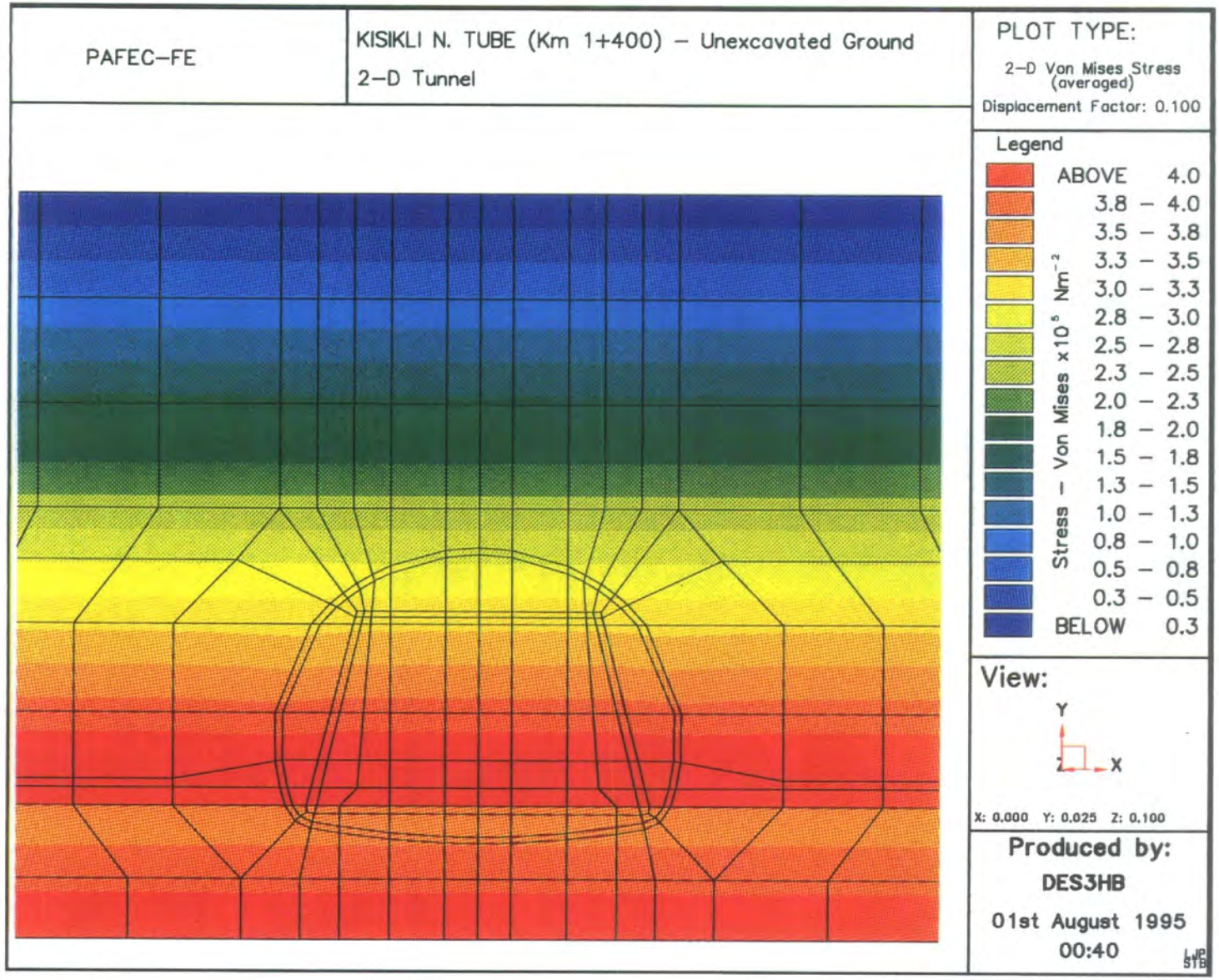

Fig. 7.21 Unexcavated ground colour stress and displaced shape diagrams of Kisikli north tube (km 1+400)

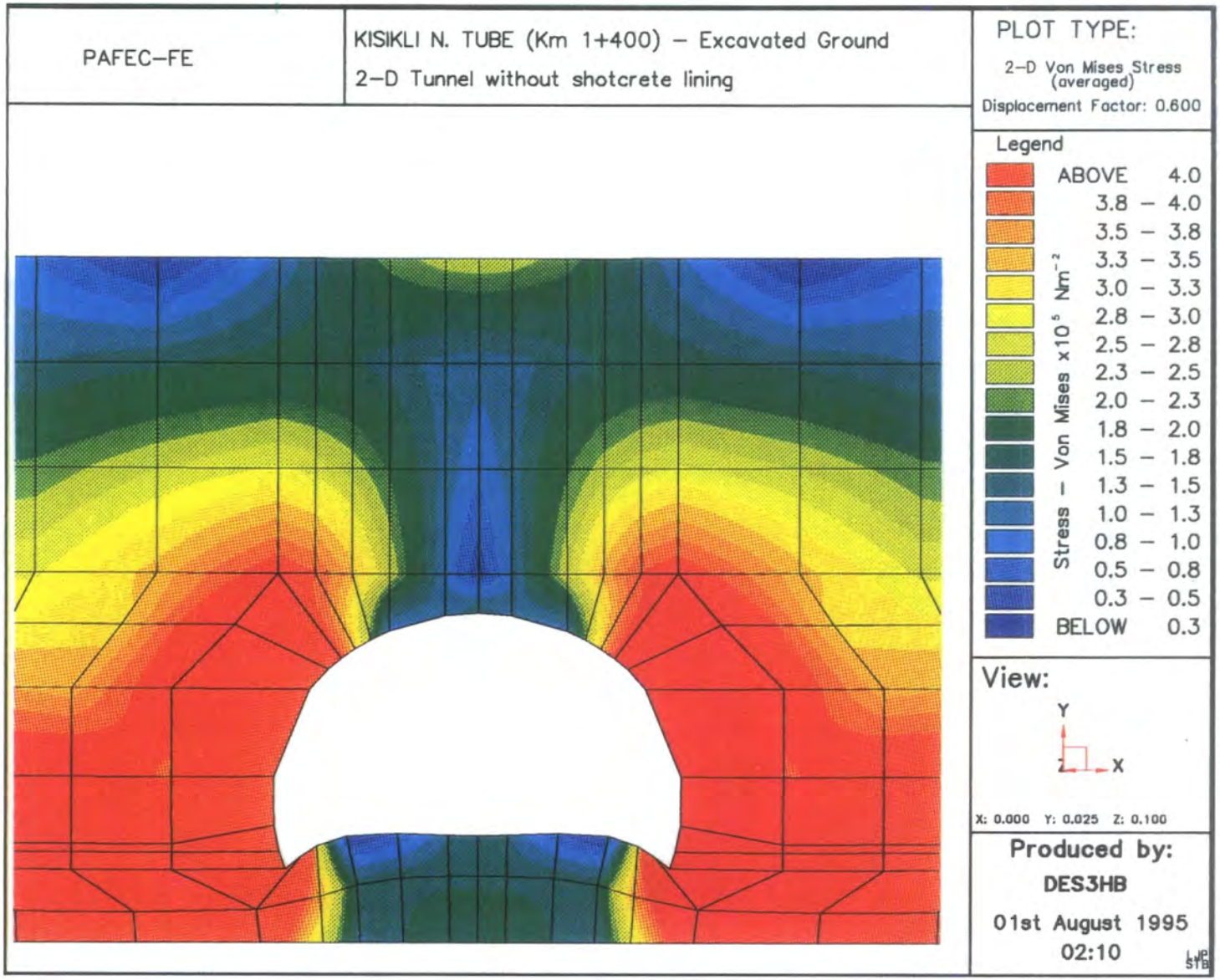

Fig. 7.22 Excavated ground colour stress and displaced shape diagrams of Kisikli north tube (km 1+400)

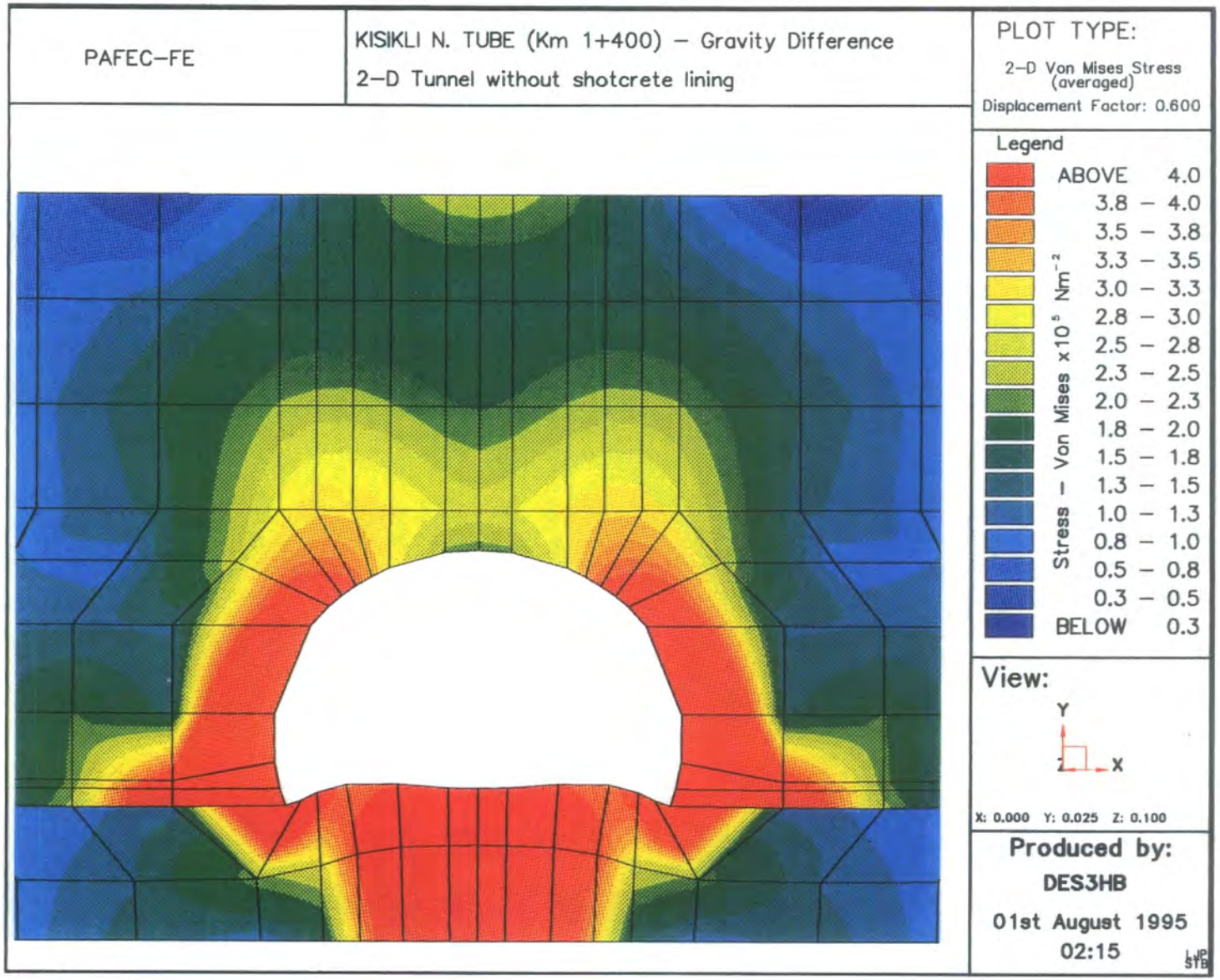

Fig 7.23 Colour stress and displaced shape diagrams of Kisikli north tube, (km 1+400), using gravity difference method

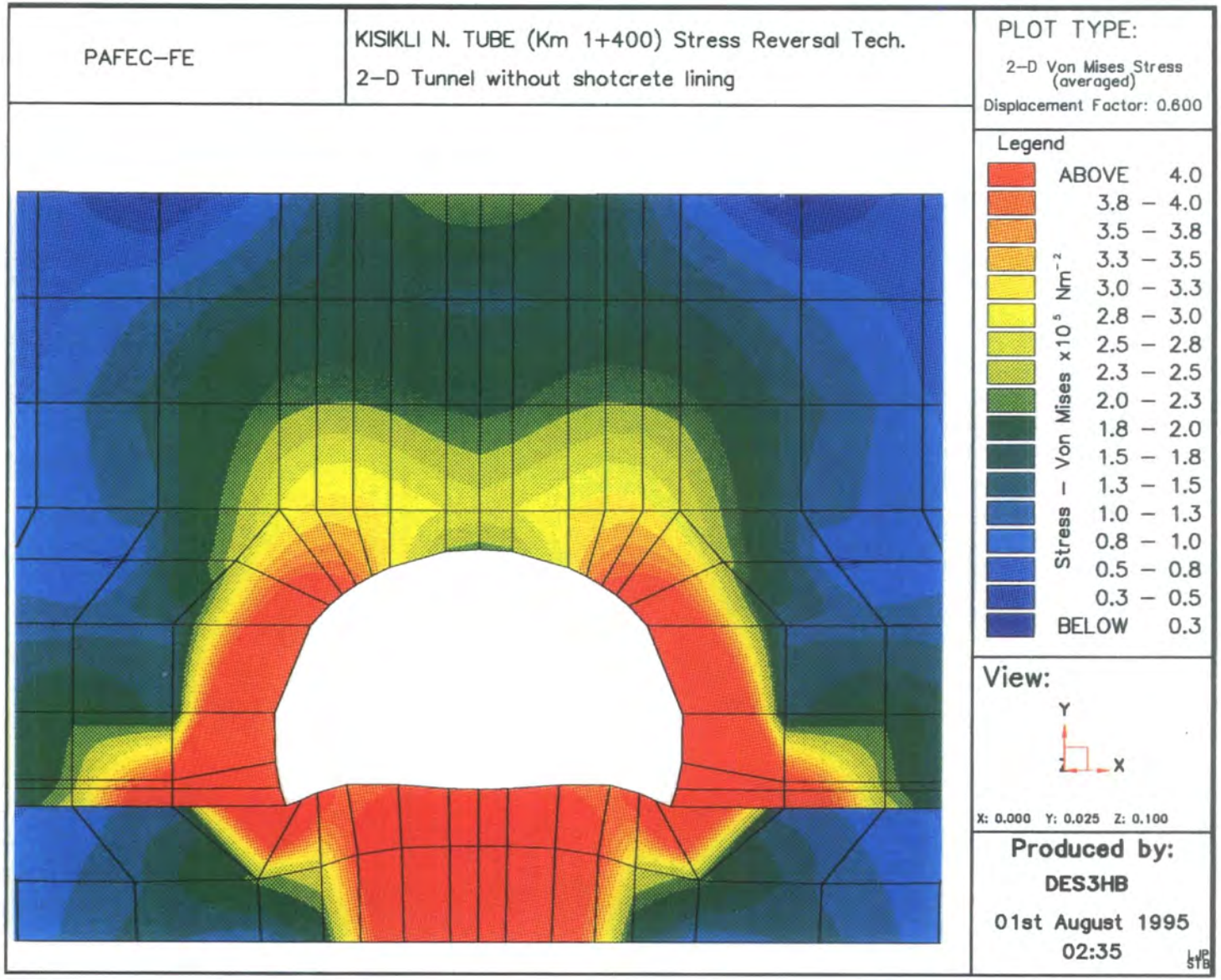

Fig. 7.24 Colour stress and displaced shape diagrams of Kisikli north tube, (km 1+400), using stress reversal technique

7.3.1.2 Comparison of Shotcrete Lining Pressures

In the case of the shotcrete lining analyses, the stress reversal technique only was used. Model dimensions, material properties, geological conditions of the Kisikli north tube at km 1+400 and shotcrete lining properties are shown in Fig. 7.25. The initial state of stress is due to gravity loading with horizontal stresses generated by the Poisson's ratio effect alone.

Two analyses with different shotcrete lining thicknesses, 100 mm and 200 mm, were completed for this cross-section of the Kisikli tunnel with the general aim of testing the sensitivity of the model. The results of these analyses are presented in Figs. 7.26 to 7.36 and are summarised in Tables 7.8 to 7.11.

Table 7.8 shows a comparison of stresses along the interface between the excavation surface and the shotcrete lining and the free surface of the shotcrete lining for the Kisikli north tube at km 1+400. The variations in stress along the free surface of the shotcrete lining are shown graphically in Fig. 7.26 using a polar diagram. These results are also presented in Fig. 7.27 which also shows the variation in Von Mises stresses for the interface for comparison. In comparison with the unsupported tunnel, the Von Mises stresses are slightly increased from 1.71 MN/m^2 (Table 7.5) to 2.03 MN/m^2 (Table 7.8) along the excavation surface by the application of a 200 mm thick shotcrete lining.

Table 7.9 shows a comparison of the component and resultant displacements along the interface between the excavation surface and the shotcrete lining and along the free surface of the shotcrete lining. In comparison with the unsupported tunnel, the displacements are reduced from 2.99 mm (Table 7.7) to 2.94 mm (Table 7.9) along the excavation surface by the application of a 200 mm thick shotcrete lining. Fig. 7.28 shows the deformed and undeformed mesh diagrams after application of a 200 mm thick shotcrete lining for this section of the Kisikli tunnel. It can be seen that the roof and invert area of the tunnel have quite extensive convergence. The component and resultant displacements at nodes along the free surface of the shotcrete lining are presented in Fig. 7.29. The resultant

displacements are also presented in Fig. 7.30 using a polar diagram. The component and resultant displacements at nodes along the interface between the excavation surface and the shotcrete lining are shown in Fig. 7.31. Both Figures 7.29 and 7.31 show similar patterns of displacement.

Finally a comparison of Von Mises stresses and displacements along the free surface of the shotcrete lining is shown in Fig 7.32. This figure illustrates relative changes in Von Mises stresses and displacements. It can be seen that where the displacements are high, the resulting stresses are low and also when the displacements are low, the resulting stresses are high. The maximum Von Mises stress and displacement along the free surface of the 200 mm thick shotcrete lining are 7.04 MN/m^2 and 2.95 mm respectively. It appears, quite logically, that the insertion of the shotcrete lining increases stresses locally in the rock and reduces displacements on the excavation surface.

Values of Young's modulus, as determined by laboratory testing on small specimens of visually intact rock, do not give a true indication of the stiffness of the rock mass surrounding the excavation. Reduction factors are necessary if the elastic parameters assigned to the model are to achieve consistency between the measured and computed values of displacements. Therefore reduction factors of 0.10 and 0.50 were applied to the values of the 'intact' Young's modulus and an increase of 0.05 in the values for Poisson's ratio have been used for the models. Tables 7.10 and 7.11 show displacements along the free surface of the shotcrete lining and a summary of the ranges of elastic constants used in both analyses with different shotcrete lining thicknesses of 200 mm and 100 mm respectively. The same results are presented in Figs. 7.33 and 7.34 for visual comparison.

These changes to the values of Young's modulus have a greater influence on deformations than those produced by the change to the values of Poisson's ratio. When Young's modulus is reduced by 50%, the resultant displacements increase roughly by 50 % as shown in the figures. In comparing displacements along the free surface of the shotcrete lining from the two analyses with different thicknesses of shotcrete lining, it can be seen that the displacements obtained by the application of a 200 mm thick shotcrete lining are only slightly reduced compared to the case

for the 100 mm lining. Hence, in this example, a 100 mm thick shotcrete lining appears sufficient for the tunnel.

The addition of a shotcrete lining to the tunnel model increased the stress state locally in the rock strata. This increased stress state might reasonably be expected also to increase the stress in the shotcrete lining. The results of this exercise confirm this expectation as shown in Figs. 7.35 and 7.36. Fig. 7.35 shows the Von Mises stress distribution in colour and the slightly deformed shape of the 200 mm thick shotcrete lining for the Kisikli north tube under the action of gravity. Fig 7.36 presents a similar diagram for the 100 mm thick shotcrete lined Kisikli north tube. These shaded colour diagrams indicate areas of increased and decreased stress through changes in colour from red to blue respectively.

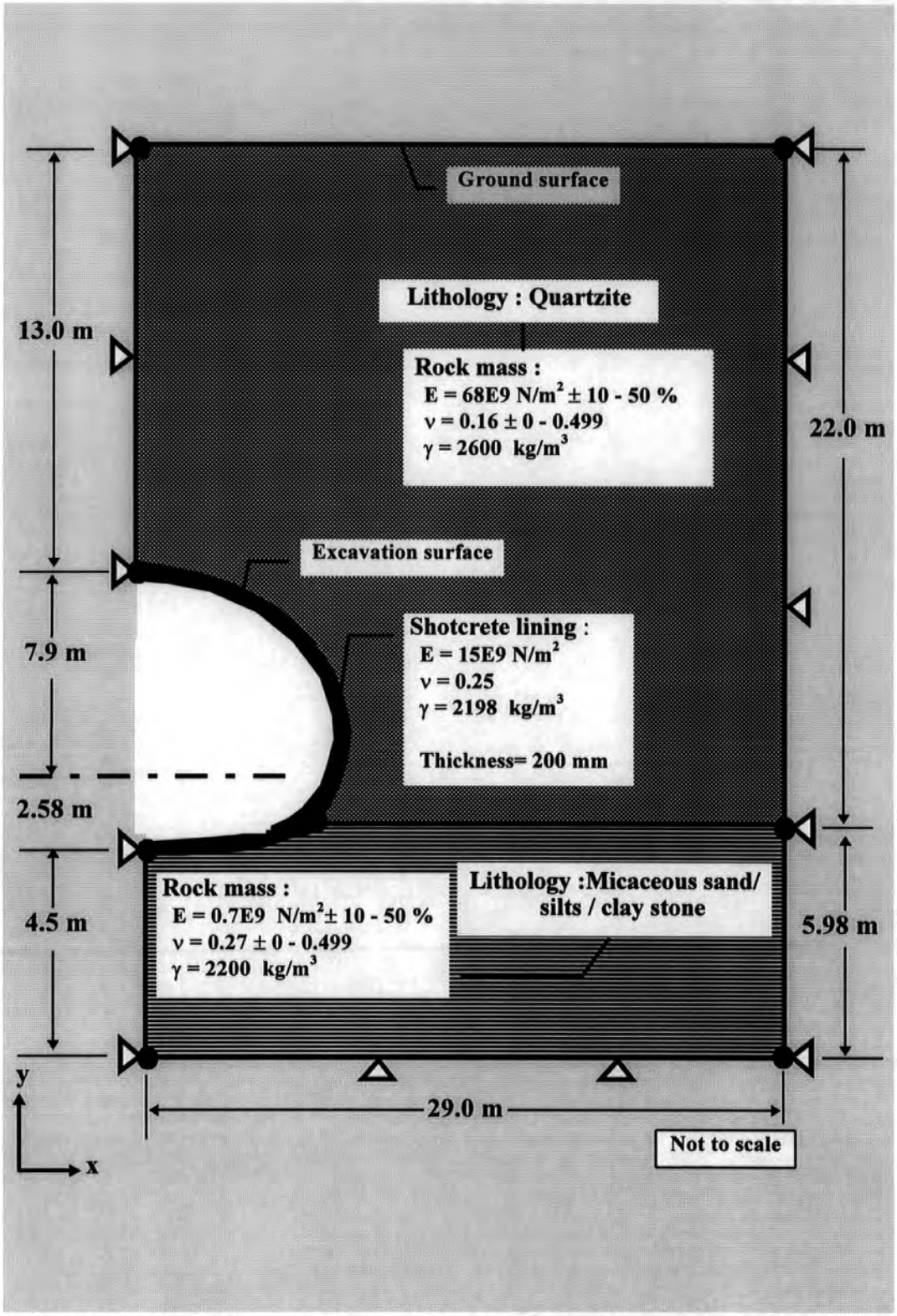

Fig. 7.25 Model dimensions, material properties and geological conditions of Kisikli north tube, (km 1+400), having shotcrete lining

KISIKLI NORTH TUBE			*STRESS REVERSAL*			*STRESS REVERSAL*
km 1+400			*TECHNIQUE*			*TECHNIQUE*
WITH SHOTCRETE LINING =200 mm			*Number of nodes = 1736*			*Number of nodes = 1736*
HETEROGENEOUS MODEL			*Number of elements = 384*			*Number of elements = 384*
LITHOLOGY : QUARTZITE + MICACEOUS			*Number of d.o.f = 2343*			*Number of d.o.f = 2343*
SAND / SILT / CLAY STONE						
			AVERAGED			AVERAGED VON MISES
	ELEMENT	NODE	VON MISES	ELEMENT	NODE	STRESS (N/m^2)
	NUMBER	NUMBER	STRESS (N/m^2)	NUMBER	NUMBER	ALONG THE
COMPUTED	ALONG THE	ALONG THE	ALONG THE	ALONG THE	ALONG THE	EXCAVATION SURFACE /
RESULT	SHOTCRETE	SHOTCRETE	SHOTCRETE LINING	EXCAVATION	EXCAVATION	THE SHOTCRETE LINING
LOCATIONS	LINING	LINING	FREE SURFACE	SURFACE	SURFACE	INTERFACE
1	37	69	4.68E+04	73	137	2.13E+05
2	37	70	4.38E+04	73	138	2.10E+05
3	38	71	4.07E+04	74	139	2.15E+05
4	38	72	2.12E+04	74	140	2.29E+05
5	39	73	2.44E+03	75	141	2.73E+05
6	39	74	1.30E+04	75	142	2.95E+05
7	40	75	2.27E+04	76	143	3.17E+05
8	40	76	3.49E+04	76	144	3.44E+05
9	41	77	4.47E+04	77	145	3.71E+05
10	41	78	5.60E+04	77	146	3.99E+05
11	42	79	6.54E+04	78	147	4.05E+05
12	42	80	7.74E+04	78	148	4.56E+05
13	43	81	8.61E+04	79	149	5.14E+05
14	43	82	1.01E+05	79	150	5.79E+05
15	44	83	1.21E+05	80	151	6.19E+05
16	45	84	1.83E+05	81	152	8.27E+05
17	46	85	2.89E+05	82	153	1.21E+06
18	46	86	3.71E+05	82	154	1.47E+06
19	47	87	3.90E+05	83	155	1.72E+06
20	47	88	5.39E+05	83	156	1.92E+06
21	48	89	6.55E+05	84	157	2.03E+06
22	48	90	2.21E+06	84	158	1.79E+06
23	49	91	5.08E+06	85	159	1.48E+05
24	49	92	7.04E+06	85	160	2.55E+05
25	50	93	6.79E+06	86	161	3.52E+05
26	50	94	5.42E+06	86	162	4.85E+05
27	51	95	2.07E+06	87	163	6.04E+05
28	51	96	9.64E+05	87	164	4.79E+05
29	52	97	7.67E+05	88	165	4.52E+05
30	52	98	1.16E+06	88	166	4.55E+05
31	53	99	1.51E+06	89	167	4.41E+05
32	53	100	1.67E+06	89	168	4.43E+05
33	54	101	1.85E+06	90	169	4.42E+05
34	54	102	1.90E+06	90	170	4.38E+05
35	55	103	1.94E+06	91	171	4.37E+05
36	55	104	1.90E+06	91	172	4.38E+05
37	56	105	1.85E+06	92	173	4.42E+05
38	56	106	1.67E+06	92	174	4.43E+05
39	57	107	1.51E+06	93	175	4.41E+05
40	57	108	1.16E+06	93	176	4.55E+05
41	58	109	7.67E+05	94	177	4.52E+05
42	58	110	9.64E+05	94	178	4.79E+05
43	59	111	2.07E+06	95	179	6.04E+05
44	59	112	5.42E+06	95	180	4.85E+05
45	60	113	6.79E+06	96	181	3.52E+05
46	60	114	7.04E+06	96	182	2.55E+05
47	61	115	5.08E+06	97	183	1.53E+06
48	61	116	2.21E+06	97	184	1.79E+06
49	62	117	6.55E+05	98	185	2.03E+06
50	62	118	5.39E+05	98	186	1.92E+06
51	63	119	3.90E+05	99	187	1.72E+06
52	63	120	3.71E+05	99	188	1.47E+06
53	64	121	2.89E+05	100	189	1.21E+06
54	65	122	1.83E+05	101	190	8.27E+05
55	66	123	1.21E+05	102	191	6.19E+05
56	66	124	1.01E+05	102	192	5.79E+05
57	67	125	8.62E+04	103	193	5.14E+05
58	67	126	7.74E+04	103	194	4.56E+05
59	68	127	6.53E+04	104	195	4.05E+05
60	68	128	5.60E+04	104	196	3.99E+05
61	69	129	4.48E+04	105	197	3.71E+05
62	69	130	3.50E+04	105	198	3.44E+05
63	70	131	2.28E+04	106	199	3.17E+05
64	70	132	1.30E+04	106	200	2.95E+05
65	71	133	2.46E+03	107	201	2.73E+05
66	71	134	2.12E+04	107	202	2.29E+05
67	72	135	4.07E+04	108	203	2.15E+05
68	72	136	4.38E+04	108	204	2.10E+05

Table 7.8 Comparison of stresses along excavation surface / shotcrete lining interface for Kisikli north tube (km 1+400)

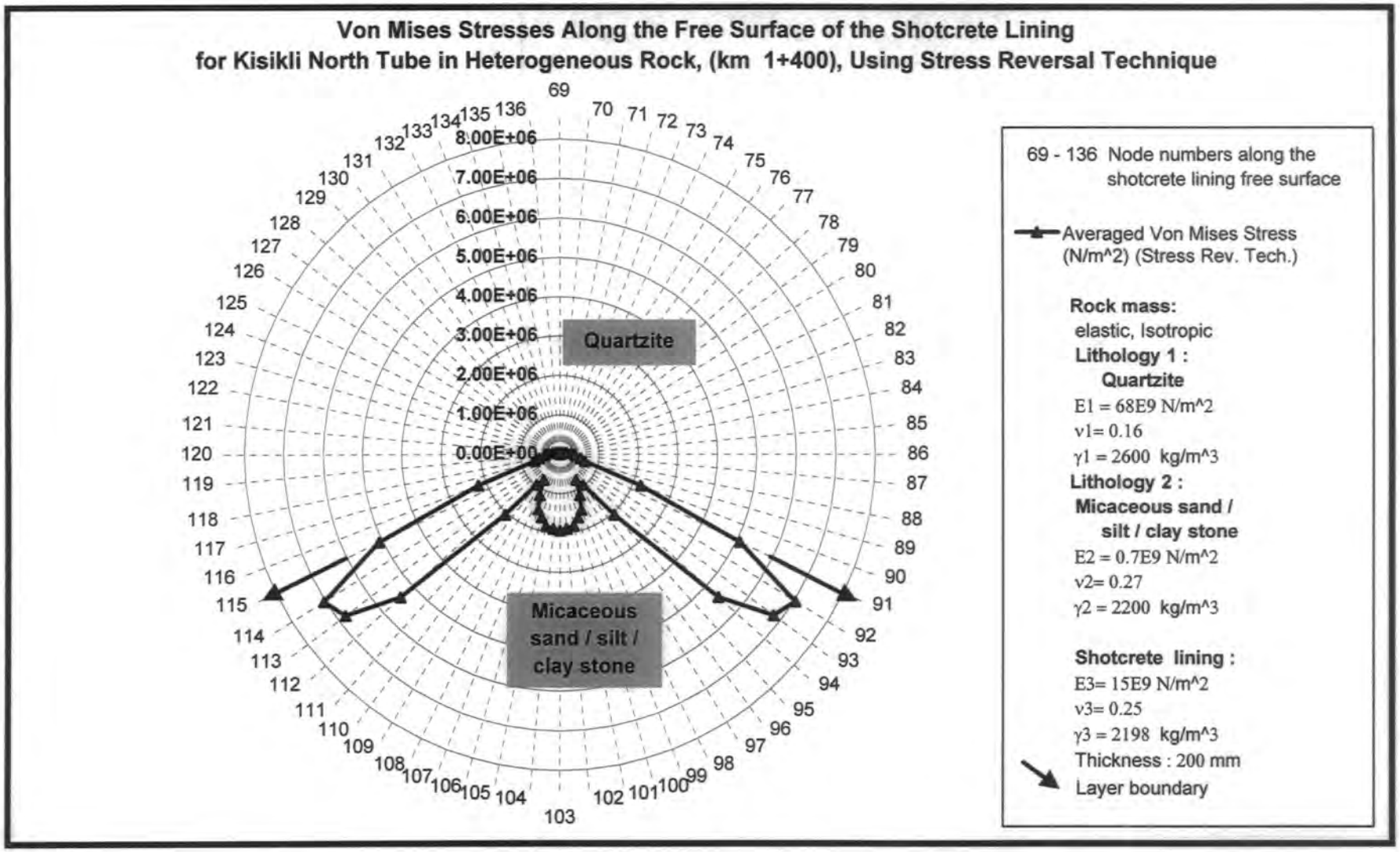

Fig. 7.26 Stress distributions along the free surface of the shotcrete lining for Kisikli north tube (km 1+400)

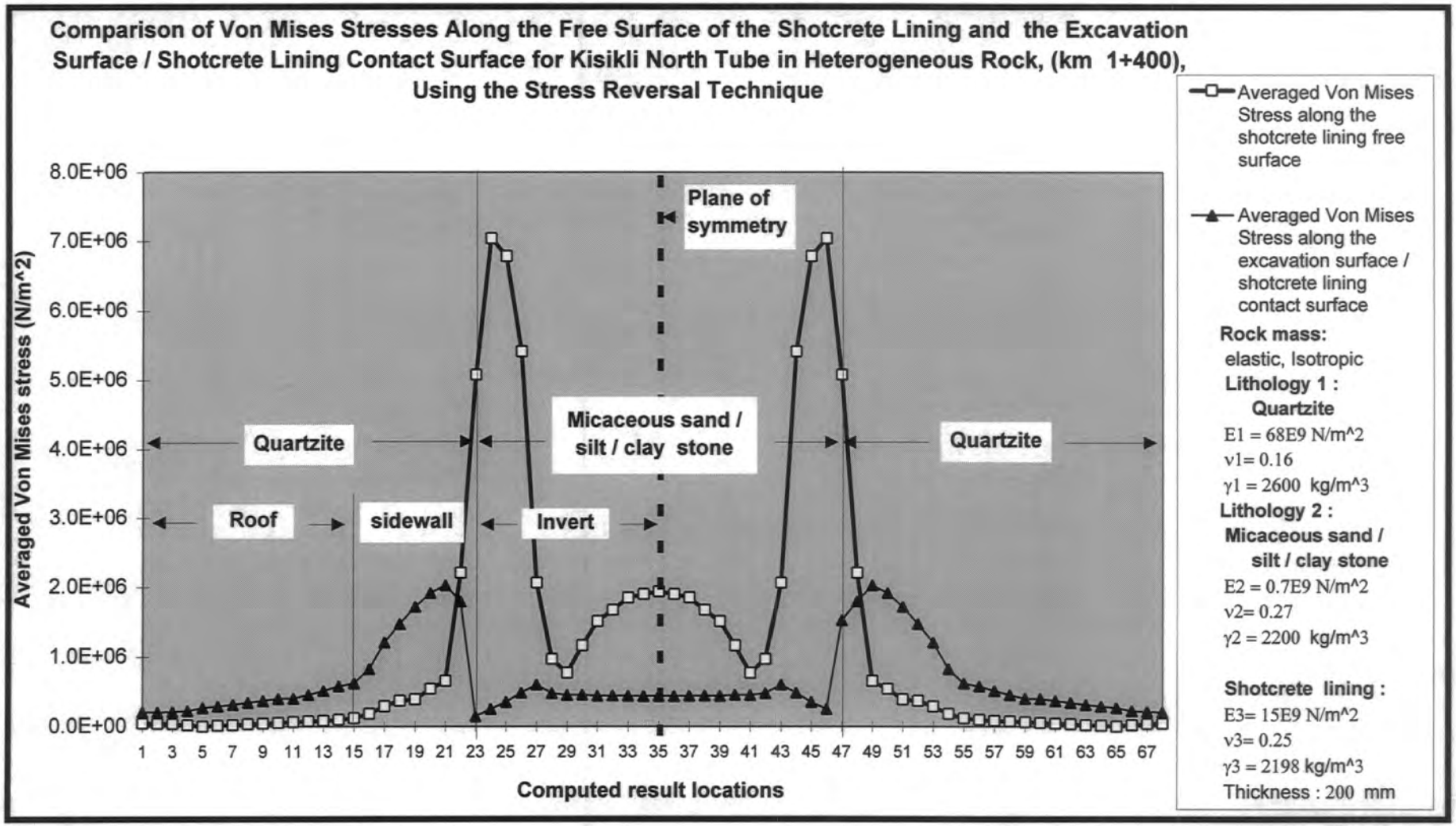

Fig. 7.27 Comparison of stresses along the free surface of the shotcrete lining and the excavation surface / shotcrete lining interface for Kisikli north tube (km 1+400)

KISIKLI NORTH TUBE			*STRESS REVERSAL*					*STRESS REVERSAL*		
km 1+400			*TECHNIQUE*					*TECHNIQUE*		
WITH SHOTCRETE LINING =200 mm										
HETEROGENEOUS MODEL			*Number of nodes = 1736*					*Number of nodes = 1736*		
LITHOLOGY : QUARTZITE + MICACEOUS			*Number of elements = 384*					*Number of elements = 384*		
SAND / SILT / CLAY STONE			*Number of d.o.f = 2343*					*Number of d.o.f = 2343*		
	ELEMENT	NODE				ELEMENT	NODE			
	NUMBER	NUMBER	DISPLACEMENTS (mm)			NUMBER	NUMBER	DISPLACEMENTS (mm)		
COMPUTED	ALONG THE	ALONG THE	ALONG THE SHOTCRETE LINING			ALONG THE	ALONG THE	ALONG THE EXCAVATION SURFACE /		
RESULT	SHOTCRETE	SHOTCRETE	FREE SURFACE			EXCAVATION	EXCAVATION	SHOTCRETE LINING INTERFACE		
LOCATIONS	LINING	LINING	Ux	Uy	U	SURFACE	SURFACE	Ux	Uy	U
1	37	69	0.0000	-0.5090	**0.5090**	73	137	0.0000	-0.5092	**0.5092**
2	37	70	0.0019	-0.5086	**0.5086**	73	138	0.0016	-0.5087	**0.5087**
3	38	71	0.0038	-0.5077	**0.5077**	74	139	0.0032	-0.5079	**0.5079**
4	38	72	0.0068	-0.5043	**0.5043**	74	140	0.0058	-0.5044	**0.5044**
5	39	73	0.0095	-0.4995	**0.4996**	75	141	0.0083	-0.4995	**0.4996**
6	39	74	0.0103	-0.4974	**0.4975**	75	142	0.0090	-0.4972	**0.4973**
7	40	75	0.0109	-0.4953	**0.4954**	76	143	0.0097	-0.4949	**0.4950**
8	40	76	0.0115	-0.4930	**0.4931**	76	144	0.0104	-0.4924	**0.4925**
9	41	77	0.0120	-0.4907	**0.4908**	77	145	0.0109	-0.4899	**0.4900**
10	41	78	0.0124	-0.4883	**0.4885**	77	146	0.0113	-0.4873	**0.4874**
11	42	79	0.0128	-0.4858	**0.4860**	78	147	0.0117	-0.4846	**0.4847**
12	42	80	0.0131	-0.4834	**0.4836**	78	148	0.0122	-0.4819	**0.4821**
13	43	81	0.0133	-0.4811	**0.4813**	79	149	0.0125	-0.4790	**0.4792**
14	43	82	0.0135	-0.4769	**0.4771**	79	150	0.0130	-0.4742	**0.4744**
15	44	83	0.0139	-0.4722	**0.4724**	80	151	0.0136	-0.4688	**0.4690**
16	45	84	0.0138	-0.4505	**0.4507**	81	152	0.0142	-0.4483	**0.4485**
17	46	85	0.0115	-0.4217	**0.4219**	82	153	0.0128	-0.4218	**0.4220**
18	46	86	0.0089	-0.4015	**0.4016**	82	154	0.0104	-0.4022	**0.4023**
19	47	87	0.0012	-0.3775	**0.3775**	83	155	0.0024	-0.3814	**0.3814**
20	47	88	-0.0059	-0.3604	**0.3604**	83	156	-0.0046	-0.3662	**0.3662**
21	48	89	-0.0167	-0.3352	**0.3356**	84	157	-0.0148	-0.3498	**0.3501**
22	48	90	-0.0227	-0.3079	**0.3087**	84	158	-0.0254	-0.3364	**0.3374**
23	49	91	-0.0371	-0.2151	**0.2183**	85	159	-0.0419	-0.3226	**0.3253**
24	49	92	-0.0885	-0.0673	**0.1112**	85	160	-0.1266	-0.1922	**0.2301**
25	50	93	-0.1519	0.1595	**0.2203**	86	161	-0.2978	0.0148	**0.2982**
26	50	94	-0.2398	0.4850	**0.5410**	86	162	-0.4837	0.3522	**0.5983**
27	51	95	-0.2922	0.8764	**0.9238**	87	163	-0.5977	0.8101	**1.0067**
28	51	96	-0.3715	1.5792	**1.6223**	87	164	-0.6063	1.5474	**1.6619**
29	52	97	-0.4327	2.0553	**2.1004**	88	165	-0.5711	2.0479	**2.1260**
30	52	98	-0.4302	2.5532	**2.5892**	88	166	-0.5027	2.5464	**2.5955**
31	53	99	-0.3803	2.7847	**2.8105**	89	167	-0.4045	2.7769	**2.8062**
32	53	100	-0.2758	2.9038	**2.9169**	89	168	-0.2883	2.8960	**2.9103**
33	54	101	-0.1585	2.9460	**2.9503**	90	169	-0.1583	2.9371	**2.9414**
34	54	102	-0.0795	2.9528	**2.9539**	90	170	-0.0798	2.9443	**2.9454**
35	55	103	0.0000	2.9541	**2.9541**	91	171	0.0000	2.9450	**2.9450**
36	55	104	0.0795	2.9528	**2.9539**	91	172	0.0798	2.9443	**2.9454**
37	56	105	0.1585	2.9460	**2.9503**	92	173	0.1583	2.9371	**2.9414**
38	56	106	0.2757	2.9038	**2.9169**	92	174	0.2883	2.8960	**2.9103**
39	57	107	0.3803	2.7847	**2.8105**	93	175	0.4045	2.7769	**2.8062**
40	57	108	0.4301	2.5533	**2.5893**	93	176	0.5027	2.5464	**2.5955**
41	58	109	0.4327	2.0554	**2.1005**	94	177	0.5711	2.0479	**2.1260**
42	58	110	0.3715	1.5792	**1.6223**	94	178	0.6063	1.5474	**1.6619**
43	59	111	0.2922	0.8764	**0.9238**	95	179	0.5977	0.8102	**1.0068**
44	59	112	0.2397	0.4851	**0.5411**	95	180	0.4837	0.3522	**0.5983**
45	60	113	0.1519	0.1595	**0.2203**	96	181	0.2978	0.0149	**0.2982**
46	60	114	0.0885	-0.0673	**0.1112**	96	182	0.1266	-0.1921	**0.2301**
47	61	115	0.0371	-0.2151	**0.2183**	97	183	0.0419	-0.3226	**0.3253**
48	61	116	0.0227	-0.3079	**0.3087**	97	184	0.0254	-0.3364	**0.3374**
49	62	117	0.0167	-0.3351	**0.3355**	98	185	0.0148	-0.3498	**0.3501**
50	62	118	0.0059	-0.3604	**0.3604**	98	186	0.0046	-0.3662	**0.3662**
51	63	119	-0.0012	-0.3774	**0.3774**	99	187	-0.0024	-0.3814	**0.3814**
52	63	120	-0.0090	-0.4015	**0.4016**	99	188	-0.0104	-0.4022	**0.4023**
53	64	121	-0.0115	-0.4216	**0.4218**	100	189	-0.0128	-0.4218	**0.4220**
54	65	122	-0.0138	-0.4504	**0.4506**	101	190	-0.0143	-0.4483	**0.4485**
55	66	123	-0.0139	-0.4722	**0.4724**	102	191	-0.0136	-0.4688	**0.4690**
56	66	124	-0.0135	-0.4769	**0.4771**	102	192	-0.0130	-0.4742	**0.4744**
57	67	125	-0.0133	-0.4811	**0.4813**	103	193	-0.0125	-0.4790	**0.4792**
58	67	126	-0.0131	-0.4834	**0.4836**	103	194	-0.0122	-0.4819	**0.4821**
59	68	127	-0.0128	-0.4857	**0.4859**	104	195	-0.0117	-0.4846	**0.4847**
60	68	128	-0.0124	-0.4883	**0.4885**	104	196	-0.0113	-0.4873	**0.4874**
61	69	129	-0.0120	-0.4907	**0.4908**	105	197	-0.0109	-0.4899	**0.4900**
62	69	130	-0.0115	-0.4930	**0.4931**	105	198	-0.0104	-0.4924	**0.4925**
63	70	131	-0.0110	-0.4953	**0.4954**	106	199	-0.0098	-0.4949	**0.4950**
64	70	132	-0.0103	-0.4974	**0.4975**	106	200	-0.0091	-0.4972	**0.4973**
65	71	133	-0.0095	-0.4994	**0.4995**	107	201	-0.0083	-0.4995	**0.4996**
66	71	134	-0.0068	-0.5043	**0.5043**	107	202	-0.0059	-0.5043	**0.5043**
67	72	135	-0.0038	-0.5077	**0.5077**	108	203	-0.0032	-0.5079	**0.5079**
68	72	136	-0.0019	-0.5086	**0.5086**	108	204	-0.0016	-0.5087	**0.5087**

Table 7.9 Comparison of displacements along the excavation surface / shotcrete lining interface for Kisikli north tube (km 1+400)

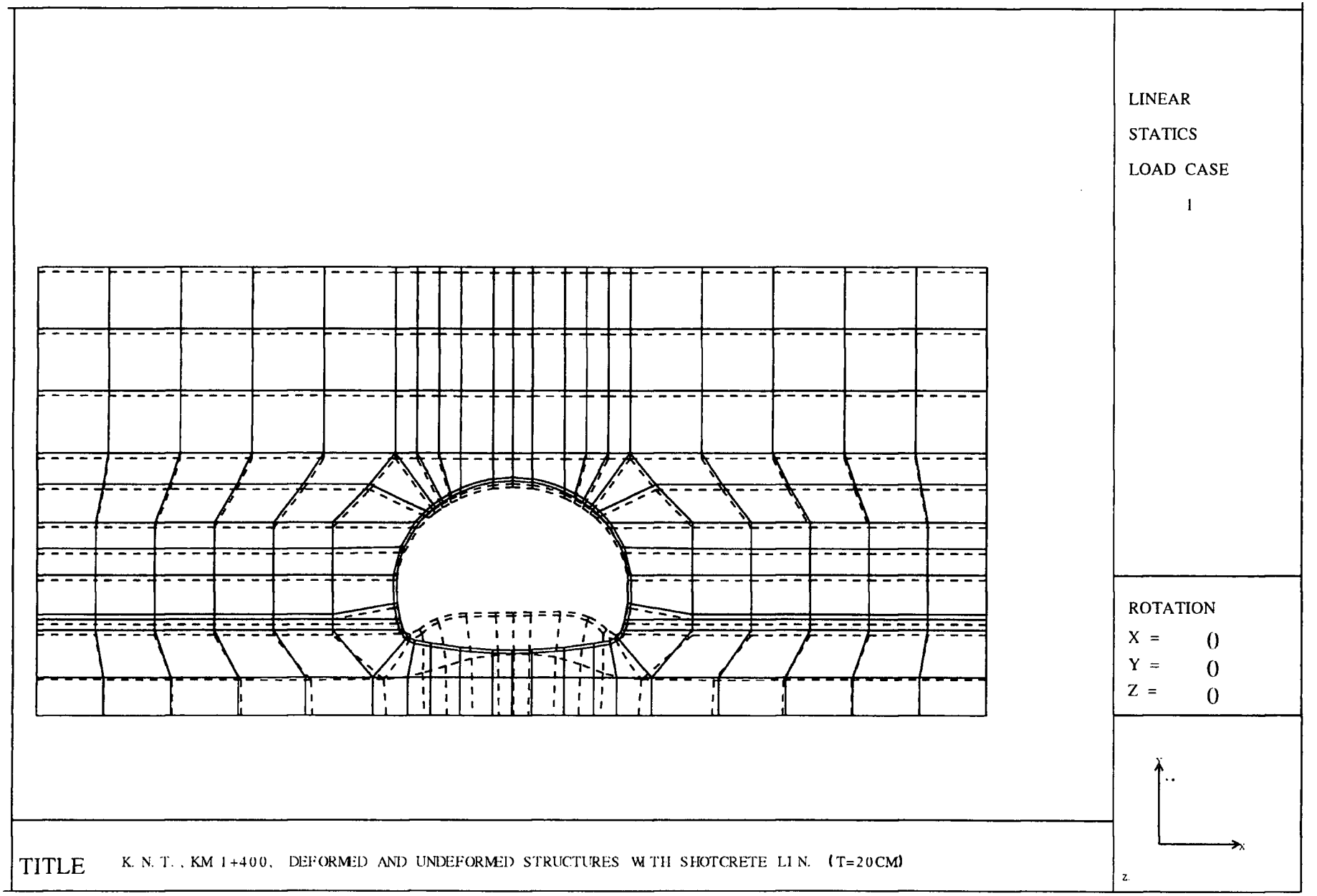

Fig. 7.28 Deformed and undeformed meshes of Kisikli north tube, (km 1+400), having shotcrete lining

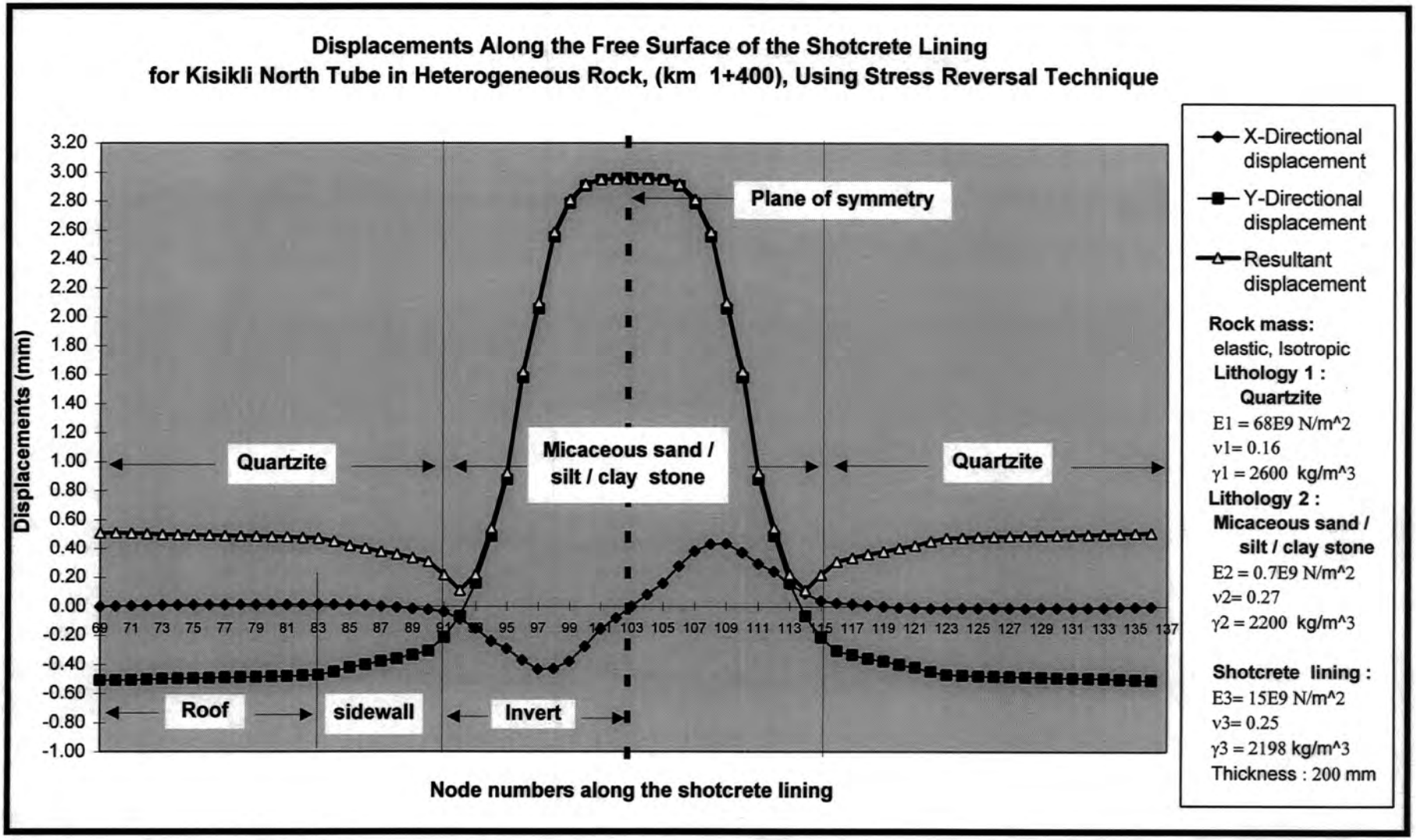

Fig. 7.29 Displacements along the free surface of the shotcrete lining for Kisikli north tube (km 1+400)

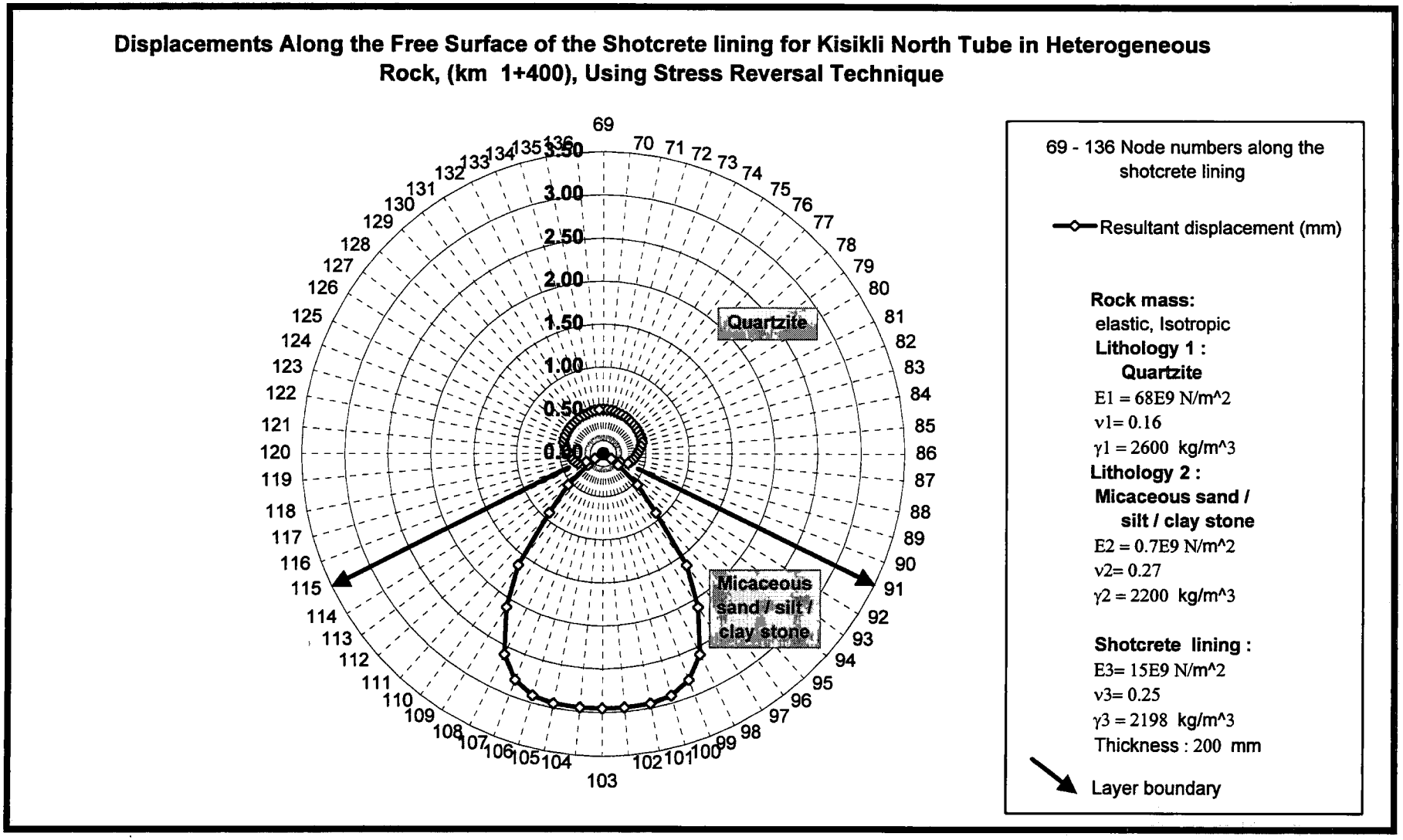

Fig. 7.30 Resultant displacements along the free surface of the shotcrete lining for Kisikli north tube (km 1+400)

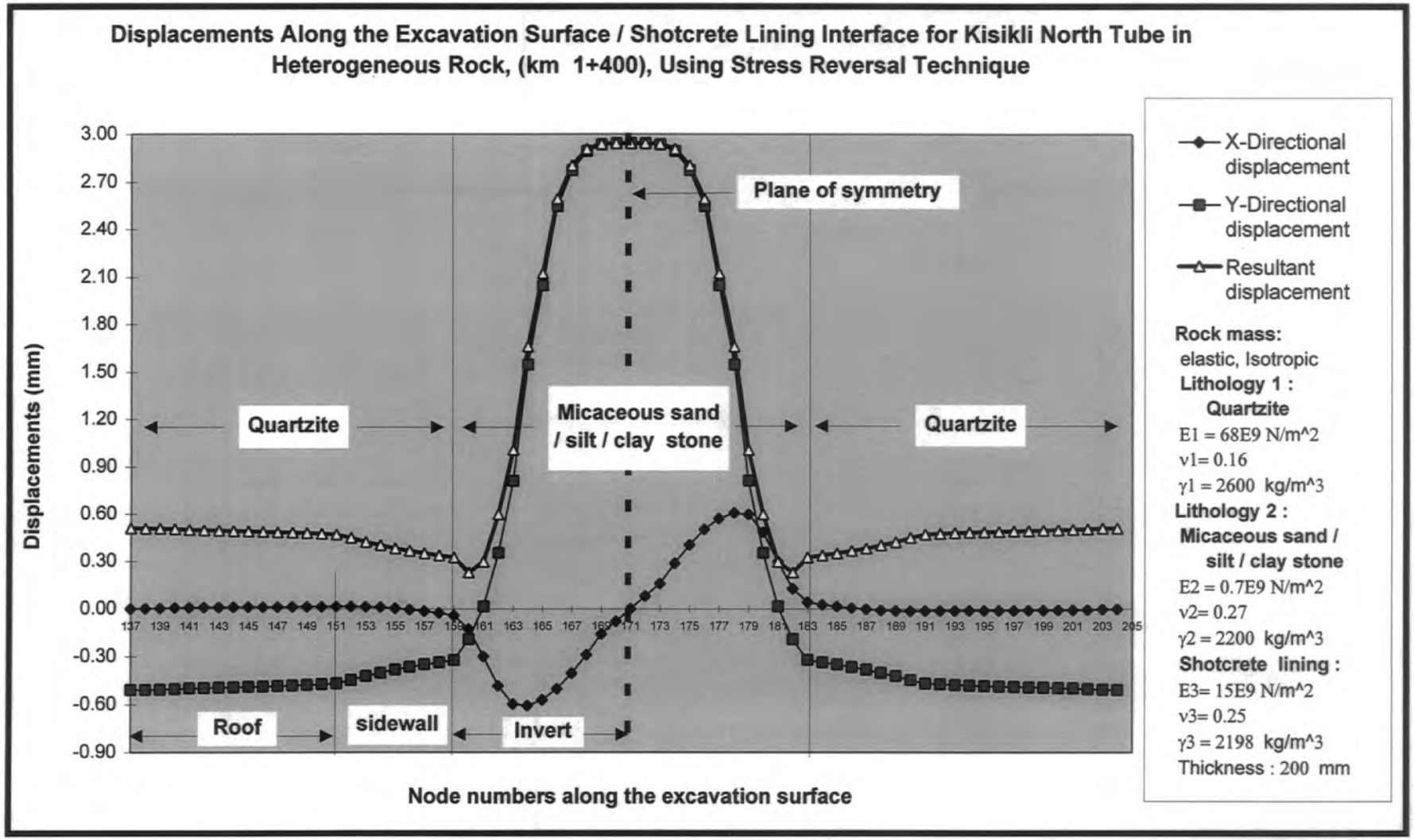

Fig. 7.31 Displacements along the excavation surface / shotcrete lining interface for Kisikli north tube (km 1+400)

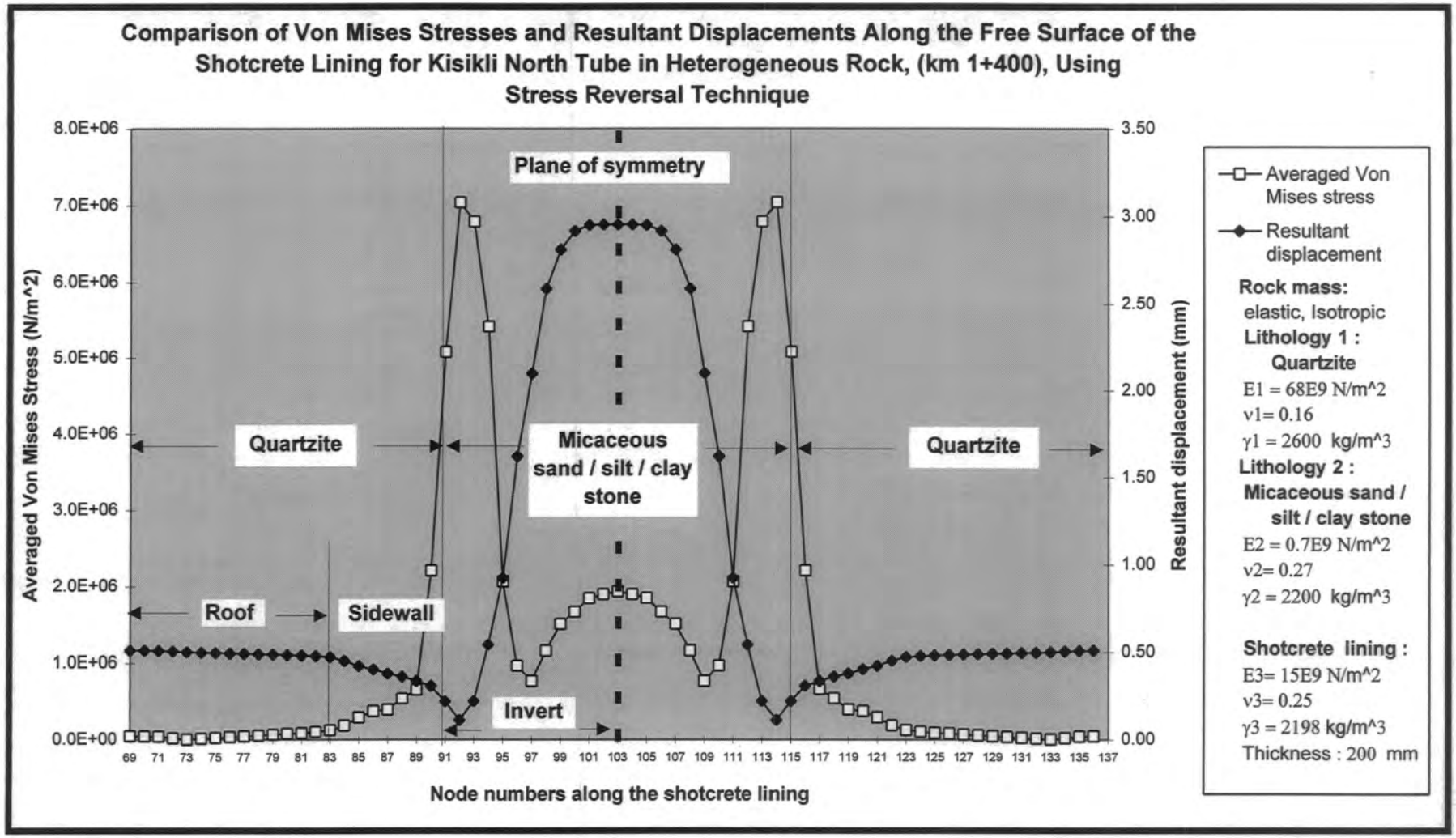

Fig. 7.32 Comparison of stresses and displacements along the free surface of the shotcrete lining for Kisikli north tube (km 1+400)

KISIKLI NORTH TUBE		KEEP EVERYTHING SAME			REDUCE (E) BY 10 TIMES			REDUCE (E) BY 50 TIMES			INCREASED (ν) BY 0.05			REDUCE (E) BY 10 TIMES AND			REDUCE (E) BY 50 TIMES AND		
km 1+400					KEEPING EVERTHING ELSE			KEEPING EVERTHING ELSE			KEEPING EVERTHING ELSE			INCREASED (ν) BY 0.05			INCREASED (ν) BY 0.05		
WITH SHOTCRETE					SAME			SAME			SAME			KEEPING EVERTHING ELSE SAME			KEEPING EVERTHING ELSE SAME		
LINING, t = 200 mm																			
HETEROGENEOUS MODEL		STRESS REVERSAL			STRESS REVERSAL			STRESS REVERSAL			STRESS REVERSAL			STRESS REVERSAL			STRESS REVERSAL		
		TECHNIQUE			TECHNIQUE			TECHNIQUE			TECHNIQUE			TECHNIQUE			TECHNIQUE		
		Lithology=Quartzite			Lithology=Quartzite			Lithology=Quartzite			Lithology=Quartzite			Lithology=Quartzite			Lithology=Quartzite		
		E=56E9 (N/m^2)			E=61.2E9 (N/m^2)			E=34E9 (N/m^2)			E=56E9 (N/m^2)			E=61.2E9 (N/m^2)			E=34E9 (N/m^2)		
		ν=0.16, γ=2600 (kg/m^3)			ν=0.16, γ=2600 (kg/m^3)			ν=0.16, γ=2600 (kg/m^3)			ν=0.21, γ=2600 (kg/m^3)			ν=0.21, γ=2600 (kg/m^3)			ν=0.21, γ=2600 (kg/m^3)		
ELEMENT	NODE	Lith.=Sand, silt, clay stone			Lith.=Sand, silt, clay stone			Lith.=Sand, silt, clay stone			Lith.=Sand, silt, clay stone			Lith.=Sand, silt, clay stone			Lith.=Sand, silt, clay stone		
NUMBER	NUMBER	E=0.7E9 (N/m^2)			E=0.63E9 (N/m^2)			E=0.35E9 (N/m^2)			E=0.7E9 (N/m^2)			E=0.63E9 (N/m^2)			E=0.35E9 (N/m^2)		
ALONG THE	ALONG THE	ν=0.27, γ=2200 (kg/m^3)			ν=0.27, γ=2200 (kg/m^3)			ν=0.27, γ=2200 (kg/m^3)			ν=0.32, γ=2200 (kg/m^3)			ν=0.32, γ=2200 (kg/m^3)			ν=0.32, γ=2200 (kg/m^3)		
SHOTCRETE	SHOTCRETE	DISPLACEMENT (mm)			DISPLACEMENT (mm)			DISPLACEMENT (mm)			DISPLACEMENT (mm)			DISPLACEMENT (mm)			DISPLACEMENT (mm)		
LINING	LINING	Ux	Uy	U	Ux	Uy	U	Ux	Uy	U	Ux	Uy	U	Ux	Uy	U	Ux	Uy	U
37	69	0.0000	-0.5080	0.5080	-0.0015	-0.5303	0.5303	-0.0027	-0.8901	0.8901	-0.0009	-0.4879	0.4879	-0.0010	-0.5364	0.5364	-0.0018	-0.9010	0.9010
37	70	0.0019	-0.5086	0.5086	0.0007	-0.5301	0.5301	0.0017	-0.8898	0.8898	0.0002	-0.4877	0.4877	0.0002	-0.5361	0.5361	0.0007	-0.9005	0.9005
38	71	0.0038	-0.5077	0.5077	0.0030	-0.5294	0.5294	0.0060	-0.8886	0.8886	0.0012	-0.4870	0.4870	0.0014	-0.5353	0.5353	0.0033	-0.8991	0.8991
38	72	0.0068	-0.5043	0.5043	0.0068	-0.5261	0.5261	0.0132	-0.8824	0.8825	0.0029	-0.4839	0.4839	0.0033	-0.5319	0.5319	0.0073	-0.8929	0.8929
39	73	0.0095	-0.4995	0.4996	0.0098	-0.5211	0.5212	0.0197	-0.8733	0.8738	0.0042	-0.4795	0.4796	0.0048	-0.5270	0.5270	0.0108	-0.8839	0.8840
39	74	0.0103	-0.4974	0.4975	0.0108	-0.5189	0.5190	0.0217	-0.8693	0.8696	0.0046	-0.4776	0.4776	0.0053	-0.5249	0.5249	0.0119	-0.8800	0.8801
40	75	0.0109	-0.4953	0.4954	0.0117	-0.5166	0.5167	0.0235	-0.8652	0.8655	0.0049	-0.4755	0.4755	0.0056	-0.5226	0.5226	0.0128	-0.8758	0.8760
40	76	0.0115	-0.4930	0.4931	0.0124	-0.5142	0.5143	0.0251	-0.8608	0.8612	0.0051	-0.4734	0.4734	0.0059	-0.5203	0.5203	0.0135	-0.8716	0.8717
41	77	0.0120	-0.4907	0.4908	0.0131	-0.5116	0.5118	0.0265	-0.8561	0.8565	0.0053	-0.4711	0.4711	0.0061	-0.5177	0.5177	0.0141	-0.8671	0.8672
41	78	0.0124	-0.4883	0.4885	0.0137	-0.5089	0.5091	0.0278	-0.8513	0.8518	0.0054	-0.4688	0.4689	0.0063	-0.5151	0.5151	0.0147	-0.8624	0.8628
42	79	0.0128	-0.4858	0.4860	0.0142	-0.5061	0.5063	0.0291	-0.8462	0.8467	0.0055	-0.4663	0.4663	0.0064	-0.5123	0.5123	0.0153	-0.8574	0.8578
42	80	0.0131	-0.4834	0.4836	0.0146	-0.5034	0.5036	0.0301	-0.8415	0.8420	0.0055	-0.4640	0.4640	0.0064	-0.5098	0.5099	0.0156	-0.8527	0.8529
43	81	0.0133	-0.4811	0.4813	0.0150	-0.5007	0.5009	0.0310	-0.8368	0.8372	0.0055	-0.4615	0.4616	0.0064	-0.5071	0.5071	0.0159	-0.8480	0.8481
43	82	0.0135	-0.4789	0.4791	0.0156	-0.4956	0.4958	0.0327	-0.8276	0.8282	0.0054	-0.4571	0.4571	0.0064	-0.5021	0.5021	0.0164	-0.8391	0.8393
44	83	0.0139	-0.4722	0.4724	0.0161	-0.4901	0.4904	0.0343	-0.8176	0.8183	0.0053	-0.4521	0.4521	0.0063	-0.4966	0.4966	0.0170	-0.8293	0.8295
45	84	0.0136	-0.4505	0.4507	0.0154	-0.4657	0.4660	0.0359	-0.7744	0.7752	0.0022	-0.4305	0.4306	0.0031	-0.4727	0.4727	0.0140	-0.7868	0.7869
46	85	0.0115	-0.4217	0.4219	0.0113	-0.4366	0.4367	0.0327	-0.7238	0.7245	-0.0047	-0.4044	0.4044	-0.0042	-0.4438	0.4438	0.0051	-0.7367	0.7367
46	86	0.0089	-0.4015	0.4016	0.0084	-0.4159	0.4160	0.0299	-0.6888	0.6894	-0.0090	-0.3859	0.3860	-0.0088	-0.4233	0.4234	-0.0005	-0.7020	0.7020
47	87	0.0012	-0.3775	0.3776	0.0004	-0.3904	0.3904	0.0206	-0.6462	0.6465	-0.0180	-0.3629	0.3633	-0.0184	-0.3980	0.3984	-0.0129	-0.6597	0.6598
47	88	-0.0059	-0.3604	0.3604	-0.0066	-0.3720	0.3721	0.0114	-0.6151	0.6152	-0.0257	-0.3462	0.3473	-0.0287	-0.3797	0.3806	-0.0240	-0.6286	0.6294
48	89	-0.0167	-0.3352	0.3356	-0.0174	-0.3450	0.3454	-0.0007	-0.5740	0.5740	-0.0374	-0.3214	0.3236	-0.0391	-0.3527	0.3549	-0.0390	-0.5878	0.5891
48	90	-0.0227	-0.3079	0.3087	-0.0243	-0.3168	0.3177	-0.0117	-0.5361	0.5382	-0.0436	-0.2941	0.2972	-0.0464	-0.3238	0.3271	-0.0514	-0.5489	0.5513
49	91	-0.0371	-0.2151	0.2183	-0.0359	-0.2259	0.2287	-0.0143	-0.4434	0.4436	-0.0619	-0.1999	0.2093	-0.0645	-0.2274	0.2364	-0.0628	-0.4490	0.4534
49	92	-0.0885	-0.0673	0.1112	-0.0755	-0.0793	0.1095	-0.0248	-0.2781	0.2792	-0.1251	-0.0507	0.1350	-0.1269	-0.0728	0.1463	-0.1001	-0.2734	0.2911
50	93	-0.1519	0.1595	0.2203	-0.1284	0.1536	0.2002	-0.0660	0.0256	0.0708	-0.1997	0.1740	0.2641	-0.2022	0.1650	0.2610	-0.1673	0.0371	0.1714
50	94	-0.2398	0.4850	0.5410	-0.2143	0.5026	0.5464	-0.1600	0.5624	0.5820	-0.2882	0.4912	0.5700	-0.2993	0.5097	0.5911	-0.2969	0.3873	0.4414
51	95	-0.3922	0.8784	0.9038	-0.2866	0.9333	0.9706	-0.2577	1.2891	1.3146	-0.3405	0.8690	0.9332	-0.3558	0.9271	0.9639	-0.3855	-1.2739	1.3310
51	96	-0.3715	1.5792	1.6223	-0.3524	1.7220	1.7587	-0.4361	2.7284	2.7630	-0.4123	1.5428	1.5949	-0.4377	1.6817	1.7377	-0.5474	2.6569	2.7127
52	97	-0.4327	2.0553	2.1004	-0.4200	2.2850	2.3036	-0.5631	3.7857	3.8303	-0.4827	1.9940	2.0470	-0.4971	2.1916	2.2473	-0.6819	3.6591	3.7221
52	98	-0.4302	2.5532	2.5892	-0.4158	2.8346	2.8649	-0.6349	4.9445	4.9851	-0.4379	2.4585	2.4972	-0.4748	2.7184	2.7686	-0.7070	4.7388	4.7912
53	99	-0.3803	2.7847	2.8106	-0.3577	3.0996	3.1284	-0.5711	5.4750	5.5047	-0.3847	2.6680	2.6928	-0.3974	2.9554	2.9820	-0.6167	5.2154	5.2517
53	100	-0.2758	2.9036	2.9169	-0.2386	3.2345	3.2453	-0.3684	5.7200	5.7332	-0.2338	2.7699	2.7798	-0.2558	3.0687	3.0793	-0.4048	5.4198	5.4349
54	101	-0.1585	2.9480	2.9503	-0.1074	3.2815	3.2833	-0.1872	5.8174	5.8204	-0.0908	2.8005	2.8029	-0.1008	3.1040	3.1056	-0.1738	5.4944	5.4971
54	102	-0.0795	2.9528	2.9538	-0.0206	3.2853	3.2854	-0.0551	5.8283	5.8286	0.0030	2.8006	2.8008	0.0001	3.1047	3.1047	-0.0241	5.4994	5.4995
55	103	0.0000	2.9541	2.9541	0.0659	3.2788	3.2795	0.0771	5.8189	5.8194	0.0964	2.7948	2.7965	0.1009	3.0983	3.0999	0.1258	5.4906	5.4920
55	104	0.0795	2.9528	2.9539	0.1512	3.2628	3.2663	0.2073	5.7894	5.7931	0.1879	2.7832	2.7895	0.1996	3.0854	3.0918	0.2725	5.4685	5.4733
56	105	0.1585	2.9480	2.9503	0.2345	3.2321	3.2406	0.3348	5.7328	5.7424	0.2763	2.7576	2.7716	0.2952	3.0572	3.0714	0.4150	5.4157	5.4316
56	106	0.2757	2.9036	2.9169	0.3574	3.1376	3.1679	0.5241	5.5537	5.6784	0.4086	2.6793	2.7103	0.4385	2.9693	3.0015	0.6302	5.2528	5.2905
57	107	0.3803	2.7847	2.8106	0.4644	2.9580	2.9942	0.6889	5.2261	5.2713	0.5249	2.5350	2.5868	0.5645	2.8089	2.8651	0.8199	4.9627	5.0300
57	108	0.4301	2.5533	2.5893	0.5075	2.6574	2.7054	0.7365	4.6387	4.6968	0.5779	2.2829	2.3646	0.6212	2.5363	2.6113	0.8876	4.4297	4.5178
58	109	0.4327	2.0554	2.1005	0.5070	2.0781	2.1400	0.6855	3.4869	3.5556	0.5813	1.8174	1.9112	0.6223	2.0004	2.0980	0.8565	3.3618	3.4693
58	110	0.3715	1.5792	1.6223	0.4510	1.5956	1.6581	0.5595	2.5295	2.5906	0.5493	1.4242	1.5265	0.5828	1.5542	1.6599	0.7418	2.4669	2.5759
59	111	0.2922	0.8764	0.9238	0.3684	0.8978	0.9704	0.4036	1.2367	1.3037	0.4771	0.8441	0.9696	0.5013	0.9024	1.0323	0.5890	1.2485	1.3805
59	112	0.2387	0.4851	0.5411	0.3063	0.5078	0.5941	0.3131	0.5772	0.6567	0.4135	0.5071	0.6843	0.4323	0.5293	0.6834	0.4875	0.6098	0.7807
60	113	0.1519	0.1595	0.2203	0.2056	0.1796	0.2730	0.1736	0.0710	0.1877	0.2990	0.2086	0.3646	0.3097	0.2042	0.3716	0.3222	0.1056	0.3391
60	114	0.0885	-0.0673	0.1112	0.1208	-0.0542	0.1324	0.0908	-0.2363	0.2531	0.1835	-0.0214	0.1847	0.1899	-0.0401	0.1941	0.1942	-0.2191	0.2928
61	115	0.0371	-0.2151	0.2183	0.0505	-0.2090	0.2158	0.0392	-0.4147	0.4165	0.0807	-0.1832	0.2002	0.0852	-0.2066	0.2253	0.0966	-0.4173	0.4288
61	116	0.0227	-0.3079	0.3087	0.0302	-0.3081	0.3076	0.0235	-0.5170	0.5175	0.0518	-0.2862	0.2908	0.0555	-0.3147	0.3196	0.0694	-0.5325	0.5370
62	117	0.0167	-0.3351	0.3355	0.0229	-0.3350	0.3358	0.0106	-0.5582	0.5583	0.0451	-0.3148	0.3180	0.0475	-0.3451	0.3484	0.0543	-0.5739	0.5765
62	118	0.0059	-0.3604	0.3604	0.0099	-0.3617	0.3618	-0.0056	-0.5971	0.5971	0.0305	-0.3396	0.3410	0.0320	-0.3720	0.3734	0.0336	-0.6152	0.6161
63	119	-0.0012	-0.3774	0.3774	0.0013	-0.3800	0.3800	-0.0174	-0.6277	0.6279	0.0212	-0.3560	0.3565	0.0219	-0.3901	0.3907	0.0192	-0.6458	0.6461
63	120	-0.0090	-0.4015	0.4016	-0.0087	-0.4055	0.4056	-0.0304	-0.6704	0.6711	0.0097	-0.3791	0.3792	0.0096	-0.4156	0.4157	0.0019	-0.6884	0.6894
64	121	-0.0115	-0.4216	0.4218	-0.0132	-0.4267	0.4269	-0.0360	-0.7062	0.7071	0.0036	-0.3982	0.3982	0.0030	-0.4367	0.4367	-0.0073	-0.7241	0.7241
65	122	-0.0138	-0.4504	0.4506	-0.0183	-0.4578	0.4582	-0.0410	-0.7603	0.7614	-0.0043	-0.4263	0.4263	-0.0055	-0.4678	0.4678	-0.0184	-0.7780	0.7782
66	123	-0.0139	-0.4722	0.4724	-0.0189	-0.4840	0.4844	-0.0391	-0.8067	0.8078	-0.0072	-0.4492	0.4493	-0.0085	-0.4933	0.4934	-0.0207	-0.8232	0.8235
66	124	-0.0135	-0.4769	0.4771	-0.0183	-0.4900	0.4903	-0.0375	-0.8174	0.8183	-0.0072	-0.4544	0.4545	-0.0084	-0.4990	0.4991	-0.0199	-0.8334	0.8336
67	125	-0.0133	-0.4811	0.4812	-0.0178	-0.4954	0.4957	-0.0360	-0.8271	0.8279	-0.0073	-0.4590	0.4591	-0.0085	-0.5042	0.5043	-0.0195	-0.8427	0.8429
67	126	-0.0131	-0.4834	0.4836	-0.0174	-0.4984	0.4987	-0.0351	-0.8323	0.8330	-0.0073	-0.4616	0.4617	-0.0085	-0.5070	0.5071	-0.0192	-0.8477	0.8479
68	127	-0.0128	-0.4857	0.4858	-0.0170	-0.5012	0.5016	-0.0341	-0.8375	0.8382	-0.0073	-0.4640	0.4641	-0.0084	-0.5097	0.5098	-0.0188	-0.8526	0.8528
68	128	-0.0124	-0.4883	0.4885	-0.0165	-0.5043	0.5046	-0.0329	-0.8431	0.8437	-0.0072	-0.4667	0.4668	-0.0083	-0.5127	0.5128	-0.0183	-0.8579	0.8581
69	129	-0.0120	-0.4907	0.4908	-0.0159	-0.5073	0.5075	-0.0316	-0.8483	0.8489	-0.0070	-0.4692	0.4693	-0.0081	-0.5154	0.5155	-0.0177	-0.8629	0.8631
69	130	-0.0115	-0.4930	0.4931	-0.0153	-0.5101	0.5103	-0.0302	-0.8535	0.8540	-0.0069	-0.4716	0.4717	-0.0079	-0.5181	0.5182	-0.0171	-0.8677	0.8679
70	131	-0.0110	-0.4953	0.4954	-0.0146	-0.5128	0.5130	-0.0286	-0.8584	0.8589	-0.0067	-0.4738	0.4738	-0.0077	-0.5206	0.5207	-0.0163	-0.8723	0.8725
70	132	-0.0103	-0.4974	0.4975	-0.0137	-0.5154	0.5156	-0.0269	-0.8631	0.8636	-0.0064	-0.4760	0.4760	-0.0073	-0.5231	0.5232	-0.0155	-0.8767	0.8768
71	133	-0.0095	-0.4994	0.4995	-0.0128	-0.5179	0.5181	-0.0249	-0.8676	0.8680	-0.0060	-0.4781	0.4781	-0.0069	-0.5253	0.5253	-0.0144	-0.8808	0.8809
71	134	-0.0068	-0.5043	0.5043	-0.0096	-0.5239	0.5240	-0.0185	-0.8785	0.8787	-0.0047	-0.4829	0.4829	-0.0053	-0.5308	0.5308	-0.0109	-0.8906	0.8909
72	135	-0.0038	-0.5077	0.5077	-0.0060	-0.5283	0.5283	-0.0114	-0.8865	0.8866	-0.0031	-0.4865	0.4865	-0.0035	-0.5347	0.5347	-0.0069	-0.8980	0.8980
72	136	-0.0019	-0.5086	0.5086	-0.0038	-0.5295	0.5295	-0.0070	-0.8888	0.8888	-0.0020	-0.4874	0.4874	-0.0023	-0.5358	0.5358	-0.0044	-0.8999	0.8999

Table 7.10 Comparison of displacements as a function of elasticity modulus and Poisson's ratio along the free surface of the shotcrete lining for Kisikli north tube (km 1+400)

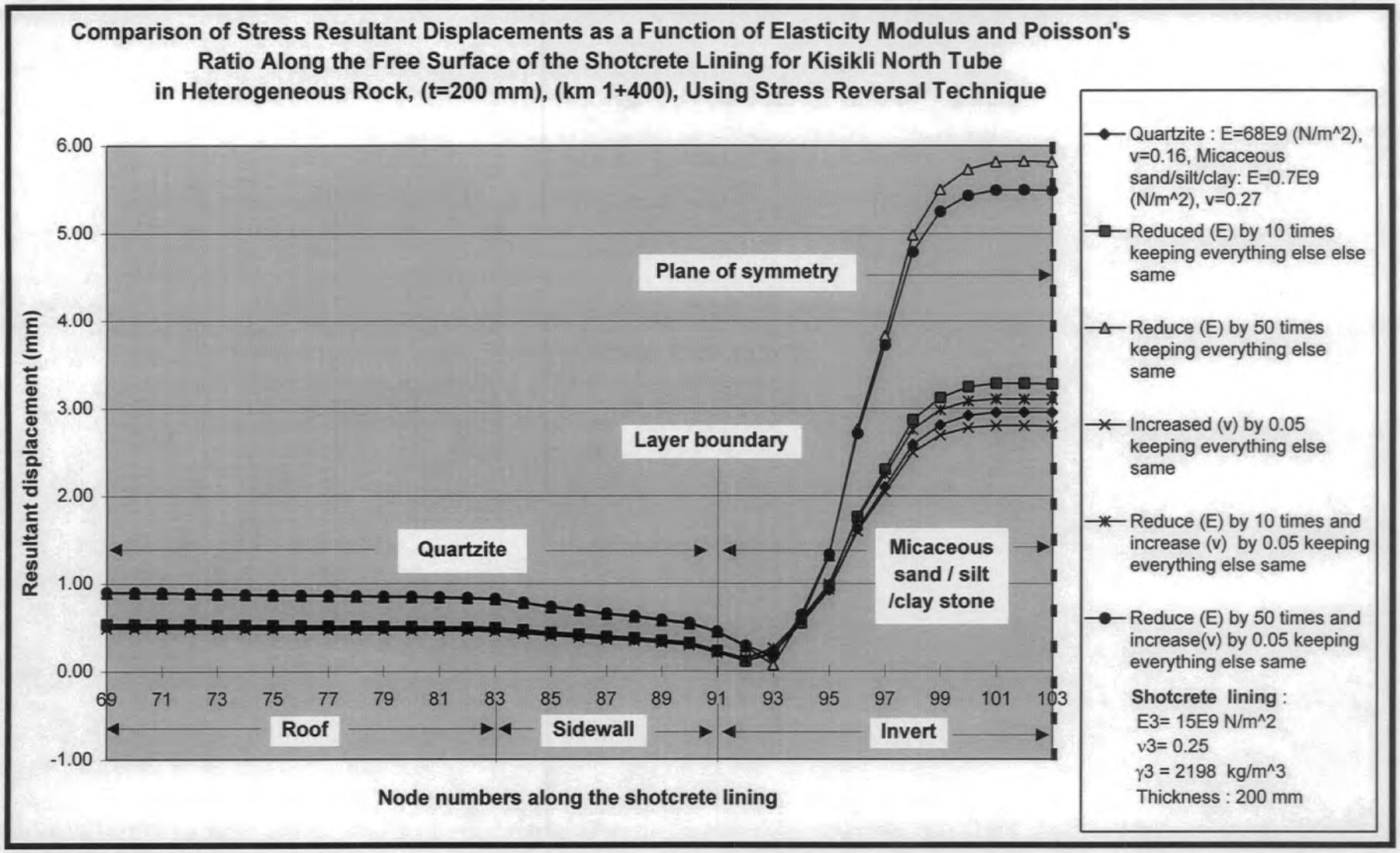

Fig.7.33 Comparison of displacements as a function of elasticity modulus and Poisson's ratio along the free surface of the shotcrete lining for Kisikli north tube (km 1+400)

KISIKLI NORTH TUBE		KEEP EVERYTHING SAME			REDUCE (E) BY 10 TIMES			REDUCE (E) BY 50 TIMES			INCREASED (ν) BY 0.05			REDUCE (E) BY 10 TIMES AND			REDUCE (E) BY 50 TIMES AND		
km 1+400					KEEPING EVERTHING ELSE			KEEPING EVERTHING ELSE			KEEPING EVERTHING ELSE			INCREASED (ν) BY 0.05			INCREASED (ν) BY 0.05		
WITH SHOTCRETE					SAME			SAME			SAME			KEEPING EVERTHING ELSE SAME			KEEPING EVERTHING ELSE SAME		
LINING, t = 100 mm																			
HETEROGENEOUS MODEL		STRESS REVERSAL			STRESS REVERSAL			STRESS REVERSAL			STRESS REVERSAL			STRESS REVERSAL			STRESS REVERSAL		
		TECHNIQUE			TECHNIQUE			TECHNIQUE			TECHNIQUE			TECHNIQUE			TECHNIQUE		
		Lithology=Quartzite			Lithology=Quartzite			Lithology=Quartzite			Lithology=Quartzite			Lithology=Quartzite			Lithology=Quartzite		
		E=61.2E9 (N/m^2)			E=61.2E9 (N/m^2)			E=34E9 (N/m^2)			E=61.2E9 (N/m^2)			E=61.2E9 (N/m^2)			E=34E9 (N/m^2)		
		ν=0.16, γ=2600 (kg/m^3)			ν=0.16, γ=2600 (kg/m^3)			ν=0.16, γ=2600 (kg/m^3)			ν=0.21, γ=2600 (kg/m^3)			ν=0.21, γ=2600 (kg/m^3)			ν=0.21, γ=2600 (kg/m^3)		
ELEMENT	NODE	Lith.=Sand, silt, clay stone			Lith.=Sand, silt, clay stone			Lith.=Sand, silt, clay stone			Lith.=Sand, silt, clay stone			Lith.=Sand, silt, clay stone			Lith.=Sand, silt, clay stone		
NUMBER	NUMBER	E=0.7E9 (N/m^2)			E=0.63E9 (N/m^2)			E=0.35E9 (N/m^2)			E=0.7E9 (N/m^2)			E=0.63E9 (N/m^2)			E=0.35E9 (N/m^2)		
ALONG THE	ALONG THE	ν=0.27, γ=2200 (kg/m^3)			ν=0.27, γ=2200 (kg/m^3)			ν=0.27, γ=2200 (kg/m^3)			ν=0.32, γ=2200 (kg/m^3)			ν=0.32, γ=2200 (kg/m^3)			ν=0.32, γ=2200 (kg/m^3)		
SHOTCRETE	SHOTCRETE	DISPLACEMENT (mm)			DISPLACEMENT (mm)			DISPLACEMENT (mm)			DISPLACEMENT (mm)			DISPLACEMENT (mm)			DISPLACEMENT (mm)		
LINING	LINING	Ux	Uy	U	Ux	Uy	U	Ux	Uy	U	Ux	Uy	U	Ux	Uy	U	Ux	Uy	U
49	69	0.0006	-0.5343	0.5343	0.0009	-0.5890	0.5890	0.0016	-1.0132	1.0132	0.0009	-0.5337	0.5337	0.0010	-0.5891	0.5891	0.0018	-1.0135	1.0136
49	70	0.0024	-0.5338	0.5338	0.0027	-0.5884	0.5884	0.0052	-1.0121	1.0121	0.0017	-0.5332	0.5332	0.0019	-0.5885	0.5885	0.0036	-1.0124	1.0124
50	71	0.0041	-0.5328	0.5328	0.0045	-0.5874	0.5874	0.0087	-1.0102	1.0102	0.0024	-0.5323	0.5323	0.0026	-0.5875	0.5875	0.0053	-1.0106	1.0106
51	72	0.0069	-0.5295	0.5296	0.0077	-0.5836	0.5837	0.0147	-1.0034	1.0035	0.0036	-0.5291	0.5291	0.0040	-0.5840	0.5840	0.0082	-1.0042	1.0042
52	73	0.0083	-0.5242	0.5243	0.0104	-0.5777	0.5778	0.0201	-0.9927	0.9929	0.0044	-0.5241	0.5241	0.0050	-0.5784	0.5784	0.0105	-0.9941	0.9942
53	74	0.0099	-0.5221	0.5222	0.0111	-0.5755	0.5756	0.0218	-0.9886	0.9888	0.0046	-0.5222	0.5222	0.0052	-0.5763	0.5763	0.0111	-0.9902	0.9903
54	75	0.0105	-0.5199	0.5200	0.0118	-0.5730	0.5731	0.0230	-0.9841	0.9844	0.0048	-0.5200	0.5200	0.0054	-0.5739	0.5739	0.0116	-0.9859	0.9860
54	76	0.0110	-0.5176	0.5177	0.0124	-0.5704	0.5706	0.0242	-0.9795	0.9798	0.0048	-0.5178	0.5178	0.0055	-0.5714	0.5714	0.0120	-0.9815	0.9816
55	77	0.0115	-0.5152	0.5153	0.0129	-0.5677	0.5678	0.0252	-0.9748	0.9749	0.0048	-0.5156	0.5156	0.0055	-0.5689	0.5689	0.0122	-0.9769	0.9770
55	78	0.0118	-0.5127	0.5128	0.0133	-0.5650	0.5652	0.0262	-0.9697	0.9701	0.0048	-0.5132	0.5132	0.0055	-0.5663	0.5663	0.0124	-0.9721	0.9722
56	79	0.0121	-0.5102	0.5103	0.0137	-0.5621	0.5623	0.0270	-0.9645	0.9649	0.0048	-0.5107	0.5107	0.0055	-0.5635	0.5636	0.0124	-0.9672	0.9673
56	80	0.0124	-0.5078	0.5080	0.0140	-0.5595	0.5597	0.0277	-0.9599	0.9603	0.0047	-0.5085	0.5085	0.0054	-0.5610	0.5610	0.0125	-0.9627	0.9628
57	81	0.0125	-0.5054	0.5056	0.0141	-0.5569	0.5571	0.0282	-0.9550	0.9554	0.0045	-0.5062	0.5062	0.0052	-0.5584	0.5584	0.0123	-0.9581	0.9582
57	82	0.0128	-0.5012	0.5014	0.0144	-0.5522	0.5524	0.0291	-0.9467	0.9471	0.0041	-0.5021	0.5021	0.0048	-0.5540	0.5540	0.0119	-0.9500	0.9501
58	83	0.0132	-0.4965	0.4967	0.0149	-0.5469	0.5471	0.0303	-0.9372	0.9377	0.0038	-0.4975	0.4975	0.0046	-0.5488	0.5488	0.0119	-0.9408	0.9409
59	84	0.0133	-0.4749	0.4751	0.0152	-0.5230	0.5232	0.0327	-0.8943	0.8949	0.0016	-0.4786	0.4786	0.0023	-0.5256	0.5256	0.0096	-0.8991	0.8992
61	85	0.0105	-0.4466	0.4467	0.0123	-0.4915	0.4917	0.0300	-0.8384	0.8389	-0.0036	-0.4485	0.4485	-0.0034	-0.4944	0.4944	0.0022	-0.8438	0.8438
62	86	0.0063	-0.4289	0.4289	0.0077	-0.4719	0.4720	0.0236	-0.8039	0.8042	-0.0095	-0.4309	0.4310	-0.0098	-0.4749	0.4750	-0.0075	-0.8095	0.8095
63	87	-0.0020	-0.4057	0.4057	-0.0012	-0.4462	0.4462	0.0103	-0.7591	0.7592	-0.0195	-0.4077	0.4082	-0.0207	-0.4492	0.4497	-0.0243	-0.7649	0.7653
63	88	-0.0103	-0.3909	0.3910	-0.0104	-0.4296	0.4297	-0.0039	-0.7293	0.7293	-0.0290	-0.3930	0.3941	-0.0311	-0.4326	0.4339	-0.0408	-0.7354	0.7365
64	89	-0.0223	-0.3892	0.3898	-0.0234	-0.4059	0.4066	-0.0232	-0.6909	0.6913	-0.0428	-0.3710	0.3735	-0.0461	-0.4067	0.4113	-0.0635	-0.6965	0.6994
64	90	-0.0318	-0.3583	0.3607	-0.0339	-0.3944	0.3959	-0.0402	-0.6670	0.6682	-0.0532	-0.3615	0.3654	-0.0575	-0.3978	0.4018	-0.0824	-0.6735	0.6785
65	91	-0.0438	-0.2859	0.2892	-0.0468	-0.3182	0.3216	-0.0566	-0.5789	0.5817	-0.0699	-0.2825	0.2910	-0.0755	-0.3154	0.3243	-0.1086	-0.5760	0.5858
65	92	-0.1118	-0.0892	0.1429	-0.1164	-0.1126	0.1619	-0.1149	-0.3320	0.3513	-0.1811	-0.0747	0.1959	-0.1913	-0.0972	0.2146	-0.2274	-0.3068	0.3819
66	93	-0.2174	0.2004	0.2967	-0.2297	0.1957	0.3018	-0.2603	0.0850	0.2728	-0.3287	0.2265	0.3975	-0.3471	0.2247	0.4128	-0.4322	0.1363	0.4532
66	94	-0.3470	0.5930	0.6871	-0.3735	0.6258	0.7288	-0.4967	0.7809	0.9266	-0.4736	0.6130	0.7748	-0.5067	0.6457	0.8250	-0.6974	0.6278	1.0824
67	95	-0.4189	1.0428	1.1238	-0.4553	1.1254	1.2149	-0.6558	1.6803	1.8037	-0.5499	1.0410	1.1773	-0.5957	1.1258	1.2737	-0.8589	1.6906	1.8963
67	96	-0.4803	1.7654	1.8296	-0.5277	1.9404	2.0109	-0.8301	3.2560	3.3601	-0.6060	1.7184	1.8228	-0.6642	1.8696	2.0029	-1.0235	3.1774	3.3382
68	97	-0.5065	2.2059	2.2632	-0.5595	2.4371	2.5008	-0.9203	4.2316	4.3305	-0.6272	2.1251	2.2157	-0.6881	2.3486	2.4473	-1.0991	4.0630	4.2283
69	98	-0.4736	2.6448	2.6869	-0.5234	2.9287	2.9781	-0.8757	5.1652	5.2389	-0.5785	2.5241	2.5895	-0.6348	2.7955	2.8667	-1.0272	4.9328	5.0388
70	99	-0.4051	2.8774	2.9058	-0.4467	3.1897	3.2208	-0.7436	5.6569	5.7056	-0.4904	2.7298	2.7725	-0.5372	3.0252	3.0728	-0.8856	5.3656	5.4352
71	100	-0.2981	2.9934	3.0082	-0.3279	3.3205	3.3367	-0.5415	5.9106	5.9354	-0.3582	2.8242	2.8468	-0.3916	3.1328	3.1572	-0.6298	5.5742	5.6093
72	101	-0.1682	3.0352	3.0399	-0.1847	3.3682	3.3733	-0.3027	6.0061	6.0137	-0.2012	2.8656	2.8629	-0.2197	3.1668	3.1764	-0.3495	5.6452	5.6960
72	102	-0.0842	3.0472	3.0484	-0.0924	3.3816	3.3829	-0.1510	6.0313	6.0332	-0.1006	2.8641	2.8659	-0.1098	3.1780	3.1789	-0.1740	5.6620	5.6647
73	103	0.0017	3.0475	3.0476	0.0018	3.3823	3.3823	0.0033	6.0355	6.0355	0.0022	2.8631	2.8631	0.0024	3.1772	3.1772	0.0043	5.6633	5.6633
73	104	0.0876	3.0472	3.0485	0.0961	3.3816	3.3830	0.1575	6.0313	6.0334	0.1050	2.8641	2.8660	0.1147	3.1780	3.1801	0.1826	5.6620	5.6649
74	105	0.1715	3.0352	3.0400	0.1883	3.3682	3.3726	0.3093	6.0061	6.0141	0.2056	2.8558	2.8632	0.2246	3.1668	3.1767	0.3581	5.6452	5.6565
75	106	0.2514	2.9934	3.0085	0.3315	3.3205	3.3370	0.5479	5.9106	5.9359	0.3625	2.8242	2.8474	0.3965	3.1329	3.1679	0.6354	5.5742	5.6103
76	107	0.4083	2.8773	2.9061	0.4502	3.1896	3.2212	0.7500	5.6567	5.7062	0.4946	2.7287	2.7732	0.5420	3.0251	3.0733	0.8741	5.3657	5.4364
77	108	0.4768	2.6445	2.6871	0.5258	2.9283	2.9753	0.8820	5.1645	5.2393	0.5827	2.5239	2.5903	0.6395	2.7952	2.8674	1.0355	4.9322	5.0297
78	109	0.5085	2.2052	2.2633	0.5626	2.4363	2.5005	0.9264	4.2302	4.3306	0.6312	2.1245	2.2163	0.6926	2.3478	2.4478	1.1072	4.0617	4.2292
78	110	0.4832	1.7643	1.8293	0.5309	1.9392	2.0106	0.8360	3.2538	3.3595	0.6119	1.7174	1.8232	0.6685	1.8685	2.0033	1.0314	3.1755	3.3388
79	111	0.4217	1.0412	1.1234	0.4583	1.1245	1.2143	0.6913	1.6789	1.8026	0.5537	1.0396	1.1779	0.5999	1.1241	1.2742	0.8666	1.6875	1.8970
79	112	0.3496	0.5910	0.6867	0.3784	0.6235	0.7283	0.5040	0.7767	0.9259	0.4775	0.6111	0.7766	0.5137	0.6465	0.8257	0.7047	0.8239	1.0642
80	113	0.2198	0.1879	0.2958	0.2323	0.1929	0.3019	0.2951	0.0600	0.2769	0.3300	0.2242	0.3990	0.3508	0.2219	0.4151	0.4368	0.1315	0.4691
80	114	0.1138	-0.0820	0.1403	0.1168	-0.1156	0.1659	0.1191	-0.3377	0.3581	0.1841	-0.0775	0.1997	0.1945	-0.1004	0.2189	0.2333	-0.3125	0.3900
81	115	0.0457	-0.2890	0.2929	0.0488	-0.3217	0.3254	0.0604	-0.5852	0.5883	0.0725	-0.2856	0.2947	0.0784	-0.3190	0.3285	0.1119	-0.5822	0.5929
81	116	0.0338	-0.3625	0.3641	0.0360	-0.3980	0.3996	0.0441	-0.6734	0.6748	0.0559	-0.3646	0.3689	0.0605	-0.4015	0.4060	0.0879	-0.6789	0.6856
82	117	0.0243	-0.3724	0.3732	0.0256	-0.4085	0.4103	0.0272	-0.6972	0.6977	0.0456	-0.3741	0.3769	0.0491	-0.4124	0.4163	0.0690	-0.7028	0.7062
82	118	0.0124	-0.3941	0.3943	0.0126	-0.4332	0.4334	0.0080	-0.7357	0.7357	0.0318	-0.3962	0.3975	0.0342	-0.4365	0.4378	0.0465	-0.7418	0.7433
83	119	0.0041	-0.4089	0.4089	0.0036	-0.4496	0.4496	-0.0060	-0.7655	0.7655	0.0225	-0.4109	0.4115	0.0240	-0.4529	0.4535	0.0302	-0.7713	0.7719
84	120	-0.0039	-0.4322	0.4322	-0.0051	-0.4756	0.4756	-0.0188	-0.8104	0.8106	0.0127	-0.4342	0.4344	0.0133	-0.4787	0.4789	0.0139	-0.8162	0.8163
85	121	-0.0075	-0.4500	0.4501	-0.0089	-0.4953	0.4954	-0.0240	-0.8451	0.8454	0.0076	-0.4520	0.4521	0.0079	-0.4983	0.4984	0.0059	-0.8507	0.8507
86	122	-0.0106	-0.4774	0.4775	-0.0122	-0.5258	0.5259	-0.0273	-0.8992	0.8996	0.0018	-0.4790	0.4790	0.0015	-0.5284	0.5284	-0.0028	-0.9040	0.9040
88	123	-0.0111	-0.4984	0.4985	-0.0126	-0.5490	0.5491	-0.0282	-0.9409	0.9413	-0.0013	-0.4994	0.4994	-0.0015	-0.5510	0.5510	-0.0069	-0.9445	0.9446
88	124	-0.0108	-0.5030	0.5031	-0.0123	-0.5542	0.5543	-0.0252	-0.9502	0.9505	-0.0017	-0.5039	0.5039	-0.0021	-0.5560	0.5560	-0.0071	-0.9536	0.9536
89	125	-0.0106	-0.5071	0.5072	-0.0121	-0.5587	0.5588	-0.0245	-0.9584	0.9587	-0.0022	-0.5078	0.5078	-0.0026	-0.5603	0.5603	-0.0077	-0.9614	0.9614
89	126	-0.0105	-0.5094	0.5095	-0.0119	-0.5613	0.5614	-0.0240	-0.9630	0.9633	-0.0024	-0.5101	0.5101	-0.0029	-0.5629	0.5629	-0.0080	-0.9660	0.9660
90	127	-0.0103	-0.5117	0.5118	-0.0117	-0.5639	0.5640	-0.0234	-0.9676	0.9679	-0.0025	-0.5123	0.5123	-0.0030	-0.5653	0.5653	-0.0080	-0.9703	0.9703
90	128	-0.0100	-0.5142	0.5143	-0.0113	-0.5666	0.5667	-0.0229	-0.9726	0.9729	-0.0026	-0.5147	0.5147	-0.0031	-0.5679	0.5679	-0.0080	-0.9751	0.9751
91	129	-0.0097	-0.5166	0.5167	-0.0109	-0.5693	0.5694	-0.0217	-0.9774	0.9776	-0.0027	-0.5170	0.5170	-0.0032	-0.5705	0.5705	-0.0078	-0.9797	0.9797
91	130	-0.0093	-0.5189	0.5190	-0.0105	-0.5719	0.5720	-0.0208	-0.9820	0.9822	-0.0027	-0.5192	0.5192	-0.0032	-0.5729	0.5729	-0.0078	-0.9841	0.9841
92	131	-0.0088	-0.5211	0.5212	-0.0100	-0.5743	0.5744	-0.0196	-0.9865	0.9867	-0.0027	-0.5213	0.5213	-0.0032	-0.5753	0.5753	-0.0075	-0.9884	0.9884
93	132	-0.0082	-0.5233	0.5234	-0.0093	-0.5767	0.5768	-0.0182	-0.9908	0.9910	-0.0026	-0.5233	0.5233	-0.0030	-0.5775	0.5775	-0.0070	-0.9925	0.9925
94	133	-0.0078	-0.5252	0.5253	-0.0086	-0.5789	0.5790	-0.0168	-0.9946	0.9948	-0.0024	-0.5252	0.5252	-0.0028	-0.5796	0.5796	-0.0065	-0.9962	0.9962
95	134	-0.0052	-0.5302	0.5302	-0.0059	-0.5844	0.5844	-0.0115	-1.0046	1.0049	-0.0017	-0.5298	0.5298	-0.0019	-0.5846	0.5848	-0.0044	-1.0056	1.0056
96	135	-0.0025	-0.5332	0.5332	-0.0028	-0.5878	0.5878	-0.0055	-1.0110	1.0110	-0.0005	-0.5327	0.5327	-0.0006	-0.5880	0.5880	-0.0016	-1.0114	1.0114
96	136	-0.0009	-0.5340	0.5340	-0.0010	-0.5886	0.5886	-0.0020	-1.0125	1.0125	0.0002	-0.5334	0.5334	0.0002	-0.5887	0.5887	0.0001	-1.0128	1.0128

Table 7.11 Comparison of displacements as a function of elasticity of modulus and Poisson's ratio along the reduced thickness of shotcrete lining free surface of Kisikli north tube (km 1+400)

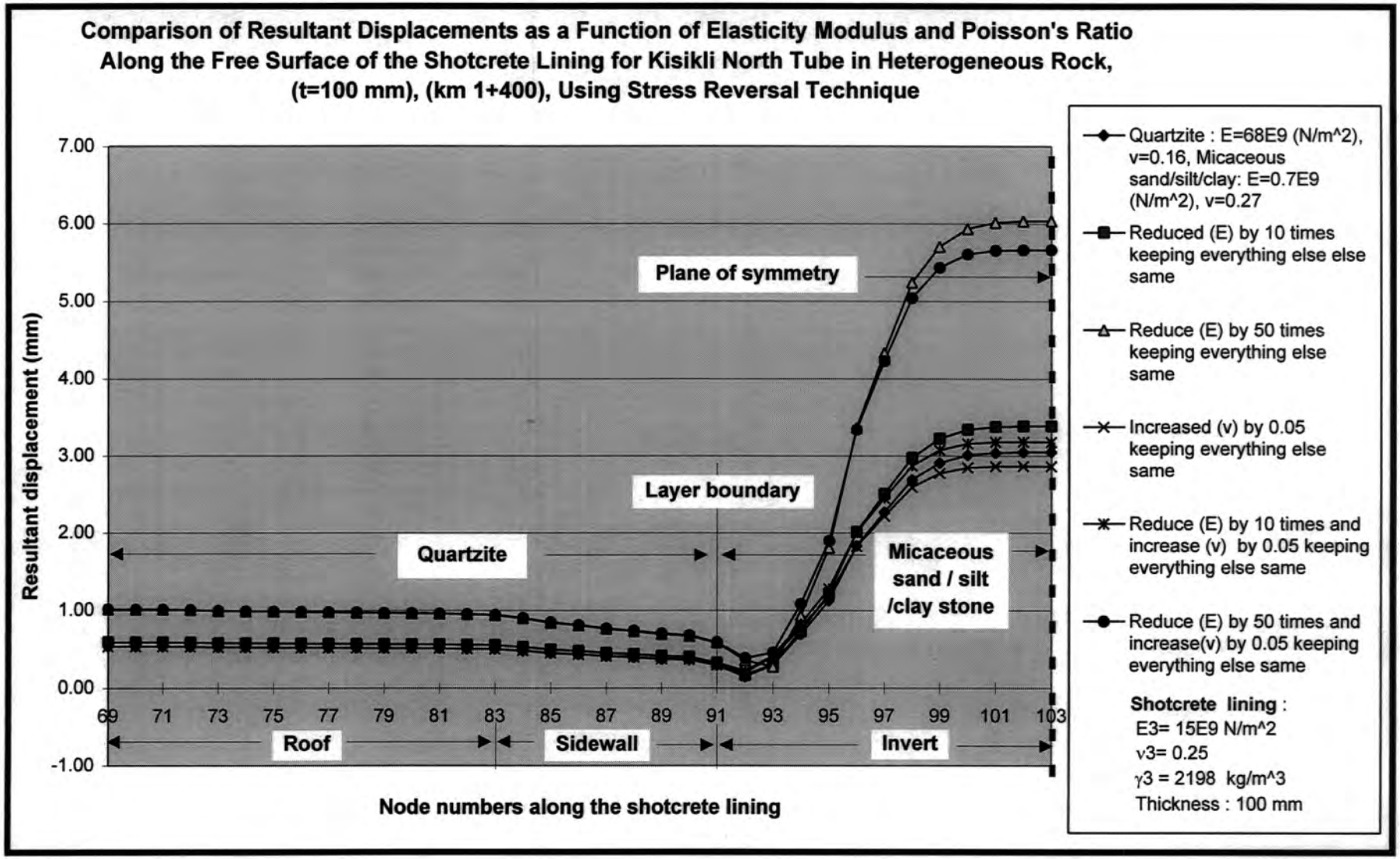

Fig. 7.34 Comparison of displacements as function of elasticity modulus and Poisson's ratio along the reduced thickness of shotcrete lining free surface for Kisikli north tube

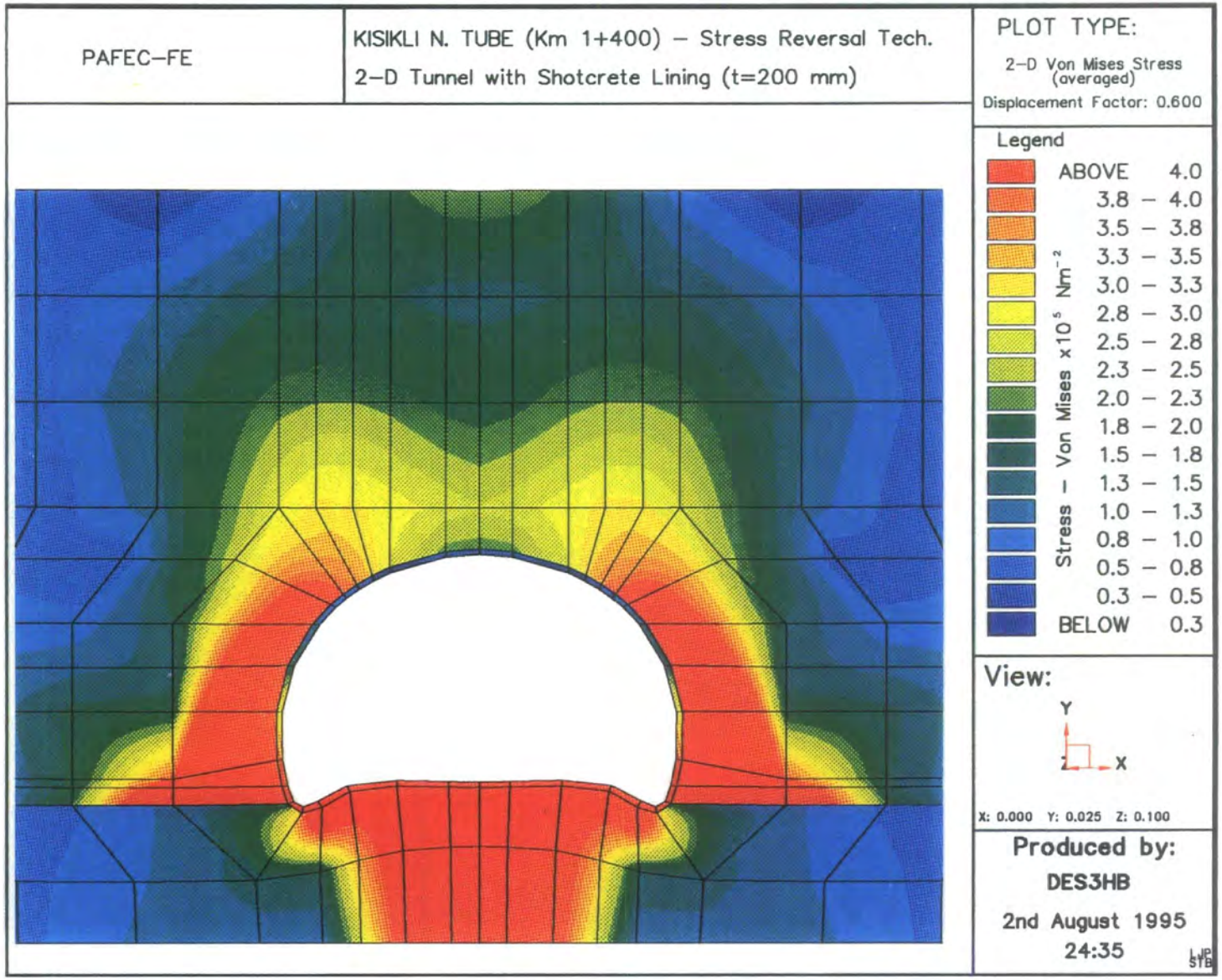

Fig. 7.35 Colour stress and displaced shape diagrams of Kisikli north tube, (km 1+400), having shotcrete lining (t=200 mm)

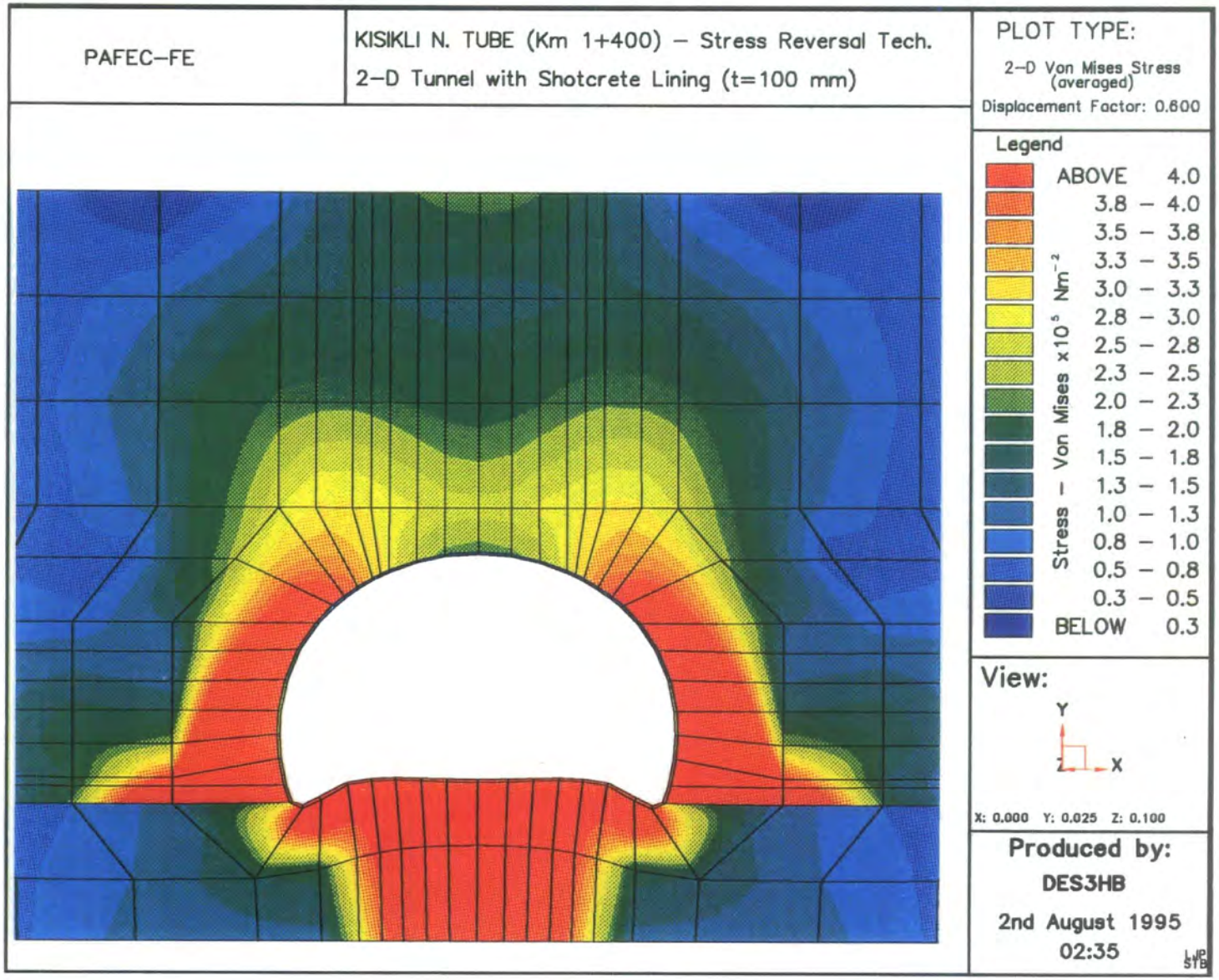

Fig. 7.36 Colour stress and displaced shape diagrams of Kisikli north tube, (km 1+400), having shotcrete lining (t=100 mm)

7.3.1.3 Comparison of Measured and Computed Displacements

A comparison of the measured and calculated results of displacements of the Kisikli north tube (km 1+400) having a 200 mm thick shotcrete lining is presented in Table 7.12 for various values of material properties for the in situ rock. It should be noted that the sign of the displacement (the sense of the movement) indicates the direction of movement relative to the axes on the centre of the tunnel, as shown in Fig 7.4. The measured displacements indicate a general trend of movement towards the tunnel origin, as shown in Fig. 7.28.

The calculated tunnel convergence at all points are smaller than the measured in situ values for the Kisikli north tube having a 200 mm thick shotcrete lining. The maximum difference between the measured and calculated displacement values is 0.42 mm. This occurs for the horizontal convergence between measuring points B2-C3, when the relatively large actual movement occurs in the opposite direction to the slight predicted movement.

The influence of Young's modulus and Poisson's ratio on the convergence of the tunnel is shown in Fig. 7.37 and Table 7.12. From these it can be clearly seen that reducing the Young's modulus has a notable increase on the tunnel convergence. The Young's modulus of the in situ rock quartzite is very high. Therefore the reduction factors of 0.10 and 0.50 applied to the values of the 'intact' Young's modulus are not sufficient. Furthermore, it can be clearly seen that reducing the thickness of the shotcrete lining from 200 mm to 100 mm has not notably changed the tunnel convergence as shown in Table 7.12.

The computed convergence is similarly affected by changes in Poisson's ratio which may produce a reduction or an increase. This is because, with the conditions of plane strain imposed on the analysis, changing the value of Poisson's ratio also effects the in situ stress state and its effect on the displacements is much less predictable than the effect of changing Young's modulus. This is even more pronounced because the in situ rock at this section of the Kisikli tunnel at km 1+400 is a relatively stiff quartzite.

				KEEP EVERYTHING SAME	REDUCE (E) BY 10 TIMES KEEPING EVERTHING ELSE SAME	REDUCE (E) BY 50 TIMES KEEPING EVERTHING ELSE SAME	INCREASED (ν) BY 0.05 KEEPING EVERTHING ELSE SAME	REDUCE (E) BY 10 TIMES AND INCREASED (ν) BY 0.05 KEEPING EVERTHING ELSE SAME	REDUCE (E) BY 50 TIMES AND INCREASED (ν) BY 0.05 KEEPING EVERTHING ELSE SAME
				STRESS REVERSAL TECHNIQUE	STRESS REVERSAL TECHNIQUE	STRESS REVERSAL TECHNIQUE	STRESS REVERSAL TECHNIQUE	STRESS REVERSAL TECHNIQUE	STRESS REVERSAL TECHNIQUE
		(TUNNEL EXCAVATION) →		Lithology=Quartzite	Lithology=Quartzite	Lithology=Quartzite	Lithology=Quartzite	Lithology=Quartzite	Lithology=Quartzite
				E=68E9 (N/m^2)	E=61.2E9 (N/m^2)	E=34E9 (N/m^2)	E=68E9 (N/m^2)	E=61.2E9 (N/m^2)	E=34E9 (N/m^2)
				ν=0.16, γ=2600 (kg/m^3)	ν=0.16, γ=2600 (kg/m^3)	ν=0.16, γ=2600 (kg/m^3)	ν=0.21, γ=2600 (kg/m^3)	ν=0.21, γ=2600 (kg/m^3)	ν=0.21, γ=2600 (kg/m^3)
				Lith.=Sand, silt, clay stone	Lith.=Sand, silt, clay stone	Lith.=Sand, silt, clay stone	Lith.=Sand, silt, clay stone	Lith.=Sand, silt, clay stone	Lith.=Sand, silt, clay stone
KISIKLI NORTH TUBE				E=0.7E9 (N/m^2)	E=0.63E9 (N/m^2)	E=0.35E9 (N/m^2)	E=0.7E9 (N/m^2)	E=0.63E9 (N/m^2)	E=0.35E9 (N/m^2)
WITH SHOTCRETE LINING				ν=0.27, γ=2200 (kg/m^3)	ν=0.27, γ=2200 (kg/m^3)	ν=0.27, γ=2200 (kg/m^3)	ν=0.32, γ=2200 (kg/m^3)	ν=0.32, γ=2200 (kg/m^3)	ν=0.32, γ=2200 (kg/m^3)
t = 200 mm									
HETEROGENEOUS MODEL		MEASURED		COMPUTED	COMPUTED	COMPUTED	COMPUTED	COMPUTED	COMPUTED
Km 1+400		TUNNEL		TUNNEL	TUNNEL	TUNNEL	TUNNEL	TUNNEL	TUNNEL
	MEASURMENTS	CONVERGENCE		CONVERGENCE	CONVERGENCE	CONVERGENCE	CONVERGENCE	CONVERGENCE	CONVERGENCE
ARRAY	ALONG	TOTAL (mm)	ARRAY	TOTAL (mm)	TOTAL (mm)	TOTAL (mm)	TOTAL (mm)	TOTAL (mm)	TOTAL (mm)
A1-B2	DIAGONAL	-0.36	69(Ud), 122(Ud)	-0.0173	-0.0203	-0.0291	-0.0276	-0.0300	-0.0465
A1-C3	DIAGONAL	-0.29	69(Ud), 84(Ud)	-0.0173	-0.0203	-0.0291	-0.0276	-0.0300	-0.0465
B2-C3	HORIZONTAL	-0.39	84(Ux), 122(Ux)	0.0276	0.0337	0.0769	0.0065	0.0086	0.0324
KISIKLI NORTH TUBE			ARRAY						
WITH SHOTCRETE LINING									
t = 100 mm			69(Ud), 122(Ud)	-0.0175	-0.0191	-0.0297	-0.0264	-0.0289	-0.0473
HETEROGENEOUS MODEL			69(Ud), 84(Ud)	-0.0175	-0.0191	-0.0297	-0.0264	-0.0289	-0.0473
Km 1+400			85(Ux), 122(Ux)	0.0239	0.0274	0.0600	-0.0002	0.0008	0.0124

Table 7.12 Comparison of measured and computed displacements along the free surface of the 100 and 200 mm thick shotcrete linings for Kisikli north tube (km 1+400)

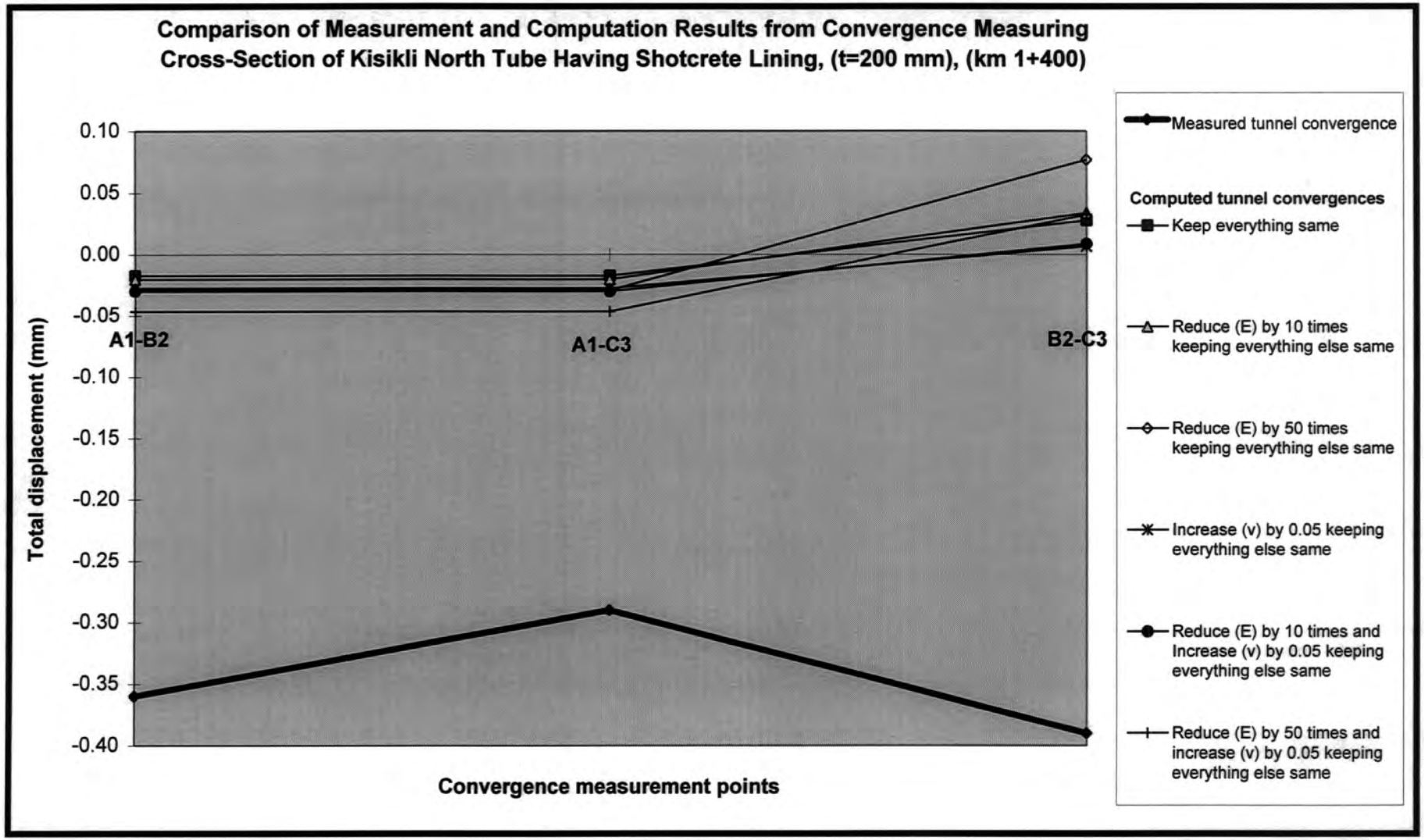

Fig. 7.37 Comparison of measured and computed displacements along the 200 mm thick free surface of the shotcrete lining for Kisikli north tube (km 1+400)

7.3.2 Kisikli North Tube (Km 1+536)

One type of analysis using the stress reversal technique was completed for the cross-section of Kisikli north tube at km 1+536 for the case of a 200 mm thick shotcrete lining only. The model dimensions, material properties and geological conditions are shown in Fig. 7.40. Fig. 7.41 shows the overall tunnel model mesh diagram produced by the pre-processing programs. There were 436 elements and 2015 nodes in the mesh diagram. The node and element numbers along the excavation surface are shown in Fig. 7.42. Fig. 7.43 shows the node numbers along the shotcrete lining. Figs. 7.41 to 7.43 were produced using PAFEC-PIGS for the reasons stated earlier. A detail of the mesh and geological conditions produced by the post-processing program using UNIRAS is also shown in Fig. 7.44.

Several analyses were performed using changes applied to the elastic parameters of the intact rock strata. This enabled the effects of discontinuities in the rock mass to be assessed and comparisons to be made between measured and computed values of the displacements for each set of factors. Reduction factors of 0.10 and 0.50 were applied to the values of the 'intact' Young's modulus and an increase of 0.05 was applied to the Poisson's ratio. The results of these analyses are presented in Figs. 7.45 to 7.49 and summarised in Tables 7.13 and 7.14.

Fig. 7.45 shows the deformed and undeformed mesh diagrams for this section. It can be seen that the roof, side walls and invert area of the tunnel have quite extensive convergence. Table 7.13 shows displacements along the free surface of the shotcrete lining and a summary of the ranges of elastic constants used in the analyses. The same results are presented in Fig. 7.46 for visual comparison. The changes in the values of Young's modulus again have similar influences on the deformation to the change in Poisson's ratio as shown in the table and the figure. The measured displacements are shown in Table 7.2 and Fig. 7.6.

A comparison of the measured and computed displacements of the Kisikli north tube at km 1+536 having a 200 mm thick shotcrete lining is presented in

Table 7.14. It should be again noted that the sign of the displacement (the sense of the movement) indicates the direction of movement relative to the axes on the centre of the tunnel. Fig. 7.47 shows the convergence results in graphical form for both measured and computed cases. The calculated tunnel convergences at all points agree more closely with the measured in situ values for the Kisikli north tube at km 1+536 than for km 1+400. Although the maximum difference between the measured and calculated displacement values is 1.20 mm, their order of magnitude are similar and in all instances the modelled displacements are in the same directions as those actually measured.

Finally, the Von Mises stress distribution in colour and slightly deformed shape of the unexcavated ground under the action gravity are shown in Fig. 7.48. Fig 7.49 shows a similar colour diagram, following excavation and the provision of the 200 mm thick shotcrete lining using the stress reversal technique. Again these shaded colour diagrams indicate areas of increased and decreased stress through changes in colour from red to blue.

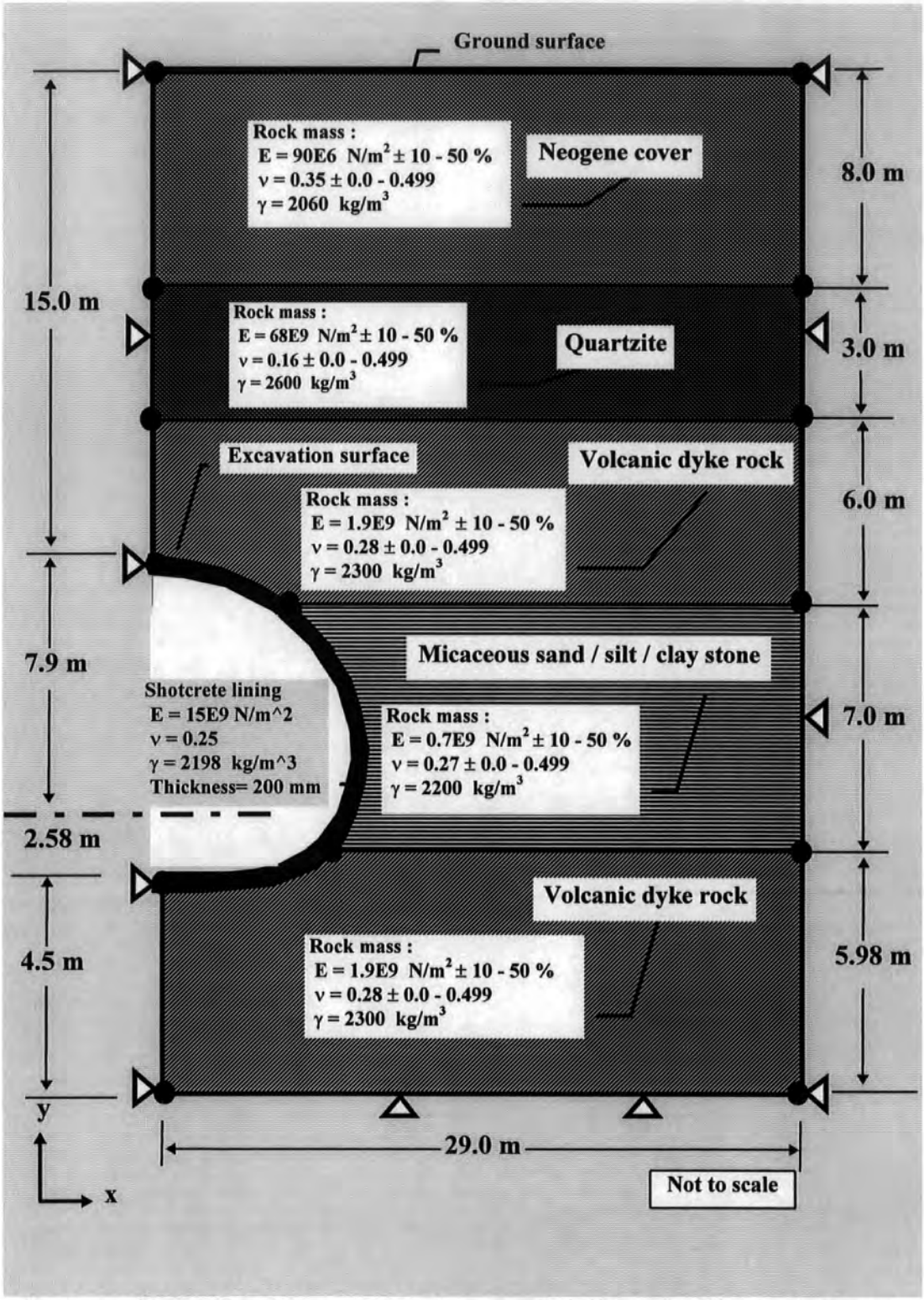

Fig. 7.40 Model dimensions, material properties and geological conditions of Kisikli north tube, (km 1+536), having shotcrete lining

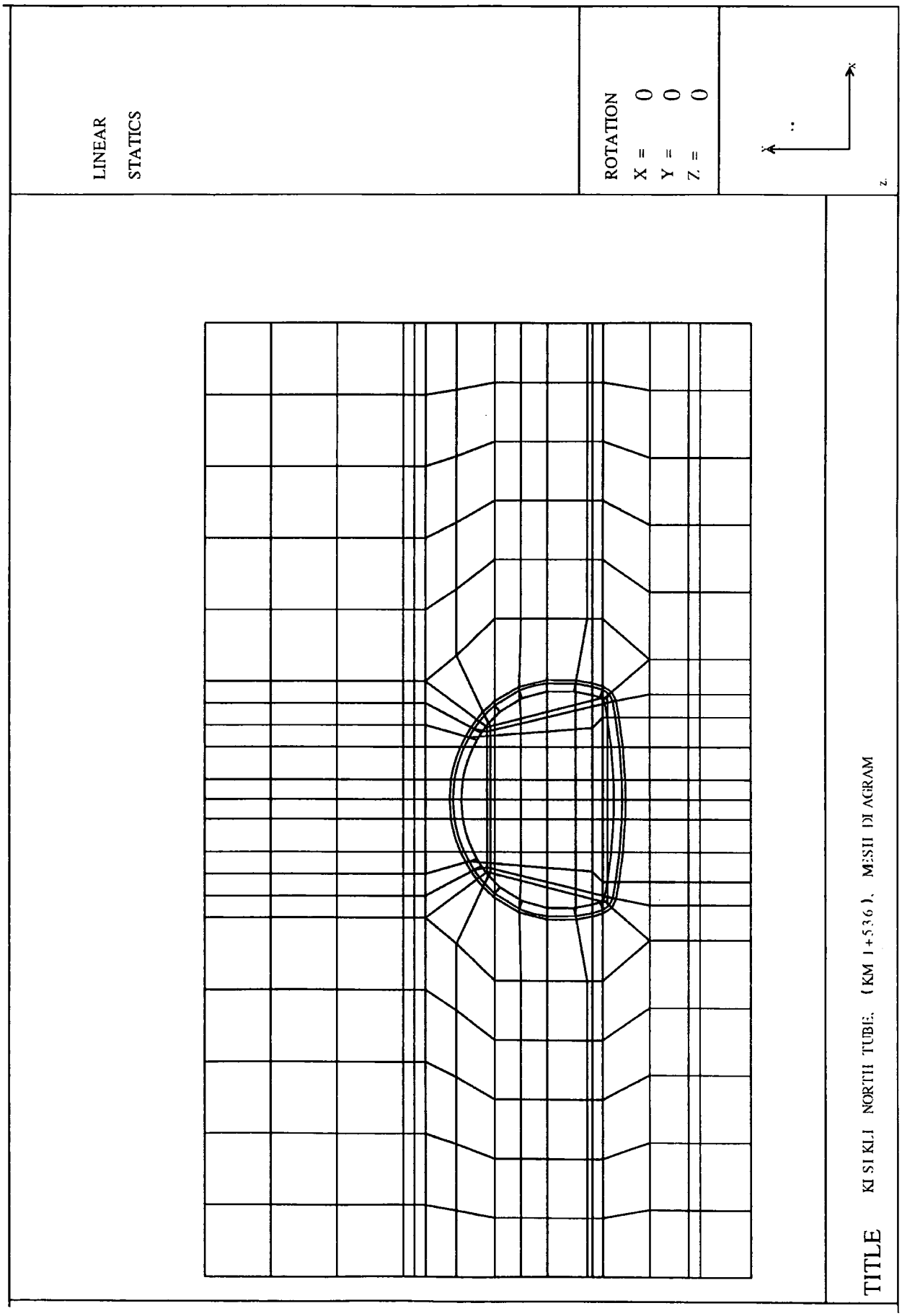

Fig. 7.41 Mesh diagram of Kisikli north tube (km 1+536)

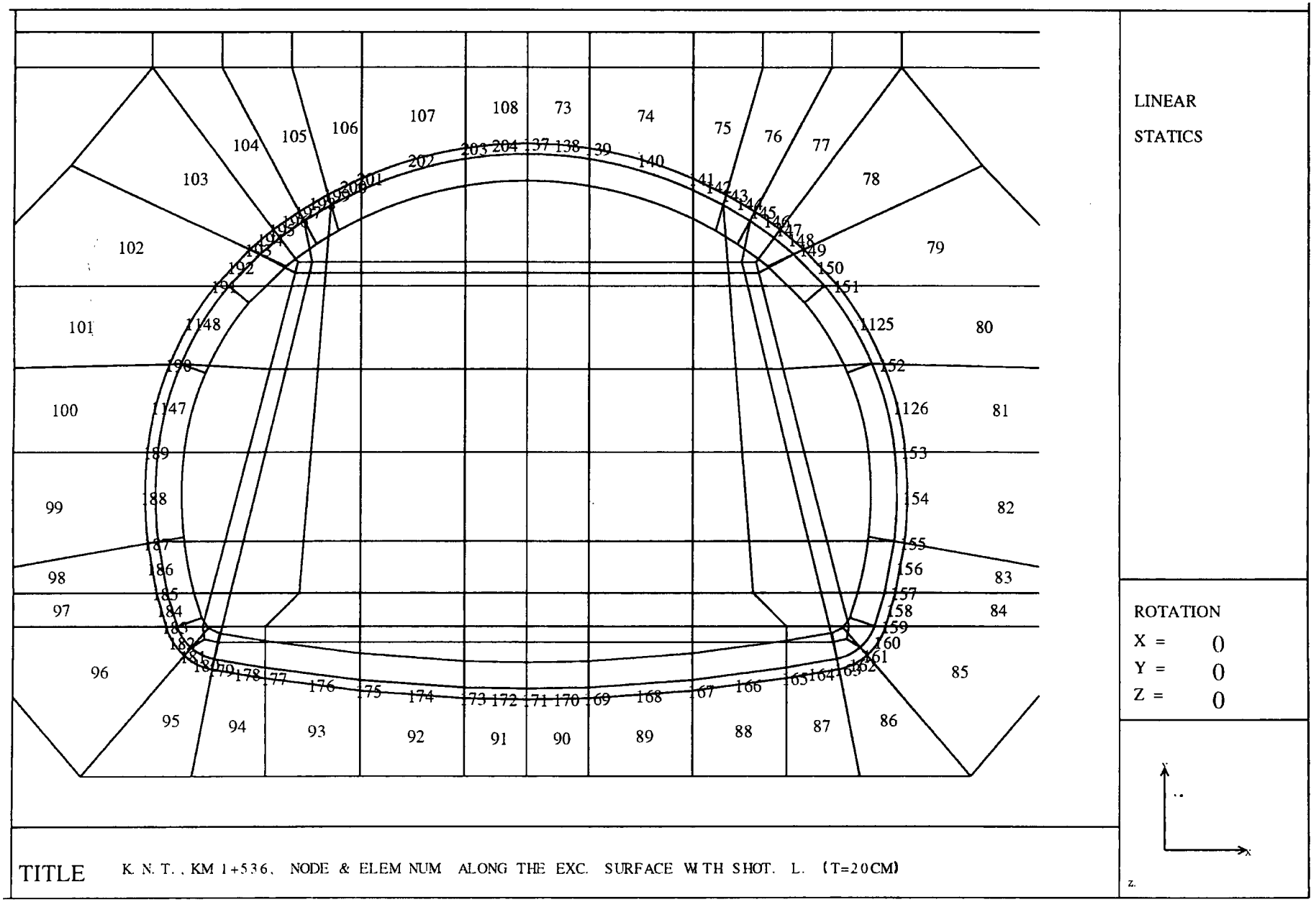

Fig. 7.42 Node and element numbers along the excavation surface of Kisikli north tube (km 1+536)

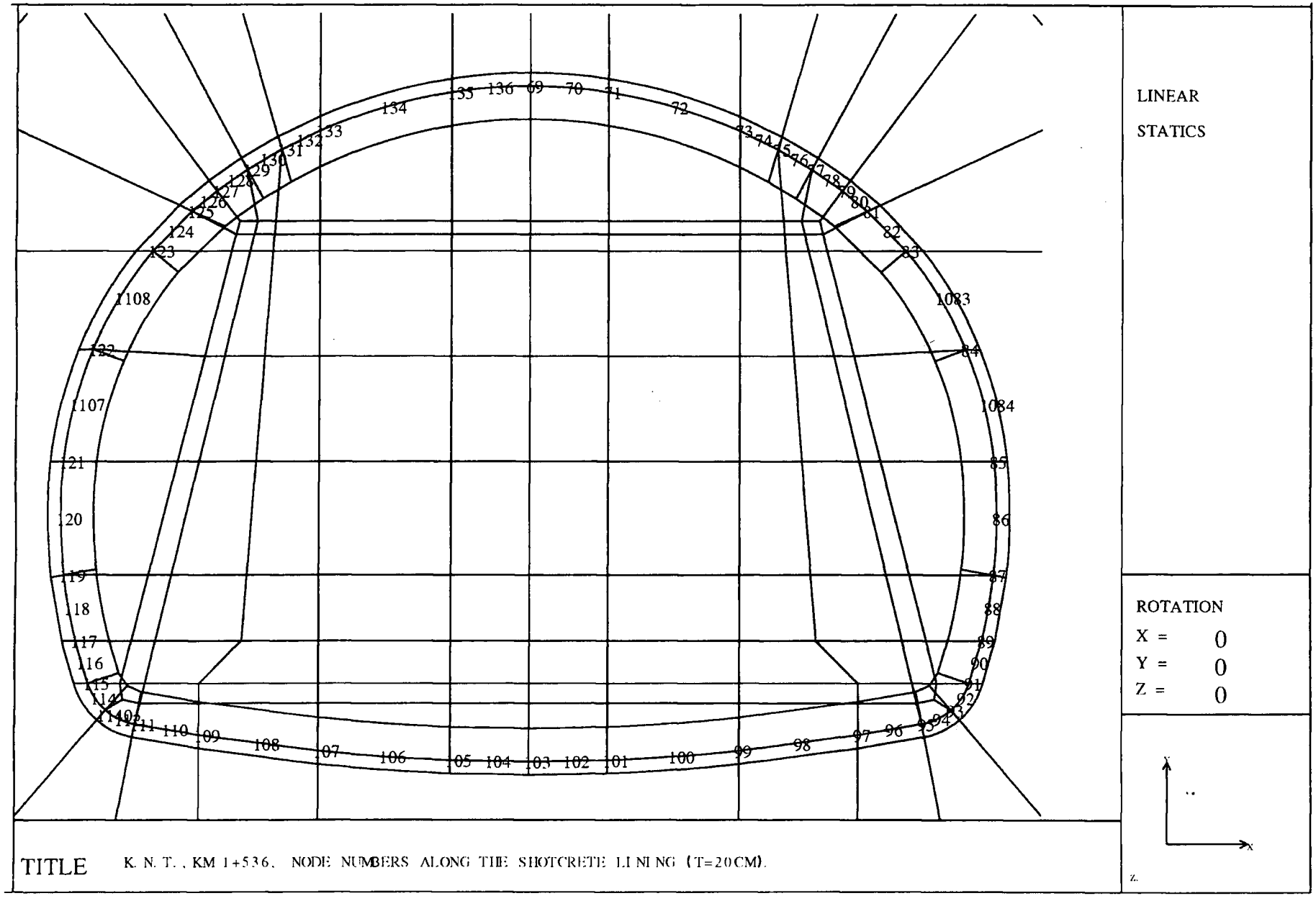

Fig. 7.43 Node numbers along the free surface of the shotcrete lining of Kisikli north tube (km 1+536)

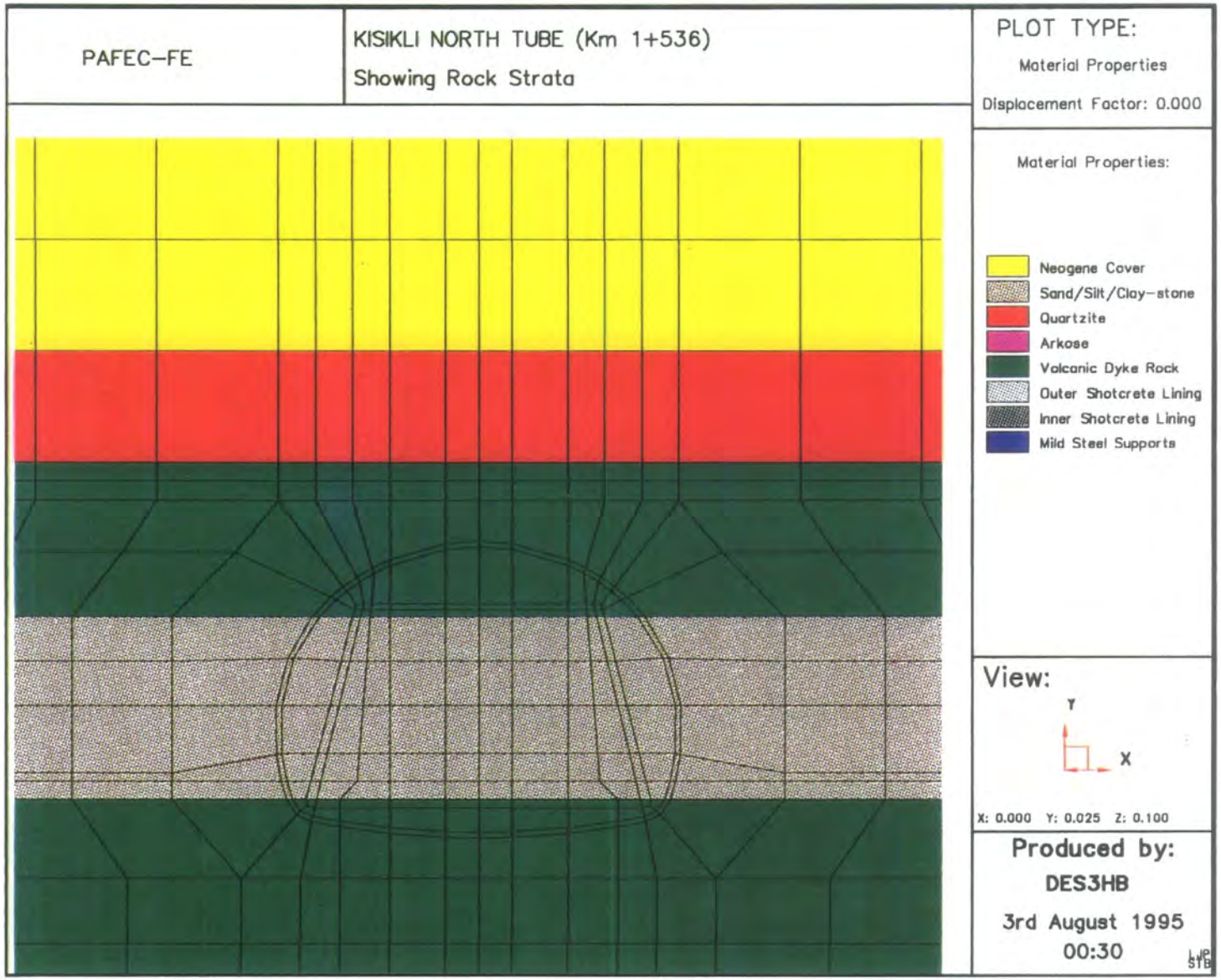

Fig. 7.44 Mesh diagram and colour output of geological conditions of Kisikli north tube (km 1+536)

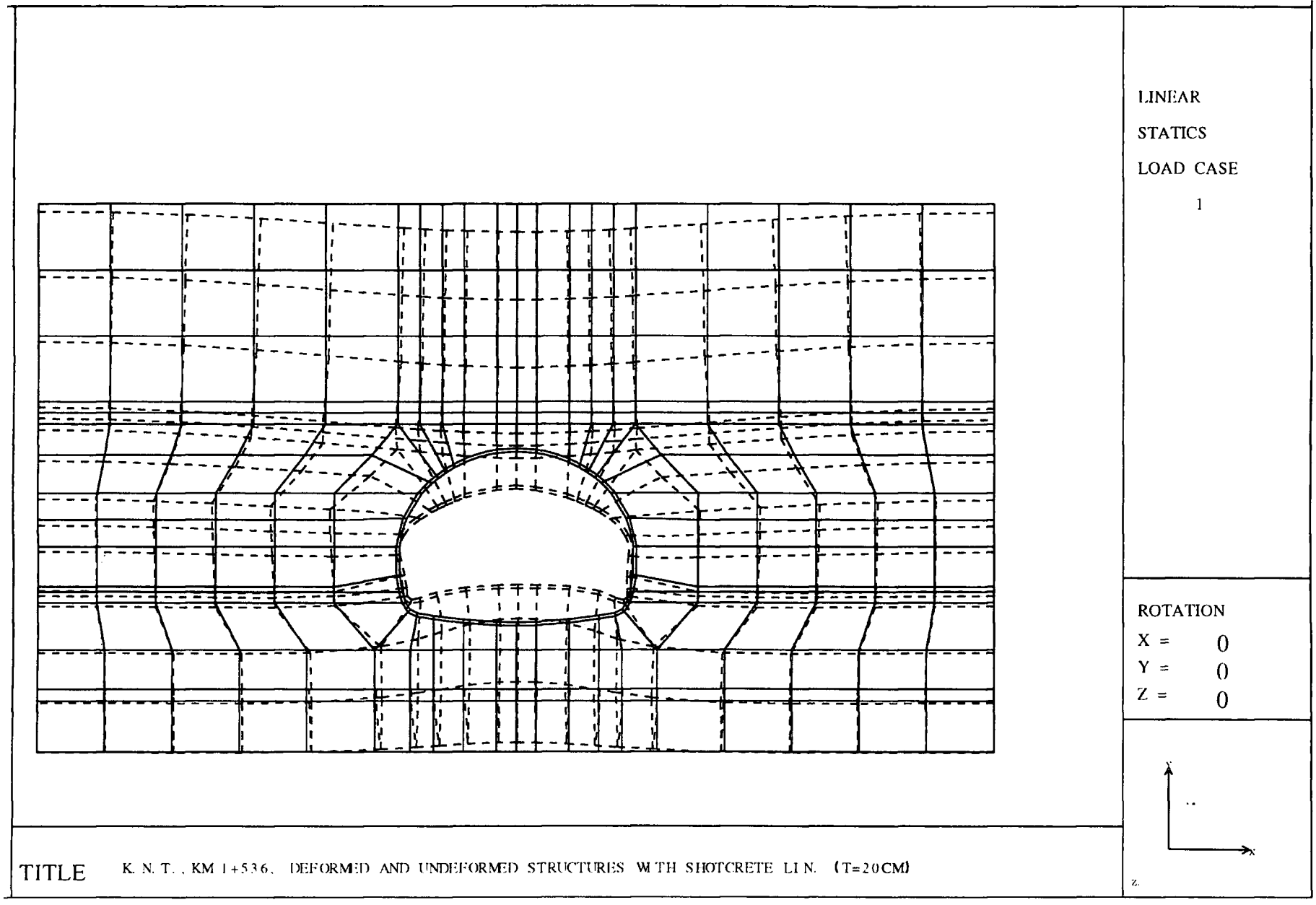

Fig. 7.45 Deformed and undeformed meshes of Kisikli north tube, (km 1+536), having shotcrete lining

KISIKLI NORTH TUBE		KEEP EVERYTHING SAME			REDUCE (E) BY 10 TIMES			REDUCE (E) BY 50 TIMES			INCREASED (ν) BY 0.05			REDUCE (E) BY 10 TIMES AND			REDUCE (E) BY 50 TIMES AND		
km 1+536					KEEPING EVERTHING ELSE			KEEPING EVERTHING ELSE			KEEPING EVERTHING ELSE			INCREASED (ν) BY 0.05			INCREASED (ν) BY 0.05		
WITH SHOTCRETE					SAME			SAME			SAME			KEEPING EVERTHING ELSE SAME			KEEPING EVERTHING ELSE SAME		
LINING, t = 200 mm																			
HETEROGENEOUS MODEL		STRESS REVERSAL			STRESS REVERSAL			STRESS REVERSAL			STRESS REVERSAL			STRESS REVERSAL			STRESS REVERSAL		
		TECHNIQUE			TECHNIQUE			TECHNIQUE			TECHNIQUE			TECHNIQUE			TECHNIQUE		
		Lithology=Neogene cover			Lithology=Neogene cover			Lithology=Neogene cover			Lithology=Neogene cover			Lithology=Neogene cover			Lithology=Neogene cover		
		E=90E9 (N/m^2)			E=81E8 (N/m^2)			E=45E6 (N/m^2)			E=90E9 (N/m^2)			E=81E6 (N/m^2)			E=45E6 (N/m^2)		
		ν=0.35, γ=2060 (kg/m^3)			ν=0.35, γ=2060 (kg/m^3)			ν=0.35, γ=2060 (kg/m^3)			ν=0.40, γ=2060 (kg/m^3)			ν=0.40, γ=2060 (kg/m^3)			ν=0.40, γ=2060 (kg/m^3)		
		Lithology=Quartzite			Lithology=Quartzite			Lithology=Quartzite			Lithology=Quartzite			Lithology=Quartzite			Lithology=Quartzite		
		E=68E9 (N/m^2)			E=61.2E9 (N/m^2)			E=34E9 (N/m^2)			E=68E9 (N/m^2)			E=61.2E9 (N/m^2)			E=34E9 (N/m^2)		
		ν=0.16, γ=2600 (kg/m^3)			ν=0.16, γ=2600 (kg/m^3)			ν=0.16, γ=2600 (kg/m^3)			ν=0.21, γ=2600 (kg/m^3)			ν=0.21, γ=2600 (kg/m^3)			ν=0.21, γ=2600 (kg/m^3)		
		Lithology=Volcanic Dyke			Lithology=Volcanic Dyke			Lithology=Volcanic Dyke			Lithology=Volcanic Dyke			Lithology=Volcanic Dyke			Lithology=Volcanic Dyke		
		E=1.9E9 (N/m^2)			E=1.71E8 (N/m^2)			E=0.95E9 (N/m^2)			E=1.9E9 (N/m^2)			E=1.71E9 (N/m^2)			E=0.95E9 (N/m^2)		
		ν=0.28, γ=2300 (kg/m^3)			ν=0.28, γ=2300 (kg/m^3)			ν=0.28, γ=2300 (kg/m^3)			ν=0.33, γ=2300 (kg/m^3)			ν=0.33, γ=2300 (kg/m^3)			ν=0.33, γ=2300 (kg/m^3)		
ELEMENT	NODE	Lith.=Sand, silt, clay stone			Lith.=Sand, silt, clay stone			Lith.=Sand, silt, clay stone			Lith.=Sand, silt, clay stone			Lith.=Sand, silt, clay stone			Lith.=Sand, silt, clay stone		
NUMBER	NUMBER	E=0.7E9 (N/m^2)			E=0.63E9 (N/m^2)			E=0.35E9 (N/m^2)			E=0.7E9 (N/m^2)			E=0.63E9 (N/m^2)			E=0.35E9 (N/m^2)		
ALONG THE	ALONG THE	ν=0.27, γ=2200 (kg/m^3)			ν=0.27, γ=2200 (kg/m^3)			ν=0.27, γ=2200 (kg/m^3)			ν=0.32, γ=2200 (kg/m^3)			ν=0.32, γ=2200 (kg/m^3)			ν=0.32, γ=2200 (kg/m^3)		
SHOTCRETE	SHOTCRETE	DISPLACEMENT (mm)			DISPLACEMENT (mm)			DISPLACEMENT (mm)			DISPLACEMENT (mm)			DISPLACEMENT (mm)			DISPLACEMENT (mm)		
LINING	LINING	Ux	Uy	U	Ux	Uy	U	Ux	Uy	U	Ux	Uy	U	Ux	Uy	U	Ux	Uy	U
57	69	0.0000	-2.2716	2.2716	0.0000	-2.4595	2.4595	0.0000	-3.7788	3.7788	-0.0001	-2.1396	2.1396	0.0001	-2.3140	2.3140	-0.0003	-3.5227	3.5227
57	70	-0.0171	-2.2677	2.2678	-0.0204	-2.4552	2.4553	-0.0459	-3.7708	3.7711	-0.0339	-2.1359	2.1362	-0.0363	-2.3100	2.3103	-0.0719	-3.5155	3.5162
58	71	-0.0338	-2.2586	2.2589	-0.0404	-2.4447	2.4450	-0.0904	-3.7490	3.7501	-0.0675	-2.1275	2.1288	-0.0764	-2.3003	2.3016	-0.1424	-3.4957	3.4988
58	72	-0.0502	-2.2155	2.2164	-0.0749	-2.3961	2.3973	-0.1627	-3.6576	3.6612	-0.1271	-2.0670	2.0909	-0.1434	-2.2548	2.2594	-0.2618	-3.4124	3.4224
59	73	-0.0829	-2.1468	2.1488	-0.1068	-2.3188	2.3212	-0.2248	-3.5106	3.5178	-0.1885	-2.0236	2.0329	-0.2115	-2.1837	2.1939	-0.3742	-3.2803	3.3016
59	74	-0.0993	-2.1151	2.1174	-0.1161	-2.2532	2.2581	-0.2383	-3.4497	3.4648	-0.2051	-1.9844	2.0049	-0.2298	-2.1509	2.1631	-0.4020	-3.2223	3.2473
60	75	-0.1052	-2.0784	2.0811	-0.1225	-2.2422	2.2456	-0.2440	-3.3723	3.3911	-0.2213	-1.9601	1.9729	-0.2473	-2.1127	2.1271	-0.4285	-3.1542	3.1829
60	76	-0.1092	-2.0384	2.0413	-0.1267	-2.1975	2.2011	-0.2485	-3.2920	3.3012	-0.2350	-1.9225	1.9368	-0.2618	-2.0709	2.0874	-0.4448	-3.0802	3.1122
61	77	-0.1124	-1.9943	1.9976	-0.1298	-2.1482	2.1521	-0.2451	-3.2034	3.2128	-0.2480	-1.8810	1.8973	-0.2756	-2.0246	2.0433	-0.4595	-2.9983	3.0333
61	78	-0.1132	-1.9472	1.9508	-0.1301	-2.0958	2.0993	-0.2380	-3.1099	3.1190	-0.2579	-1.8365	1.8548	-0.2857	-1.9751	1.9857	-0.4676	-2.9113	2.9488
62	79	-0.1132	-1.8956	1.8992	-0.1294	-2.0386	2.0427	-0.2279	-3.0092	3.0178	-0.2670	-1.7877	1.8075	-0.2949	-1.9210	1.9436	-0.4730	-2.8170	2.8584
62	80	-0.1134	-1.8474	1.8509	-0.1289	-1.9850	1.9892	-0.2163	-2.9166	2.9248	-0.2755	-1.7417	1.7634	-0.3034	-1.8701	1.8948	-0.4776	-2.7304	2.7719
63	81	-0.1171	-1.7988	1.8028	-0.1321	-1.9313	1.9358	-0.2128	-2.8248	2.8326	-0.2881	-1.6958	1.7201	-0.3163	-1.8195	1.8468	-0.4878	-2.6451	2.6897
63	82	-0.1257	-1.7152	1.7198	-0.1397	-1.8391	1.8444	-0.2029	-2.6883	2.6780	-0.3147	-1.6189	1.6492	-0.3435	-1.7349	1.7688	-0.5094	-2.5039	2.5562
64	83	-0.1401	-1.6281	1.6341	-0.1533	-1.7437	1.7504	-0.1971	-2.5109	2.5186	-0.3495	-1.5392	1.5784	-0.3794	-1.6480	1.6911	-0.5407	-2.3642	2.4252
65	84	-0.2252	-1.1974	1.2184	-0.2223	-1.2747	1.2939	-0.0801	-1.7668	1.7688	-0.5846	-1.1601	1.2902	-0.5899	-1.2362	1.3697	-0.6621	-1.7250	1.8477
46	85	-0.2467	-0.6475	0.6929	-0.2332	-0.6867	0.7271	0.0185	-0.9551	0.9553	-0.6921	-0.6536	0.9518	-0.7182	-0.6969	1.0007	-0.7714	-0.9875	1.2531
46	86	-0.2784	-0.3781	0.4679	-0.2685	-0.4025	0.4838	-0.0494	-0.5865	0.5886	-0.7325	-0.3959	0.8326	-0.7639	-0.4251	0.8742	-0.8573	-0.6370	1.0681
47	87	-0.2716	-0.1111	0.2934	-0.2648	-0.1226	0.2919	-0.0815	-0.2240	0.2384	-0.6974	-0.1451	0.7123	-0.7290	-0.1804	0.7484	-0.8325	-0.2947	0.8831
47	88	-0.2348	0.0341	0.2371	-0.2272	0.0301	0.2292	-0.0498	-0.0286	0.0574	-0.6240	-0.0120	0.6241	-0.6512	-0.0204	0.6516	-0.7280	-0.1194	0.7377
48	89	-0.1570	0.1639	0.2270	-0.1452	0.1667	0.2211	0.0541	0.1444	0.1642	-0.4957	0.1020	0.5061	-0.5129	0.0968	0.5223	-0.5228	0.0246	0.5234
48	90	-0.0748	0.2412	0.2528	-0.0596	0.2483	0.2561	0.1842	0.2509	0.3099	-0.3723	0.1875	0.4092	-0.3807	0.1674	0.4159	-0.3330	0.1092	0.3504
49	91	0.0112	0.3287	0.3289	0.0316	0.3406	0.3421	0.2730	0.3736	0.4627	-0.2449	0.2456	0.3468	-0.2449	0.2482	0.3494	-0.1448	0.2117	0.2565
49	92	0.0400	0.4270	0.4289	0.0607	0.4463	0.4504	0.2923	0.5311	0.6062	-0.1920	0.3368	0.3876	-0.1892	0.3485	0.3948	-0.0773	0.3024	0.3656
50	93	0.0438	0.5628	0.5645	0.0614	0.5841	0.5873	0.2582	0.7585	0.8025	-0.1683	0.4523	0.4826	-0.1664	0.4725	0.5012	-0.0716	0.5568	0.5934
50	94	0.0279	0.7188	0.7191	0.0401	0.7681	0.7691	0.1887	1.0871	1.1030	-0.1707	0.6109	0.6343	-0.1729	0.6488	0.6714	-0.1188	0.8704	0.8785
51	95	0.0217	0.9058	0.9061	0.0305	0.9779	0.9784	0.1438	1.4795	1.4885	-0.1676	0.7933	0.8108	-0.1723	0.8332	0.8704	-0.1456	1.2528	1.2612
51	96	0.0060	1.2332	1.2332	0.0115	1.3477	1.3477	0.0734	2.1991	2.2063	-0.1690	1.1145	1.1272	-0.1762	1.2162	1.2292	-0.1976	1.9629	1.9728
52	97	-0.0078	1.4725	1.4725	-0.0087	1.6180	1.6180	0.0093	2.7299	2.7299	-0.1715	1.3468	1.3577	-0.1844	1.4790	1.4905	-0.2428	2.4631	2.4849
52	98	-0.0112	1.7772	1.7772	-0.0145	1.9804	1.9805	-0.0282	3.3899	3.3900	-0.1468	1.6362	1.6428	-0.1601	1.8047	1.8118	-0.2378	3.1164	3.1256
53	99	-0.0131	1.9780	1.9780	-0.0170	2.1859	2.1860	-0.0426	3.8192	3.8194	-0.1185	1.8244	1.8283	-0.1313	2.0163	2.0206	-0.2077	3.5222	3.5283
53	100	-0.0095	2.1340	2.1340	-0.0125	2.3602	2.3602	-0.0344	4.1417	4.1418	-0.0832	1.9704	1.9722	-0.0916	2.1795	2.1814	-0.1467	3.8249	3.8278
54	101	-0.0069	2.2206	2.2206	-0.0088	2.4575	2.4576	-0.0228	4.3273	4.3274	-0.0472	2.0503	2.0508	-0.0518	2.2694	2.2700	-0.0854	3.9975	3.9994
54	102	-0.0033	2.2482	2.2482	-0.0042	2.4884	2.4884	-0.0115	4.3844	4.3844	-0.0234	2.0758	2.0767	-0.0256	2.2976	2.2977	-0.0426	4.0500	4.0502
55	103	-0.0002	2.2565	2.2565	-0.0002	2.4977	2.4977	-0.0004	4.4024	4.4024	0.0000	2.0831	2.0831	0.0002	2.3061	2.3061	0.0000	4.0665	4.0665
55	104	0.0029	2.2462	2.2462	0.0035	2.4864	2.4864	0.0107	4.3843	4.3843	0.0233	2.0756	2.0767	0.0261	2.2976	2.2977	0.0426	4.0500	4.0502
56	105	0.0065	2.2206	2.2206	0.0084	2.4575	2.4576	0.0220	4.3273	4.3274	0.0472	2.0503	2.0508	0.0524	2.2694	2.2700	0.0853	3.9975	3.9994
56	106	0.0091	2.1340	2.1340	0.0121	2.3602	2.3602	0.0338	4.1416	4.1417	0.0831	1.9705	1.9723	0.0921	2.1795	2.1814	0.1466	3.8250	3.8279
57	107	0.0127	1.9779	1.9779	0.0166	2.1858	2.1859	0.0418	3.8191	3.8193	0.1165	1.8245	1.8284	0.1318	2.0162	2.0206	0.2076	3.5223	3.5284
57	108	0.0108	1.7772	1.7772	0.0140	1.9803	1.9803	0.0274	3.3897	3.3898	0.1468	1.6362	1.6428	0.1606	1.8046	1.8117	0.2378	3.1168	3.1257
58	109	0.0074	1.4724	1.4724	0.0082	1.6178	1.6178	-0.0101	2.7297	2.7297	0.1715	1.3469	1.3578	0.1849	1.4789	1.4904	0.2428	2.4633	2.4951
58	110	-0.0084	1.2331	1.2331	-0.0120	1.3475	1.3476	-0.0743	2.1889	2.2062	0.1690	1.1147	1.1274	0.1788	1.2161	1.2292	0.1976	1.9633	1.9732
59	111	-0.0222	0.9058	0.9059	-0.0310	0.9777	0.9782	-0.1447	1.4791	1.4882	0.1678	0.7935	0.8110	0.1729	0.8530	0.8703	0.1456	1.2533	1.2617
59	112	-0.0284	0.7183	0.7189	-0.0408	0.7676	0.7688	-0.1877	1.0868	1.1027	0.1707	0.6112	0.6346	0.1734	0.6486	0.6714	0.1189	0.8709	0.8790
60	113	-0.0444	0.5525	0.5543	-0.0621	0.5838	0.5871	-0.2603	0.7590	0.8024	0.1683	0.4525	0.4828	0.1670	0.4726	0.5012	0.0717	0.5594	0.5840
60	114	-0.0407	0.4266	0.4285	-0.0614	0.4459	0.4501	-0.2936	0.5304	0.6062	0.1920	0.3368	0.3878	0.1898	0.3483	0.3948	0.0774	0.3531	0.3816
61	115	-0.0120	0.3282	0.3284	-0.0325	0.3402	0.3417	-0.2744	0.3726	0.4629	0.2450	0.2460	0.3472	0.2457	0.2481	0.3489	0.1450	0.2125	0.2873
61	116	0.0741	0.2407	0.2518	0.0576	0.2478	0.2545	-0.1855	0.2501	0.2899	0.3723	0.1679	0.4084	0.3815	0.1673	0.4168	0.3331	0.1099	0.3508
62	117	0.1584	0.1635	0.2283	0.1446	0.1682	0.2203	-0.0552	0.1438	0.1538	0.4956	0.1024	0.5061	0.5136	0.0988	0.5230	0.5227	0.0254	0.5233
62	118	0.2342	0.0337	0.2368	0.2268	0.0297	0.2287	0.0490	-0.0294	0.0571	0.6238	-0.0116	0.6239	0.6519	-0.0207	0.6522	0.7277	-0.1188	0.7373
63	119	0.2713	-0.1114	0.2833	0.2645	-0.1232	0.2918	0.0810	-0.2247	0.2389	0.6970	-0.1446	0.7119	0.7298	-0.1607	0.7473	0.8319	-0.2940	0.8823
63	120	0.2782	-0.3764	0.4681	0.2683	-0.4029	0.4841	0.0492	-0.5870	0.5891	0.7317	-0.3955	0.8317	0.7649	-0.4255	0.8763	0.8558	-0.6362	1.0684
64	121	0.2498	-0.6477	0.6931	0.2351	-0.6930	0.7274	-0.0188	-0.9557	0.9559	0.6907	-0.6531	0.9506	0.7199	-0.6875	1.0024	0.7687	-0.9868	1.2507
65	122	0.2252	-1.1976	1.2186	0.2223	-1.2749	1.2941	0.0801	-1.7672	1.7690	0.5833	-1.1599	1.2994	0.5914	-1.2365	1.3707	0.6597	-1.7245	1.8464
66	123	0.1401	-1.6282	1.6342	0.1533	-1.7435	1.7505	0.1971	-2.5112	2.5189	0.3490	-1.5392	1.5783	0.3799	-1.6480	1.6912	0.5396	-2.3642	2.4250
66	124	0.1257	-1.7154	1.7209	0.1397	-1.8392	1.8446	0.2029	-2.6686	2.6763	0.3143	-1.6189	1.6491	0.3440	-1.7349	1.7687	0.5087	-2.5039	2.5551
67	125	0.1171	-1.7989	1.8027	0.1321	-1.9314	1.9359	0.2128	-2.8248	2.8328	0.2878	-1.6958	1.7200	0.3166	-1.8195	1.8469	0.4868	-2.6451	2.6896
67	126	0.1134	-1.8475	1.8510	0.1289	-1.9851	1.9893	0.2183	-2.9169	2.9251	0.2751	-1.7417	1.7833	0.3038	-1.8701	1.8948	0.4789	-2.7305	2.7718
68	127	0.1132	-1.8958	1.8993	0.1294	-2.0387	2.0428	0.2278	-3.0094	3.0180	0.2687	-1.7877	1.8078	0.2953	-1.9210	1.9436	0.4725	-2.8171	2.8564
68	128	0.1132	-1.9473	1.9508	0.1301	-2.0959	2.0999	0.2380	-3.1101	3.1192	0.2575	-1.8365	1.8545	0.2861	-1.9751	1.9957	0.4670	-2.9113	2.9486
69	129	0.1125	-1.9944	1.9976	0.1296	-2.1483	2.1522	0.2451	-3.2036	3.2130	0.2477	-1.8810	1.8972	0.2760	-2.0248	2.0433	0.4589	-2.9983	3.0332
69	130	0.1092	-2.0385	2.0414	0.1267	-2.1976	2.2012	0.2485	-3.2922	3.3014	0.2347	-1.9225	1.9368	0.2623	-2.0709	2.0874	0.4442	-3.0803	3.1122
70	131	0.1052	-2.0785	2.0812	0.1225	-2.2422	2.2456	0.2440	-3.3724	3.3812	0.2210	-1.9601	1.9725	0.2476	-2.1127	2.1272	0.4259	-3.1542	3.1828
70	132	0.0993	-2.1152	2.1175	0.1161	-2.2833	2.2882	0.2363	-3.4469	3.4550	0.2049	-1.9944	2.0049	0.2301	-2.1509	2.1632	0.4015	-3.2223	3.2472
71	133	0.0929	-2.1468	2.1488	0.1085	-2.3186	2.3212	0.2248	-3.5107	3.5178	0.1883	-2.0236	2.0328	0.2119	-2.1837	2.1940	0.3737	-3.2803	3.3016
71	134	0.0832	-2.2155	2.2164	0.0749	-2.3962	2.3974	0.1827	-3.6577	3.6813	0.1269	-2.0870	2.0909	0.1437	-2.2549	2.2595	0.2613	-3.4124	3.4224
72	135	0.0338	-2.2586	2.2589	0.0404	-2.4447	2.4450	0.0904	-3.7490	3.7501	0.0673	-2.1275	2.1288	0.0767	-2.3003	2.3018	0.1419	-3.4957	3.4988
72	136	0.0171	-2.2677	2.2678	0.0204	-2.4552	2.4553	0.0456	-3.7708	3.7711	0.0337	-2.1359	2.1362	0.0388	-2.3100	2.3103	0.0714	-3.5155	3.5162

Table 7.13 Comparison of displacements as a function of elasticity modulus and Poisson's ratio along the free surface of the shotcrete lining for Kisikli north tube (km 1+536)

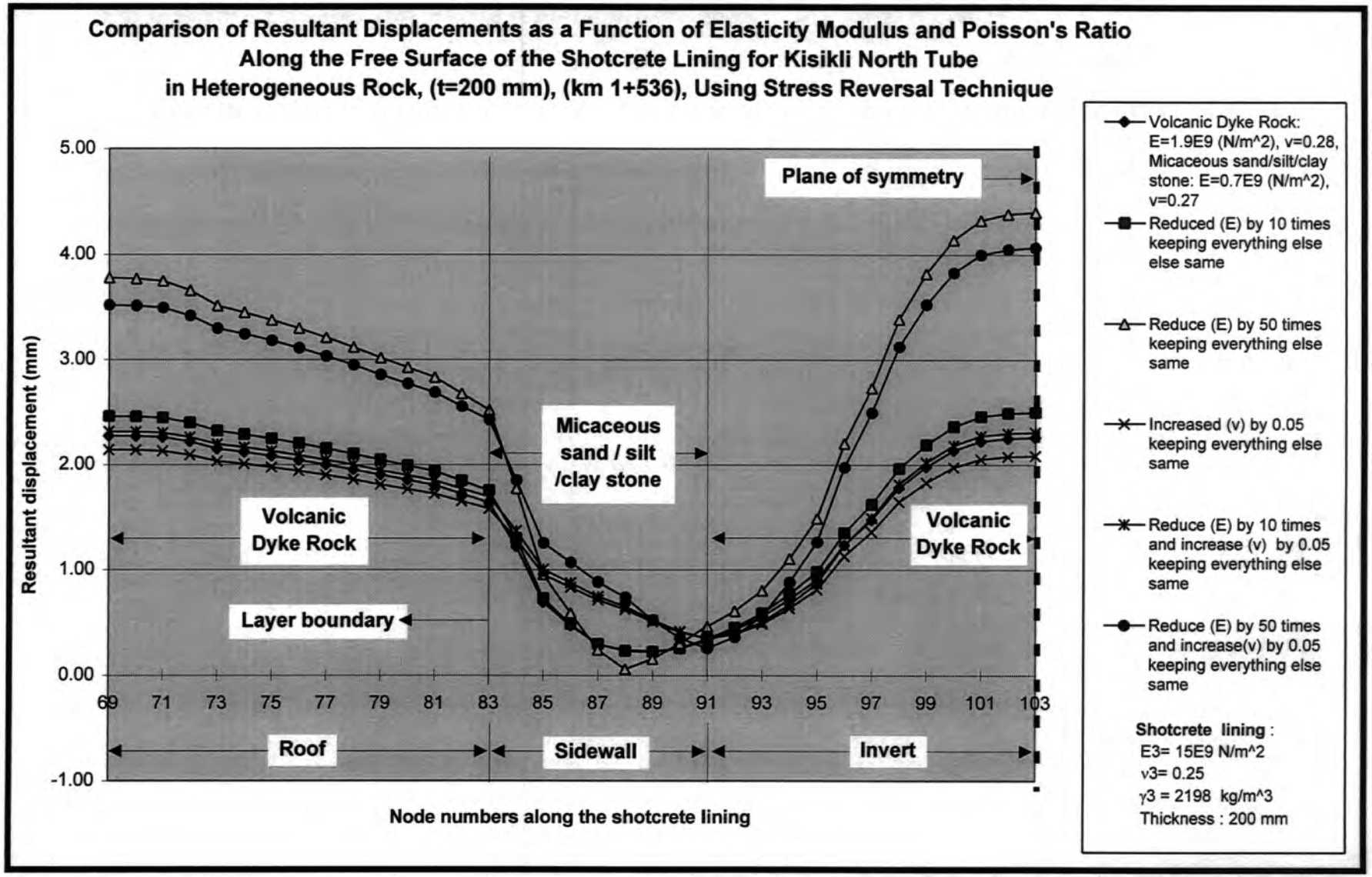

Fig. 7.46 Comparison of displacements as a function of elasticity modulus and Poisson's ratio along the free surface of the shotcrete lining for Kisikli north tube (km 1+536)

				KEEP EVERYTHING SAME	REDUCE (E) BY 10 TIMES KEEPING EVERYTHING ELSE SAME	REDUCE (E) BY 50 TIMES KEEPING EVERYTHING ELSE SAME	INCREASE (v) BY 0.05 KEEPING EVERYTHING ELSE SAME	REDUCE (E) BY 10 TIMES AND INCREASE (v) BY 0.05 KEEPING EVERYTHING ELSE SAME	REDUCE (E) BY 50 TIMES AND INCREASE (v) BY 0.05 KEEPING EVERYTHING ELSE SAME
				STRESS REVERSAL TECHNIQUE	STRESS REVERSAL TECHNIQUE	STRESS REVERSAL TECHNIQUE	STRESS REVERSAL TECHNIQUE	STRESS REVERSAL TECHNIQUE	STRESS REVERSAL TECHNIQUE
				Lithology=Neogene cover	Lithology=Neogene cover	Lithology=Neogene cover	Lithology=Neogene cover	Lithology=Neogene cover	Lithology=Neogene cover
				E=90E6 (N/m^2)	E=81E6 (N/m^2)	E=45E6 (N/m^2)	E=90E6 (N/m^2)	E=81E6 (N/m^2)	E=45E6 (N/m^2)
				v=0.35, γ=2060 (kg/m^3)	v=0.35, γ=2060 (kg/m^3)	v=0.35, γ=2060 (kg/m^3)	v=0.40, γ=2060 (kg/m^3)	v=0.40, γ=2060 (kg/m^3)	v=0.40, γ=2060 (kg/m^3)
				Lithology=Quartzite	Lithology=Quartzite	Lithology=Quartzite	Lithology=Quartzite	Lithology=Quartzite	Lithology=Quartzite
				E=68E9 (N/m^2)	E=61.2E9 (N/m^2)	E=34E9 (N/m^2)	E=68E9 (N/m^2)	E=61.2E9 (N/m^2)	E=34E9 (N/m^2)
				v=0.16, γ=2600 (kg/m^3)	v=0.16, γ=2600 (kg/m^3)	v=0.16, γ=2600 (kg/m^3)	v=0.21, γ=2600 (kg/m^3)	v=0.21, γ=2600 (kg/m^3)	v=0.21, γ=2600 (kg/m^3)
		(TUNNEL EXCAVATION) →		Lithology=Volcanic Dyke	Lithology=Volcanic Dyke	Lithology=Volcanic Dyke	Lithology=Volcanic Dyke	Lithology=Volcanic Dyke	Lithology=Volcanic Dyke
				E=1.9E9 (N/m^2)	E=1.71E9 (N/m^2)	E=0.95E9 (N/m^2)	E=1.9E9 (N/m^2)	E=1.71E9 (N/m^2)	E=0.95E9 (N/m^2)
				v=0.28, γ=2300 (kg/m^3)	v=0.28, γ=2300 (kg/m^3)	v=0.28, γ=2300 (kg/m^3)	v=0.33, γ=2300 (kg/m^3)	v=0.33, γ=2300 (kg/m^3)	v=0.33, γ=2300 (kg/m^3)
		(TUNNEL EXCAVATION) →		Lith.=Sand, silt, clay stone	Lith.=Sand, silt, clay stone	Lith.=Sand, silt, clay stone	Lith.=Sand, silt, clay stone	Lith.=Sand, silt, clay stone	Lith.=Sand, silt, clay stone
KISIKLI NORTH TUBE				E=0.7E9 (N/m^2)	E=0.63E9 (N/m^2)	E=0.35E9 (N/m^2)	E=0.7E9 (N/m^2)	E=0.63E9 (N/m^2)	E=0.35E9 (N/m^2)
WITH SHOTCRETE LINING				v=0.27, γ=2200 (kg/m^3)	v=0.27, γ=2200 (kg/m^3)	v=0.27, γ=2200 (kg/m^3)	v=0.32, γ=2200 (kg/m^3)	v=0.32, γ=2200 (kg/m^3)	v=0.32, γ=2200 (kg/m^3)
t = 200 mm									
HETEROGENEOUS MODEL		MEASURED		COMPUTED	COMPUTED	COMPUTED	COMPUTED	COMPUTED	COMPUTED
km 1+536		TUNNEL		TUNNEL	TUNNEL	TUNNEL	TUNNEL	TUNNEL	TUNNEL
	MEASURMENTS	CONVERGENCE		CONVERGENCE	CONVERGENCE	CONVERGENCE	CONVERGENCE	CONVERGENCE	CONVERGENCE
ARRAY	ALONG	TOTAL (mm)	ARRAY	TOTAL (mm)	TOTAL (mm)	TOTAL (mm)	TOTAL (mm)	TOTAL (mm)	TOTAL (mm)
A1-B2	DIAGONAL	-1.13	69(Ud), 122(Ud)	-0.7321	-0.7849	-1.0754	-0.9788	-1.0497	-1.4725
A1-C3	DIAGONAL	-0.71	69(Ud), 84(Ud)	-0.7321	-0.7849	-1.0754	-0.9788	-1.0497	-1.4725
B2-C3	HORIZONTAL	-1.36	84(Ux), 122(Ux)	-0.4504	-0.4446	-0.1602	-1.1279	-1.1813	-1.3218

Table 7.14 Comparison of measured and computed displacements along the free surface of the shotcrete lining for Kisikli North Tube (km 1+536)

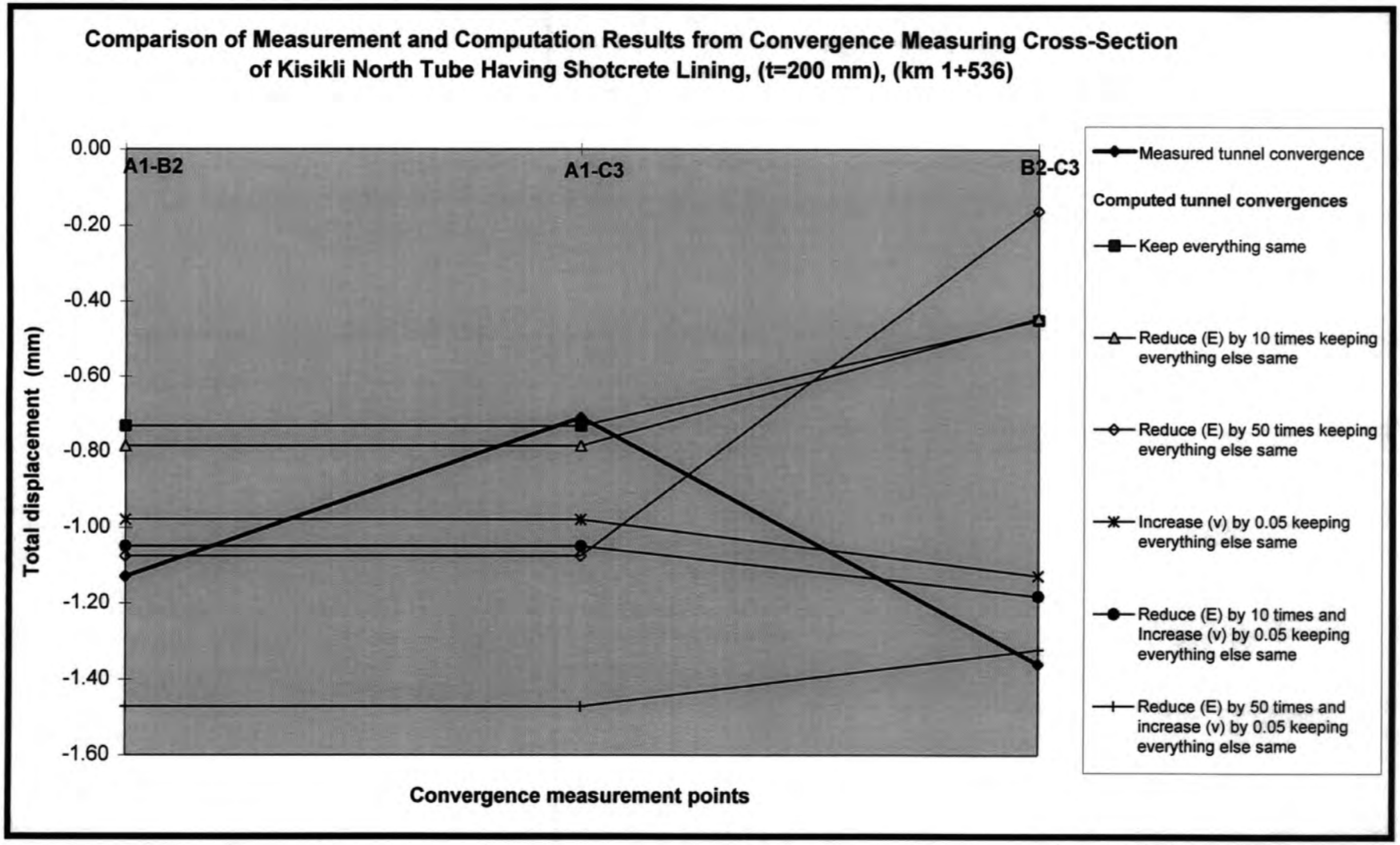

Fig. 7.47 Comparison of measured and computed displacements along the free surface of the shotcrete lining for Kisikli north tube (km 1+536)

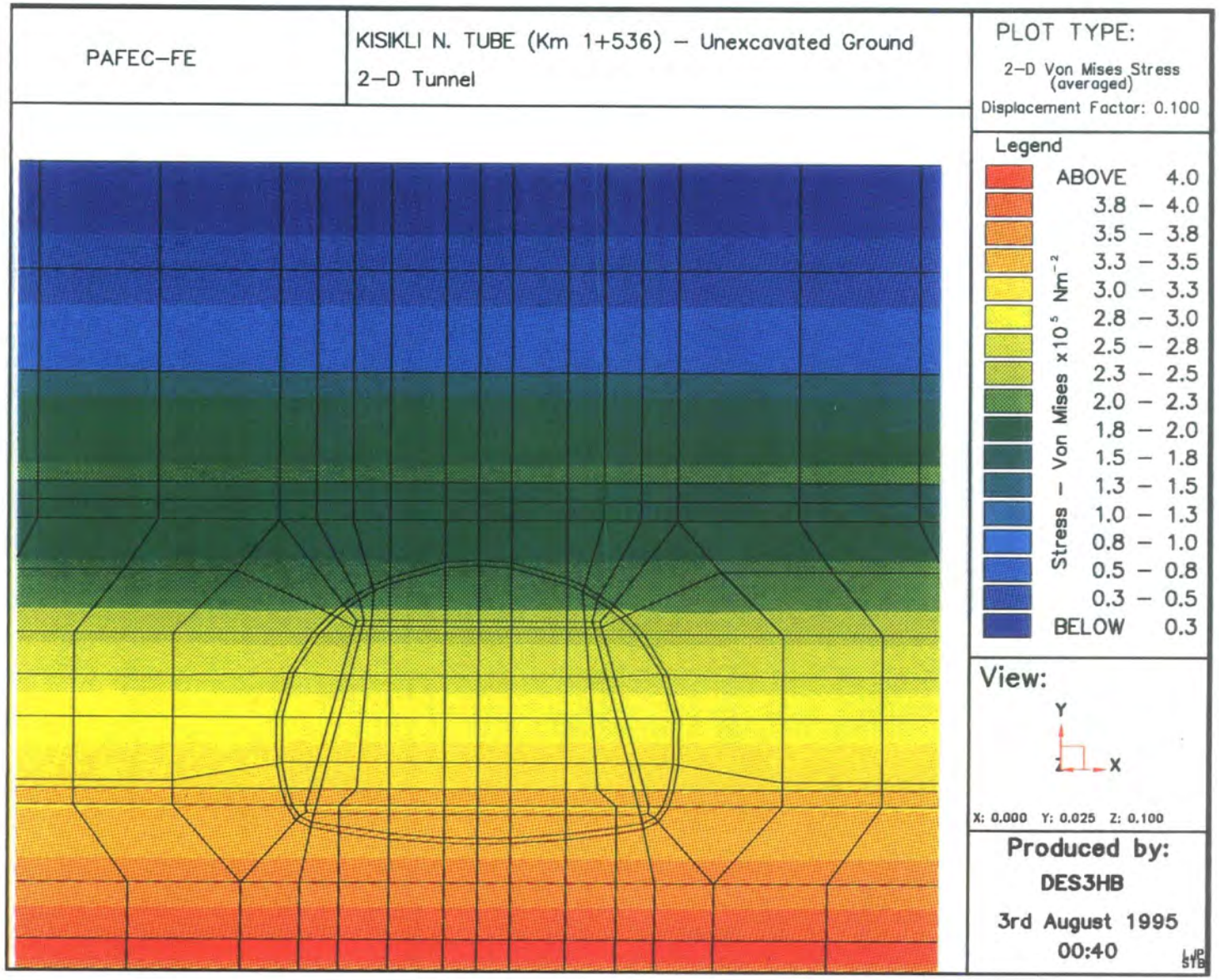

Fig. 7.48 Unexcavated ground colour stress and displaced shape diagrams of Kisikli north tube (km 1+536)

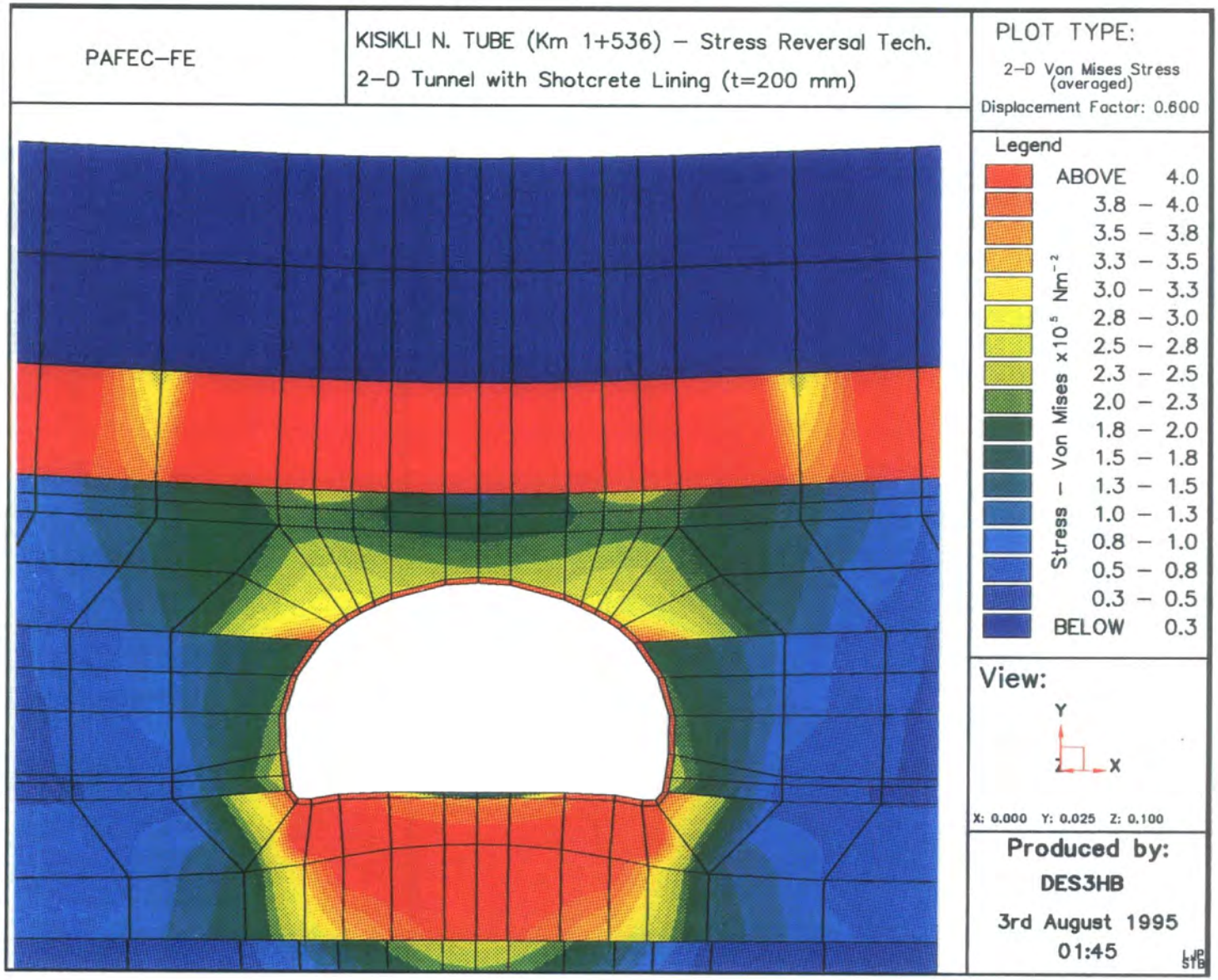

Fig. 7.49 Colour stress and displaced shape diagrams of Kisikli north tube, (km 1+536), having shotcrete lining (t=200 mm)

7.3.3 Kisikli South Tube (Km 1+544)

Several analyses, following the construction sequence through various excavation stages and to the provision of the shotcrete lining, anchorages, steel arch and inner lining, were completed for the section of the Kisikli south tube at km 1+544 with the general aim of demonstrating the versatility of the program using the three-dimensional model. Attention was again directed towards examining the magnitudes of stresses and displacements at particular points on the shotcrete and inner linings.

The model dimensions, material properties and geological conditions of the cross-section of the Kisikli south tube at km 1+544 are shown in Fig. 7.50. Fig. 7.51 shows the overall three-dimensional tunnel model mesh diagram produced by the pre-processing programs. The node and element numbers along the excavation surface for front plane of the three-dimensional model are shown in Fig. 7.52. Fig 7.53 shows the node numbers along the shotcrete lining for the same front plane. These three figures were produced using PAFEC-PIGS. A detail of the mesh and geological conditions produced by the post-processing program using UNIRAS is also shown in Fig. 7.54. The three-dimensional mesh diagram contains 444 elements and 3498 nodes.

All aspects in the modelling have been formulated to ensure that the results are as accurate as possible, consistent with the standard of information requested from prior investigation and the time available. The comparative testing and the analysis conditions themselves were all selected with this aim in mind.

The magnitude of displacements and stresses indicate whether a 'rigid' type of support system can be used, typically steel arches or concrete lining, or whether a system designed to allow some yield may be required, typically in the form of rock bolts. Time dependent effects on the stability of the support systems should not be ignored and the design should be such that the support has to be loaded to less than 60% of its yield strength in order that any significant creep deformation is eliminated.

The results of these analyses using the gravity difference method for the partial excavation and the stress reversal technique for the support systems are presented in Figs. 7.55 to 7.77 and summarised in Tables 7.15 to 7.24.

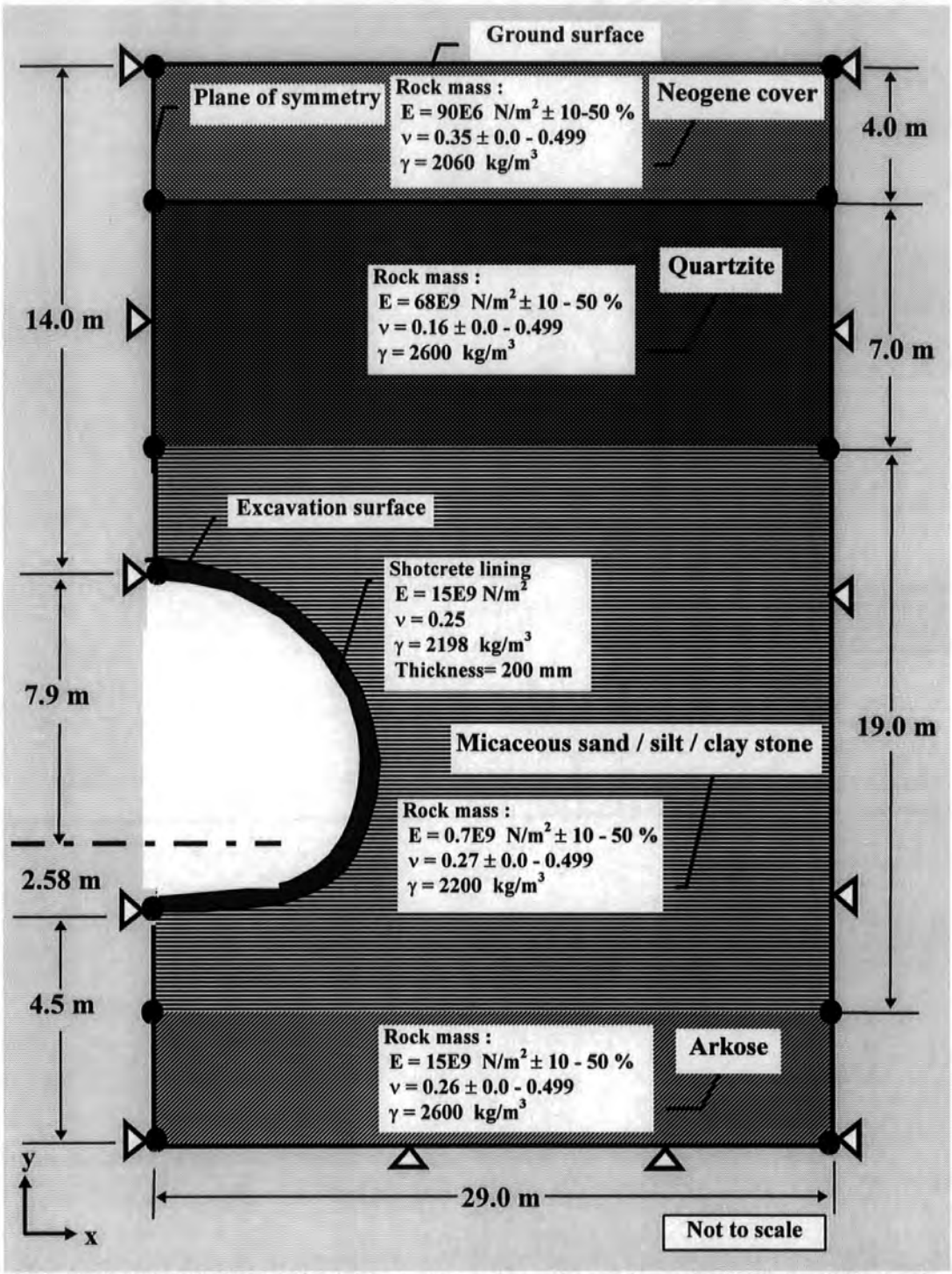

Fig. 7.50 Model dimensions, material properties and geological conditions of Kisikli south tube, (km 1+544), having shotcrete lining

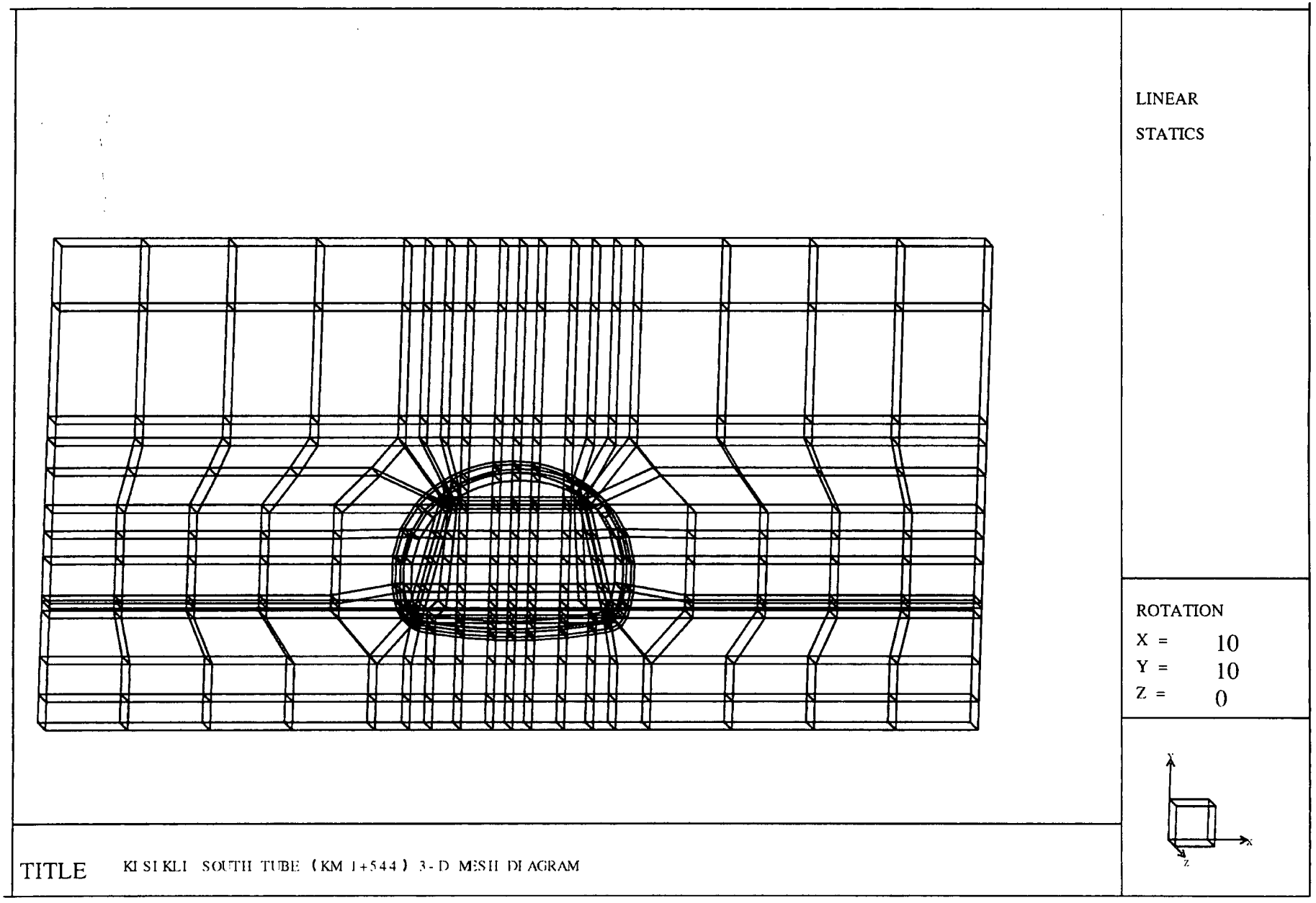

Fig. 7.51 Three-dimensional mesh diagram of Kisikli south tube (km 1+544)

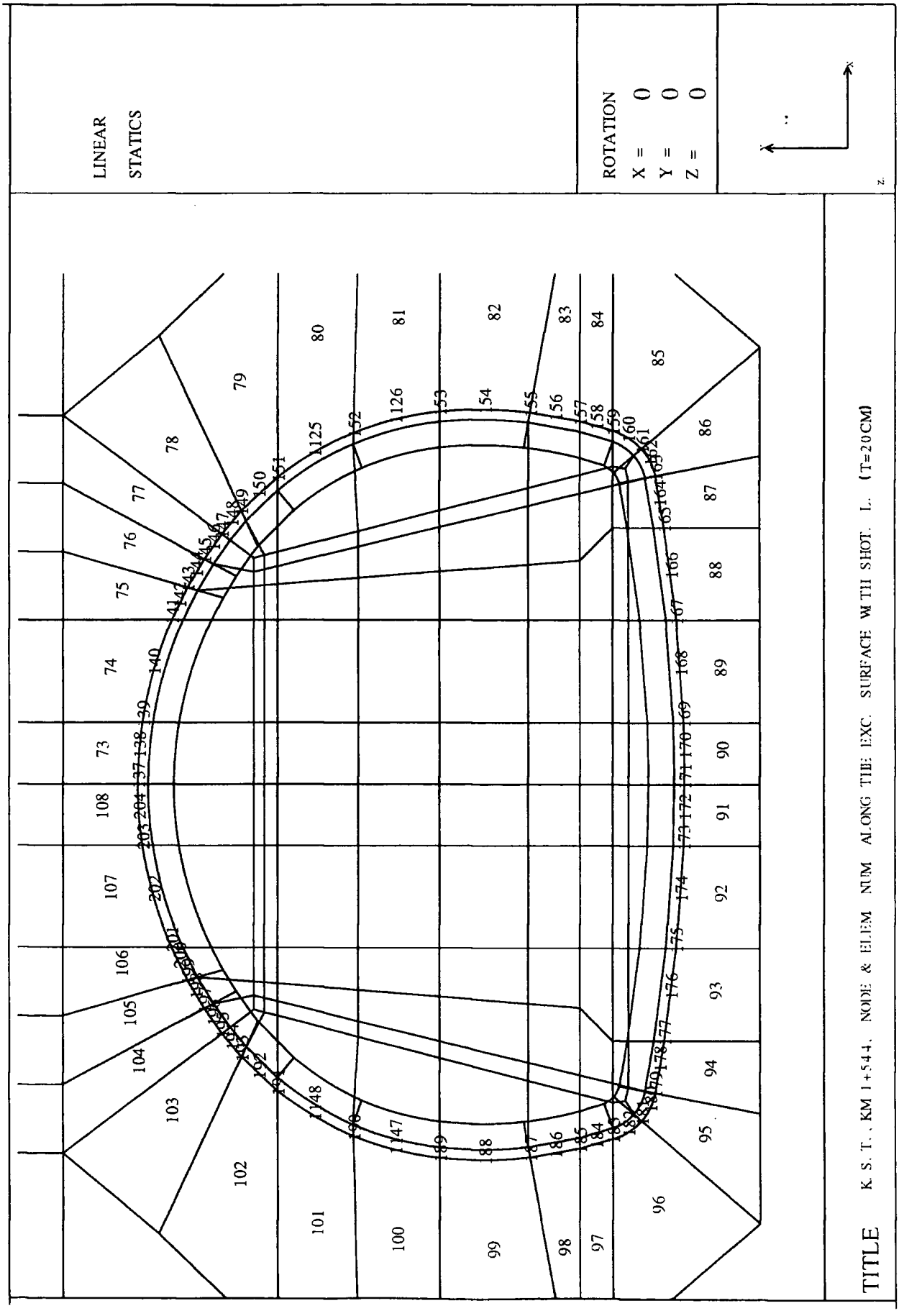

Fig. 7.52 Node and element numbers for the front plane along the excavation surface of Kisikli south tube (km 1+544)

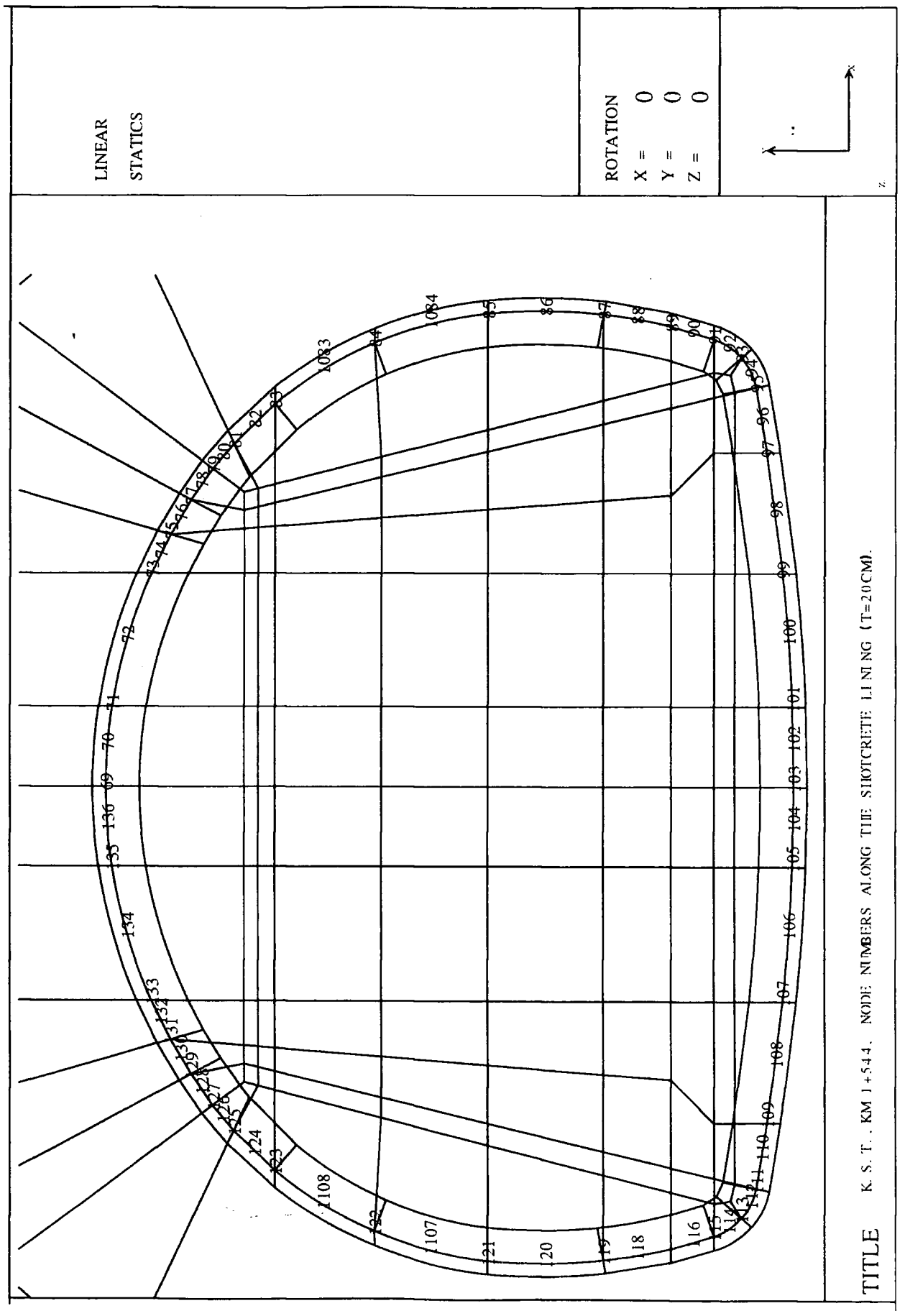

Fig. 7.53 Node numbers for the front plane along the free surface of the shotcrete lining of Kisikli south tube (km 1+544)

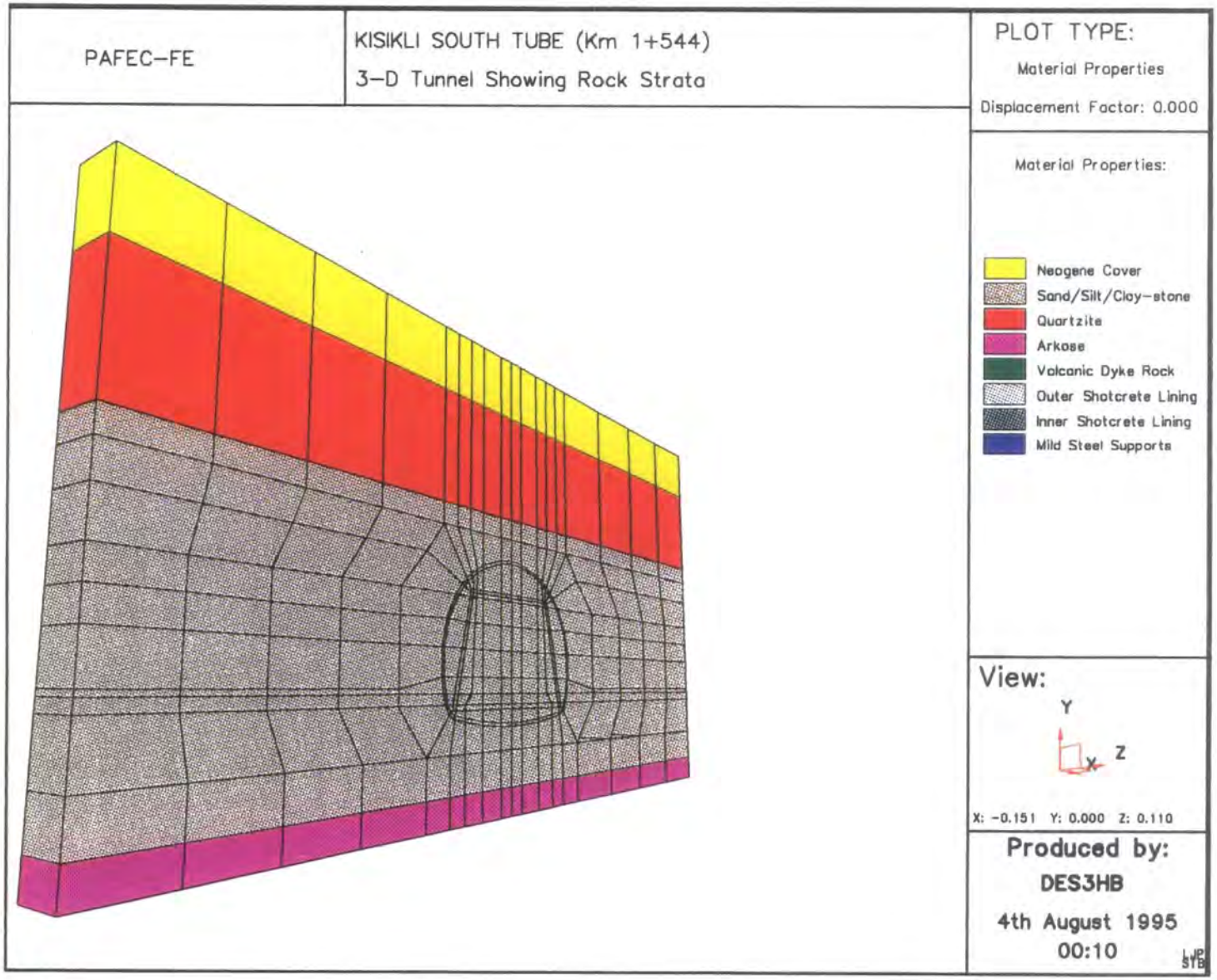

Fig. 7.54 Mesh diagram and colour output of geological conditions of Kisikli south tube (km 1+544)

7.3.3.1 Excavation Stages

The excavation sequences have been modelled for rock types A, B and C as explained in Chapters 2 and 5. The whole cross-sectional area is divided into six parts for excavation. In stages 1, 2a and 2b, the crown of the tunnel is excavated. In stages 3a and 3b, two side walls of the tunnel are dug, but the centre core of the tunnel remains. In stage 4, the centre core of tunnel is excavated. In stages 5a, 5b and 6, the remainder of tunnel invert is removed. With each stage of excavation, the shotcrete lining can be placed before the next excavation stage is implemented. The excavation is simulated step by step by eliminating the tunnel face elements within the excavation boundary as shown in Figs 5.12 and 5.13. This can be achieved in the excavation area by reducing the Young's modulus of the elements to zero and giving them air material properties, as shown in Tables 4.1 and 4.2.

An analysis was conducted using the gravity difference method to investigate the effects of the first four stages (1, 2a, 2b, 3a, 3a and 4) of partial excavation on the stresses and displacements of Kisikli south tube (km 1+544). Table 7.15 shows a comparison of the Von Mises stresses for the partially and fully excavated tunnel models along the unsupported excavation surface. The same results are also shown graphically in Fig. 7.55 for visual comparison. It can be seen that the partially excavated tunnel results in quite low stresses along the unsupported excavation surface. In comparing Von Mises stresses from partially and fully excavated tunnel models, it can be seen that the output shows quite convincingly the variations in stress along the excavation surface. It is possible to estimate the Von Mises stress in the rock layer on the boundary of the partial excavation. Table 7.16 shows a comparison of the component and resultant displacements for nodes along the full excavation surface for unsupported partial and full excavation of the Kisikli south tube models. For these conditions, the resultant displacements at nodes along this surface are presented in Fig. 7.56 for visual comparison, which illustrates the increase in displacements occurring as excavation progresses.

The stress colour diagrams of this study using the gravity difference method are shown in Figs. 7.57 to 7.59 respectively. Fig. 7.57 shows the Von Mises stress distribution in colour and the slightly deformed shape of the unexcavated ground under the action of gravity. Fig. 7.58 shows a similar diagram for the partially excavated ground. The gravity difference method uses the differences between these two analyses to produce the stresses and displacements shown in Fig 7.59 that results from the partial excavation. These shaded colour diagrams indicate areas of increased and decreased stress through changes in colour from red to blue.

A failure zone will be produced in the rock mass around the partial excavation when induced stresses are greater than the rock strength. The extent of the high stress zone produced by partial excavation of the tunnel can be assessed from a consideration of the effects of partial excavations stages on the stresses and displacements.

GRAVITY DIFFERENCE METHOD				*GRAVITY DIFFERENCE METHOD*		
PARTIALLY EXCAVATED TUNNEL				**FULLY EXCAVATED TUNNEL**		
THREE-DIMENSIONAL MODEL				THREE-DIMENSIONAL MODEL		
Number of nodes = 3498				*Number of nodes = 3498*		
Number of elements = 444				*Number of elements = 444*		
Number of d.o.f = 6798				*Number of d.o.f = 6798*		
KISIKLI SOUTH TUBE (km 1+544)				KISIKLI SOUTH TUBE (km 1+544)		
			VON MISES			
	ELEMENT	NODE	STRESS (N/m^2)	ELEMENT	NODE	VON MISES
	NUMBER	NUMBER	ALONG THE	NUMBER	NUMBER	STRESS (N/m^2)
COMPUTED	ALONG THE	ALONG THE	UNSUPPORTED	ALONG THE	ALONG THE	ALONG THE
RESULT	EXCAVATION	EXCAVATION	PARTIAL	EXCAVATION	EXCAVATION	UNSUPPORTED
LOCATIONS	SURFACE	SURFACE	EXCAVATION SURFACE	SURFACE	SURFACE	FULL EXCAVATION SURFACE
1	73	137	2.56E+05	73	137	2.68E+05
2	73	138	2.56E+05	73	138	2.70E+05
3	74	139	2.55E+05	74	139	2.70E+05
4	74	140	2.65E+05	74	140	2.83E+05
5	75	141	2.67E+05	75	141	2.90E+05
6	75	142	2.74E+05	75	142	2.98E+05
7	76	143	2.76E+05	76	143	3.01E+05
8	76	144	2.83E+05	76	144	3.08E+05
9	77	145	2.85E+05	77	145	3.12E+05
10	77	146	2.92E+05	77	146	3.19E+05
11	78	147	2.84E+05	78	147	3.13E+05
12	78	148	3.08E+05	78	148	3.36E+05
13	79	149	3.47E+05	79	149	3.65E+05
14	79	150	3.72E+05	79	150	3.80E+05
15	80	151	3.85E+05	80	151	3.87E+05
16	81	152	5.46E+05	81	152	4.41E+05
17	82	153	9.01E+05	82	153	4.92E+05
18	82	154	4.14E+05	82	154	5.04E+05
19	83	155	2.70E+05	83	155	5.12E+05
20	83	156	2.71E+05	83	156	5.11E+05
21	84	157	2.68E+05	84	157	5.46E+05
22	84	158	2.57E+05	84	158	5.69E+05
23	85	159	2.53E+05	85	159	6.58E+05
24	85	160	2.34E+05	85	160	7.59E+05
25	86	161	2.26E+05	86	161	6.89E+05
26	86	162	2.41E+05	86	162	6.99E+05
27	87	163	2.46E+05	87	163	6.16E+05
28	87	164	2.65E+05	87	164	4.95E+05
29	88	165	2.80E+05	88	165	4.26E+05
30	88	166	2.93E+05	88	166	4.13E+05
31	89	167	3.03E+05	89	167	3.83E+05
32	89	168	3.07E+05	89	168	3.97E+05
33	90	169	3.08E+05	90	169	4.05E+05
34	90	170	3.08E+05	90	170	4.06E+05
35	91	171	3.08E+05	91	171	4.08E+05
36	91	172	3.08E+05	91	172	4.06E+05
37	92	173	3.08E+05	92	173	4.05E+05
38	92	174	3.07E+05	92	174	3.97E+05
39	93	175	3.03E+05	93	175	3.83E+05
40	93	176	2.93E+05	93	176	4.12E+05
41	94	177	2.80E+05	94	177	4.26E+05
42	94	178	2.65E+05	94	178	4.95E+05
43	95	179	2.46E+05	95	179	6.16E+05
44	95	180	2.41E+05	95	180	6.99E+05
45	96	181	2.26E+05	96	181	6.89E+05
46	96	182	2.34E+05	96	182	7.59E+05
47	97	183	2.53E+05	97	183	6.58E+05
48	97	184	2.57E+05	97	184	5.69E+05
49	98	185	2.68E+05	98	185	5.46E+05
50	98	186	2.71E+05	98	186	5.11E+05
51	99	187	2.70E+05	99	187	5.12E+05
52	99	188	4.14E+05	99	188	5.04E+05
53	100	189	9.01E+05	100	189	4.92E+05
54	101	190	5.46E+05	101	190	4.41E+05
55	102	191	3.85E+05	102	191	3.87E+05
56	102	192	3.72E+05	102	192	3.80E+05
57	103	193	3.47E+05	103	193	3.64E+05
58	103	194	3.08E+05	103	194	3.36E+05
59	104	195	2.84E+05	104	195	3.13E+05
60	104	196	2.92E+05	104	196	3.19E+05
61	105	197	2.85E+05	105	197	3.12E+05
62	105	198	2.83E+05	105	198	3.08E+05
63	106	199	2.76E+05	106	199	3.01E+05
64	106	200	2.74E+05	106	200	2.98E+05
65	107	201	2.67E+05	107	201	2.90E+05
66	107	202	2.65E+05	107	202	2.83E+05
67	108	203	2.55E+05	108	203	2.70E+05
68	108	204	2.56E+05	108	204	2.70E+05

Table 7.15 Comparison of stresses along the unsupported excavation surface for partially and fully excavated Kisikli south tube models (Km 1+544)

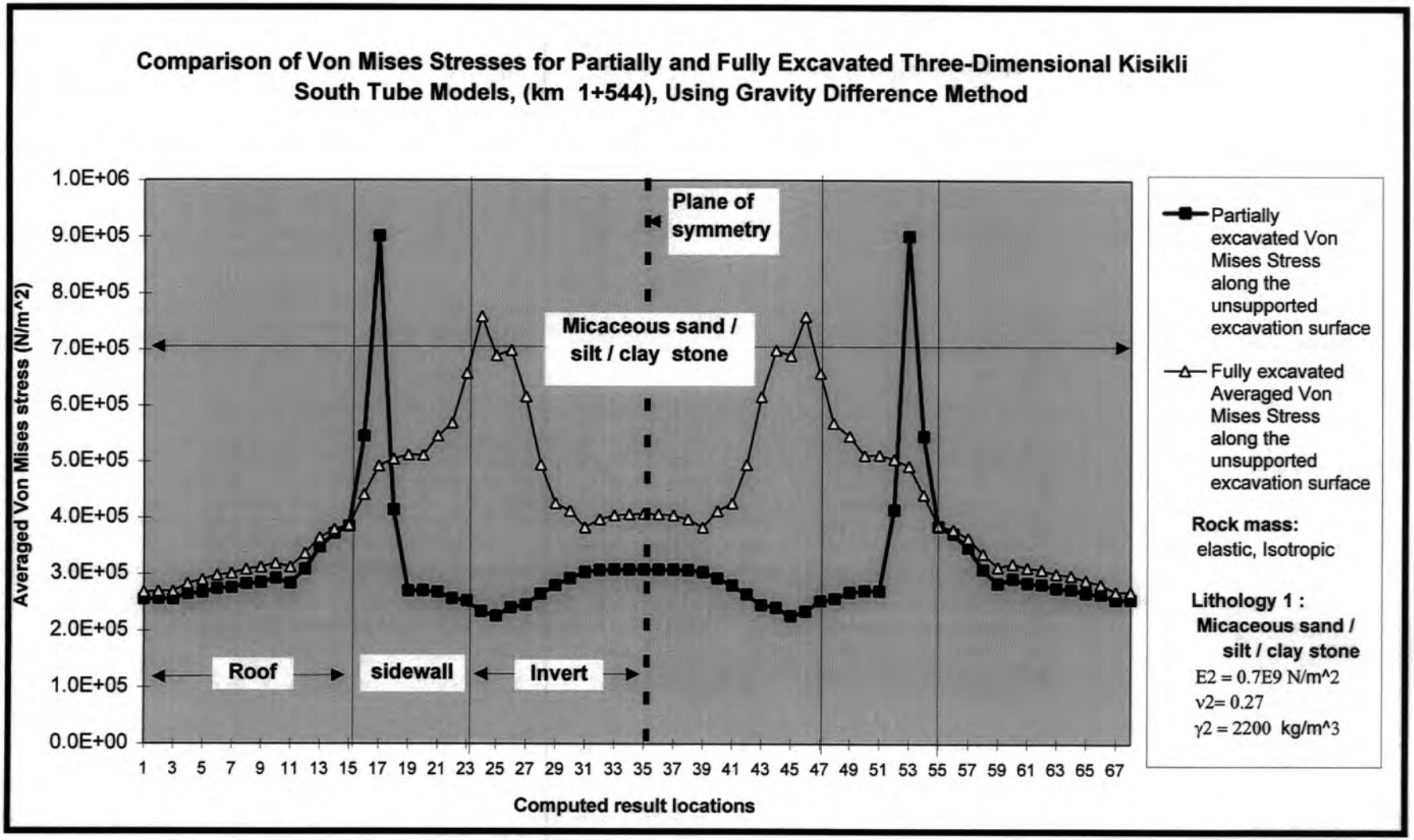

Fig. 7.55 Comparison of stresses along the unsupported excavation surface for partially and fully excavated Kisikli south tube models (km 1+544)

GRAVITY DIFFERENCE METHOD						*GRAVITY DIFFERENCE METHOD*				
PARTIALLY EXCAVATED TUNNEL						**FULLY EXCAVATED TUNNEL**				
Number of nodes = 3498						*Number of nodes = 3498*				
Number of elements = 444						*Number of elements = 444*				
Number of d.o.f = 6798						*Number of d.o.f = 6798*				
KISIKLI SOUTH TUBE (km 1+544)						**KISIKLI SOUTH TUBE (km 1+544)**				
	ELEMENT	**NODE**				**ELEMENT**	**NODE**			
	NUMBER	**NUMBER**	**DISPLACEMENT (mm)**			**NUMBER**	**NUMBER**	**DISPLACEMENT (mm)**		
COMPUTED	**ALONG THE**	**ALONG THE**	**ALONG THE UNSUPPORTED**			**ALONG THE**	**ALONG THE**	**ALONG THE UNSUPPORTED**		
RESULT	**EXCAVATIO**	**EXCAVATIO**	**PARIAL EXCAVATION SURFACE**			**EXCAVATION**	**EXCAVATION**	**FULL EXCAVATION SURFACE**		
LOCATIONS	**SURFACE**	**SURFACE**	**Ux**	**Uy**	**U**	**SURFACE**	**SURFACE**	**Ux**	**Uy**	**U**
1	73	137	0.0000	-3.4586	**3.4586**	73	137	0.0000	-3.8246	**3.8246**
2	73	138	0.1956	-3.4591	**3.4646**	73	138	0.2090	-3.8241	**3.8298**
3	74	139	0.3928	-3.4617	**3.4839**	74	139	0.4188	-3.8237	**3.8466**
4	74	140	0.7357	-3.4607	**3.5380**	74	140	0.7742	-3.8177	**3.8954**
5	75	141	1.0896	-3.4173	**3.5868**	75	141	1.1325	-3.7743	**3.9405**
6	75	142	1.2135	-3.3869	**3.5977**	75	142	1.2534	-3.7459	**3.9500**
7	76	143	1.3231	-3.3423	**3.5947**	76	143	1.3586	-3.7083	**3.9493**
8	76	144	1.4266	-3.2904	**3.5864**	76	144	1.4572	-3.6644	**3.9435**
9	77	145	1.5143	-3.2234	**3.5614**	77	145	1.5403	-3.6094	**3.9243**
10	77	146	1.5946	-3.1524	**3.5328**	77	146	1.6159	-3.5514	**3.9017**
11	78	147	1.6581	-3.0654	**3.4851**	78	147	1.6766	-3.4819	**3.8645**
12	78	148	1.7621	-2.9514	**3.4374**	78	148	1.7785	-3.3874	**3.8259**
13	79	149	1.8383	-2.8225	**3.3684**	79	149	1.8573	-3.2875	**3.7759**
14	79	150	1.9997	-2.5528	**3.2428**	79	150	2.0396	-3.0638	**3.6806**
15	80	151	1.9813	-2.2883	**3.0269**	80	151	2.0374	-2.8882	**3.5345**
16	81	152	1.6446	-1.1712	**2.0190**	81	152	2.0161	-2.0864	**2.9013**
17	82	153	0.1526	0.0532	**0.1616**	82	153	1.4522	-1.5082	**2.0937**
18	82	154	-0.3041	-0.3285	**0.4476**	82	154	1.0250	-1.3686	**1.7099**
19	83	155	-0.5291	-0.6528	**0.8403**	83	155	0.5818	-1.3081	**1.4316**
20	83	156	-0.5627	-0.7978	**0.9763**	83	156	0.3428	-1.2930	**1.3377**
21	84	157	-0.5744	-0.9265	**1.0901**	84	157	0.1042	-1.3001	**1.3043**
22	84	158	-0.5663	-0.9975	**1.1470**	84	158	-0.0770	-1.2760	**1.2783**
23	85	159	-0.5499	-1.0568	**1.1913**	85	159	-0.2563	-1.2531	**1.2790**
24	85	160	-0.2855	-1.2090	**1.2423**	85	160	-0.2735	-1.3164	**1.3445**
25	86	161	0.0036	-1.2927	**1.2927**	86	161	-0.2635	-1.5492	**1.5714**
26	86	162	0.2914	-1.3362	**1.3676**	86	162	-0.0940	-1.8506	**1.8530**
27	87	163	0.5971	-1.3246	**1.4530**	87	163	0.1947	-2.1708	**2.1795**
28	87	164	0.5491	-1.5072	**1.6041**	87	164	0.0353	-2.6172	**2.6174**
29	88	165	0.4958	-1.6673	**1.7395**	88	165	-0.0389	-2.9170	**2.9173**
30	88	166	0.3969	-1.8950	**1.9361**	88	166	-0.0679	-3.2908	**3.2915**
31	89	167	0.2991	-2.0571	**2.0787**	89	167	-0.0309	-3.4886	**3.4887**
32	89	168	0.1980	-2.1721	**2.1811**	89	168	-0.0147	-3.6038	**3.6038**
33	90	169	0.1048	-2.2353	**2.2378**	90	169	0.0009	-3.6538	**3.6538**
34	90	170	0.0519	-2.2539	**2.2545**	90	170	0.0008	-3.6636	**3.6636**
35	91	171	0.0000	-2.2599	**2.2599**	91	171	0.0000	-3.6675	**3.6675**
36	91	172	-0.0519	-2.2539	**2.2545**	91	172	-0.0008	-3.6636	**3.6636**
37	92	173	-0.1048	-2.2353	**2.2378**	92	173	-0.0009	-3.6538	**3.6538**
38	92	174	-0.1980	-2.1721	**2.1811**	92	174	0.0147	-3.6038	**3.6038**
39	93	175	-0.2991	-2.0571	**2.0787**	93	175	0.0309	-3.4886	**3.4887**
40	93	176	-0.3969	-1.8950	**1.9361**	93	176	0.0679	-3.2908	**3.2915**
41	94	177	-0.4958	-1.6673	**1.7395**	94	177	0.0390	-2.9170	**2.9173**
42	94	178	-0.5491	-1.5072	**1.6041**	94	178	-0.0353	-2.6172	**2.6174**
43	95	179	-0.5971	-1.3246	**1.4530**	95	179	-0.1947	-2.1708	**2.1795**
44	95	180	-0.2914	-1.3362	**1.3676**	95	180	0.0940	-1.8506	**1.8530**
45	96	181	-0.0036	-1.2927	**1.2927**	96	181	0.2635	-1.5492	**1.5714**
46	96	182	0.2855	-1.2090	**1.2423**	96	182	0.2735	-1.3164	**1.3445**
47	97	183	0.6032	-1.0273	**1.1913**	97	183	0.3200	-1.2384	**1.2791**
48	97	184	0.5663	-0.9975	**1.1470**	97	184	0.0770	-1.2760	**1.2783**
49	98	185	0.5744	-0.9265	**1.0901**	98	185	-0.1042	-1.3001	**1.3043**
50	98	186	0.5627	-0.7978	**0.9763**	98	186	-0.3428	-1.2930	**1.3377**
51	99	187	0.5292	-0.6528	**0.8404**	99	187	-0.5817	-1.3081	**1.4316**
52	99	188	0.3041	-0.3285	**0.4476**	99	188	-1.0250	-1.3686	**1.7099**
53	100	189	-0.1527	0.0531	**0.1617**	100	189	-1.4510	-1.5094	**2.0937**
54	101	190	-1.6447	-1.1712	**2.0191**	101	190	-2.0162	-2.0864	**2.9014**
55	102	191	-1.9813	-2.2883	**3.0269**	102	191	-2.0374	-2.8882	**3.5345**
56	102	192	-1.9997	-2.5528	**3.2428**	102	192	-2.0396	-3.0639	**3.6807**
57	103	193	-1.8383	-2.8225	**3.3684**	103	193	-1.8573	-3.2875	**3.7759**
58	103	194	-1.7621	-2.9513	**3.4373**	103	194	-1.7785	-3.3874	**3.8259**
59	104	195	-1.6581	-3.0654	**3.4851**	104	195	-1.6766	-3.4819	**3.8645**
60	104	196	-1.5946	-3.1524	**3.5328**	104	196	-1.6159	-3.5514	**3.9017**
61	105	197	-1.5143	-3.2234	**3.5614**	105	197	-1.5403	-3.6094	**3.9243**
62	105	198	-1.4266	-3.2904	**3.5864**	105	198	-1.4572	-3.6644	**3.9435**
63	106	199	-1.3231	-3.3423	**3.5947**	106	199	-1.3586	-3.7083	**3.9493**
64	106	200	-1.2135	-3.3869	**3.5977**	106	200	-1.2534	-3.7459	**3.9500**
65	107	201	-1.0896	-3.4173	**3.5868**	107	201	-1.1325	-3.7743	**3.9405**
66	107	202	-0.7357	-3.4607	**3.5380**	107	202	-0.7742	-3.8177	**3.8954**
67	108	203	-0.3928	-3.4617	**3.4839**	108	203	-0.4188	-3.8237	**3.8466**
68	108	204	-0.1956	-3.4591	**3.4646**	108	204	-0.2090	-3.8241	**3.8298**

Table 7.16 Comparison of displacements along the unsupported excavation surface for partially and fully excavated Kisikli south tube models (km 1+544)

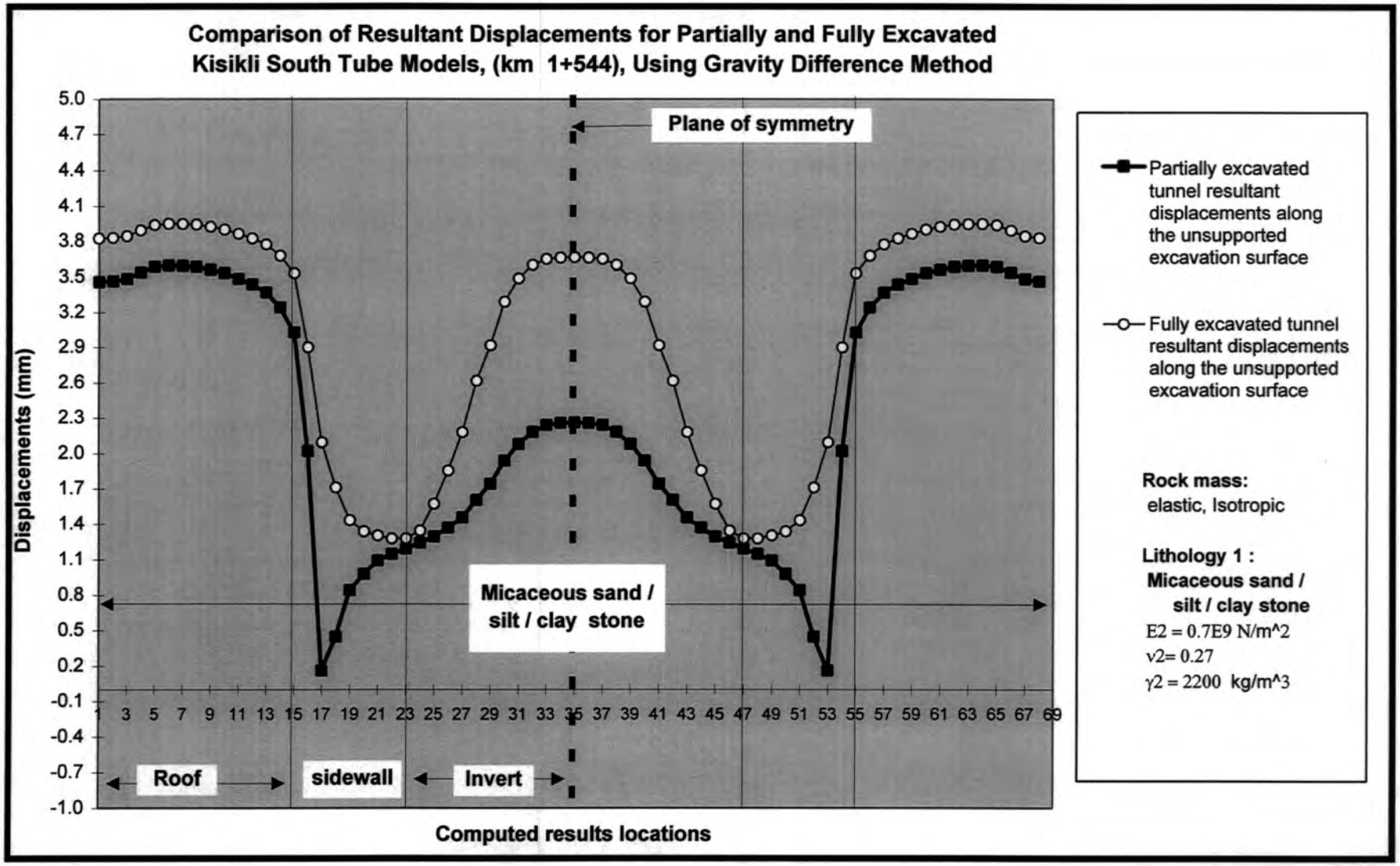

Fig. 7.56 Comparison of displacements along the unsupported excavation surface for partially and fully excavated Kisikli south tube models, (km 1+544)

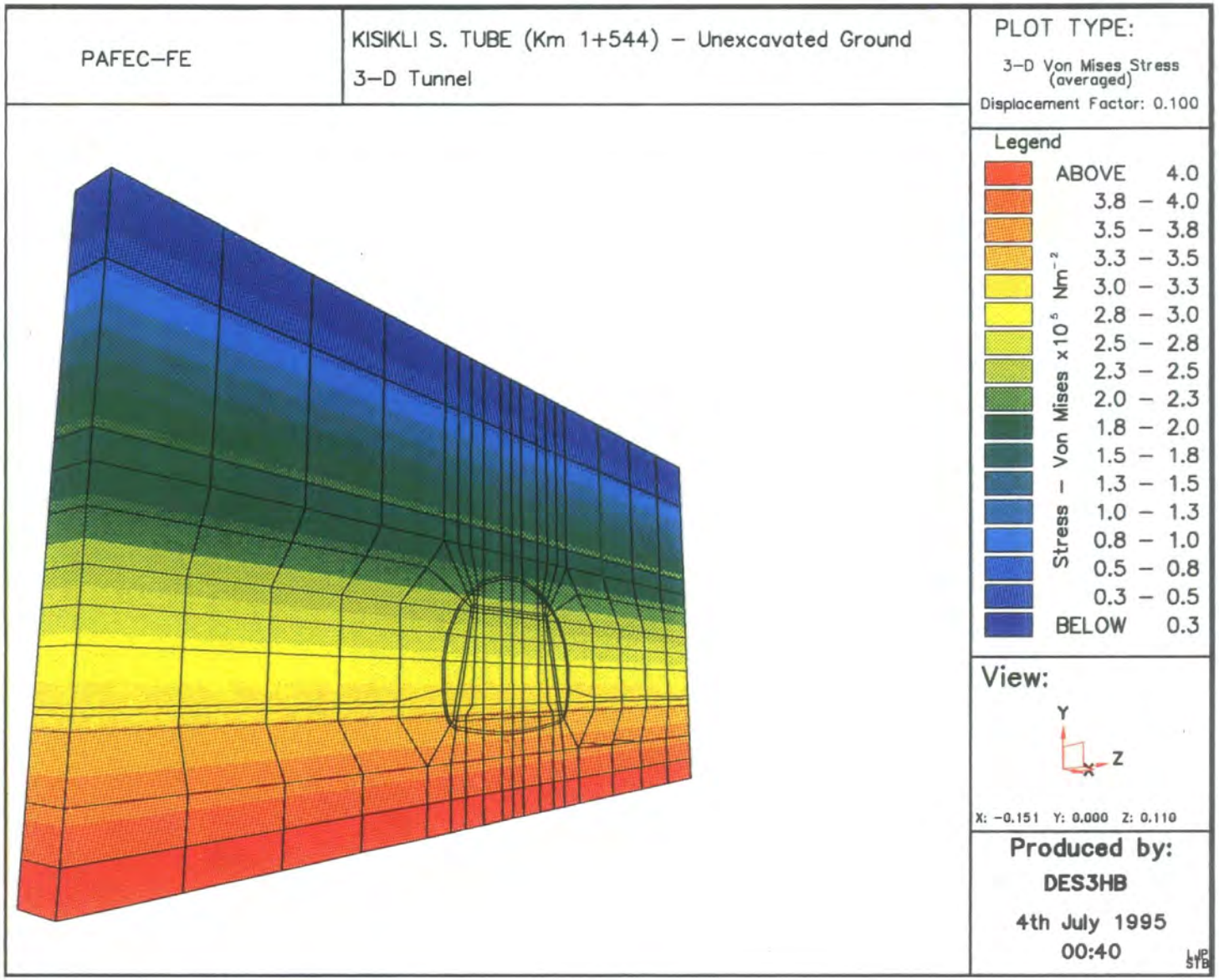

Fig. 7.57 Unexcavated ground colour stress and displaced shape diagrams of Kisikli south tube (km 1+544)

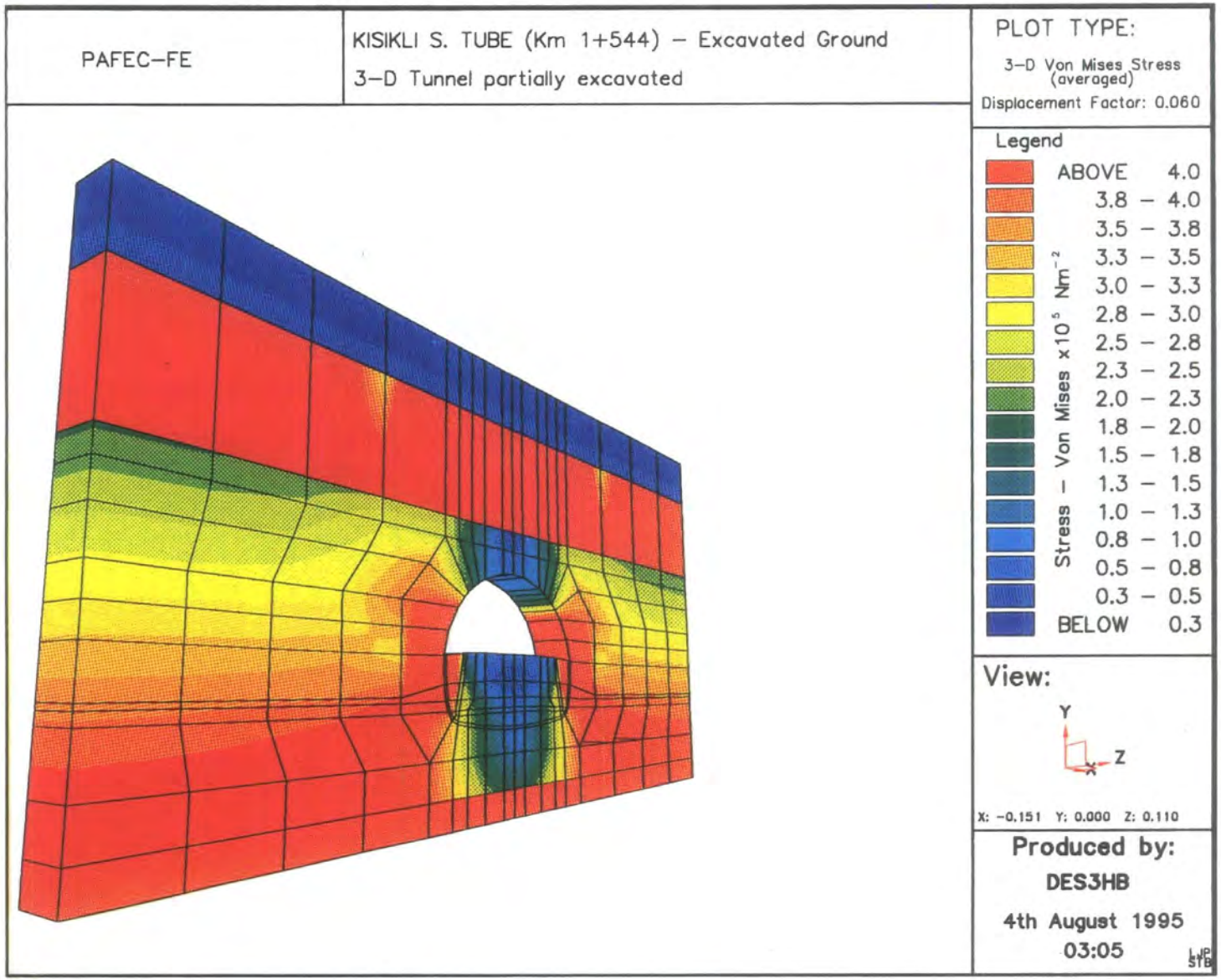

Fig. 7.58 Partially excavated ground colour stress and displaced shape diagrams of Kisikli south tube (km 1+544)

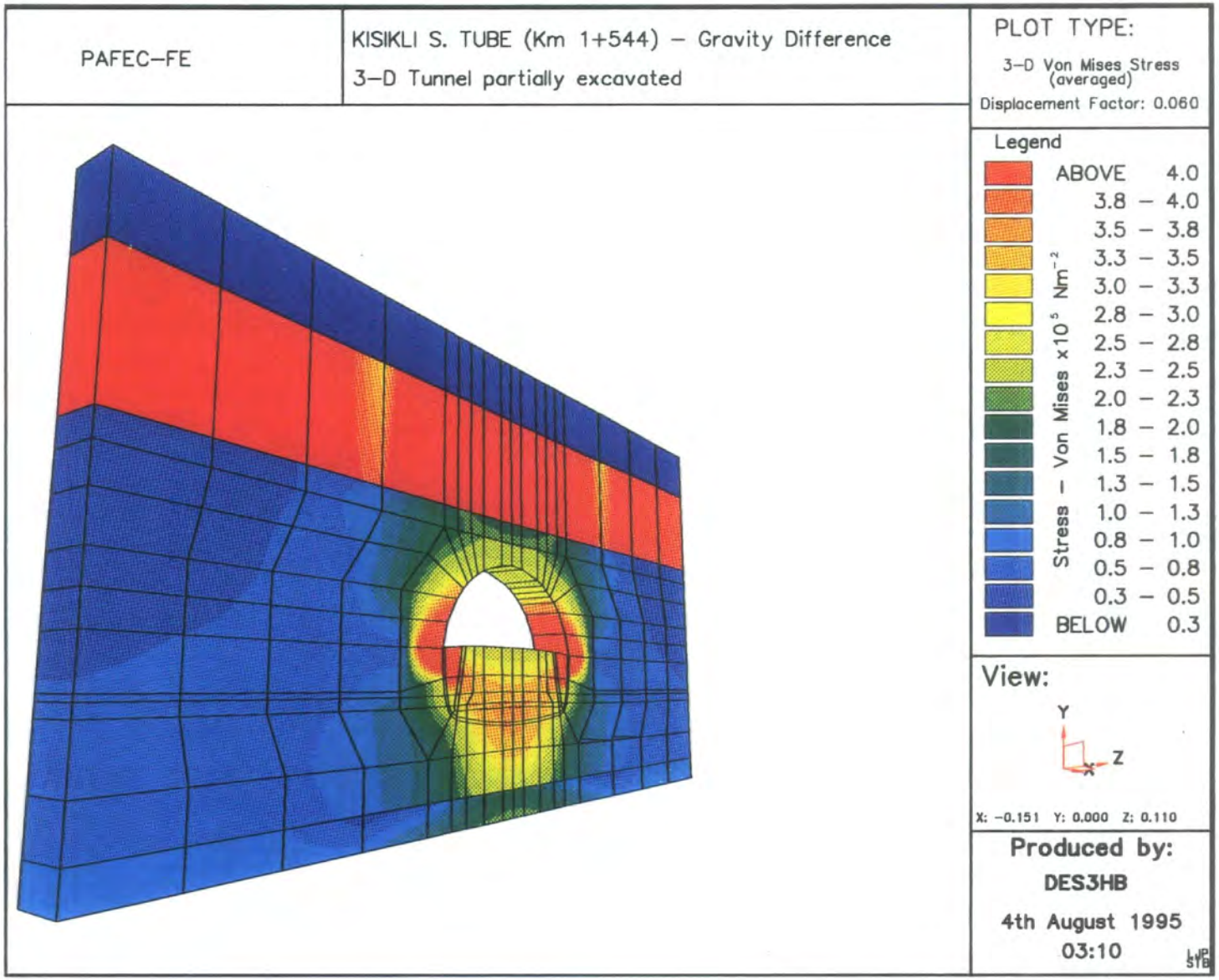

Fig. 7.59 Colour stress and displaced shape diagrams of partially excavated Kisikli south tube, (km 1+554), using gravity difference method

7.3.3.2 Analysis of Shotcrete Lining and Comparison of Displacements

Computation procedures to investigate the stability of a tunnel having a periodic support system in rock must be able to handle general three-dimensional states of stresses and displacements. A three-dimensional model is needed in the case of the anchorages and steel arches due to the their periodic form and analysis of the tunnel's temporary working face. The outer (shotcrete) and inner concrete linings are parallel to the excavation surface and are constructed continuously. It is for this reason that a two-dimensional plane strain tunnel model is able to predict the displacements and stresses in the case of a continuous reinforced concrete lining. The results of analyses using two- and three-dimensional models for the Kisikli south tube at km 1+544 having shotcrete linings are shown in Figs. 7.60 to 7.62 and are summarised in Tables 7.17 to 7.18.

Fig. 7.60 shows the deformed and undeformed mesh diagrams after application of a 200 mm thick shotcrete lining for this section of the Kisikli south tube. It can be seen that the roof and invert area of the tunnel have quite extensive convergence. A comparison of stresses along the free surface of the shotcrete lining for two- and three-dimensional Kisikli south tube models is presented in Table 7.17. The variations in Von Mises stress along this surface for the two- and three dimensional models of the section are shown graphically in Fig. 7.61 for visual comparison. Table 7.18 shows a comparison of the component and resultant displacements along this surface for both models. These results are also presented in Fig. 7.62. The figures and tables show that the two-dimensional Von Mises stress and displacement results are in agreement with the equivalent three-dimensional results.

Again changes have been made to the elastic parameters of the 'intact' rock strata to allow for the effects of discontinuities within the rock mass. As before, reduction factors of 0.10 and 0.50 were applied to the values of Young's modulus for the 'intact' rock and an increase of 0.05 for Poisson ratio has been used. Table 7.19 shows displacements along the free surface of the shotcrete lining and a

summary of the ranges of elastic constants used in the analyses for a 200 mm thick shotcrete lining. The same results are presented in Fig. 7.63 for visual comparison. The influence of the change in Young's modulus has a similar influence on deformation to the change in Poisson's ratio as shown both the figure and the table. The measured displacements are shown in Table 7.3 and Fig. 7.7.

A comparison of the measured and calculated results of displacements of the Kisikli south tube at km 1+544 having a 200 mm thick shotcrete lining is presented in Table 7.20. It should be again noted that the sign of the displacement (the sense of the movement) indicates the direction of movement relative to the axes on the centre of the tunnel. Fig. 7.64 shows the convergence results in graphical form for both measured and computed cases. The calculated tunnel convergences at all points agreed less closely with the measured in situ values than for km 1+536. The maximum difference between the measured and calculated displacement values is 1.67 mm. In all instances the modelled displacements are in the same direction as those actually measured but their magnitudes are in all cases higher. However the order of magnitude of the results is generally close bearing in mind the difficulties in obtaining site data.

Finally, the Von Mises stress distribution in colour and the slightly deformed shape of the 200 mm thick shotcrete lined Kisikli south tube at km 1+544 under the action of gravity are shown in Fig. 7.65. These shaded colour diagrams indicate areas of increased and decreased stress through changes in colour from red to blue.

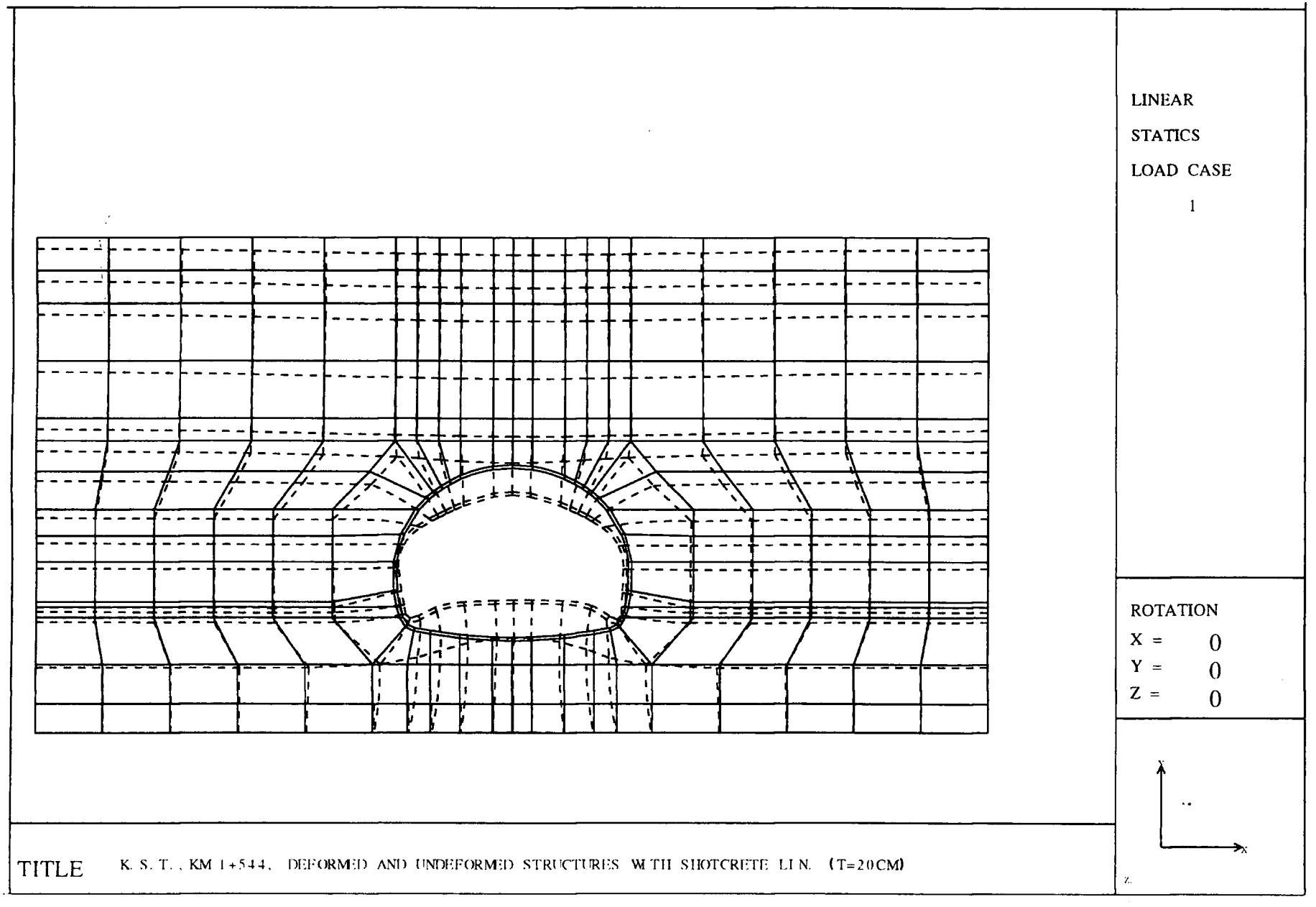

Fig. 7.60 Deformed and undeformed meshes of Kisikli south tube, (km 1+544), having shotcrete lining

STRESS REVERSAL TECHNIQUE				*STRESS REVERSAL TECHNIQUE*		
TWO-DIMENSIONAL MODEL				**THREE-DIMENSIONAL MODEL**		
Number of nodes = 2039				*Number of nodes = 3498*		
Number of elements = 444				*Number of elements = 444*		
Number of d.o.f = 2703				*Number of d.o.f = 6798*		
KISIKLI SOUTH TUBE (km 1+544)				**KISIKLI SOUTH TUBE (km 1+544)**		
HAVING SHOTCRETE LINING (t=200 mm)				**HAVING SHOTCRETE LINING (t=200 mm)**		
	ELEMENT NUMBER	NODE NUMBER	VON MISES STRESS (N/m^2)	ELEMENT NUMBER	NODE NUMBER	VON MISES STRESS (N/m^2)
COMPUTED RESULT LOCATIONS	ALONG THE SHOTCRETE LINING	ALONG THE SHOTCRETE LINING	ALONG THE SHOTCRETE LINING FREE SURFACE	ALONG THE SHOTCRETE LINING	ALONG THE SHOTCRETE LINING	ALONG THE SHOTCRETE LINING FREE SURFACE
1	37	69	1.73E+06	37	69	1.71E+06
2	37	70	1.75E+06	37	70	1.74E+06
3	38	71	1.71E+06	38	71	1.70E+06
4	38	72	1.81E+06	38	72	1.80E+06
5	39	73	1.86E+06	39	73	1.85E+06
6	39	74	1.90E+06	39	74	1.88E+06
7	40	75	1.95E+06	40	75	1.94E+06
8	40	76	2.05E+06	40	76	2.04E+06
9	41	77	2.12E+06	41	77	2.11E+06
10	41	78	2.27E+06	41	78	2.25E+06
11	42	79	2.40E+06	42	79	2.38E+06
12	42	80	2.62E+06	42	80	2.61E+06
13	43	81	2.71E+06	43	81	2.69E+06
14	43	82	2.90E+06	43	82	2.88E+06
15	44	83	3.11E+06	44	83	3.11E+06
16	45	84	3.95E+06	45	84	3.95E+06
17	46	85	4.54E+06	46	85	4.55E+06
18	46	86	4.41E+06	46	86	4.43E+06
19	47	87	4.27E+06	47	87	4.29E+06
20	47	88	4.08E+06	47	88	4.09E+06
21	48	89	3.79E+06	48	89	3.83E+06
22	48	90	4.59E+06	48	90	4.59E+06
23	49	91	5.57E+06	49	91	5.62E+06
24	49	92	7.89E+06	49	92	7.95E+06
25	50	93	7.06E+06	50	93	7.04E+06
26	50	94	6.11E+06	50	94	6.17E+06
27	51	95	2.54E+06	51	95	2.57E+06
28	51	96	1.27E+06	51	96	1.27E+06
29	52	97	8.92E+05	52	97	9.16E+05
30	52	98	1.08E+06	52	98	1.10E+06
31	53	99	1.23E+06	53	99	1.22E+06
32	53	100	1.20E+06	53	100	1.20E+06
33	54	101	1.24E+06	54	101	1.25E+06
34	54	102	1.25E+06	54	102	1.27E+06
35	55	103	1.27E+06	55	103	1.28E+06
36	55	104	1.25E+06	55	104	1.27E+06
37	56	105	1.24E+06	56	105	1.25E+06
38	56	106	1.20E+06	56	106	1.20E+06
39	57	107	1.23E+06	57	107	1.22E+06
40	57	108	1.08E+06	57	108	1.10E+06
41	58	109	8.92E+05	58	109	9.15E+05
42	58	110	1.27E+06	58	110	1.27E+06
43	59	111	2.54E+06	59	111	2.57E+06
44	59	112	6.11E+06	59	112	6.17E+06
45	60	113	7.06E+06	60	113	7.04E+06
46	60	114	7.89E+06	60	114	7.95E+06
47	61	115	5.57E+06	61	115	5.62E+06
48	61	116	4.59E+06	61	116	4.59E+06
49	62	117	3.79E+06	62	117	3.83E+06
50	62	118	4.08E+06	62	118	4.09E+06
51	63	119	4.26E+06	63	119	4.29E+06
52	63	120	4.41E+06	63	120	4.44E+06
53	64	121	4.54E+06	64	121	4.55E+06
54	65	122	3.95E+06	65	122	3.95E+06
55	66	123	3.11E+06	66	123	3.11E+06
56	66	124	2.90E+06	66	124	2.88E+06
57	67	125	2.71E+06	67	125	2.69E+06
58	67	126	2.62E+06	67	126	2.61E+06
59	68	127	2.40E+06	68	127	2.38E+06
60	68	128	2.27E+06	68	128	2.25E+06
61	69	129	2.12E+06	69	129	2.11E+06
62	69	130	2.05E+06	69	130	2.00E+06
63	70	131	1.95E+06	70	131	1.94E+06
64	70	132	1.90E+06	70	132	1.88E+06
65	71	133	1.86E+06	71	133	1.85E+06
66	71	134	1.81E+06	71	134	1.80E+06
67	72	135	1.71E+06	72	135	1.70E+06
68	72	136	1.75E+06	72	136	1.74E+06

Table 7.17 Comparison of stresses along the free surface of the shotcrete lining for two- and three-dimensional Kisikli south tube models (km 1+544)

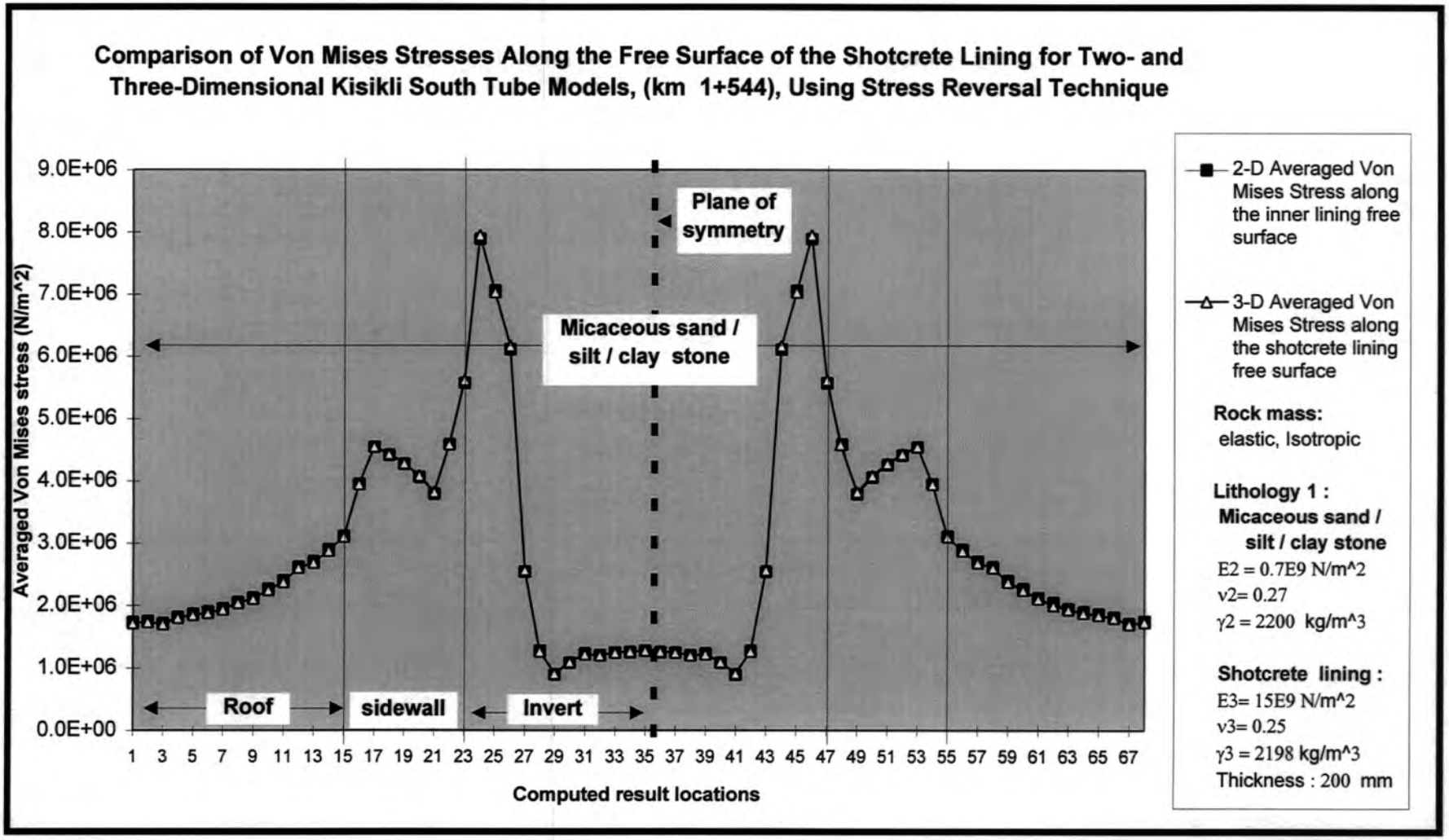

Fig. 7.61 Comparison of stresses along free surface of the shotcrete lining for two- and three-dimensional Kisikli south tube models (km 1+544)

STRESS REVERSAL TECHNIQUE						*STRESS REVERSAL TECHNIQUE*				
TWO-DIMENSIONAL MODEL						**THREE-DIMENSIONAL MODEL**				
Number of nodes = 2039						*Number of nodes = 3498*				
Number of elements = 444						*Number of elements = 444*				
Number of d.o.f = 2703						*Number of d.o.f = 6798*				
KISIKLI SOUTH TUBE (km 1+544)						KISIKLI SOUTH TUBE (km 1+544)				
HAVING SHOTCRETE LINING (t=200 mm),						HAVING SHOTCRETE LINING (t=200 mm),				
	ELEMENT	NODE				ELEMENT	NODE			
	NUMBER	NUMBER	DISPLACEMENT (mm)			NUMBER	NUMBER	DISPLACEMENT (mm)		
COMPUTED	ALONG THE	ALONG THE	ALONG THE SHOTCRETE LINING			ALONG THE	ALONG THE	ALONG THE SHOTCRETE LINING		
RESULT	SHOTCRETE	SHOTCRETE	FREE SURFACE			SHOTCRETE	SHOTCRETE	FREE SURFACE		
LOCATIONS	LINING	LINING	Ux	Uy	U	LINING	LINING	Ux	Uy	U
1	37	69	0.0000	-2.6319	**2.6319**	37	69	0.0000	-2.6442	**2.6442**
2	37	70	-0.0728	-2.6318	**2.6328**	37	70	-0.0731	-2.6441	**2.6451**
3	38	71	-0.1457	-2.6333	**2.6373**	38	71	-0.1463	-2.6453	**2.6493**
4	38	72	-0.2730	-2.6149	**2.6291**	38	72	-0.2741	-2.6269	**2.6412**
5	39	73	-0.4010	-2.5745	**2.6055**	39	73	-0.4030	-2.5867	**2.6179**
6	39	74	-0.4341	-2.5485	**2.5852**	39	74	-0.4362	-2.5607	**2.5976**
7	40	75	-0.4633	-2.5122	**2.5546**	40	75	-0.4656	-2.5242	**2.5668**
8	40	76	-0.4859	-2.4676	**2.5150**	40	76	-0.4885	-2.4795	**2.5272**
9	41	77	-0.5042	-2.4146	**2.4667**	41	77	-0.5073	-2.4264	**2.4789**
10	41	78	-0.5157	-2.3550	**2.4108**	41	78	-0.5192	-2.3668	**2.4231**
11	42	79	-0.5228	-2.2875	**2.3465**	42	79	-0.5265	-2.2992	**2.3587**
12.1	42	80	-0.5263	-2.2227	**2.2842**	42	80	-0.5305	-2.2344	**2.2965**
13	43	81	-0.5303	-2.1568	**2.2210**	43	81	-0.5350	-2.1684	**2.2334**
14	43	82	-0.5285	-2.0380	**2.1054**	43	82	-0.5341	-2.0496	**2.1180**
15	44	83	-0.5204	-1.9111	**1.9807**	44	83	-0.5266	-1.9223	**1.9931**
16	45	84	-0.4556	-1.3631	**1.4372**	45	84	-0.4656	-1.3713	**1.4482**
17	46	85	-0.4273	-0.8043	**0.9108**	46	85	-0.4377	-0.8069	**0.9180**
18	46	86	-0.4446	-0.5391	**0.6988**	46	86	-0.4549	-0.5384	**0.7048**
19	47	87	-0.4261	-0.2808	**0.5103**	47	87	-0.4357	-0.2768	**0.5162**
20	47	88	-0.3796	-0.1403	**0.4047**	47	88	-0.3893	-0.1346	**0.4119**
21	48	89	-0.2866	-0.0166	**0.2871**	48	89	-0.2970	-0.0087	**0.2971**
22	48	90	-0.1874	0.0557	**0.1955**	48	90	-0.1981	0.0647	**0.2084**
23	49	91	-0.0787	0.1414	**0.1618**	49	91	-0.0893	0.1511	**0.1755**
24	49	92	-0.0410	0.2642	**0.2674**	49	92	-0.0496	0.2746	**0.2790**
25	50	93	-0.0526	0.4583	**0.4613**	50	93	-0.0611	0.4700	**0.4740**
26	50	94	-0.1112	0.7602	**0.7683**	50	94	-0.1181	0.7710	**0.7800**
27	51	95	-0.1464	1.1393	**1.1487**	51	95	-0.1524	1.1505	**1.1605**
28	51	96	-0.2147	1.8495	**1.8619**	51	96	-0.2200	1.8587	**1.8717**
29	52	97	-0.2730	2.3557	**2.3715**	52	97	-0.2774	2.3621	**2.3783**
30	52	98	-0.2806	2.9281	**2.9415**	52	98	-0.2832	2.9325	**2.9461**
31	53	99	-0.2512	3.2409	**3.2506**	53	99	-0.2534	3.2452	**3.2551**
32	53	100	-0.1809	3.4421	**3.4489**	53	100	-0.1826	3.4454	**3.4502**
33	54	101	-0.1043	3.5422	**3.5437**	54	101	-0.1056	3.5426	**3.5442**
34	54	102	-0.0521	3.5690	**3.5694**	54	102	-0.0528	3.5680	**3.5684**
35	55	103	0.0001	3.5769	**3.5769**	55	103	-0.0001	3.5757	**3.5757**
36	55	104	0.0523	3.5690	**3.5694**	55	104	0.0527	3.5680	**3.5684**
37	56	105	0.1045	3.5422	**3.5437**	56	105	0.1055	3.5426	**3.5442**
38	56	106	0.1811	3.4420	**3.4468**	56	106	0.1825	3.4454	**3.4502**
39	57	107	0.2514	3.2409	**3.2506**	57	107	0.2533	3.2452	**3.2551**
40	57	108	0.2808	2.9280	**2.9414**	57	108	0.2831	2.9326	**2.9462**
41	58	109	0.2732	2.3556	**2.3714**	58	109	0.2773	2.3621	**2.3783**
42	58	110	0.2149	1.8493	**1.8617**	58	110	0.2199	1.8587	**1.8717**
43	59	111	0.1466	1.1391	**1.1486**	59	111	0.1523	1.1505	**1.1605**
44	59	112	0.1114	0.7599	**0.7680**	59	112	0.1180	0.7710	**0.7800**
45	60	113	0.0528	0.4581	**0.4611**	60	113	0.0609	0.4700	**0.4739**
46	60	114	0.0412	0.2639	**0.2671**	60	114	0.0494	0.2746	**0.2790**
47	61	115	0.0789	0.1411	**0.1617**	61	115	0.0891	0.1511	**0.1754**
48	61	116	0.1876	0.0554	**0.1956**	61	116	0.1979	0.0647	**0.2082**
49	62	117	0.2868	-0.0169	**0.2873**	62	117	0.2968	-0.0087	**0.2969**
50	62	118	0.3798	-0.1406	**0.4050**	62	118	0.3891	-0.1346	**0.4117**
51	63	119	0.4262	-0.2810	**0.5105**	63	119	0.4356	-0.2768	**0.5161**
52	63	120	0.4448	-0.5394	**0.6991**	63	120	0.4547	-0.5385	**0.7048**
53	64	121	0.4275	-0.8045	**0.9110**	64	121	0.4376	-0.8070	**0.9180**
54	65	122	0.4557	-1.3633	**1.4374**	65	122	0.4655	-1.3714	**1.4483**
55	66	123	0.5204	-1.9112	**1.9808**	66	123	0.5266	-1.9225	**1.9933**
56	66	124	0.5286	-2.0381	**2.1055**	66	124	0.5341	-2.0497	**2.1181**
57	67	125	0.5303	-2.1569	**2.2211**	67	125	0.5349	-2.1685	**2.2335**
58	67	126	0.5264	-2.2228	**2.2843**	67	126	0.5305	-2.2345	**2.2966**
59	68	127	0.5000	-2.2875	**2.3416**	68	127	0.5265	-2.2993	**2.3588**
60	68	128	0.5157	-2.3550	**2.4108**	68	128	0.5191	-2.3669	**2.4232**
61	69	129	0.5043	-2.4147	**2.4668**	69	129	0.5072	-2.4265	**2.4789**
62	69	130	0.4859	-2.4677	**2.5151**	69	130	0.4885	-2.4796	**2.5273**
63	70	131	0.4633	-2.5122	**2.5546**	70	131	0.4656	-2.5242	**2.5668**
64	70	132	0.4341	-2.5485	**2.5852**	70	132	0.4362	-2.5608	**2.5977**
65	71	133	0.4010	-2.5746	**2.6056**	71	133	0.4029	-2.5867	**2.6179**
66	71	134	0.2730	-2.6149	**2.6291**	71	134	0.2741	-2.6270	**2.6413**
67	72	135	0.1458	-2.6333	**2.6373**	72	135	0.1462	-2.6453	**2.6493**
68	72	136	0.0728	-2.6318	**2.6328**	72	136	0.0731	-2.6441	**2.6451**

Table 7.18 Comaprison of displacements along the free surface of the shotcrete lining for two- and three-dimensional Kisikli south tube models (km 1+544)

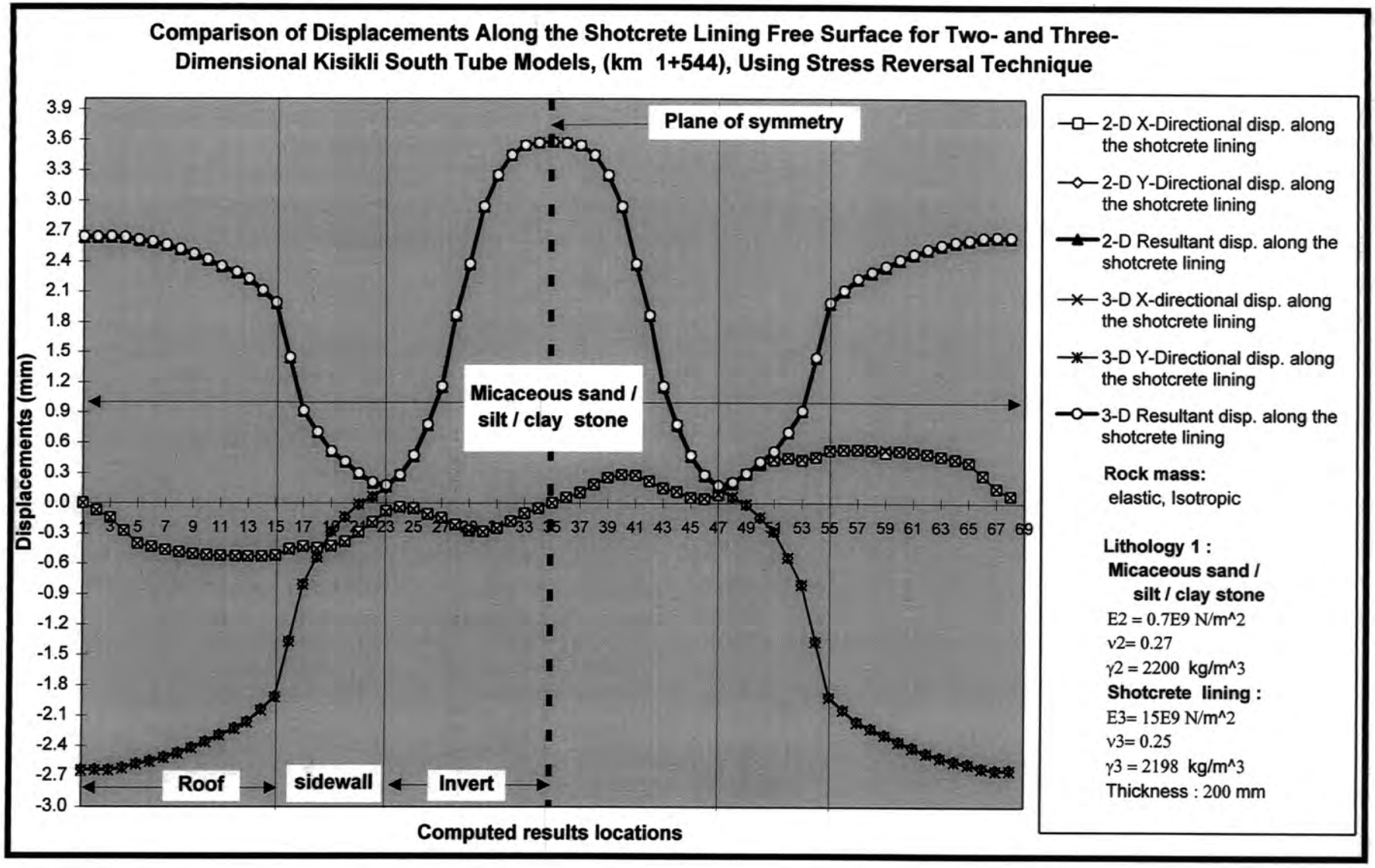

Fig 7.62 Comparison of displacements along the free surface of the shotcrete lining for two- and three-dimensional Kisikli south tube models (km 1+544)

KISIKLI SOUTH TUBE		KEEP EVERYTHING SAME			REDUCE (E) BY 10 TIMES			REDUCE (E) BY 50 TIMES			INCREASED (+) BY 0.05			REDUCE (E) BY 10 TIMES AND			REDUCE (E) BY 50 TIMES AND		
km 1+544					KEEPING EVERTHING ELSE			KEEPING EVERTHING ELSE			KEEPING EVERTHING ELSE			INCREASED (+) BY 0.05			INCREASED (+) BY 0.05		
WITH SHOTCRETE					SAME			SAME			SAME			KEEPING EVERTHING ELSE SAME			KEEPING EVERTHING ELSE SAME		
LINING, t = 200 mm																			
HETEROGENEOUS MODEL		STRESS REVERSAL			STRESS REVERSAL			STRESS REVERSAL			STRESS REVERSAL			STRESS REVERSAL			STRESS REVERSAL		
		TECHNIQUE			TECHNIQUE			TECHNIQUE			TECHNIQUE			TECHNIQUE			TECHNIQUE		
		Lithology=Neogene cover			Lithology=Neogene cover			Lithology=Neogene cover			Lithology=Neogene cover			Lithology=Neogene cover			Lithology=Neogene cover		
		E=90E9 (N/m^2)			E=81E6 (N/m^2)			E=45E6 (N/m^2)			E=90E9 (N/m^2)			E=81E6 (N/m^2)			E=45E6 (N/m^2)		
		v=0.35, γ=2660 (kg/m^3)			v=0.35, γ=2660 (kg/m^3)			v=0.35, γ=2660 (kg/m^3)			v=0.40, γ=2660 (kg/m^3)			v=0.40, γ=2660 (kg/m^3)			v=0.40, γ=2660 (kg/m^3)		
		Lithology=Quartzite			Lithology=Quartzite			Lithology=Quartzite			Lithology=Quartzite			Lithology=Quartzite			Lithology=Quartzite		
		E=58E9 (N/m^2)			E=61,2E9 (N/m^2)			E=34E9 (N/m^2)			E=58E9 (N/m^2)			E=61,2E9 (N/m^2)			E=34E9 (N/m^2)		
		v=0.15, γ=2600 (kg/m^3)			v=0.15, γ=2600 (kg/m^3)			v=0.15, γ=2600 (kg/m^3)			v=0.21, γ=2600 (kg/m^3)			v=0.21, γ=2600 (kg/m^3)			v=0.21, γ=2600 (kg/m^3)		
		Lith.=Sand, silt, clay stone			Lith.=Sand, silt, clay stone			Lith.=Sand, silt, clay stone			Lith.=Sand, silt, clay stone			Lith.=Sand, silt, clay stone			Lith.=Sand, silt, clay stone		
		E=0.7E9 (N/m^2)			E=0.63E9 (N/m^2)			E=0.35E9 (N/m^2)			E=0.7E9 (N/m^2)			E=0.63E9 (N/m^2)			E=0.35E9 (N/m^2)		
		v=0.27, γ=2200 (kg/m^3)			v=0.27, γ=2200 (kg/m^3)			v=0.27, γ=2200 (kg/m^3)			v=0.32, γ=2200 (kg/m^3)			v=0.32, γ=2200 (kg/m^3)			v=0.32, γ=2200 (kg/m^3)		
ELEMENT	NODE	Lithology=Arkose			Lithology=Arkose			Lithology=Arkose			Lithology=Arkose			Lithology=Arkose			Lithology=Arkose		
NUMBER	NUMBER	E=15E9 (N/m^2)			E=13,5E9 (N/m^2)			E=7,5E9 (N/m^2)			E=15E9 (N/m^2)			E=13,5E9 (N/m^2)			E=7,5E9 (N/m^2)		
ALONG THE SHOTCRETE	ALONG THE SHOTCRETE	v=0.26, γ=2600 (kg/m^3)			v=0.26, γ=2600 (kg/m^3)			v=0.26, γ=2600 (kg/m^3)			v=0.31, γ=2600 (kg/m^3)			v=0.31, γ=2600 (kg/m^3)			v=0.31, γ=2600 (kg/m^3)		
LINING	LINING	DISPLACEMENT (mm)			DISPLACEMENT (mm)			DISPLACEMENT (mm)			DISPLACEMENT (mm)			DISPLACEMENT (mm)			DISPLACEMENT (mm)		
		Ux	Uy	U	Ux	Uy	U	Ux	Uy	U	Ux	Uy	U	Ux	Uy	U	Ux	Uy	U
37	69	0.0000	-2.8319	2.8319	0.0000	-2.8601	2.8601	0.0000	-4.5072	4.5072	0.0000	-2.4593	2.4593	0.0000	-2.6643	2.6643	0.0000	-4.1136	4.1136
37	70	-0.0728	-2.8316	2.8328	-0.0766	-2.8599	2.8610	-0.1152	-4.5061	4.5076	-0.0952	-2.4591	2.4609	-0.1025	-2.6641	2.6661	-0.1454	-4.1131	4.1157
38	71	-0.1457	-2.8333	2.8373	-0.1576	-2.8609	2.8652	-0.2303	-4.5036	4.5095	-0.1908	-2.4607	2.4691	-0.2053	-2.6654	2.6733	-0.2911	-4.1131	4.1234
38	72	-0.2730	-2.8149	2.8291	-0.2949	-2.8394	2.8547	-0.4248	-4.4577	4.4779	-0.3595	-2.4465	2.4728	-0.3863	-2.6492	2.6772	-0.5433	-4.0825	4.1185
39	73	-0.4010	-2.5745	2.6055	-0.4317	-2.7822	2.8254	-0.6081	-4.3566	4.3968	-0.5326	-2.4172	2.4752	-0.5711	-2.6152	2.6768	-0.7929	-4.0132	4.0908
39	74	-0.4341	-2.5465	2.5852	-0.4696	-2.7629	2.8029	-0.6500	-4.3011	4.3459	-0.5809	-2.3961	2.4655	-0.6222	-2.5917	2.6653	-0.8581	-3.9710	4.0627
40	75	-0.4633	-2.5122	2.5646	-0.4970	-2.7220	2.7679	-0.6817	-4.2290	4.2796	-0.6259	-2.3658	2.4472	-0.6895	-2.5578	2.6440	-0.9146	-3.9103	4.0158
40	76	-0.4859	-2.4676	2.5150	-0.5199	-2.6721	2.7222	-0.6996	-4.1333	4.1921	-0.6636	-2.3274	2.4202	-0.7087	-2.5150	2.6129	-0.9569	-3.8345	3.9521
41	77	-0.5042	-2.4148	2.4667	-0.5378	-2.6127	2.6675	-0.7061	-4.0241	4.0856	-0.6976	-2.2812	2.3686	-0.7435	-2.4635	2.5733	-0.9892	-3.7425	3.8710
41	78	-0.5157	-2.3550	2.4106	-0.5480	-2.5460	2.6043	-0.6994	-3.9031	3.9653	-0.7243	-2.2285	2.3433	-0.7703	-2.4049	2.5253	-1.0082	-3.6388	3.7769
42	79	-0.5228	-2.2875	2.3469	-0.5533	-2.4708	2.5329	-0.6822	-3.7679	3.8292	-0.7474	-2.1684	2.2936	-0.7929	-2.3382	2.4690	-1.0185	-3.5221	3.6664
42	80	-0.5263	-2.2227	2.2842	-0.5548	-2.3988	2.4621	-0.6609	-3.6408	3.7004	-0.7656	-2.1109	2.2485	-0.8106	-2.2746	2.4147	-1.0232	-3.4124	3.5625
43	81	-0.5303	-2.1568	2.2210	-0.5565	-2.3257	2.3914	-0.6361	-3.5124	3.5699	-0.7856	-2.0530	2.1982	-0.8296	-2.2105	2.3610	-1.0285	-3.3027	3.4591
43	82	-0.5285	-2.0380	2.1064	-0.5502	-2.1945	2.2624	-0.5840	-3.2675	3.3390	-0.8130	-1.9490	2.1118	-0.8553	-2.0963	2.2641	-1.0278	-3.1124	3.2777
44	83	-0.5204	-1.9111	1.9807	-0.5371	-2.0554	2.1244	-0.5210	-3.0592	3.1032	-0.8356	-1.8378	2.0187	-0.8758	-1.9748	2.1603	-1.0218	-2.9195	3.0931
45	84	-0.4556	-1.3631	1.4372	-0.4502	-1.4639	1.5316	-0.2289	-2.1716	2.1836	-0.8969	-1.3448	1.6176	-0.9306	-1.4455	1.7192	-0.9772	-2.1521	2.3636
46	85	-0.4273	-0.8043	0.9108	-0.4136	-0.8728	0.9657	-0.1245	-1.3905	1.3981	-0.9915	-0.8171	1.2818	-0.9951	-0.8881	1.3338	-1.0561	-1.4281	1.7782
46	86	-0.4446	-0.5391	0.6988	-0.4336	-0.5949	0.7361	-0.1680	-1.0472	1.0606	-0.9913	-0.5611	1.1391	-1.0290	-0.6200	1.2013	-1.1244	-1.0977	1.5714
47	87	-0.4261	-0.2808	0.5103	-0.4138	-0.3246	0.5259	-0.1384	-0.7160	0.7293	-0.9551	-0.3125	1.0048	-0.9894	-0.3599	1.0528	-1.0561	-0.7809	1.3135
47	88	-0.3796	-0.1403	0.4047	-0.3618	-0.1789	0.4036	-0.0402	-0.5494	0.5509	-0.8827	-0.1809	0.9010	-0.9082	-0.2239	0.9354	-0.9004	-0.6310	1.0895
48	89	-0.2866	-0.0166	0.2871	-0.2570	-0.0520	0.2622	0.1617	-0.4156	0.4459	-0.7505	-0.0708	0.7538	-0.7590	-0.1121	0.7672	-0.6102	-0.5249	0.8049
48	90	-0.1674	0.0557	0.1956	-0.1489	0.0221	0.1486	0.3514	-0.3342	0.4849	-0.6142	-0.0124	0.6143	-0.6071	-0.0535	0.6096	-0.3397	-0.4719	0.5815
49	91	-0.0787	0.1414	0.1618	-0.0282	0.1111	0.1146	0.5302	-0.2219	0.5748	-0.4582	0.0656	0.4616	-0.4352	0.0157	0.4355	-0.0607	-0.3962	0.4008
49	92	-0.0410	0.2642	0.2674	0.0095	0.2434	0.2436	0.5506	-0.0168	0.5509	-0.3818	0.1605	0.4142	-0.3544	0.1281	0.3768	0.0381	-0.2272	0.2304
50	93	-0.0526	0.4583	0.4613	-0.0089	0.4562	0.4563	0.4646	0.3402	0.5758	-0.3591	0.3318	0.4889	-0.3347	0.3152	0.4599	0.0194	0.0626	0.0948
50	94	-0.1112	0.7802	0.7883	-0.0796	0.7810	0.7850	0.2803	0.9307	0.9749	-0.3930	0.6146	0.7295	-0.3781	0.6285	0.7335	-0.1080	0.8319	0.8411
51	95	-0.1464	1.1383	1.1487	-0.1232	1.2146	1.2206	0.1747	1.7018	1.7106	-0.4120	0.9803	1.0634	-0.4040	1.0370	1.1129	-0.1950	1.3733	1.3871
51	96	-0.2147	1.8495	1.8619	-0.2056	2.0136	2.0241	-0.0272	3.2092	3.2093	-0.4625	1.6764	1.7390	-0.4675	1.8203	1.8794	-0.3696	2.8502	2.8741
52	97	-0.2730	2.3557	2.3715	-0.2764	2.5865	2.6012	-0.2060	4.3372	4.3421	-0.5028	2.1700	2.2275	-0.5193	2.3796	2.4356	-0.5229	3.9552	3.9896
52	98	-0.2806	2.9281	2.9415	-0.2935	3.2359	3.2492	-0.3253	5.6529	5.6823	-0.4722	2.7147	2.7565	-0.4961	2.9966	3.0394	-0.5906	5.2212	5.2545
53	99	-0.2512	3.2409	3.2506	-0.2665	3.5898	3.5997	-0.3390	6.3567	6.3657	-0.4025	3.0018	3.0257	-0.4265	3.3236	3.3509	-0.5487	5.8718	5.8974
53	100	-0.1809	3.4421	3.4469	-0.1926	3.8146	3.8197	-0.2523	6.7751	6.7798	-0.2856	3.1788	3.1916	-0.3033	3.5215	3.5345	-0.3969	6.2379	6.2505
54	101	-0.1043	3.5422	3.5437	-0.1112	3.9281	3.9297	-0.1483	6.9971	6.9987	-0.1618	3.2631	3.2671	-0.1719	3.6170	3.6211	-0.2274	6.4251	6.4281
54	102	-0.0521	3.5690	3.5694	-0.0556	3.9584	3.9588	-0.0746	7.0564	7.0568	-0.0808	3.2852	3.2862	-0.0860	3.6418	3.6428	-0.1142	6.4736	6.4746
55	103	0.0001	3.5799	3.5799	0.0001	3.9674	3.9674	0.0002	7.0751	7.0751	0.0000	3.2916	3.2916	0.0000	3.6491	3.6491	-0.0001	6.4857	6.4857
55	104	0.0523	3.5690	3.5694	0.0558	3.9584	3.9588	0.0750	7.0564	7.0568	0.0808	3.2852	3.2862	0.0859	3.6418	3.6428	0.1141	6.4736	6.4746
56	105	0.1045	3.5422	3.5437	0.1114	3.9281	3.9297	0.1487	6.9970	6.9986	0.1616	3.2632	3.2672	0.1718	3.6170	3.6211	0.2273	6.4252	6.4282
56	106	0.1811	3.4420	3.4468	0.1928	3.8147	3.8196	0.2527	6.7751	6.7798	0.2855	3.1789	3.1917	0.3032	3.5215	3.5345	0.3968	6.2380	6.2506
57	107	0.2514	3.2409	3.2506	0.2667	3.5897	3.5996	0.3394	6.3566	6.3657	0.4024	3.0018	3.0287	0.4265	3.3236	3.3509	0.5486	5.8718	5.8974
57	108	0.2808	2.9280	2.9414	0.2937	3.2358	3.2491	0.3257	5.6527	5.6821	0.4721	2.7148	2.7565	0.4960	2.9966	3.0393	0.5905	5.2213	5.2546
58	109	0.2732	2.3556	2.3714	0.2766	2.5864	2.6011	0.2064	4.3370	4.3419	0.5028	2.1701	2.2276	0.5192	2.3796	2.4356	0.5228	3.9553	3.9897
58	110	0.2149	1.8493	1.8617	0.2058	2.0134	2.0239	0.0276	3.2089	3.2090	0.4624	1.6764	1.7390	0.4675	1.8204	1.8795	0.3995	2.8503	2.8742
59	111	0.1486	1.1391	1.1485	0.1233	1.2143	1.2205	-0.1743	1.7011	1.7100	0.4120	0.9804	1.0635	0.4039	1.0371	1.1130	0.1950	1.3735	1.3873
59	112	0.1114	0.7599	0.7690	0.0798	0.7907	0.7947	-0.2889	0.9303	0.9744	0.3829	0.6147	0.7296	0.3780	0.6286	0.7335	0.1079	0.6322	0.6413
60	113	0.0528	0.4581	0.4611	0.0091	0.4559	0.4560	-0.4642	0.3397	0.5762	0.3590	0.3320	0.4890	0.3346	0.3154	0.4599	-0.0195	0.0828	0.0851
60	114	0.0412	0.2639	0.2671	-0.0080	0.2431	0.2433	-0.5502	-0.0173	0.5505	0.3818	0.1607	0.4142	0.3544	0.1283	0.3769	-0.0382	-0.2269	0.2301
61	115	0.0789	0.1411	0.1617	0.0284	0.1108	0.1144	-0.5298	-0.2224	0.5746	0.4562	0.0657	0.4616	0.4352	0.0159	0.4355	0.0607	-0.3962	0.4005
61	116	0.1876	0.0554	0.1956	0.1471	0.0216	0.1487	-0.3510	-0.3347	0.4850	0.5142	-0.0122	0.5143	0.5071	-0.0533	0.5094	0.3397	-0.4716	0.5812
62	117	0.2868	-0.0169	0.2873	0.2572	-0.0523	0.2625	-0.1613	-0.4161	0.4463	0.7505	-0.0706	0.7538	0.7589	-0.1119	0.7671	0.6101	-0.5246	0.8048
62	118	0.3798	-0.1406	0.4050	0.3620	-0.1792	0.4039	0.0406	-0.5499	0.5514	0.8827	-0.1807	0.9010	0.9082	-0.2236	0.9354	0.8003	-0.6306	1.0993
63	119	0.4262	-0.2810	0.5105	0.4140	-0.3249	0.5263	0.1388	-0.7165	0.7298	0.9551	-0.3124	1.0049	0.9894	-0.3596	1.0528	1.0559	-0.7807	1.3132
63	120	0.4448	-0.5394	0.6991	0.4337	-0.5951	0.7364	0.1683	-1.0477	1.0611	0.9912	-0.5611	1.1390	1.0288	-0.6199	1.2012	1.1242	-1.0976	1.5712
64	121	0.4275	-0.8045	0.9110	0.4138	-0.8729	0.9660	0.1248	-1.3909	1.3965	0.9614	-0.8170	1.2817	0.9950	-0.8881	1.3337	1.0560	-1.4279	1.7760
65	122	0.4557	-1.3633	1.4374	0.4503	-1.4641	1.5318	0.2291	-2.1719	2.1839	0.8989	-1.3448	1.6176	0.9308	-1.4455	1.7192	0.9771	-2.1520	2.3634
66	123	0.5204	-1.9112	1.9808	0.5371	-2.0555	2.1245	0.5211	-3.0595	3.1036	0.8355	-1.8376	2.0186	0.8758	-1.9747	2.1602	1.0217	-2.9195	3.0931
66	124	0.5286	-2.0381	2.1065	0.5503	-2.1946	2.2625	0.5841	-3.2678	3.3383	0.8130	-1.9490	2.1118	0.8553	-2.0962	2.2640	1.0277	-3.1124	3.2777
67	125	0.5303	-2.1589	2.2211	0.5566	-2.3258	2.3916	0.6382	-3.5127	3.5702	0.7856	-2.0529	2.1981	0.8296	-2.2105	2.3610	1.0285	-3.3026	3.4690
67	126	0.5284	-2.2228	2.2843	0.5548	-2.3990	2.4623	0.6610	-3.6411	3.7006	0.7656	-2.1109	2.2485	0.8106	-2.2746	2.4147	1.0232	-3.4123	3.5624
68	127	0.5228	-2.2675	2.3465	0.5533	-2.4709	2.5321	0.6623	-3.7681	3.8294	0.7474	-2.1684	2.2936	0.7929	-2.3382	2.4690	1.0185	-3.5221	3.6664
68	128	0.5157	-2.3550	2.4108	0.5481	-2.5461	2.6044	0.6695	-3.9033	3.9655	0.7243	-2.2285	2.3433	0.7703	-2.4049	2.5253	1.0082	-3.6388	3.7769
69	129	0.5043	-2.4147	2.4668	0.5378	-2.6127	2.6676	0.7062	-4.0243	4.0858	0.6976	-2.2812	2.3685	0.7435	-2.4635	2.5733	0.9892	-3.7425	3.8710
69	130	0.4859	-2.4677	2.5151	0.5199	-2.6721	2.7222	0.6996	-4.1334	4.1922	0.6636	-2.3274	2.4202	0.7087	-2.5150	2.6129	0.9569	-3.8345	3.9521
70	131	0.4633	-2.5122	2.5646	0.4970	-2.7221	2.7671	0.6817	-4.2251	4.2787	0.6259	-2.3658	2.4472	0.6995	-2.5577	2.6439	0.9145	-3.9103	4.0158
70	132	0.4341	-2.5485	2.5852	0.4666	-2.7629	2.8029	0.6501	-4.3012	4.3501	0.5809	-2.3961	2.4655	0.6222	-2.5917	2.6653	0.8581	-3.9710	4.0627
71	133	0.4010	-2.5746	2.6056	0.4317	-2.7923	2.8255	0.6081	-4.3567	4.3969	0.5326	-2.4172	2.4762	0.5711	-2.6152	2.6768	0.7929	-4.0132	4.0908
71	134	0.2730	-2.6149	2.6291	0.2949	-2.8394	2.8547	0.4248	-4.4577	4.4779	0.3595	-2.4465	2.4728	0.3863	-2.6492	2.6772	0.5433	-4.0825	4.1185
72	135	0.1458	-2.6333	2.6373	0.1578	-2.8609	2.8652	0.2303	-4.5036	4.5095	0.1908	-2.4607	2.4691	0.2053	-2.6654	2.6733	0.2910	-4.1131	4.1234
72	136	0.0728	-2.8318	2.8328	0.0789	-2.8599	2.8610	0.1153	-4.5061	4.5076	0.0952	-2.4591	2.4609	0.1025	-2.6641	2.6661	0.1454	-4.1131	4.1157

Table 7.19 Comparison of displacements as a function of elasticity modulus and Poisson's ratio along the free surface of the shotcrete lining for Kisikli south tube (km 1+544)

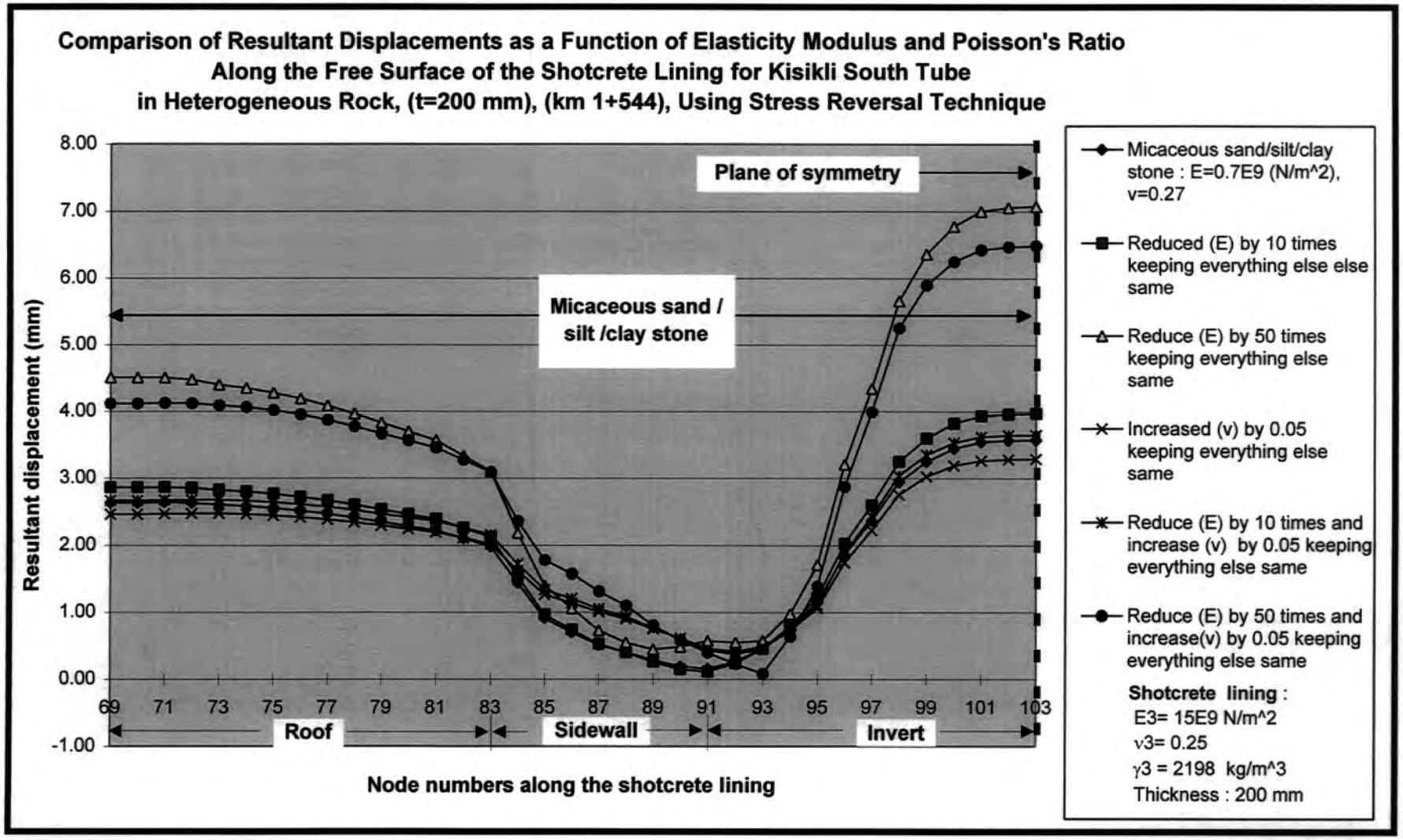

Fig. 7.63 Comparison of displacements as a function of elasticity modulus and Poisson's ratio along the free surface of shotcrete lining for Kisikli south tube (km 1+544)

				KEEP EVERYTHING SAME	REDUCE (E) BY 10 TIMES KEEPING EVERYTHING ELSE SAME	REDUCE (E) BY 50 TIMES KEEPING EVERYTHING ELSE SAME	INCREASE (ν) BY 0.05 KEEPING EVERYTHING ELSE SAME	REDUCE (E) BY 10 TIMES AND INCREASE (ν) BY 0.05 KEEPING EVERYTHING ELSE SAME	REDUCE (E) BY 50 TIMES AND INCREASE (ν) BY 0.05 KEEPING EVERYTHING ELSE SAME
				STRESS REVERSAL TECHNIQUE	STRESS REVERSAL TECHNIQUE	STRESS REVERSAL TECHNIQUE	STRESS REVERSAL TECHNIQUE	STRESS REVERSAL TECHNIQUE	STRESS REVERSAL TECHNIQUE
				Lithology=Neogene cover	Lithology=Neogene cover	Lithology=Neogene cover	Lithology=Neogene cover	Lithology=Neogene cover	Lithology=Neogene cover
				E=90E6 (N/m^2)	E=81E6 (N/m^2)	E=45E6 (N/m^2)	E=90E6 (N/m^2)	E=81E6 (N/m^2)	E=45E6 (N/m^2)
				ν=0.35, γ=2060 (kg/m^3)	ν=0.35, γ=2060 (kg/m^3)	ν=0.35, γ=2060 (kg/m^3)	ν=0.40, γ=2060 (kg/m^3)	ν=0.40, γ=2060 (kg/m^3)	ν=0.40, γ=2060 (kg/m^3)
				Lithology=Quartzite	Lithology=Quartzite	Lithology=Quartzite	Lithology=Quartzite	Lithology=Quartzite	Lithology=Quartzite
				E=68E9 (N/m^2)	E=61.2E9 (N/m^2)	E=34E9 (N/m^2)	E=68E9 (N/m^2)	E=61.2E9 (N/m^2)	E=34E9 (N/m^2)
				ν=0.16, γ=2600 (kg/m^3)	ν=0.16, γ=2600 (kg/m^3)	ν=0.16, γ=2600 (kg/m^3)	ν=0.21, γ=2600 (kg/m^3)	ν=0.21, γ=2600 (kg/m^3)	ν=0.21, γ=2600 (kg/m^3)
		(TUNNEL EXCAVATION) →		Lith.=Sand, silt, clay stone	Lith.=Sand, silt, clay stone	Lith.=Sand, silt, clay stone	Lith.=Sand, silt, clay stone	Lith.=Sand, silt, clay stone	Lith.=Sand, silt, clay stone
				E=0.7E9 (N/m^2)	E=0.63E9 (N/m^2)	E=0.35E9 (N/m^2)	E=0.7E9 (N/m^2)	E=0.63E9 (N/m^2)	E=0.35E9 (N/m^2)
KISIKLI SOUTH TUBE				ν=0.27, γ=2200 (kg/m^3)	ν=0.27, γ=2200 (kg/m^3)	ν=0.27, γ=2200 (kg/m^3)	ν=0.32, γ=2200 (kg/m^3)	ν=0.32, γ=2200 (kg/m^3)	ν=0.32, γ=2200 (kg/m^3)
WITH SHOTCRETE LINING				Lithology=Arkose	Lithology=Arkose	Lithology=Arkose	Lithology=Arkose	Lithology=Arkose	Lithology=Arkose
t = 200 mm				E=15E9 (N/m^2)	E=13.5E9 (N/m^2)	E=7.5E9 (N/m^2)	E=1.9E9 (N/m^2)	E=13.5E9 (N/m^2)	E=7.5E9 (N/m^2)
HETEROGENEOUS MODEL				ν=0.26, γ=2600 (kg/m^3)	ν=0.26, γ=2600 (kg/m^3)	ν=0.26, γ=2600 (kg/m^3)	ν=0.31, γ=2600 (kg/m^3)	ν=0.31, γ=2600 (kg/m^3)	ν=0.31, γ=2600 (kg/m^3)
km 1+544									
		MEASURED TUNNEL		COMPUTED TUNNEL	COMPUTED TUNNEL	COMPUTED TUNNEL	COMPUTED TUNNEL	COMPUTED TUNNEL	COMPUTED TUNNEL
	MEASURMENTS	CONVERGENCE		CONVERGENCE	CONVERGENCE	CONVERGENCE	CONVERGENCE	CONVERGENCE	CONVERGENCE
ARRAY	ALONG	TOTAL (mm)	ARRAY	TOTAL (mm)	TOTAL (mm)	TOTAL (mm)	TOTAL (mm)	TOTAL (mm)	TOTAL (mm)
A1-B2	DIAGONAL	-0.50	69(Ud), 122(Ud)	-1.0290	-1.0880	-1.3660	-1.3357	-1.4153	-1.8270
A1-C3	DIAGONAL	-0.15	69(Ud), 84(Ud)	-1.0290	-1.0880	-1.3660	-1.3357	-1.4153	-1.8270
B2-C3	HORIZONTAL	-0.45	84(Ux), 122(Ux)	-0.9113	-0.9005	-0.4580	-1.7978	-1.8612	-1.9543

Table 7.20 Comparison of measured and computed displacements along the shotcrete lining for Kisikli south tube (km 1+544)

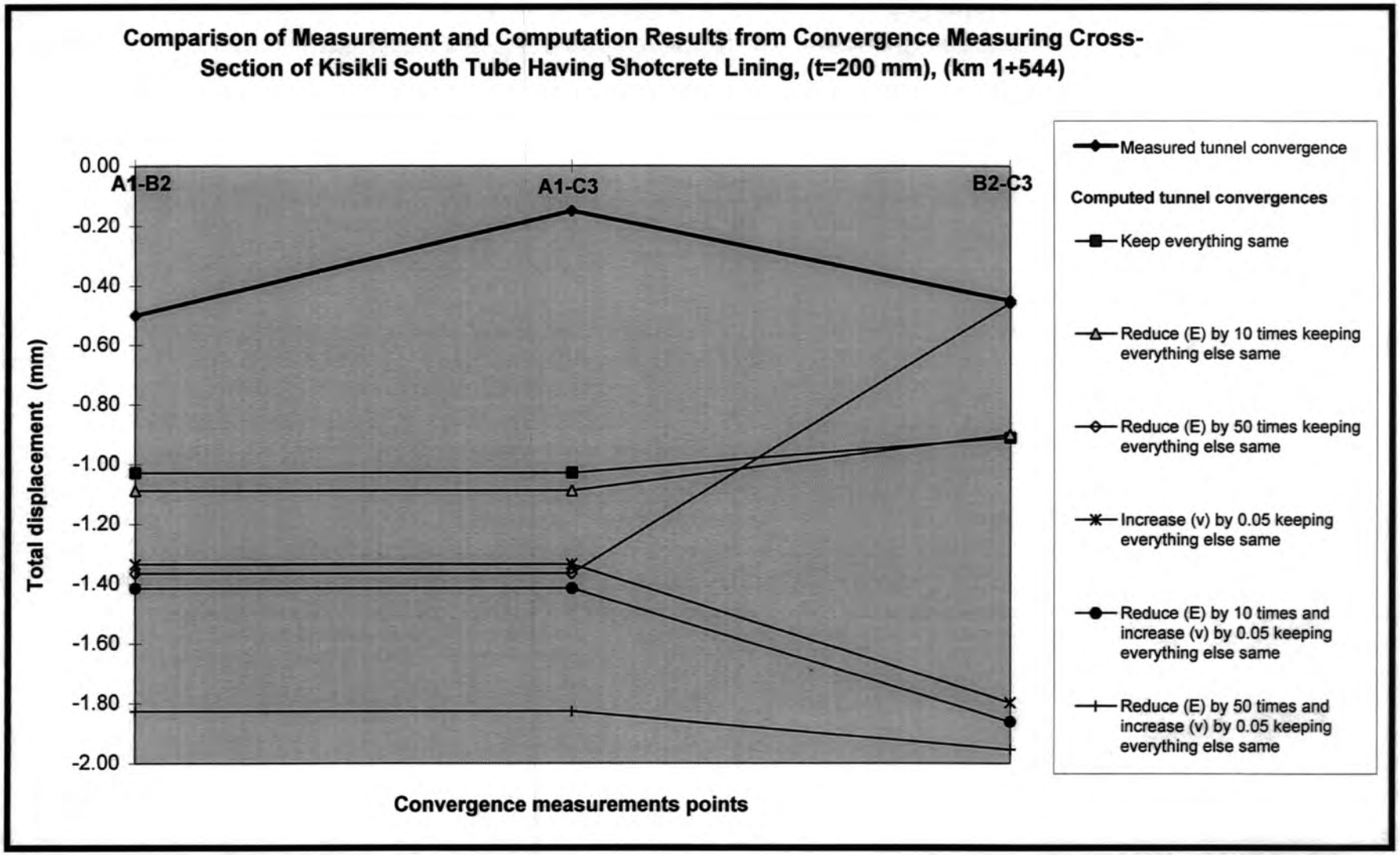

Fig. 7.64 Comparison of measured and computed displacements along the free surface of the shotcrete lining for Kisikli south tube (km 1+544)

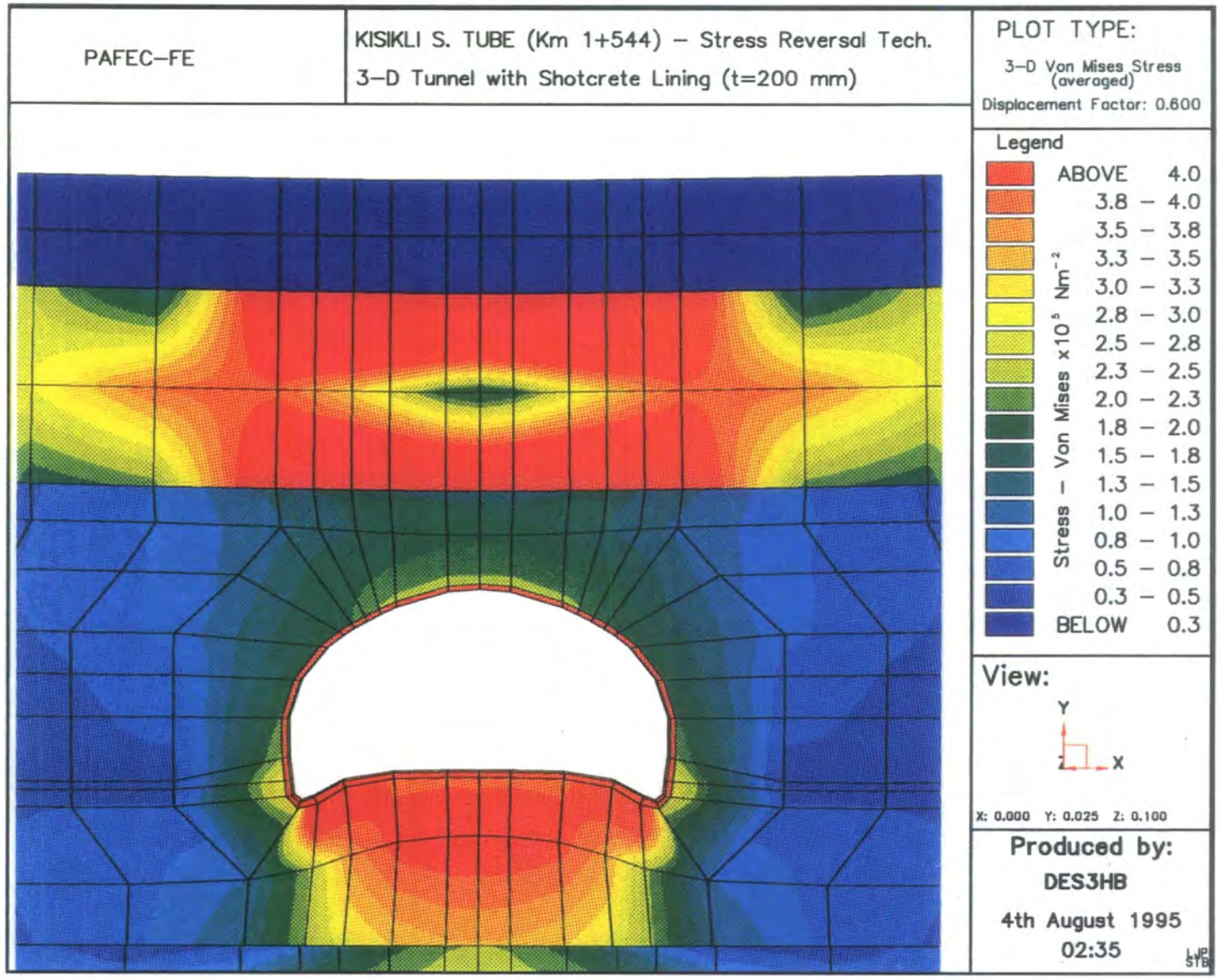

Fig. 7.65 Colour stress and displaced shape diagrams of Kisikli south tube, (km 1+544), having shotcrete lining (t=200 mm)

7.3.3.3 Analysis with Anchorages and Steel Arches

The anchorage (rock bolt) and steel arch options are defined in Chapter 5. Addition or removal of rock bolts and steel arches from their sections in the tunnel is done automatically by adding or removing their entries from the input data file, as shown in Table 5.1. The three-dimensional model of Kisikli south tube having a 350 mm length of half period at km 1+544 was used for the analysis of the anchorages and steel arch performance using the stress reversal technique. The results of this analysis are presented in Figs. 7.66 to 7.70 and are summarised in Tables 7.21 and 7.22.

Table 7.21 shows a comparison of Von Mises stresses along the free surface of the shotcrete lining before and after installation of anchorages and steel arches. These results are also shown graphically in Fig. 7.66. Table 7.22 shows a comparison of component and resultant displacements along the free surface of the shotcrete lining before and after installation of anchorages and steel arches for this section. The same results are presented in Fig. 7.67 for visual comparison.

A maximum Von Mises stress of 13.3 MN/m^2 and a resultant displacement of 1.78 mm have been found along the free boundary of the shotcrete lining after application of anchorages and steel arch, whereas a maximum Von Mises stress and a resultant displacement of 0.403 MN/m^2 and 1.44 mm were noted along the interface between the excavation surface and the shotcrete lining respectively. A maximum Von Mises stress of 0.759 MN/m^2 and a resultant displacement of 3.95 mm have been found along the unsupported excavation surface for the fully excavated tunnel as shown in Figs. 7.55 and 7.56 respectively.

Comparison between the steel arch supported and unsupported sections shows larger tensile stresses in the roof of the tunnel for the latter. The stress distributions also show that an extensive area in the invert of tunnel is subjected to tensile stresses. The highest compressive stresses in all cases occur in the side walls. It can be seen that both the magnitude and the extent (area) of the Von Mises stress zone and resultant displacements along the interface between the excavation surface and the shotcrete lining of the tunnel are decreased by factors of

approximately 0.47 and 0.63 respectively, as result of the presence of the anchorages and steel arches.

Computed stress colour diagrams and displacements are presented in Fig. 7.68 to 7.70 for the front and back views of the Kisikli south tube three-dimensional model having steel arches and anchorages. Fig. 7.68 shows the Von Mises stress distribution in colour and deformed shape of the front view of the tunnel under the action of gravity after installation of anchorages and steel arch. Figs. 7.69 and 7.70 show similar more detailed front and back views of the tunnel with its support systems. In each example the zones of increased stress are indicated on each colour diagram, by change in colour from red to blue indicating the reduction in field stress away from the tunnel excavation boundary.

KISIKLI SOUTH TUBE				
km 1+544			THREE-DIMENSIONAL MODEL	THREE-DIMENSIONAL MODEL
STRESS REVERSAL TECHNIQUE			HAVING SHOTCRETE LINING	HAVING SHOTCRETE LINING,
Number of nodes = 3498				ANCHORAGES AND STEEL ARCH
Number of elements = 444				
Number of d.o.f = 6798				AVERAGED
Thickness of shotcrete lining = 200 mm			AVERAGED	VON MISES STRESS (N/m^2)
	ELEMENT	NODE	VON MISES	ALONG THE
	NUMBER	NUMBER	STRESS (N/m^2)	SHOTCRETE LINING
COMPUTED	ALONG THE	ALONG THE	ALONG THE	FREE SURFACE
RESULT	SHOTCRETE	SHOTCRETE	SHOTCRETE LINING	HAVING ANCHORAGES
LOCATIONS	LINING	LINING	FREE SURFACE	AND STEEL ARCH
1	37	69	1.71E+06	1.08E+06
2	37	70	1.74E+06	1.06E+06
3	38	71	1.70E+06	1.13E+06
4	38	72	1.80E+06	1.18E+06
5	39	73	1.85E+06	1.40E+06
6	39	74	1.88E+06	1.49E+06
7	40	75	1.94E+06	1.58E+06
8	40	76	2.04E+06	1.71E+06
9	41	77	2.11E+06	1.82E+06
10	41	78	2.25E+06	1.97E+06
11	42	79	2.38E+06	2.09E+06
12	42	80	2.61E+06	2.40E+06
13	43	81	2.69E+06	2.65E+06
14	43	82	2.88E+06	2.90E+06
15	44	83	3.11E+06	3.30E+06
16	45	84	3.95E+06	4.71E+06
17	46	85	4.55E+06	5.67E+06
18	46	86	4.43E+06	5.84E+06
19	47	87	4.29E+06	6.03E+06
20	47	88	4.09E+06	5.96E+06
21	48	89	3.83E+06	5.79E+06
22	48	90	4.59E+06	7.57E+06
23	49	91	5.62E+06	1.07E+07
24	49	92	7.95E+06	1.22E+07
25	50	93	7.04E+06	1.33E+07
26	50	94	6.17E+06	8.94E+06
27	51	95	2.57E+06	5.27E+06
28	51	96	1.27E+06	2.05E+06
29	52	97	9.16E+05	2.07E+06
30	52	98	1.10E+06	1.98E+06
31	53	99	1.22E+06	1.82E+06
32	53	100	1.20E+06	1.86E+06
33	54	101	1.25E+06	1.81E+06
34	54	102	1.27E+06	1.84E+06
35	55	103	1.28E+06	1.80E+06
36	55	104	1.27E+06	1.84E+06
37	56	105	1.25E+06	1.81E+06
38	56	106	1.20E+06	1.86E+06
39	57	107	1.22E+06	1.82E+06
40	57	108	1.10E+06	1.98E+06
41	58	109	9.15E+05	2.07E+06
42	58	110	1.27E+06	2.05E+06
43	59	111	2.57E+06	5.27E+06
44	59	112	6.17E+06	8.93E+06
45	60	113	7.04E+06	1.33E+07
46	60	114	7.95E+06	1.22E+07
47	61	115	5.62E+06	1.07E+07
48	61	116	4.59E+06	7.57E+06
49	62	117	3.83E+06	5.79E+06
50	62	118	4.09E+06	5.96E+06
51	63	119	4.29E+06	6.03E+06
52	63	120	4.44E+06	5.84E+06
53	64	121	4.55E+06	5.67E+06
54	65	122	3.95E+06	4.71E+06
55	66	123	3.11E+06	3.30E+06
56	66	124	2.88E+06	2.90E+06
57	67	125	2.69E+06	2.65E+06
58	67	126	2.61E+06	2.40E+06
59	68	127	2.38E+06	2.09E+06
60	68	128	2.25E+06	1.96E+06
61	69	129	2.11E+06	1.82E+06
62	69	130	2.04E+06	1.71E+06
63	70	131	1.94E+06	1.57E+06
64	70	132	1.88E+06	1.49E+06
65	71	133	1.85E+06	1.40E+06
66	71	134	1.80E+06	1.18E+06
67	72	135	1.70E+06	1.13E+06
68	72	136	1.74E+06	1.06E+06

Table 7.21 Comparison of stresses along free surface of the shotcrete lining before and after installation of anchorages and steel arch for Kisikli south tube (km 1+544)

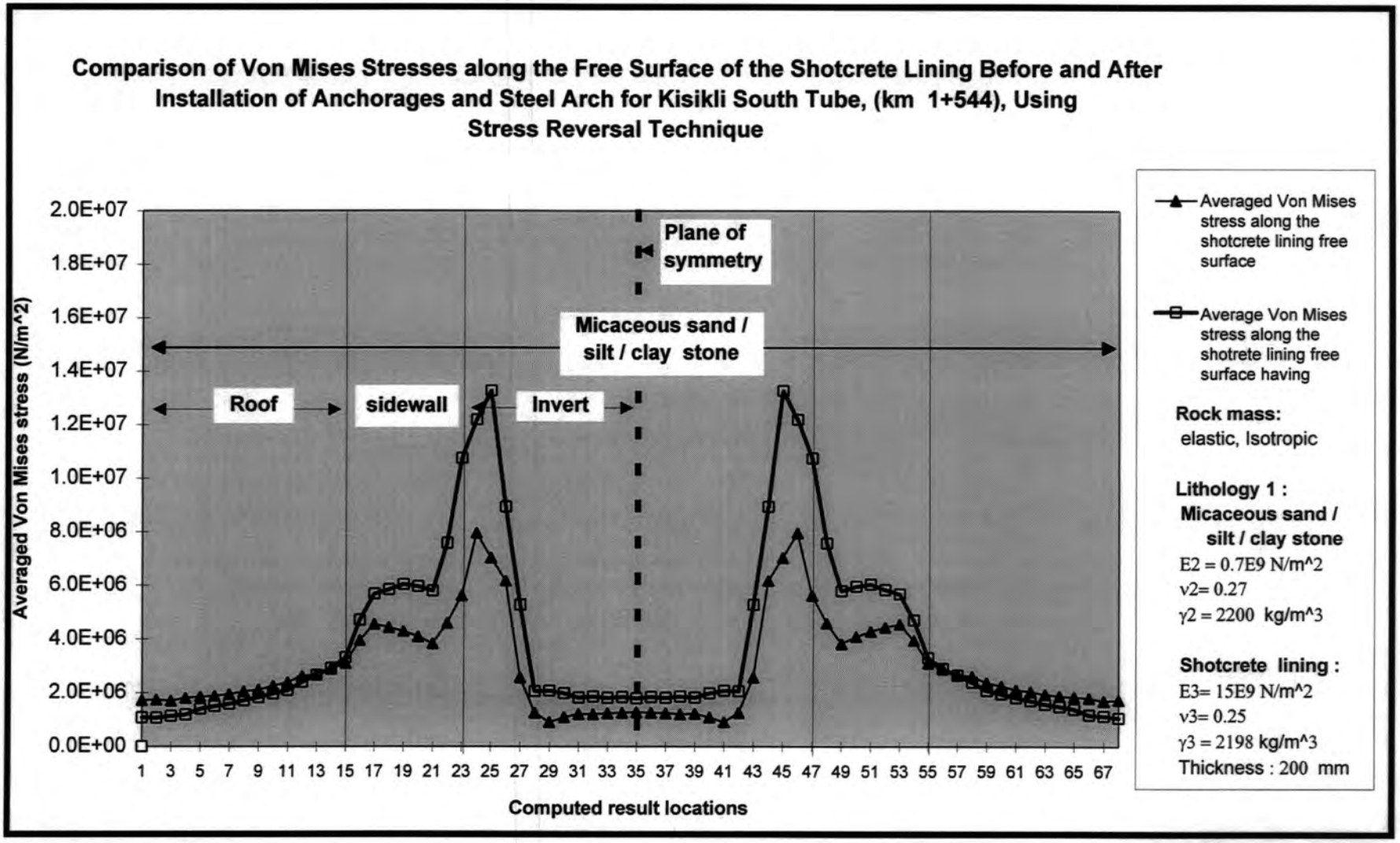

Fig. 7.66 Comparison of stresses along the free surface of the shotcrete lining before and after installation of anchorages and steel arch for Kisikli south tube (km 1+544)

KISIKLI SOUTH TUBE											
km 1+644											
STRESS REVERSAL TECHNIQUE											
Number of nodes = 3498			THREE-DIMENSIONAL MODEL					THREE-DIMENSIONAL MODEL			
Number of elements = 532			HAVING SHOTCRETE LINING					HAVING SHOTCRETE LINING,			
Number of d.o.f = 6793								ANCHORAGES AND STEEL ARCH			
Thickness of shotcrete lining = 200 mm											
	ELEMENT	NODE				ELEMENT	NODE	DISPLACEMENT (mm)			
	NUMBER	NUMBER	DISPLACEMENT (mm)			NUMBER	NUMBER	ALONG THE SHOTCRETE LINING			
COMPUTED	ALONG THE	ALONG THE	ALONG THE SHOTCRETE LINING			ALONG THE	ALONG THE	HAVING ANCHORAGES AND STEEL ARC			
RESULT	SHOTCRETE	SHOTCRETE				SHOTCRETE	SHOTCRETE				
LOCATIONS	LINING	LINING	Ux	Uy	U	LINING	LINING	Ux	Uy	U	
1	37	69	0.0000	-2.6442	**2.6442**	37	69	0.0000	-1.2392	**1.2392**	
2	37	70	-0.0731	-2.6441	**2.6451**	37	70	-0.0341	-1.2379	**1.2384**	
3	38	71	-0.1463	-2.6453	**2.6493**	38	71	-0.0690	-1.2337	**1.2356**	
4	38	72	-0.2741	-2.6269	**2.6412**	38	72	-0.1397	-1.2169	**1.2249**	
5	39	73	-0.4030	-2.5867	**2.6179**	39	73	-0.2226	-1.1845	**1.2052**	
6	39	74	-0.4362	-2.5607	**2.5976**	39	74	-0.2532	-1.1701	**1.1972**	
7	40	75	-0.4656	-2.5242	**2.5668**	40	75	-0.2852	-1.1534	**1.1881**	
8	40	76	-0.4885	-2.4795	**2.5272**	40	76	-0.3174	-1.1350	**1.1785**	
9	41	77	-0.5073	-2.4264	**2.4789**	41	77	-0.3507	-1.1142	**1.1681**	
10	41	78	-0.5192	-2.3668	**2.4231**	41	78	-0.3845	-1.0915	**1.1572**	
11	42	79	-0.5265	-2.2992	**2.3587**	42	79	-0.4190	-1.0664	**1.1458**	
12	42	80	-0.5305	-2.2344	**2.2965**	42	80	-0.4507	-1.0414	**1.1347**	
13	43	81	-0.5350	-2.1684	**2.2334**	43	81	-0.4833	-1.0134	**1.1227**	
14	43	82	-0.5341	-2.0496	**2.1180**	43	82	-0.5438	-0.9545	**1.0985**	
15	44	83	-0.5266	-1.9223	**1.9931**	44	83	-0.6040	-0.8881	**1.0740**	
16	45	84	-0.4656	-1.3713	**1.4482**	45	84	-0.8447	-0.4842	**0.9736**	
17	46	85	-0.4377	-0.8069	**0.9180**	46	85	-0.9909	0.0951	**0.9955**	
18	46	86	-0.4549	-0.5384	**0.7048**	46	86	-1.0065	0.4181	**1.0899**	
19	47	87	-0.4357	-0.2768	**0.5162**	47	87	-0.9865	0.7475	**1.2377**	
20	47	88	-0.3893	-0.1346	**0.4119**	47	88	-0.9573	0.9432	**1.3439**	
21	48	89	-0.2970	-0.0087	**0.2971**	48	89	-0.9148	1.1402	**1.4618**	
22	48	90	-0.1981	0.0647	**0.2084**	48	90	-0.8787	1.2719	**1.5459**	
23	49	91	-0.0893	0.1511	**0.1755**	49	91	-0.8309	1.4212	**1.6463**	
24	49	92	-0.0496	0.2746	**0.2790**	49	92	-0.7766	1.5303	**1.7161**	
25	50	93	-0.0611	0.4700	**0.4740**	50	93	-0.6961	1.6214	**1.7645**	
26	50	94	-0.1181	0.7710	**0.7800**	50	94	-0.6280	1.6665	**1.7809**	
27	51	95	-0.1524	1.1505	**1.1605**	51	95	-0.5812	1.6823	**1.7799**	
28	51	96	-0.2200	1.8587	**1.8717**	51	96	-0.5405	1.6899	**1.7742**	
29	52	97	-0.2774	2.3621	**2.3783**	52	97	-0.4812	1.7006	**1.7674**	
30	52	98	-0.2832	2.9325	**2.9461**	52	98	-0.3778	1.7198	**1.7608**	
31	53	99	-0.2534	3.2452	**3.2551**	53	99	-0.2818	1.7340	**1.7567**	
32	53	100	-0.1826	3.4454	**3.4502**	53	100	-0.1883	1.7454	**1.7555**	
33	54	101	-0.1056	3.5426	**3.5442**	54	101	-0.1004	1.7519	**1.7548**	
34	54	102	-0.0528	3.5680	**3.5684**	54	102	-0.0500	1.7535	**1.7542**	
35	55	103	-0.0001	3.5757	**3.5757**	55	103	-0.0001	1.7541	**1.7541**	
36	55	104	0.0527	3.5680	**3.5684**	55	104	0.0499	1.7535	**1.7542**	
37	56	105	0.1055	3.5426	**3.5442**	56	105	0.1003	1.7519	**1.7548**	
38	56	106	0.1825	3.4454	**3.4502**	56	106	0.1882	1.7454	**1.7555**	
39	57	107	0.2533	3.2452	**3.2551**	57	107	0.2817	1.7340	**1.7567**	
40	57	108	0.2831	2.9326	**2.9462**	57	108	0.3777	1.7198	**1.7608**	
41	58	109	0.2773	2.3621	**2.3783**	58	109	0.4811	1.7006	**1.7673**	
42	58	110	0.2199	1.8587	**1.8717**	58	110	0.5404	1.6899	**1.7742**	
43	59	111	0.1523	1.1505	**1.1605**	59	111	0.5811	1.6823	**1.7798**	
44	59	112	0.1180	0.7710	**0.7800**	59	112	0.6279	1.6665	**1.7809**	
45	60	113	0.0609	0.4700	**0.4739**	60	113	0.6959	1.6214	**1.7644**	
46	60	114	0.0494	0.2746	**0.2790**	60	114	0.7765	1.5303	**1.7160**	
47	61	115	0.0891	0.1511	**0.1754**	61	115	0.8308	1.4212	**1.6462**	
48	61	116	0.1979	0.0647	**0.2082**	61	116	0.8786	1.2719	**1.5459**	
49	62	117	0.2968	-0.0087	**0.2969**	62	117	0.9146	1.1402	**1.4617**	
50	62	118	0.3891	-0.1346	**0.4117**	62	118	0.9572	0.9432	**1.3438**	
51	63	119	0.4356	-0.2768	**0.5161**	63	119	0.9884	0.7475	**1.2376**	
52	63	120	0.4547	-0.5385	**0.7048**	63	120	1.0063	0.4181	**1.0897**	
53	64	121	0.4376	-0.8070	**0.9180**	64	121	0.9908	0.0950	**0.9953**	
54	65	122	0.4655	-1.3714	**1.4483**	65	122	0.8446	-0.4843	**0.9736**	
55	66	123	0.5266	-1.9225	**1.9933**	66	123	0.6039	-0.8882	**1.0741**	
56	66	124	0.5341	-2.0497	**2.1181**	66	124	0.5437	-0.9545	**1.0985**	
57	67	125	0.5349	-2.1685	**2.2335**	67	125	0.4832	-1.0135	**1.1228**	
58	67	126	0.5305	-2.2345	**2.2966**	67	126	0.4506	-1.0414	**1.1347**	
59	68	127	0.5265	-2.2993	**2.3588**	68	127	0.4189	-1.0664	**1.1457**	
60	68	128	0.5191	-2.3669	**2.4232**	68	128	0.3844	-1.0915	**1.1572**	
61	69	129	0.5072	-2.4265	**2.4789**	69	129	0.3507	-1.1143	**1.1682**	
62	69	130	0.4885	-2.4796	**2.5273**	69	130	0.3173	-1.1350	**1.1785**	
63	70	131	0.4656	-2.5242	**2.5668**	70	131	0.2851	-1.1534	**1.1881**	
64	70	132	0.4362	-2.5608	**2.5977**	70	132	0.2532	-1.1701	**1.1972**	
65	71	133	0.4029	-2.5867	**2.6179**	71	133	0.2225	-1.1845	**1.2052**	
66	71	134	0.2741	-2.6270	**2.6413**	71	134	0.1397	-1.2169	**1.2249**	
67	72	135	0.1462	-2.6453	**2.6493**	72	135	0.0690	-1.2337	**1.2356**	
68	72	136	0.0731	-2.6441	**2.6451**	72	136	0.0341	-1.2379	**1.2384**	

Table 7.22 Comparison of displacements along the free surface of the shotcrete lining before and after installation of anchorages and steel arch for Kisikli south tube (km 1+544)

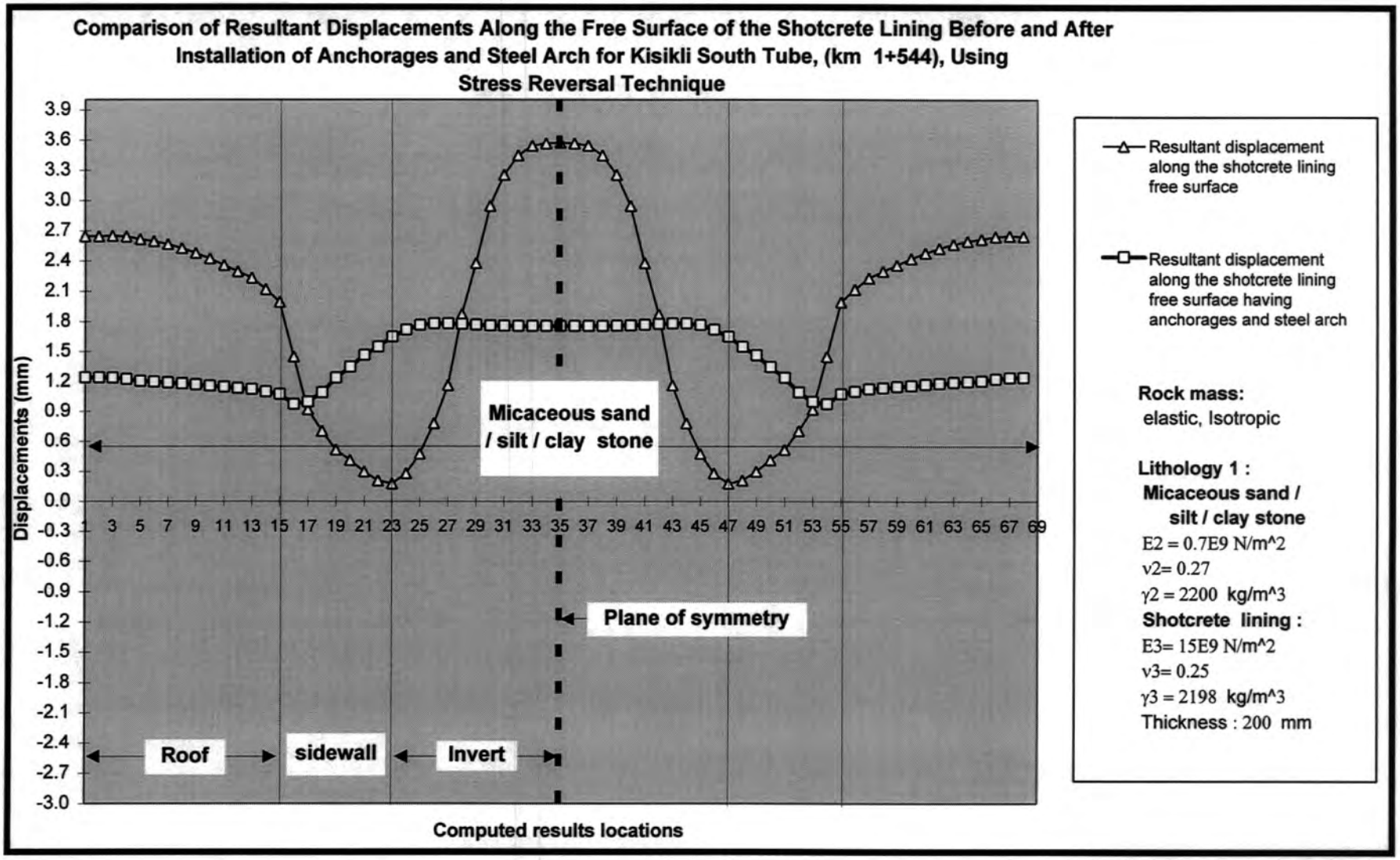

Fig. 7.67 Comparison of displacements along the free surface of the shotcrete lining before and after installation of anchorages and steel arch for Kisikli north tube (km 1+544)

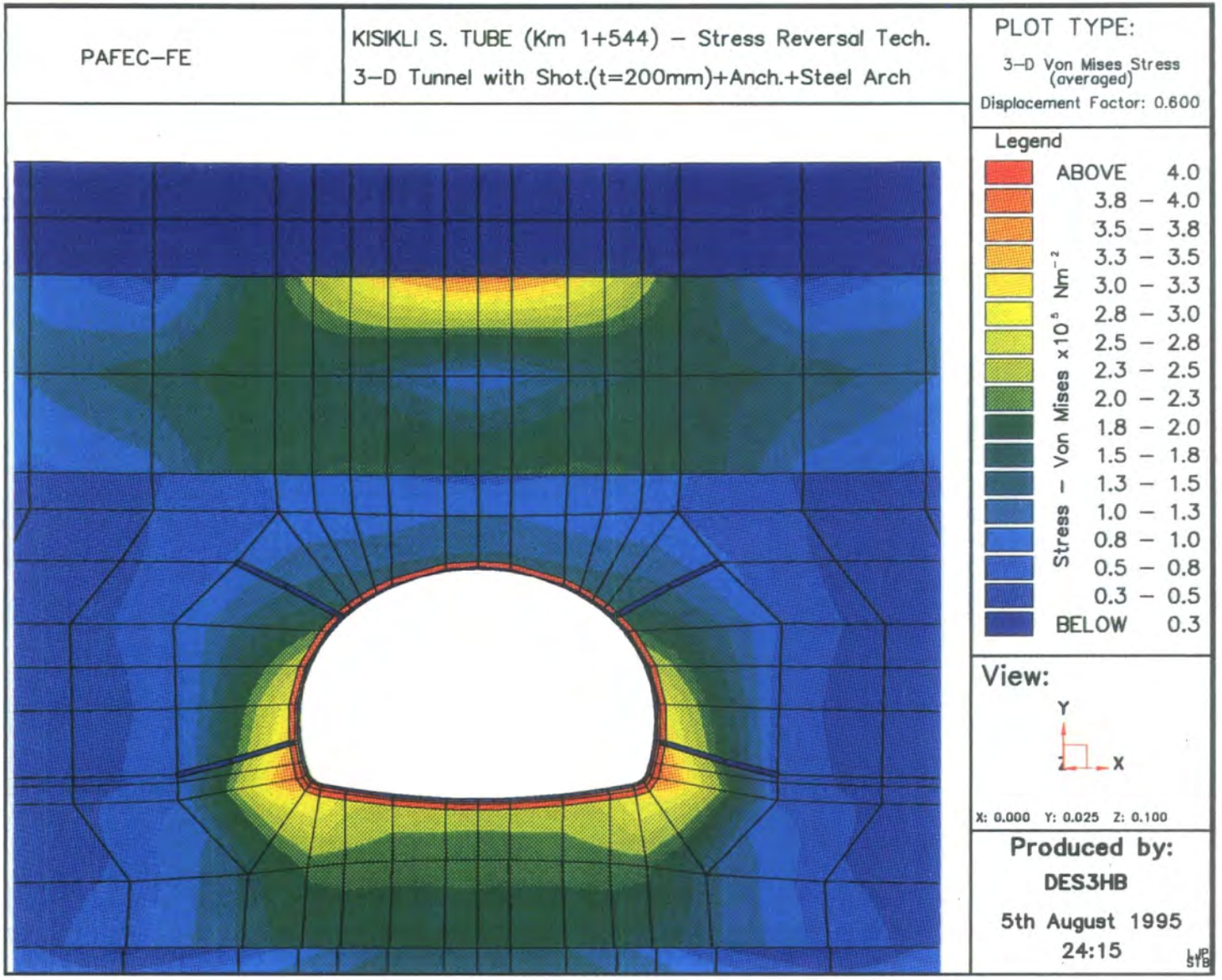

Fig. 7.68 Colour stress and displaced shape diagrams of Kisikli south tube ,(km 1+544), having shotcrete lining, anchorages and steel arch

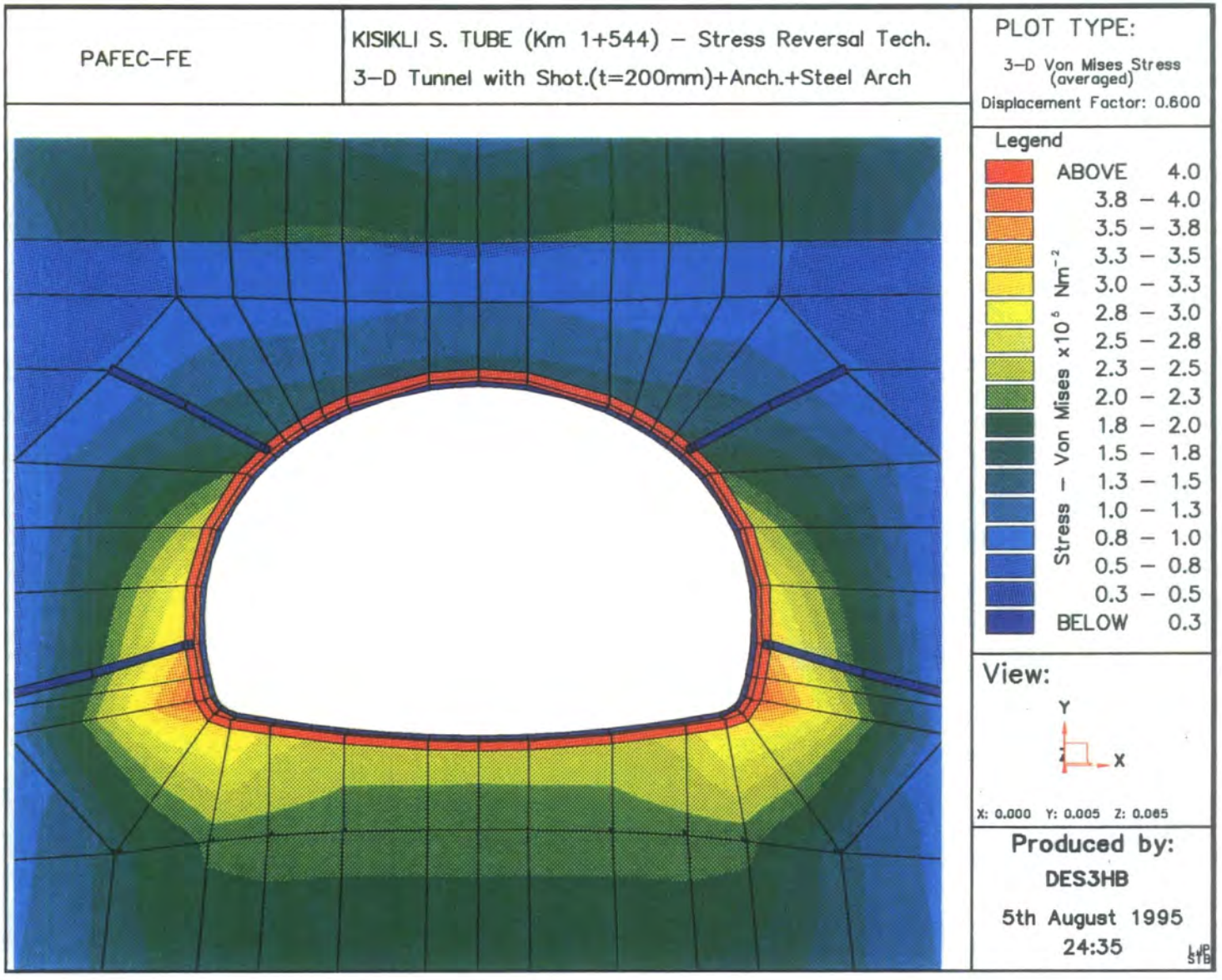

Fig. 7.69 Front view of colour stress and displaced shape diagrams of Kisikli south tube, (km 1+544), having shotcrete lining, anchorages and steel arch

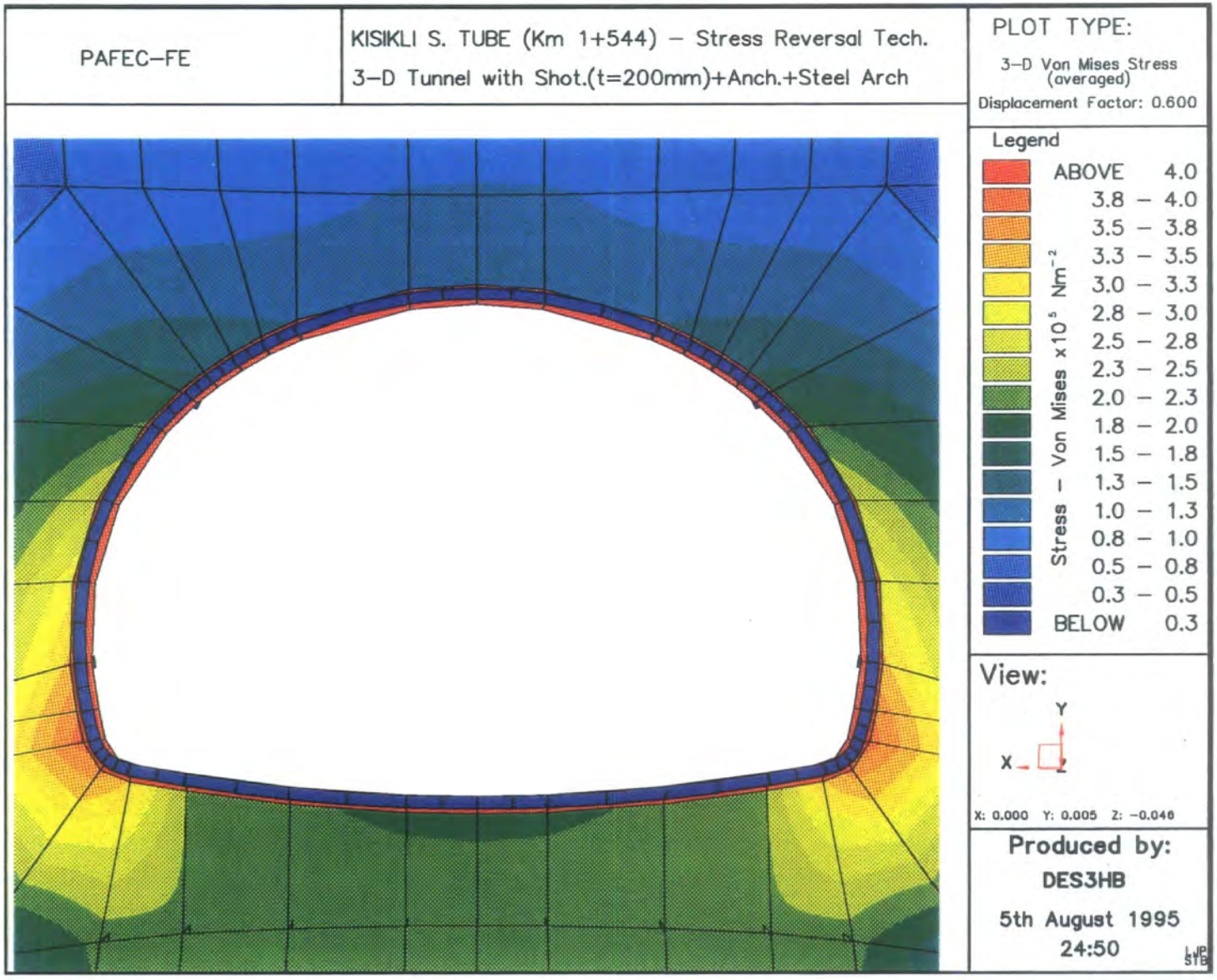

Fig. 7.70 Back view of colour stress and displaced shape diagrams of Kisikli south tube, (km 1+544), having shotcrete lining, anchorages and steel arch

7.3.3.4 Analysis with Inner Lining

The presence of the 500 mm inner concrete lining alters considerably the size and position of the stress and displacement distributions around the tunnel. The stresses and displacements along the inner lining are shown in Figs. 7.71 to 7.76 and are summarised in Tables 7.23 and 7.24.

Table 7.23 shows a comparison of the Von Mises stresses along the free surface of the shotcrete lining for Kisikli south tube at km 1+544 after installation of the inner lining. The same results are presented in Fig. 7.71. A comparison of the component and resultant displacements at nodes along the free surface of the inner lining is shown in Table 7.24. These results are also illustrated in Fig 7.72 for visual comparison. Fig. 7.73 shows a comparison of the Von Mises stresses and displacements along the free surface of the inner lining. This figure illustrates the relative changes in Von Mises stresses and displacements. It can be seen that where the displacements is high the resulting stress is low, and also when the displacement is low, the resulting stress is high.

A maximum Von Mises stress of 4.91 MN/m^2 and a maximum resultant displacement of 1.16 mm have been found along the inner lining, whereas a maximum Von Mises stress and a resultant displacement of 0.199 MN/m^2 and 0.047 mm, respectively, appear along the interface between the excavation surface and the shotcrete lining. These compare with a maximum Von Mises stress of 0.759 MN/m^2 and a resultant displacement of 3.95 mm along the unsupported excavation surface for the fully excavated Kisikli south tube at km 1+544 as shown in Figs. 7.55 and 7.56 respectively.

It can be seen that both the magnitude and the extent (area) of the Von Mises stress zone and resultant displacements along the interface between excavation surface and shotcrete lining of the tunnel are decreased by a factor of approximately 0.73 and 0.99 respectively, as result of the presence of the anchorages, steel arches and the inner lining.

The redistribution of stresses resulting from the installation of the anchorages, steel arches and inner lining indicated the increased resistance to movement produced by the presence of the these support systems, as shown in the colour diagrams of Figs. 7.74 to 7.76 for the Kisikli south tube three- dimensional model. Fig. 7.74 shows the Von Mises stress distribution in colour and deformed shape of the front view of the tunnel under the action of gravity after installation of anchorages, steel arches and inner lining. Figs. 7.75 and 7.76 show similar detailed front and back views of the tunnel with these support systems respectively. In each example the zones of increased stress are indicated on each colour diagram by a change in colour from red to blue indicating the reduction in field stress away from the tunnel excavation boundary.

Comparison of stress colour diagrams presented in Fig. 7.65 of the tunnel having a shotcrete lining and Fig. 7.74 of the tunnel having an inner lining show the influence of the inner lining. Looking particularly at the Von Mises stresses as shown in Fig. 7.65 the area above the roof and the invert of the tunnel are subjected to tensile stresses. When the tunnel is lined with permanent concrete the magnitude of these stresses is greatly reduced. The area of high stresses is largely changed after application of the inner lining as shown in Figs. 7.74 to 7.76.

Finally, a view of the Kisikli south tube at km 1+544, showing in colour the rock strata and support systems after completion of construction, is presented in Fig. 7.77.

	STRESS REVERSAL TECHNIQUE			*STRESS REVERSAL TECHNIQUE*		
	Number of nodes = 3498			*Number of nodes = 3498*		
	Number of elements = 532			*Number of elements = 532*		
	Number of d.o.f = 6793			*Number of d.o.f = 6973*		
				KISIKLI SOUTH TUBE (km 1+544)		
	KISIKLI SOUTH TUBE (km 1+544)			HAVING SHOTCRETE LINING (t=200 mm),		
	HAVING SHOTCRETE LINING (t=200 mm),			ANCHORAGES, STEEL ARCH		
				AND INNER LINING (t= 500 mm)		
			AVERAGED			AVERAGED
	ELEMENT	NODE	VON MISES	ELEMENT	NODE	VON MISES
	NUMBER	NUMBER	STRESS (N/m^2)	NUMBER	NUMBER	STRESS (N/m^2)
COMPUTED	ALONG THE	ALONG THE	ALONG THE	ALONG THE	ALONG THE	ALONG THE
RESULT	SHOTCRETE	SHOTCRETE	SHOTCRETE LINING	INNER	INNER	INNER LINING
LOCATIONS	LINING	LINING	FREE SURFACE	LINING	LINING	FREE SURFACE
1	37	69	1.71E+06	1	1	7.74E+05
2	37	70	1.74E+06	1	2	8.10E+05
3	38	71	1.70E+06	2	3	8.31E+05
4	38	72	1.80E+06	2	4	1.04E+06
5	39	73	1.85E+06	3	5	1.29E+06
6	39	74	1.88E+06	3	6	1.38E+06
7	40	75	1.94E+06	4	7	1.45E+06
8	40	76	2.04E+06	4	8	1.53E+06
9	41	77	2.11E+06	5	9	1.61E+06
10	41	78	2.25E+06	5	10	1.74E+06
11	42	79	2.38E+06	6	11	1.86E+06
12	42	80	2.61E+06	6	12	1.94E+06
13	43	81	2.69E+06	7	13	1.99E+06
14	43	82	2.88E+06	7	14	2.18E+06
15	44	83	3.11E+06	8	15	2.44E+06
16	45	84	3.95E+06	9	16	3.21E+06
17	46	85	4.55E+06	10	17	3.69E+06
18	46	86	4.43E+06	10	18	3.74E+06
19	47	87	4.29E+06	11	19	3.80E+06
20	47	88	4.09E+06	11	20	3.72E+06
21	48	89	3.83E+06	12	21	3.62E+06
22	48	90	4.59E+06	12	22	3.89E+06
23	49	91	5.62E+06	13	23	4.53E+06
24	49	92	7.95E+06	13	24	4.91E+06
25	50	93	7.04E+06	14	25	4.55E+06
26	50	94	6.17E+06	14	26	3.85E+06
27	51	95	2.57E+06	15	27	2.76E+06
28	51	96	1.27E+06	15	28	1.80E+06
29	52	97	9.16E+05	16	29	9.75E+05
30	52	98	1.10E+06	16	30	1.30E+06
31	53	99	1.22E+06	17	31	1.27E+06
32	53	100	1.20E+06	17	32	1.17E+06
33	54	101	1.25E+06	18	33	1.09E+06
34	54	102	1.27E+06	18	34	1.11E+06
35	55	103	1.28E+06	19	35	1.10E+06
36	55	104	1.27E+06	19	36	1.11E+06
37	56	105	1.25E+06	20	37	1.09E+06
38	56	106	1.20E+06	20	38	1.17E+06
39	57	107	1.22E+06	21	39	1.27E+06
40	57	108	1.10E+06	21	40	1.30E+06
41	58	109	9.15E+05	22	41	9.74E+05
42	58	110	1.27E+06	22	42	1.80E+06
43	59	111	2.57E+06	23	43	2.76E+06
44	59	112	6.17E+06	23	44	3.85E+06
45	60	113	7.04E+06	24	45	4.55E+06
46	60	114	7.95E+06	24	46	4.91E+06
47	61	115	5.62E+06	25	47	4.53E+06
48	61	116	4.59E+06	25	48	3.89E+06
49	62	117	3.83E+06	26	49	3.62E+06
50	62	118	4.09E+06	26	50	3.72E+06
51	63	119	4.29E+06	27	51	3.80E+06
52	63	120	4.44E+06	27	52	3.74E+06
53	64	121	4.55E+06	28	53	3.69E+06
54	65	122	3.95E+06	29	54	3.21E+06
55	66	123	3.11E+06	30	55	2.44E+06
56	66	124	2.88E+06	30	56	2.18E+06
57	67	125	2.69E+06	31	57	1.99E+06
58	67	126	2.61E+06	31	58	1.94E+06
59	68	127	2.38E+06	32	59	1.86E+06
60	68	128	2.25E+06	32	60	1.74E+06
61	69	129	2.11E+06	33	61	1.61E+06
62	69	130	2.04E+06	33	62	1.53E+06
63	70	131	1.94E+06	34	63	1.45E+06
64	70	132	1.88E+06	34	64	1.38E+06
65	71	133	1.85E+06	35	65	1.29E+06
66	71	134	1.80E+06	35	66	1.04E+06
67	72	135	1.70E+06	36	67	8.31E+05
68	72	136	1.74E+06	36	68	8.09E+05

Table 7.23 Comparison of stresses along the free surface of the shotcrete and inner linings for Kisikli south tube (km 1+544)

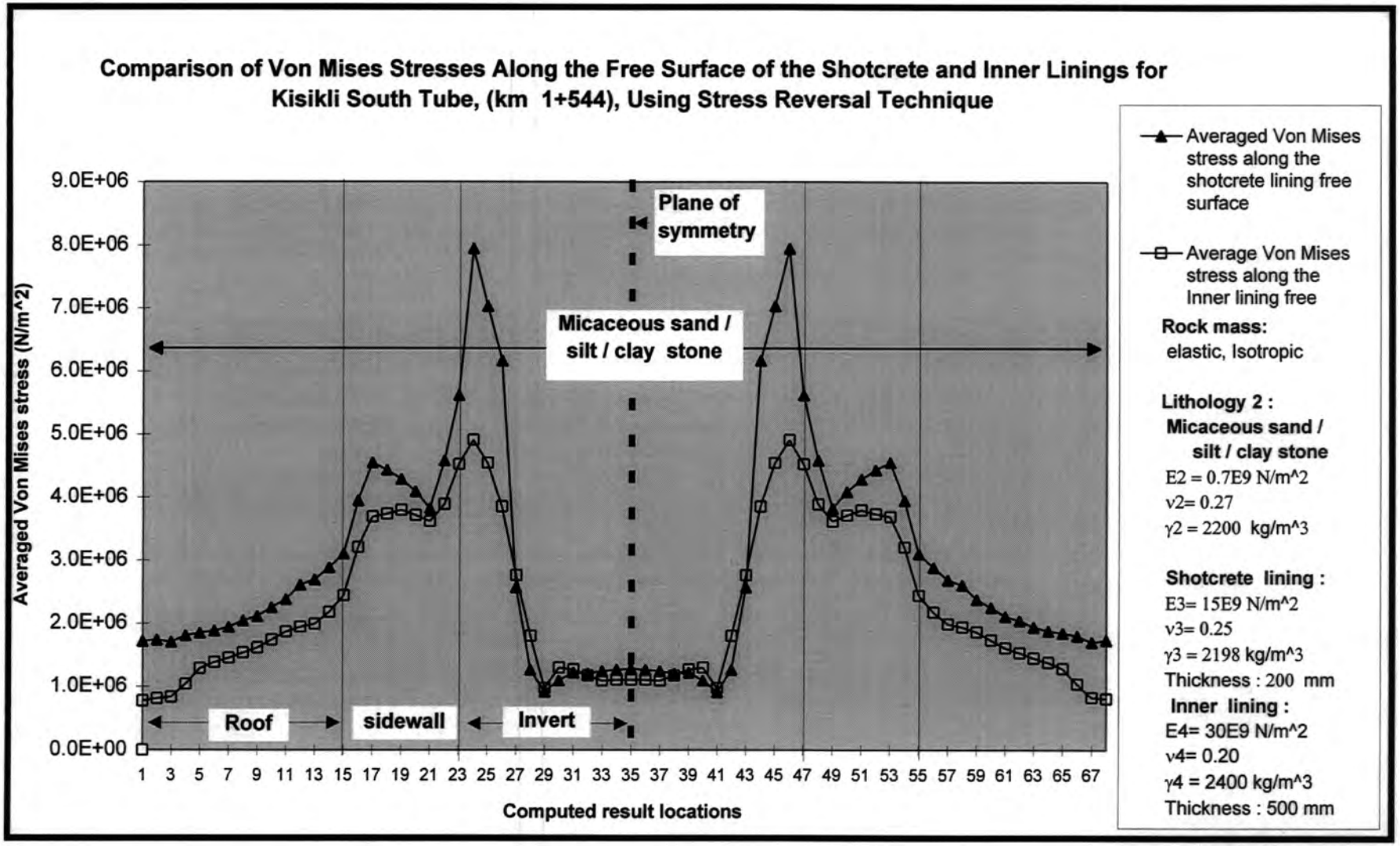

Fig 7.71 Comparison of stresses along the free surface of the shotcrete and inner linings for Kisikli south tube (km 1+544)

	STRESS REVERSAL TECHNIQUE					*STRESS REVERSAL TECHNIQUE*				
	Number of nodes = 3498					*Number of nodes = 3498*				
	Number of elements = 532					*Number of elements = 532*				
	Number of d.o.f = 6793					*Number of d.o.f = 6793*				
						KISIKLI SOUTH TUBE (km 1+544)				
	KISIKLI SOUTH TUBE (km 1+544)					HAVING SHOTCRETE LINING (t=200 mm),				
	HAVING SHOTCRETE LINING (t=200 mm),					ANCHORAGES, STEEL ARCH				
						AND INNER LINING (t= 500 mm)				
	NUMBER	NUMBER	DISPLACEMENT (mm)			ELEMENT	NODE	DISPLACEMENT (mm)		
COMPUTED	ALONG THE	ALONG THE	ALONG THE SHOTCRETE LINING			NUMBER	NUMBER	ALONG THE INNER LINING		
RESULT	SHOTCRETE	SHOTCRETE	FREE SURFACE			ALONG THE	ALONG THE	FREE SURFACE		
LOCATIONS	LINING	LINING	Ux	Uy	U	INNER LINING	INNER LINING	Ux	Uy	U
1	37	69	0.0000	-2.6442	**2.6442**	1	1	0.0000	0.1616	**0.1616**
2	37	70	-0.0731	-2.6441	**2.6451**	1	2	-0.0165	0.1624	**0.1632**
3	38	71	-0.1463	-2.6453	**2.6493**	2	3	-0.0337	0.1646	**0.1680**
4	38	72	-0.2741	-2.6269	**2.6412**	2	4	-0.0658	0.1746	**0.1866**
5	39	73	-0.4030	-2.5867	**2.6179**	3	5	-0.1047	0.1924	**0.2190**
6	39	74	-0.4362	-2.5607	**2.5976**	3	6	-0.1147	0.1976	**0.2285**
7	40	75	-0.4656	-2.5242	**2.5668**	4	7	-0.1254	0.2036	**0.2391**
8	40	76	-0.4885	-2.4795	**2.5272**	4	8	-0.1362	0.2101	**0.2504**
9	41	77	-0.5073	-2.4264	**2.4789**	5	9	-0.1476	0.2177	**0.2630**
10	41	78	-0.5192	-2.3668	**2.4231**	5	10	-0.1590	0.2258	**0.2762**
11	42	79	-0.5265	-2.2992	**2.3587**	6	11	-0.1712	0.2354	**0.2911**
12	42	80	-0.5305	-2.2344	**2.2985**	6	12	-0.1770	0.2403	**0.2985**
13	43	81	-0.5350	-2.1684	**2.2334**	7	13	-0.1833	0.2454	**0.3063**
14	43	82	-0.5341	-2.0496	**2.1180**	7	14	-0.2088	0.2693	**0.3408**
15	44	83	-0.5266	-1.9223	**1.9931**	8	15	-0.2354	0.2998	**0.3812**
16	45	84	-0.4656	-1.3713	**1.4482**	9	16	-0.3112	0.4347	**0.5346**
17	46	85	-0.4377	-0.8069	**0.9180**	10	17	-0.3569	0.6182	**0.7138**
18	46	86	-0.4549	-0.5384	**0.7048**	10	18	-0.3630	0.7227	**0.8087**
19	47	87	-0.4357	-0.2768	**0.5162**	11	19	-0.3565	0.8300	**0.9033**
20	47	88	-0.3893	-0.1346	**0.4119**	11	20	-0.3465	0.9016	**0.9659**
21	48	89	-0.2970	-0.0087	**0.2971**	12	21	-0.3271	0.9696	**1.0233**
22	48	90	-0.1981	0.0647	**0.2084**	12	22	-0.3138	1.0002	**1.0483**
23	49	91	-0.0893	0.1511	**0.1755**	13	23	-0.2948	1.0295	**1.0709**
24	49	92	-0.0496	0.2746	**0.2790**	13	24	-0.2805	1.0464	**1.0833**
25	50	93	-0.0611	0.4700	**0.4740**	14	25	-0.2705	1.0648	**1.0986**
26	50	94	-0.1181	0.7710	**0.7800**	14	26	-0.2597	1.0796	**1.1104**
27	51	95	-0.1524	1.1505	**1.1605**	15	27	-0.2494	1.0924	**1.1205**
28	51	96	-0.2200	1.8587	**1.8717**	15	28	-0.2228	1.1211	**1.1430**
29	52	97	-0.2774	2.3621	**2.3783**	16	29	-0.2078	1.1319	**1.1508**
30	52	98	-0.2832	2.9325	**2.9461**	16	30	-0.1662	1.1435	**1.1555**
31	53	99	-0.2534	3.2452	**3.2551**	17	31	-0.1263	1.1512	**1.1581**
32	53	100	-0.1826	3.4454	**3.4502**	17	32	-0.0848	1.1588	**1.1619**
33	54	101	-0.1056	3.5426	**3.5442**	18	33	-0.0460	1.1630	**1.1639**
34	54	102	-0.0528	3.5680	**3.5684**	18	34	-0.0229	1.1640	**1.1642**
35	55	103	-0.0001	3.5757	**3.5757**	19	35	0.0000	1.1643	**1.1643**
36	55	104	0.0527	3.5680	**3.5684**	19	36	0.0228	1.1640	**1.1642**
37	56	105	0.1055	3.5426	**3.5442**	20	37	0.0459	1.1630	**1.1639**
38	56	106	0.1825	3.4454	**3.4502**	20	38	0.0847	1.1588	**1.1619**
39	57	107	0.2533	3.2452	**3.2551**	21	39	0.1262	1.1512	**1.1581**
40	57	108	0.2831	2.9326	**2.9462**	21	40	0.1661	1.1435	**1.1555**
41	58	109	0.2773	2.3621	**2.3783**	22	41	0.2077	1.1319	**1.1508**
42	58	110	0.2199	1.8587	**1.8717**	22	42	0.2227	1.1211	**1.1430**
43	59	111	0.1523	1.1505	**1.1605**	23	43	0.2493	1.0924	**1.1205**
44	59	112	0.1180	0.7710	**0.7800**	23	44	0.2596	1.0796	**1.1104**
45	60	113	0.0609	0.4700	**0.4739**	24	45	0.2704	1.0648	**1.0986**
46	60	114	0.0494	0.2746	**0.2790**	24	46	0.2804	1.0464	**1.0833**
47	61	115	0.0891	0.1511	**0.1754**	25	47	0.2947	1.0295	**1.0708**
48	61	116	0.1979	0.0647	**0.2082**	25	48	0.3137	1.0002	**1.0482**
49	62	117	0.2968	-0.0087	**0.2969**	26	49	0.3270	0.9696	**1.0233**
50	62	118	0.3891	-0.1346	**0.4117**	26	50	0.3464	0.9016	**0.9659**
51	63	119	0.4356	-0.2768	**0.5161**	27	51	0.3565	0.8300	**0.9033**
52	63	120	0.4547	-0.5385	**0.7048**	27	52	0.3629	0.7227	**0.8087**
53	64	121	0.4376	-0.8070	**0.9180**	28	53	0.3568	0.6182	**0.7138**
54	65	122	0.4655	-1.3714	**1.4483**	29	54	0.3111	0.4347	**0.5346**
55	66	123	0.5266	-1.9225	**1.9933**	30	55	0.2353	0.2998	**0.3811**
56	66	124	0.5341	-2.0497	**2.1181**	30	56	0.2087	0.2693	**0.3407**
57	67	125	0.5349	-2.1685	**2.2335**	31	57	0.1832	0.2454	**0.3062**
58	67	126	0.5305	-2.2345	**2.2966**	31	58	0.1769	0.2403	**0.2984**
59	68	127	0.5265	-2.2993	**2.3588**	32	59	0.1711	0.2354	**0.2910**
60	68	128	0.5191	-2.3669	**2.4232**	32	60	0.1589	0.2258	**0.2761**
61	69	129	0.5072	-2.4265	**2.4789**	33	61	0.1475	0.2176	**0.2629**
62	69	130	0.4885	-2.4796	**2.5273**	33	62	0.1361	0.2101	**0.2503**
63	70	131	0.4656	-2.5242	**2.5668**	34	63	0.1253	0.2036	**0.2391**
64	70	132	0.4362	-2.5608	**2.5977**	34	64	0.1146	0.1976	**0.2284**
65	71	133	0.4029	-2.5867	**2.6179**	35	65	0.1046	0.1924	**0.2190**
66	71	134	0.2741	-2.6270	**2.6413**	35	66	0.0657	0.1746	**0.1866**
67	72	135	0.1462	-2.6453	**2.6493**	36	67	0.0336	0.1646	**0.1680**
68	72	136	0.0731	-2.6441	**2.6451**	36	68	0.0164	0.1624	**0.1632**

Table 7.24 Comparison of displacements along the free surface of the shotcrete and inner linings for Kisikli south tube (km 1+544)

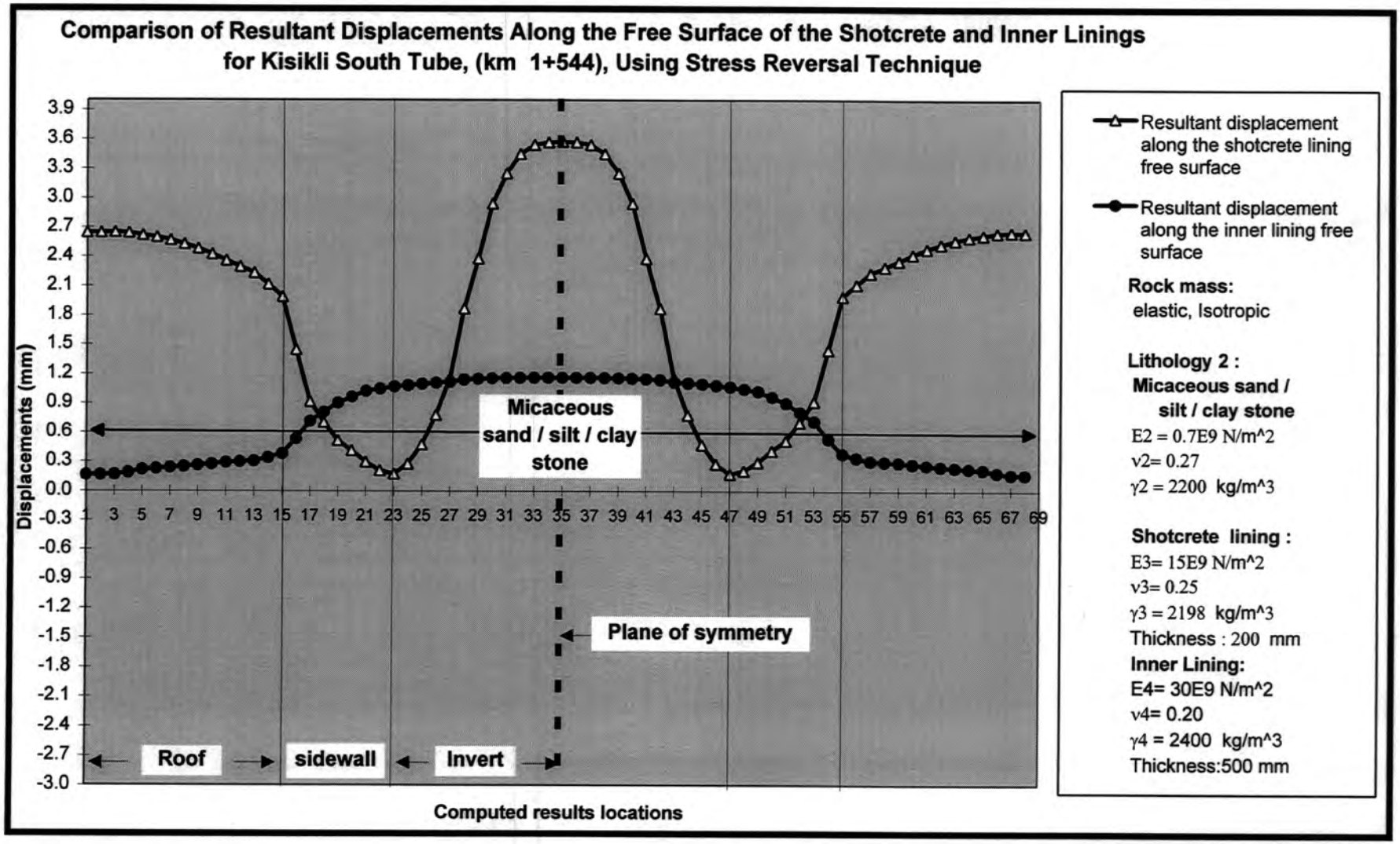

Fig. 7.72 Comparison of displacements along the free surface of the shotcrete and inner linings for Kisikli south tube (km 1+544)

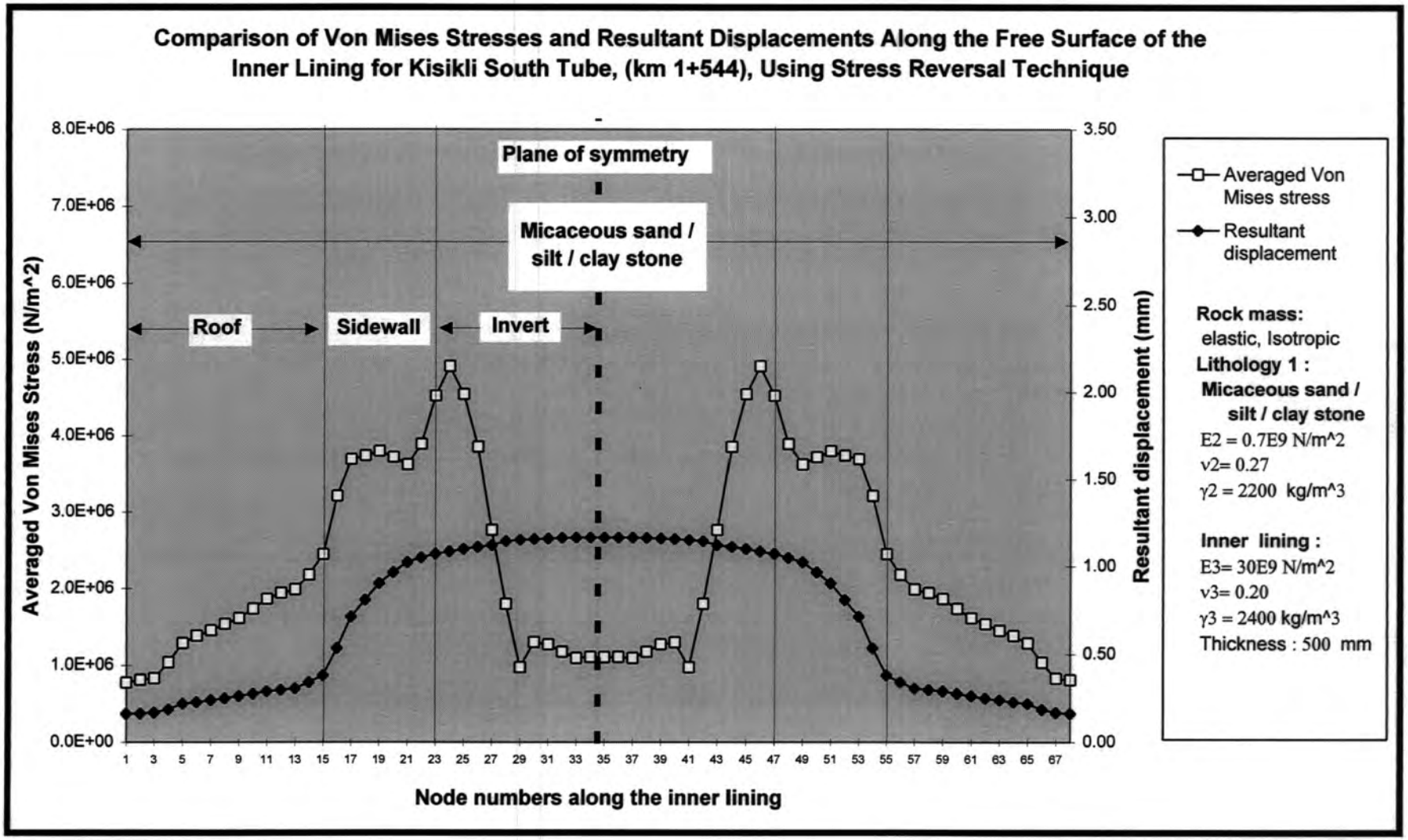

Fig. 7.73 Comparison of stresses and displacements along the free surface of the inner lining for Kisikli south tube (km 1+544)

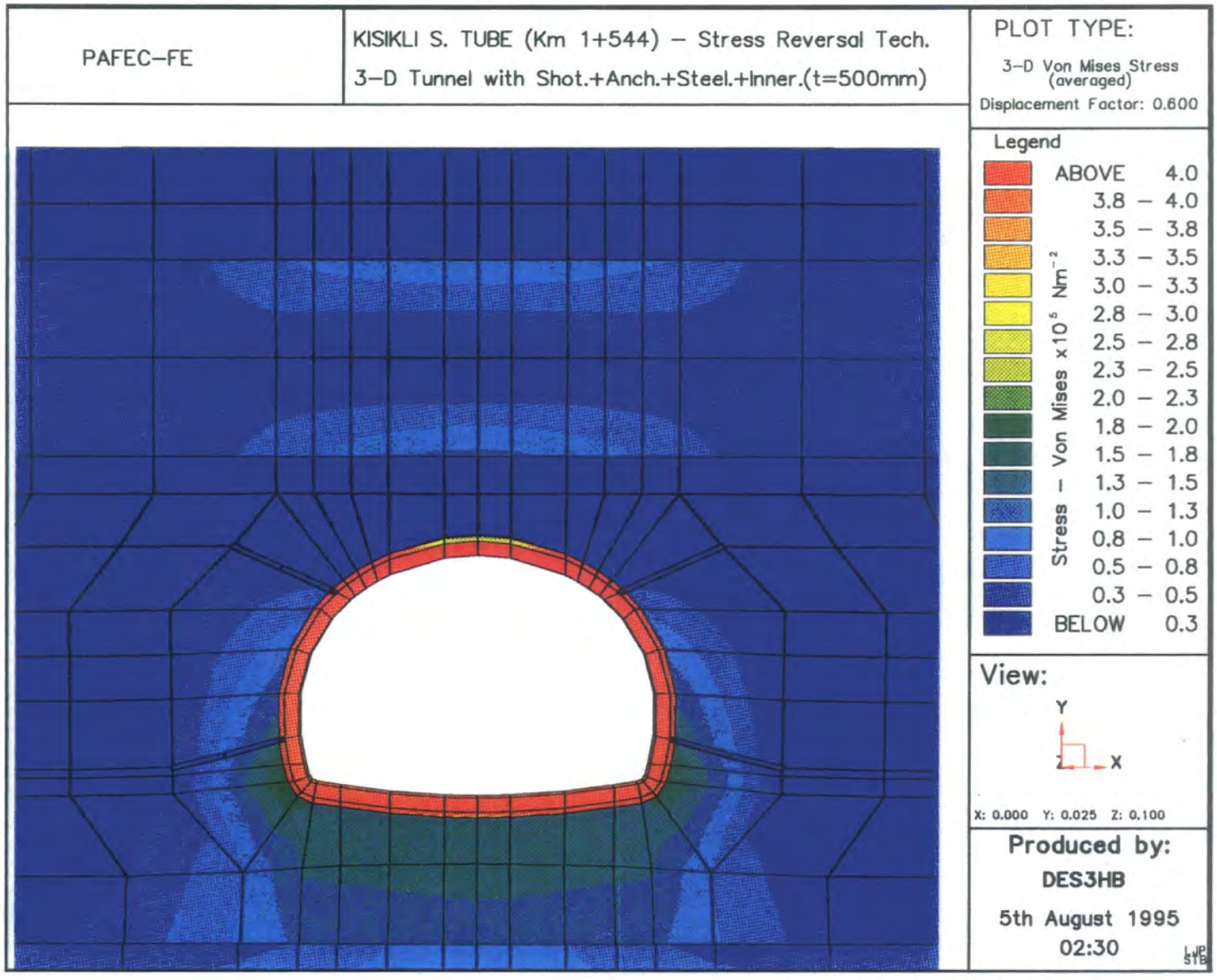

Fig. 7.74 Colour stress and displaced shape diagrams of Kisikli south tube, (km 1+544), having shotcrete lining, anchorages, steel arch and inner lining

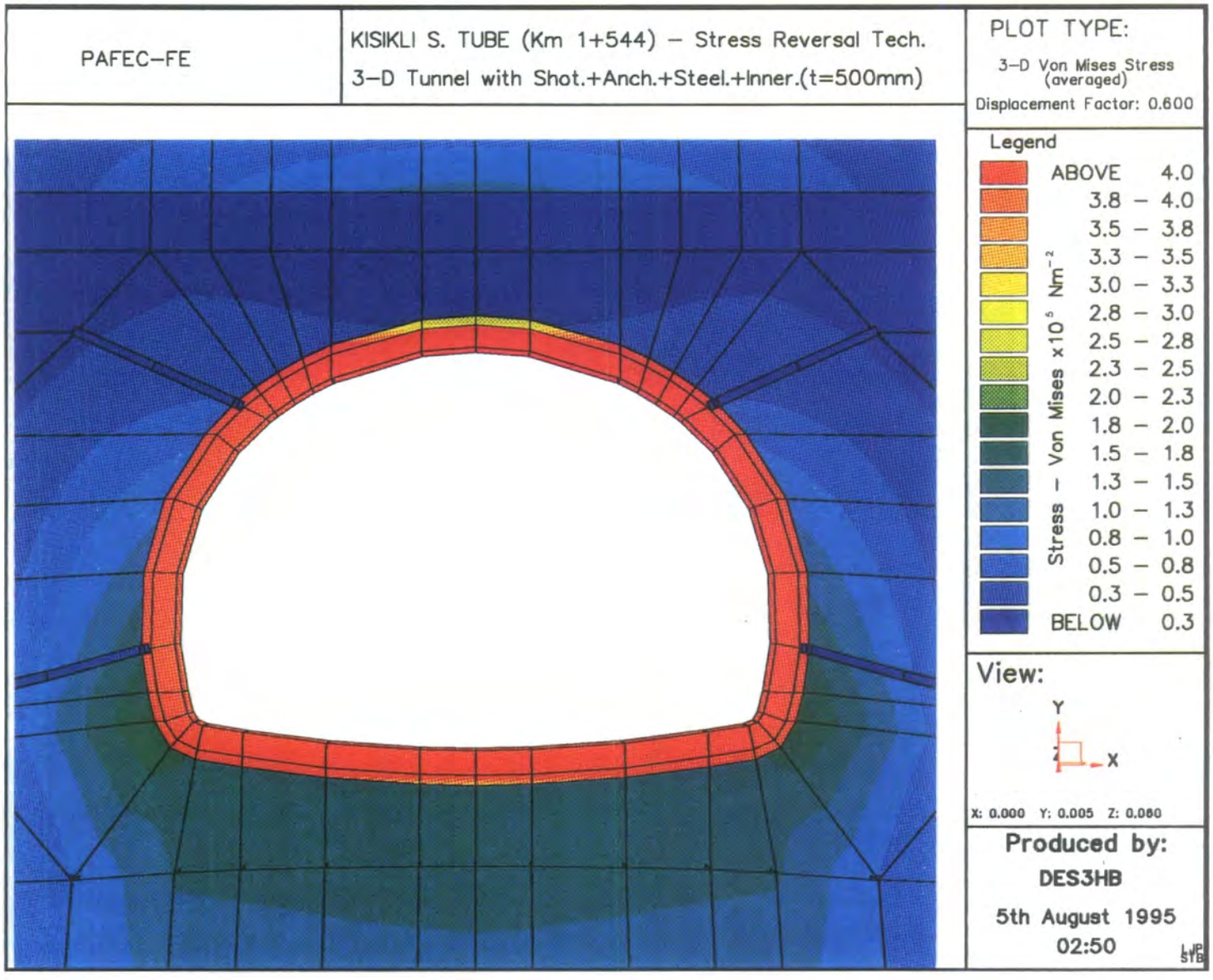

Fig. 7.75 Front view of colour stress and displaced shape diagrams of Kisikli south tube, (km 1+544), having shotcrete, anchorages, steel arch and inner lining

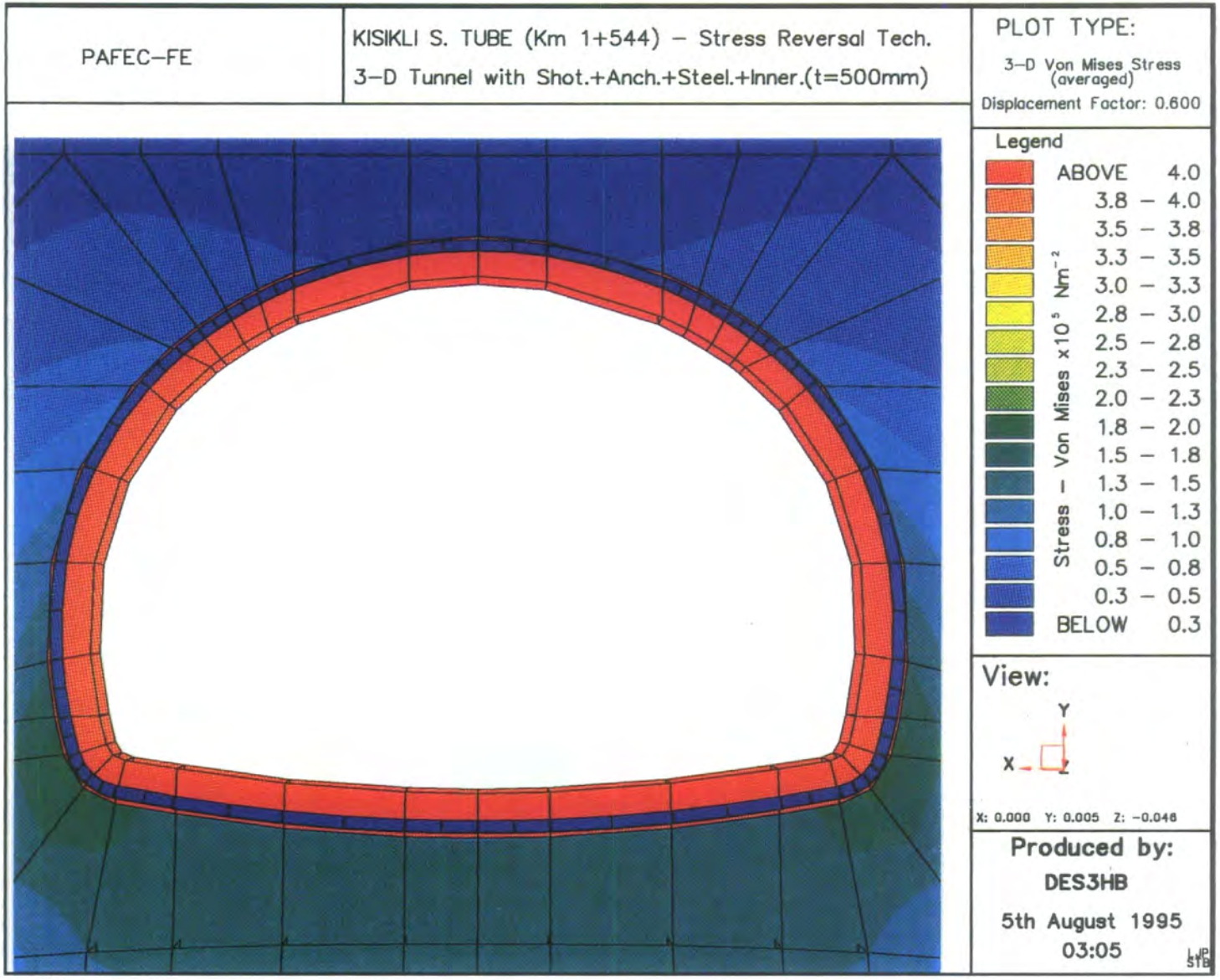

Fig. 7.76 Back view of colour stress and displaced shape diagrams of Kisikli south tube, (km 1+544), having shotcrete, anchorages, steel arch and inner lining

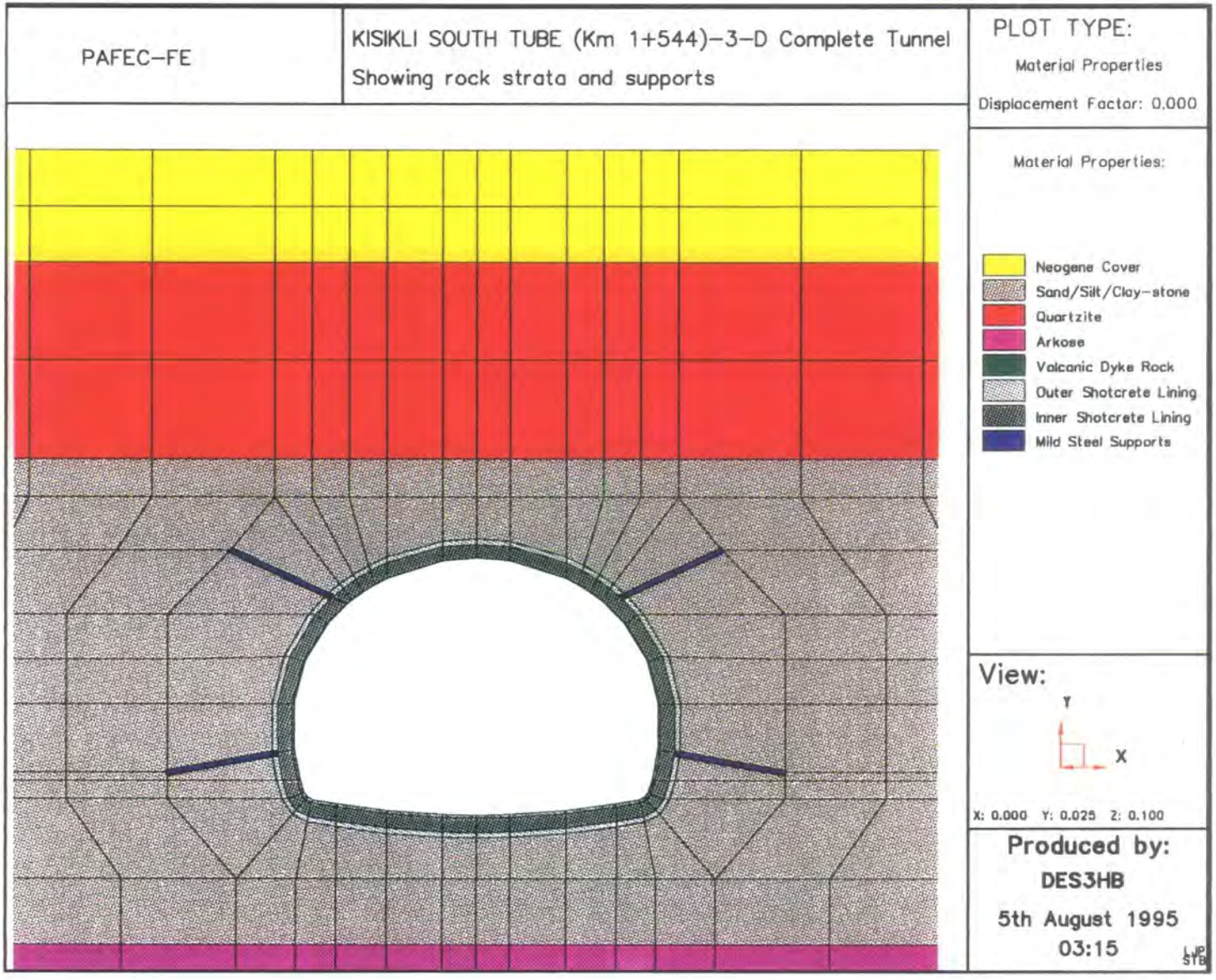

Fig. 7.77 Complete Kisikli south tube, (km 1+544), showing colour rock strata and support systems

CHAPTER 8

GENERAL DISCUSSION

8.1 Introduction

The classical analytical method after Kirsch (1898) - outlined by Attewell (1980) - suitably describes a tunnel perforation of circular configuration in an elastic homogeneous body (ground). It was considered very doubtful whether the Kirsch method used to obtain these formulae could be adapted to suit the tunnel geometry and ground conditions applicable to this present tunnel project. It was quite apparent that the support system and the in situ conditions needed to be analysed by an alternative procedure, and clearly a rather different approach was required to solve this more complex type of problem to any degree of accuracy.

Within the last 25 years, supported by the development of more powerful computers and more refined mathematical methods of analysis, a new form of modelling has evolved for civil engineering structures. This computer modelling provides an important alternative for systems that had previously been physically modelled, particularly by photoelastic methods. Moreover, computer models are rather more versatile than the physical models and can simulate a wider range of situations often more accurately and at lower cost.

At the beginning of this thesis the main tools of numerical analysis, useful for understanding mechanisms of deformation and stress in structures, which include the finite element method, finite difference method and boundary element method were considered for adaptation. In principal any of these methods could be used but PAFEC-FE was available when this study was started. Simple examples used to test the system before application of more complex models. Complex modelling should only be adopted after developing an understanding of displacement and stress mechanisms.

In all finite element studies, a number of factors have to be taken into account in order to ensure that a valid model is established. Initial loads - their

magnitude and distribution- are applied to the model by a gravity loading procedure. Elastic properties and the effects of stratification govern the performance of the model when subjected to gravity loading. Stratification is modelled by assigning different values of elastic modulus to the elements comprising each stratum in order to simulate the different rock properties existing in practice. The finite element method can be used in such cases as a prediction tool to assess potential problems and determine the amount and types of the support system likely to be required.

8.2 Elastic Approach

8.2.1 Justification

The tunnels under study are shallow, the height of overburden varying between 3 and 15 m, and they are not subjected to mining - style stresses which could induce plastic-type behaviour under strong confinement. It is a fact of nature that rock in situ is macroscopically discontinuous. The assumption of elastic behaviour with localised plastic deformations on the discontinuities is often used for the rock mechanics models in practical cases. The assumption of viscoplastic behaviour appears to be appropriate when time dependent highly plastic deformations occur. The rock layers having no systematic discontinuities may be regarded as approximately elastic and isotropic under loading below their strength, and their stress-strain behaviour therefore can be described by elastic constants. Therefore, an elastic heterogeneous type solution outlined in this thesis can reasonably be used to assess the degree of deformation and stress levels likely to be encountered.

The thrust of the analyses is towards sprayed concrete, or shotcrete, lining behaviour, incorporating anchorages and steel arches which in general have more predictable and consistent material properties. The concrete material here is monolithic and would be expected to respond elastically under the imposed ground stresses to which the tunnels are subjected.

8.2.2 Elastic Properties of Rock

The mechanical parameters required to formulate rock mass models may be determined using in situ and laboratory test methods. The mechanical properties of the intact rock can be determined by laboratory test methods. These properties of jointed rock, however, have to be determined in the field tests. The Young's modulus of the rock mass can be determined from flat jack tests which measure the in situ deformation of the rock mass. Poisson's ratio cannot be derived from the results of standard flat jack tests and its magnitude therefore has to be estimated. A relatively low value of Poisson's ratio is assumed when the Young's modulus is comparatively high or a high value of Poisson's ratio is estimated when the Young's modulus is low.

The intact rock characteristics may usually be determined relatively quickly and at low cost. Furthermore, core drilling is usually carried out at the beginning of an investigation programme, so intact rock samples are available at an early stage of the planning process. These present the reasons why relatively extensive tests on intact rock samples are undertaken in many investigation programmes.

Values of Young's modulus, as determined by laboratory testing on small specimens of visually intact rock, do not give a true indication of stiffness of the rock mass surrounding the excavation. However the results of such tests may provide a valuable guide to the rock mass. Reduction factors are necessary if the elastic parameters assigned to the model are to achieve consistency between measured and computed values of displacements. Therefore, 0.10 and 0.50 reduction factors on an 'intact' Young's modulus value and an increase of 0.05 for Poisson's ratio have been used for the models. These values were picked as an example.

8.3 Excavation Simulation

Under excavation the removal of material and subsequent redistribution of stress in the remaining material must be treated by one of three methods. These are

the gravity difference method, the stress reversal technique and the relaxation approach. Both the gravity difference method and stress reversal technique have been used to simulate the performance of tunnel excavation for this study. Because of the lack of explanation in the published literature the author has tried to give more precise details of procedures.

The gravity difference method requires the differences between excavated and unexcavated model analyses to produce the stresses and displacements that result from the creation of ground excavation. This is because in the gravity difference method displacements can be subtracted but stresses need to be carefully considered. Von Mises stress (the equivalent stress) should not be subtracted but the equivalent stress is calculated from global stress tensor components which can be subtracted. When the ground support is applied at the excavation surface it is positioned in the rock before gravity loading has been applied. When the gravity loading is exerted it has to work against the support to achieve the displacement expected from gravity-loaded ground having no excavation. The resulting displacement is significantly less above the supports, indicating that the presence of the supports make the surface rise. Therefore this method should only be used for the analysis of unsupported tunnel models.

The stress reversal approach considers the stresses existing in the elements on both sides of a proposed excavation boundary at any stage of excavation, and based upon these stresses evaluates the equivalent nodal forces to be applied along the boundary. Stresses on the excavation boundary have to be defined in terms of local direction for front and back planes in a three-dimensional model. In the finite element method, stresses are commonly determined at either the centres of the elements or midway between two opposing nodal points, depending upon the type of element used, but excavation boundaries pass between elements. Therefore, a technique must be employed to interpolate from the centre stresses to the nodal or boundary stresses. This method can be applied to tunnel model in any stages of construction but it needs more care.

In the relaxation or residual stress approach, the elements representing the surrounding rock mass are initially stressed to some desired values which are

subsequently relaxed to provide a final equilibrium stress state around the opening. With this approach it is difficult to follow a construction sequence, and also the relaxation is controlled exclusively by stresses existing in the elements which form the rock mass surrounding the excavation. Application of this method requires prediction of ground stresses and more experience. In view of these difficulties, this method was not used in the study.

8.4 In Situ Stresses

These methods were used to simulate tunnel excavation in relatively heterogeneous stratified rock. The horizontally stratified ground was modelled on a simplified basis by banding together adjacent strata of similar elastic properties and assuming that each model strata behaved elastically, homogeneously and isotropically.

The in situ state of stress was assumed to be due to gravity loading and was computed using the rock mass unit weight, elastic constants and the influence of topography using the GRAVITY LOADING module of PAFEC-FE. The in situ stress state in the construction site in Istanbul is not known very well from direct measurements. However, experience of tunnelling in Turkey is generally used to estimate the in situ stress state. If the in situ stress state for a tunnel site is known from measurements or is known to differ significantly from that due to gravity it can be modelled by incorporating other boundary conditions. However, changes in stresses due to excavation are likely to be dictated by the elastic behaviour in any case.

8.5 Limitation of the General Model

It has been necessary to determine exactly what form the simulations were mainly going to take; for example, whether the tunnel would be modelled in two- or three-dimensions using the gravity difference method or the reverse stress technique, and exactly what conditions were going to be imposed on the model.

This is an essential stage in the determination of the simulation requirements expressed in Chapter 4.

The choice of PAFEC-FE as a software for performing the basic finite element calculations, to which it is well suited, led to a number of important consequences. It has no direct system for dealing with Geotechnical problems involving excavation. This meant that the lack of facilities for pre- and post-processing of results, dictated that a number of additional computer programs were required to be written. By doing this, repeated use could be made of PAFEC-FE without time-consuming and inaccurate manual retrieval of data either for further computation or graphical output. Although it does have pre and post processing facility (PIGS) it is fairly limited. In the event, many post-processing programs of varying complexity were written in a form that created a system where simple output could be manipulated and adapted according to different simulations being performed in the least time and with minimum error.

Furthermore, complications arising from element angle and aspect ratio errors within PAFEC-FE led to a number of simplifications having to be made. These are discussed in detail in Chapter 5. The angle of each corner of a pafblock has to be greater than 45^{O} and less then 135^{O} ($45^{O} < \theta < 135^{O}$) and the aspect ratio (ratio of the pafblock side lengths) of the resulting pafblock is required to be less than 15:1. Errors and warnings are produced by PAFEC-FE if these limits are violated or approached respectively. In order to ensure that such problems do not occur the angular limit was set at 50°. At this stage the region and shell boundaries have to be set to ensure that this condition is avoided. If the model contains thin structures (very thin inner and outer linings), a pre-processing program generates extra pafblocks for the thin structure. PAFEC-FE assign nodes and element numbers to these elements in an arbitrary manner. For the stress reversal method of analysis, nodes and element numbers along the excavation boundary need to be very carefully checked.

All the graphical results from this research were produced using post-processing programs created specifically for this work. In order to produce output pictures of quality and flexibility, UNIRAS subroutines were used. Post-

processing programs have to be called and run depending on the particular output required, such as unexcavated ground showing rock strata, model mesh diagrams, shaded contour diagrams, displaced shape diagrams and excavated tunnels with support systems and complete tunnels showing rock strata and support.

The post-processing program output results can also be imported into spreadsheets using file transfer programs in order to get more detailed analyses. It was relatively simple to construct a sheet containing all nodes and their stress and displacement results.

The size of the actual finite element also affects the rigidity of the model. Relatively large elements were used in the mesh, partly on the grounds of computational costs and time and partly because highly accurate results were not required. These larger elements are not so sensitive to movement as would be a greater number of smaller elements.

8.6 Tunnel Support Design

The results stemming from the modelling of the support system are important and need discussing. The support system stress distributions are important for achieving stable tunnel conditions.

Optimum conditions cannot be generated solely by means of computer simulations, although there is substantial confidence in the principles and the effects of determining necessary support systems or modifying them. It is not possible to predict with a high degree accuracy the ground response during construction of a tunnel. This is not a disclaimer against any inaccuracy but a simple statement of practical fact with this type of testing. All aspects in the modelling have been formulated to ensure that the results are as accurate as possible, consistent with the standard of information requested from prior investigation and the time available. The comparative testing and the test conditions themselves were all selected with this aim in mind.

The magnitude of displacements and stresses indicate whether a 'rigid' type of support system can be used, such as steel arches or a concrete lining, or whether

a system designed to allow some yield may be required, typically in the form of rock bolts.

Time dependent effects on the stability of the support systems should not be ignored and the design should be such that the support has to be loaded less than 60% of its yield strength in order that any significant creep deformation is eliminated.

Although much of the work in this thesis has not yet been applied to actual tunnel excavation and support systems, the model interactive (support system with the ground) responses seem to have been demonstrated with quite reasonable clarity. Tunnel design will never be a rigidly defined scientific exercise. The judgement and experience of the designer are naturally very important elements, but it is necessary to base design decisions on robustly established criteria. This thesis has sought to examine and promote those criteria.

It has been demonstrated that a tunnel, its excavation and support protocols, can be designed according to specific performance criteria. With the system that has been used, many variables within the model can be changed, and if some understanding is obtained for the effect on the model of each variable then the tunnel can be designed according to the specific ground and operational conditions pertaining and with an economy of ground support. Although the research work documented in this report has used a particular tunnel as an example, the results and trends that have been obtained should find some application in the case of any similar design of transportation tunnel.

The cost of constructing a tunnel, including the initial investigation and design costs, should, of course, be as low as possible, and extensive testing would be required for assurance in respect of safety and quality of the tunnel and tunnel support. It was concluded that although good results have been achieved in the computer simulations, the response of an actual support system may not accord with the finite element model outcomes. As is the case with any tunnel designed by modelling, prototype development should be significantly reduced, but not removed altogether.

8.7 Measured and Computed Displacements

Measured and computed displacements along the tunnel have been compared in Chapter 7. The measured tunnel convergence results were monitored by extensometers. It should be noted that the convergence measuring programme in the field began in full after the shotcrete lining was placed and the tunnel face was some 15 metres away from the measurement section. This indicates that the total consequential movement had not been recorded and the displacement results from the computer simulation should exceed those actually measured. On the other hand, the simulation has been applied elastically whereas the measured displacements may have been to some extent non-linear (pseudo-plastic), leading to the latter exceeding the former.

In general, the calculated values based on laboratory test on Young's modulus of rock stiffnesses are marginally greater than the measured ones. In all instances the modelled displacements are similar in direction to those actually measured but the magnitudes of displacements, particularly above the crown, are generally higher in the case of the simulation. A close agreement is generally achieved between the measured values and the calculated results based on laboratory test values of stiffness that have been factored.

While there is a general agreement for the diagonal convergence measurements, results for the horizontal convergence do not always show the same trend as produced by the computer simulation. The results obtained from the simulation indicate an upward movement at tunnel invert. The computed displacements due to gravity loading also show a net downward movement both above and below the level of the tunnel.

Many authors, including Gudehus (1977), Wittke (1990) and Duddeck (1991), pointed out that the magnitude of displacements are very important when measured and computed convergences are compared. Therefore, the primary objective of an assessment of the ability of the model to describe behaviour of the tunnel has to be achieved. Calculated maximum tunnel convergence is 0.45 mm as opposed to 1.36 mm measured in the Kisikli north tube (km 1+536). This

relatively small difference would seem reasonably to confirm the validity of using an elastic solution for this particular case. Reasonable comparison can be made between simulated and measured displacement, but close agreement between the two is obviously dependent on the same geology, ground conditions and material properties pertaining.

8.8 Stress Distribution

The stress distribution aspects of the problem have been mainly considered for the induced stresses stemming from the tunnel advance. The term 'induced stress' in the case refers to that value of stress produced only by the tunnel excavation. Von Mises stress shaded colour diagrams were drawn for tunnel sections. Use of Von Mises stresses enable an assessment to be made of zones of probable failure in the rock mass surrounding the excavations. These stress distributions show that the stress levels around the excavation were insufficiently large to produce failure of the intact rock. However, the shaded stress diagrams show the occurrence of a significant region of tensile stress between the tunnel crown and ground surface. Because of the natural discontinuities known to be present in rock, causing the rock mass to have a very low resistance to tensile forces, any such areas of appreciable tensile stress need special consideration in respect of the rock mass support capacity. Potential instability depends on the directional sense of the tensile stress.

8.9 Conclusion

From a consideration of the above comments the question arises as to how realistically finite element modelling can be used in tunnelling design. The studies discussed above would indicate that such a solution technique can be adopted successfully at shallow depth using the gravity difference method and stress reversal technique. However, these finite element tunnel models have related to excavation in horizontally bedded rock layers. The effects of such features as

heavily jointed rock and dipping laminated layers on the validity of the model have not been assessed. Determination of the geology (petrology and structure) of the site prior to simulation is important and the possible effects of the engineering geological factors on the accuracy of such simulation should not be ignored.

CHAPTER 9

CONCLUSIONS AND RECOMMENDATIONS

9.1 Conclusions

9.1.1 Finite Element Model

Eight main issues have been identified in this study and which justify choosing the finite element method over an analytical method for the modelled solution of stresses and displacements in a tunnel support system.

a) The complex tunnel geometry of the project.
b) The rock layers at different heights and heterogeneous rock properties.
c) Extension of the problem into a three-dimensional model which is both symmetric and periodic in form.
d) The need to optimise dimensions of the tunnel support systems because the construction cost of tunnels is high.
e) A requirement for estimating stress levels in the tunnelled ground and lining.
f) A desire to determine displacements within the structure to be designed.
g) Estimation of the characteristic strengths of rock around the tunnel using mechanical and physical parameters.
h) Information presentation in graphical / pictorial form (shaded stress contours and displaced shape diagrams).

9.1.2 PAFEC-FE

a) PAFEC-FE despite its limitations has proved suitable for finite element analysis of shallow rock tunnel problems.

b) PAFEC-PIGS has been unsuitable for processing and presenting finite element stress and displacement output data. It was concluded that UNIRAS graphics software would be suitable and this proved to be correct. All the graphical results in this thesis were produced using the post-processing programs created for this work. It was found that UNIRAS subroutines can produce pictures of quality and versatility.

9.1.3 Excavation Simulation

a) Use of both the gravity difference method and stress reversal technique has shown that the deformations and the computed distributions of stresses were very similar. The very small error obtained was more likely to be the result of using calculated reverse forces on the excavation boundary. In both cases elastic heterogeneous two- and three-dimensional finite element models were used to simulate stresses and displacements.

b) Although the in situ measurements of convergence data tended to display some variation, using the gravity difference method and the stress reversal technique, a generally good correlation was found between values of displacement derived from the finite element model and those measured in the tunnel.

9.1.4 Support Systems

A series of computer model studies was carried out in order to assess tunnel support system performance. Data collection from the tunnelling site, carried out by others, was valuable in assisting in a comparison between measured displacements and computed values using finite element modelling.

The following main conclusions may be drawn from the results.

a) The computer model developed using PAFEC-FE is sensitive enough to be able to be used for the analysis of transportation tunnel deformation

behaviour. Quadrilateral and brick type elements that were used provided a good description of the state of stress in the tunnel structure.

b) Insertion of a support system into the model has a marginal effect on the development of rock strength around excavation boundary.

c) From the results presented in this research, it is possible to see how an analysis can be used to identify an optimum support system.

d) The study of the interaction between the shotcrete lining and excavation surface in Kisikli tunnel showed that two-dimensional finite element plane strain analysis could be used effectively to model a shotcrete lining. Displacements of the Kisikli tunnel having 100 and 200 mm thick shotcrete linings were satisfactorily modelled. Using these values for the model, comparison between measured and computed displacements show that close agreement was obtained.

e) This study has confirmed that an elastic three-dimensional finite element analysis can reasonably be used to model the ground-structure interaction effects resulting from driving a relatively shallow transportation tunnel with the installation of support systems comprising anchorages and steel arches.

f) The input data for the mass properties of a rock needed inevitably to be assessed from the results of laboratory tests on 'intact' samples of the rock. However, it was concluded that these latter property values needed to be adjusted in order to satisfy the stiffness reductions and Poisson's ratio increases brought about by such natural structural features as discontinuities. Reductions of 10 % and 50% in elastic modulus and an increase of 0.05 in Poisson's ratio, applied interactively, were needed to achieve the required comparisons between the computed results from the model and the measured results at the actual tunnel.

g) The degree of accuracy obtained by the simulation was also assisted by the general nature of the geology, particularly the relative lack of discontinuities.

h) Data obtained from the model, and the graphical output, showed that the presence of the tunnel had a significant influence upon the stress magnitude and (re-)distribution overhead. There was also a large increase in the area of the zone subjected to tensile stress, above the tunnel crown and below the invert.

i) The choice of Von Mises stress as a single parameter to represent the stress state is useful because it can also be used to indicate zones liable to failure under tension or compression.

j) For the tunnel used as an example for the modelling, it has been shown that a reduction in the support element would stem from the design recommendations. In particular, there could be a reduction in the thickness of the concrete shell and in the rib density, while still maintaining wall deformation within tolerable limits. A 200 mm thick shotcrete lining has been used in the tunnels. From the computer simulations given in Chapter 7 it is concluded that this lining thickness could be reduced to 100 mm. However, in the example given, it was felt that there was a risk of worsening (increasing) the deformation by reducing the material stiffness.

9.2 Recommendations for Further Work

The work described in this thesis has been directed towards producing a firm link between field studies and finite element modelling. A degree of success has been achieved in simulating rock behaviour around the excavation using the gravity difference and stress reversal methods and in modelling the influence of support systems on the overall stability of the tunnel. The relation between the amount of support and the stability of tunnel has been examined, but further work is needed in this area.

The finite element studies outlined here have been carried out using complex simulations having horizontally laminated rock strata. There is a

capability in a future study of extension from this type of model into a more complex model incorporating such features as dipping strata and geological faults.

This finite element work has emphasised the importance of making available to the civil engineering designer the correct software to allow him to successfully carry out the computer modelling. It is to be recommended that in future studies the provision of general purpose relatively inexpensive finite element software such as PAFEC-FE be made available for the solution of most ground-structure interaction problems when many variants on these problems are accommodated by the user's own pre- and post-processing programs.

Finally, simulation of the anchorages and steel arches could be extended to examine different type of beam elements.

REFERENCES

AGARWAL, R. K. and BOSHKOV, H. S. (1969) Stresses and Displacements Around a Circular Tunnel in A Three-Layer Medium-II. *International Journal of Rock Mechanics and Mining Science*, Vol. 6, pp. 529-540.

AKIN, J. E. (1986) *Finite Element Analysis for Undergraduates*. Academic Press., Florida., pp. 27-61.

ANDERSON, W. A. and DODD, S. J. (1966) Finite Element Method Applied to Rock Mechanics. *Proceedings of the First Congress of the International Society of Rock Mechanics*, Lisbon, Vol. 2, pp. 317-321.

ATTEWELL, P. B. (1980) *Stress Distribution and Displacement Around a Tunnel at Depth in Rock*. Notes prepared for M.Sc. Advanced Course in Engineering Geology, University of Durham, pp. 1-9.

ATTEWELL, P. B., YEATES, J. and SELBY, A. R. (1986) *Soil Movements Induced by Tunnelling and Their Effects on Pipelines and Structures*. Blackie and Son Ltd., London.

ATTEWELL, P. B. (1995) *Tunnelling Contracts and Site Investigation*, E. & F.N. Spon Ltd., London.

BARLA, G. (1972) Stresses Around a Single Underground Opening Near a Traction-Free Surface. *International Journal of Rock Mechanics and Mining Science,* Vol. 9, pp. 103-126.

BARLA, G. and OTTOVIANI, M. (1974) Stresses and Displacements Around Two Adjacent Circular Openings Near to the Ground Surface. *Proceedings of the Third Congress of the International Society for Rock Mechanics*, Vol. 2, Part B, pp. 975-980, Denver, Colorado.

BARTON, N., LIEN, R. and LUNDE, J. (1974) Engineering Classification of Rock Masses for the Design of Tunnel Support. *Rock Mechanics*, Vol. 6, No. 4, pp. 183-236.

BERNAUD, D., BUHAN, P. AND MAGHOUS, S. (1995) Numerical Simulation of the Convergence of a Bolt-Supported Tunnel Through a Homogenisation Method. ***International Journal for numerical and Analytical Methods in Geomechanics*****, Vol. 19, No. 4, pp. 267-288.**

BIENIAWSKI, Z. T. (1984) ***Rock Mechanics Design in Mining and Tunnelling.*** **A. A. Balkema Publishers Ltd., Rotterdam, pp. 97-132.**

BIENIAWSKI, Z. T. (1989) ***Engineering Rock Mass Classifications: A Complete Manual for Engineers and Geologists in Mining, Civil and Petroleum Engineering.*** **John Wiley and Sons Inc., New York, pp. 251.**

BIENIAWSKI, Z. T. (1992) ***Design Methodology in Rock Engineering: Theory, Education and Practice.*** **A. A. Balkema Publishers Ltd., Rotterdam, pp. 171-187.**

BLAKE, W. (1966) Application of the Finite Element Method of Analysis in Solving Boundary Value Problems In Rock Mechanics. ***International Journal of Rock Mechanics and Mining Science,*** **Vol. 3, pp. 169-180.**

BRADY, B. H. G. and BROWN, E. T. (1985) ***Rock Mechanics For Underground Mining.*** **George Allen & Unwin Publishers Ltd., London, pp 17-47.**

BREBBIA, C. A. (1978) ***The Boundary Element Method for Engineers*****, Pentech Press, London.**

BROWN, C. B. and KING, I. P. (1966) Automatic Embankment Analysis: Equilibrium and Instability Conditions. ***Geotechnique*****, Vol. XVI, pp. 209-219.**

BROWN, E. T. (1987) ***Analytical and Computational Methods in Engineering Rock Mechanics.*** **Allen & Unwin Publishers Ltd., London, pp. 5-28.**

BS 4 : Part 1 : 1993 ***Specification for hot-rolled sections.***

BS 4848 : Part 2 : 1991 ***Specification for hot-finished hollow sections.***

BUDARI, S. (1983) ***Rock Mechanics in Mining Practice.*** **Published by The South African Institute of Mining and Metallurgy, Johannesburg.**

CARLTON, D. (1993) Application of the Finite Element Method to Structural Engineering Problems. ***The Structural Engineer*****, Vol. 71, No. 4, pp. 55-59**

CARTER. J. P. and XIAO, B. (1994) A 2-D Coupled Finite Element and Boundary Element Scheme to Simulate the Elastic Behaviour of Jointed Rocks. *International Journal for Numerical and Analytical Methods in Geomechanics*, Vol. 18, No. 1, pp. 49-71.

CHANG, C. Y. and NAIR, K. (1974) Development and Application of a General Computer Program for Evaluating Stability of Openings in Rock. *Proceedings of the Third Congress of the International Society for Rock Mechanics*, Vol. 2, Part B, pp. 981-988, Denver, Colorado.

CLOUGH, R. W. (1960) The Finite Element Method in Plane Stress Analysis. *Proc. 2nd ASCE Conference on Electronic Computation*, Pittsburgh, pp. 345-378.

CLOUGH, R. W. (1980) The Finite Element Method After Twenty-Five Years: A Personal View, *Computers & Structures*, Vol. 12, pp. 361-370.

DEERE, D. U. (1963) Technical Description of Rock Cores for Engineering Purposes. *Rock Mechanics and Engineering Geology*, Vol. 1 pp. 16-22.

DEERE, D. U. and MILLER, R. P. (1966) *Engineering Classification and Index Properties of Intact Rock*, Air Force Laboratory Technical Report No. AFNL-TR-65-116, Albuquerque, NM.

DESAI, C. S. and ABEL, J. F. (1972) *Introduction to the Finite Element Method.* Van Nostrand Reinhold Company., New York, pp. 326-330.

DESAI, C. S. and CHRISTIAN, J. T. (1977) *Numerical Methods in Geotechnical Engineering*, Mc Graw-Hill book Company, London.

DUDDECK, H. (1991) Application of Numerical Analyses for Tunnelling. *International Journal for Numerical and Analytical Methods in Geomechanics*, Vol. 15, No. 8, pp. 223-239.

DUNLOP, P. and DUNCAN, M. J. (1970) Development of Failure Around Excavated Slopes. *Proceeding of The American Society of Civil Engineers, Journal of the Soil Mechanics and Foundation Division*, Part 96, No. SM1, pp. 471-493.

EDWARDS R. H. (1951) Stress Concentration Around Spheroidal Inclusions and Cavities. Journal of Applied Mechanics, March 1951, pp. 19-30.

ERDEM, Y. (1994) Highway Tunnels in Turkey: Opportunities for International Transport Links. *Tunnelling and Underground Space Technology*, Vol. 9, No. 4, pp. 455-459.

FRANKLIN, J. A. (1975) Safety and Economy of Tunnelling. *Proceedings, Tenth Canadian Rock Mechanics Symposium,* Kingstone, pp. 27-53.

GOODMAN, L. E. and BROWN, C. B. (1963) Dead Load Stresses and The Instability of Slopes. *Proceeding of The American Society of Civil Engineers, Journal of the Soil Mechanics and Foundation Division*, Vol. 89, No. SM3, pp. 103-133.

GOODMAN, R. E. (1966) On the Distribution of Stresses Around Circular Tunnels in Non-Homogeneous Rocks. *Proceedings of the First Congress of the International Society of Rock Mechanics*, Lisbon, Vol. 2, pp. 249-255.

GUDEHUS, G. (Ed.) (1977) *Finite Elements in Geomechanics.* John Wiley & Sons, Ltd., London

HOEK, E. and BROWN, E. T. (1980) *Underground Excavations in Rock.* The Institution of Mining and Metallurgy, London.

ISRM, (1981) Basic Technical Description of Rock Masses. *International Journal of Rock Mechanics and Mining Science,* Vol. 18, pp. 85-110.

IRONS, B. and AHMAD, S. (1980) *Techniques of Finite Elements.* Ellis Horwood Limited, Chichester, West Sussex.

JAEGER, J. C. and COOK, N. G. W. (1979) *Fundamentals of Rock Mechanics.* Chapman and Hall, Third Edition, London.

JUEMIN, P. and HUANQIAN, H. (1990) The 3-D Finite Element Analysis of the Excavation for a Subway Tunnel Shallowly Embedded in Sand and Gravel. *Proceedings of the International Congress Tunnel and Underground Works Today and Future*, Vol. 2, pp. 571-577, China

KIELBASSA, S. and DUDDECK, H. (1991) Stress-Strain Fields at the Tunnelling Face-Three-Dimensional Analysis for Two-Dimensional Technical Approach. *Rock Mechanics* Vol. 24, No. 1, pp. 115-132.

KOVARI, K. (1994) Erroneous Concepts Behind the New Austrian Tunnelling Method. *Tunnels and Tunnelling*, November, pp. 38-42.

KULHAWY, F. H. (1974) Finite Element Modelling Criteria for Underground Openings in Rock. *International Journal of Rock Mechanics and Mining Science and Geomechanics Abstracts*, Vol. 11. pp. 465-472.

KULHAWY, F. H. (1975) Stresses and Displacements Around Openings in Homogeneous Rock. *International Journal of Rock Mechanics and Mining Science and Geomechics Abstracts*, Vol. 12, pp. 43-57.

KULHAWY, F. H. (1975) Stresses and Displacements Around Openings in Rock Containing an Elastic Discontinuity. *International Journal of Rock Mechanics and Mining Science and Geomechics Abstracts*, Vol. 12, pp. 59-72.

KULHAWY, F. H. (1975) Stresses and Displacements Around Openings in Rock Containing an Inelastic Discontinuity. *International Journal of Rock Mechanics and Mining Science and Geomechanics Abstracts*, Vol. 12, pp. 73-78.

LAUFFER, H. (1958) Gebirgsklassifizierung für den Stolenbau. *Geologie Bauwesen 74*, pp. 46-51.

MAHTAB, M. A. and GRASSO, P. (1992) *Geomechanics Principles in the Design of Tunnels and Caverns in Rock.* Elsevier Science Publishers Co., Amsterdam, pp. 52-87.

MERTZ, W. G. and SWOBODA, G. A. (1989) Interactive Finite Element Mesh Generation for Three-Dimensional Tunnel Analysis. *Computer and Physical Modelling in Geotechnical Engineering*, Balasubramaniam et al. Editor, Balkema, Rotterdam, pp. 253-265.

MONACO, A., FANELLI, M. and RICCIONI, R. (1974) Analysis of Large Underground Openings in Rock with Finite Element Linear and Non-Linear Mathematical Models. *Proceedings of the Third Congress of the International Society for Rock Mechanics*, Vol. 2, Part B, pp. 1256-1261, Denver, Colorado.

NAYLOR, D. J. and PANDE, G. N. (1981) *Finite Elements in Geotechnical Engineering.* Pineridge Press Ltd., Swansea, pp. 42-47.

NORRIE, D. H., and VRIES, G. (1973) *The Finite Element Method.* Academic Press Inc., New York.

NORRIE, D. H., and VRIES, G. (1978) *An Introduction to Finite Element Analysis.* Academic Press Inc., New York.

OBERT, L. and DUVALL, W. I. (1967) *Rock Mechanics and Design of Rock Structures in Rock.* John Wiley & Sons, Inc., New York.

OHNISHI, Y., KISHIMOTO, H., NISHIGAKI, Y. and TANAKA, Y. (1982) Analysis of Advancing Tunnel by Two-Dimensional F.E.M. *Proceedings of the Fourth International Conference on Numerical Methods in Geomechanics*, Edmonton, Canada, Vol. 2, pp. 571-578.

ORR, T. L. L., ATKINSON, J. H. and WORTH, C. P. (1978) Finite Element Calculations for the Deformation Around Model Tunnels. *In Burt, A. Computer Methods in Tunnel Design,* Institution of Civil Engineers, London.

OTTOSEN, N. S. and PETERSSON, H. (1992) *Introduction to the Finite Element Method.* Prentice Hall International (UK) Ltd., Hertfordshire.

OWEN, D. R. J. and HINTON, E. (1980) *A Simple Guide to Finite Element.* Pineridge Press Limited, Swansea.

PAFEC 75 (1976) *Theory and Results.* PAFEC Development and Marketing, PAFEC Ltd., Pafec House, Nottingham.

PAFEC Ltd. (1992) *Data Preparation User Manual Level 7.4..* PAFEC Limited, Strelley Hall, Nottingham.

PAFEC Ltd. (1992) *PIGS User Manual Level 5.1.* PAFEC Limited, Strelley Hall, Nottingham.

PAN, X. and HUDSON, J. A. (1988) Plane Strain Analysis in Modelling Three-Dimensional Tunnel Excavations. *International Journal of Rock Mechanics and Mining Science and Geomechanics Abstracts*, Vol. 25, No. 5, pp. 331-337.

PEILA, D. (1994) A Theoretical Study of Reinforcement Influence on the Stability of a Tunnel Face. ***Geotechnical and Geological Engineering*****, Vol. 12, pp. 145-168.**

PEILA, D. and ORESTE, P. P. (1995) Axisymmetric Analysis of Ground Reinforcing in Tunnelling Design. ***Computer and Geomechanics*****, Vol. 17, pp. 253-274.**

PENDER, M. J. (1980) Elastic Solution for a Deep Circular Tunnel. Geotechniques, Vol. XXX, No. 2, pp. 216-222.

RAO, S. S. (1989) ***The Finite Element Method in Engineering.*** **Pergamon Press plc, Oxford, Second Edition.**

ROCKEY, K. C., EVANS, H. R., GRIFFITHS, D. W. and NETHERCOT, D. A. (1975) ***The Finite Element Method : A Basic Introduction.*** **Granada Published Limited, London.**

SALVADOR, F. R. And DON, U. D., (1966) Elasto-Plastic Analysis of Underground Openings by the Finite Element Method. ***Proceedings of the First Congress of the International Society of Rock Mechanics*****, Lisbon, Vol. 2, pp. 477-483.**

SAVIN, G. N. (1961) ***Stress Concentration Around Holes.*** **International Series of Monographics in Aeronautics and Astronautics, Perganom Press, London.**

SEGERLIND, L. J. (1976) ***Applied Finite Element Analysis.*** **John Wiley & Sons Inc., Michigan.**

SINHA, R. S. (1991) ***Underground Structures - Design and Construction.*** **Elsevier Science Publishers Co., Amsterdam, pp. 33-36.**

SMITH, I. M. (1982) ***Programming the Finite Element Method with Application to Geomechanics.*** **John Wiley & Son Ltd., London.**

SMITH, I. M., and GRIFFITHS, D. V. (1988) ***Programming the Finite Element Method.*** **John Wiley & Sons Ltd., Essex, Second Edition.**

SOLIMAN, E., DUDDECK, H. and AHRENS, H. (1993) Two and Three-dimensional Analysis of Closely Spaced Double-Tube Tunnels. ***Tunnelling and Underground Space Technology*****, Vol. 8, No. 1, pp. 13-18.**

STAGG, K. G., and ZIENKIEWICZ, O. C. (1968) *Rock Mechanics in Engineering Practise.* John Wiley & Sons, Inc., pp. 353-384.

STFA Construction Co. (1992) *Kisikli and Tantavi Tunnels Final Design Report,* Vol. 1, Report and Specifications, Istanbul, Turkey.

SWOBODA, G. (1982) Special Problems During the Geomechanical Analysis of Tunnels. *Proceedings of the Fourth International Conference on Numerical Methods in Geomechanics,* Edmonton, Canada, Vol. 2, pp. 605-609.

SWOBODA, G. (1990) Numerical Modelling of Tunnels. *Numerical Methods and Constitutive Modelling in Geomechanics.* International Centre for Mechanical Science Courses and Lectures No: 311, Springer Verlag pp. 227-318.

TERZAGHI, K. (1946) Rock Defects and Loads on Tunnel Support. *Rock Tunnelling with Steel Supports,* Editor R. V. Proctor and T. White, Commercial Shearing Co., Youngstown, OH, pp. 15-99.

TERZAGHI, K. and RICHARD, F. E. (1952) Stresses in Rock About Cavities. *Geotechnique,* Vol. III, pp. 57-90.

TIMOSHENKO, S., and GOODIER, J. N. (1970) *Theory of Elasticity,* Second edition. McGraw-Hill, New York

TOTTENHAM, H. and BREBBIA, C. (1977) *Finite Element Techniques in Structural Mechanics.* Stress Analysis Publishers, Southampton.

VOLLSTEDT, H. W. and DUDDECK, H. (1978) Time Dependency and Some Other Non-Linearities in Theoretical Models for Tunnels. *In Burt, A. Computer Methods in Tunnel Design,* Institute of Civil Engineering, London.

WICKHAM, G. E., TIEDEMANN, H. R. and SKINNER, E. H. (1972) Support Determination Based on Geologic Predictions. *Proceedings, Rapid Excavation and Tunnelling Conference, AIME,* New York, pp. 43-64.

WHITTAKER, B. N. and FRITH, R. C. (1990) *Tunnelling.* The Institution of Mining and Metallurgy, London, pp. 407- 421.

WITTKE, W. (1977a) Static Analysis for Underground Openings in Jointed Rock. ***In C. S. Desai and J. T. Christian : Numerical Methods In Geomechanical Engineering.*** **McGraw Hill, New York.**

WITTKE, W. (1977b) New Design Concept for Underground Openings in Rock. ***In Gudehus, G. : Finite Elements in Geomechanics.*** **John Wiley & Sons, Ltd., London.**

WITTKE, W. (1990) ***Rock Mechanics, Theory and Applications with Case Histories.*** **Springer-Verlag, Berlin.**

WOODFORD, C. H., PASSARIS, E. K. S. and BULL, J. W. (1992) ***Engineering Analysis Using PAFEC Finite Element Software.*** **Blackie and Son Ltd., Glasgow.**

ZIENKIEWICZ, O. C. (1971) ***The Finite Element Method in Engineering Science.*** **McGraw-Hill Publishing Ltd., London.**

ZIENKIEWICZ, O. C. and TAYLOR, R, L. (1989) ***The Finite Element Method.*** **Mc Graw-Hill Book Company, London.**